Journal of

Tropical Biodiversity and Biotechnology

VOLUME 10 | ISSUE 4 | DECEMBER 2025

PUBLISHED BY

UNIVERSITAS GADJAH MADA
FAKULTAS BIOLOGI

IN COLLABORATION WITH

KOBI
Konsorsium Biologi

KBI
KONSORSIUM BIOTEKNOLOGI INDONESIA
INDONESIAN BIOTECHNOLOGY CONSORTIUM

Credits

Table of Contents

Review Article

Journal of Tropical Biodiversity and Biotechnology
Volume 10, Issue 04 (2025): jtbb17573
DOI: 10.22146/jtbb.17573

Short Communication

Peliosanthes cambodiana, A New Record for The Flora of Vietnam with Focus on Its Anatomical Characteristics

Nga Nguyen-Phi[1,2], Viet Hoang[1,2], Triet Tran[1,2], Thu Trang Le-thi[3], Hong Truong Luu[4,5], Hong Thien Van[6]*

1)Faculty of Biology and Biotechnology, University of Science, Ho Chi Minh City, No. 227 Nguyen Van Cu Street, Cho Quan Ward, Ho Chi Minh City, Vietnam, 700000
2)Vietnam National University, Ho Chi Minh City, Linh Xuan Ward, Ho Chi Minh City, Vietnam, 700000
3)Faculty of Pharmacy, Nguyen Tat Thanh University, No. 300A Nguyen Tat Thanh Street, Xom Chieu Ward, Ho Chi Minh City, Vietnam, 700000
4)Graduate University of Science and Technology, Vietnam Academy of Science and Technology, 18 Hoang Quoc Viet, Nghia Do Ward, Ha Noi, Vietnam, 100000
5)Institute of Advanced Technology, Vietnam Academy of Science and Technology, No. 1D, TL29 Street, An Phu Dong Ward, Ho Chi Minh City, Vietnam, 700000
6)Institute of Biotechnology and Food Technology, Industrial University of Ho Chi Minh City, No. 12 Nguyen Van Bao Street, Hanh Thong Ward, Ho Chi Minh City, Vietnam, 700000
* Corresponding author, email: vanhongthien@iuh.edu.vn

Keywords:
Anatomy
New Record
Peliosanthes
Vietnam
Submitted:
11 November 2024
Accepted:
27 April 2025
Published:
03 October 2025
Editors:
Ardaning Nuriliani
Annisaa Widyasari

ABSTRACT
This report documents *Peliosanthes cambodiana* as a newly recorded species in the flora of Vietnam, with its distribution identified on Phu Quoc and Tho Chu Islands. Additionally, the anatomical characteristics of the leaf sheath, leaf, and root of the studied species are described here for the first time.

How to cite:
Nguyen-Phi, N. et al., 2025. *Peliosanthes cambodiana*, A New Record for The Flora of Vietnam with Focus on Its Anatomical Characteristics. *Journal of Tropical Biodiversity and Biotechnology*, 10(4), jtbb17573. doi: 10.22146/jtbb.17573

Peliosanthes Andrews, a genus belonging to the subfamily Convallarioideae of the family Asparagaceae (Chase et al. 2009; Tanaka & Nguyen 2023), comprises about 80–85 accepted species widely distributed in Southeast and South Asia, including Thailand, Myanmar, Malaysia, Indonesia, Laos, Vietnam, Nepal, Bangladesh, India, and Bhutan (Tanaka 2019; Borah & Tanaka 2024). In Vietnam, Pham (2000) listed one species, *Peliosanthes teta* André, and its subspecies, *P. teta* subsp. *humilis* (Andr.) Jess (Pham 2000). Additionally, twenty-two species and one variety belonging to the genus *Peliosanthes* have been identified as the new or additional species for the flora of Vietnam (Tanaka 2004; Averyanov 2011; Averyanov & Tanaka 2013; Averyanov et al. 2015; Averyanov et al. 2016a; Averyanov et al. 2016b; Nguyen et al. 2017; Luu et al. 2024). Studies have revealed the potential benefits of some species belonging to the genus *Peliosanthes*. For instance, *P. teta* is a medicinal plant and it has been reported to have medicinal values, including treatment for earaches, improved circulation, energy tonic properties, and postpartum care (Rahman et al. 2007; Walker 2017). Furthermore, the cytotoxic and free radical scavenging activities of *P. teta* were also reported (Al-Zubaidi et al. 2024). More recently, Do et al. (2025) successfully isolated β-sitosterol, a bioactive compound, from the ethanol extracts of the *P. micrantha* rhizomes using a newly developed HPLC method.

Peliosanthes cambodiana Aver. et N.Tanaka, a new species to science, was described by Averyanov et al. (2013) which the type specimen was collected from Kampong Saom Province, southern Cambodia. Vislobokov et al. (2020) described a new species from Vietnam, *Peliosanthes curviandra*, whose abaxial leaf epidermis characteristics were smooth, like those of two specimens of *P. cambodiana* found in Cambodia and Vietnam. Of these, the voucher specimen, 2017.13515, of *P. cambodiana* in Vietnam was collected from Phu Quoc Island, Kien Giang Province and deposited at the Main Botanic Garden of the Russian Academy of Science in Moscow (MBG) (Averyanov et al. 2013). Unfortunately, no official publications have documented the presence of *P. cambodiana* in the flora of Vietnam so far.

In 2014 and 2023, we conducted some field trips to Phu Quoc and Tho Chu islands, southern Vietnam and discovered some herbaceous populations belonging to the genus *Peliosanthes*. Our careful examination of its morphological traits indicates that the specimens from these islands are *P. cambodiana*. Thus, in the current study, *P. cambodiana* is recorded as an additional species for the flora of Vietnam with focus on its micro-morphological traits for the first time.

Peliosanthes cambodiana Aver. et N.Tanaka, Taiwania, 58(4): 233 (2013) (Figure 1)

TYPE: LE (holotype), Kampong Saom province, Cambodia, 26 November 2012.

Evergreen herb, rhizome short, 1.5–2.5 cm long, ca. 0.5 cm in diameter with many numerous thick roots, 3–5 cm long, ca. 0.3 cm in diameter. Stem erect, short, ca. 0.5 cm tall. Leaf blade elliptic to oblong, 18–22 cm long, 3–6 cm wide, dark green on the upper surface, pale green on the lower surface, glabrous, glossy, and coriaceous, apex acute or obtuse, margin serrulate; 6–8 longitudinal veins with subperpendicular secondary veinlets; petiole cylindrical, green to dark green, 20–25 cm long, ca. 0.3 cm in diameter, straight. Inflorescence hysteranthous, 8–10 cm long, flowers spirally arranged; sterile bracts surrounding peduncle, creamy white to purple, 0.7–1.6 cm long, 0.3–0.5 cm wide, herbaceous, acuminate, cuneate; peduncle erect, creamy white to purple, straight, 3–5 cm long, ca. 0.5 cm in diameter; rachis straight, white to creamy white, 4–7 cm long, ca. 0.5 cm in diameter; at the base of each pedicel are two floral bracts, creamy white to purple, cuneate, acute apex; outer

bracts (0.5–0.7 cm x ca. 0.1 cm) are longer than inner bracts (0.1–0.4 cm x ca. 0.1 cm). Pedicels pale green to white, 0.5–0.7 cm long, 0.4–0.7 mm in diameter, straight, cylindrical. Flowers solitary, growing in the bract axil. Perianth segments purple to black, incurved, ovate, ca. 1.5 mm long, ca. 1 mm wide; corona purple to black, cylindrical, 1.8–2.0 mm wide; anthers dull yellow, 6, ca. 0.4-0.6 mm wide; ovaries 1.2–1.5 mm long, ca. 1.2 mm, indistinctly hexagonal, 3-locular; ovules creamy white, 2 ovules per 1 lobe of the ovary.

Studied specimens: *Viet Hoang & Nga Nguyen-Phi TCS315, TCS316, TCS317, TCS318, TCS319, and TCS320* (PHH!), 07 March 2023, Tho Chu Island, Vietnam; *Hong Truong Luu, Tran Quoc Trung Nguyen & Quoc Dat Nguyen PQ01, PQ02, PQ03, PQ04* (SGN!), 09 December 2014, Phu Quoc Island, Vietnam.

Distribution: the species is found in Kampong Saom Province, Cambodia; Tho Chu and Phu Quoc Islands, Kien Giang Province, Vietnam

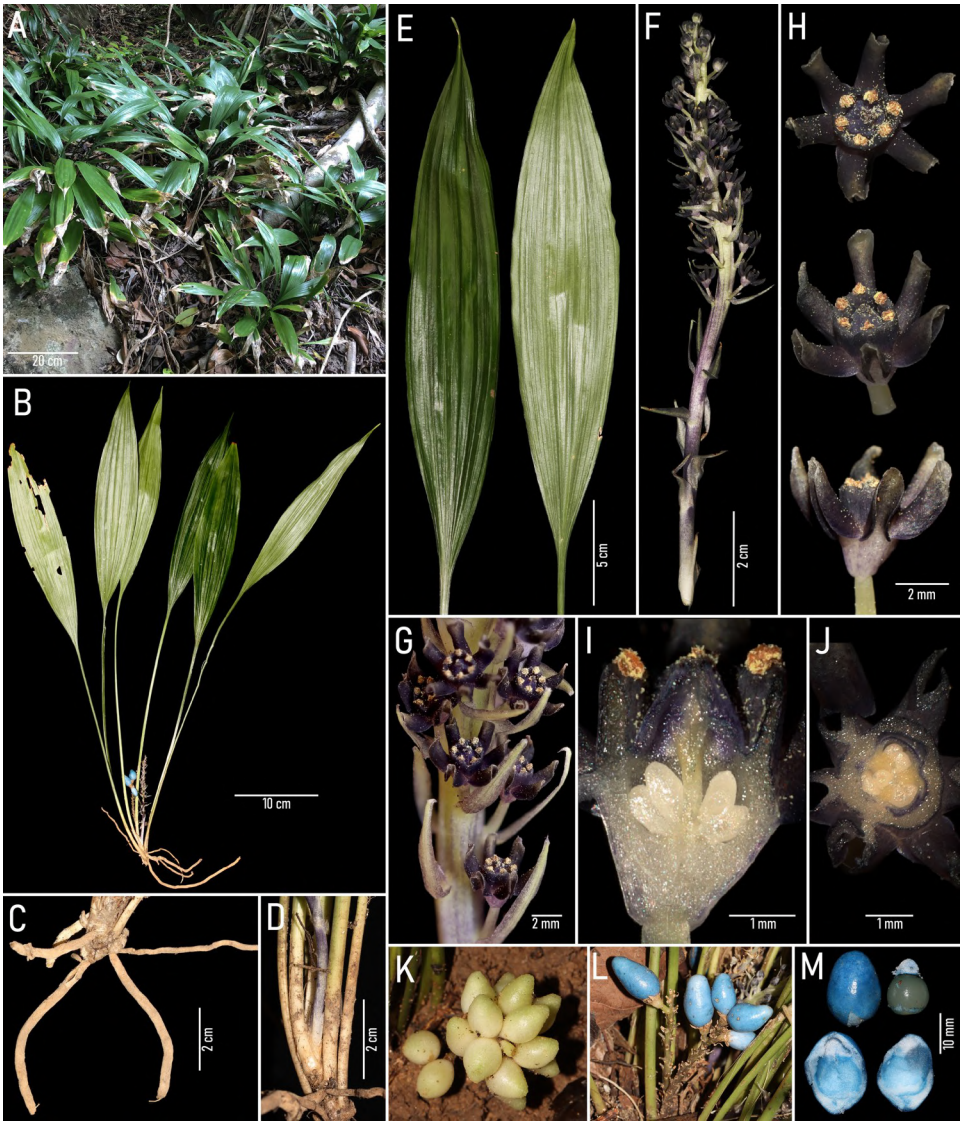

Figure 1. *Peliosanthes cambodiana* Aver. et N.Tanaka. A. Habit. B. Whole plant. C. Roots. D. Petioles. E. Leaves. F-G. Inflorescence. H. Flowers in frontal and side views. I. Longitudinal section of ovary. J. Cross section of ovary. K-L. Infructescences with different colours. M. Longitudinal section of fruit.

Anatomical characteristics of the *Peliosanthes cambodiana*

Root (Figure 2)

The cross-section has a nearly circular shape, divided into two regions; the cortex, which occupies 2/3 of the radius, and the stele, which occupies 1/3 of the radius. Cortex: the piliferous layer consists of a layer of polygonal cells,

irregular in size, with thin cellulose walls or cork impregnated, and short root hairs. The cortical parenchyma includes 26–32 layers of polygonal cells, nearly uniform in size, arranged haphazardly with small intercellular spaces. The endodermis is U-shaped. Stele: the pericycle consists of one to two layers of polygonal cells with cellulose walls, nearly uniform in size, arranged alternately with the endodermis. The vascular system consists of 18–22 phloem bundles alternating with 18–22 protoxylem bundles per ring, separated by medullary rays. The phloem bundles form oval clusters of polygonal, irregular cells. The protoxylem bundles consist of two to five xylem vessels, polygonal and centripetally differentiated. There are 18–24 phloem vessels forming a ring below the primary phloem and protoxylem; the metaxylem vessels are often connected to the protoxylem bundles. The medullary rays consist of a row of horizontally flattened polygonal cells with cellulose walls. The medullary parenchyma is divided into two regions: two to three cell layers below the metaxylem vessels have thick cellulose walls, and six to eight innermost cell layers have thin cellulose walls.

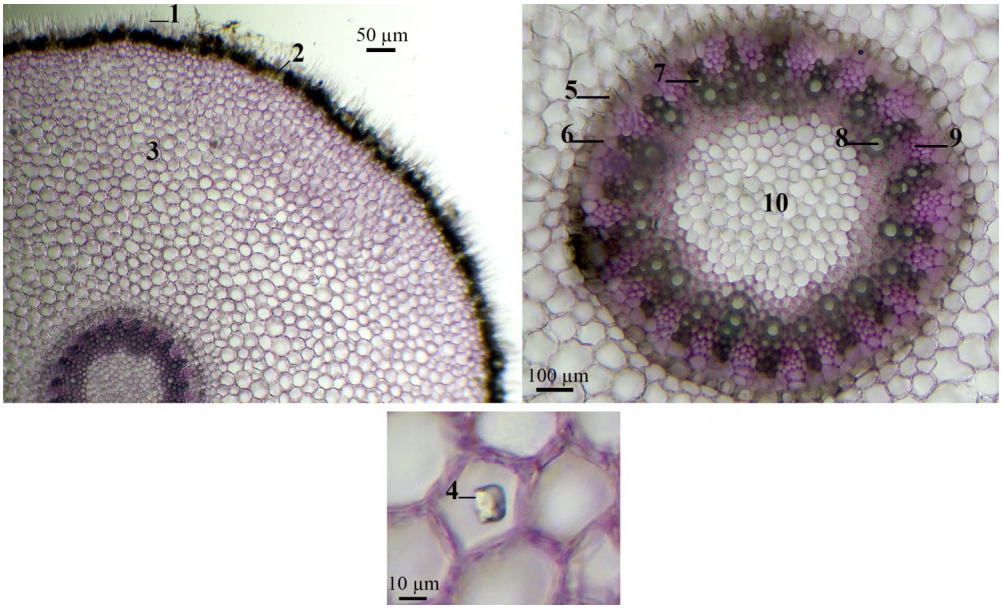

Figure 2. Cross-section of root. 1: root hairs, 2: piliferous layer, 3: parenchyma, 4: cell containing cubic calcium oxalate crystals, 5: U-shaped endodermis, 6: pericycle, 7: protoxylem, 8: metaxylem, 9: phloem, 10: medullary parenchyma.

Leaves (Figure 3)

The leaf blade is convex and concave on both sides, thickened at the vascular bundles and concave between the bundles. The upper and lower epidermis consist of a single layer of polygonal cells, with the outer surface covered with cutin. The collenchyma consists of three to six layers of cells concentrated in convex areas. The vascular bundles are arranged in a row; the vascular bundles at the midrib are the largest and become smaller towards both sides of the leaf blade. The vascular bundles have xylem overlapping phloem. Each bundle consists of 8–14 xylem vessels, lignin-impregnated walls; parenchyma with cellulose walls; and phloem consists of small polygonal cells with cellulose walls, interspersed with many very thick-walled sclerenchyma fibres, lignin-impregnated. Surrounding the vascular bundle are three to four layers of sclerenchyma fibres with very thick walls, concentrated towards the phloem. In the midrib, there are one to two small vascular bundles located above, near the collenchyma. The spongy parenchyma includes irregular, polygonal cells, arranged haphazardly around the vascular bundles. In the concave areas on the leaves (no vascular bundles), appear one to two layers of large, rectangular colourless parenchyma cells lying in rows in the middle of the spongy parenchyma.

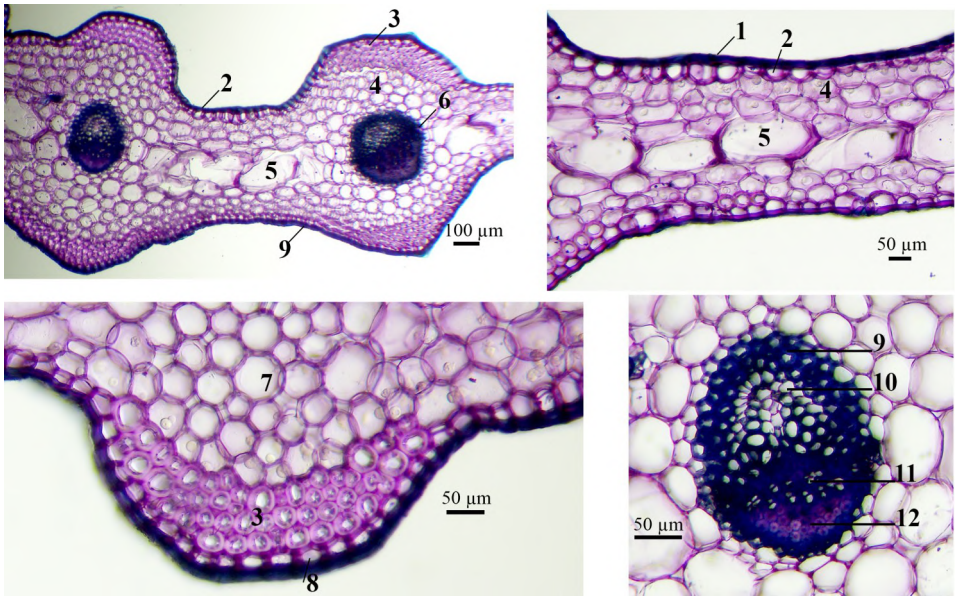

Figure 3. Cross-section of leaf blade. 1: cuticle, 2: upper epidermis, 3: collenchyma, 4: parenchyma, 5: colourless parenchyma, 6: vascular bundle, 7: spongy parenchyma, 8: lower epidermis, 9: sclerenchyma, 10: xylem, 11: phloem, 12: sclerenchyma fibres.

Leaf sheath (Figure 4)

The shape of the leaf sheath is often skewed, slightly concave on the upper surface and convex on the lower surface. The epidermis has one layer of rectangular, regular cells, cellulose walls, the outer surface is covered with a thick cutin layer. The collenchyma has three to five layers of round cells, irregular in size, arranged haphazardly. The spongy parenchyma includes polygonal, irregular cells, arranged haphazardly, surrounding the vascular bundles. The vascular bundles consist of phloem overlapping the xylem, arranged in rows in the spongy parenchyma area with the lower bundle being larger than the upper bundle. Each vascular bundle consists of 8–10 small, fairly regular xylem vessels, with wood-impregnated walls; soft tissue with cellulose walls; phloem comprises small polygonal cells with cellulose walls, interspersed with many very thick-walled sclerenchyma fibres, impregnated with lignin. Surrounding the vascular bundle are three to four layers of sclerenchyma fibres, very thick walls, concentrated towards the phloem.

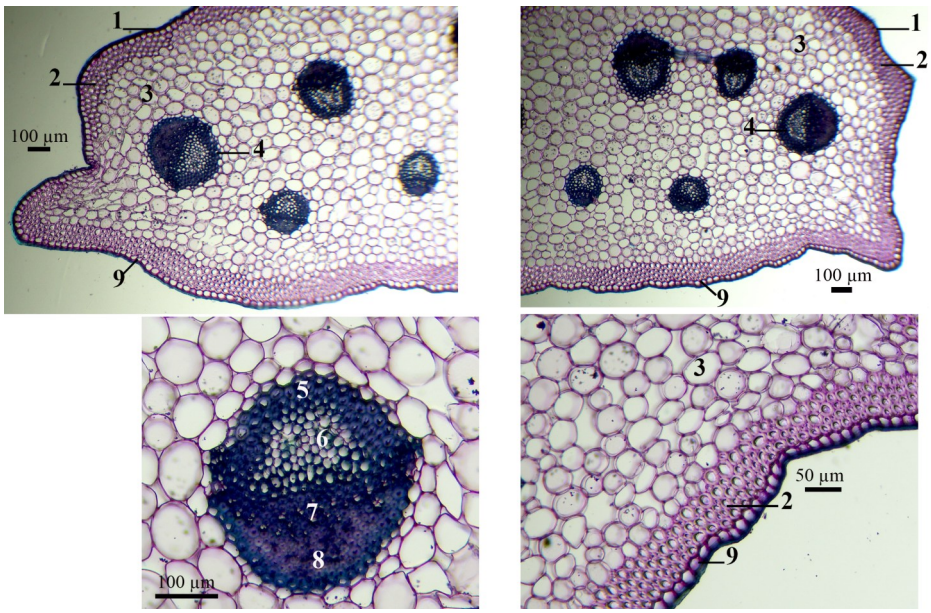

Figure 4. Cross-section of leaf sheath. 1: upper epidermis, 2: annular collenchyma, 3: spongy parenchyma, 4: vascular bundle, 5: sclerenchyma, 6: xylem, 7: phloem, 8: sclerenchyma fibres, 9: lower epidermis.

The anatomical traits of *Peliosanthes teta* were also provided by Chaikla et al. (2011). Accordingly, the transverse sections of leaf blades of *P. teta* and *P. cambodiana* share the following structural features: the leaf blade is convex and concave on both sides, thickened at the vascular bundles and concave between the bundles; the upper and lower epidermis consist of a single layer of polygonal cells; and both contained the large vascular bundles. However, the leaf cross-section *P. cambodiana* can be only distinguished from *P. teta* in having: there is a thick collenchyma layer above the lower epidermis; in the concave areas on the leaves, there are one to two layers of large, rectangular colourless parenchyma cells lying in rows in the middle of the spongy parenchyma (Chaikla et al. 2011). In addition, the transverse section of root of *P. cambodiana* differs from those of *P. teta* in having: cells containing the cubic calcium oxalate crystals; the piliferous layer with mamy short root hairs; endodermis with U-shaped (vs. no calcium oxalate crystals in cells; the piliferous layer with a few root hairs; endodermis with casparian strip in *P. teta*) (Chaikla et al. 2011).

AUTHORS CONTRIBUTION

N.N.P. and H.T.V. designed the research. N.N.P., V.H., T.T., H.T.L. collected samples during the field trips, T.T.L.T. performed the anatomical experiments. H.T.V. and N.N.P. analysed the data and wrote the manuscript.

ACKNOWLEDGMENTS

The authors are grateful to Nguyen Tran Quoc Trung and Nguyen Quoc Dat (Institute of Advanced Technology, Vietnam Academy of Science and Technology), Nguyen Thi Lan Thi (Vietnam National University- Ho Chi Minh City), for their help in collection of the samples in Phu Quoc and Tho Chu Islands, Vietnam. Additionally, we also wish to thank Lam Ty Na and Tran Thi Thao Ly (Industrial University of Ho Chi Minh City) for their cooperation.

CONFLICT OF INTEREST

The authors do not have any conflict of interests to declare.

REFERENCES

Al-Zubaidi, Y.M.A., Kadir, A.A. & Zakaria, Z.A., 2024. The free radical scavenging and cytotoxic properties of *Ardisia crenata* and *Peliosanthes teta* in the 4T1 breast cancer cell line. *Al-Rafidain Journal of Medical Sciences*, 7 (2), pp.101–108. doi: 10.54133/ajms.v7i2.1373

Averyanov, L. & Tanaka, N., 2013. New species of *Peliosanthes* (Asparagaceae) from Vietnam. *Turczaninowia*, 16(2), pp.5–7.

Averyanov, L.V., Tanaka, N. & Luu, H.T., 2013. New species of *Ophiopogon* and *Peliosanthes* (Asparagaceae) from Cambodia and Vietnam. *Taiwania*, 58(4), pp.233–241. doi: 10.6165/tai.2013.58.4.233

Averyanov, L.V. et al., 2015. New species of *Ophiopogon* Ker Gawl., *Peliosanthes* Andrews and *Tupistra* Ker Gawl. (Asparagaceae) in the flora of Laos and Vietnam. *Adansonia*, 37(1), pp.25–45. doi: 10.5252/a2015n1a4

Averyanov, L.V. et al., 2016a. New species of *Ophiopogon* and *Peliosanthes* (Asparagaceae) from Laos and Vietnam. *Taiwania*, 61(3), pp.201–217. doi: 10.6165/tai.2016.61.201

Averyanov, L.V. et al., 2016b. New species of *Ophiopogon*, *Peliosanthes* and *Tupistra* (Asparagaceae S.L.) in the flora of Vietnam. *Nordic Journal of Botany*, 34(1), pp.23–37. doi: 10.1111/njb.00854

Averyanov, L.V., 2011. *Peliosanthes yunnanensis* and *Trichosma yanshanensis*-new additions to the flora of Vietnam. *Taiwania*, 56(2), pp.143–148. doi: 10.6165/tai.2011.56(2).143

Borah, D. & Tanaka, N., 2024. *Peliosanthes meghalayensis* (Asparagaceae), a new species from Meghalaya, NE India, and synonymization of *P. bipiniana* with *P. subspicata*. *Flora*, 317, 152569. doi: 10.1016/j.flora.2024.152569

Chaikla, P., suwanthada, C. & Trisonthi, C., 2011. Morphological, anatomic and karyotypic characteristics of *Peliosanthes teta* Andrew. *African Journal of Agricultural Research*, 6(32), pp.6698–6705. doi: 10.5897/ajar11.1598

Chase, M.W., Reveal, J.L. & Fay, M.F., 2009. A subfamilial classification for the expanded Asparagalean families Amaryllidaceae, Asparagaceae and Xanthorrhoeaceae. *Botanical Journal of the Linnean Society*, 161(2), pp.132–136. doi: 10.1111/j.1095-8339.2009.00999.x

Do, N.T., Le, N.H. & Nguyen, T.H., 2025. Development of HPLC method for estimation of β-sitosterol from *Peliosanthes micrantha* rhizomes. *World News of Natural Sciences*, 59, pp.142–152.

Luu, T.T. et al., 2024. *Peliosanthes thachii* (Asparagaceae), a new species from Vietnam. *Phytotaxa*, 662(2), pp.170–176. doi: 10.11646/phytotaxa.662.2.5

Nguyen, K.S. et al., 2017. New taxa of *Peliosanthes* and *Tupistra* (Asparagaceae) in the flora of Laos and Vietnam and supplemental data for *T. patula*. *Phytotaxa*, 312(2), pp.199–212. doi: 10.11646/phytotaxa.312.2.3

Pham, H.H., 2000. C*ây cỏ Việt Nam: an illustrated flora of Vietnam* vol 3. Youth publishing house, Ho Chi Minh City.

Rahman, M.A., Uddin, S.B. & Wilcock, C.C., 2007. Medicinal plants used by Chakma tribe in Hill Tracts districts of Bangladesh. *Indian Journal of Traditional Knowledge*, 6(3), pp.508–517.

Tanaka, N., 2004. A new species of *Peliosanthes* (Convallariaceae) from Vietnam and China. *Kew Bulletin*, 59(1), pp.157–159. doi: 10.2307/4111093

Tanaka, N., 2019. Typification and identity of five taxa of *Peliosanthes* (Asparagaceae), with proposal of the new name *P. pumila* for *P. violacea* var. *minor*. *Phytotaxa*, 401(4), pp.296–300. doi: 10.11646/phytotaxa.401.4.7

Tanaka, N. & Nguyen K.S., 2023. Nolinoideae (Asparagaceae) in APG III needs replacing with Convallarioideae. *Phytotaxa* 583(3), pp.297–299. doi: 10.11646/phytotaxa.583.3.9

Vislobokov, N.A. et al., 2020. Description of the a species Peliosanthes curviandra (Asparagaceae) from Vietnam with focus on androecium structure and leaf micromorphology. *Phytotaxa*, 464(1), pp.69–76. doi: 10.11646/phytotaxa.464.1.5

Walker, T., 2017. *An examination of medicinal ethnobotany and biomedicine use in two villages on the Phnom Kulen Plateau*. Project Report, Virginia, VA, USA: Hollins University.

Journal of Tropical Biodiversity and Biotechnology
Volume 10, Issue 04 (2025): jtbb18022
DOI: 10.22146/jtbb.18022

Research Article

Identification of *Parathelphusa* sp. in the Catchment Area of Lake Matano, South Sulawesi, Using Classical Taxonomy and DNA Barcoding

Andi Wafiq Maulidah[1,6], Andi Aliah Hidayani[2,5]*, Nadiarti Nurdin Kadir[2,5,6,7], Andi Adam Malik[3], Abigail Mary Moore[4,5,6,7]

1)Master Program in Fisheries Science, Hasanuddin University, Makassar 90245, Indonesia
2)Fisheries Department, Faculty of Marine Science and Fisheries, Hasanuddin University, Makassar 90245, Indonesia
3)Faculty of Agriculture, Animal Husbandry and Fisheries, Universitas Muhammadiyah Parepare, Parepare 91131, Indonesia
4)Graduate School, Hasanuddin University, Makassar 90245, Indonesia
5)Aquatic Macrofaunal Biodiversity and Conservation Research Group, Hasanuddin University, Makassar 90245, Indonesia
6)Center of Excellence for Marine Resilience and Sustainable Development, Hasanuddin University, Makassar 90245, Indonesia
7)EAFM Learning Centre, Universitas Hasanuddin, Makassar 90245
* Corresponding author, email: aliah@fikp.unhas.ac.id

Keywords:
Malili Ancient Lake
Freshwater Crustaceans
Morphology
Phylogenetics
Watersheds
Submitted:
02 December 2024
Accepted:
27 April 2025
Published:
28 November 2025
Editors:
Ardaning Nuriliani
Tanti Agustina

ABSTRACT

This study aimed to identify and classify *Parathelphusa* sp. in Lake Matano using classical taxonomy and DNA barcoding. Methods included morphological and morphometric analysis, alongside molecular analysis using the *Cytochrome Oxidase Subunit I* (COI) gene and NCBI GenBank BLAST. The results revealed two morphotypes, one identified as *Parathelphusa pantherina*, while the second remained unidentified despite resembling *Parathelphusa pallida*. This research underscores the value of combining DNA barcoding and classical taxonomy (morphological and morphometric) for species identification, offering new insights into the genetic diversity of *Parathelphusa* crabs in the Lake Matano watershed. The results can support conservation, ecosystem management, and the protection of endemic species.

How to cite:
Maulidah, A.W. et al., 2025. Identification of *Parathelphusa* sp. in the Catchment Area of Lake Matano, South Sulawesi, Using Classical Taxonomy and DNA Barcoding. *Journal of Tropical Biodiversity and Biotechnology*, 10(4), jtbb18022. doi: 10.22146/jtbb.18022

Freshwater crabs comprise more than 1,500 species in five families, including the speciose family Gecarcinucidae (Pati & Pradhan 2020). These crabs can be an important source of nutrients as they contain vitamins, protein, calcium, and bioactive compounds (Grinang et al. 2017). However, utilization is mostly limited to consumption by local communities, with large species being more popular. Crab species of the family Gecarcinucidae reported from Lake Matano, Sulawesi, Indonesia, include *Nautilothelphusa zimmeri* Balss, 1933, *Parathelphusa pantherina* Schenkel, 1902, *P. pallida* Schenkel, 1902, *P. ferruginea* Chia & Ng, 2006, *Syntripsa matannensis* Schenkel, 1902, and *S. flavichela* Chia & Ng, 2006 (Schubart & Ng 2008; von Rintelen et al. 2012; Sentosa et al. 2017). Of these, five are considered endemic to the Malili ancient lake complex, and have been assessed as endangered in the IUCN Red List (Schubart 2018a, 2018b, 2018c, 2018d, 2018e), while one (*P. pallida*) is endemic to the wider region of Sulawesi and assessed as least concern, despite reports of declining abundance (Esser & Cumberlidge 2008).

Lake Matano, the deepest lake in Southeast Asia and the eighth deepest in the world, is estimated to be around 5 million years old (Adhityatama et al. 2017). The lake has a rich ecosystem of endemic flora and fauna (Achmad et al. 2020) and is designated as a nature reserve (Minister of Agriculture Decree No. 274/Kpts-UM/1979). With a small catchment area (436 km^2) and a surface elevation of 382 m (Crowe et al. 2008), the ecosystem is influenced by geomorphology, human activities, and internal processes (Sulastri et al. 2020). Human activities such as mining and agriculture affect water quality and ecosystems (Hatta et al. 2022). The survey shows that Matano Lake is fed by various rivers with unique catchment area characteristics.

Crabs of the genus *Parathelphusa* play important roles in aquatic ecosystems and are sensitive to environmental quality (Ng 2014). Crab populations in the Malili ancient lake complex are declining due to the introduction of invasive fish species and environmental degradation (Hilgers et al. 2018; Kusumadewi et al. 2024). Invasive flowerhorn hybrid cichlids released between 2005 and 2010 quickly spread and had become the dominant fish species in Lakes Mahalona and Towuti by 2012 (Herder et al. 2012; Haase et al. 2023). Several other invasive fish species have been introduced to Matano Lake, including the striped snakehead (*Channa striata*), tilapia (*Oreochromis* spp.), armoured catfishes (Loricariidae), catfish (*Clarias* spp.) and others; however, the most dominant is the flowerhorn, locally known as louhan (Hedianto & Sentosa 2019; Rahmawati et al. 2025).

Lake Matano, as an ancient lake with high endemic biodiversity, is recognized as a national and global conservation priority (Lukman et al. 2017; Achmad et al. 2020). Science-based conservation of endemic species such as *Parathelphusa* crabs requires ecological and genetic studies, including accurate species identification and distribution data. DNA barcoding techniques can be used to aid in species identification, especially for distinguishing morphologically similar species, in marine and freshwater environments (Hikam et al. 2021). Examples include freshwater shrimps (Jurniati et al. 2020), freshwater crabs (Sinaga et al. 2024), and gastropods (Saleky et al. 2020).

DNA barcoding has not yet been applied to endemic crabs in the watershed of Lake Matano, as previous studies did not cover a broader watershed area, and the available data only pertain to *Parathelphusa* species in the lake (von Rintelen et al. 2012; Sentosa et al. 2017). This study integrates DNA barcoding and classical morphological taxonomy to identify endemic crabs in the Matano watershed. This approach aims to enhance identification accuracy, to improve understanding of biodiversity, and to support sustainable conservation efforts.

In this study, sampling was conducted around the catchment area of Lake Matano, South Sulawesi with morphological analysis conducted at the

Fisheries Biology Laboratory, Faculty of Marine Science and Fisheries, Hasanuddin University. DNA extraction and PCR were carried out at the Biodiversity Laboratory of Indonesia (BIONESIA), Ubung Kaja, Denpasar City, Bali, while DNA sequencing was carried out at PT Genetics Science, Jakarta. Endemic crabs were collected from sites in six rivers around Lake Matano (Figure 1) with the help of local fishermen. Each specimen was photographed and stored in a labelled bag containing 96 % ethanol. The samples were then stored in a cool box with ice cubes and brought to the laboratory.

Upon arrival at the Fisheries Biology Laboratory, Hasanuddin University, tissue samples were taken from three specimens for genetic analysis. Body tissues were taken from the right side of the abdomen using sterile forceps and put into 1.5 mL micro tubes containing 96 % absolute ethanol, then taken to the Bionesia Laboratory in Denpasar, for DNA barcode analysis. Morphometric measurements (Figure 2) were carried out at the Fisheries Biology Laboratory using digital callipers with an accuracy of 0.1 mm following references (Keenan et al. 1998; Junardi et al. 2020). Morphological analysis and identification of *Parathelphusa* specimens referred to (Chia & Ng 2006).

Genomic DNA was extracted from each sample using the Geneaid Tissue Genomic DNA Extraction kit following the manufacturer's protocol. Crab tissue samples were placed in a microcentrifuge with GT buffer and proteinase, incubated, and underwent a process of lysis, binding, DNA purification by washing in a GS column, and final elution using Elution Buffer/TE at 60 °C. Fragments of the target *cytochrome oxidase subunit I* (COI) gene (barcode DNA) were amplified via PCR using forward LCO1490 and reverse HCO2198 primers (Folmer et al. 1994) following the BIONESIA protocol. The PCR profile included denaturation, annealing process, and extension steps. PCR products were verified through electrophoresis on 1 % agarose gel

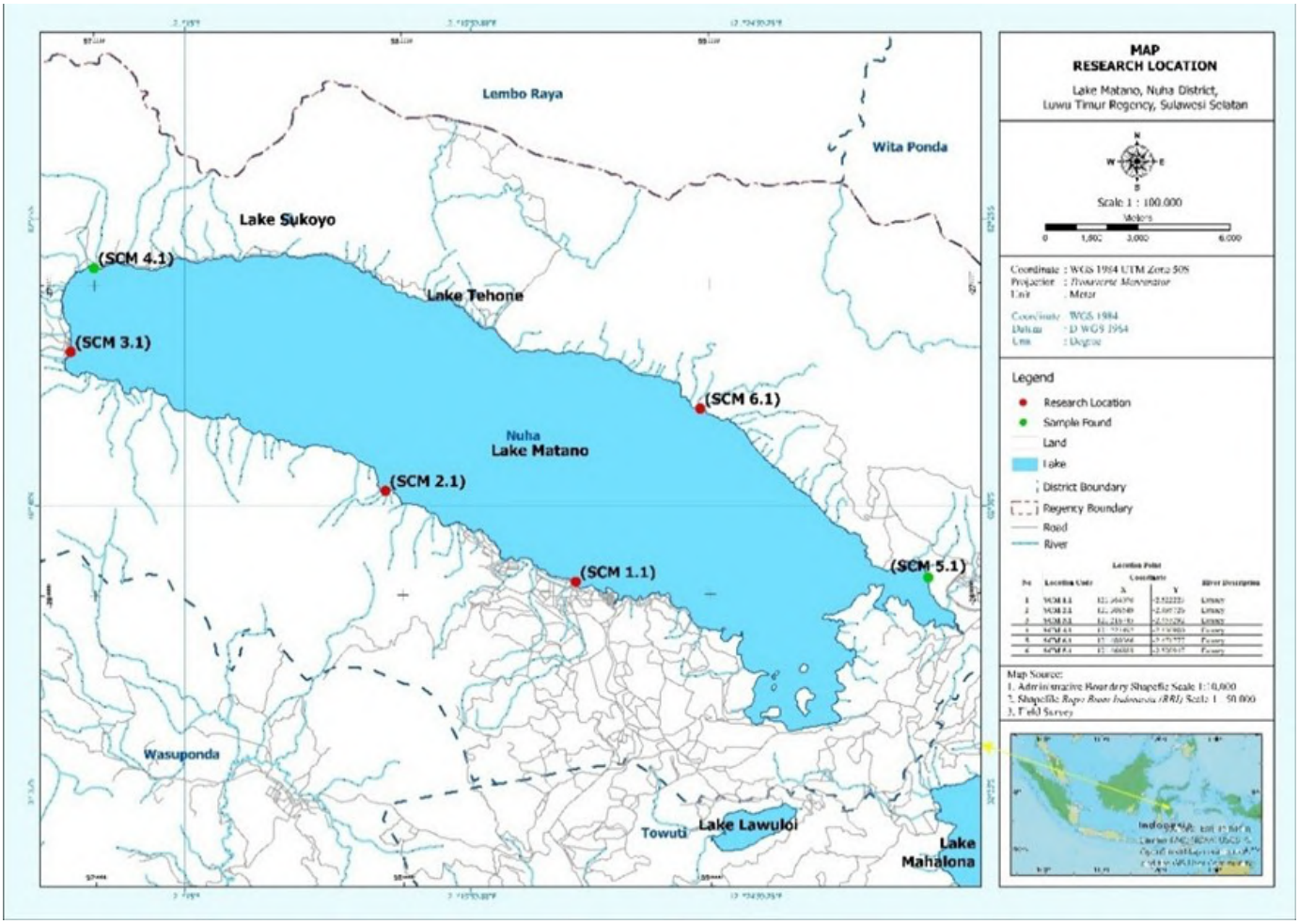

Figure 1. Research sites in the Lake Matano watershed.

with Nucleic Acid Gel Stain (GelRed®), then sent for Sanger sequencing, using a Capillary Electrophoresis Sequencer at PT Genetika Science in Jakarta.

Figure 2. Morphometric parameters of *Parathelphusa* sp. from Lake Matano watershed. Abbreviations: CL= Carapace length, CW= Carapace width, PCW= Posterior carapace width, FW= Frontal width, SL= Sternum length, SW= Sternum width, CaL= Carpus length, PrW= Propodus width, ChL= Chela length, MPrL= Major propodus length, and TL= Total width.

Morphological and morphometric data were analyzed descriptively in Microsoft Excel 2021. Chromatograms from Sanger sequencing were processed in MEGA 11 (Tamura et al. 2021) and the nucleotide sequences of each specimen were cleaned, aligned, and concatenated to generate DNA barcodes. Homologous sequences were obtained from the NCBI GenBank using the online nucleotide Basic Local Alignment Search Tool (BLAST) (NCBI, https://blast.ncbi.nlm.nih.gov) with default parameters, then aligned using the ClustalW routine in MEGA 11. Phylogenetic trees were constructed using the Neighbour-Joining method with the Kimura 2 parameter model and 1000 bootstrap replicates (Kimura 1980) and edited using the IToL Version 5 online tool (Letunic & Bork 2021).

Three samples of *Parathelphusa* sp. were recovered from the six study sites in the Lake Matano catchment: one from SCM 5.1 and two from SCM 4.1. Based on morphology referring to Chia and Ng (2006), two specimens showed typical features of *Parathelphusa pantherina* (Figure 3A) while one specimen (Figure 3B) most closely resembled *Parathelphusa pallida*, but morphological differences prevented definitive identification.

Figure 3. Morphology of *Parathelphusa* crabs from the Matano watershed: (A) *P. pantherina*. (B) *Parathelphusa* sp.

The morphometric characteristics of the three *Parathelphusa* specimens are presented in Table 1. For *P. pantherina*, comparative data from a previous study on the same species are also shown in Table 1.

The DNA barcodes obtained from the three crab specimens were 672 bp long (Table 2). Two sequences had over 99 % identity with the NCBI GenBank reference sequence of *P. pantherina* accession KF201113.1, collected from Matano Lake (Poettinger & Schubart 2014). No GenBank accession was close (>98 % identity) to the third sequence. The barcoded DNA sequences have been deposited in NCBI GenBank under submission number SUB14896961, accession numbers PQ662808- PQ662810.

A phylogenetic tree constructed using DNA barcodes from this study and homologous sequences from GenBank (Figure 4) shows two specimens in the *P. pantherina* clade while the third specimen is nested in the genus *Parathelphusa* but does not cluster with any GenBank accessions.

Morphological analysis of *Parathelphusa* sp. showed interspecies variation at the two Lake Matano watershed Sites. Two specimens from SCM 4 were confirmed as *P. pantherina*, while a specimen from SCM 5 resembled *P. pallida* more closely than other congeneric species described to date, but had black spots, unlike the description of *P. pallida* (Chia & Ng 2006). *P. pallida* is characterized by a body without black spots, while the specimen found in SCM 5 had clearly visible black spots on its carapace. Such differences could be influenced by genetic factors, nutrition, environmental conditions, and development (Song et al. 2022). DNA barcoding showed that the SCM 5 specimen was closer to *Parathelphusa ferruginea* than *P. pallida* based on the BLAST results, but did not cluster with either of these species in the phylogenetic analysis. Based on the morphological description of *P. ferruginea* by (Chia & Ng 2006), this species has a rusty red colour, a rough and wrinkled carapace surface, an "H"-shaped central depression, and an expanded claw size. These characteristics differ significantly from the specimen found in SCM 5, which more closely resembles *P. pallida*.

Parathelphusa crabs collected from the catchment area (DTA) of Lake Matano (Table 1) were within but towards the lower end of the carapace width size range previously reported for *P. pantherina* from Lake Matano (Sentosa et al. 2017). This indicates that these individuals may still be in relatively early growth stages. Meanwhile, the *Parathelphusa* sp. specimen from site SCM 5 had a carapace width of 54.5 mm, much larger than *P. pantherina*

Table 1. Morphometric characters of *Parathelphusa pantherina* and *Parathelphusa* sp. from Lake Matano DTA.

NO.	Character	Code	Measurements (mm)		Sentosa et al. 2017 (mm)
			Parathelphusa pantherina	*Parathelphusa* sp.	*Parathelphusa pantherina*
1	Carapace Width	CW	25.6-29.2	54.5	16.6 - 33.3
2	Carapace Length	CL	20.9-25.0	45	-
3	Posterior Carapace Width	PCW	11.6-16.7	27	-
4	Frontal Width	FW	11.6-16.7	21.8	-
5	Sternum Length	SL	9.3-14.6	45	-
6	Sternum Width	SW	16.3-18.8	38	-
7	Carpus Length	CaL	7.0-12.5	32.7	-
8	Major Propodus Length	MpL	16.3-27.1	51	-
9	Propodus Width	PW	4.7-10.4	20	-
10	Chela Length	ChL	11.6-16.7	24	-
11	Total width	TL	4.3-4.8	5.5	-

Table 2. Closest NCBI GenBank Accessions (BLAST Nukleotida results) for DNA Barcode Sequences of *Parathelphusa* spp. from the Lake Matano Watershed.

DNA Barcoding specimens from Matano DTA			Closest NCBI GenBank Accession			
Specimen ID	Station	Length (bp)	Species Name	Accession Number	Query Cover (%)	Identity (%)
UNH24-MAT020	SCM 5	672	*Parathelphusa ferruginea*	KF201127.1[a]	97 %	97.13 %
UNH24-MAT021	SCM 4	672	*P. pantherina*	KF201113.1[a]	97 %	99.84 %
UNH24-MAT022	SCM 4	672	*P. pantherina*	KF201113.1[a]	97 %	100 %

[a] (Poettinger & Schubart 2014)

from site SCM 4 in the Lake Matano watershed. To identify this species, additional references are required due to the lack of comparative data from previous studies. Lake crabs tend to be larger due to pressure (von Rintelen et al. 2012). Morphometric measurements of SCM 4 only included carapace width, but DNA barcoding confirmed it as *P. pantherina*, while SCM 5 requires further study for accurate identification. The mtDNA COI gene is a common molecular marker for species identification of freshwater crabs (Waugh 2007; Paransa et al. 2024). In this study, the 672 bp fragment of the COI gene was used to identify crabs in the Lake Matano DTA, resulting in two genotypes, only one of which was identified to the species level (Table 2). DNA barcode-based identification using BLAST matched the morphological results for specimens from site SCM 4, with a high identity (99.83-100 %) with the closest GenBank *P. pantherina* accession, KF201113 (Poettinger & Schubart 2014). Meanwhile, the DNA barcode of SCM 5 could not be identified based on current GenBank accessions. The closest match was *P. ferruginea* accession KF201127, from a river in the Lake Lantoa watershed (Poettinger & Schubart 2014), differing from *P. pallida* by nearly 3 %, while intraspecific genetic variation in the COI marker is typically less than 3 % in crabs (Hidayani et al. 2020).

The phylogenetic tree (Figure 4) supports the morphological and molecular (BLAST) identification of the two SCM 4 specimens as *P. pantherina*, as the sequences form a monophyletic group (clade) with other *P. pantherina* sequences in GenBank, well separated from other species groups within the genus. Meanwhile, specimen SCM 5 formed a separate clade (labelled *BIOSUB284 001 Parathelphusa* sp.), with closest kinship to another singlet, *Parathelphusa* sp., GenBank accession KF201089.1 from Lemolemo River in the Towuti Lake watershed (Poettinger & Schubart 2014). Both singlets are

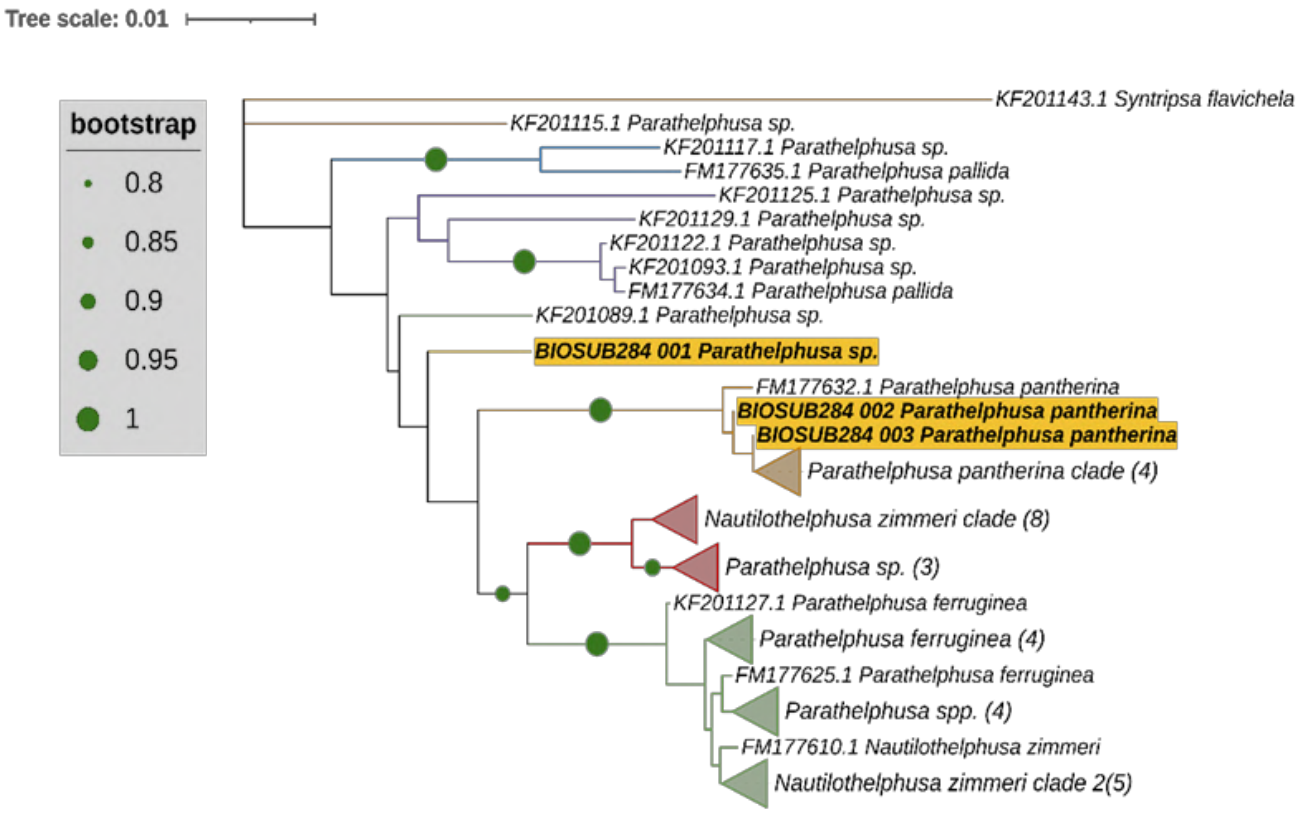

Figure 4. Phylogenetic tree based on COI DNA barcodes of *Parathelphusa* crabs from Lake Matano (yellow highlights) and nearby GenBank accessions homologous to *Sytripsa flavichela* as outgroups.

clearly separated from the clades containing *P. ferruginea* accessions, an apparent contradiction with the BLAST results, as well as clades containing *P. pantherina* and *P. pallida*. Several other separate clades were also identified as *Parathelphusa* sp. (Figure 4), suggesting the identity of these sequences was not yet known when submitted to GenBank. The outgroup, *Syntripsa flavichela*, plays an important role in identifying primitive and derivative characters and in determining the starting point in the construction of the phylogenetic tree (Subari et al. 2021).

This study on freshwater crabs in the Danau Matano watershed identified two sympatric species of the genus *Parathelphusa*. Morphological and genetic analyses (DNA barcoding) identified specimens from site SCM 4 as *P. pantherina*. Based on morphology, the specimen from SCM 5 most closely resembled *P. pallida*, though with some differences, while the DNA barcode nested in the genus *Parathelphusa* but differed from all current COI GenBank accessions. This unidentified taxon may be a new or poorly documented species within the genus *Parathelphusa*. These findings add to the evidence for undescribed species in the genus *Parathelphusa*, as discussed by Poettinger and Schubart (2014), and highlight the need for further research on freshwater crab diversity using integrated morphological and molecular taxonomy approaches, in particular in the Malili ancient lakes of Sulawesi.

AUTHORS CONTRIBUTION

A.A.H., N.N. and A.M.M.: planned the research and contributed to the manuscript including final edits. A.W.M.: collected and analyzed the data and wrote the draft manuscript. A.A.M.: provided materials and contributed to the manuscript.

ACKNOWLEDGMENTS

This study was partially funded by the Directorate General of Higher Education (DGHE) of the Republic of Indonesia under the Regular Fundamental Research Grant Scheme with contract number: 050/E5/PG.02.00.PL/2024. We also wish to express our gratitude to Muth Mainna and Meylan for their assistance in the field.

CONFLICT OF INTEREST

All authors declare no conflict of interest.

REFERENCES

Achmad, A. et al., 2020. Strategy of Ecotourism Development in Matano Lake, East Luwu Regency, South Sulawesi. *Perennial*, 16(1), pp.26–33. doi: 10.24259/perennial.v16i1.7631.

Adhityatama, S. et al., 2017. Underwater Archaeological Study on Prehistoric Material Culture in Matano Lake, South Sulawesi, Indonesia. *Journal of Southeast Asian Archaeology*, 37, pp.37–49.

Chia, O.K.S. & Ng, P.K.L., 2006. The freshwater crabs of Sulawesi, with descriptions of two new genera and four new species (Crustacea: Decapoda: Brachyura: Parathelphusidae). *Raffles Bulletin of Zoology*, 54(2), pp.381–428.

Crowe, S.A. et al., 2008. The biogeochemistry of tropical lakes: A case study from Lake Matano, Indonesia. *Limnology and Oceanography*, 53(1), pp.319–331. doi: 10.4319/lo.2008.53.1.0319.

Esser, L. & Cumberlidge, N., 2008. Parathelphusa pallida. *IUCN Red List of Threatened Species*. doi: 10.2305/IUCN.UK.2008.RLTS.T134059A3887925.en.

Folmer, O. et al., 1994. DNA primers for amplification of mitochondrial cytochrome c oxidase subunit I from diverse metazoan invertebrates. *Molecular marine biology and biotechnology*, 3(5), 294–299.

Grinang, J. et al., 2017. Nutrient Contents of the Freshwater Crab, Isolapotamon bauense from Sarawak, Malaysia (Borneo). *Tropical Life Sciences Research*, 28, pp.75–87. doi: 10.21315/tlsr2017.28.2.6.

Haase, M. et al., 2023. New species from a 'lost world': Sulawesidrobia (Caenogastropoda, Tateidae) from ancient Lake Matano, Sulawesi, Indonesia. *European Journal of Taxonomy*, 864, pp.77–103. doi: 10.5852/ejt.2023.864.2089.

Hatta, E., Manaf, M. & Alimuddin, I., 2022. Analisis Pengaruh Sektor Pertambangan Terhadap Kawasan Permukiman Kabupaten Luwu Timur. *Urban and Regional Studies Journal*, 5(1), pp.70–76. doi: 10.35965/ursj.v5i1.1971.

Hedianto, D.A. & Sentosa, A.A., 2019. Interaksi Trofik Komunitas Ikan Di Danau Matano, Sulawesi Selatan Pasca Berkembangnya Ikan Asing Invasif. *Jurnal Penelitian Perikanan Indonesia*, 25(2), 117. doi: 10.15578/jppi.25.2.2019.117-133.

Herder, F. et al., 2012. Alien invasion in Wallace's Dreamponds: Records of the hybridogenic "flowerhorn" cichlid in lake Matano, with an annotated checklist of fish species introduced to the Malili Lakes system in Sulawesi. *Aquatic Invasions*, 7(4), pp.521–535. doi: 10.3391/ai.2012.7.4.009.

Hidayani, A.A., Fujaya, Y. & Dh Trijuno, D., 2020. Variasi Genetik Intrapopulasi Rajungan (Portunus Pelagicus) dari Kaimana, Papua Barat Indonesia Berdasarkan Sekuen Gen Sitokrom C Oksidase (CO1) Intrapopulated Genetic Variation Of The Blue Swimming Crab (Portunus Pelagicus) From Kaimana, West Papua Indon. *Torani Journal of Fisheries and Marine Science*, 3(2), pp.71–83. doi: 10.35911/torani.v3i2.11373

Hikam, A.M. et al., 2021. DNA barcoding pada invertebrata laut DNA barcoding on marine invertebrates. *Biologi Udayana*, 25(1), pp.46–56. doi: 10.24843/JBIOUNUD.2021.v25.i01.p06

Hilgers, L. et al., 2018. Alien attack: trophic interactions of flowerhorn cichlids with endemics of ancient Lake Matano (Sulawesi, Indonesia). *Evolutionary Ecology Research*, 19, pp.575–590.

Junardi, J., Idola, I. & Setyawati, T.R., 2020. Morphometric of Freshwater crab Parathelphulsa maindroni Rathbun, 1902 (Decapoda, Gegarcinucidae) from two habitat type in Gunung Palung National Park. *Bioscience*, 4(2), pp.140–150. doi: 10.24036/02020421093 11-0-00.

Jurniati, J. et al., 2020. The morphological characters and DNA barcoding identification of sweet river prawn Macrobrachium esculentum (Thallwitz, 1891) from Rongkong watershed of South Sulawesi, Indonesia. *Biodiversitas Journal of Biological Diversity*, 22(1), pp.113-121. doi: 10.13057/biodiv/d220116.

Keenan, C.P., Davie, P.J. & Mann, D.L., 1998. A Revision Of The Genus Scylla De Haan, 1833 (Crustasea: Decapoda: Brachyura: Portunidae). *The Raffles Bulletin Of Zoology*, 46(1), pp.217–245.

Kimura, M., 1980. A simple method for estimating evolutionary rates of base substitutions through comparative studies of nucleotide sequences. *Journal of Molecular Evolution*, 16, pp.111–120. doi: 10.1007/BF01731581.

Kusumadewi, Y. et al., 2024. Endemic crabs from ancient Sulawesi lakes under double threat. *Oryx*, 58(1), pp.13–14. doi: 10.1017/s0030605323001242.

Letunic, I. & Bork, P., 2021. Interactive tree of life (iTOL) v5: An online tool for phylogenetic tree display and annotation. *Nucleic Acids Research*, 49 (W1), pp.W293–W296. doi: 10.1093/nar/gkab301.

Lukman et al., 2017. *Tiga Dasawarsa Berkarya Tiga Dasawarsa Berkarya Pusat Penelitian Limnologi LIPI Editor*, Jakarta: LIPI Press.

Ng, P.K.L., 2014. The identity of the Sarawak freshwater crab Parathelphusa oxygona Nobili, 1901, with description of a new species, Parathelphusa nobilii, from Western Kalimantan, Indonesia, Borneo (Crustacea: Brachyura: Gecarcinucidae). *Zootaxa*, 3774(1), pp.31–44. doi: 10.11646/zootaxa.3774.1.2.

Paransa, D.S.J. et al., 2024. Morphological and molecular identification of Metopograpsus crab caught from the coast of Tambala Village, North Sulawesi, Indonesia. *Fisheries and Aquatic Sciences*, 27(7), pp.411–420. doi: 10.47853/FAS.2024.e39.

Pati, S.K. & Pardhan, R.N., 2020. An Overview of the Freshwater Crabs (Brachyura: Gecarcinucidae) of the Western Ghats, India. *Oceanography & Fisheries Open access Journal*, 12(3), 555836. doi: 10.19080/ofoaj.2020.12.555836.

Poettinger, T. & Schubart, C.D., 2014. Molecular diversity of freshwater crabs from Sulawesi and the sequential colonization of ancient lakes. *Hydrobiologia*, 739(1), pp.73–84. doi: 10.1007/s10750-013-1643-1.

Rahmawati et al., 2025. Fisheries in the Malili ancient lake complex: from endemic to introduced species. *Cybium*, 49, pp.65–84. doi: 10.26028/cybium/2025-007.

Saleky, D., Supriyatin, F.E. & Dailami, M., 2020. Pola Pertumbuhan dan Identifikasi Genetik Turbo setosus Gmelin, 1791 [Turbinidae, Gastropoda]. *Jurnal Kelautan Tropis*, 23(3), pp.305–315. doi: 10.14710/jkt.v23i3.7514.

Schubart, C., 2018a. *Nautilothelphusa zimmeri. IUCN Red List of Threatened Species*. doi: 10.2305/IUCN.UK.2018-2.RLTS.T134323A109682617.en.

Schubart, C., 2018b. *Parathelphusa ferruginea. IUCN Red List of Threatened Species*. doi: 10.2305/IUCN.UK.2018-2.RLTS.T134327A109682794.en.

Schubart, C., 2018c. *Parathelphusa pantherina*: Matano Leopard Crab. *IUCN Red List of Threatened Species*. doi: 10.2305/IUCN.UK.2018-2.RLTS.T134415A109682928.en.

Schubart, C., 2018d. *Syntripsa flavichela*: Towuti Molluscivore Crab. *IUCN Red List of Threatened Species*. doi: 10.2305/IUCN.UK.2018-2.RLTS.T134942A109683110.en.

Schubart, C., 2018e. *Syntripsa matannensis*: Matano Molluscivore Crab. *IUCN Red List of Threatened Species*. doi: 10.2305/IUCN.UK.2018-2.RLTS.T135110A109683277.en.

Schubart, C.D. & Ng, P.K.L., 2008. A new molluscivore crab from Lake Poso confirms multiple colonization of ancient lakes in Sulawesi by freshwater crabs (Decapoda: Brachyura). *Zoological Journal of the Linnean Society*, 154(2), pp.211-221. doi: 10.1111/j.1096-3642.2008.00441.x

Sentosa, A.A., Agus Hedianto, D.H. & Satria, H., 2017. *Aspek Biologi Kepiting Endemik Di Danau Matano. LIMNOTEK*, 24(2), pp.93-100.

Sinaga, S. et al., 2024. The Impact of Artificial Barriers on the Varuna litterata Migration Route in the Lower Serayu River, Central Java and Its Molecular Identification. *Omni-Akuatika*, 20(1), pp.50-59. doi: 10.20884/1.oa.2024.20.1.1140.

Song, F. et al., 2022. The Effect of Background Color on Skin Color Variation of Juvenile Plectropomus leopardus. *Animals (Basel)*, 12(23), 3349. doi: 10.3390/ani12233349.

Subari, A., Razak, A. & Sumarmin, R., 2021. Phylogenetic Analysis of Rasbora spp. Based on the Mitochondrial DNA COI gene in Harapan Forest. *Jurnal Biologi Tropis*, 21(1), pp.89–94. doi: 10.29303/jbt.v21i1.2351.

Sulastri et al., 2020. Endemic and invasive species of Lake Matano and allowable suspended solid load to sustain high species endemism. *IOP Conference Series: Earth and Environmental Science*, 535, 012026. doi: 10.1088/1755-1315/535/1/012026.

Tamura, K., Stecher, G. & Kumar, S., 2021. MEGA11: Molecular Evolutionary Genetics Analysis Version 11. *Molecular Biology and Evolution*, 38, pp.3022–3027. doi: 10.1093/molbev/msab120.

von Rintelen, T. et al., 2012. Aquatic biodiversity hotspots in Wallacea. In *Biotic Evolution and Environmental Change in Southeast Asia*. Cambridge University Press, pp.290–315. doi: 10.1017/cbo9780511735882.014.

Waugh, J., 2007. DNA barcoding in animal species: Progress, potential and pitfalls. *BioEssays*, 29(2), pp.188–197. doi: 10.1002/bies.20529.

Journal of Tropical Biodiversity and Biotechnology
Volume 10, Issue 04 (2025): jtbb15909
DOI: 10.22146/jtbb.15909

Research Article

Bioinformatic Characterization of the Mitogen-Activated Protein Kinase Genes in Wild *Arachis* Species with Expression Insights in *Arachis hypogaea*

Ha Duc Chu[1], Huyen Thi Thanh Tran[2], Le Thi Ngoc Quynh[3], Dong Huy Gioi[4], Hong Viet La[5], Man Thi Le[6], Phi Bang Cao[6]*

1)Faculty of Agricultural Technology, University of Engineering and Technology, Vietnam National University Hanoi, Xuan Thuy Road, Cau Giay Ward, Hanoi City 122300, Vietnam
2)Faculty of Biology, Hanoi National University of Education, Xuan Thuy Road, Cau Giay Ward, Hanoi City 122300, Vietnam
3)Department of Biotechnology, Thuyloi University, Tay Son Road, Kim Lien Ward, Hanoi City 122300, Vietnam
4)Faculty of Biotechnology, Vietnam National University of Agriculture, Gia Lam Ward, Hanoi City 122300, Vietnam
5)Institute of Research and Application, Hanoi Pedagogical University 2, Xuan Hoa Ward, Phu Tho Province 280000, Vietnam
6)Faculty of Natural Sciences, Hung Vuong University, Nong Trang Ward, Phu Tho Province 35000, Vietnam
* Corresponding author, email: phibang.cao@hvu.edu.vn

Keywords:
Evolutionary genomics
Mitogen-activated protein kinase
Peanut
Tissue-specific expression
Wild *Arachis*
Submitted:
20 March 2024
Accepted:
07 May 2025
Published:
06 October 2025
Editors:
Ardaning Nuriliani
Liya Audinah

ABSTRACT

Mitogen-activated protein kinases (MAPKs) are crucial signalling components involved in plant growth, development, and responses to environmental stimuli. While their roles are well established in model plants, comprehensive characterisation in *Arachis* species remains limited. This *in silico* study conducted a genome-wide identification and analysis of *MAPK* genes in cultivated peanut (*A. hypogaea*) and its two wild *Arachis* species, *A. duranensis*, and *A. ipaensis*. We identified 42 AhMAPK, 18 AraduMAPK, and 18 AraipMAPK proteins in *A. hypogaea*, *A. duranensis*, and *A. ipaensis*, respectively. These MAPK proteins exhibited diverse physicochemical properties and gene structures. We constructed a maximum likelihood-based phylogenetic tree, categorising the MAPK proteins in *Arachis* species, *Arabidopsis thaliana*, and *Medicago truncatula*, into five distinct groups. Gene structure analysis indicated substantial exon-intron variation, implying potential regulatory complexity and alternative splicing mechanisms. Transcriptome data analysis across multiple major organ and tissue types revealed differential expression patterns, with certain *AhMAPK* genes showing strong tissue-specific expression, particularly in leaves, roots, and reproductive organs. The inclusion of diploid progenitors provided insights into the evolutionary trajectory and functional conservation of *MAPK* genes in *Arachis* species. These findings contribute to a deeper understanding of MAPK-mediated signalling in peanuts and offer a genetic foundation for future studies aimed at improving stress resilience and crop performance. The identified *MAPK* genes present valuable targets for genetic engineering and molecular breeding programmes to enhance peanut productivity and adaptability to environmental stresses.

How to cite:
Chu, H.D. et al., 2025. Bioinformatic Characterization of the Mitogen-Activated Protein Kinase Genes in Wild *Arachis* Species with Expression Insights in *Arachis hypogaea*. *Journal of Tropical Biodiversity and Biotechnology*, 10(4), jtbb15909. doi: 10.22146/jtbb.15909

INTRODUCTION

The cultivated peanut (*Arachis hypogaea*) is a multi-functional crop of significant agricultural and economic importance, primarily cultivated in tropical and subtropical regions around the world (Toomer 2018). Originating from South America, the peanut has an interesting history of domestication and dispersal, making its way across the globe through Spanish and Portuguese explorers (Bertioli et al. 2020; Wadood et al. 2022). Peanuts play a crucial role in global food systems, serving as a vital source of protein, fat, and other nutrients (Hill 2002; Toomer 2018). They are utilised in various forms, including whole peanuts, peanut oil, and peanut butter, contributing to both human nutrition and livestock feed. Despite its widespread cultivation and utility, peanuts face various abiotic stresses, such as drought, salinity, and temperature extremes, which can significantly impact yield and quality (Li et al. 2014; Zheng et al. 2019). Understanding the molecular mechanisms underlying peanut growth, development, and stress adaptation is essential for improving crop resilience. Several regulatory pathways, including hormonal signalling networks and transcription factor-mediated gene expression, have been implicated in peanut development and stress responses. However, the specific molecular players governing these processes remain largely unexplored (Kosev & Vasileva 2019).

Mitogen-activated protein kinase (MAPK) proteins are pivotal components of signalling pathways in plants, playing crucial roles in regulating cellular responses to a variety of external stimuli (Avruch 2007; Zhang & Zhang 2022). Specifically, MAPKs are serine/threonine protein kinases that are organised into three-tiered cascades, including MAP kinase kinase kinases, MAP kinase kinases, and MAPKs (Group 2002). This categorised arrangement facilitates the transmission of signals from the cell surface to the nucleus, enabling an effective and coordinated cellular response. Of particular interest, MAPKs are involved in a wide array of plant processes such as growth, development, and reproduction, and are particularly critical in the adaptation and survival strategies of plants under stress conditions (Jagodzik et al. 2018; Lin et al. 2021; Niekerk et al. 2024). Recently, the MAPK families have been comprehensively identified and characterized in a large number of higher plant species, including rice (*Oryza sativa*) (Reyna & Yang 2006), Arabidopsis (*Arabidopsis thaliana*) (Andreasson & Ellis 2010), purple false brome (*Brachypodium distachyon*) (Chen et al. 2012), tomato (*Solanum lycopersicum*) (Kong et al. 2012), three legume species, including *Lotus japonicus*, *Medicago truncatula* and *Phaseolus vulgaris* (Neupane et al. 2013), maize (*Zea mays*) (Liu et al. 2013), grapevine (*Vitis vinifera*) (Wang et al. 2014), cucumber (*Cucumis sativus*) (Wang et al. 2015), chrysanthemum (*Chrysanthemum morifolium*) (Song et al. 2018), chickpea (*Cicer arietinum*) (Singh et al. 2018), cultivated strawberry (*Fragaria* × *ananassa*) (Li et al. 2022), lettuce (*Lactuca sativa*) (Wang et al. 2022), as well as banana (*Musa* spp.) (Fan et al. 2023), where they are known to regulate responses to abiotic and biotic stresses. Despite their established roles in other crops, there have been no recent reports on the MAPKs in peanuts, even though the genome of peanuts has been released (Clevenger et al. 2016; Zhuang et al. 2019). Furthermore, *A. hypogaea* is an allotetraploid species derived from the hybridisation of two wild diploid ancestors, *A. duranensis* (A-genome) and *A. ipaensis* (B-genome). These wild species serve as essential genetic resources for understanding the evolutionary development of *A. hypogaea*, as well as for identifying key genes associated with agronomic traits. Investigating the MAPK protein family across these three species allows for a comparative genomic approach to explore their conservation, divergence, and functional relevance in peanut biology.

This study aimed to conduct a computational analysis of MAPK proteins in three *Arachis* species, including *A. hypogaea*, *A. duranensis*, and *A. ipaensis* (García et al. 2021). We began by identifying and annotating all putative MAPK proteins within the most recent *A. hypogaea*, *A. duranensis*, and *A. ipaensis* genome

assemblies. Using bioinformatics tools, we analysed the physical and chemical properties of each identified MAPK protein. Further investigations included exploring the classification and gene structure of these proteins. Finally, we re-analysed the expression levels of genes encoding the MAPK proteins across various major organs and tissues of the peanut by accessing previous microarray datasets. The findings provide valuable insights into the potential functions of *MAPK* genes in peanut development. As no prior genome-wide studies on *MAPK* genes in peanuts exist, this research establishes a foundation for future functional studies and genetic improvement efforts.

MATERIALS AND METHODS

Screening of the mitogen-activated protein kinase proteins in *Arachis* species

To identify members of the *MAPK* gene families in *Arachis* spp., a two-step approach was adopted as previously described (Brasileiro et al. 2023; Chu et al. 2024). Initially, a gene family search was conducted in the PeanutBase database (Dash et al. 2016), utilising the well-characterised MAPK proteins from *A. thaliana* (Andreasson & Ellis 2010). This search targeted the annotated genomes of cultivated peanut, namely *A. hypogaea* (BioProject: PRJNA419393) (Bertioli et al. 2019) and two wild *Arachis* species, including *A. duranensis* (BioProject: PRJNA258023) and *A. ipaensis* (BioProject: PRJNA258025) (Bertioli et al. 2016). Only non-redundant *MAPK* genes were selected for further analysis.

Characterisation of the mitogen-activated protein kinase proteins in *Arachis* species

The molecular weight (mW) and common physicochemical properties of each MAPK protein sequences were predicted using the ExPASy Protparam web-based tool (Gasteiger et al. 2003, 2005), as previously reported (La et al. 2022a, 2022b; Le et al. 2022). Among them, isoelectric point (pI), grand average of hydropathicity (GRAVY), and aliphatic index (AI) values were analysed. To maintain consistency in the analysis, all tools and databases were employed with their default settings throughout the process.

Phylogenetic analysis of the mitogen-activated protein kinase proteins in *Arachis* species

The construction of the phylogenetic tree for the well-characterised MAPK members from *Arabidopsis* (Andreasson & Ellis 2010), *M. truncatula* (Neupane et al. 2013), and three *Arachis* species was carried out by first aligning the full-length protein sequences using the ClustalX program (Thompson et al. 1997; Thompson et al. 2002). Following the alignment, a Maximum Likelihood-based phylogenetic tree was generated using MEGA11 software (Tamura et al. 2021). A total of 1000 bootstrap replicates were used to explore the phylogenetic relationships among members of the MAPK families as previously described (Cao 2022; La et al. 2022a, 2022b; Le et al. 2022; Chu et al. 2024).

Exon/intron organisation of the mitogen-activated protein kinase proteins in *Arachis hypogaea*

To analyse the gene structure of genes encoding the MAPK in *A. hypogaea*, we examined the organisation of the exons and introns for each MAPK gene as following previous studies (Cao 2022; La et al. 2022a, 2022b; Le et al. 2022; Chu et al. 2024). Using the BioEdit software (Hall 1999), we first calculated the lengths of the genomic DNA sequence for each gene. These genomic DNA sequence and coding DNA sequence data were then input into the Gene Structure Display Server (Hu et al. 2015), which facilitated the construction and visualisation of the exon/intron structure for each *MAPK* gene.

Expression analysis of the mitogen-activated protein kinase proteins in *Arachis hypogaea*

To explore the expression profiles of the *MAPK* genes across various growth and development stages in *A. hypogaea* plants, we re-analysed recent transcriptome datasets from the GEO NCBI (Barrett et al. 2013) and the PeanutBase websites (Dash et al. 2016). Specifically, we focused on an expression atlas from PeanutBase (Dash et al. 2016), which has been catalogued under GEO accession number GSE71357 (Clevenger et al. 2016). This microarray dataset was re-analysed to validate the Fragments Per Kilobase of transcript per Million mapped reads (FPKM) values for the peanut *MAPK* genes across ten major organs and tissues, including mainstem leaf, lateral stem leaf, seedling leaf, vegetative shoot tip, reproductive shoot tip, nodule, root, perianth, stamen, and pistil (Clevenger et al. 2016). We also accessed one recent dataset, namely GSE180915, that provided the transcriptomic profiles in lateral and terminal leaflets, petiole, and shoot apical meristem. The re-analysis was conducted using R-script, following the methods previously described (La et al. 2022a, 2022b; Le et al. 2022).

RESULTS AND DISCUSSION

Genome-wide identification of the mitogen-activated protein kinase proteins in *Arachis* species

In this study, genome-wide searches focused on identifying conserved MAPK domains were conducted across the genomes of three *Arachis* species, including *A. duranensis* (Bertioli et al. 2016), *A. ipaensis* (Bertioli et al. 2016) and *A. hypogaea* (Bertioli et al. 2019). After manually removing redundant sequences, only proteins that contained conserved MAPK domains were retained. The naming of each *MAPK* gene family was based on the chromosomal locations for each species. As a result, a total of 42 AhMAPK proteins in *A. hypogaea*, 18 AraduMAPK proteins in *A. duranensis* and 18 AraipMAPK proteins in *A. ipaensis* were comprehensively identified (Table 1 and 2).

Recently, the MAPK proteins have been extensively screened across various plant species, revealing significant diversity in their numbers and functions. In *Arabidopsis*, 20 MAPK proteins have been documented (Andreasson & Ellis 2010), while rice has reported 15 members (Reyna & Yang 2006). Other plant species have shown varied counts, such as chrysanthemum (11 genes) (Song et al. 2018) , grape (12 genes) (Wang et al. 2014), and cultivated strawberry (43 genes) (Li et al. 2022). In the genomes of *L. japonicus*, *M. truncatula* and *P. vulgaris*, it has been identified varying numbers of MAPK proteins (Neupane et al. 2013). Specifically, *L. japonicus* possesses 19 MAPK proteins, *M. truncatula* has 18 MAPK proteins, while *P. vulgaris* contains 15 MAPK proteins (Neupane et al. 2013). In cucumber, a total of 14 members of the MAPK family have been reported (Wang et al. 2015). According to the banana genome databases, *M. acuminata*, *M. balbisiana*, *M. itinerans*, *M. schizocarpa*, and *M. textilis* contained 21 (namely MaMPK1-21), 12 (namely MbMPK1-12), 18 (namely MiMPK1-18), 16 (namely MsMPK1-16), and 10 (namely MtMPK1-10) members of the MAPK family, respectively (Fan et al. 2023). This study extended the exploration to three *Arachis* species, identifying 42 AhMAPK, 18 AraduMAPK, and 18 AraipMAPK proteins, which were designated from AhMAPK01 to AhMAPK42, AraduMAPK01 to AraduMAPK18 and AraipMAPK01 to AraipMAPK18 proteins in *A. hypogaea*, *A. duranensis*, and *A. ipaensis*, respectively.

Characterisation of the general properties of the mitogen-activated protein kinase proteins in *Arachis* species

The MAPK protein lengths varied across the three *Arachis* species, reflecting structural diversity. In *A. hypogaea*, 42 AhMAPK proteins ranged from 125

Table 1. Summary of the mitogen-activated protein kinase proteins in *Arachis hypogaea*.

Gene name	Locus name	gDNA (bp)	PL (aa)	mW (kDa)	pI	GRAVY	AI
AhMAPK01	arahy.Tifrunner.gnm1.ann1.LP1FMS	4788	612	69.51	9.20	-0.46	81.62
AhMAPK02	arahy.Tifrunner.gnm1.ann1.E5L63Q	3998	578	65.73	9.00	-0.45	79.84
AhMAPK03	arahy.Tifrunner.gnm1.ann1.YDHQ7Y	3419	383	43.86	5.91	-0.28	92.40
AhMAPK04	arahy.Tifrunner.gnm1.ann1.RQ7QZ9	2657	371	42.57	5.60	-0.23	99.65
AhMAPK05	arahy.Tifrunner.gnm1.ann1.Z8RB6C	2512	370	42.68	4.97	-0.29	96.97
AhMAPK06	arahy.Tifrunner.gnm1.ann1.HLI3FT	2027	393	44.50	6.32	-0.36	86.11
AhMAPK07	arahy.Tifrunner.gnm1.ann1.80H1WW	3235	397	45.40	5.51	-0.33	88.26
AhMAPK08	arahy.Tifrunner.gnm1.ann1.2MP0U5	4078	608	69.10	7.01	-0.63	80.05
AhMAPK09	arahy.Tifrunner.gnm1.ann1.M5D7FW	2102	368	42.27	8.00	-0.17	99.10
AhMAPK10	arahy.Tifrunner.gnm1.ann1.VK23H5	6635	563	63.96	8.80	-0.46	78.67
AhMAPK11	arahy.Tifrunner.gnm1.ann1.BC5GM2	5094	376	43.33	5.91	-0.34	91.54
AhMAPK12	arahy.Tifrunner.gnm1.ann1.HE88YK	2028	380	43.49	6.36	-0.35	90.34
AhMAPK13	arahy.Tifrunner.gnm1.ann1.U4IX7Q	5192	482	55.28	6.50	-0.53	81.97
AhMAPK14	arahy.Tifrunner.gnm1.ann1.3P0VVA	5296	663	75.85	9.19	-0.41	81.76
AhMAPK15	arahy.Tifrunner.gnm1.ann1.KXH2SR	4980	600	68.00	9.16	-0.49	78.72
AhMAPK16	arahy.Tifrunner.gnm1.ann1.X8RB79	1807	372	42.64	6.14	-0.20	97.55
AhMAPK17	arahy.Tifrunner.gnm1.ann1.ZIU9VW	4793	612	69.50	9.19	-0.46	81.78
AhMAPK18	arahy.Tifrunner.gnm1.ann1.521JDX	4285	577	65.65	9.09	-0.48	76.95
AhMAPK19	arahy.Tifrunner.gnm1.ann1.WCN1YP	3048	383	43.92	5.91	-0.27	92.40
AhMAPK20	arahy.Tifrunner.gnm1.ann1.YJFK71	1391	291	32.50	8.64	-0.19	96.15
AhMAPK21	arahy.Tifrunner.gnm1.ann1.AF4FIK	2664	371	42.58	5.60	-0.24	99.11
AhMAPK22	arahy.Tifrunner.gnm1.ann1.FN4EG0	2267	369	42.57	4.97	-0.30	96.18
AhMAPK23	arahy.Tifrunner.gnm1.ann1.773MH2	1996	387	44.05	6.32	-0.37	86.43
AhMAPK24	arahy.Tifrunner.gnm1.ann1.C5DY5V	3247	397	45.40	5.51	-0.33	88.26
AhMAPK25	arahy.Tifrunner.gnm1.ann1.68AXRD	4095	606	68.88	7.01	-0.63	79.98
AhMAPK26	arahy.Tifrunner.gnm1.ann1.68T27Q	1710	368	42.27	8.00	-0.17	99.10
AhMAPK27	arahy.Tifrunner.gnm1.ann1.9G5FU0	7429	563	63.97	8.80	-0.45	79.70
AhMAPK28	arahy.Tifrunner.gnm1.ann1.L410JY	4675	376	43.33	5.91	-0.34	91.54
AhMAPK29	arahy.Tifrunner.gnm1.ann1.CC6N12	2446	380	43.50	6.28	-0.35	89.84
AhMAPK30	arahy.Tifrunner.gnm1.ann1.7K4NIS	4577	482	55.31	6.50	-0.53	81.97
AhMAPK31	arahy.Tifrunner.gnm1.ann1.IN5DGA	746	125	14.02	10.00	-0.38	92.16
AhMAPK32	arahy.Tifrunner.gnm1.ann1.BPF1MW	6451	426	48.31	5.60	-0.36	81.06
AhMAPK33	arahy.Tifrunner.gnm1.ann1.Q98R2Z	5179	667	76.02	9.23	-0.40	81.14
AhMAPK34	arahy.Tifrunner.gnm1.ann1.X0F9HV	1760	372	42.59	6.14	-0.19	98.36
AhMAPK35	arahy.Tifrunner.gnm1.ann1.8F3XE1	4447	600	68.04	9.18	-0.49	78.72
AhMAPK36	arahy.Tifrunner.gnm1.ann1.4D26T3	2084	355	40.87	9.51	-0.11	101.07
AhMAPK37	arahy.Tifrunner.gnm1.ann1.RFCR2Y	6491	550	62.18	9.61	-0.316	78.73
AhMAPK38	arahy.Tifrunner.gnm1.ann1.1E12MN	7483	439	50.11	5.85	-0.267	86.36
AhMAPK39	arahy.Tifrunner.gnm1.ann1.C4CQD3	6491	550	62.18	9.61	-0.316	78.73
AhMAPK40	arahy.Tifrunner.gnm1.ann1.ZSL8AZ	7456	438	49.92	5.93	-0.269	85.66
AhMAPK41	arahy.Tifrunner.gnm1.ann1.UDY993	1248	415	47.35	9.04	-0.381	80.58
AhMAPK42	arahy.Tifrunner.gnm1.ann1.QN2FLP	1218	405	46.30	8.97	-0.34	82.57

Note: gDNA: gene size (bp), PL: protein length (amino acid residues), MW: Molecular weight (kDa), pI: Isoelectric point, GRAVY: Grand average of hydropathicity, AI: Aliphatic index.

(AhMAPK31) to 667 (AhMAPK33) amino acids, averaging 383 amino acids. In *A. duranensis*, 18 AraduMAPK proteins ranged from 360 (AraduMAPK08) to 669 (AraduMAPK14) amino acids, with an average of 415 amino acids. Similarly, *A. ipaensis* contained 18 AraipMAPK proteins, ranging from 368 (AraipMAPK09) to 667 (AraipMAPK14) amino acids, also averaging 415 amino acids. The mW values of these MAPK proteins varied from 14.02 (AhMAPK31) to 76.02 (AhMAPK33) kDa (in the AhMAPK family from *A. hypogaea*), 41.02 (AraduMAPK08) and 76.41 (AraduMAPK14) kDa (in the AraduMAPK family from *A. duranensis*) and 42.27 (AraipMAPK09) and 76.02

Table 2. Summary of the mitogen-activated protein kinase proteins in *A. duranensis* and *A. ipaensis*.

Gene name	Locus name	gDNA (bp)	PL (aa)	mW (kDa)	pI	GRAVY	AI
AraduMAPK01	Aradu.271A7	3072	600	68.03	9.17	-0.41	83.25
AraduMAPK02	Aradu.B41M6	3229	578	65.67	9.00	-0.45	79.84
AraduMAPK03	Aradu.CGX1Z	3043	371	42.56	5.86	-0.30	91.46
AraduMAPK04	Aradu.IP5K7	2656	371	42.57	5.60	-0.23	99.65
AraduMAPK05	Aradu.RVT4Y	2513	369	42.54	4.97	-0.29	97.24
AraduMAPK06	Aradu.J97W2	1989	371	42.74	6.15	-0.31	90.94
AraduMAPK07	Aradu.A68MB	3576	607	68.97	7.01	-0.63	80.18
AraduMAPK08	Aradu.44GS0	3129	360	41.02	5.72	-0.34	88.94
AraduMAPK09	Aradu.Q0IL1	1044	368	42.29	8.00	-0.17	99.10
AraduMAPK10	Aradu.WE8JU	4030	563	63.96	8.80	-0.46	78.67
AraduMAPK11	Aradu.NJQ5G	4433	383	44.00	5.54	-0.28	92.40
AraduMAPK12	Aradu.A7MKH	2040	384	43.74	6.36	-0.34	89.92
AraduMAPK13	Aradu.H6YZR	4783	500	57.42	6.94	-0.52	80.56
AraduMAPK14	Aradu.E1ZU5	5072	669	76.41	9.03	-0.40	81.48
AraduMAPK15	Aradu.93Y1F	4763	600	68.00	9.16	-0.49	78.72
AraduMAPK16	Aradu.49RUG	2385	372	42.64	6.14	-0.20	97.55
AraduMAPK17	Aradu.4FA0W	4435	417	47.50	9.49	-0.45	75.30
AraduMAPK18	Aradu.IX021	7290	453	51.61	5.79	-0.21	87.55
AraipMAPK01	Araip.RV49X	4100	600	68.04	9.16	-0.42	83.25
AraipMAPK02	Araip.Y7IQI	3278	561	63.76	8.98	-0.50	77.06
AraipMAPK03	Araip.32FLV	3048	371	42.56	5.80	-0.30	91.46
AraipMAPK04	Araip.IL3I2	2664	371	42.58	5.60	-0.24	99.11
AraipMAPK05	Araip.8K6RH	2267	369	42.57	4.97	-0.30	96.18
AraipMAPK06	Araip.WRI31	1616	387	44.05	6.32	-0.37	86.43
AraipMAPK07	Araip.74VLD	5603	385	44.34	5.65	-0.34	89.22
AraipMAPK08	Araip.LMV71	3565	615	69.82	7.30	-0.61	80.55
AraipMAPK09	Araip.AT3RC	1710	368	42.27	8.00	-0.17	99.10
AraipMAPK10	Araip.96FUL	4009	563	63.97	8.80	-0.45	79.70
AraipMAPK11	Araip.AH33F	4211	376	43.33	5.91	-0.34	91.54
AraipMAPK12	Araip.6I993	2098	380	43.50	6.28	-0.35	89.84
AraipMAPK13	Araip.TJ3I8	4577	482	55.30	6.50	-0.53	81.97
AraipMAPK14	Araip.P1N43	4920	667	76.02	9.23	-0.40	81.14
AraipMAPK15	Araip.CL071	1760	372	42.60	6.14	-0.19	98.36
AraipMAPK16	Araip.U4Z8Q	4532	600	68.04	9.18	-0.49	78.72
AraipMAPK17	Araip.T0473	4135	397	44.70	9.56	-0.45	72.75
AraipMAPK18	Araip.Q5AHE	1218	392	44.72	9.20	-0.40	79.85

Note: gDNA: gene size (bp), PL: protein length (amino acid residues), MW: Molecular weight (kDa), pI: Isoelectric point, GRAVY: Grand average of hydropathicity, AI: Aliphatic index.

(AraipMAPK14) kDa (in the AraipMAPK family from *A. ipaensis*). Next, the pI values of the AhMAPK proteins in *A. hypogaea* spanned from 4.97 (AhMAPK22 and AhMAPK05) to 10.00 (AhMAPK31), while these scores of the AraduMAPK and AraipMAPK proteins in *A. duranensis* and *A. ipaensis* ranged from 4.97 (AraduMAPK05) to 9.49 (AraduMAPK17) and 4.97 (AraipMAPK05) to 9.56 (AraipMAPK17), respectively. Interestingly, we found that the GRAVY values of whole MAPK proteins in three *Arachis* species were minus, ranging from -0.48 (AhMAPK18) to -0.11 (AhMAPK36) in *A. hypogaea*, -0.63 (AraduMAPK07) to -0.17 (AraduMAPK09) in *A. duranensis*

and -0.61 (AraipMAPK08) to -0.17 (AraipMAPK09) in *A. ipaensis*. This finding strongly indicated that the MAPK proteins in these *Arachis* species were hydrophilic. Additionally, the AI values of the MAPK proteins in *A. hypogaea* ranged from 76.95 (AhMAPK18) to 101.07 (AhMAPK36), while the AI scores of the MAPK proteins in *A. duranensis* and *A. ipaensis* ranged from 75.30 (AraduMAPK17) to 99.65 (AraduMAPK04) and 72.75 (AraipMAPK17) to 99.11 (AraipMAPK04), respectively. Detailed data regarding the physicochemical properties of the MAPK proteins across the three *Arachis* species were comprehensively presented in Table 1 and 2.

The characteristics of the MAPK proteins in terms of their molecular profiles were thoroughly analysed in various higher plant species, revealing a range in their physicochemical properties. Particularly, in *Musa* species, the number of amino acids in these MAPK proteins ranged from 366 to 1155 residues (Fan et al. 2023). The mW of the MAPK proteins spanned from 41.68 to 130.81 kDa, while the theoretical pI ranged between 5.34 and 9.73, indicating diverse charge profiles across different MAPKs (Fan et al. 2023). The AI scores showed a range from 78.41 to 99.1, which typically suggests how thermostable the protein is, whereas the GRAVY results indicated that these MAPK proteins in *Musa* species were hydrophilic, further underscoring their compatibility with aqueous cellular environments (Fan et al. 2023). Additionally, the LsMAPK proteins in lettuce exhibited a range in length from 284 amino acids for LsMAPK4-3 to 782 amino acids for LsMAPK16-4 (Wang et al. 2022). Correspondingly, their mW values ranged from 33.00 kDa to 89.70 kDa (Wang et al. 2022). The theoretical pI values of these MAPK proteins also displayed a wide scope, extending from 4.74 for LsMAPK4-3 up to 9.08 for LsMAPK16, indicating significant variations in their charge characteristics across different molecular forms (Wang et al. 2022). These findings indicated that while MAPK proteins in *Arachis* share common hydrophilic characteristics with other plant species, they exhibited a more conserved molecular size and weight distribution, which may be linked to their functional roles in peanut signalling pathways. This suggested that MAPK proteins in *Arachis* species may have evolved under different selective pressures compared to species like *Musa*, potentially due to variations in developmental processes.

Phylogenetic analysis of the mitogen-activated protein kinase proteins in *Arachis* species

To investigate the relationships among the MAPK families in *A. hypogaea*, *A. duranensis*, and *A. ipaensis*, a Maximum Likelihood-based phylogenetic tree was constructed using MEGA software. *A. thaliana* and *M. truncatula* were selected as reference species due to their well-characterized MAPK families. *Arabidopsis* serves as a model dicot plant with a fully annotated genome (Andreasson & Ellis 2010), while *M. truncatula* is known as a legume species closely related to *Arachis* (Neupane et al. 2013). As provided in Figure 1, the phylogenetic tree was classified into five different groups, including groups A, B, C, D, and E. Particularly, group A contained four members of the AhMAPK family (AhMAPK04, AhMAPK07, AhMAPK21, and AhMAPK24), two members of the AraduMAPK family (AraduMAPK04 and AraduMAPK08) and two members of the AraipMAPK family (AraipMAPK04 and AraipMAPK07). Group B had ten, five, and five members of the AhMAPK, AraduMAPK, and AraipMAPK families in *A. hypogaea*, *A. duranensis*, and *A. ipaensis*, respectively, while group C exhibited four AhMAPK proteins (AhMAPK09, AhMAPK16, AhMAPK26, and AhMAPK34), two AraduMAPK proteins (AraduMAPK09 and AraduMAPK16) and two AraipMAPK proteins (AraipMAPK09 and AraipMAPK15). Group D shared the highest members of the MAPK families in three *Arachis* species, including 18 AhMAPK proteins, seven AraduMAPK proteins and seven AraipMAPK

proteins. Group E contained six AhMAPK proteins, two AraduMAPK proteins (AraduMAPK17 and AraduMAPK18) and two AraipMAPK proteins (AraipMAPK17 and AraipMAPK18).

Previously, the phylogenetic relationships and classification of the MAPK families in plant species have been comprehensively analysed. For example, a phylogenetic tree using the full-length amino acid sequences of 20 AtMAPK proteins from Arabidopsis, 12 FvMAPK proteins from *Fragaria vesca*, and 43 FaMAPK proteins from cultivated strawberry was constructed (Li et al. 2022). The analysis revealed that all MAPK proteins from Arabidopsis, *F. vesca*, and cultivated strawberry were divided into four distinct cluster groups, namely groups A, B, C, and D (Li et al. 2022). Another phylogenetic tree constructed for the MAPK protein family across Arabidopsis, *Helianthus annuus*, and chrysanthemum revealed a categorization into four distinct groups, including groups A, B, C, and D (Song et al. 2018). Next, phylogenetic analysis of the MAPK families in Arabidopsis and five *Musa* species, including *M. acuminata*, *M. balbisiana*, *M. itinerans*, *M. schizocarpa*, and *M. textilis*, clearly revealed that these MAPK proteins could be divided into groups A, B, C, and D based on phylogenetic relationships (Fan et al. 2023). In this study, the phylogenetic classification of MAPK proteins in *Arachis* species also identified distinct groupings, consistent with those observed in other plants. However, while the core MAPK classification aligns with previous studies, some species-specific variations were evident, particularly in *A. hypogaea*, which has undergone genome expansion due to polyploidization. The grouping of *Arachis* MAPKs alongside their counterparts from *A. thaliana* and *M. truncatula* suggested functional conservation within legume species, supporting their roles in signaling pathways associated with biological processes.

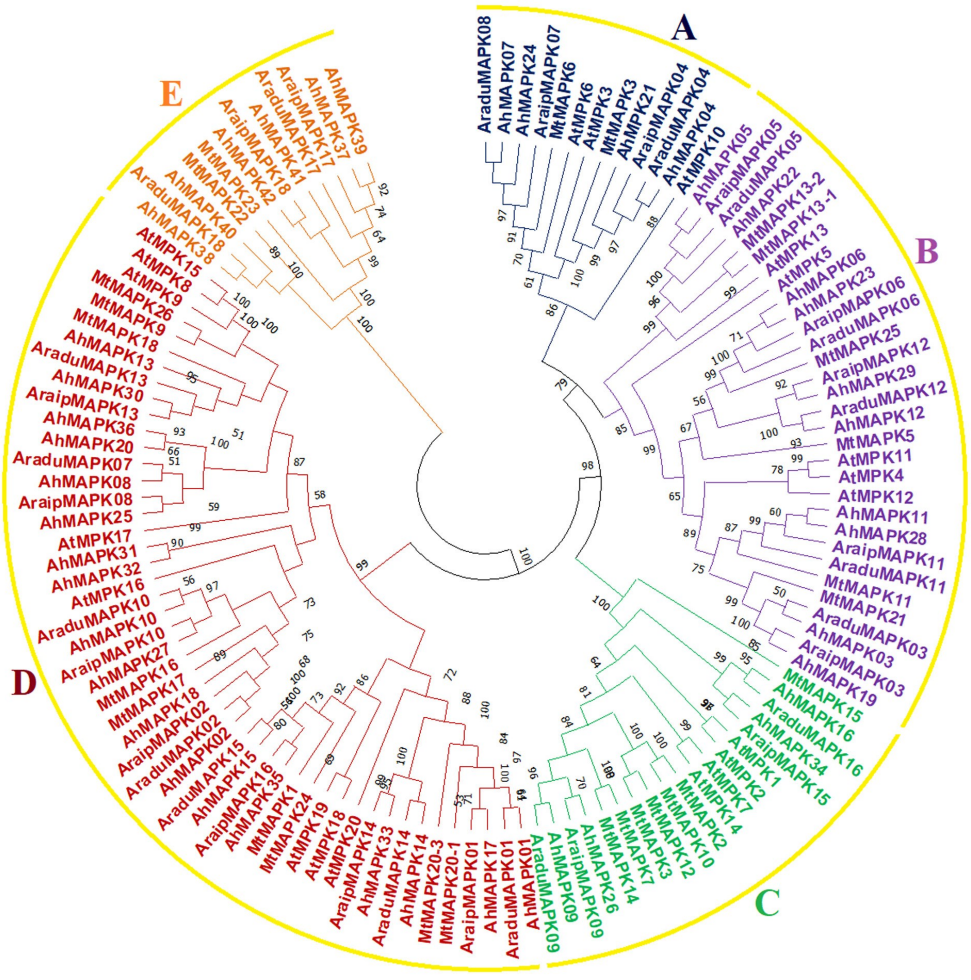

Figure 1. Classification of the MAPK families in *Arabidopsis thaliana*, *Medicago truncatula*, *Arachis hypogaea*, *A. duranensis*, and *A. ipaensis*.

Gene structure of the mitogen-activated protein kinase proteins in *Arachis* species

To examine the gene structure of the *MAPK* genes in *Arachis* species, the BioEdit software and Gene Structure Display Server (Hu et al. 2015) were applied to analyse the gene size and number of exons. As provided in Table 1, the genomic DNA sequences of the *AhMAPK* genes in *A. hypogaea* ranged from 746 (*AhMAPK31*) to 7483 (*AhMAPK38*) bp. Meanwhile, the gene sizes of the *AraduMAPK* and *AraipMAPK* genes in *A. duranensis* and *A. ipaensis* varied from 1044 (*AraduMAPK09*) to 7290 (*AraduMAPK18*) bp and 1218 (*AraipMAPK18*) to 5603 (*AraipMPK07*) bp, respectively (Tables 2).

Of particular interest, we focused on the exon/intron organization of the *AhMAPK* genes in *A. hypogaea* (Figure 2). Our analysis indicated that these *AhMAPK* genes displayed notable structural variations. For instance, two *AhMAPK* genes, including *AhMAPK41* and *AhMAPK42* each comprised a single exon, indicating a simpler gene structure. Conversely, the remaining 40 out of 42 *AhMAPK* genes had a variable number of exons, ranging from two to 19 exons. Four *AhMAPK* genes, including *AhMAPK09*, *AhMAPK16*, *AhMAPK26*, and *AhMAPK34* each consisting of two exons, while *AhMAPK31* and *AhMAPK20* showed an organization of four and five exons, respectively. Interestingly, 13 (out of 42) *AhMAPK* genes contained six exons. Only *AhMAPK36* had eight exons and two *AhMAPK* genes, namely *AhMAPK07* and *AhMAPK32* had nine exons, while seven and seven *AhMAPK* genes exhibited 10 and 11 exons, respectively. Finally, two (*AhMAPK38* and *AhMAPK40*) and two (*AhMAPK37* and *AhMAPK39*) genes contained 16 and 19 exons.

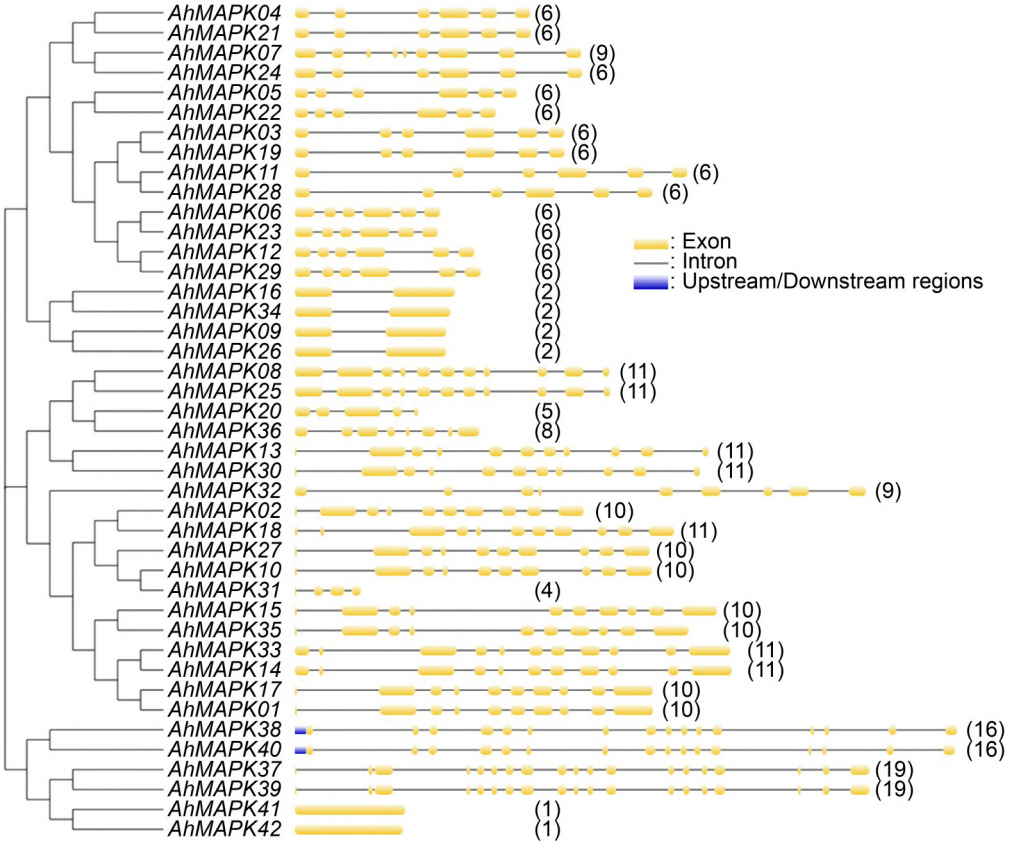

Figure 2. Gene structure of the MAPK family in *Arachis hypogaea*.

Previously, the gene structures encoding the MAPK families in plant species have been investigated. For example, it was discovered that all members of the MAPK family in purple false brome possess introns ranging from three to eleven, indicating a significant variation in the gene structure across this protein family (Chen et al. 2012). The number of introns within the

CsMAPK gene family in cucumber ranged from one to 10 (Wang et al. 2015), this finding was also confirmed in the *MAPK* gene families in tomato (Kong et al. 2012), grapevine (Wang et al. 2014), cucumber (Wang et al. 2015), chickpea (Singh et al. 2018), and lettuce (Wang et al. 2022). These variations suggest species-specific adaptations in *MAPK* gene structure, which may influence their functional roles in different plant lineages. In *A. hypogaea*, the exon-intron organization of *MAPK* genes also exhibits diversity, particularly among the 18 *AhMAPK* genes in Cluster D, which represents the largest MAPK subgroup. These genes showed a range of exon-intron structures, with some possessing multiple exons, indicating potential functional complexity. The presence of genes with higher intron numbers suggested possible regulation through alternative splicing. This structural variability aligns with the observed expression patterns of Cluster D *MAPK* genes. Such findings highlight the evolutionary significance of exon-intron organization in *A. hypogaea*, as the structural flexibility of these genes may contribute to their regulatory complexity. Understanding these structural characteristics provides essential insights into how *MAPK* genes in peanut function in developmental and environmental adaptation processes.

Expression patterns of the mitogen-activated protein kinase proteins in *Arachis hypogaea*

To explore the differential expression patterns of the *AhMAPK* genes in peanut, we analysed transcriptomic data for all 42 members from this gene family across 10 distinct organ and tissue samples (Figure 3). Our findings revealed a subset (17 out of 42) of the *AhMAPK* genes displaying notably lower expression levels in all tested tissues. Interestingly, a majority of the *AhMAPK* genes (25 out of 42) demonstrated significant expression, marked by high FPKM values, in at least one major organ or tissue. Notably, four *AhMAPK* genes, including *AhMAPK01*, *AhMAPK10*, *AhMAPK17*, and *AhMAPK27* exhibited the highest FPKM values in lateral stem leaf and mainstem leaf tissues, suggesting a specialized expression of these genes in these particular organs. Additionally, all *AhMAPK* genes presented lower expression levels in vegetative shoot tips and stamens, indicating a potential tissue-specific regulation of these *AhMAPK* genes. A total of 19 (out of 42) *AhMAPK* genes were exclusively expressed in root and/or nodule tissues, while five *AhMAPK* genes, particularly *AhMAPK01*, *AhMAPK10*, *AhMAPK15*, *AhMAPK17*, and *AhMAPK27*, were highly expressed in pistil tissues. Taken together, these findings suggest that the *AhMAPK* genes displayed a diverse range of expression patterns, underscoring the complexity of their role in peanut tissue specificity.

According to the GSE180915 dataset, the expression profiles of *AhMAPK* genes across four different organs, including lateral leaflets, petioles, shoot apical meristems, and terminal leaflets, indicated varying levels of tissue-specific expression (Figure 4). Several *AhMAPK* genes exhibited high expression across all four organs, suggesting their broad functional roles in peanut development. Notably, *AhMAPK37* and *AhMAPK39* displayed the highest expression levels in all tissues, particularly in terminal leaflets and lateral leaflets, indicating a potential role in leaf expansion and development. Similarly, *AhMPK14* showed strong expression in all organs, with the highest level in shoot apical meristem, suggesting its involvement in meristematic activity and growth regulation. The remaining *AhMAPK* genes showed minimal or negligible expression across all tissues.

Previously, the *MAPK* genes have been demonstrated to play a pivotal role in various developmental processes, with their tissue-specific expression patterns. Thus, the analysis of these patterns revealed crucial insights into the functional specialization of individual *MAPK* genes (Taj et al. 2010). For instance, higher expression of *MAPK* genes in root tissues may correlate with

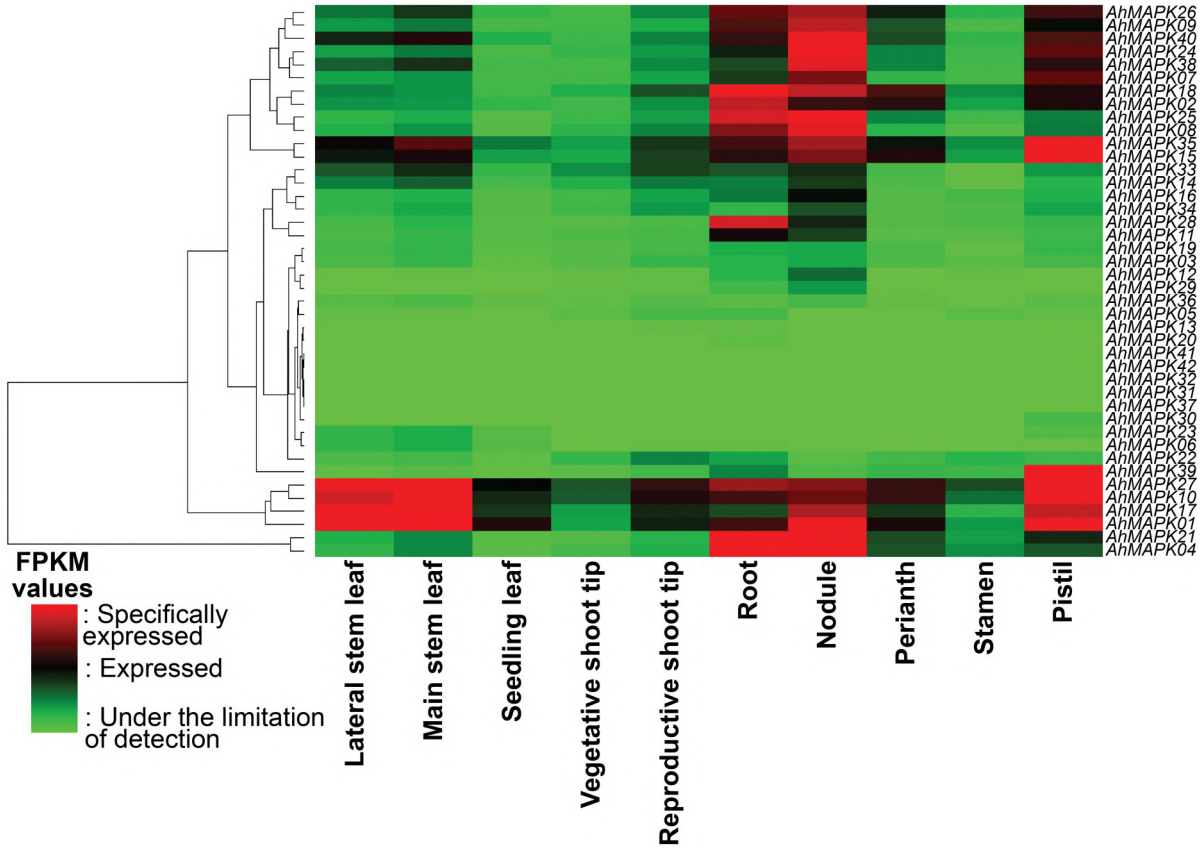

Figure 3. Expression heatmap of *AhMAPK* genes across ten major organs of *Arachis hypogaea*, including vegetative and reproductive tissues. The expression patterns of *AhMAPK* genes were explored across a comprehensive range of vegetative (e.g., lateral stem leaf, main stem leaf, seedling leaf, vegetative shoot tip, root, nodule) and reproductive organs (e.g., reproductive shoot tip, perianth, stamen, pistil) in *A. hypogaea*.

enhanced root growth or stress responses, such as those triggered by water deficiency (Opdenakker et al. 2012; Majeed et al. 2022). Similarly, the specific expression of other *MAPK* genes in the leaves and/or flowers could be linked to specific roles in photosynthesis regulation or reproductive development (Jonwal et al. 2023). Furthermore, *OsMPK3* in rice enhances drought tolerance by modulating stomatal closure (Reyna & Yang 2006), while *AtMPK6* in *Arabidopsis* plays a key role in pathogen defence by activating stress-responsive genes (Andreasson & Ellis 2010). In this study, the expression analysis revealed that several *MAPK* genes exhibited tissue-specific expression, with high transcript levels in leaves, roots, and reproductive organs. Notably, *AhMAPK10*, *AhMAPK17*, and *AhMAPK27* demonstrated high expression in lateral stem leaf and mainstem leaf tissues, indicating their potential involvement in leaf development and photosynthetic regulation. In contrast, several *MAPK* genes were more prominently expressed in root tissues, suggesting roles in root architecture or stress adaptation. Such differential expression not only underscores the adaptability of plants to their environment by modulating physiological and metabolic processes in a tissue-specific manner but also highlights the potential of these *MAPK* genes as targets for genetic engineering aimed at improving plant resilience and productivity (Taj et al. 2010). Therefore, understanding MAPK functions in peanuts could provide valuable insights into improving stress resilience and yield stability in peanut cultivation. Potential applications include using MAPK-associated genes as markers in breeding programs to develop drought-resistant varieties or leveraging biotechnological approaches to enhance peanut defense mechanisms against fungal pathogens such as *Aspergillus* species, which cause aflatoxin contamination. Future studies should focus on functional validation of *MAPK* genes in peanuts to explore their full potential in agricultural applications.

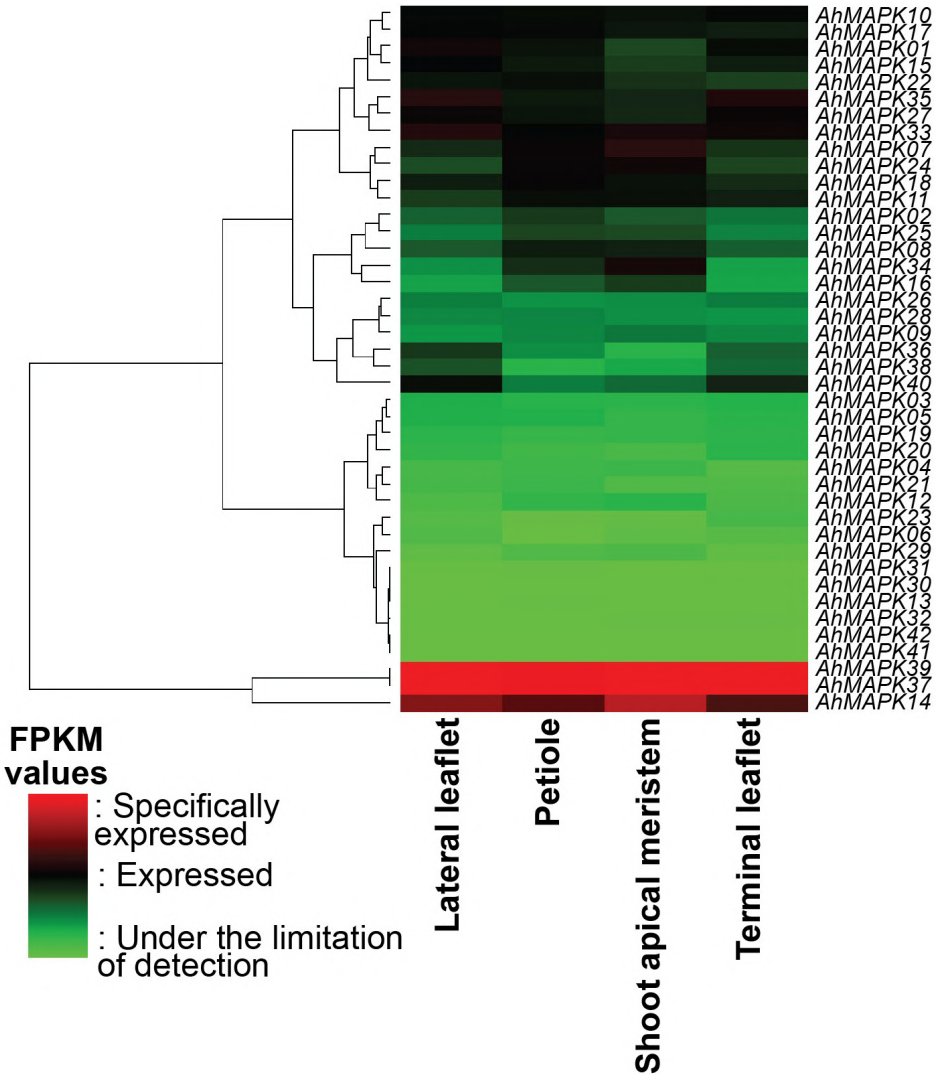

Figure 4. Tissue-specific expression profiles of *AhMAPK* genes in leaf-related structures of *Arachis hypogaea*. The expression levels of *AhMAPK* genes were explored in four aerial organs, including lateral leaflet, terminal leaflet, petiole, and shoot apical meristem.

CONCLUSION

This study presents a comprehensive genome-wide analysis of *MAPK* genes in *Arachis hypogaea*, *A. duranensis*, and *A. ipaensis*. A total of 42, 18, and 18 MAPK genes were identified in these species, respectively, and their molecular characteristics, gene structures, and evolutionary relationships were examined. The phylogenetic classification grouped these genes into five distinct clusters, revealing both conserved and divergent features among species. Expression analysis demonstrated tissue-specific patterns, with several *MAPK* genes showing high transcript levels in leaf and reproductive tissues, suggesting their roles in developmental processes and stress responses. Specifically, *AhMAPK10*, *AhMAPK17*, and *AhMAPK27* displayed strong expression in lateral and mainstem leaves, indicating their potential function in photosynthetic regulation, while *AhMAPK02*, *AhMAPK04*, *AhMAPK18*, *AhMAPK21*, *AhMAPK25*, and *AhMAPK28* were predominantly expressed in roots, likely contributing to root development and environmental adaptation. The findings of this study serve as a valuable genomic resource for understanding MAPK-mediated signalling in peanuts and provide a foundation for future applications in crop improvement. Further functional validation through transcriptomic and gene expression studies will be essential to explore the potential of these *MAPK* genes in enhancing stress tolerance and agricultural productivity.

AUTHORS CONTRIBUTION

H.D.C. contributed to the research design, data collection and analysis, and preparation of the first draft of the manuscript. H.T.T.T. contributed to data collection. L.T.Q.N. and D.H.G. contributed to data collection and analysis. H.V.L. contributed to the research design, data collection and analysis. M.T.L. contributed to data collection. P.B.C. contributed to the research design, data collection and analysis, preparation and editing of the manuscript, and supervision of the entire process.

ACKNOWLEDGMENTS

This work was fully funded by Vietnam National University Hanoi under the project number QG.25.61.

CONFLICT OF INTEREST

The authors declare no conflict of interest regarding the research or the research funding.

REFERENCES

Andreasson, E. & Ellis, B., 2010. Convergence and specificity in the Arabidopsis MAPK nexus. *Trends in Plant Science*, 15(2), pp.106-113. doi: 10.1016/j.tplants.2009.12.001

Avruch, J., 2007. MAP kinase pathways: the first twenty years. *Biochimica et biophysica acta*, 1773(8), pp.1150-1160. doi: 10.1016/j.bbamcr.2006.11.006

Barrett, T. et al., 2013. NCBI GEO: archive for functional genomics data sets - update. *Nucleic Acid Research*, 41(Database issue), pp.D991-995. doi: 10.1093/nar/gks1193

Bertioli, D.J. et al., 2016. The genome sequences of *Arachis duranensis* and *Arachis ipaensis*, the diploid ancestors of cultivated peanut. *Nature Genetics*, 48(4), pp.438-446. doi: 10.1038/ng.3517

Bertioli, D.J. et al., 2019. The genome sequence of segmental allotetraploid peanut *Arachis hypogaea*. *Nature Genetics*, 51(5), pp.877-884. doi: 10.1038/s41588-019-0405-z

Bertioli, D.J. et al., 2020. Evaluating two different models of peanut's origin. *Nature Genetics*, 52(6), pp.557-559. doi:10.1038/s41588-020-0626-1

Brasileiro, A.C.M. et al., 2023. The stilbene synthase family in *Arachis*: A genome-wide study and functional characterization in response to stress. *Genes (Basel)*, 14(12), 2181. doi: 10.3390/genes14122181

Cao, P.B., 2022. *In silico* structural, evolutionary, and expression analysis of small heat shock protein (shsp) encoding genes in cocoa (*Theobroma cacao* L.). *The Journal of Animal and Plant Sciences*, 32(5), pp.1394-1402. doi: 10.36899/JAPS.2022.5.0546

Chen, L. et al., 2012. Genome-wide identification and analysis of MAPK and MAPKK gene families in *Brachypodium distachyon*. *PLoS One*, 7(10), e46744. doi:10.1371/journal.pone.0046744

Chu, H.D. et al., 2024. Identification of two enzymes for trehalose synthesis and their potential function in growth and development in peanut (*Arachis hypogaea*). *Journal of Tropical Life Science*, 14(1), pp.83-94. doi: 10.11594/jtls.14.01.10

Clevenger, J. et al., 2016. A developmental transcriptome map for allotetraploid *Arachis hypogaea*. *Frontiers in Plant Science*, 7, 1446. doi: 10.3389/fpls.2016.01446

Dash, S. et al., 2016. PeanutBase and other bioinformatic resources for peanut. In *Peanuts: Genetics, processing, and utilization*. AOCS Press, pp.241-252. doi: 10.1016/B978-1-63067-038-2.00008-3

Fan, Z. et al., 2023. Genome-wide identification of the MPK gene family and expression analysis under low-temperature stress in the banana. *Plants (Basel)*, 12(16), 2926. doi: 10.3390/plants12162926

García, A.V. et al., 2021. Genomic affinity in hybrids of B-genome *Arachis* species: new genetic resources toward peanut improvement. *Crop Breeding and Applied Biotechnology*, 21(3), e38292139. doi: 10.1590/1984-70332021v21n3a48

Gasteiger, E. et al., 2003. ExPASy: The proteomics server for in-depth protein knowledge and analysis. *Nucleic Acids Research*, 31(13), pp.3784-3788. doi: 10.1093/nar/gkg563

Gasteiger, E. et al., 2005. Protein identification and analysis tools on the ExPASy server. In *The proteomics protocols handbook*. Humana Press, pp.571-607. doi: 10.1385/1-59259-890-0:571

Group, M., 2002. Mitogen-activated protein kinase cascades in plants: a new nomenclature. *Trends in Plant Science*, 7(7), pp.301-308. doi: 10.1016/s1360-1385(02)02302-6

Hall, T.A., 1999. BioEdit: A user-friendly biological sequence alignment editor and analysis program for Windows 95/98/NT. *Nucleic Acids Symposium Series*, 41, pp.95-98. doi: 10.14601/Phytopathol_Mediterr-14998u1.29

Hill, G.M., 2002. Peanut by-products fed to cattle. *The Veterinary clinics of North America: Food animal practice*, 18(2), pp.295-315. doi: 10.1016/s0749-0720(02)00019-1

Hu, B. et al., 2015. GSDS 2.0: an upgraded gene feature visualization server. *Bioinformatics*, 31(8), pp.1296-1297. doi: 10.1093/bioinformatics/btu817

Jagodzik, P. et al., 2018. Mitogen-Activated Protein Kinase Cascades in Plant Hormone Signaling. *Frontiers in Plant Science*, 9, 1387. doi: 10.3389/fpls.2018.01387

Jonwal, S. et al., 2023. Regulation of photosynthesis by mitogen-activated protein kinase in rice: antagonistic adjustment by OsMPK3 and OsMPK6. *Physiology and Molecular Biology of Plants*, 29(9), pp.1247-1259. doi: 10.1007/s12298-023-01383-9

Kong, F. et al., 2012. Genome-wide analysis of the mitogen-activated protein kinase gene family in *Solanum lycopersicum*. *Gene*, 499(1), pp.108-120. doi: 10.1016/j.gene.2012.01.048

Kosev, V.I. & Vasileva, V.M., 2019. Morphological characterization of Grass pea (*Lathyrus sativus* L.) Varieties. *Journal of Agricultural Sciences - Sri Lanka*, 14(2), pp.67-76. doi: 10.4038/jas.v14i2.8509

La, H.V. et al., 2022a. SWEET gene family in sugar beet (*Beta vulgaris*): Genome-wide survey, phylogeny and expression analysis. *Pakistan journal of biological sciences*, 25(5), pp.387-395. doi: 10.3923/pjbs.2022.387.395

La, H.V. et al., 2022b. Insights into the gene and protein structures of the CaSWEET family members in chickpea (*Cicer arietinum*), and their gene expression patterns in different organs under various stress and abscisic acid treatments. *Gene*, 819, 146210. doi: 10.1016/j.gene.2022.146210

Le, M.T. et al., 2022. Genome-wide identification and analysis of genes encoding putative heat shock protein 70 in papaya (*Carica papaya*). *Pakistan journal of biological sciences*, 25(6), pp.468-475. doi:10.3923/pjbs.2022.468.475

Li, M. et al., 2022. Genome-wide identification and expression of MAPK gene family in cultivated strawberry and their involvement in fruit developing and ripening. *International Journal of Molecular Sciences*, 23(9), 5201. doi: 10.3390/ijms23095201

Li, X. et al., 2014. Identification of rapidly induced genes in the response of peanut (*Arachis hypogaea*) to water deficit and abscisic acid. *BMC Biotechnology*, 14, 58. doi:10.1186/1472-6750-14-58

Lin, L. et al., 2021. Plant mitogen-activated protein kinase cascades in environmental stresses. *International Journal of Molecular Sciences*, 22(4), 1543. doi: 10.3390/ijms22041543

Liu, Y. et al., 2013. Genome-wide analysis of mitogen-activated protein kinase gene family in maize. *Plant Molecular Biology Reporter*, 31(6), pp.1446-1460. doi: 10.1007/s11105-013-0623-y

Majeed, Y. et al., 2022. Functional analysis of mitogen-activated protein kinases (MAPKs) in potato under biotic and abiotic stress. *Molecular Breeding*, 42(6), 31. doi: 10.1007/s11032-022-01302-y

Neupane, A. et al., 2013. Evolutionary history of mitogen-activated protein kinase (MAPK) genes in *Lotus*, *Medicago*, and *Phaseolus*. *Plant Signaling & Behavior*, 8(11), e27189. doi: 10.4161/psb.27189

Niekerk, L.A. et al., 2024. Heavy metal stress and mitogen activated kinase transcription factors in plants: Exploring heavy metal-ROS influences on plant signalling pathways. *Plant, Cell & Environment*, 47(8), pp.2793-2810. doi: 10.1111/pce.14926

Opdenakker, K. et al., 2012. Mitogen-Activated Protein (MAP) kinases in plant metal stress: regulation and responses in comparison to other biotic and abiotic stresses. *International Journal of Molecular Sciences*, 13(6), pp.7828-7853. doi: 10.3390/ijms13067828

Reyna, N.S. & Yang, Y., 2006. Molecular analysis of the rice MAP kinase gene family in relation to *Magnaporthe grisea* infection. *Molecular Plant-Microbe Interactions*, 19(5), pp.530-540. doi: 10.1094/mpmi-19-0530

Singh, A. et al., 2018. Genome-wide identification of the MAPK gene family in chickpea and expression analysis during development and stress response. *Plant Gene*, 13, pp.25-35. doi:10.1016/j.plgene.2017.12.001

Song, A. et al., 2018. Comprehensive analysis of mitogen-activated protein kinase cascades in *Chrysanthemum*. *PeerJ*, 6, e5037. doi: 10.7717/peerj.5037

Taj, G. et al., 2010. MAPK machinery in plants: recognition and response to different stresses through multiple signal transduction pathways. *Plant Signaling & Behavior*, 5(11), pp.1370-1378. doi: 10.4161/psb.5.11.13020

Tamura, K. et al., 2021. MEGA11: Molecular evolutionary genetics analysis version 11. *Molecular Biology and Evolution*, 38(7), pp.3022-3027. doi: 10.1093/molbev/msab120

Thompson, J. et al., 1997. The ClustalX windows interface: flexible strategies for multiple sequence alignment aided by quality analysis tools. *Nucleic Acids Research*, 25, pp.4876 - 4882.

Thompson, J.D. et al., 2002. Multiple sequence alignment using ClustalW and ClustalX. *Current Protocols in Bioinformatics*, Chapter 2, Unit 2.3. doi: 10.1002/0471250953.bi0203s00

Toomer, O.T., 2018. Nutritional chemistry of the peanut (*Arachis hypogaea*). *Critical Reviews in Food Science and Nutrition*, 58(17), pp.3042-3053. doi: 10.1080/10408398.2017.1339015

Wadood, S.A. et al., 2022. Geographical origin classification of peanuts and processed fractions using stable isotopes. *Food Chemistry: X*, 16, 100456. doi: 10.1016/j.fochx.2022.100456

Wang, G. et al., 2014. Genome-wide identification and analysis of mitogen activated protein kinase kinase kinase gene family in grapevine (*Vitis vinifera*). *BMC Plant Biology*, 14, 219. doi: 10.1186/s12870-014-0219-1

Wang, J. et al., 2015. Genome-wide identification of MAPK, MAPKK, and MAPKKK gene families and transcriptional profiling analysis during development and stress response in cucumber. *BMC Genomics*, 16(1), 386. doi: 10.1186/s12864-015-1621-2

Wang, T. et al., 2022. Genome-wide identification and expression analysis of MAPK gene family in lettuce (*Lactuca sativa* L.) and functional analysis of LsMAPK4 in high- temperature-induced bolting. *International Journal of Molecular Sciences*, 23(19). doi: 10.3390/ijms231911129

Zhang, M. & Zhang, S., 2022. Mitogen-activated protein kinase cascades in plant signaling. *Journal of Integrative Plant Biology* , 64(2), pp.301-341. doi: 10.1111/jipb.13215

Zheng, Y.M. et al., 2019. Nitrogen fixation characteristics of root nodules in different peanut varieties and their relationship with yield. *Ying yong sheng tai xue bao = The journal of applied ecology*, 30(3), pp.961-968. doi: 10.13287/j.1001-9332.201903.019

Zhuang, W. et al., 2019. The genome of cultivated peanut provides insight into legume karyotypes, polyploid evolution and crop domestication. *Nature Genetics*, 51(5), pp.865-876. doi: 10.1038/s41588-019-0402-2

Journal of Tropical Biodiversity and Biotechnology
Volume 10, Issue 04 (2025): jtbb20682
DOI: 10.22146/jtbb.20682

Research Article

Unveiling Actinobacteria Potency from The Sungai Wain Protected Forest, East Kalimantan, Indonesia: A Promising Source of Antibacterial, Anti-Biofilm, and Antioxidant Compounds

Hasnadhiazahra Rohadi[1], Tirta Kumala Dewi[2], Sri Widawati[2], Yadi Suryadi[3], Shanti Ratnakomala[4], Endah Retnaningrum[5]*

1)Master Degree Program, Faculty of Biology, Universitas Gadjah Mada, JL. Teknika Selatan Sekip Utara, Sendowo, Sinduadi, Kec. Mlati, Kabupaten Sleman, Daerah Istimewa Yogyakarta 55281, Indonesia
2)Research Center for Applied Microbiology, National Research and Innovation Agency, KST Soekarno, JL. Raya Jakarta-Bogor, Pakansari, Kec. Cibinong, Kabupaten Bogor, Jawa Barat 16915, Indonesia
3)Research Center for Horticulture, National Research and Innovation Agency, KST Soekarno, JL. Raya Jakarta-Bogor, Pakansari, Kec. Cibinong, Kabupaten Bogor, Jawa Barat 16915, Indonesia
4)Research Center for Biosystematics and Evolution, National Research and Innovation Agency, KST Soekarno, JL. Raya Jakarta-Bogor, Pakansari, Kec. Cibinong, Kabupaten Bogor, Jawa Barat 16915, Indonesia
5)Microbiology Laboratory, Faculty of Biology, Universitas Gadjah Mada, JL. Teknika Selatan Sekip Utara, Sendowo, Sinduadi, Kec. Mlati, Kabupaten Sleman, Daerah Istimewa Yogyakarta 55281, Indonesia
* Corresponding author, email: endahr@ugm.ac.id

Keywords:
Actinobacteria
Anti-bacterial
Antibiofilm
Antioxidant
GC-MS
Submitted:
09 April 2025
Accepted:
01 July 2025
Published:
10 October 2025
Editors:
Miftahul Ilmi
Liya Audinah

ABSTRACT

Actinobacteria are Gram-positive bacteria widely distributed in soil environments and are well known for producing diverse bioactive compounds. Almost 80 % of the antibiotics in the world are derived from actinobacteria. However, inappropriate use of antibiotics has accelerated antibiotic resistance in many pathogenic bacteria. This study aimed to screen and analyse actinobacteria from the soil of the Sungai Wain protected forest to determine their antimicrobial, antibiofilm, and antioxidant potential. The research involved several stages, including preliminary screening; secondary metabolite production; determination of Minimum Inhibition Concentration (MIC), Minimum Bactericidal Concentration (MBC), anti-biofilm assay, and antioxidant assay; 16S rRNA gene identification; biosynthetic genes detection (PKS and NRPS); and compound profiling using GC-MS. Three isolates, K22S-22, 31, and 36 exhibited the highest inhibition zones, with K22S-22 showing the strongest activity against *Staphylococcus aureus* and *Bacillus subtilis* (IC50 = 1.033±0.033 µg mL^{-1} and 4.155±0.028 µg mL^{-1}, respectively). Strain K22S-22 also displayed antioxidant activity (DPPH IC_{50} = 67.59 ± 0.020 µg mL^{-1}) and significant antibiofilm effects (inhibition IC_{50} = 4.541 ± 0.124 µg mL^{-1}; eradication EC_{50} = 50.71 ± 0.029 µg mL^{-1}). Molecular identification revealed K22S-22 as *Streptomyces rapamycinicus* NRRL B-5491 (T) with a similarity value of 99.08 %, harbouring PKS-I, PKS-II, and NRPS genes. The Gas Chromatography-Mass Spectroscopy analysis (GC-MS) shows that Hexadecanoic acid is the dominant compound based on its area percentage. These findings highlight *Streptomyces* K22S-22 is a promising source of metabolites that exhibit potent antimicrobial, antioxidant, and antibiofilm characteristics, presenting opportunities for new therapeutic uses against multidrug-resistant (MDR) pathogens.

How to cite:
Rohadi, H. et al., 2025. Unveiling Actinobacteria Potency from The Sungai Wain Protected Forest, East Kalimantan, Indonesia: A Promising Source of Antibacterial, Anti-Biofilm, and Antioxidant Compounds. *Journal of Tropical Biodiversity and Biotechnology*, 10(4), jtbb20682. doi: 10.22146/jtbb.20682

INTRODUCTION

Antibiotic-resistant bacteria are currently rising and have become a global problem. The search for new antibiotic-derived compounds is urgently needed. Drug-resistant strains of pathogens are emerging faster than the discovery rate of new drugs and antibiotics. Centre for Disease Control and Prevention (CDC) reported that more than 35,000 deaths in the United States are caused by antibiotic-resistant infections (De Simeis & Sera 2021). Another primary concern of antibiotic-resistant infections is the presence of biofilm-forming bacteria. Biofilms are Extracellular Polymeric Substancesc (EPS) produced by microbial communities attached to biotic and abiotic surfaces. The formation of the EPS matrix of biofilms supports the biofilm and serves as a barrier that restricts antibiotic access, safeguards the cells, and can counteract antimicrobial substances. Biofilms also utilise quorum sensing to synchronise gene sharing and survival tactics. These processes render bacteria within biofilms up to 1,000 times more tolerant to antibiotics than free-floating cells, contributing to the increase in multidrug-resistant infections. (Zhao et al. 2023; Nahum et al. 2025). Based on this phenomenon, new alternative antibiotics are needed to kill resistant pathogenic bacteria without causing further resistance.

Actinomycetes are filamentous, Gram-positive bacteria with high guanine-cytosine (G+C) content in their genetic material. Over 90 % of the currently identified actinomycete genera have been isolated from soil habitats (Janatiningrum et al. 2024). Actinomycetes, particularly from the *Streptomyces* genus, are widely recognised as a prolific source of antibiotics. The majority of currently available antimicrobial agents were initially derived from these microorganisms. The diverse compounds they produce span all the major drug classes utilised in modern medical practice, including β-lactams, tetracyclines, macrolides, aminoglycosides, and glycopeptides (Mast & Stegmann 2019). This extensive legacy of antibiotic discovery has positioned actinomycetes as a prime target for ongoing research efforts to identify novel compounds capable of combating the growing global antimicrobial resistance (Delbari et al. 2023).

A promising method for discovering novel antibiotic compounds is investigating actinomycetes inhabiting unexplored regions, such as the Sungai Wain Protected Forest in East Kalimantan, which represents an effort to enrich the understanding of microbes and potentially discover novel antibiotic compounds from areas with limited human impact. Sungai Wain Protection Forest, abbreviated as HLSW, is located in Balikpapan City, East Kalimantan Province. Geographically, it is situated at 116° 47' - 116° 55' East Longitude and 01° 02' - 01° 10' South Latitude. The Sungai Wain Protection Forest has a unique ecosystem, with an area of 10.000 ha and high biodiversity, including endemic species of plants and animals. The diverse habitats and ecological niches within the Sungai Wain Protection Forest correspond to various chemical compounds derived from the isolated actinomycetes.

This study aims to screen the isolated actinomycetes derived from the Sungai Wain Protected Forest and to evaluate their potential as antimicrobials, anti-biofilm, and antioxidant sources. Additionally, the study identified antibiotic-producing actinomycetes through molecular approaches. It determines the chemical compounds that actinomycetes produce, which may contribute to the antimicrobial, anti-biofilm, and antioxidant activities.

MATERIALS AND METHODS

Materials

Soil samples from Sungai Wain Protected Forest, East Kalimantan, *Escherichia coli* InaCC B005, *Bacillus subtilis* InaCC B001, and *Staphylococcus aureus* InaCC B004, *Staphylococcus aureus* ATCC 25923, glycerol, Yeast Starch Agar

(YSA) media, nutrient agar (NA) media, Nutrient Broth media (NB), Yeast Starch Broth media, Tryptic soy broth (TSB) media, ethyl acetate, methanol (MeOH), crystal violet, DPPH (2,2-Diphenyl-1-picrylhydrazyl), resazurin, ascorbic acid, cetril aquadest, 20 mg mL^{-1} proteinase K, 50 mg mL^{-1} lysozyme, TE buffer, 70 % alcohol, RNaseA (10 mg mL^{-1}), 10 % sucrose, 5M NaCl, absolute ethanol, NFW (nuclease-free water), florosafe DNA stain, agarose gel 1 %, Tris-acetate-EDTA (TAE), DNA ladder 1 KB, loading dye, and helium gas.

Methods

Rejuvenation of Actinobacteria Cultures Isolated from The Sungai Wain Protected Forest

Ninety-six actinomycete cultures isolated from the forest soil of Sungai Wain, East Kalimantan (048016'47" SL 987041'04" EL) were rejuvenated from cryopreservation stock (in 10 % glycerol (volume/volume)) in a deep freezer at -80 °C). Furthermore, the culture was thawed using a water bath (37 °C) for 3 min. Cryopreservation is a long-term preservation method for microbes using 10 % glycerol as their cryoprotectant to protect the cell. According to Bircher et al. (2018), glycerol has been shown to help stabilising cells during gradual freezing by reducing or slowing down osmotic-induced shrinkage at lower temperatures. It can also prevent damage from increased osmotic pressure by decreasing the excessive rise in salt concentration in the unfrozen water portions during freezing in a deep freezer at -80 °C. The disc-shaped culture in the cryotube was inoculated into YSA media consisting of 2 g yeast, 10 g starch, and 25 g agar in 1 L of water at pH 7.0 into a Petri dish with a toothpick, then crushed and streaked into a quadrant. The rejuvenated culture was incubated at 30 °C for 7-14 days for further use (Ratnakomala et al. 2018). The 96 revived isolates were screened for antimicrobial activity against several bacterial strains. The isolates were then re-cultured into another YSA medium plate for the preliminary screening.

Preliminary Screening of K22S Actinomycete for Anti-bacterial Compounds Production using Double Layer Agar Plug Diffusion

The K22S Isolates were first screened to assess their anti-bacterial properties using the double-layer agar plug diffusion following the method of Ratnakomala et al. (2018) with modifications. The half-solid Mueller Hinton Agar (MHA) media were prepared by adding half a volume of agar and adding the test bacteria: *Bacillus subtilis* InaCC B001, *Staphylococcus aureus* InaCC B004, and *Escherichia coli* InaCC B005, which had already been measured for their optical density (OD) 600 nm with the value equivalent to 0.5 McFarland (OD: 0.08-0.1). These bacteria were selected as representatives of clinically important pathogens frequently associated with antibiotic resistance. *S. aureus* and *B. subtilis* represent Gram-positive bacteria, while *E. coli* represents Gram -negative bacteria, allowing for evaluation of the antimicrobial spectrum across both groups. Then, the media prepared were stored at 4 °C for 1 h. The cylinder agar (6 mm in diameter) from a 14-day-old actinomycete culture grown in YSA was cut using a sterile straw and placed on a plate containing double-layer media seeded with the test bacteria. The preliminary screening used 10 µg of streptomycin as the positive control to determine the antimicrobial susceptibility against the tested bacterial strains. The Petri dish was then stored at 4 °C for 2 hours and incubated at 30 °C for 24 h. The inhibitory zone was measured using a ruler. The SPSS version 20 application program was used to perform a one-way analysis of variance (ANOVA) at the 95 % confidence level on the data derived from double-layer agar plug diffusion. Duncan's Multiple Range Test (DMRT) was used to test further at a 5 % confidence level ($\alpha = 0.05$). The isolate with the highest antimicrobial activity

against the three test bacteria was further analysed for the secondary metabolite content.

Actinobacteria Fermentation and Metabolite Extraction

The isolate with the best ability was inoculated into 100 mL of yeast starch broth (YSB) media in a 500 mL Erlenmeyer flask for secondary metabolite production and fermentation following the method of Atikana et al. (2021). The actinomycete isolate culture was incubated for 7 days at 30 °C in an orbital shaker at 120 rpm. After incubation, the liquid culture was added with a 1:1 volume/volume ethyl acetate and incubated at 30 °C in an orbital shaker at 120 rpm for 1 h to extract the bioactive compounds. The ethyl acetate phase was collected and evaporated using an IKA® RV 10 Vacuum evaporator at 40 °C. The concentrated crude extract was collected in a new glass bottle, and the dried ethyl acetate extract was placed at -20 °C.

Determination of Minimum Inhibitory Concentration (MIC) and Minimum Bactericidal Concentration (MBC) of The Ethyl Acetate Extract

The Secondary screening was assessed by determining the Minimum Inhibitory Concentration (MIC) using the Resazurin Microtiter Assay dilution method (REMA), following the modified protocols of Atikana et al. (2021). The resazurin stock was diluted 0.01 g of resazurin to 10 mL of sterile aquadest. The resazurin was mixed with a sterile Tween 80 40 % with a comparison of 1:1 volume/volume. The test bacteria were prepared by diluting them with 1:1000 volume/volume to a sterile Mueller Hinton Broth media and homogenizing them (with a total OD600 value of 0.02). The ethyl acetate stock was diluted using 50 % DMSO to stabilize and store the extract for long-term storage. A series of two-fold serial dilutions was achieved, with the final concentration of the extract ranging from 400 µg mL^{-1} to 0.20 µg mL^{-1}, respectively. The bacterial suspension of 48 µL was added to the well, and 2 µL of extract was added to each well. Streptomycin served as the antibiotic control, the bacterial suspension containing DMSO was used as the growth control, and sterile Mueller Hinton broth (MHB) functioned as the sterile control. The 96-well plates were prepared in duplicate, while an additional plate was used for the Minimum Bactericidal Concentration (MBC) assay. The other plate was used for the Minimum Bactericidal Concentration (MBC) Assay. After being incubated at 37 °C for 24 h, the 96-well plates were stained with the prepared resazurin by adding 20 µL resazurin into each well and incubated at 37 °C overnight. The remaining plate for assessing the minimum bactericidal concentration was carried out by inoculating an aliquot of the serial dilution in the MIC test onto MHA medium and incubating at 37 ° C for 24 h. The bacterial growth was observed after incubation, and the MBC was subsequently determined (CLSI 2015). The minimum inhibitory concentration (MIC) was the lowest extract concentration that inhibited bacterial growth. Visual assessment of colour changes showed bright pink for bacterial growth, while blue-purple indicated no bacterial growth (Atikana et al. 2021). Fluorescence was measured at 530 nm excitation and 590 nm emission to determine the percentage of cell growth inhibition, calculated using the formula (Kim & Jang 2018):

$$\text{Inhibition percentage (\%)} = [1 - \frac{(\text{fluorescence Value} - \text{Bacteria Growth Control})}{(\text{Bacteria Growth Control} - \text{Control Sterile})}] \text{x } 100$$

All the experiments were carried out in triplicate. The Inhibition percentage was calculated for the Inhibitory Concentration of 50 % inhibition (IC_{50}) using the GraphPad Prism software version 10 (Silva et al. 2019). Results are expressed as the mean ± standard error (SE).

DNA Extraction and Phylogenetic Analysis

DNA extraction was performed using the method described by Atikana et al.

(2021), while the 16S rRNA PCR was conducted following the protocol of Nurkanto and Agusta (2015). The universal primer used for the 16s rRNA sequence namely 27F (5'-AGA GTT TGA TCC TGG CTC AG-3') and 1492R (5'-GGT TAC CTT GTT ACG ACT T-3'), and additional primers were used to achieve a full-length sequence of 16s rRNA namely 520F (5'-GTG CCA GCA GCC GCG G-3') and 520R (5'-ACC GCG GCK GCT GGC AC-3') also the primer of 920F (5'-AAA CTC AAA TGA ATT GAC GG -3') and 920R (5'- CCG TCA ATT CAT TTG AGT TT -3'). PCR was performed using a Thermal Cycler with an initial denaturation at 95 °C for 1.5 minutes, followed by 30 cycles of denaturation at 95 °C for 30 seconds, annealing at 50 °C for 30 seconds, and extension at 72 °C for 1.5 minutes. A final extension was carried out at 72 °C for 10 minutes, followed by cooling at 4 °C for 30 minutes. The sequencing was done using the 1st BASE service in Malaysia. The sequence was analysed using BioEdit 7.0 and subjected to a BLAST search in the EzBioCloud database. Phylogenetic trees were constructed using the neighbour-joining (NJ) method in MEGA X software. The evolutionary distances were computed using Kimura's two-parameter model for the neighbour-joining algorithm and 1000 replicated bootstrap resampling for the phylogenetic tree.

Detection of PKS-I, PKS-II, and NRPS genes within K22S-22 isolate

The detection of the PKS-I, PKS-II, and NRPS genes within the K22S-22 was conducted using the protocols of Escalante-Réndiz et al. (2019). The degenerate primer pairs, encompassing both forward and reverse sequences, were utilized for PKS-I (K1F-M6R), PKS-II (KSα-KSβ), and NRPS (A3F-A7R) genes in the Polymerase Chain Reaction (PCR) analysis. The PCR products were visualised under a 1.5 % agarose gel (Promega, USA) and examined through the GelDoc EZ system (Biorad, USA). The electrophoresis results were examined, and DNA bands for each primer (PKS I, PKS II, and NRPS) indicated that K22S-22 possesses and utilised the corresponding genes.

DPPH (2,2-diphenyl-1-picrylhydrazyl) Scavenging Antioxidant Assay

The K22S-22 ethyl acetate extract was analysed for its DPPH free radical scavenging activity according to the National Standardization Agency of Indonesia, SNI 8623 (2018) method. The assay was performed using a 96-well plate. The two-fold serial dilution of the extract ranged from 1000, 750, 500, 250, 125, 50, 25, and 12.5 µg mL-1 concentrations. The ascorbic acid in methanol was used as the positive control with two-fold serial dilution ranging from 60, 40, 20, 10, 5, and 3 µg mL-1 concentrations. A 3 mg DPPH was dissolved in 10 mL of methanol to prepare a 0.76 mM solution, and 40 µL of this solution was added to each well. The 96-well plates were incubated in the dark at room temperature (27 °C) for 20 minutes, after which absorbance was measured at 517 nm using a Varioskan LUX microplate reader (Thermo Scientific). The assay was performed in triplicate, and the absorbance values were used to calculate the DPPH scavenging activity (%) (Baliyan et al. 2022).

$$DPPH\ Scavenging\ Activity\% = \frac{(Negative\ Control - Blanko) - (Sample\ Extract - Control\ Extract)}{(Negative\ Control - Blanko)}$$

Biofilm Inhibition and Eradication Assay

Anti-biofilm inhibition and eradication assay was carried out according to the method of Haney et al. (2021). According to previous studies, *Staphylococcus aureus* ATCC 25923 was selected for evaluating anti-biofilm activity due to its well-documented ability to form biofilms under suitable conditions. (Hiltunen et al. 2019). Both of the assays were conducted on 96-well plates. The actinobacteria extract was diluted in a two-fold serial dilution in a strip tube with a

concentration ranging from 1030-8 µg mL^{-1}. For the inhibition assay, 10 µL of extract was added to each well in the 96-well plate with three replicates, and then 90 µL of bacteria suspension with an OD600 of 0.01 was added. The eradication assay was done by forming the biofilm. The biofilm was established in the 96-well plate by incubating the bacteria for one day before conducting the eradication assay (Haney et al. 2021). After incubation, the extract was added and re-incubated for one day. The streptomycin was used as an antibiotic control with a concentration ranging from 100-0.78 µg mL^{-1} for both assays. Both well plates were added 105 µL aqueous crystal violet (0.1 % b v^{-1}) for 30 min. Wells were rinsed with sterile distilled water 5 times and allowed to dry. Then, 110 µL of 70 % ethanol was added to dissolve the crystal violet (CV) and incubated for 30 minutes (Amran et al. 2024). Each test had a sterile control (sterile media + sterile solvent) and a bacterial control (bacterial suspension + solvent). CV absorbance was measured at a wavelength of 595 nm. The percentage (%) of anti-biofilm inhibition and eradication was calculated using the following formula:

$$\%\text{biofilm Inhibition/eradication: } \frac{(Control\ bacteria - Control\ media\ sterile) - (sampel - Control\ media\ sterile)}{(Control\ Bacteria - Control\ media\ sterile)}$$

GC-MS analysis to identify the chemical content of K22S-22 extract.

The chemical compounds of the ethyl acetate extract of K22S-22 were analysed using GC-MS following the procedure from Kumari et al. (2021). The Shimadzu QP2010 ultra-GC system detected the chemical composition of ethyl acetate extract of actinobacteria isolates with an Agilent DB-5MS UI column (film thickness 30 m × 0.25 mm id × 0.25 µm). Actinobacteria extract was injected with a volume of 2 µL into the injector. The chromatograms obtained were then analysed using each sample's information in the compound library (NIST14.LIB) (NIST 2023).

RESULTS AND DISCUSSION

Preliminary screening of actinobacteria for antibacterial activity using agar diffusion method

There are 30 (35.41 %) actinomycete isolates that inhibited the growth of *E. coli* (InaCC B005), 35 (36.45 %), and 34 (31.25 %) actinomycete isolates that inhibited Gram-positive bacteria *B. subtilis* InaCC B001 and *S. aureus* InaCC B004, respectively. The isolates K22S-22, K22S-31, and K22S-36 displayed the highest inhibitory activity against the three strains of bacteria (Table 1). Based on the antimicrobial index analysis (mean ± SE), K22S-22 isolate demonstrated the most distinctive and potent antimicrobial properties ($P<0.05$), exhibiting the most significant inhibitory effect against the three bacterial test strains. K22S-36 showed the highest inhibitory zone against *E. coli*, which suggests it may produce potent antibacterial compounds that are particularly effective against Gram-negative bacteria. One possible explanation is that K22S-36 may possess a different or more efficient inhibition mechanism than the other isolates. Ouchari et al. (2018) categorised the Zone of

Table 1. Antimicrobial index (AI) (mean ± SE) of the actinobacteria isolate against three bacterial strains.

Sample Name	Zone of Inhibition (mm)		
	E. coli	*B. subtilis*	*S. aureus*
K22S-22	$24.00^{n} \pm 0.14$	$31.33^{n} \pm 1.04$	$33.00^{l} \pm 2.00$
K22S-31	$18.33^{l} \pm 0.66$	$28.67^{m} \pm 1.33$	$29.00^{k} \pm 0.44$
K22S-36	$29.67^{o} \pm 0.33$	$29.33^{m} \pm 0.6$	$24.33^{j} \pm 0.58$

*Means followed by the same letter are not significantly different according to the Duncan Multiple Range Test (DMRT), $P< 0.05$.

Inhibition (ZOI) based on the diameter of the ZOI, classifying it into four distinct levels: very strong (>20 mm), strong (10-20 mm), medium (5-10 mm), and no response (<5 mm), which categorized the three actinobacteria as the very strong antimicrobial ability against the three tested bacteria. The zone of inhibition diameter differences occured because each bacterial isolate produces unique secondary metabolites with varying chemical structures, compounds, and concentrations (Ouchari et al. 2018).

The minimum inhibitory concentration (MIC) and Minimum bactericidal concentration (MBC) of selected actinobacteria

The three actinobacteria isolated, i.e., K22S-22, K22S-31, and K22S-36, were selected for MIC and MBC determination. Based on the results of MIC value, the K22S-22 isolate had the highest minimum inhibitory concentration against the Gram-positive bacteria *B. subtilis* and *S. aureus*, with MIC values of 3.4 µg mL^{-1} and 1.72 µg mL^{-1}, respectively (Table 2). According to Praptiwi et al. (2019), the category of MIC value is as follows: strong anti-bacterial (<100 µg mL^{-1}), moderate anti-bacterial (100-500 µg mL^{-1}), and weak antimicrobial (>500 µg mL^{-1}). It suggests that the K22S-22 isolate has strong antibacterial activity against these bacteria. The IC_{50} value against *S. aureus* was 1.033±0.033 µg mL^{-1}, and the IC_{50} value against *B. subtilis* was 4.155±0.028 µg mL^{-1}, with R-squared values of 0.95 and 0.98, respectively (Figure 1). The findings revealed that none of the ethyl acetate extracts inhibit the growth of Gram-negative *E. coli*.

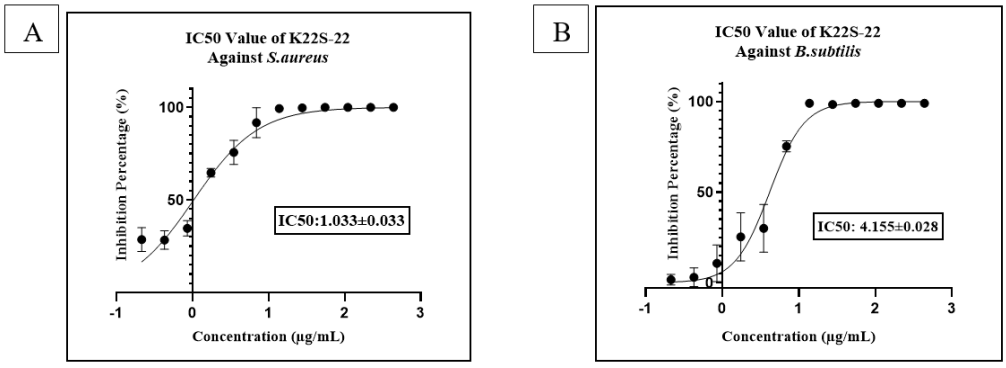

Figure 1. The Resazurin microtiter assay for the ethyl acetate extract of K22S-22 isolate, ranging from 400- 0.20 µgmL^{-1} using GraphPad Prism 10; (A) against *Staphylococcus aureus* (InaCC B005) with the IC_{50} value of 1.033±0.033. (B) against *Bacillus subtilis* (InaCC B004) with the IC_{50} value of 4.155±0.028.

The results showed that the MBC value of K22S-22 extract against *B. subtilis* and *S. aureus* was 100 µg mL^{-1} (Table 2). Sapkota et al. (2020) explained that the differences in cell wall structure between Gram-negative and Gram-positive bacteria affect the sensitivity of bioactive compounds from actinomycete extracts. Gram-negative bacteria possessed an outer membrane composed of phospholipids and a dense layer of lipopolysaccharides. They effectively restrict the entry of small molecules into the cell by employing a

Table 2. The MIC and MBC values of the selected actinobacteria against the three test bacteria.

Sample ID	MIC (µg mL^{-1})			MBC (µg mL^{-1})		
	E. coli	*B. subtilis*	*S. aureus*	*E. coli*	*B. subtilis*	*S. aureus*
K22S-22	100	3.13	1.56	-	100	100
K22S-31	-	50	12.50	-	>400	>400
K22S-36	-	400	100	-	>400	>400

combination of low outer membrane permeability, active efflux pumps, and degradative enzymes (Saxena et al. 2023). In contrast, Gram-positive bacteria have a multilayered peptidoglycan cell wall without an outer membrane. As a result, hydrophobic anti-bacterial components can disrupt the Gram-positive cell walls increasing membrane permeability and leading to bacterial death.

Differences between the preliminary assay and the MIC/MBC analysis of K22S-36 may be due to variations in the experimental conditions and sensitivity of the methods. In the preliminary agar diffusion assay, the inhibition zone reflects not only the antibacterial potency but also the ability of the compound to diffuse through the agar. Thus, a compound with good diffusion properties can create a large inhibition zone, even if it is not highly potent at lower concentrations. In contrast, MIC and MBC assays are conducted in a liquid medium, where diffusion is not a factor, and the actual bactericidal or inhibitory concentration is measured directly. It may not show activity in MIC/MBC despite strong results in the diffusion assay if the active compound is unstable in liquid, poorly soluble, or requires synergy with other compounds to be effective. Other possible factors may include the compound effectivity at high concentrations not achieved in the dilution series, loss of activity due to degradation in broth conditions, and the presence of compound interactions or antagonistic effects in liquid media.

Molecular Identification and Phylogenetic Analysis of K22S-22

A total of six distinct primers were employed to amplify the DNA from strain K22S-22, resulting in an overall sequence length of 1504 bp. Based on the EZBiocloud databases, the isolate was included in the genus of *Streptomyces*, and the highest hit in percentage was *Streptomyces rapamycinicus* NRRL B-5491 (T) species with a similarity of 99.08 % and completeness of 97.9 %. Followed by *Streptomyces iranensis* HM 35 (T) (98.96 %), *Streptomyces endocoffeicus* CA3R110 (T) (98.95 %), and *Streptomyces coffeae* CA1R205 (T) (98.89 %). According to Putri and Nurkanto (2016), a similarity of 99.08 % indicates a strong relatedness, but it does not rule out the possibility of K22S-22 being a novel species. Further genomic and phenotypic characterisation would be needed to make a conclusive determination. However, actinobacteria may be classified as new species despite having 16S rRNA homology exceeding 98 % if the DNA-DNA hybridisation homology value is low or below 70 %.

The phylogenetic tree of K22S-22 using the neighbour-joining method with Kimura-2 parameter as the model and 1000 bootstraps (Figure 2) shows that K22S-22 is located closely and in one node with the species *Streptomyces coffeae*, *Streptomyces endocoffeicus*, and *Streptomyces rapamycinicus*. The tree bootstrap values show a reliability value, most of which is above 70 % (Ecker et al. 2024). The placement of K22S-22 within the neighbor-joining tree has a higher bootstrap value with *Streptomyces coffeae* instead of *S. rapamycinicus*, as explained by Labeda et al. (2012), indicating that there are minor variations between the two sequences, differences in ecological niches, or it may be novel strains or species. The BLAST results are limited in accurately reflecting the evolutionary relationships, as they primarily compare the sequence similarity without fully considering phylogenetic divergence. Furthermore, recent research indicated that relying on 16S rRNA phylogeny and clustering for Streptomyces taxonomy can be misleading because of their significant genetic similarities and intricate evolutionary connections. To achieve a more precise classification, genome-based taxonomic methods such as whole-genome sequencing and ANI analysis are essential (Kiepas et al. 2024). Therefore, additional analyses were required to validate whether K22S-22 represented a novel strain, including genome sequencing and phenotypic characterization of the species.

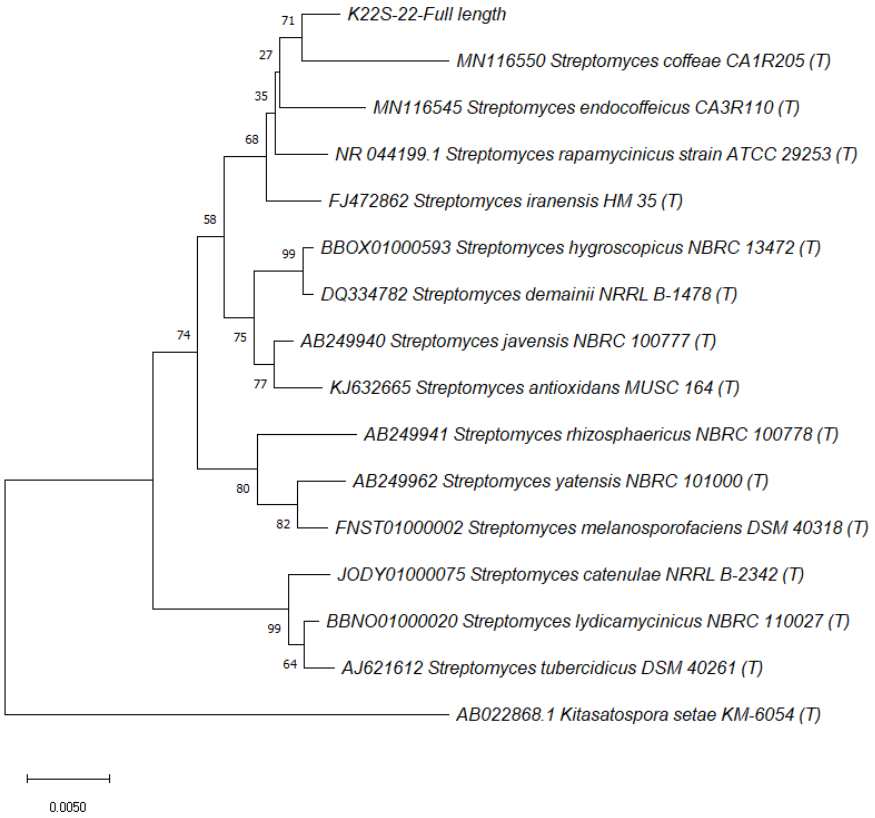

Figure 2. The phylogenetic tree of the K22S-22 isolate was constructed using the neighbour-joining method (NJ). The *Kitasatospora setae* was used as the outgroup. The number at the branch node indicates the bootstrap value (%) with 1000 replicates. Ruller bar showed 0.005 substitutions per nucleotide.

Detection of The Polyketide Synthase (PKS)–I, PKS-II, and Non-ribosomal Peptides Synthase (NRPS) Genes in K22S-22.

The K22S-22 isolate, identified as *Streptomyces* sp., possesses all three potential antibiotic biosynthetic genes (PKS-I, PKS-II, NRPS) (Figure 3). The selected isolate demonstrated relatively strong activity during the preliminary screening. According to Singh et al. (2021), multiple studies have shown that actinobacterial genomes are a rich source of antibiotics. Although *Streptomyces* are not the only producers of bioactive compounds, they are prolific, making the genus the most prominent among prokaryotes. Additionally, *Streptomyces* genomes contain a wide range of 20-30 biosynthetic gene clusters for secondary metabolites, including polyketide synthases (PKS) and non-ribosomal peptide synthetases (NRPS). In total, 1346 of these gene clusters were detected by antiSMASH in 39 *Streptomyces* genomes in the antiSMASH database. Among the diverse range of metabolites synthesized by PKS-I, PKS -II, and NRPS are antibiotics like penicillins, vancomycin, and erythromycin, antifungals such as nystatin, anti-tumor agents like ansamitocin and bleomycin, anthelmintics including avermectin, and immunosuppressive agents like rapamycin and FK506 (Dhakal et al. 2019). Previous research identified *Streptomyces rapamycinicus NRRL 5491* from soil samples at Easter Island, Chile. This species primarily examined its capacity to synthesize rapamycin, an immunosuppressive drug that is widely utilized in healthcare (Baranasic et al. 2013). The genome of this particular strain contains a high number of clusters associated with secondary metabolites, particularly those related to the biosynthesis of rapamycin through PKS and NRPS genes (Baranasic et al. 2013). Conversely, our isolate from the Sungai Wain Protected Forest exhibited a wider range of bioactivities, demonstrating significant antioxidant and

antibiofilm properties. This implies that environmental factors might play a role in the diversity of metabolites in Streptomyces, underscoring the necessity for additional comparative genomic and metabolomic research.

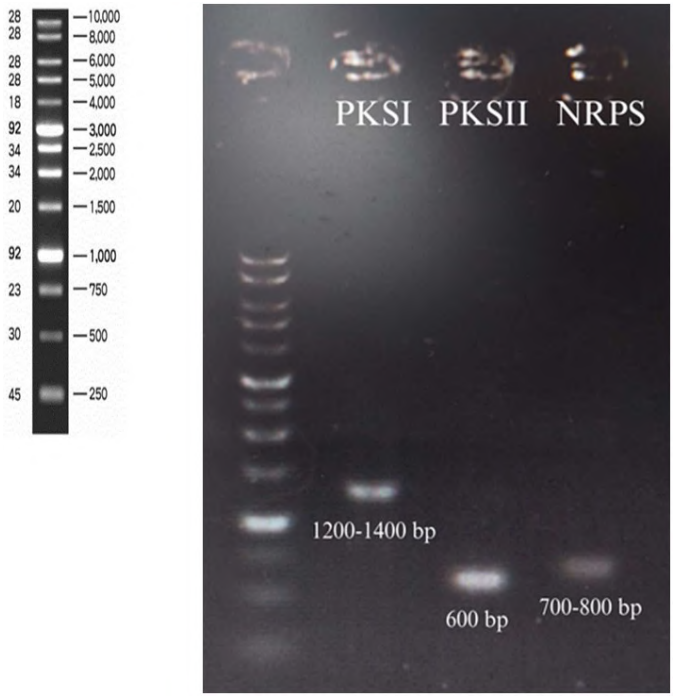

Figure 3. Detection of the polyketide synthase (PKS) and non-ribosomal peptides synthase (NRPS) genes in K22S-22 isolate.

The antioxidant activity assay using the DPPH free radical scavenging assay

The DPPH scavenging activity of the K22S-22 extract increased with increasing concentrations but showed a sharp decline at 50 µg mL^{-1}, where the activity dropped to 35.07 %. The IC_{50} of the K22S-22 isolate extract was 67.59 ± 0.020 µg mL^{-1}. According to Itam et al. (2021), the IC_{50} values of antioxidants are categorized as follows: very strong (<50 µg mL^{-1}), strong (50-100 µg mL^{-1}), weak (250-500 µg mL^{-1}), and inactive (>500 µg mL^{-1}).

According to the classification, the IC_{50} value of 67.59 ± 0.020 µg mL^{-1}for the K22S-22 extract signifies 'strong' antioxidant activity. In comparison, the positive control, ascorbic acid, showed a significantly lower IC_{50} value of 4.095 ± 0.02 µg mL^{-1}, reflecting its well-known potency as a standard antioxidant. Gas Chromatography-Mass Spectrometry (GC-MS) analysis of the ethyl acetate extract from K22S-22 revealed the presence of several fatty acid derivatives and other organic compounds. These included saturated and unsaturated fatty acids such as hexadecanoic acid (palmitic acid), oleic acid, and pentadecanoic acid derivatives, which are known to exhibit moderate antioxidant properties by donating hydrogen atoms or electrons to neutralize free radicals (Venn-Watson & Schork 2023).

Additionally, some of the detected compounds may contain hydroxyl or carboxyl groups, which are often associated with radical-scavenging activity due to their ability to stabilize unpaired electrons. The presence of these bioactive metabolites suggests that the antioxidant activity observed may result from a synergistic effect of multiple compounds rather than a single dominant constituent (Tumilaar et al. 2024).

This antioxidant scavenging assay is important because antioxidants are significant for therapeutic applications. They neutralize reactive oxygen species (ROS) in patients with infectious diseases or metabolic disorders (Agwu et al. 2024).

The biofilm Inhibition assay

Based on the biofilm inhibition assay results, the K22S-22 ethyl acetate extract shows a clear crystal violet decolourisation at the concentration of 8 µg mL^{-1}. The clear crystal violet colourisation indicated biofilm inhibition by a particular extract concentration. The Biofilm IC_{50} was calculated and measured according to the biofilm inhibition percentage at 4.541 ± 0.124 µg mL^{-1}. Streptomycin, used as the antibiotic control, exhibited a noticeable dark violet coloration from crystal violet staining at a concentration of 6.25 µg mL^{-1}, indicating potent biofilm inhibition with an effectiveness of 60.92 %. It decreases remarkably to 48.94 % at the concentration of 3.13 µg mL^{-1} (Figure 4). The streptomycin control shows a similar result in concentration to the K22S-22 extract. Therefore, the extract is a potential inhibitor and prevents biofilm formation within the *S. aureus* cell. According to Sukmarini et al. (2024), preventing the initial adhesion of the microbes is an effective method to avoid the initial biofilm colonization and subsequent infections resulting from planktonic cells released from the biofilm. The initial colonisation of bacterial cells relies heavily on surface attachment, a critical first step in biofilm formation. Screening for compounds that block this process is a valuable method for identifying potential antibiofilm agents. Although several classes of chemical compounds are known to contribute to antibiofilm activity, no study has yet identified in this work which specific compounds might be contributing to its antibiofilm effect; however, the GC-MS analysis of the K22S-22 isolate identified palmitic acid (hexadecanoic acid). A study by Nirwati et al. (2022) showed that Streptomyces' antibiofilm activity interferes with the proliferative stage and disrupts EPS formation through quorum sensing.

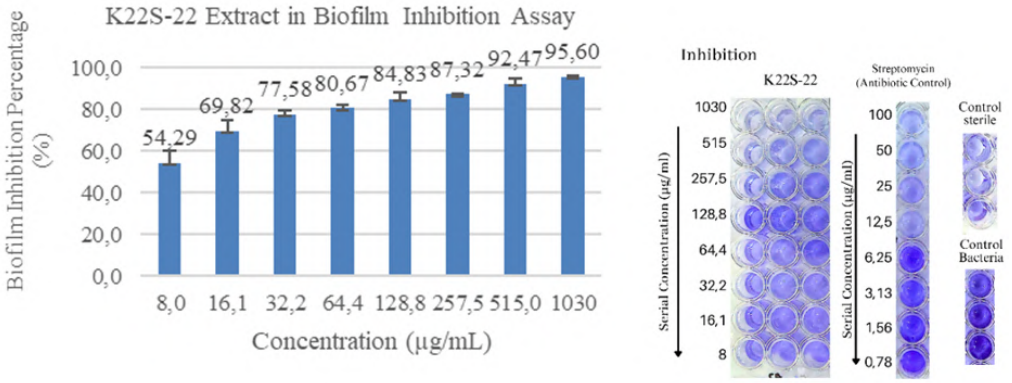

Figure 4. The K22S-22 biofilm inhibition percentage and the visualization of inhibition according to the crystal violet staining.

Biofilm Eradication Assay

The extract was further tested for the eradication assay because of its potential to inhibit biofilm formation. The value of Biofilm eradication concentration (BEC_{50}) was 50.71 ± 0.029 µg mL^{-1} (R-squared value of 0.97). Streptomycin was used as a control, as its effect on preformed biofilms was comparable to its activity in the biofilm inhibition assay, showing a mean inhibition of 55.68 % at 6.25 µg mL^{-1}, which decreased to 35.61 % at 3.13 µg mL^{-1}. The Minimum Biofilm Eradication Concentration ($MBEC_{50}$) of streptomycin was 4.501 ± 0.089 µg mL^{-1}.

Preventing biofilm formation seems to be easier than destroying the preformed biofilms. This is because the antimicrobial compounds can easily penetrate the microorganism, as the protective matrix of extracellular polymeric substances (EPS) has not yet been fully formed in the early biofilm stage. The pre-formed biofilm has established the protective EPS matrix, which consists of polysaccharides, proteins, nucleic acids, and lipids. Therefore, it is more difficult to disrupt, hinders the antimicrobial agent diffusion, and makes the microorganism resistant to antibiotics and survive in a

dormant state (Srivastava et al. 2024). Therefore, the biofilm inhibition possessed a higher value than the eradication, which is 4.541 ± 0.124 µg mL^{-1} and 50.71 ± 0.029 µg mL^{-1}, respectively.

Gas Chromatography-Mass Spectrometry (GC-MS) Analysis of K22S-22 Extract

Results of the GC-MS analysis showed that the K22S-22 extract had 51 peaks with retention times varying from 5.77 minutes to 52.441 minutes, with the major compound being Hexadecanoic acid with an area percentage of 12.98 % (Table 3). The compounds were also assigned based on their similarity index (SI) of >70 % with the NIST data. According to Gumbi et al. (2019), a similarity index (SI) of more than 85 values is considered to be the assignment of probable identity to the compounds.

Hexadecanoic acid, also known as palmitic acid, is the compound with the highest relative abundance in the K22S-22, with a retention time of 34.430 minutes and a similarity index of 93. Palmitic acid is included among fatty acids, which play crucial roles in the biosynthesis of diverse antibiotic compounds, serving as building blocks or regulators (Acetyl-CoA) in secondary metabolite production by actinobacteria. Modifying lipid biosynthetic pathways affects antibiotic production yields in *Streptomyces* species. Specific fatty acid constituents correlate directly with polyketide synthesis (PKS) effi-

Table 3. The eight identified dominant volatile compounds by GC–MS analysis of the ethyl acetate extract of K22S-22.

No	Retention time (min)	Compound	Molecular formula	Molecular weight	Area %	SI Value	Reported activity	References
1	34.430	Hexadecanoic acid	$C_{16}H_{32}O_2$	256	12.98	93	antioxidant, antimicrobial, and anti-inflammatory	Shaaban et al. 2021
2	11.196	3-Pentanol, 3-ethyl- (CAS) 3-Ethyl-3-pentanol	$C_7H_{16}O$	116	9.94	74	unknown	
3	32.380	9-Octadecenoic acid	$C_{18}H_{34}O_2$	242	7.52	87	Antimicrobial, Anticancer, Hepatoprotective, Anti-arthritic, anti-asthma, diuretic	Toh et al. 2023
4	29.890	Tetradecanoic acid	$C_{14}H_{28}O_2$	228	5.38	93	Nematicide and cancer-preventive agents, antimicrobial, antioxidant, antifungal, and hypercholesterolemic effects	Toh et al. 2023
5	36.815	9-Octadecenoic acid (Z)- (CAS) Oleic acid	$C_{18}H_{34}O_2$	282	4.57	93	Antioxidant, antimicrobial, anticarcinogenic, antihypertensive, and Anti-inflammatory	Toh et al. 2023
6	17.321	Malonic acid	$C_9H_8O_4$	180	4.14	95	Anti-inflammatory, antibacterial, antifungal, chelating agent,	Fatima et al. 2024
7	24.381	Phenol, 3,5-bis (1,1-dimethyl ethyl)-	$C_{14}H_{22}O$	206	3.25	94	Anti-inflammatory effects, antimicrobial, and antioxidant	Toh et al. 2023
8	32.156	Pentadecanoic acid	$C_{15}H_{30}O_2$	242	3.25	90	Supporting cardiometabolic and liver health, antimicrobial properties, and a longevity-enhancing compound	Venn-Watson & Schork 2023

ciency. These interconnections between lipid metabolism and antibiotic generation underscore the significance of understanding lipid-regulating enzymes, such as acyl-CoA carboxylases, and the broader influence of lipid metabolism on the biosynthesis of secondary metabolites (Gago et al. 2018). Another identified fatty acid was Pentadecanoic acid, at RT of 32.156, with an area percentage of 3.25 % and SI 90. According to Venn-Watson and Schork (2023), this compound has the ability for longevity and health span activities. It is consistent with the 16S rRNA identification of K22S-22, which was classified as *Streptomyces rapamycinicus* strain NRRL 5491, known as the producer of immunosuppressant compounds that help extend the survival of transplanted organs. (Mohamed et al. 2019). Rumbaugh and Sauer (2020) reported that fatty acids can inhibit growth and disrupt *Staphylococcus aureus* biofilm formation. The K22S-22 extract also possesses high antimicrobial and antibiofilm activity against *S. aureus*.

CONCLUSIONS

The less explored Sungai Wain-Protected Forest environments constitute a valuable repository of actinomycete species and antimicrobial agents. In this study, the isolated actinobacteria produced remarkable secondary metabolites, which can be anti-bacterial, antioxidant, and antibiofilm. The K22S-22 was identified as *Streptomyces rapamycinicus* NRRL B-5491 (T) species with a similarity of 99.08 %, which possesses polyketide synthase (PKS-I and II) and the non-ribosomal peptide synthase (NRPS) biosynthetic gene clusters (BGCs), and contains several fatty acids. This study highlights that unexplored areas, such as the Sungai Wain Protected Forest, representing a valuable bioactive source, especially the *Streptomyces* species exhibiting diverse biological activities, including anti-bacterial, antibiofilm, and antioxidant properties. These findings underscored the potential of this strain for future biotechnological applications.

AUTHOR CONTRIBUTION

Conceptualisation: H.R., S.R., E.R., Methodology: H.R., R.S., E.R. Validation: H.R., R.S., E.R., S.W. Investigation: H.R. Resources: S.R., T.K.D. H.R. Writing and editing: H.R., E.R., S.W., Y.S. Supervisions: R.S., E.R., S.W., Y.S. Before submission, the final draft was examined and approved by each co-author.

ACKNOWLEDGMENTS

The author expresses gratitude to the research group of prokaryotes in the Research Centre for Biosystematics and Evolution, National Research and Innovation Agency (BRIN), for providing lab facilities and consumables. The authors are also thankful to the Endowment Fund for Education Agency (LPDP) for funding the author (Scholarship ID: 202212111512312) throughout the Master's degree and Research. The research grant and funding from BRIN's Advanced Indonesian Innovation Research, LPDP Exploration and Expedition Program Number of B-1116/II.7.5/FR.06/3/2024 dan B-949/III.5/FR.06.00/3/2024.

CONFLICT OF INTEREST

The authors declare that there are no conflicts of interest.

REFERENCES

Agwu, E. et al., 2024. Antioxidant roles/functions of ascorbic acid (vitamin C). In *Ascorbic Acid - Biochemistry and Functions*. IntechOpen. doi: 10.5772/intechopen.110589.

Amran, S.S.D. et al., 2024. Preparation of biofilm assay using 96-well and 6-

well microplates for quantitative measurement and structural characterization: a review. *Science Letters*, 18(2), pp.21–134. doi: 10.24191/sl.v18i2.27020

Atikana, A. et al., 2021. Uncovering the potential of *actinobacterium* BLH 1-22 isolated from marine sediment as a producer of antibiotics. *IOP Conference Series: Earth and Environmental Science*, 948, 012056. doi: 10.1088/1755-1315/948/1/012056

Baliyan, S. et al., 2022. Determination of Antioxidants by DPPH Radical Scavenging Activity and Quantitative Phytochemical Analysis of *Ficus religiosa*. *Molecules (Basel, Switzerland)*, 27(4), 1326. doi: 10.3390/molecules27041326

Baranasic, D. et al., 2013. Draft genome sequence of *Streptomyces rapamycinicus strain NRRL 5491*, the producer of the immunosuppressant rapamycin. *Genome Announcements*, 1(4), e00581-13. doi: 10.1128/genomeA.00581-13.

Bircher, L. et al., 2018. Cryopreservation of artificial gut microbiota produced with in vitro fermentation technology. *Microbial Biotechnology*, 11(1), pp.163-175. doi: 10.1111/1751-7915.12844.

Clinical and Laboratory Standards Institute (CLSI)., 2015. *Methods for dilution antimicrobial susceptibility tests for bacteria that grow aerobically*. Approved Standard. 10thed. CLSI document M07-A10. Clinical and Laboratory Standards Institute, Annapolis Junction, MD.

Delbari, Y. et al., 2023. Identification and anti-bacterial properties of endophytic actinobacteria from *Thymes kotschyanus*, *Allium hooshidaryae*, and *Cerasus microcarpa*. *Scientific Reports*, 13(1), 13145 . doi: 10.1038/s41598-023-40478-x.

De Simeis, D. & Serra, S. 2021. Actinomycetes: a never-ending source of bioactive compounds - an overview on antibiotics production. *Antibiotics*, 10 (5), 483. doi: 10.3390/antibiotics10050483.

Dhakal, D., Sohng, J.K. & Pandey, R.P. 2019. Engineering actinomycetes for the biosynthesis of macrolactone polyketides. *Microbial Cell Factories*, 18 (1), 137. doi: 10.1186/s12934-019-1184-z.

Ecker, N. et al., 2024. A machine-learning-based alternative to phylogenetic bootstrap. *Bioinformatics* 40(Issue Supplement_1), pp.i208-i217. doi:10.1093/ bioinformatics/btae255.

Escalante-Rendiz, D. et al., 2019. Molecular Identification of Selected Streptomyces Strains Isolated from Mexican Tropical Soils and Their Anti-Candida Activity. *International Journal of Environmental Research and Public Health*, 16(11), 1913. doi: 10.3390/ijerph16111913.

Fatima, T. et al., 2024. Molecular marker identification, antioxidant, antinociceptive, and anti-inflammatory responsiveness of malonic acid capped silver nanoparticle. *Frontiers in Pharmacology*, 14, 1319613. doi: 10.3389/fphar.2023.1319613.

Gago, G. et al., 2018. Components and key regulatory steps of lipid biosynthesis in actinomycetes. In *Biogenesis of fatty acids, lipids and membranes*. Cham: Springer, pp.1–28. doi: 10.1007/978-3-319-43676-0_65-1

Gumbi, B.P. et al., 2019. Target, suspect and non-target screening of silylated derivatives of polar compounds based on single ion monitoring GC-MS. *International Journal of Environmental Research and Public Health*, 16(21), 4022. doi: 10.3390/ijerph16214022

Haney, E.F., Trimble, M.J. & Hancock, R.E., 2021. Microtiter plate assays to assess antibiofilm activity against bacteria. *Nature Protocols*, 16(5), pp.2615-2632. doi: 10.1038/s41596-021-00515-3

Hiltunen, A.K. et al., 2019. Structural and Functional Dynamics of Staphylo-

coccus aureus Biofilms and Biofilm Matrix Proteins on Different Clinical Materials. *Microorganisms*, 7(12), 584. doi: 10.3390/microorganisms7120584.

Itam, A. et al., 2021. Comparative study of phytochemical, antioxidant, and cytotoxic activities and phenolic content of *Syzygium aqueum* (Burm. F. Alston f.) extracts growing in West Sumatra, Indonesia. *Scientific World Journal*, 2021, 553759. doi:10.1155/2021/5537597.

Janatiningrum, I. et al., 2024. Rhizosphere actinobacteria isolated from *Pometia pinnata* and its antimicrobial activity. *Biodiversitas*, 25(3), pp.1007-1014. doi:10.13057/biodiv/d250313.

Kiepas, A.B., Hoskisson, P.A. & Pritchard, L., 2024. 16S rRNA phylogeny and clustering is not a reliable proxy for genome-based taxonomy in *Streptomyces*. *Microbial Genomics*, 10(3), 001287. doi: 10.1099/mgen.0.001287

Kim, H.J. & Jang, S., 2018. Optimization of a resazurin-based microplate assay for large-scale compound screenings against *Klebsiella pneumoniae*. *3 Biotech*, 8(1), 3. doi: 10.1007/s13205-017-1034-9.

Kumari, N., Pandey, S. & Meghani, E., 2021. Evaluation of actinomycetes isolated antimicrobial metabolites as potent inhibitors of multidrug resistant organisms. *Indian Journal of Geo-Marine Sciences*, 50(1), pp.29-36. doi: 10.56042/ijms.v50i01.66080.

Labeda, D.P. et al., 2012. Phylogenetic study of the species within the family Streptomycetaceae. *Antonie van Leeuwenhoek*, 101(1), pp.73–104. doi: 10.1007/s10482-011-9656-0.

Mast, Y. & Stegmann, E., 2019. Actinomycetes: the antibiotics producers. *Antibiotics*, 8(3), 105. doi: 10.3390/antibiotics8030105.

Mohamed, A.M., Elkhateeb, A.W. & Daba, M.G., 2019. The Continuous Story of the Miraculous Drug, Rapamycin. ARC *Journal of Pharmaceutical Sciences*, 5(2), pp.1-7. doi: 10.20431/2455-1538.0502001.

Nahum, Y. et al., 2025. Biofilms as potential reservoirs of antimicrobial resistance in vulnerable settings. Frontiers in Public Health, 13, 1568463. doi: 10.3389/fpubh.2025.1568463.

National Standardization Agency of Indonesia, 2018. *Antioxidant assay method for natural compounds from aquatic sources using DPPH (2,2-diphenyl-1-picrylhydrazyl) spectrophotometry*. SNI 8623:2018. Jakarta.

Nurkanto, A. & Agusta, A., 2015. Molecular identification and morphophysiological characterization of Actinomycetes producing antimicrobial compounds. Jurnal Biologi Indonesia, 11(2), pp.193–205.

Nirwati, H. et al., 2022. Soil-derived Streptomyces sp. GMR22 producing antibiofilm activity against Candida albicans: bioassay, untargeted LC-HRMS, and gene cluster analysis. *Heliyon*, 8, e09333. doi: 10.1016/j.heliyon.2022.e09333

National Institute of Standards and Technology (NIST)., 2023, 'NIST mass spectral libraries and software [ChemData.NIST.GOV release],' in *NIST Mass Spectrometry Data Center*, viewed from https://chemdata.nist.gov

Ouchari, L. et al., 2018. Antimicrobial potential of actinomycetes isolated from the unexplored hot Merzouga desert and their taxonomic diversity. *Biology Open*, 8(2), bio035410. doi: 10.1242/bio.035410.

Praptiwi, R. et al., 2019. Assessment of actinomycetes isolated from soils on Simeuleu Island as anti-bacterial and antioxidant. *AIP Conference Proceedings*, 2120, 080011. doi: 10.1063/1.5115749.

Putri, A.L., Arif, N. & Nurkanto, A., 2016. Diversity of Actinomycetes from soil, sediment, and leaf litter samples of Enggano Island, Bengkulu. *Berita Biologi*, 15(3), pp.217–225.

Ratnakomala, S. et al., 2018. Antimicrobial activity of selenium nanoparticles

synthesized by Actinomycetes isolated from Lombok Island soil samples. *Jurnal Kimia Terapan Indonesia*, 20(1), pp.8-15. doi: 10.14203/jkti.v20i1.374.

Rumbaugh, K.P. & Sauer, K., 2020. Biofilm dispersion. *Nature Reviews Microbiology*, 18(10), pp.571-586. doi: 10.1038/s41579-020-0385-0.

Sapkota, A. et al., 2020. Isolation, Characterization, and screening of antimicrobial-producing actinomycetes from soil samples. *International Journal of Microbiology*, 2020, 2716584. doi: 10.1155/2020/2716584.

Saxena, D. et al., 2023. Tackling the outer membrane: Facilitating compound entry into Gram-negative bacterial pathogens. *Npj Antimicrobials and Resistance*, 1(1), 17. doi: 10.1038/s44259-023-00016-1

Silva, K.R. et al., 2019. Antibacterial and Cytotoxic Activities of *Pinus tropicalis* and *Pinus elliottii* Resins and of the Diterpene Dehydroabietic Acid Against Bacteria That Cause Dental Caries. *Frontiers in Microbiology*, 10, 987. doi: 10.3389/fmicb.2019.00987

Shaaban, M.T., Ghaly, M.F. & Fahmi, S.M., 2021. Anti-bacterial activities of hexadecanoic acid methyl ester and green-synthesized silver nanoparticles against multidrug-resistant bacteria. *Journal of Basic Microbiology*, 61(6), pp.557-568. doi: 10.1002/jobm.202100061.

Singh, T.A. et al., 2021. Tapping into actinobacterial genomes for natural product discovery. *Frontiers in Microbiology*, 12, 655620. doi:10.3389/fmicb.2021.655620.

Srivastava, A. et al., 2024. Biofilm inhibition/eradication: exploring strategies and confronting challenges in combating biofilm. *Archives of Microbiology*, 206(5), 212. doi: 10.1007/s00203-024-03938-0

Sukmarini, L., Atikana, A. & Hertiani, T., 2024. Antibiofilm activity of marine microbial natural products: potential peptide- and polyketide-derived molecules from marine microbes toward targeting biofilm-forming pathogens. *Journal of Natural Medicines*, 78, pp.1–20. doi: 10.1007/s11418-023-01754-2

Tumilaar, S.G. et al., 2024. A comprehensive review of free radicals, oxidative stress, and antioxidants: Overview, clinical applications, global perspectives, future directions, and mechanisms of antioxidant activity of flavonoid compounds. *Journal of Chemistry*, 2024, 5594386. doi: 10.1155/2024/5594386

Toh, S.C. et al., 2023. In vitro antimicrobial efficacy of *Cassia alata* (Linn.) leaves, stem, and root extracts against cellulitis causative agent *Staphylococcus aureus. BMC Complementary Medicine and Therapies*, 23, 85. doi: 10.1186/s12906-023-03914-z.

Venn-Watson, S. & Schork, N.J., 2023. Pentadecanoic Acid (C15:0), an essential fatty acid, shares clinically relevant cell-based activities with leading longevity-enhancing compounds. *Nutrients* 15(21), 4607. doi: 10.3390/nu15214607.

Zhao, A., Sun, J. & Liu, Y. 2023. Understanding bacterial biofilms: From definition to treatment strategies. *Frontiers in Cellular and Infection Microbiology*, 13, 1137947. doi: 10.3389/fcimb.2023.1137947.

Journal of Tropical Biodiversity and Biotechnology
Volume 10, Issue 04 (2025): jtbb20733
DOI: 10.22146/jtbb.20733

Research Article

The Effect of 2-iP (*2-isopentenyl adenine*) Concentration on the Growth of Ki Aksara Orchids (*Macodes petola* (Blume) Lindl.) *In Vitro*

Yenisbar[1]*, Arief Wicaksono[1], Edhi Sandra[2]
1)Agrotechnology Study Program, Faculty of Biology and Agriculture, National University, Jl. Sawo Manila No.61 South Jakarta 12520, Indonesia
2)Department of Forest Resource Conservation and Ecotourism, Faculty of Forestry and Environment, IPB University, Jl. Raya Dramaga Kampus IPB Bogor 16680, Indonesia
* Corresponding author, email: yenisbar.chaniago@gmail.com

Keywords:
2-isopentenyl adenine
Cytokinin
Ki Aksara Orchids
Orchids
Tissue Culture
Submitted:
11 April 2025
Accepted:
15 July 2025
Published:
13 October 2025
Editors:
Furzani Binti Pa'ee
Tanti Agustina

ABSTRACT

This study aims to determine the optimal concentration of 2-iP (*2-isopentenyl adenine*) for the in vitro shoot growth of Ki Aksara orchids (*Macodes petola* (Blume) Lindl.). The experiment was conducted at the Esha Flora Tissue Culture Laboratory, Kedung Waringin Sub-district, Tanah Sereal District, Bogor City, from December 2022 to March 2023. The method used a Completely Randomized Design (CRD) comprising six treatment levels, leading to a total of 30 experimental units. The treatment levels included P0 (Control), P1 (0.05 mg L^{-1}), P2 (0.10 mg L^{-1}), P3 (0.15 mg L^{-1}), P4 (0.20 mg L^{-1}), and P5 (0.25 mg L^{-1}). The observed parameters included the number of shoots, stem diameter, number of leaves, number of roots, plant height, and leaf colour. Subsequently, the collected data were analysed using Analysis of Variance (ANOVA), followed by a Least Significant Difference (LSD) test at a 95 % confidence level. The results showed that 2-iP concentration of 0.10 mg L^{-1} was the most effective in promoting the growth of apical shoots, stem diameter, root number, and plant height of Ki Aksara orchids. The two types of shoots observed were apical and lateral. However, the expected growth corresponded to apical shoots, which were predominantly found at 2-iP concentration of 0.10 mg L^{-1}.

How to cite:
Yenisbar, Wicaksono, A. & Sandra, E., 2025. The Effect of 2-iP (*2-isopentenyl adenine*) Concentration on the Growth of Ki Aksara Orchids (*Macodes petola* (Blume) Lindl.) *In Vitro*. *Journal of Tropical Biodiversity and Biotechnology*, 10(4), jtbb20733. doi: 10.22146/jtbb.20733

INTRODUCTION

Ornamental plants, such as orchids, are highly valued for their aesthetic appeal, particularly flowers and leaves. Orchids are part of the *Orchidaceae* family with around 5000 species globally, possessing significant economic value due to the striking colours and patterns (Herliana et al. 2019). However, the natural populations are threatened by habitat loss from urban and plantation development, as well as environmental degradation (Dewi et al. 2018). To protect endangered species, the Indonesian government, through Regulation No. 7 of 1999, has designated black, hartinah, sugarcane, star moon, and Ki Aksara orchids as protected. Ki Aksara orchids (*Macodes petola* (Blume) Lindl.) captivate attention due to the distinctive leaf patterns, resembling script or letters (Gunawan 2016). These species have been classified as Endangered (EN), facing a high risk of extinction unless protective measures are implemented within a certain timeframe (Rugayah et al. 2017).

One of the primary challenges in the cultivation of orchids is the limited availability of seedlings. An alternative method to produce a large number of seedlings in a short period is vegetative propagation through in vitro plant tissue culture. The in vitro method includes cultivating plant organs in sterile conditions in containers filled with growth media (Yuniardi 2020). The main objective of this method is to generate a high quantity of uniform seedlings in a shorter time compared to a conventional propagation strategy (Santoso et al. 2020). One of the key factors determining the success of in vitro propagation is the type and concentration of plant growth regulators, which must be selected according to the purpose and stage of cultivation.

Growth regulators are organic compounds not classified as nutrients but are capable of stimulating plant growth. These compounds are plant hormones deliberately added to accelerate the plant production process (Widiastoety 2014). The application of growth regulators can cause varying responses based on the type and concentration (Nurana et al. 2017). Among several plant hormones influencing cell division, cytokinin plays a central role. Cytokinin functions to stimulate cell division in meristematic tissues, promoting both cell division and enlargement, thereby facilitating growth (Rosniawaty et al. 2018). Administering high concentrations of cytokinin increases the frequency of shoot multiplication. This suggests that higher cytokinin concentration correlates with a greater number of shoots produced (Munggarani et al. 2018). A particular type of cytokinin used for promoting shoot elongation is 2-iP (*2-isopentenyl adenine*). Generally, 2-iP is often selected due to the relatively stable and extensive effect in stimulating shoot multiplication without inducing morphological abnormalities such as vitrification or excessive callus formation.

The application of 2-iP in the vitro method functions to stimulate plant growth and shows high activity in promoting cell division (Nurana et al. 2017). 2-iP-type cytokinin has been used in tissue culture to stimulate callus differentiation, induce axillary bud formation, and enhance cell division (Tongkok et al. 2018). According to Nurana et al. (2017), the application of 2-iP in combination with NAA to hybrid Dendrobium orchids at a concentration of 0.2 mL L^{-1} produced optimal growth of the plantlets, particularly in shoot development and production of leaves. Therefore, this study aims to determine the most effective concentration of 2-iP for promoting shoot elongation in Ki Aksara orchids (*Macodes petola*) under in vitro conditions.

MATERIALS AND METHODS

Materials

The materials used were one-year-old Ki Aksara orchids derived from multiplication, and practical Murashige and Skoog (MS) medium. Other materials included sugar, agar, 2-iP hormone, myo-inositol, glycine, peptone, plant pre-

servative mixture, sodium hypochlorite, distilled water, betadine, sterile water, sterile tissue, methylated spirits, pH meter, matches, aluminium foil, rubber bands, plastic culture containers, plastic wrap, label paper, latex gloves, and alcohol at concentrations of 70 % and 96 %.

Methods

Explant Preparation

The medium was prepared in a 1000 mL measuring cup containing 500 mL of distilled water. This solution was further supplemented with 4.43 g L^{-1} MS medium, 0.1 mg L^{-1} myo-inositol, 2 mL L^{-1} glycine, 0.20 g L^{-1} peptone, 30 g L^{-1} granulated sugar, and 0.2 mL L^{-1} PPM. The growth regulator 2-iP was added according to the treatment levels, comprising 0 mg L^{-1} (P0), 0.05 mg L^{-1} (P1), 0.10 mg L^{-1} (P2), 0.15 mg L^{-1} (P3), 0.20 mg L^{-1} (P4), and 0.25 mg L^{-1} (P5). After mixing all components, the pH of the solution was measured and adjusted to 5.8. When the desired pH was achieved, 6 g L^{-1} of agar was added. The prepared solution was transferred into a pan and brought to a boil. Subsequently, the medium was dispensed into culture bottles, each containing 15–20 mL, based on the treatment. The culture bottles were sterilized using an autoclave at 121 °C and 17.5 psi for 30 minutes. After sterilization, the medium was stored on a rack in the culture room for 1 week to monitor for possible contamination.

Explant Inoculation

The culture bottle containing 1-year-old Ki Aksara orchids was sprayed with 70 % alcohol before being brought into a Laminar Air Flow (LAF) cabinet. A sufficient amount of sterile water was poured into an empty culture bottle, followed by the addition of 6–8 drops of betadine. A similar procedure was applied to the petri dish by pouring in sterile water and adding 3–5 drops of betadine. This was followed by homogenising the solution to ensure coverage of the entire surface of the petri dish was coated. Subsequently, Ki Aksara orchids were removed from the culture bottle, and explant was cut using sterilised forceps with a scalpel. The explant used was taken from the top of the shoot. Each culture bottle was planted with 1 explant. After planting, the bottle was closed again using plastic and sealed with a rubber band to ensure it was airtight. The planted culture bottle was removed from LAF and covered using aluminium foil and plastic, sealed with a rubber band. Furthermore, the mouth of the bottle was sealed with plastic wrap to ensure a tight closure. Each bottle was labelled with the treatment code, planting date, and medium name.

Incubation and Maintenance

To ensure optimal growth of Ki Aksara orchids, temperature, humidity, and lighting conditions were regulated in the incubation room. The temperature was maintained at 24–26 °C, relative humidity was kept between 60–70 %, and lighting was set at 1000–3000 lux using TL lamps or white LEDs, with a photoperiod of 16 hours of light and 8 hours of darkness. Observations were conducted once a week to monitor explant growth and confirm the absence of contamination in the culture medium.

Study Parameters

The parameters of plantlet growth were recorded from 1 week after planting (WAP) to 12 WAP. In this study, the parameters assessed were the number of shoots, leaves, and roots, including stem diameter, plant height, and leaf colour.

Data Analysis

Data were analysed using analysis of variance (ANOVA) based on Completely Randomized Design (CRD) with a single factor to evaluate the effect of each treatment level. When ANOVA showed a significant effect of treatment, further analysis was conducted using Least Significant Difference (LSD) test at a 95 % confidence level to determine the differences among treatments.

RESULTS AND DISCUSSION

Results

The results were described based on several parameters including the number of shoots, leaves, and roots, as well as stem diameter, plant height and leaf colour. Specifically, Figure 1 shows the values obtained in line with the analysis conducted on Ki Aksara orchids at 12 WAP.

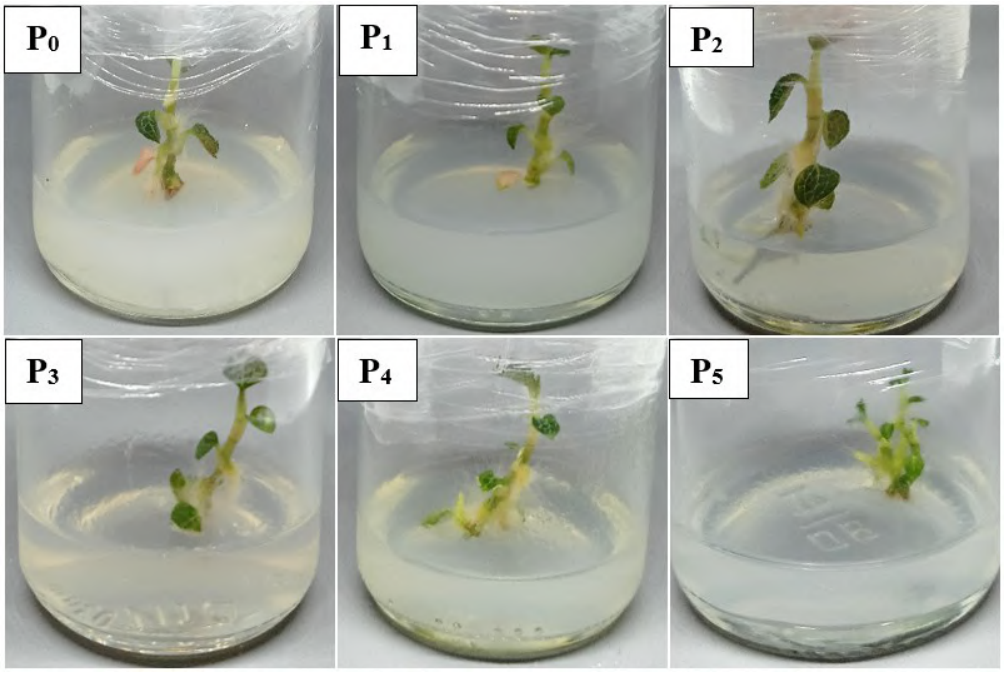

Figure 1. The growth of Ki Aksara orchids was observed at 12 weeks of age following the administration of 2-iP.

Number of Shoots

The observation results of the effect of 2-iP concentration on the number of shoots of Ki Aksara orchids at 12 WAP are shown in Figure 2.

Based on the results in Table 1, LSD concentration of 2-iP showed that the treatment had significant effect on the number of buds at 1 to 12 WAP. At 12 WAP, the highest average number of shoots (7.20) was found in the 0.25 mg L^{-1} treatment, consisting of lateral shoots.

Stem Diameter

LSD test results on the effect of 2-iP concentration on the stem diameter of Ki Aksara orchids are presented in Table 2. Based on the 12 WAP observation, the 2-iP treatment at 0.10 mg L^{-1} was significantly different from 0.05 mg L^{-1}, 0.15 mg L^{-1}, 0.20 mg L^{-1}, and 0.25 mg L^{-1}, but not significantly different from 0 mg L^{-1}. The highest average stem diameter of 0.29 cm was found in the 0.10 mg L^{-1}, while the lowest at 0.21 cm was observed in the 0.20 mg L^{-1} treatment.

Number of Leaves

LSD results on the concentration of 2-iP on the number of leaves are shown in Table 3. The 2-iP treatment showed significant differences in number of

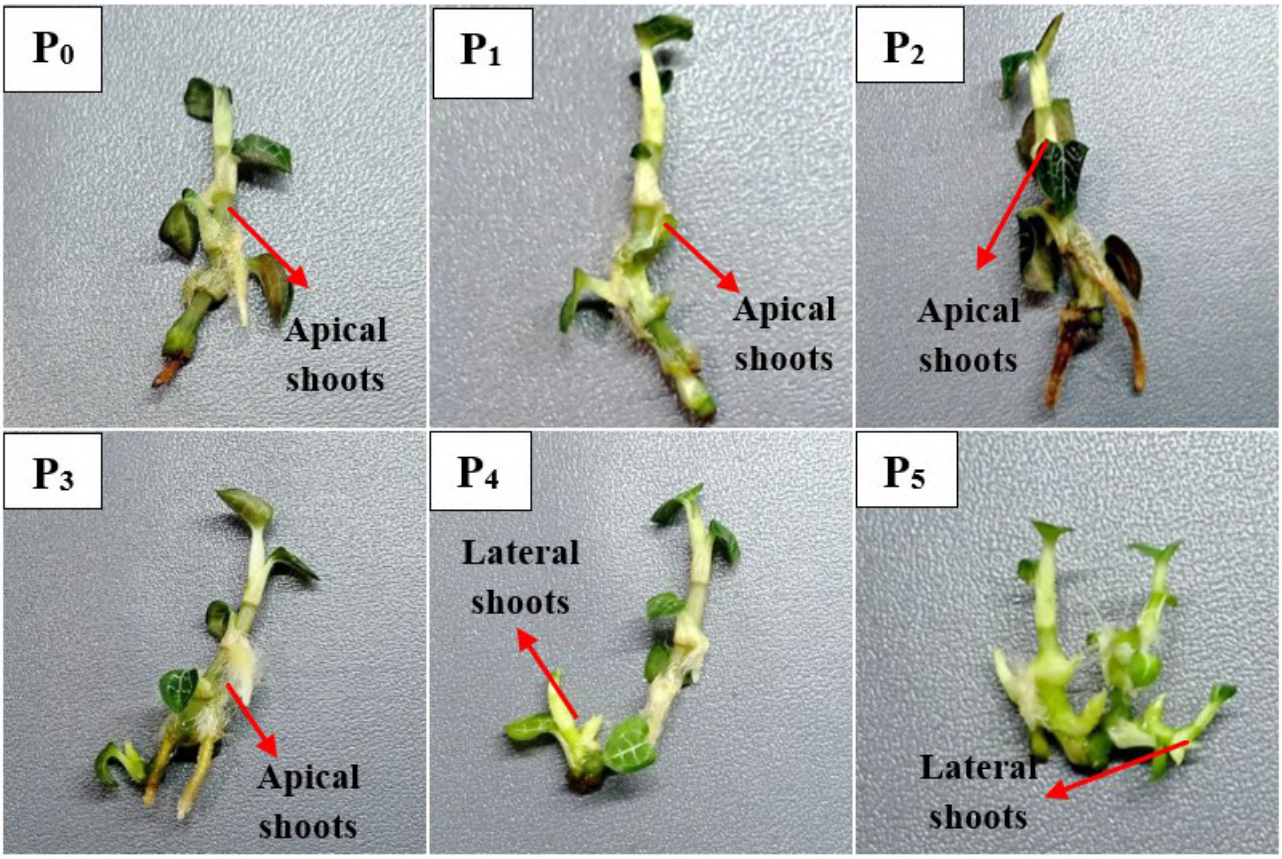

Figure 1. Number of Shoots of Ki Aksara Orchid Plants at 12 Weeks of Age Following the Application of 2-iP Concentration.

Table 1. The Effect of 2-iP Concentration on the Number of Shoots of Ki Aksara Orchid Plants.

	Number of Shoots				
Concentration	Week 1	Week 3	Week 6	Week 9	Week 12
0 mg L^{-1}	0.00 c	1.00 c	2.20 b	3.20 b	5.00 b
0.05 mg L^{-1}	0.80 ab	1.60 ab	2.80 b	3.80 b	4.80 b
0.10 mg L^{-1}	1.00 a	1.20 bc	2.60 b	3.80 b	5.20 b
0.15 mg L^{-1}	1.00 a	1.80 a	2.60 b	3.60 b	5.00 b
0.20 mg L^{-1}	1.00 a	1.80 a	2.40 b	3.60 b	5.20 b
0.25 mg L^{-1}	0.60 b	1.40 abc	3.60 a	5.00 a	7.20 a
LSD 5 %	0.37	0.58	0.67	0.69	0.96

Notes: Numbers followed by the same letter in the same column are not significantly different according to the 95 % LSD test.

leaves at 1 to 12 WAP. Observation at 12 WAP showed that 0.25 mg L^{-1} treatment was significantly different from 0.05 mg L^{-1}, 0.15 mg L^{-1}, and 0.20 mg L^{-1}, but there was no substantial variation between 0 mg L^{-1} and 0.10 mg L^{-1}. The highest average number of leaves (7.60) was found in the 0.25 mg L^{-1} treatment, while the lowest (5.80) was observed in the 0.20 mg L^{-1} treatment. The results showed that the use of 2-iP in the multiplication of Ki Aksara orchids could stimulate the formation of leaves. This was because the highest number of leaves that grew on lateral shoots.

Number of Roots

As shown in Table 4, the LSD results showed that 2-iP treatment significantly different affected the number of roots from 1 to 12 WAP. In comparison, a concentration of 0.10 mg L^{-1} was significantly different from 0.05 mg L^{-1} 12 WAP. However, there was no significant difference from the treatment of 0 mg L^{-1}, 0.15 mg L^{-1}, 0.20 mg L^{-1}, and 0.25 mg L^{-1}. The highest average for the

Table 2. The Effect of 2-iP Concentration on Stem Diameter of Ki Aksara Orchid Plants.

	Stem Diameter				
Concentration	Week 1	Week 3	Week 6	Week 9	Week 12
0 mg L^{-1}	0.10 a	0.15 ab	0.22 ab	0.24 a	0.28 ab
0.05 mg L^{-1}	0.10 a	0.14 ab	0.20 b	0.20 b	0.24 bc
0.10 mg L^{-1}	0.11 a	0.21 a	0.23 a	0.24 a	0.29 a
0.15 mg L^{-1}	0.10 a	0.13 b	0.21 ab	0.22 ab	0.22 c
0.20 mg L^{-1}	0.10 a	0.16 ab	0.21 ab	0.21 b	0.21 c
0.25 mg L^{-1}	0.10 a	0.16 ab	0.20 b	0.22 ab	0.22 c
LSD 5 %	0.00	0.07	0.00	0.00	0.04

Notes: Numbers followed by the same letter in the same column are not significantly different according to the 95 % LSD test.

Table 3. The Effect of 2-iP Concentration on the Number of Leaves of Ki Aksara Orchid Plants.

	Number of Roots				
Concentration	Week 1	Week 3	Week 6	Week 9	Week 12
0 mg L^{-1}	0.00 a	0.00 b	1.40 b	2.60 ab	4.00 ab
0.05 mg L^{-1}	0.00 a	0.20 ab	1.40 b	2.20 b	3.40 b
0.10 mg L^{-1}	0.20 a	0.60 a	2.20 a	3.00 a	4.40 a
0.15 mg L^{-1}	0.20 a	0.40 ab	1.80 ab	2.80 ab	3.80 ab
0.20 mg L^{-1}	0.00 a	0.40 ab	1.60 ab	2.60 ab	3.60 ab
0.25 mg L^{-1}	0.00 a	0.00 b	1.80 ab	2.60 ab	3.60 ab
LSD 5 %	0.33	0.55	0.65	0.71	0.98

Notes: Numbers followed by the same letter in the same column are not significantly different according to the 95 % LSD test.

number of roots at 4.40 was found in the 0.10 mg L^{-1}, while the lowest at 3.40 was observed in 0.05 mg L^{-1} treatment. This suggested that at high concentrations, 2-iP was more effective for cell division, shoots, and leaf development compared to roots growth.

Table 4. The Effect of 2-iP Concentration on the Number of Roots of Ki Aksara Orchid Plants.

	Number of Leaves				
Concentration	Week 1	Week 3	Week 6	Week 9	Week 12
0 mg L^{-1}	3.00 a	3.00 c	4.40 ab	5.60 abc	7.20 ab
0.05 mg L^{-1}	3.00 a	3.20 bc	4.40 ab	4.80 c	6.80 bc
0.10 mg L^{-1}	3.20 a	3.80 a	4.80 ab	6.00 ab	7.40 ab
0.15 mg L^{-1}	3.00 a	3.60 ab	4.80 ab	5.80 ab	6.40 cd
0.20 mg L^{-1}	3.00 a	3.20 bc	4.20 b	5.40 bc	5.80 d
0.25 mg L^{-1}	3.00 a	3.80 a	5.20 a	6.40 a	7.60 a
LSD 5 %	0.23	0.55	0.82	0.80	0.75

Plant Height

As presented in Table 5, LSD results showed that the treatment of 2-iP was significantly different on the height of Ki Aksara orchids at 1 to 12 WAP. At 12 WAP, the 2-iP treatments at 0 mg L^{-1}, 0.10 mg L^{-1}, and 0.15 mg L^{-1} were significantly different from 0.25 mg L^{-1}, but not significantly different from 0.05 mg L^{-1} and 0.20 mg L^{-1}. The highest average height of 3.50 cm was found in 0.10 mg L^{-1} treatment, while the lowest at 2.90 was observed in 0.25 mg L^{-1}.

Colour of Leaves

Leaf colour was observed at 12 WAP visually using the Munsell Colour Chart Ver 1.0.0 application by KSGc. Based on the observation results in Table 6, there were two categories: dark green and light green.

Table 5. The Effect of 2-iP Concentration on Ki Aksara Orchid Plant Height.

	Plant Height				
Concentration	Week 1	Week 3	Week 6	Week 9	Week 12
0 mg L^{-1}	1.45 a	1.67 ab	1.85 ab	2.24 a	3.45 a
0.05 mg L^{-1}	1.44 ab	1.52 b	1.75 b	2.03 a	3.33 ab
0.10 mg L^{-1}	1.69 a	1.85 a	2.13 a	2.32 a	3.50 a
0.15 mg L^{-1}	1.50 ab	1.67 ab	1.77 b	2.22 a	3.46 a
0.20 mg L^{-1}	1.53 ab	1.72 ab	2.04 ab	2.18 a	3.28 ab
0.25 mg L^{-1}	1.39 b	1.64 ab	1.86 ab	2.27 a	2.90 b
LSD 5 %	0.27	0.30	0.30	0.36	0.43

Notes: Numbers followed by the same letter in the same column are not significantly different according to the 95 % LSD test.

Table 6. The Effect of 2-iP Concentration on Colour of Leaves of Ki Aksara Orchid Plants.

Treatment	Munsell Colour	Figure
P_3 (2-iP 0.15 mg L^{-1})	Munsell Value: 7.5 GY 1/4	
P_0 (2-iP 0 mg L^{-1})	Munsell Value: 7.5 GY 2/4	
P_5 (2-iP 0.25 mg L^{-1})	Munsell Value: 7.5 GY 4/8	

Discussion

Cytokinin plays an essential role in plant development, including regulating the formation and proliferation of shoots as well as promoting cell division and elongation (Ashraf et al. 2014). A study conducted by Kadapatti and Murthy (2022) showed that 2-iP at an optimal concentration significantly enhanced the direct regeneration of adventitious shoots from explants without callus formation. This led to a high number of shoots, uniform growth, and good regeneration efficiency, suggesting that higher concentrations required more time for shoot formation. Murashige and Skoog (MS) medium contains high levels of micronutrients that support plant growth (Lawrie et al. 2021). MS medium provides complete micronutrients, supporting the physiological activity of 2-iP through synergy with auxin in regulating apical dominance and inducing organogenesis. Generally, the mechanism of cytokinin in cell division in shoots occurs through cooperation with auxin, stimulating cell division and influencing cell differentiation pathways. Cytokinin enters plant's shoot system through the roots by signalling axillary buds to initiate growth (Wiraatmaja 2017).

2-iP cytokinin shows a distinct molecular mechanism by binding to histidine kinase receptors located in the endoplasmic membrane, thereby activating a two-component phosphorylation system. The phosphate is transferred through AHP proteins to type-A response regulators (RRs), which stimulate the expression of genes regulating cell division and differentiation (Cárdenas-Aquino et al. 2023). This pathway is essential, allowing a more targeted hormonal response and minimizing side effects such as unwanted callus formation. Based on the analysis conducted, observations on stem diameter showed that lower concentrations led to optimal growth. The phenomenon was due to the role of 2-iP in increasing stem diameter, which is related to its function in stimulating cell division. According to Nurana (2017), 2-iP functioned to stimulate growth with high activity in promoting cell division in tissue culture. This showed that lower concentrations supported optimal growth due to the role of 2-iP, increasing the stem diameter through the ability to stimulate cell division.

Observations on number of leaves showed that the use of 2-iP in the propagation of *Macodes petola* orchids could stimulate the formation of leaves. This was because the highest number of leaves occurred from lateral shoots, indicating that 2-iP played two interrelated roles, namely cell division and chloroplast formation. The ongoing cell division process enlarges leaf surface area and causes chloroplasts to form and develop. According to Dewanto et al. (2019), formation of leaves in explants can be triggered by the availability of nitrogen (N) and potassium (K), acting as macronutrients in the culture medium. In in vitro propagation, photosynthesis is facilitated by artificial light. However, the activity is generally very low because the propagated plantlet is typically not yet autotrophic, showing the need for assistance by the presence of sugar (glucose) as an energy source. Similar results were also reported by Nurana et al. (2017), who applied 2 ppm 2-iP to *Dendrobium* Hybrid orchids, producing the highest number of leaves compared to other cytokinin growth regulators. The application of 2-iP as a plant growth regulator could influence the number and length of leaves.

The change in colour of leaves observed during the study was presumed to be associated with the physiological activity of the plant, which was influenced by the concentration of the applied hormone. Leaves showing a dark green colour indicated a high chlorophyll content. Similarly, Astuti et al. (2016) stated that the intensity of green coloration was directly proportional to chlorophyll accumulation. The high nitrogen content in MS medium also supported chlorophyll formation through the enhancement of endogenous cytokinin (Joni et al. 2014). The presence of 2-iP hormone can stimulate cell division and chloroplast formation, particularly in lateral leaves. The dark green colour indicates a high chlorophyll level in accordance with the hormonal mechanism and nitrogen presence in MS medium.

Auxin is generally produced in the shoots, stems, and roots (Nurana et al. 2017). In this study, explants used were shoot tips of *Macodes petola* orchids, showing the occurrence of root development in the area. The results showed that higher concentrations of auxin produced fewer roots. The auxin hormone present in the shoot was produced and transported from the apical meristem to the basal stem, roots, and young tissues. Root formation often occurs after the cultured explants form shoots, which stimulate development (Yatim 2016).

An increase in explant height indicates that growth and development are influenced by the availability of nutrients in the medium (Karyanti 2017). The nutrient content in MS medium is generally sufficient to influence the growth of explants. According to Isda and Fatonah (2014), the use of MS medium with the addition of the appropriate growth regulator can enhance explant growth. Growth regulators are non-nutrient organic compounds that,

when applied in low concentrations, can promote explant growth. However, when administered in high concentrations, there is a tendency to inhibit plant growth and development (Nurhanis et al. 2019).

The application of 2-iP at varying treatments can lead to changes in leaf colour. This is presumably due to the different physiological responses of the plant during development. Improper use of growth regulators can cause leaves to turn light green or even pale (Indriani et al. 2014). Chlorophyll levels are influenced by leaf pigments, where greener colour indicates higher chlorophyll content (Astuti et al. 2016). MS is an in vitro culture medium containing high nitrogen levels, which is capable of enhancing endogenous cytokinin (Joni et al. 2014). This endogenous cytokinin assists the explants in forming chlorophyll in leaves. The application of cytokinin at an optimum concentration can increase nitrogen content, which will be used as a building block for plant organs including roots, stems, and leaves.

CONCLUSIONS

In conclusion, the administration of 2-iP in in vitro culture medium significantly affects the growth of Ki Aksara orchids. The concentration of 0.10 mg L^{-1} is the most effective treatment in increasing the number of apical shoots, leaves, and roots, including stem diameter and plant height. The dark green colour of leaves with a Munsell value code of 7.5 GY 1/4 produced under this treatment, indicates a high chlorophyll content and optimal physiological condition.

AUTHOR CONTRIBUTION

A.W. collected and analysed data, and wrote the manuscript. E.S. and Y designed and supervised the entire process.

ACKNOWLEDGMENTS

The authors are grateful to Mrs. Ir. Hapsiati as the owner of CV Plant Tissue Culture Esha Flora for providing the opportunity to conduct the study.

CONFLICT OF INTEREST

The authors declare no conflict of interest.

REFERENCES

Ashraf, M.F. et al., 2014. Effect of cytokinin types, concentrations and their interactions on in vitro shoot regeneration of chlorophytum borivilianum sant. & fernandez. *Electronic Journal of Biotechnology*, 17(6), pp.275–279. doi: 10.1016/j.ejbt.2014.08.004.

Astuti, A.F., Hardjoko, D. & Rahayu, M. 2016. Kombinasi serat batang aren dan pasir merapi pada hidroponik substrat kailan. *Agrosains: Jurnal Penelitian Agronomi*, 18(2), pp.50-56. doi: 10.20961/agsjpa.v18i2.18692.

Cárdenas-Aquino, M.D.R. et. al., 2023. The Cytokinins BAP and 2-iP modulate different molecular mechanisms on shoot proliferation and Root Development in Lemongrass (*Cymbopogon citratus*). *Plants*, 12(20), 3637. doi: 10.3390/plants12203637.

Dewanto, H.A., Saraswati, D. & Hadjoeningtijas, O.D., 2019. Pertumbuhan Kultur Tunas Aksilar Kentang (*Solanum tuberosum* L.) dengan Penambahan Super Fosfat dan KNO3 Pada Media AB Mix Secara In Vitro. *Agritech*, 20(2), pp.71–81. doi: 10.30595/agritech.v20i2.3991.

Dewi, E.R.S., Ary, S.N. & Maria, U., 2018. Menuju Desa Konservasi Anggrek di Desa Ngesrep Balong, Limbangan Kendal. *Journal of Dedicators Community*, 2(2), pp.100-107. doi: 10.34001/jdc.v2i2.702.

Gunawan, G., 2016. *Pengaruh Zat Pengatur Tumbuh Tunas (BAP, IBA, GA3, Myoinositol Dan Mineral) dan Umur Kultur Terhadap Pertumbuhan Tanaman Macodes Petola Secara In Vitro*. Universitas Islam Negeri Sunan Gunung Djati Bandung.

Herliana, O., Harjoso, T. & Rokhminarsi, E., 2019. Pemberdayaan Mantan Buruh Migran Melalui Introduksi Budidaya Anggrek *Dendrobium* sp dengan Berbagai Jenis Media Tanam dan Aplikasi Pupuk Hayati Mikoriza di Kabupaten Banyumas. *Jurnal Panrita Abdi*, 3(1), pp.9-17. doi: 10.20956/pa.v3i1.3696.

Indriani, B.S., Suwarsi, E. & Pukan, K.K., 2014. *Efektivitas Substitusi Sitokinin dengan Air Kelapa pada Medium Multiplikasi Tunas Krisan (Chrysanthemum indicum L.) Secara In Vitro*. Universitas Negeri Semarang.

Isda, M.N. & Fatonah, S., 2014. Induksi Akar Pada Eksplan Tunas Anggrek *Grammatophylum scriptum* var. Citrinum Secara In Vitro Pada Media MS dengan Penambahan NAA dan BAP. *Al-Kauniyah Jurnal Biologi*, 7(2), pp.53–57. doi: 10.15408/kauniyah.v7i2.2715.

Joni, Y., Efendi, D. & Roostika, I., 2014. Morfogenesis Eksplan Keping Biji dari Tiga Klon Manggis (*Garcinia mangostana* L.) pada Tiga Jenis Media Dasar. *Horticultura*, 24(2), pp.94–101. doi: 10.21082/jhort.v24n2.2014.p94-101.

Kadapatti, S.S. & Murthy, H.N., 2022. Micropropagation of Andrographis producta through axillary and adventitious shoot regeneration. *Journal of Genetic Engineering and Biotechnology*, 20(1), 152. doi: 10.1186/s43141-022-00438-w.

Karyanti, K., 2017. Pengaruh Beberapa Jenis Sitokinin Pada Multiplikasi Tunas Anggrek Vanda Douglas Secara In Vitro. *Jurnal Bioteknologi & Biosains Indonesia (JBBI)*, 4(1), pp.36-43. doi: 10.29122/jbbi.v4i1.2200.

Lawrie, M. D. et al., 2021. In Vitro Germination and Flowering of Dendrobium capra J.J. Smith, An Endemic Orchid of Java. *HAYATI Journal of Biosciences*, 28(2), pp.172–172. doi: 10.4308/hjb.28.2.172.

Munggarani, M. et al., 2018. Multiplikasi Tunas Meriklon Kentang Pada Berbagai Jenis dan Konsentrasi Sitokinin. *Agrologia*, 7(2), pp.80-89. doi: 10.30598/a.v7i2.766

Nurana, A.R., Wijana, G. & Dwiyani, R., 2017. Pengaruh 2-iP dan NAA terhadap Pertumbuhan Plantlet Anggrek *Dendrobium Hibrida* pada Tahap Subkultur. *Agrotrop*, 7(2), pp.139–146. doi: 10.24843/AJoAS.2017.v07.i02.p05.

Nurhanis, S.E., Wulandari, R.S. & Suryantini, R., 2019. Korelasi Konsentrasi IAA dan BAP Terhadap Pertumbuhan Kultur Jaringan Sengon (*Paraserianthes falcataria*). *Jurnal Hutan Lestari*, 7(2), pp.857-867. doi: 10.26418/jhl.v7i2.34552.

Rosniawaty, S., Anjarsari, I.R D. & Sudirja. R., 2018. Aplikasi Sitokinin untuk Meningkatkan Pertumbuhan Tanaman Teh di Dataran Rendah. *Jurnal of Industrial and Beverage Crops*, 5(1), pp.31-38. doi: 10.21082/jtidp.v5n1.2018.p31-38.

Rugayah, K.S.Y. et al., 2017. *Tumbuhan langka Indonesia: 50 Jenis Tumbuhan Terancam Punah*. BRIN.

Santoso, I.B. et al., 2020. Teknologi Kultur Invitro Anggrek untuk Meningkatkan Keragaman Tanaman Di Agrowisata Serang. *Prosiding Seminar Nasional LPPM Unsoed*, 9, pp.294-303.

Tongkok, P., Prasart, K. & Kaewsuralikhit, C., 2018. Effect of n6-(2-*isopentenyl adenin*) (2iP) on The Grwoth of Tropical Seagrass Enhalus Acroides After Germination. *Journal of Fisheries and Environment*, 42(1), pp.16–23.

Widiastoety, D., 2014. Pengaruh Auksin dan Sitokinin Terhadap Pertumbuhan Planlet Anggrek Mokara. *Jurnal Hortilultura*, 24(3), pp.230-238. doi:10.21082/JHORT.V24N3.2014.P230-238

Wiraatmaja, I.W., 2017. *Bahan Ajar Zat pengatur tumbuh Giberelin dan Sitokinin*. Universitas Udayana.

Yatim, H., 2016. Multiplikasi Pisang Raja Bulu (*Musa paradisiaca* L. AAB GROUP) pada Beberapa Konsentrasi Benzyl Aminopurine (BAP) Secara In Vitro. *Jurnal Agroekoteknologi*, 4(3), pp.1989-1995. doi: 10.32734/ja.v4i3.2075.

Yuniardi, F., 2020. Aplikasi Dimmer Switch pada Rak Kultur Sebagai Pengatur Kebutuhan Intesitas Cahaya Optimum Bagi TanamanIn Vitro. *Indonesian Journal of Laboratory*, 1(4), pp.8–13. doi: 10.22146/ijl.v1i4.52991

Journal of Tropical Biodiversity and Biotechnology
Volume 10, Issue 04 (2025): jtbb17393
DOI: 10.22146/jtbb.17393

Research Article

Wings Above Wilderness: Diversity and Ecological Significance of Winged Vertebrates in Nusa Barung Island Wildlife Reserved, East Java, Indonesia

Tri Atmoko[1]*, Mukhlisi[1], Warsidi[3], Fajar Dwi Nur Aji[4], Oki Hidayat[1], Bina Swasta Sitepu[2], Toni Artaka[5], Andi Iskandar Zulkarnain[6], Bagus Suseno[4], Istiana Prihatini[7]

1)Research Center for Applied Zoology, National Research and Innovation Agency (BRIN), Jl. Raya Jakarta-Bogor Km. 46, Cibinong, Bogor 16911, West Java, Indonesia
2)Research Center for Ecology and Ethnobiology, National Research and Innovation Agency (BRIN), Jl. Raya Jakarta-Bogor Km. 46, Cibinong, Bogor 16911, West Java, Indonesia
3)Office for Social Forestry of Kutai Kartanegara, Ministry of Forestry, Jl. Soekarno-Hatta Km 38 Samboja 75271, Kalimantan Timur, Indonesia
4)Natural Resources Conservation Agency of East Java (BBKSDA Jawa Timur), Ministry of Forestry, Jl. Bandara Juanda Surabaya 61253, East Java, Indonesia
5)Bromo Tengger Semeru National Park Management Office, Ministry of Forestry, Jl. Raden Intan No. 6, Malang 65126, East Java, Indonesia
6)Yayasan Pakarti, Jl. Anggodo III No 51, Malang 65154, East Java, Indonesia
7)Research Center for Applied Botany, National Research and Innovation Agency (BRIN), Jl. Raya Jakarta-Bogor Km. 46, Cibinong, Bogor 16911, West Java, Indonesia
* Corresponding author, email: tri.atmoko@brin.go.id

Keywords:
Bat
Bird
Diversity
Ecological role
Feeding guilds
Nusa Barung
Submitted:
05 November 2024
Accepted:
27 April 2025
Published:
17 October 2025
Editors:
Ardaning Nuriliani
Annisaa Widyasari

ABSTRACT

Nusa Barung Island is a small conservation area at one of Indonesia borders in the Indian Ocean. There is limited data on biodiversity due to the accessibility and the freshwater sources availability. Data on bird species at this location is still limited; even bat data is completely absent. This study aims to identify the bird and bat species and their ecological roles. We conducted bird surveys using point count and sound recording methods and captured bats using mist and sweep nets. We found 389 individuals in 32 birds, with a diversity index (H') value ranging from 2.23 to 2.58. The *Pycnonotus plumosus*, *Chalcophaps indica*, and *Collocalia esculenta* recorded having wide distribution and high abundance. We identified 10 species from 141 captured bats, while *Pteropos vampyrus* colonies were directly observed. The H' index of bat species ranged from 0.46 to 0.78. The *Rousettus amplexicaudatus* were most captured. The ecological role of birds and bats includes trophic interactions in food webs and ecosystem services (insect control, seed dispersal, prey population controlling, and pollinator). The diversity of bird and bat species is relatively moderate and low, respectively, but their role in maintaining ecology is essential. The study included new records of all bats found and ten previously unreported bird species that are a basis for improving area protection.

How to cite:
Atmoko, T. et al., 2025. Wings Above Wilderness: Diversity and Ecological Significance of Winged Vertebrates in Nusa Barung Island Wildlife Reserved, East Java, Indonesia. *Journal of Tropical Biodiversity and Biotechnology*, 10(4), jtbb17393. doi: 10.22146/jtbb.17393

INTRODUCTION

Indonesia is an archipelagic country with thousands of islands stretching more than 140 thousand km along the equator (BPS Indonesia 2024). Nusa Barung Island, one of Indonesia outermost small islands, plays a strategic role in defending the country's outermost borders. On the other hand, this island is also an essential habitat for various wildlife species. The existence of wildlife has important values for human life, including ecology, economy, aesthetics, society, and culture, as well as for science (Atmoko 2022). Ecologically, wildlife helps keep the environment in balance by controlling tropic networks, pollinating plants (Franks & Farquhar 2024), spreading seeds (Chandru et al. 2020), controlling pests, monitoring ecosystem health, keeping soil fertility high, protecting habitats, and starting new life cycles. They are an important part of biodiversity (Doley & Barman 2023).

Wildlife plays an irreplaceable role in the ecosystem of isolated small islands such as Nusa Barung (also known as Nusa Barong). Winged vertebrates such as birds and bats are two taxa that play essential role in facilitating vegetation regeneration, maintaining plant population dynamics as pollinators and seed dispersers, and controlling insect populations (Enriquez & Rodriguez 2023; García et al. 2024). Bats that are active at night complement the role of birds during the day; both works alternately. Bats, as the only flying mammals, can utilize habitats inaccessibly compared to other species, such as caves and rock crevices, contributing additional ecological complexity to the ecosystem (Sakoui et al. 2020). Given the central role of birds and bats in energy and material cycles on islands, birds and bats are intriguing taxa to understand biodiversity patterns and ecological interactions.

According to the theory of island biogeography, small islands with limited populations tend to have high levels of endemism but they are also very vulnerable to extinction (Ratter 2018). The small and uninhabited island of Nusa Barung is located six kilometers off the mainland. Nusa Barung maintains limited ecosystem and population that receive little nor outside immigration to balance population dynamics. Isolated geographic small islands by waters with other islands around them are very vulnerable, likewise Nusa Barung Island. Ecological disturbances, such as climate change, invasion of alien species (Pringle et al. 2023), or habitat changes due to human activities, can increase threat to the survival of existing species (Banks-Leite et al. 2020). Small islands' limited resources and space require each species to adapt uniquely (Ciarle et al. 2024). Ecological specialisation, if disturbed, can lead to the collapse of the island ecosystem.

The isolated geographical characteristics of Nusa Barung Island provide ideal conditions for studying the island biogeography, biodiversity, species evolution, ecosystem dynamics, and the impact of geographic isolation on biodiversity. However, there are still limited publications related to its flora and fauna. There have only been two reported studies on the flora of Nusa Barung (Jacobs 1958; Partomihardjo & Ismail 2008) and one study on the fauna has focused on macro-moth taxa (Sutrisno 2007). The Natural Resources Conservation Agency (NRCA) East Java (BBKSDA Jawa Timur) conducted a bird survey in 2023, but the results remain unpublished. Uninhabited island, high seas, unpredictable weather, and a shortage of freshwater sources are limitations for staying longer on this island, which causes rare research on this island.

This is the first research concerning bat and bird species on Nusa Barung Island. This study examined and evaluated the diversity of bird and bat species, their ecological functions within the island, and their contributions to ecosystem services.

MATERIALS AND METHODS

Study area

The research was conducted over two weeks on Nusa Barung Island, which is administratively located in Puger Kulon Village, Puger District, Jember Regency, East Java, Indonesia (Figure 1).

The research site is a conservation area as a wildlife sanctuary managed by the NRCA East Java (BBKSDA Jawa Timur). This island, as part of the of outermost islands series in Indonesia, is located off the southern coast of Java Island. The area of the island is 79.6 km²; in general, the topography along the north coast is steeper than the south, with a maximum height of 280 meters above sea level (m a.s.l.) with an average height of 127 m a.s.l., while the coast in the southwest is gentler than other locations (https://earthexplorer.usgs.gov/). The primary habitat types found on the island are coastal forests, karst, mangroves, and inland forests (Partomihardjo & Ismail 2008).

Jeruk, Cambah, and Ceret Bay are the northern coasts of the island, with sloping to steep rocky topography. Coastal forests and lowland forests cover these areas in general. There are bat caves, rain-fed lakes in Pucung Prau, and bunkers from World War II in Jeruk Bay around. Cambah Bay is the starting point of the entrance route to Kedok Watu, and between them is a rain-fed lake in Sumber Gempol. Kedok Watu is the deepest terrestrial part of the island that the research can reach. It has mineral soil and karst conditions; lowland forest types and freshwater sources were found. Kandangan Bay is the only accessible southern part of the island, with cliffs almost along the southern coast. The area also encompasses Monyetan Bay and Endog-endogan, which feature coastal forest types, karst, and a small portion of a mangrove.

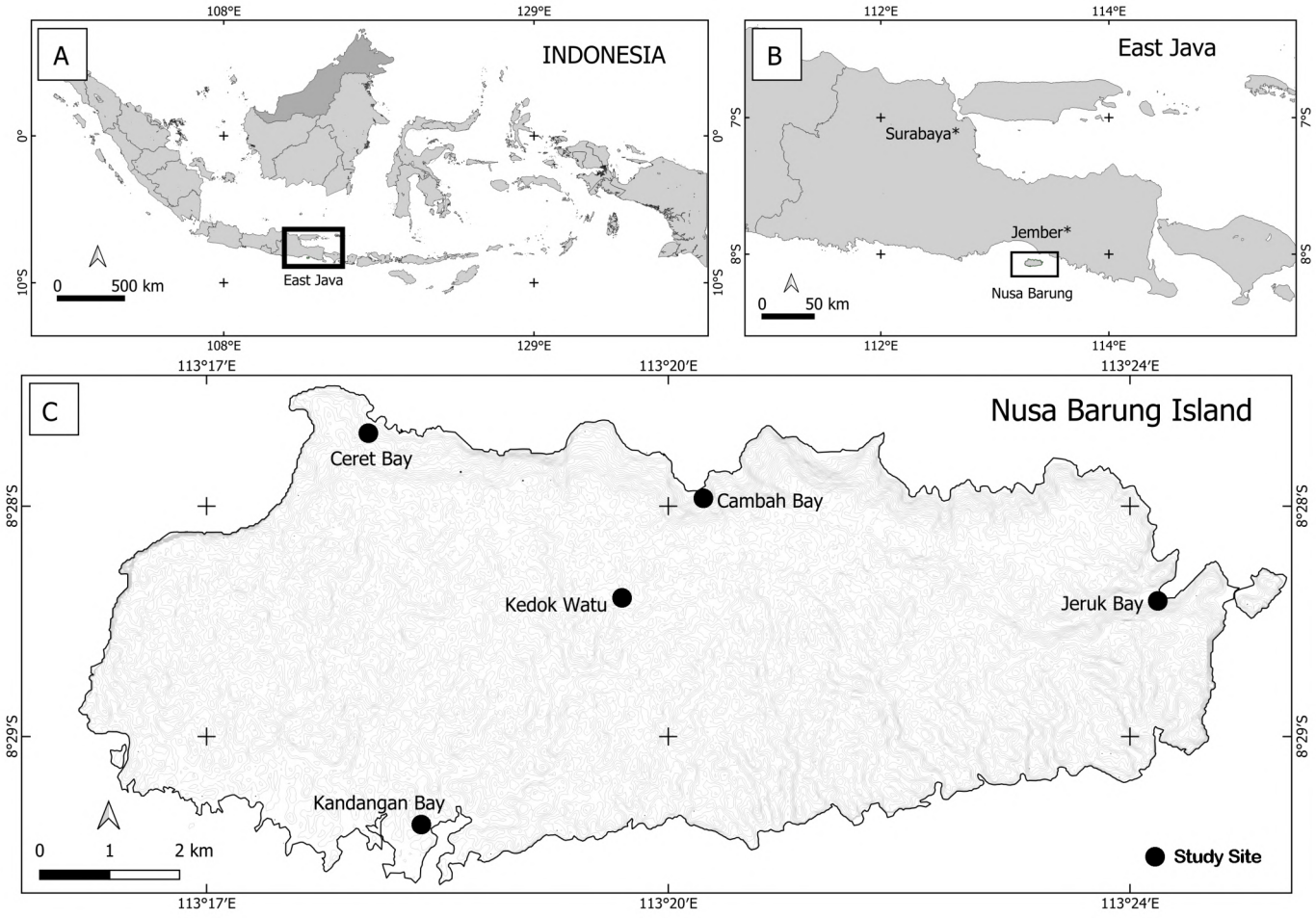

Figure 1. Maps of study site in Nusa Barung Island, East Java, Indonesia.

Data collection procedures

Birds detection

Bird observations used the point count method (Joel et al. 2024). In this method, observers walk at a constant speed along the transect and then stop every ± 200–300 m to record all species of birds observed for 15–20 minutes. We conducted diurnal bird observations in the morning at 06:30–09:00 and in the afternoon at 15:30–18:00. Bird observation locations are Kandangan Bay, Jeruk Bay, Cambah Bay, and Ceret Bay. The observation duration for each location is two days, except in Ceret Bay, which is only one day due to time constraints and weather conditions turning bad. We identified the bird species using a bird field guide (Eaton et al. 2021). The total number of bird observation points was 35. We also identify bird sounds by recording and analyzing them using the BirdNET v. 1.93 application on a smartphone.

Bats survey

The bat survey used the capture method with mist nets. We installed a total of 44 net nights in Kandangan Bay (16 net nights), Jeruk Bay (25 net nights), and Kedok Watu (3 net nights). Each set of 14 m long mist nets was stretched between two 3 m high aluminum poles placed at the border of the forest, targeting Megachiroptera and the forest alley for Microchiroptera. We installed the mist net approximately from 18:00 to 05:00. We also conducted surveys in the bat caves around Jeruk Bay using sweep nets. We conducted mist net inspections every hour at night to prevent bats from dying due to entanglement. We carefully released the captured bats from the nets and then placed them in calico bags to further identify their families based on general morphology such us leaf nosed, snout, tail, and ear. We determined the species level by measuring the forearm (FA), tail (T), wing length (W), and ear length (E) with calipers and weighing the animals with digital scales. Sex is identified based on the presence of more prominent nipples in females and the presence of a scrotum in males. We used Suyanto's (2001) guide for bat identification.

Data analysis

We used the Shannon index (H') to measure alpha diversity and Bray-Curtis dissimilarity for beta diversity. We also determined the evenness index (J) of bird and bat species to assess the relative abundances of species within a community. We used the open-access program PAST 4.03 (Hammer et al. 2001) for data analysis. An analysis of the ecological role of birds and bats is based on the literature (Green & Elmberg 2014; Sheherazade et al. 2017; Setianto et al. 2017; Taylor 2019; Kruskop et al. 2019; Duya et al. 2020; Chan et al. 2021; Martínez-Núñez 2021; Prakarsa et al. 2023; Mariyappan et al. 2023). We conducted a species diversity analysis on bat species caught in nets during the survey in Kandangan Bay, which represents the south, and Jeruk Bay, which represents the north. We directly observed bats caught using sweep nets in bat caves and bunkers but excluded those caught in Kedok Watu from the analysis because the data was insufficient.

RESULTS AND DISCUSSION

Bird diversity

The observation results from four different locations successfully identified a total of 32 bird species, with a total of 389 individuals. The number of species recorded at each observation site varied, ranging from 12 to 22 species. The results of the species diversity index (H') calculation showed moderate values that were not much different between locations, namely in the range of 2229 to 2576. Meanwhile, the species evenness index (J) showed that, in general, each observation location had moderate to high index values in the range of

0.541 to 0.774. At the study location, the distribution of individual birds within the community was uniform (Table 1).

Table 1. Bird species diversity and evenness index.

Parameters	Location			
	Kandangan Bay	Jeruk Bay	Cambah Bay	Ceret Bay
Number of individuals	92	115	149	33
Number of Species	20	22	16	12
Diversity Index (H')	2.576	2.476	2.350	2.229
Evenness Index (J)	0.657	0.541	0.657	0.774

Ceret Bay is the most distinct location, clustering separately with similarity level for around 0.45, indicating a significantly different bird composition (Figure 2). In contrast, Cambah Bay, Jeruk Bay, and Kandangan Bay form more similar group, with Jeruk Bay and Kandangan Bay showing the highest similarity (above 0.90), suggesting nearly identical bird assemblages. Cambah Bay is slightly similar but still closely related to this cluster (around 0.825 similarity). These patterns may be influenced by habitat characteristics, food availability, or other ecological factors that shape bird distributions. Additionally, the shorter bird observation period in Ceret Bay may have contributed to its distinct species composition.

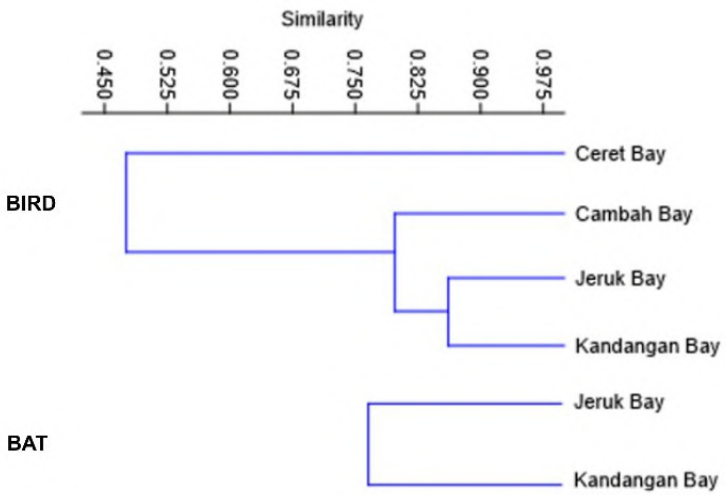

Figure 2. Beta diversity of birds and bats based on Bray-Curtis similarity.

Several bird species appeared to have wide distribution and high relative abundance values, such as olive-winged bulbul (*Pycnonotus plumosus)*, grey-capped emerald-dove *(Chalcophaps indica)*, and glossy swiftlet (*Collocalia esculenta)*. These species are always present in the top five bird species with the highest relative abundance at each location (Figure 3). The distribution of these birds tends to be wide and occupies the entire island habitat. They are species with the ability to adapt in various types of habitats. The adaptability of a species is very important to avoid extinction and to maintain its ecological role. However, several species are found only in certain locations, such as *Caprimulgus macrurus* in Kandangan Bay, *Hemiprocne longipennis* in Jeruk Bay, and *Accipiter trivirgatus* in Jeruk Bay.

A total of nine bird species in this study are protected species based on Indonesian Regulations (Table 2). One of these bird species is the Javan hawk-eagle, which is also categorised as endangered in the IUCN Red List and Appendix I in the CITES list. However, the majority of bird species are still in the least concern category. Of the five bird species that have been included in the CITES appendix list, all belong to the raptor group (eagle/falcon).

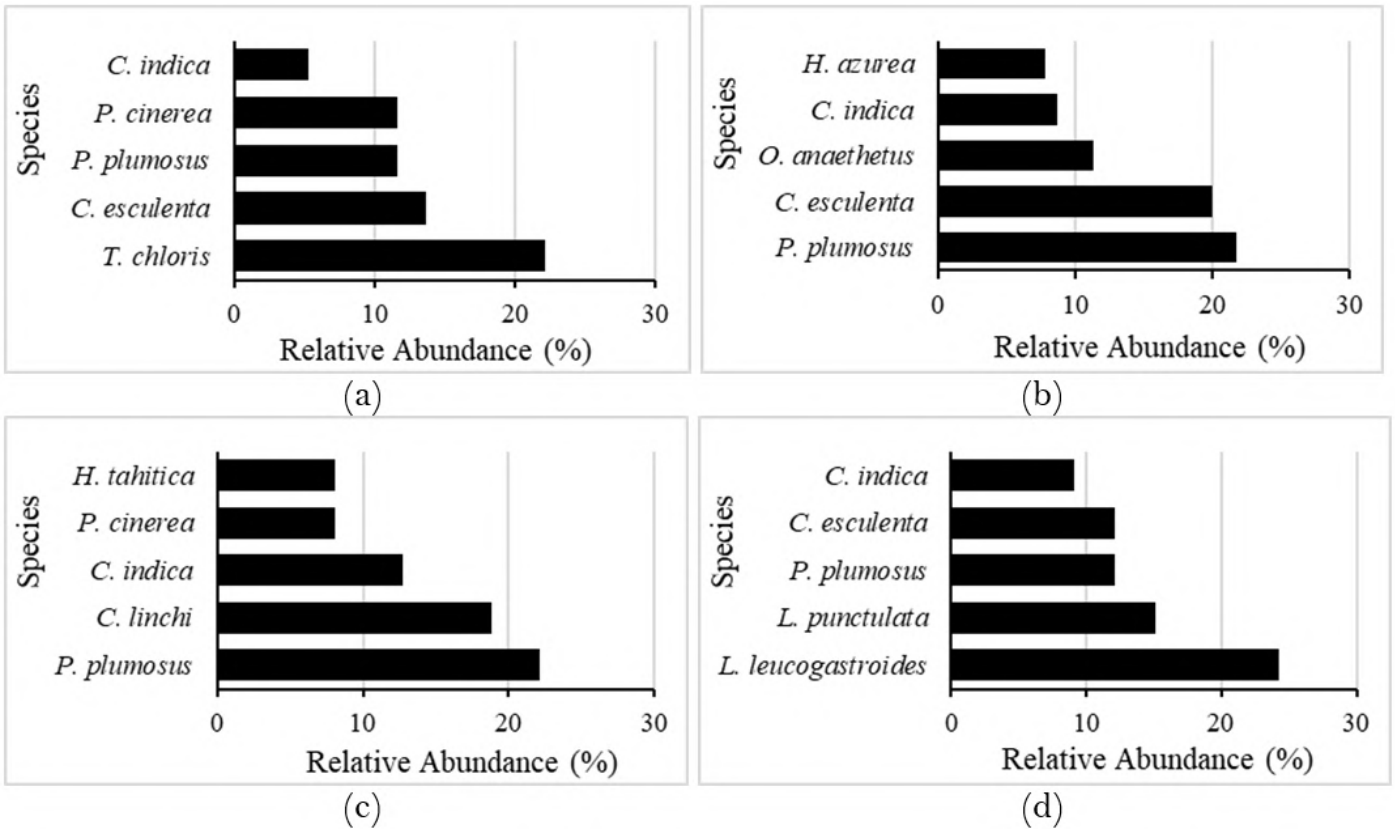

Figure 3. Top five bird species based on relative abundance (a) Kandangan Bay (b) Jeruk Bay (c) Cambah Bay (d) Ceret Bay.

All bird species recorded on Nusa Barung Island are the same as those found on the Java mainland. If we combine the richness of bird species in this study with previous surveys that recorded 53 bird species (BBKSDA Jawa Timur 2023), we found total of 67 species. We have added ten species to the list that were previously unreported. They are *Accipiter trivirgatus*, *Lalage nigra*, *Corvus enca*, *Cacomantis variolosus*, *Dicrurus leucophaeus*, *Hemiprocne longipennis*, *Onychoprion anaethetus*, *Pachycephala cinerea*, and *Gallus varius*. *Corvus enca* is an exception, as it is not a naturally occurring species but rather the result of a release (Pers. Comm. Wawan; area's staff manager). It's crucial to update the species that persist as the island's challenging terrain conditions have prevented exploration in all areas. However, the small-island effect phenomenon and biphasic species-area relationship (Chisholm et al. 2016) suggest that an increase in area does not always lead to a proportional increase in the number of species.

The total number of bird species on Nusa Barung Island is currently equivalent to 12.96 % of all bird species recorded in Java-Bali, which is 517 species (Burung Indonesia 2024). Several study sites on the islands in the Indian Ocean south of Java Island have reported a variety of bird species richness, including 66 species on Sempu Island (Sukistyanawati et al. 2016), 148 species on Nusa Kambangan Island (Suripto & Hamidy 2006), and 149 species on Christmas Island (James & McAllan 2014). Although karst forest types dominate both islands, their sizes and levels of habitat heterogeneity naturally differ. Nusa Barung Island, together with Sempu Island, is the smallest island among the others, so habitat variation is more limited. In addition, on Nusa Barung Island, the presence of freshwater as one of wildlife's basic needs is minimal, which impacts the carrying capacity of wildlife habitats (Grebner et al. 2022).

The shrubby magpie (*Pycnonotus plumosus*) has a wide distribution and abundant population. This species is known to adapt well from coastal areas to the island's interior. In various other locations, this species is also known

Table 2. List of birds, conservation status, and its distribution in Nusa Barung Island.

No	Family	Species	Protected status and conservation category			Feeding guild	Distribution
			Protected status	IUCN Red List	CITES		
1	Accipitridae	*Haliaeetus leucogaster*	√	LC	App.II	Car	a b d c
2	Accipitridae	*Spilornis cheela*	√	LC	App.II	Car	b c
3	Accipitridae	*Nisaetus bartelsi*	√	EN	App.I	Car	b d
4	Accipitridae	*Accipiter trivirgatus*	√	LC	App.II	Car	b
5	Alcedinidae	*Todiramphus chloris*	-	LC	-	IP	a b c d
6	Alcedinidae	*Ceyx rudiforsa*	-	LC	-	IP	a b c
7	Apodidae	*Collocalia esculenta*	-	LC	-	Ins	a b c d
8	Apodidae	*Collocalia linchi*	-	LC	-	Ins	a b
9	Ardeidae	*Egretta sacra*	-	LC	-	IP	a b d
10	Artamidae	*Artamus leucorynchus*	-	LC	-	Ins	a
11	Campephagidae	*Lalage nigra*	-	LC	-	Ins	a
12	Caprimulgidae	*Caprimulgus macrurus*	-	LC	-	Ins	a
13	Columbidae	*Spilopelia chinensis*	-	LC	-	Gran	a
14	Columbidae	*Chalcophaps indica*	-	LC	-	Frug	a b c d
15	Corvidae	*Corvus enca*	-	LC	-	FI	b
16	Cuculidae	*Cacomantis variolosus*	-	LC	-	Ins	b c
17	Dicruridae	*Dicrurus leucophaeus*	-	LC	-	Ins	b c
18	Estrildidae	*Lonchura leucogastroides*	-	LC	-	Gran	d
19	Estrildidae	*Lonchura punctulata*	-	LC	-	Gran	d
20	Falconidae	*Falco peregrinus*	√	LC	App.I	Car	b c
21	Hemiprocnidae	*Hemiprocne longipennis*	-	LC	-	Ins	b
22	Hirundinidae	*Hirundo tahitica*	-	LC	-	Ins	a c
23	Laridae	*Onychoprion anaethetus*	√	LC	-	IP	a b
24	Laridae	*Sterna sumatrana*	√	LC	-	IP	a b
25	Monarchidae	*Hypothymis azurea*	-	LC	-	Ins	a b c d
26	Nectariniidae	*Cinnyris jugularis*	-	LC	-	NI	a c d
27	Pachycephalidae	*Pachycephala cinerea*	-	LC	-	Ins	a b c d
28	Phasianidae	*Gallus gallus*	-	LC	-	Om	a b
29	Phasianidae	*Gallus varius*	-	LC	-	Om	c
30	Pycnonotidae	*Pycnonotus goiavier*	-	LC	-	FI	a c
31	Pycnonotidae	*Pycnonotus plumosus*	-	LC	-	FI	a b c d
32	Rhipiduridae	*Rhipidura javanica*	-	LC	-	Ins	b

Notes: a. Kandangan Bay; b = Jeruk Bay; c = Cambah Bay; d = Ceret Bay; Car = carnivore; IP = insectivore/carnivore); Ins = insectivore; Gran = granivore; Frug = frugivore; FI = frugivore/insectivore; NI = nectarivore/insectivore; Om = omnivore.

as an adaptive species (Suripto & Hamidy 2006) and is considered a non-forest-dependent species (Tang et al. 2015). Meanwhile, the high abundance and wide distribution of barn swifts (*Collocalia esculenta*) on Nusa Barung Island are a natural phenomenon, primarily due to the island's karst dominance, where numerous caves serve as the primary habitat for swiftlets. Nusa Kambangan and Christmas Islands also record abundant populations of this species, classifying it as an adaptive bird species (Suripto & Hamidy 2006; James & McAllan 2014).

Bats diversity

Nets and sweep nets caught a total of 141 individual bats during the survey, representing 10 species from five families (Table 3). At dusk, we observed a colony of large flying foxes (*Pteropus vampyrus*) flying around Kandangan Bay. The five bat species found in the bat caves around Jeruk Bay are Dusky leaf-nosed bat (*Hipposideros ater*), Lesser-wooly horseshoe bat (*Rhinolophus sedulus*), Creagh's horseshoe bat (*Rhinolophus creaghi*), Diadem leaf-nosed bat (*Hipposideros diaderma*), and Javan pipistrelle (*Pipistellus javanicus*). Kedok Wa-

Table 3. Species and conservation status of bats in Nusa Barung Island.

No	Family	Species	English Name	Red List IUCN	CITES	Distri-butions
1	Hipposideridae	*Hipposideros ater*	Dusky leaf-nosed bat	LC	no CITES	d
2	Hipposideridae	*Hipposideros diadema*	Diadem leaf-nosed bat	LC	no CITES	d
3	Megadermatidae	*Megaderma spasma*	Lesser false vampire	LC	no CITES	a, e
4	Pteropodidae	*Cynopterus brachyotis*	Lesser dog-faced fruit bat	LC	no CITES	a, b
5	Pteropodidae	*Cynopterus horsfieldi*	Horsfield's fruit bat	LC	no CITES	a, c
6	Pteropodidae	*Pteropus vampyrus*	Large flying-fox	EN	App. II	a
7	Pteropodidae	*Rousettus amplexicaudatus*	Geoffroy's rousette	LC	no CITES	a
8	Rhinolophidae	*Rhinolophus creaghi*	Creagh's horseshoe bat	LC	no CITES	d
9	Rhinolophidae	*Rhinolophus sedulus*	Lesser-wooly horseshoe bat	NT	no CITES	d
10	Vespertilionidae	*Philetor brachypterus*	Short-winged pipistrelle	LC	no CITES	c
11	Vespertilionidae	*Pipistrellus javanicus*	Javan pipistrelle	LC	no CITES	d

Notes: a = Kandangan Bay, b = Jeruk Bay, c = Kedok Watu, d = Goa Kelelawar, e = Bunker.

tu, a forest area in the central part of Nusa Barung Island, is home for two species of bats: the short-winged pipistrelle (*Philetor brachypterus*) and the Horsfield's fruit bat (*Cynopterus horsfieldi*). We only caught the lesser false vampire (*Megaderma spasma*) in the net twice, in Kandangan Bay and Jeruk Bay. However, its presence is hundreds in the bat cave and Japanese bunker around Jeruk Bay.

The diversity of bat species in the southern area (Kandangan Bay) is 0.46, lower than in the northern part (Jeruk Bay), which is 0.78. The species of bats in Jeruk Bay are more evenly distributed than in Kandangan Bay, with Evenness Index (J) values of 0.433 and 0.335, respectively. Meanwhile, the community similarity between the two locations is 75 % (Figure 2).

The discovery of all bat species marks a new record for Nusa Barung Island. Most of them are unprotected. The large flying fox (*Pteropus vampyrus*) is the only endangered species and is included in CITES Appendix II. Other species are included in Least Concern, except the lesser-wooly horseshoe bat (*Rhinolophus sedulus*), which is listed in Near Threatened.

Males dominated the sex composition of bats caught in nets, accounting for 66 %. Specifically, for the *R. amplexicaudatus* species, which is the most frequently caught in nets, the number of females was only 34 % of the 123 individuals caught.

Bat morphological measurements are one of the bases for identification. However, these sizes often vary for the same species in different habitat locations. Furthermore, the maturity status of individual bats also influences their size. In addition to other characteristics, such as the presence of a tail, claws on the second digit, tragus, and body weight, the forearm serves as a useful reference for identification (Table 4). The diadem leaf-nosed bat (*Hipposideros diadema*) was the largest of the species captured (FA: 8.5–9.6 cm), while the large flying bat (*Pteropus vampyrus*) was the largest bat observed. The length of the forearm of the bats found in the study area shows that it is relatively within the size range of bats in general, except for the *R. amplexicaudatus*, which has a smaller forearm with an average of 63 mm, while the general size range is 77-87 mm (Suyanto 2021).

The karst ecosystem on Nusa Barung Island has many caves that are the best habitat for bats. The creagh's horseshoe bat (*Rhinolophus creaghi*) is a species that relies on the karst area for its habitat (Suyanto & Struebig 2007). However, due to limited time, the researchers have only explored one cave, the Goa Kelelawar in Jeruk Bay, and even then, they only caught several spe-

Table 4. Mophometric of bats in Nusa Barung Island.

Species	N	Fore Arm $\bar{x}$ (Range) (mm)	Weight $\bar{x}$ (Range) (g)	Tail $\bar{x}$ (Range) (mm)	Ears $\bar{x}$ (Range) (mm)	Wings $\bar{x}$ (Range) (mm)
*Rousettus amplexicaudatus**	123	63 (50-74)	27.7 (16.0-57.0)	1.4 (0.7-2.0)	1.4 (1.1-1.9)	37.2 (305-470)
*Cynopterus horsfieldi**	7	71 (61-81)	49.4 (31.3-75.0)	1.2 (0.7-1.8)	1.7 (1.4-1.9)	440 (370-520)
*Cynopterus brachyotis**	6	59 (54-64)	27.9 (22.6-33.7)	1.0 (0.8-1.5)	1.4 (1.2-1.5)	363 (320-400)
*Hipposideros diadema**/**	2	88 (85-96)	44.0 (41.4-46.5)	4.7 (4.2-5.3)	2.4 (1.9-3.0)	510 (480-540)
*Megaderma spasma**	2	57 (55-59)	18.0 (18.0)	-	3.8 (3.7-3.8)	430 (390-470)
*Hipposideros ater***	1	37.9	46.0	2.4	1.7	220
*Rhinolophus creaghi***	1	52.8	10.8	1.7	2.2	280
*Rhinolophus sedulous***	1	41.6	57.0	2.1	2.2	250
*Philetor brachypterus**	1	28.6	53.0	2.8	0.8	220
*Pipistrellus javanicus***	1	35.4	36.0	3.5	0.6	243

Note: * Mistnet captured, **Captured in the cave

cies of bats for identification. There was a thick layer of guano on the cave floor and there were several piles of bags containing it at the mouth of the cave. According to Wawan (Pers. Comm.), the area's staff manager, there was an attempted guano theft at that location, but the forest ranger successfully prevented it. In addition, there are at least two Japanese heritage bankers from World War II between Jeruk Bay and Ketimo Beach, also inhabited by dozens of lesser false-vampires *(Megaderma spasma)*. Generally, these bats roost in caves, tunnels, and wooden holes and live in abandoned buildings around the garden (de Mel et al. 2024).

Ecological roles

The ecological role of birds and bats includes two roles, namely trophic interactions in their involvement in food webs and ecosystem services such as pest/insect control, seed dispersal, controlling the population of prey, and pollinator. Specifically, Table 5 groups the role of birds at the tropic level into eight feeding guilds, encompassing 32 identified species. Table 6 presents the general functions of each species of bat.

Insectivorous birds have an essential ecological role in controlling insect populations in karst ecosystems. Karst ecosystems with many rock crevices and caves have provided ideal microhabitats for various insects. Insects, together with arachnids, are the most dominant taxa in various karst ecosystems worldwide (Culver & Pipan 2019). Groups of granivores, frugivores, and other generalist birds help the plant regeneration process on Nusa Barung Island. Columbidae and Pycnonotidae are bird families that play an essential role in seed dispersal in the forest (Corlett 2017). Some bird species, such as *Chalcophaps indica* and *Pycnonotus plumosus*, are also highly abundant. Both bird species prefer fruit and seeds, but *C. indica* is known to be rather terrestrial. They often pick up fruit that falls on the forest floor. Its presence on Nusa Barung Island is more recognizable by its sound than by direct sight.

Raptor species, such as eagle/falcon and pollinator birds, are keystone species that need more attention. Interestingly, Nusa Barung Island is a habitat for at least five species of raptors. The Javan hawk-eagle (*Nisaetus bartelsi*), an endangered species, is among them. Raptors are top predators and excellent indicators of the health status of the ecosystem. In this study, *Cinnyris jugularis* stands out as the sole pollinator bird. Usually, groups of nectarivore

Table 5. Ecological roles of bird in Nusa Barung Island.

No	Feeding Guild	Percentage (%)	Mainly Ecological Services	References
1	Insectivore	35.48	Controlling population of insects	Martínez-Núñez 2021; Mariyappan et al. 2023
2	Carnivore	16.13	Balancing ecosystem; controlling population of prey, scavenger	Mariyappan et al. 2023
3	Insectivore-Piscivore	16.13	Controlling population of insect and fish, nutrient cycling	Green & Elmberg 2014
4	Frugivore-Insectivore	9.69	Seed dispersal; controlling population of insects	Mariyappan et al. 2023
5	Granivore	9.68	Seed dispersal	Mariyappan et al. 2023
6	Omnivore	6.45	Prey for predator, controlling population of insect in forest floor	Setianto et al. 2017
7	Frugivore	3.23	Seed dispersal	Mariyappan et al. 2023
8	Nectarivore-Insectivore	3.23	Pollinator	Mariyappan et al. 2023

Table 6. Ecological roles of bats on the habitat in Nusa Barung.

No	Species	Mainly Ecological Services	Feeding Guilds	References
1	*Hipposideros ater*	Pest control	Insectivore	Prakarsa et al. 2023
2	*Hipposideros diadema*	Pest control	Insectivore	Prakarsa et al. 2023
3	*Megaderma spasma*	Pest control	Insectivore	Prakash et al. 2021
4	*Cynopterus brachyotis*	Seed dispersal, pollinators	Frugivore	Chan et al. 2021
5	*Cynopterus horsfieldi*	Seed dispersal, pollinators	Frugivore, Nectarivore	Chan et al. 2021
6	*Pteropus vampyrus*	Seed dispersal, pollinators	Frugivore, nectarivore	Duya et al. 2020
7	*Rousettus amplexicaudatus*	Seed Dispersers, pollinators	Frugivore	Sheherazade et al. 2017
8	*Rhinolophus creaghi*	Pest control	Insectivore	Taylor 2019
9	*Rhinolophus sedulus*	Pest control	Insectivore	Taylor 2019
10	*Philetor brachypterus*	Pest control	Insectivore	Taylor 2019
11	*Pipistrellus javanicus*	Pest control	Insectivore	Kruskop et al. 2019

birds like to visit flowers that are brightly coloured, do not have a striking odor, and have abundant nectar (Cronk & Ojeda 2008).

Since bats are the only mammals that can fly, they can search further for food. This makes them an important component at various trophic levels, influencing the population dynamics of species (Förster et al. 2019). Several species of bats that fly long distances can visit small islands, contributing to the transfer of energy and matter between ecosystems (Valido & Olesen 2023).

The study discovered at least four frugivorous and nectarivorous bats, which play crucial role in seed dispersal and pollination, particularly for plants that flower at night in locations that are challenging for other pollinators to access. Several tree species in the tropics depend highly on bats as the primary agents of their seed dispersal (Chan et al. 2021). Frugivorous bats play essential role in the dispersal of pioneer plant seeds on small islands, making them critical players in forest regeneration dynamics (Valido & Olesen 2023). Nectarivorous bats, especially from the Pteropodidae family, play role in pollinating various species of trees in tropical areas across islands (Fleming et al. 2009) that helps maintain plants' genetic diversity by spreading pollen between isolated islands.

Insectivorous bats, as biological agents, play an essential role in maintaining ecosystem balance by controlling the explosion of insect populations that have the potential to become pests for plants in tropical ecosystems (Prakash et al. 2021). Most of these species are very efficient at catching insects. Extrapolation results from the *Tadarida brasiliensis* colony in Texas, United States, showed that up to 20 million colonies can prey on more than 600 thousand tons of insects annually (Suyanto 2001). In addition, with their

ability to migrate long distances, even between islands, bats can play role in controlling the population of insect pests that often have no natural predators in small island ecosystems (Prakash et al. 2021). Some of the insect species have the potential to spread diseases, such as malaria or other zoonotic diseases.

Bats act as a link between habitats on and off the island. The long-distance movement of bats makes them important agents in connecting geographically isolated habitats or between fragmented habitats. The ability of bats to travel long distances allows them to function as essential vectors in the transfer of genetic material, nutrients, and energy between small and isolated islands (Moulistanos et al. 2023; Valido & Olesen 2023; Ciarle et al. 2024). Genetic exchange between isolated bat populations prevents genetic isolation, which has the potential to reduce genetic diversity. Bats that move long distances will bring new genes to isolated populations, helping to increase genetic diversity, which is essential for adaptation to environmental changes (Moulistanos et al. 2023).

CONCLUSIONS

Winged vertebrates, such as birds and bats, can support ecosystem resilience on the Nusa Barung Island, which play essential roles in various ecological functions. Although the diversity of bird is moderate and bat species is relatively low, their role in maintaining ecology is essential. These roles potentially support plant regeneration and biodiversity, which are essential for maintaining ecosystem stability in the face of environmental disturbances. Bats and birds have similar ecological roles, synergizing at different times, day and night. All the bat species found in this study area are new records; ten bird species have also made their first record. Future research on bat species on this island still has potential; we have only explored one of the many caves, and the biodiversity of the land forest still holds mysteries that we have yet to unravel. Protecting the island from external disturbances and various human activities, such as bird hunting and guano harvesting, must be an important concern. The results of this study strengthen the species diversity database of Nusa Barung Island to improve the status of the area and its protection as the country's outermost border island—the border of state sovereignty.

AUTHOR CONTRIBUTION

T.A. planned and developed study design, collected data, wrote the manuscript, supervised the study, and funding recipients; M developed study design, collected data, and wrote the manuscript; W collected data, did mapping, and wrote the manuscript; F.D.N.A., O.H., T.A.R., A.I.Z., B.S.S., B.S. collected data, wrote and edited the manuscript; I.P. supervised the study, edited, and proofread the manuscript.

ETHICS CLEARANCE APPROVAL

Ethics clearance approved by Ethics Commission for Animal Care and Use, BRIN (No: 008/KE.02/SK/01/2024). The research permit has been approved by the Ministry of Environment and Forestry, Republic of Indonesia (No: SI.889/K.2/BIDTEK.1/KSA/5/2024).

ACKNOWLEDGMENTS

Thanks to Mr. Nur Patria Kurniawan as Head of BBKSDA Jawa Timur for his support and research permit. Thanks to Wawan, Chandra, Aryanti, Suryadi, Abdi Purmono, Khosim, and Jamil who have helped and supported during data collection in the field. This work was supported by the RIIM (Riset dan Inovasi untuk Indonesia Maju) project with LPDP funding (SK

No. 37/II.7/HK/2023).

CONFLICT OF INTEREST

The authors have declared no conflict of interest.

REFERENCES

Atmoko, T., 2022. Kekayaan jenis satwa liar di zoogeografi wilayah Indonesia. In *Mengenal lebih dekat satwa langka Indonesia dan memahami pelestariannya* (pp. 1–9). Jakarta: BRIN Press. doi:10.55981/brin.602.c614

Banks-Leite, C., et al., 2020. Countering the effects of habitat loss, fragmentation, and degradation through habitat restoration. *One Earth*, 3, pp.672–676. doi:10.1016/j.oneear.2020.11.016

BBKSDA Jawa Timur, 2023. *Laporan pelaksanaan kegiatan inventarisasi dan verifikasi keanekaragaman hayati di SM Pulau Nusa Barong tahun 2023*. (Unpublished Report). Jember: BBKSDA Jawa Timur.

Burung Indonesia, 2024. Status burung di Indonesia 2024. https://www.burung.org/peta-interaktif-status-burung-di-indonesia-2024/

Chisholm, R.A. et al., 2016. Maintenance of biodiversity on islands. *Proceedings Biological sciences*, 283(1829), 20160102. doi: 10.1098/rspb.2016.0102.

Corlett, R.T., 2017. Frugivory and seed dispersal by vertebrates in tropical and subtropical Asia: An update. *Global Ecology and Conservation*, 11, pp.1-22. doi: 10.1016/j.gecco.2017.04.007

Cronk, Q. & Ojeda, I., 2008. Bird-pollinated flowers in an evolutionary and molecular context. *Journal of Experimental Botany*, 59(4), pp.715–727. doi: 10.1093/jxb/ern009

Culver, D.C. & Pipan, T., 2019. *The Biology of Caves and Other Subterranean Habitats*, UK: Oxford Academic.

BPS Indonesia, 2024, 'Statistical Yearbook of Indonesia 2024', in *BPS-STATISTICS INDONESIA*, viewed from https://www.bps.go.id/en/publication/2024/02/28/c1bacde03256343b2bf769b0/statistical-yearbook-of-indonesia-2024.html

Chan, A.A.Q. et al., 2021. Diet, ecological role and potential ecosystem services of the fruit bat, *Cynopterus brachyotis*, in a tropical city. *Urban Ecosystems*, 24, pp.251–263. doi: 10.1007/s11252-020-01034-x

Chandru, G. et al., 2020. Seed dispersal by ungulates in the point calimere wildlife sanctuary: A scientific and perspective analysis. *Saudi Journal of Biological Sciences*, 27(10), pp.2790–2797. doi: 10.1016/j.sjbs.2020.06.042

Ciarle, R., Burns, K.C., & Mologni, F, 2024. The loss (and gain) of defensive adaptations in island plants and animals: A comparative review. In *Ecology and Evolution of Plant-Herbivore Interactions on Islands*. Springer, pp.69–93. doi: 10.1007/978-3-031-47814-7_5

de Mel, R.K., Ranasinghe, T. & Weerakoon, D.K., 2024. Use of anthropogenic structures by bats in rubber plantations: A preliminary survey from Sri Lanka. *Ceylon Journal of Science*, 53(3), pp.399-404. doi: 10.4038/cjs.v53i3.8365

Doley, D.M. & Barman, P., 2023. Importance of communicating biodiversity for sustainable wildlife management: a review. *Journal of Environmental Studies and Sciences*, 13(2), pp.321–329. doi: 10.1007/s13412-023-00819-8

Duya, M.R.M. et al., 2020. Fruit bat assemblage in different lowland forest types in the Northern Sierra Madre Mountains, Philippines. *Acta Chiropterologica*, 22(1), pp.95–112. doi: 10.3161/15081109ACC2020.22.1.009

Eaton, J.A. et al., 2021. *Birds of the Indonesian Archipelago, Greater Sundas, and Wallacea*, Barcelona: Lynx Edicions.

Enriquez, G.P.L. & Rodriguez, L.J.V., 2023. Seed dispersal by water, wind, birds, and bats in the Caliraya Watershed, Laguna. *Proceedings of the National Institute of Ecology of the Republic of Korea*, 4(1), pp.28–42. doi: 10.22920/PNIE.2023.4.1.28

Fleming, T.H., Geiselman, C. & Kress, W.J., 2009. The evolution of bat pollination: a phylogenetic perspective. *Annals of Botany*, 104(6), pp.1017–1043. doi: 10.1093/aob/mcp197

Förster, J., et al., 2019. Climate change impacts on small island states: Ecosystem services risks and opportunities. In *Atlas of Ecosystem Services*. Cham: Springer, pp.353–359. doi: 10.1007/978-3-319-96229-054

Franks, L. & Farquhar, S., 2024. The Effect of Noise Pollution on Pollinator Biodiversity. *Journal of Student Research*, 13(1). doi: 10.47611/jsrhs.v13i1.6357

García, D. et al., 2024. Common birds combine pest control and seed dispersal in apple orchards through a hybrid interaction network. *Agriculture, Ecosystems & Environment*, 365, 108927. doi: 10.1016/j.agee.2024.108927

Grebner, D.L., et al., 2022. Wildlife habitat relationships. In *Introduction to Forestry and Natural Resources (Second Edition)*. Academic Press, pp.131-152. doi: 10.1016/B978-0-12-819002-9.00005-5.

Green, A.J., & Elmberg, J., 2014. Ecosystem services provided by waterbirds. *Biological reviews of the Cambridge Philosophical Society*, 89, pp.105-122. doi: 10.1111/brv.12045

Hammer, Ø., Harper, D.A.T., & Ryan, P.D. 2001. PAST: Paleontological statistics software package for education and data analysis. *Palaeontologia Electronica*, 4(1), pp.4-9.

Jacobs, M., 1958. Botanical reconnaissance of Nusa Barung and Blambangan, South East Java. *Blumea. Supplement*, 4(1), pp.68–86.

James, D.J., & McAllan, I.A.W., 2014. The birds of Christmas Island, Indian Ocean: A review. *Australian Field Ornithology*, 31, pp.S1-S175.

Joel, Y.H. et al., 2024. A comparison of the sampling effectiveness of acoustic recorder, camera trap and point count methods in sampling nocturnal birds in Afrotropical landscapes. *Ecology and evolution*, 14(5), e11389. doi: 10.1002/ece3.11389

Kruskop, S.V., Srinivasulu, B. & Srinivasulu, C., 2019. *Pipistrellus javanicus*. The IUCN Red List of Threatened Species 2019. doi: 10.2305/IUCN.UK.2019-3.RLTS.T17344A22128905.en

Mariyappan, M. et al., 2023. Ecological role and ecosystem services of birds: A Review. *International Journal of Environment and Climate Change*, 13(6), pp.76–87. doi: 10.9734/ijecc/2023/v13i61800

Martínez-Núñez, C. et al., 2021. Insectivorous birds are not effective pest control agents in olive groves. *Basic and Applied Ecology*, 56, pp.270-280. doi: 10.1016/j.baae.2021.08.006

Moulistanos, A. et al., 2023. Genetic diversity of bat species in the cross-border area of Greece and Bulgaria. *Journal of Biological Research – Thessaloniki*, 30, 6. doi: 10.26262/jbrt.v30i0.9024

Partomihardjo, T. & Ismail, 2008. Floral diversity of Nusa Barong Nature Reserve, Jember - East Java. *Berita Biologi*, 9(1), pp.60–67.

Prakarsa, T.B.P. et al., 2023. Hematological profil of three species of *Hipposideros* spp. (Hipposideridae) as an adaptation in cave habitat, in Gunung Sewu Geopark area, Indonesia. *Journal of Animal and Plant Science*, s33, pp.1148–1157. doi: 10.36899/JAPS.2023.5.0708

Prakash, H. et al., 2021. Ecological drivers of selection for remnant forest habitats by an insectivorous bat in a tropical, human-modified landscape. *Forest Ecology and Management*, 496, 119451. doi: 10.1016/j.foreco.2021.119451

Pringle, R.M. et al., 2023. Impacts of large herbivores on terrestrial ecosystems. *Current biology : CB*, 33(11), pp.R584–R610. doi: 10.1016/j.cub.2023.04.024

Ratter, B.M.W., 2018. Island vulnerability and resilience. In *Geography of Small Islands: Outposts of Globalisation*. Springer, pp.173–199. doi: 10.1007/978-3-319-63869-0_6

Sakoui, S. et al., 2020. The life hidden inside caves: Ecological and economic importance of bat guano. *International Journal of Ecology*, 2020(1), 9872532. doi: 10.1155/2020/9872532

Setianto, J. et al., 2017. Domestication of red jungle fowl: A case study of the red jungle fowl chicks procurement by the communities in Central Bengkulu, Indonesia. *Biodiversitas*, 18, pp.183-189. doi: 10.13057/biodiv/d180125

Sheherazade, Pradana, D.H., & Tsang, S.M., 2017. The role of fruit bats in plant community changes in an urban forest in Indonesia. *Raffles Bulletin of Zoology*, 65, pp.497–505.

Sukistyanawati, A. et al., 2016. Wild animals inventarisation in Sempu Island Nature Reserve. *Jurnal Ilmiah Perikanan dan Kelautan*, 8(1), pp.26-35. doi: 10.20473/jipk.v8i1.11188

Suripto, B. & Hamidy, A., 2006. Birds in Nusakambangan Island, Cilacap, Central Java: Diversity, adaptation and important species for conservation. *Jurnal Manusia dan Lingkungan*, 13, pp.9-25. doi: 10.22146/jml.18646

Sutrisno, H., 2007. Rapid assessment on macro-moth fauna at Nusa Barong Nature Reserve: A low diversity. *Journal of Biological Researches*, 12(2), pp.115–120. doi: 10.23869/bphjbr.12.2.20073

Suyanto, A., 2001. *Kelelawar di Indonesia*, Pusat Litbang Biologi LIPI, Bogor.

Suyanto, A. & Struebig, M.J., 2007. Bats of the Sangkulirang limestone karst formations, East Kalimantan—a priority region for Bornean bat conservation. *Acta Chiropterologica*, 9(1), pp.67–95. doi: 10.3161/1733-5329(2007)9[67:BOTSLK]2.0.CO;2

Tang, G.S., Sadanandan, K.R. & Rheindt, F.E., 2015. Population genetics of the olive-winged bulbul (*Pycnonotus plumosus*) in a tropical urban-fragmented landscape. *Ecology and evolution*, 6(1), pp.78-90. doi: 10.1002/ece3.1832

Taylor, M., 2019. *Bats: An Illustrated Guide to All Species*, UK: Ivy Press.

Valido, A. & Olesen, J.M., 2023. Oceanic island bats as flower visitors and pollinators. *Journal of Pollination Ecology*, 35, pp.239–251. doi: 10.26786/1920-7603(2023)764

Journal of Tropical Biodiversity and Biotechnology
Volume 10, Issue 04 (2025): jtbb20679
DOI: 10.22146/jtbb.20679

Research Article

Characterisation of Plant Growth Promoting Actinobacteria from Sungai Wain Protected Forest, East Kalimantan

Izzuli Salamah Haris[1], Tirta Kumala Dewi[2], Sri Widawati[2], Shanti Ratnakomala[3], Endah Retnaningrum[4]*

1)Graduate Students, Faculty of Biology, Universitas Gadjah Mada, Jl. Teknika Selatan, Sekip Utara, Yogyakarta, Indonesia, 55281
2)Research Center for Applied Microbiology, National Research and Innovation Agency (BRIN), Jl. Raya Jakarta-Bogor Km 46, Cibinong, West Java, Indonesia, 16911
3)Research Center for Biosystematics and Evolution, National Research and Innovation Agency (BRIN), Jl. Raya Jakarta-Bogor Km 46, Cibinong, West Java, Indonesia, 16911
4)Microbiology Laboratory, Faculty of Biology, Universitas Gadjah Mada, Jl. Teknika Selatan, Sekip Utara, Yogyakarta, Indonesia, 55281
* Corresponding author, email: endahr@ugm.ac.id

Keywords:
Actinobacteria
IAA production
Nitrogen fixation
Phosphate solubilization
PGPR
Submitted:
15 April 2025
Accepted:
25 June 2025
Published:
20 October 2025
Editors:
Miftahul Ilmi
Liya Audinah

ABSTRACT

The excessive use of chemical-based fertilisers, herbicides, and pesticides in Indonesian agriculture has resulted in negative environmental impacts. As a sustainable alternative, the application of biofertilisers remains uncommon despite their proven ecological benefits. A group of microorganisms known as Plant Growth Promoting Rhizobacteria (PGPR) that plays a crucial role in enhancing plant growth. Among them, actinobacteria are gram-positive bacteria that involved in ecological processes such as organic matter decomposition, nutrient cycle, plant growth promotion and plant pathogen's suppression. This study aims to investigate the potency of actinobacteria isolated from Sungai Wain Protected Forest, East Kalimantan as plant growth-promoting agents. A total of 96 actinobacteria isolates were revived from glycerol stock and subjected to primary screening through qualitative assays to assess phosphate solubilisation activity, nitrogen fixation, and *Indole-3-Acetic Acid* (IAA) production. Twenty-eight isolates demonstrated positive result among three PGP traits were subsequently selected for secondary screening, involving quantitative determination of IAA production and phosphate solubilisation through colorimetric assay. K22S-63 was identified as the most promising candidate, exhibiting the highest IAA production and phosphate solubilisation values of 43.80 and 41.51 µg mL^{-1}, respectively. Molecular analysis was performed by amplifying PGPR-associated genes using PCR. The targeted genes included *iaaM*, *phoD*, *PKS*, and *NRPS*. Phylogenetic analysis based on 16S rRNA gene sequencing revealed that K22S-63 shared 99.65 % similarity with *Peterkaempfera griseoplana*. These findings suggested that K22S-63 holds potential as bioinoculants with promising capabilities as plant growth promoter and biocontrol agents.

How to cite:
Haris, I.S. et al., 2025. Characterisation of Plant Growth Promoting Actinobacteria from Sungai Wain Protected Forest, East Kalimantan. *Journal of Tropical Biodiversity and Biotechnology*, 10(4), jtbb20679. doi: 10.22146/jtbb.20679

INTRODUCTION

Indonesia is one of the most biodiverse countries and exhibits a high level of microbial diversity, particularly within its soil ecosystems. Data provided by Ritung et al. (2015), revealed that Indonesia encompasses approximately 144.47 million hectares of dry land, representing 76.20 % of the total land area in Indonesia. A significant 82 % of the dry lands in Indonesia is classified as suboptimal, characterised by low productivity and diminished soil fertility. In response to the challenges, farmers in Indonesia frequently rely on the use of chemical fertilisers, herbicides, and pesticides due to their high effectiveness, affordability, and accessibility. The utilisation of biofertilisers remains uncommon despite their potential benefits for sustainable agriculture. The overuse of chemical fertiliser has long-term impacts on the soil, such as disruption of soil ecosystem and reduction in biodiversity, which could contribute to land degradation. One of the strategies is the utilisation of biofertiliser that can enhance soil fertility by microbial activity and nutrient cycling, leading to an increase in agricultural productivity.

Actinobacteria are gram-positive bacteria belonging to the order *Actinomycetales* and phylum *Actinobacteria* that are widely distributed in various habitats and ecosystems, including marine and terrestrial environments (Meenakshi at al. 2024). Actinobacteria play a major role in ecological processes, including biodegradation and humus formation, by facilitating the breakdown of complex polymers such as the cellulose and lignin (Bhatti et al. 2017). Actinobacteria are widely recognised as plant growth promoting rhizobacteria (PGPR) due to their ability to enhance plant growth and productivity through both direct and indirect mechanisms. These mechanisms involve the provision of essential nutrients, secondary metabolites and bioactive compounds productions that support plant development (Katz & Baltz 2016). The utilisation of plant growth-promoting Actinobacteria (PGPA) as a biofertiliser inoculant continuously and gradually offers a promising sustainable alternatives to enhance food security and agricultural stability in response to minimising the reliance on chemical fertiliser, which potentially harms the environment when excessively applied over time. Gangola (2018) assessed the impact of pesticides on soil health and their biodegradation using indigenous microorganism, and the result showed that a consortium of *Bacillus* strains efficiently degraded pesticides such as cypermethrin (99 %), imidacloprid (99 %), fipronil (95 %), and chlorsulfuron (93 %) within 15 days compared to only 7 % degradation in the control.

A deep understanding of Actinobacteria potency as PGPR is essential for advancing their application as biofertiliser. Comprehensive and collaborative research across various fields is necessary to identify and to scrutinise the potential strain and explore their capabilities as PGPR. This study evaluated actinobacteria from the unspoiled Sungai Wain Protected Forest, East Kalimantan, focusing on their plant growth-promoting abilities, including phosphate solubilisation, IAA production, and nitrogen fixation. Further molecular analysis using PCR-based gene amplification was conducted to detect the presence of functional genes associated with PGPR activity, including *iaaM*, *phoD*, PKS and NRPS. The selected strain with the highest PGPR activity were further identified using 16S rRNA sequence analysis. The findings of this study are expected to provide valuable references and knowledge for other researchers in related fields, especially for the development of Actinobacteria-based biofertiliser for the agriculture sector.

MATERIALS AND METHODS

Sample Collection, Preservation and Rejuvenation

Soil sample were collected from Sungai Wain Protected Forest, Balikpapan City, East Kalimantan, Indonesia. A total of nine soil samples, coded as K22S,

were obtained and preserved in glycerol stock at -80 °C at the Indonesian Culture Collection (InaCC) BRIN. In this study, ninety-six Actinobacteria isolates were revived from glycerol stock and grown in Yeast Starch Agar (YSA) media. Each sample was inoculated aseptically using quadrant streak plate method and incubated for 48 hours at room temperature (27 °C).

Primary Screening of PGPR Activity

Phosphate Solubilization Assay

Primary Screening of phosphate solubilisation activity of 96 Actinobacteria were carried out using plate assay based on modified method of Widawati et al. (2022). Pure culture samples were inoculated on Pikovskaya Agar Media (pH 7) containing tricalcium phosphate. Plates were divided into four quadrants as replication and isolates were inoculated on the centre of each quadrant with spot inoculation technique and incubated at 27 °C for 10 days. The clear zone that presence around the isolate is indicates the positive result of phosphate solubilisation ability. The solubilisation index was measured in day 10 by calculating the diameters of clear zone and colony as follows:

$$\text{Solubilisation Index (SI)} = (\text{Halo zone diameter} + \text{Colony Diameter})/(\text{Colony Diameter})$$

Qualitative and quantitative classification of phosphate solubilising activity into high, moderate, and low categories were determined through statistical analysis using SPSS Statistics (IBM SPSS Statistics Version 29.0.2.0). Classification thresholds for each activity level were defined according data distribution.

Indole Acetic Acid (IAA) Production

The initial screening of IAA production was tested using Tryptic Soy Agar (TSA) media supplemented with 200 ppm L-tryptophan as precursor (Widawati et al. 2022). The plate was divided into eight quadrants, each sample was grown on the quadrant with two replications and incubated at 27 °C for 48 hours in dark condition. After incubation time, colonies were dropped with a Salkowski reagent (250 mL H_2SO_4, 249 mL distilled water and 1 mL of 0.5 M $FeCl_3$) and stored in dark condition for 30 min. The isolate discoloration into pink indicates the IAA production of Actinobacteria.

Nitrogen-Fixing Activity

The nitrogen fixation test was performed qualitatively based on Widawati et al. (2022). method with modification using New Fabio (NFb) semi solid media. Actinobacteria was inoculated into 5 mL NFb semi solid media in reaction tube using inoculation needle aseptically, isolates were incubated at 27 ° C. Media was observed for 7 days, positive result was shown with discoloration into blue on the media. The isolates were grouped into high, moderate of low nitrogen-fixing potential based on the intensity of the colour.

Secondary Screening of PGPR Activity

Phosphate Soluble Content

The isolates that showed a positive result in primary screening were determined quantitatively using spectrophotometric molybdenum blue method based on Widawati et al. (2022) with modification. Each isolate was inoculated into a 100 mL erlenmeyer containing 50 mL Pikovskaya liquid medium incubated in incubator shaker at 30 °C and shaken at 160 rpm for 7 days; non-inoculated media was used as negative control. After 7 days, 20 mL of each culture was filtered using filter paper Whatman number 42 and centrifuged at 10,000 rpm for 15 min. Furthermore, 5 ml of supernatant was collected into reaction tube and mixed with 0.5 mL reagent solution, vortex for 30 seconds

and incubated at room temperature for 30 min, the samples colour was changed to blue. 200 µL of each sample was placed into 96-well plate with 3 replicates and the optical density (OD) was measured by spectrophotometer (Varioskan™ LUX *multimode Microplate reader*), at 693 nm. The estimation of phosphate soluble content was determined by comparing the sample absorbance within the phosphate standard curve.

IAA Production Assay

The isolates were determined quantitatively with the colorimetric assay based on Widawati et al. (2022), each isolate was inoculated into 100 mL Erlenmeyer covered with aluminium foil, containing 25 mL Tryptic Soy Broth (TSB) media supplemented with 200 ppm L-Tryptophan and incubated in incubator shaker at 30 °C and shaken at 160 rpm for 4 days in dark condition, non-bacterial media was used as a negative control. After incubation time, the culture was centrifuged at 10,000 rpm for 10 minutes at 4 °C. Furthermore, 1 mL supernatant was placed into reaction tube and mixed with 4 mL Salkowski reagent, the tube was incubated at room temperature for 30 minutes in dark condition. Each isolate was placed into 96-well plate with 3 replicates and measured with spectrophotometer (Varioskan™ LUX *multimode Microplate reader*), at 435 nm. The estimation of IAA production was determined by comparing the sample absorbance within IAA standard curve. The concentration of IAA produced by isolate was statistically analysis using SPSS Statistics (IBM SPSS Statistics Version 29.0.2.0), and isolates were group into high, moderate, and low IAA producers based on the distribution pattern of the measured values.

Morphological Characterisation of Potential Actinobacteria

Actinobacteria isolate that exhibited positive result and highest value across all PGP properties was subjected to morphological characterisation and molecular identification based on 16S rRNA gene analysis. The morphological characterisation of potential isolate was carried out by observed the actinobacteria morphology in YSA media and the micro-morphology were observed using Scanning Electron Microscopy (SEM) (JSM-IT200 JEOL, Japan), observed at voltage of 10kV and magnifications of 25,000 ×.

DNA Extraction, PGPR Genes Detection and Molecular Identification of Potential Actinobacteria

DNA extraction of potential actinobacteria was carried out using Quick-DNA™ High Molecular Weight MagBead Kit Zymo (Zymo Research, CA, USA) based on the protocol with modification.

Crude DNA was stored at –20 °C, the quality and quantity of DNA were measured using Varioskan Lux Micro Plate Reader. DNA amplification of genes encoded PGPR activity and 16S rRNA gene was performed using primers presented in Table 1. The 25 µL PCR reaction consisted 12.5 of µL MyTaqTM HS Red Mix 2x (Bioline, Germany), 1 µL of forward primer (10 pmol), 1 µL of reverse primer (10 pmol), 1 µL of DNA template, and 9.5 µL of Nuclease-Free Water (NFW). PCR Products were furthermore visualized qualitatively using electrophoresis, 2.5 µL of PCR product was injected into 1 % gel electrophoresis with Florosafe DNA Staining (1st BASE, Malaysia) in 1x TAE buffer pH 8.0. The electrophoresis was performed at 100 volts for 25 minutes and visualized on Gel DocTM EZ Imaginer (Bio-Rad). The PCR product of 16S rRNA gene was sequenced and analysed using BioEdit and EZBioCLoud (https://www.ezbiocloud.net). The isolate sequence was aligned using Clustal W, and the phylogenetic tree was constructed using MEGA11 based on neighbour-joining program using 1000 replicates of bootstrap.

Table 1. List of primer sequences used for molecular analysis in this study.

Gene	Primer	Sequence (5'-3')	Size (bp)	Reference
16S rRNA	27F	AGAGTTTGATCCTGGCTCAG	1500	Xu et al. 2016
	1492R	TACGGCTACCTTGTTACGACTT		
	920 F	AAACTCAAATGAATTGACGG		Nurkanto & Agusta 2015
	920 R	CCGTCAATTCATTTGAGTTT		
	520 F	GTGCCAGCAGCCGCGG		
	520 R	ACCGCGGCTGCTGGC		
phoD	ALPSF730	CAGTGGGACGACCACGAGGT	350	Amri et al. 2022
	ALPSR1101	GAGGCCGATCGGCATGTCG		
nifH	PoL-F GC	CGCCCGCCGCGCGCGGCGGGCGGGG CGGGGGCAC- GGGGGGTGCGAYCCSAARGCBGACTC	500	Koirala et al. 2025
	PoL-R	ATSGCCATCATYTCRCCGGA		
*iaa*M	*iaa*M F	ATGACGTCCACCGTGCCCAACGCG	150	Passari et al. 2016
	*iaa*M R	CTAGTCCTCGGGGAGTTCCACGGG		
PKS	PKS F	CGCGCGCATGTACTGGACNGGNGAYYT	480	Amos et al. 2015
	PKS R	GGAGTGGCCGCCCARNYBRAARAA		
NRPS	NRPS F	GGCAACGCCTACCACATGCANGGNYT	350	
	NRPS R	GGTCCGCGGGACGTARTCNARRTC		

RESULTS AND DISCUSSION

Rejuvenation of Actinobacteria Isolates

Bulk soil samples were collected from nine separate sites within the Sungai Wain Protected Forest for this study. A total of ninety-six actinobacteria isolates coded K22S were successfully revived from glycerol stock were subsequently tested in a primary screening for PGP (plant growth-promoting) activities. All isolates exhibit distinct morphological colonies, with a representative subset presented in Figure 1. Cultivation on Yeast Starch Agar (YSA) medium revealed notable phenotypic variation among the isolates, particularly in shape, surface, elevation, pigmentation, margin, and aerial mycelial development. The morphological features commonly used as preliminary taxonomic indicators within Actinobacteria.

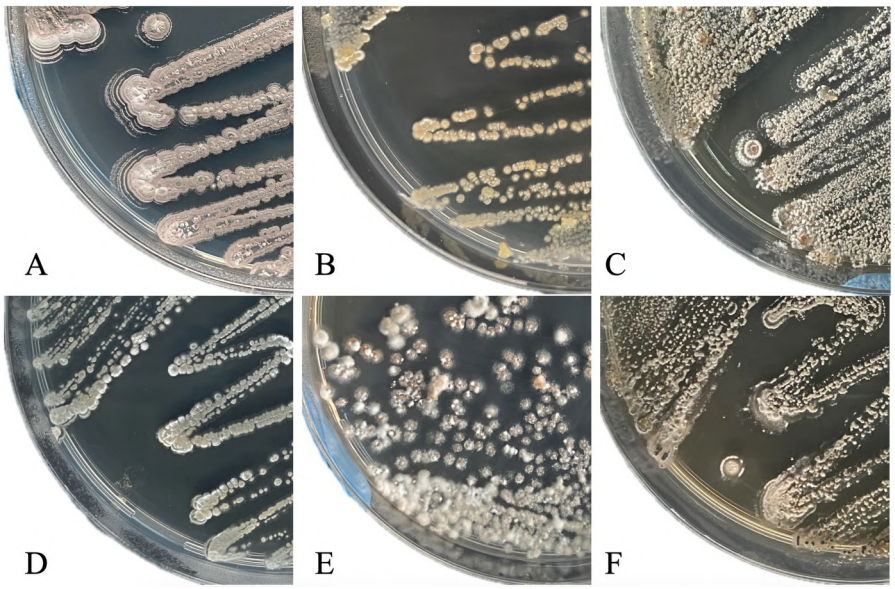

Figure 1. Morphology of actinomycetes colony grown in YSA media. (A) K22S-23; (B) K22S-20; (C) K22S-41; (D) K22S-58; (E) K22-84; (F) K22S-88.

Primary Screening of PGPR Activity

Phosphate Solubilization Assay

Ninety-six actinobacteria isolates were screened qualitatively to assess its PGP activity focusing on phosphate solubilization, IAA production and nitrogen fixation. The qualitative result of actinobacteria isolates on their Plant-Growth Promoting (PGP) ability were showed in Table 2.

Table 2. Qualitative result of actinomycetes isolates towards their PGP activity.

PGP Activity	Total of Isolate			
	High (+++)	Moderate (++)	Low (+)	Total
Phosphate solubilising	3	20	46	96
IAA Production	1	17	29	96
Nitrogen Fixation	16	17	31	96

The actinobacteria isolates were grouped into negative (-), low (+), moderate (++) and high (+++) based on their activity. Actinobacteria isolates were tested qualitatively for phosphate solubilization activity using plate assay in Pikovskaya media containing tricalcium phosphate. The formation of halo-zone around the colony indicates the phosphate solubilisation activity of actinobacteria

The Phosphate Solubilization Index (PSI) was measured in day 10 by calculating the diameters of halo-zone and colony. A total 69 isolates were exhibited the ability to solubilise the phosphate representing 71.88 % of all screened isolates, as indicated by halo-zone formation around the colony after ten days of incubation with PSI values ranging between 1.00 ± 0.00 to 9.31 ± 0.70 showed by K22S-84 and K22S-65, respectively. The grown actinobacteria isolates without halo-zone formation were categorised as negative; a total 27 out of 96 Actinobacteria isolates were showed negative result. The selected strains were further tested to confirm their activity to soluble the phosphate.

Fatmawati et al. (2019) reported that actinobacteria isolated from rhizosphere have an ability to dissolve phosphate, strain ASR 49 had the highest phosphate solubilizing activity as determined by qualitative assessment with PSI value of 2.62. The halo-zone around colony formed due to the secretion of organic acid and polysaccharides, as well as enzyme production by the actinobacteria isolates. Microbial phosphate solubilization generally occurs through multiple pathways, including the acidification mechanism that facilitated by the production of organic acid such as citric, gluconic, lactic, malic and oxalic acid. Another mechanism involves the reduction in pH level of the medium and the chelation of metal ions associated with insoluble phosphorus (Al, Fe, Ca), that facilitating the release of phosphorus (Boubekri et al. 2021).

IAA Production Assay

Auxins are a group of molecules that function as signals regulating physiological processes during plant-microorganism interactions. Auxins produced by microorganisms modify environmental auxin levels to an optimal range, resulting in increased lateral or secondary root growth and expansion of the root surface area, thereby enhancing plant growth and nutrient uptake (Olanrewaju et al. 2021). Each actinobacteria isolates were screened qualitatively using TSA media supplemented with 200 ppm L-tryptophan as precursor. Tang et al. (2023) stated that IAA biosynthesis by microorganism classified into tryptophan-independent and tryptophan-dependent pathway based on tryptophan utilization as key metabolic precursor due to their ability as the most densed amino acid among other amino acids.

IAA production of Actinobacteria isolate was indicated by discolourating the colony into pink after addition of Salkowski reagent and incubated in dark condition. Pink colour formation of Actinobacteria colony due to the reduction of Fe^{3+} to Fe^{2+}, by the interaction between IAA produced by Actinobacteria and iron (Fe) contained in Salkowski reagent (Etesami & Glick 2024). Out of 96 Actinobacteria isolates, 47 isolates known to has ability to produce IAA based on plate assay in TSA media, representing 48.97 % of all screened Actinobacteria isolates. The result of assay was classified into four group based on their colour change of Actinobacteria colonies: no discoloration (-);

whitish to yellowish (+); yellowish to pinkish (++); pinkish to purplish (+++). Twenty-eight isolates categorised as low producer of IAA, while 17 isolates were moderate and one isolates was identified as a high IAA producer, as presented in Table 2.

Nitrogen Fixing Activity

Nitrogen fixing activity of Actinobacteria isolates were evaluated qualitatively using Nfb media following method by Widawati et al. (2022). Out of 96 isolates evaluated for their nitrogen-fixing ability, a total of 64 isolates exhibited positive result representing 66.67 % of total screened Actinobacteria. In particular, 16 actinobacteria isolates (16.67 %) were classified in the high category; 17 (17.71 %) and 31 isolates (32.29 %) were categorised as moderate and low nitrogen-fixers, respectively. The colour change in media reflected the ability of actinobacteria to assimilate nitrogen in the form of nitrate and ammonia (Suleiman et al. 2019).

The results of the nitrogen fixation assay were categorized the positive results into three groups based on the degree of discoloration: light blue as low activity (+), medium blue as moderate (++), and deep blue as high activity (+++). Further test is required to validate the ability of actinobacteria through biochemical and molecular approaches. In this study, only the Actinobacteria isolates that demonstrated the capacity to solubilise phosphate, produce IAA, and fix nitrogen were further evaluated quantitatively.

Nitrogen gas (N_2) is an essential component for plant, but plants cannot directly utilize it due to the stability of its covalent bonds. Certain microorganisms possess the ability to convert atmospheric nitrogen (N_2) into inorganic compounds that plants can readily absorbed. This biochemical process, known as nitrogen fixation, enables the transformation of atmospheric nitrogen into assimilable forms. However, this current study aims to detect the ability of actinobacteria to fix the atmosphere nitrogen. Further test is required to validate the ability of actinobacteria through biochemical and molecular approaches. The genus Frankia represents a first group of actinobacteria recognised for their enzymatic capabilities to facilitate the conversion of atmospheric nitrogen into ammonia compounds (NH_3). In the preceding decade, it has been established that additional varieties of actinobacteria exhibiting nitrogen-fixing activities belonging to the genus Streptomyces, *Mycobacterium*, *Microbacterium*, *Agromyces*, *Mincromonaspora* and *Corynebacterium* (Silva et al. 2022).

Secondary Screening of PGPR Activity in Actinobacteria

Phosphate Soluble Content

Out of 96 Actinobacteria isolates that were screened qualitatively, 28 actinobacteria isolates exhibited all three PGP traits and were subsequently evaluated to quantitative assessment regarding their ability in phosphate solubilisation and IAA production. Additionally, 28 potential isolates were further examined for their ability to solubilize the phosphate. P soluble content resulted from this study refers to the measured concentration of soluble phosphate (P) released by actinobacteria. P soluble concentration determined as actual amount of P that converted into soluble form and directly available for utilisation by plants.

Figure 2 shows the actinobacteria isolates after addition of reagent, the intensity of the blue coloration indicates the highest phosphate solubilisation content. Statistical analysis shows strong correlation between actinobacteria activity and phosphate solubilisation, as indicated by significance values of <0.05. The quantitative assay revealed that K22S-78 had the highest level of phosphate solubilization, followed by K22S-63, K22S-88 with the concentration values of 69.29 ± 2.39, 41.51 ± 1.09 and 37.13 ± 0.98 µg mL^{-1}, respec-

tively. Compared to Solubilisation Index (SI), K22S-78 and K22S-63, which possess the highest P soluble content, exhibit low solubilisation activity as determined by qualitative method, with PSI values of 2.02 ± 0.20 and 1.72 ± 0.09, respectively.

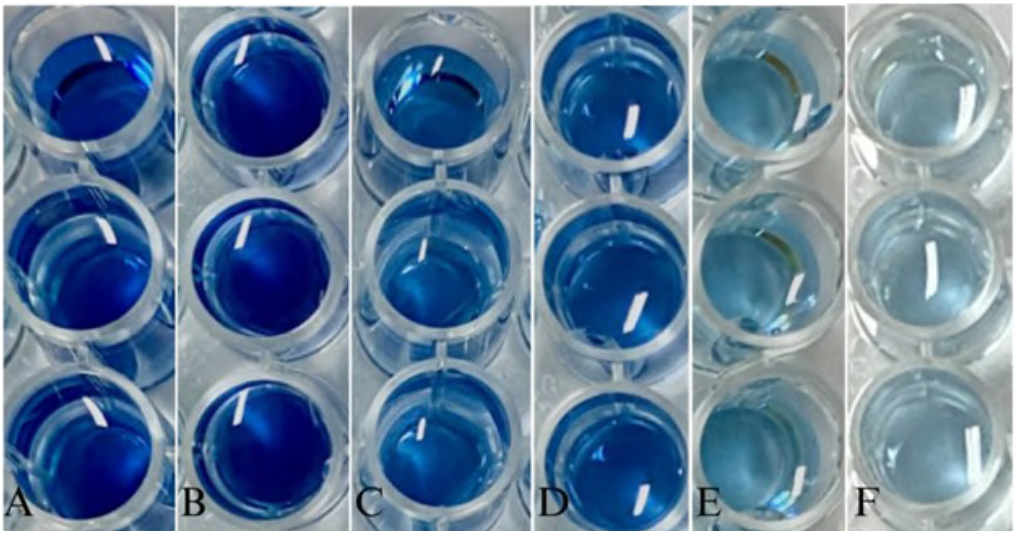

Figure 2. Quantitative assay of phosphate solubilisation activity in potential isolates. (A) K22S-78; (B) K22S-63; (C) K22S-88; (D) K22S-98; (E) K22S-41; (F) K22S-10.

Similarly, K22S-88, which has the third highest P soluble content, was categorised as moderate phosphate solubilizer according to qualitative method, with PSI value of 4.55 ± 0.05. Table 3 shows K22S-84 and K22S-97, which demonstrated the highest solubilisation index qualitatively, also shows quite high potential for phosphate solubilisation based on quantitative method, with P soluble values of 20.44 ± 0.27 and 37.04 ± 0.98 µg mL^{-1}, respectively.

The comparative analysis between qualitative and quantitative method revealed that both approaches did not exhibit the same pattern. Figure 3 illustrates the regression curve correlating the qualitative (PSI) and quantitative (colourimetric) methods, the result revealing an absence of a significant relationship, as indicated by a p-value exceeding 0.5 %. ($r = 0.0261$). This present study is in line with study observed Walpola et al. (2020) result showed the different pattern in phosphate solubilization in qualitative and quantitative method.

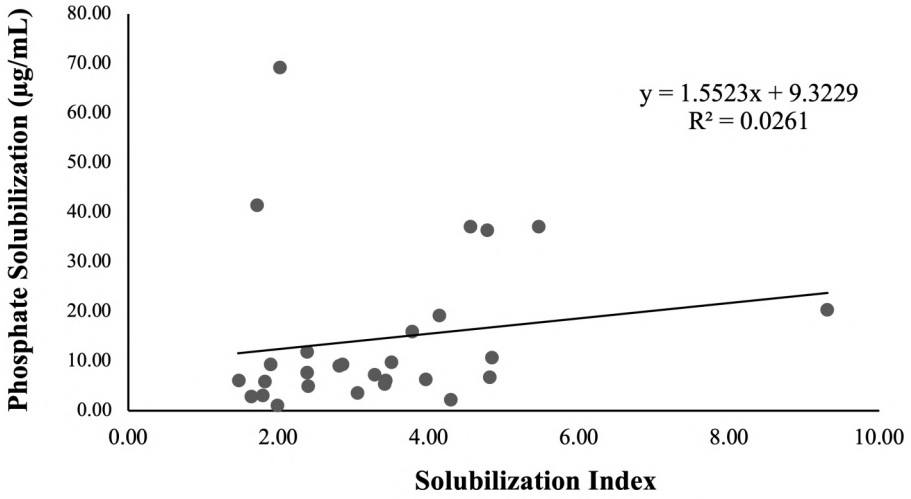

Figure 3. Comparative analysis between qualitative and quantitative method of phosphate solubilizing activity of potential actinomycetes isolates after seven days of incubation.

Table 3. Phosphate solubilization, IAA production and N-Fixation of potential isolates.

Isolate Code	Phosphate Solubilization		IAA Production (µg mL^{-1})	N Fixation
	SI	P Soluble (µg mL^{-1})		
K22S-009	4.81 ± 0.13^{l}	6.86 ± 0.06^{efg}	19.88 ± 0.55^{jk}	+
K22S-010	1.99 ± 0.13^{abc}	1.15 ± 0.70^{a}	14.02 ± 0.12^{e}	+
K22S-011	2.40 ± 0.24^{cd}	4.97 ± 0.16^{d}	18.56 ± 0.41^{h}	+
K22S-012	4.84 ± 0.73^{l}	10.66 ± 0.65^{ij}	20.34 ± 0.40^{kl}	+
K22S-013	2.38 ± 0.39^{bcd}	11.77 ± 0.71^{j}	14.08 ± 0.02^{e}	+
K22S-015	3.25 ± 0.14^{efgh}	7.64 ± 0.45^{g}	15.27 ± 1.15^{f}	+++
K22S-023	1.90 ± 0.09^{abc}	9.35 ± 0.17^{h}	8.08 ± 0.53^{b}	+
K22S-024	1.64 ± 0.13^{a}	2.93 ± 0.27^{bc}	15.21 ± 0.30^{f}	+
K22S-030	3.78 ± 0.48^{hij}	16.02 ± 0.58^{k}	9.79 ± 0.29^{c}	+++
K22S-034	1.46 ± 0.06^{a}	6.07 ± 0.15^{def}	16.18 ± 0.06^{g}	++
K22S-036	3.96 ± 0.69^{ij}	6.24 ± 0.11^{def}	18.72 ± 0.72 ^{hi}	++
K22S-037	3.42 ± 0.14^{fghi}	5.45 ± 0.75^{d}	15.47 ± 0.18^{fg}	+++
K22S-041	4.30 ± 0.13^{jkl}	2.25 ± 0.69^{ab}	40.37 ± 0.29^{p}	+++
K22S-043	3.43 ± 0.06^{fghi}	6.14 ± 0.15^{def}	5.85 ± 0.09^{a}	+
K22S-046	4.14 ± 0.59^{jk}	19.18 ± 0.47^{l}	20.81 ± 0.25^{l}	+++
K22S-049	3.05 ± 0.08^{efg}	3.62 ± 0.74^{c}	8.67 ± 0.58^{b}	+
K22S-052	2.85 ± 0.09^{def}	9.26 ± 0.51^{h}	13.12 ± 0.11^{d}	++
K22S-056	2.81 ± 0.25^{de}	9.11 ± 0.66^{h}	19.40 ± 0.36^{ij}	++
K22S-058	1.79 ± 0.01^{ab}	3.08 ± 0.15^{bc}	28.55 ± 0.54^{o}	++
K22S-063	1.72 ± 0.09^{a}	41.51 ± 1.09^{o}	43.80 ± 0.45^{q}	++
K22S-073	4.78 ± 0.19^{l}	36.49 ± 0.56^{n}	12.75 ± 0.05^{d}	+
K22S-078	2.02 ± 0.20^{abc}	69.29 ± 2.39^{p}	19.81 ± 0.36^{jk}	++
K22S-083	3.51 ± 0.25^{ghi}	9.73 ± 1.23^{hi}	24.77 ± 0.83^{m}	+
K22S-084	9.31 ± 0.70^{n}	20.44 ± 0.27^{m}	14.95 ± 0.38^{f}	+
K22S-088	4.55 ± 0.05^{kl}	37.13 ± 0.98^{n}	26.56 ± 0.60^{n}	++
K22S-094	3.27 ± 0.00^{efgh}	7.29 ± 0.19^{fg}	27.98 ± 0.68^{o}	+
K22S-097	5.47 ± 0.50^{m}	37.04 ± 0.93^{n}	18.07 ± 0.17^{h}	+
K22S-098	1.81 ± 0.06^{abc}	5.91 ± 0.27^{de}	12.23 ± 0.23^{d}	+++

Walpola et al. (2020) conducted the comparative evaluation of qualitative and quantitative phosphate solubilisation methods and found no correlation between the two approaches. Isolate PSB 10 which possessed the lowest solubilisation index (0.61), has classified as the high phosphate solubiliser using quantitative method (873.87 µg mL^{-1}). However, this result found that qualitative assay not consistently correlate with quantitative methos, indicating the fundamental methodological differences between two approaches. The discrepancies may be attributed to several factors, including inoculation technique, incubation time, different type and diffusion rates of different organic acid in microorganism, which affect the halo formation in qualitative assay. Qualitative assay provides the rapid screening of phosphate solubilisation potential that are useful for rapid preliminary screening of phosphate solubilising ability, while the quantitative assay performed in liquid media offer more precise evaluation by estimated the actual concentration of solubilized phosphate (Amri et al. 2023). Therefore, both of qualitative and quantitative method could be conducted in parallel for more reliable result to improve efficiency and to identify the most potential microorganism isolate as phosphate solubilisers.

IAA Production

In the present study, twenty-eight of actinobacteria isolates were evaluated quantitatively to identify the most potential isolate to produce the IAA using TSB media supplemented with 200 ppm tryptophan as precursor. Tabel 3. showed that all isolates possess the ability to synthesize IAA, with concentration values ranging from 5.85 ± 0.09 to 43.80 ± 0.45 µg mL^{-1}. K22S-63 exhibited the highest IAA concentration, followed by K22S-41 with respective val-

ues of 43.80 ± 0.45 and 40.37 ± 0.29 µg mL^{-1}, significantly different among other strain ($p<0.05$) (Figure 4).

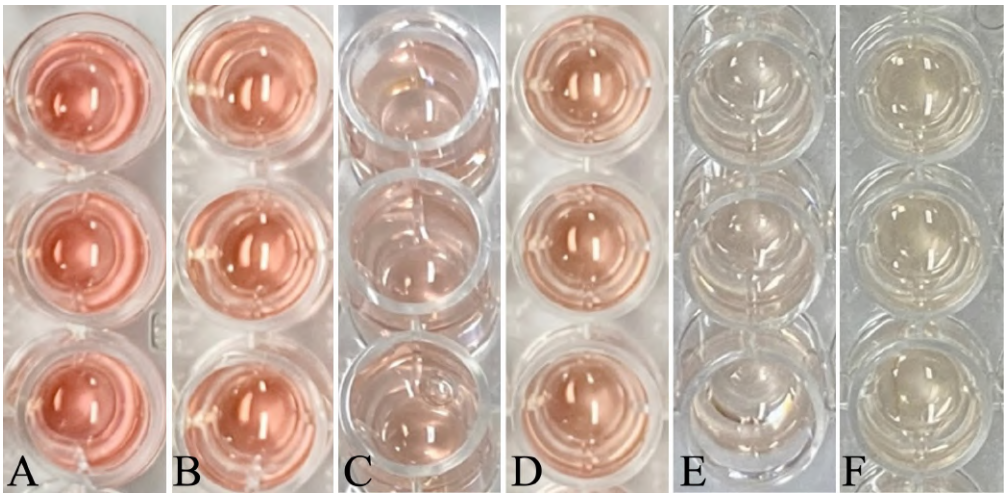

Figure 4. Quantitative assay of IAA production activity in potential isolates after Salkowski reagent addition. A. K22S-63; B. K22S-41; C. K22S-58; D. K22S-94; E. K22S-30; F. K22S-43.

In contrast, the lowest IAA concentration was exhibited by K22S-43 with value of 5.85 ± 0.09 µg mL^{-1}. Anwar et al. (2016) conducted a screening of PGP traits in Actinobacteria and reported that, among 96 Actinobacteria isolates obtained from wheat and tomato rhizospheric soils, six isolates exhibited the highest ability to produce IAA, as determined by colorimetric test using Salkowski reagent with IAA concentration values ranging from 10 to 79.5 µg mL^{-1}. Strain WA-3 which exhibit the highest IAA production, was closely related to *Streptomyces nobilis*. This strain was empirically shown to significantly enhance Wheat (*Triticum aestivum*) growth parameters, including shoot length (65 %), root length (81 %), plant fresh weight (84 %), dry weight (85 %), number of leaves (27 %), and number of roots (30 %), compared to control plants.

The presence of IAA was determined by appearance of pink colour after addition of salkowski reagent. IAA produced by Actinobacteria isolates make a complex with tris-(indole-3-acetate)-iron-(III) which formed pink color. This reaction indicates the actinobacteria ability to metabolise tryptophan as precursor into IAA or other indole compounds. Tang et al. (2023), stated that IAA is not the only indole produced by microorganism, hence the biosynthetic pathway of IAA production classified into several groups; indole-3-butyric acid (IBA), indole-3-propionis acid (IPA), indole-3-pyruvic acid (IPyA), indole -3-acetamide (IAM), indole-3-acetonitrile (IAN), indole-3-lactic acid (ILA) dan indole-3-acetaldoximme (IAAId). Salkowski reagent used for IAA production assessment cannot be able to detect the IAA specifically, but other indole derivates and analog compound. Hence, overestimation of IAA values could be detected with Salkowski reagent (Beatriz et al. 2024).

However, despite its limitation, salkowski reagent continues to be extensively used to detect the IAA production to determining plant growth promoting actinobacteria due to low level of difficulty, cost effectiveness, time efficiency and minimal equipment requirements. As demonstrated in Table 3. K22S-63 isolate exhibited the highest activity in both P solubilization and IAA production as determined through quantitative assessment with concentration values of 41.51 ± 1.09 µg mL^{-1} and 43.80 ± 0.45 µg mL^{-1} respectively, statistical analysis revealed that K22S-63 is significantly different with a p-value < 0.05. Given its potential as plant growth promoter, K22S-63 was further subjected to molecular identification.

Morphological Characterisation of Potential Actinobacteria

The morphological characterisation of potential actinobacteria isolate were further analyzed based on colony growth and Scanning Electron Microscopy (SEM) observations. Figure 5 shows morphological characterization of K22S-63 in YSA medium. Based on the Inter-Society Color Council National Bureau of Standards (ISCC-NBS) color chart, the mycelium in 4-7 days of incubation forms greyish-pink color. Additionally, the spores exhibit light-greyish olive color after 7-10 days of incubation on YSA medium.

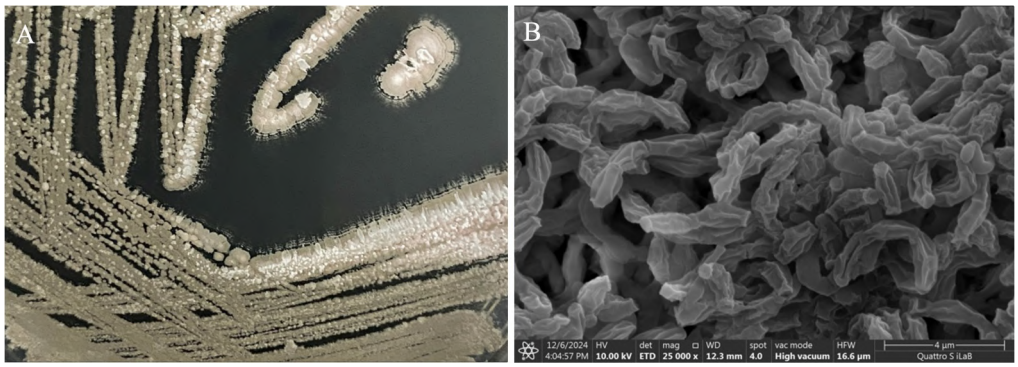

Figure 5. Morphology characterisation of K22S-63 from Sungai Wain Protected Forest. A. YSA media. B. Scanning Electron Microscopy (SEM).

Additionally, the SEM visualization (Figure 5) reveal that K22S-63 exhibit a straight monopodial mycelium, the filament surface appears rough, with an average hyphae diameter approximately 0.5 to 0.7 µm. The spore chains exhibit a poly-sporus structure appeared in *retinaculiaperti* type, characterized by primitive open loops shaped, which consist of cylindrical spore with parallel rugose surface measuring 0.5 thickness and 1µm length.

PGPR Genes Detection of Potential Actinobacteria

Among the 96 isolates, we selected K22S-63 as the promising isolate for promoting plant growth. To validate the plant growth promoting potential of K22S-63, PCR amplification was performed to detect the presence of functional genes including PKS, NRPS, *IaaM*, *NifH* and *PhoD*. The gene specific primers were used and the presence of target genes was confirmed by the amplification of DNA fragments corresponding to the expected product size, as visualized through agarose gel electrophoresis.

The result of PCR amplification confirmed the presence of PKS, NRPS, *IaaM* and *phoD* genes in the isolates, indicating its potential for secondary metabolite production, phytohormone synthesis and phosphate solubilisation. Differently, the *nifH* gene which associates with nitrogen fixation, appeared absence and was not detected based on PCR amplification method. The *phoD* gene encodes alkaline phosphatase D enzyme, which is involve inorganic phosphate mineralisation through hydrolysis of phosphate-ester bonds present in the soil. The biosynthesis of alkaline phosphatase in microorganism was encoded by three types of genes, including *phoA*, *phoX*, and *phoD*. According to Fraser et al. (2015), the *phoD* gene is highly abundant in soil ecosystem and is expressed in environment with phosphate deficiency. Moreover, this type of gene particularly widespread in terrestrial ecosystems, as well as among in archaea and bacteria (Ragot et al. 2017). In this study, amplification of *phoD* gene was generated an amplicon of approximately 300 base pairs, aligning closely with the expected product size range of 371-400 bp reported by Amri et al. (2022). The presence of *phoD* gene in K22S-63, was confirmed through secondary screening and supported its potential for phosphate solubilizing capacity via enzymatic mechanism, particularly through the action of alkaline phosphatase.

Given the significant IAA production observed in K22S-63, further molecular analysis was conducted to confirm the presence of *iaaM* gene. PCR amplification followed by visualisation through agarose gel electrophoresis, successfully detected the *iaaM* gene in K22S-63. This finding is consistent with the result of secondary screening, which shows that K22S-63 exhibited the highest IAA production value among other potential isolates. *iaaM* gene is one of key gene encodes tryptophan monooxygenase which involved in biosynthetic of IAA through IAM pathway (Tang et al. 2023). The result obtained is in line with the study of Passari et al. (2016), that confirms that *iaaM* gene was detected at a size of 150 bp. The presence of *iaaM* gene was demonstrate the ability of K22S-63 to produce the IAA compound, in accordance with the result of both qualitative and quantitative method.

Contrary, the result indicated the absence of the *nifH* gene in K22S-63; however, the qualitative nitrogen-fixing activity test yielded a positive result. This may be attributed to the primer used, which targeting only one gene (*nifH*). The detection of a single gene in nitrogen-fixing activity has a limitation if assessed by only one gene, because nitrogenase has three structural genes (*nifH*, *nifD*, *nifK*). The detection of more than one gene would provide more accurate evidence of nitrogenase in actinobacteria isolates (Mahyarudin et al. 2015). Gaby et al. (2017) conducted a comprehensive evaluation of the *nifH* encode gene, revealing that PolF/PolR primers has the less amount of bias of all primer tested, but has the lowest coverage value which is only amplify 25 % of the 23.847 *nifH* gene sequence tested. Additionally, each microorganism may exhibit the variance in DNA sequence due to single nucleotide polymorphisms (SNPs), which contribute the genetic variation. when SNP occur within the primer binding site, they can prevent DNA amplification as the primer may fail to bind properly.

This study involved the detection of PKS and NRPS genes, which are gene clusters associated with the synthesis of non-ribosomal peptides and polyketide active compounds. Secondary metabolites are involved in bioactivities including antimicrobial, antifungal, antiparasitic, antitumor, and immunosuppressive functions. The *Streptomyces* genus is recognized for its production of secondary metabolites that serve as important resources in the pharmaceutical industry. The amplification of PKS and NRPS genes in the K22S-63 resulted in amplicon sizes of approximately 500 bp and 350 bp, respectively. These results align with the expected fragment sizes reported by Amos et al. (2015). The identification of both genes suggests that the K22S-63 isolate possesses the potential to function as an antimicrobial agent and is capable of producing antimicrobial compounds.

Molecular Identification of Potential Actinobacteria Based on 16S rRNA Gene

The phylogenetic analysis of K22S-63 was revealed through 16S rRNA sequencing analysis. The assembled sequence yielded the final contigs with a length of 1484 bp which showed 99.58 % similarity with *Peterkaempfera griseoplana* as determined using EzBioCloud database (Figure 6). The identification of 16S rRNA gene sequencing revealed that K22S-63 is belong to the genus and family *Peterkaempfera* and *Streptomycetaceae*, respectively.

Peterkaempfera griseoplana is a gram-positive bacteria species belongs to the newly genus *Peterkaempfera* (Madhaiyan et al. 2022). This species was previously classified under the genera *Streptomyces* (Backus et al. 1957) and *Streptadichiphilus* (Nouioui et al. 2019) based on genetic and phylogenomic information. *Peterkaempfera* gen. nov. is a novel genus revealed by Madhaiyan et al. (2022), which is classified in *Streptomycetes* group characterised by the production of branched mycelium and aerial hyphae. The study by Boeck et al. (1971) discover that, *Streptomyces griseoplana* can produce the bioactive com-

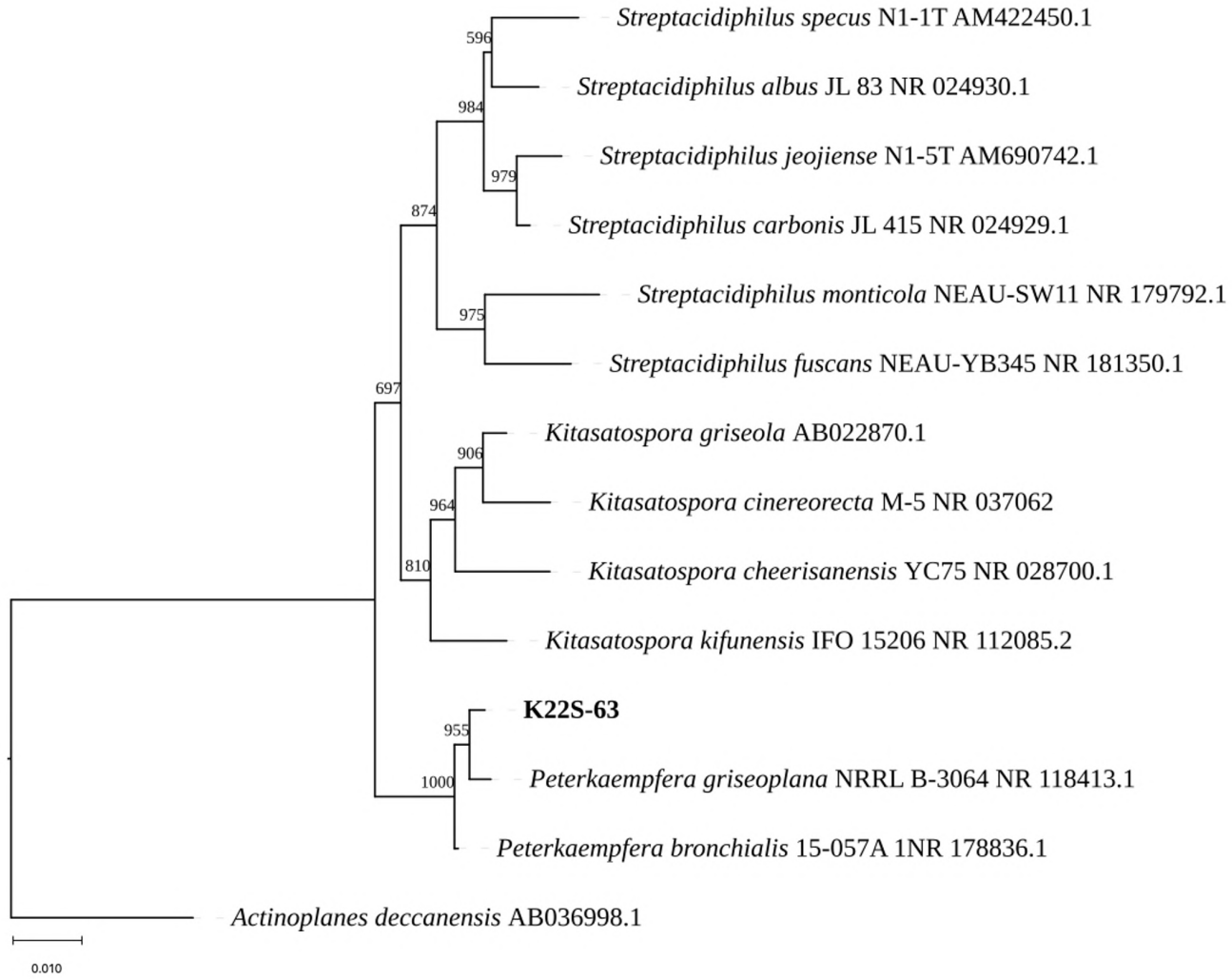

Figure 6. Phylogenetic tree of K22S-63 isolates based on 16S rRNA gene sequencing using Neighbor-Joining method with bootstrap analysis and Kimura-2-Model Parameter.

pound anticapsin, which is well known for the ability to produce a wide range of secondary metabolites, including antibiotics, antifungals and immunosuppressants (Caulier et al. 2019). Mohamed et al. (2020), reported that S1SHA1 strain had the antimicrobial activity against *Bacillus subtilis* NRRL B 543, *Staphylococcus aureus* ATCC 29213, *Escherichia coli* ATCC 25922 and *Candida albicans* MTCC183. Moreover, this strain is identified as *Streptomyces griseoplanus* based on 16S rRNA gene sequence, morphological, physiological and biochemical characteristic. Nouioui et al. (2018), stated that *S. griseoplanus* can act as a biocontrol agent against plant disease, as well as antifungal compound production including *diketopiperazine* dan surfactant. Extracellular extract of SAI-25, which identified as *S. griseoplanus*, have the potency as biosurfactant due to a broad range of insecticidal activity against *lepidopteran armigera*, *Spodoptera litura* (Fabricius), dan *Chilo partellus* (Swinhoe) in laboratory condition (Vijayabharathi et al. 2014).

CONCLUSIONS

This study unveiled the potential of actinobacteria isolated from the unspoiled protected forest in Indonesia. Out of 96 actinobacteria isolates, K22S-63 possess the highest phosphate solubilisation and *Indole-3-Acetic Acid* (IAA) production activities, with the values of 41.51 and 43.80 µg mL^{-1}, respectively. The detection of PGPR-encoding genes using PCR amplification was validates the potential of K22S-63 as biofertiliser candidate. Additionally, the presence of *PKS* and *NRPS* genes suggest the antimicrobial potency of K22S-

63 actinobacteria. This finding is particularly noteworthy given the limited research and exploration of the genus *Peterkaempfera*, which currently comprises only two recognised species. Further investigations including identification of agroactive compounds, genome mining and bioprospecting of K22S-63 for the PGPR traits, are remains essential to explore the potential of this isolate, which may extend beyond agriculture into broader field such as environmental sustainability and clinical biotechnology.

AUTHOR CONTRIBUTION

All authors are contributed equally to this work and reviewed the manuscript. I.S.H. conducted all research activities and wrote the manuscript. T.K.D. collected soil samples and provided reagents. S.W. designed the research framework and supervised the methodology. S.R. facilitated the provision of equipment and materials, and isolated the actinobacteria from soil sample. E.R. provided full supervision and mentorship throughout the research and manuscript process.

ACKNOWLEDGMENTS

The authors gratefully acknowledge the Prokaryotes Research Group, Research Centre for Biosystematics and Evolution BRIN as facilitator in this study. The authors also thankful to the Endowment Fund for Education Agency (LPDP) for providing financial support to the author (No. 202212111512274) during the research and Master's degree.

CONFLICT OF INTEREST

This research grant and funding from BRIN's Advanced Indonesian Innovation Research, LPDP Exploration and Expedition Program Number of B-1116/II.7.5/FR.06/3/2024 and B-949/III.5//FR.06.00/3/2024.

REFERENCES

Amri, M. et al., 2023. Isolation, Identification, and Characterization of Phosphate-Solubilizing Bacteria from Tunisian Soils. *Microorganisms*, 11, 783. doi: 10.3390/microorganisms11030783

Amri, M.F. et al., 2022. Alkaline phosphatase activity of plant growth-promoting actinomycetes and their genetic diversity based on the phoD gene. *HAYATI Journal of Biosciences*, 29, pp.360-369. doi: 10.4308/hjb.29.3.360-369

Amos, G.C.A. et al., 2015. Designing and Implementing an Assay for the Detection of Rare and Divergent NRPS and PKS Clones in European Antarctic and Cuban Soils. *PLoS ONE*, 10, e0138327. doi: 10.1371/journal.pone.0138327

Anwar, S., Ali, B. & Sajid, I., 2016. Screening of rhizospheric actinomycetes for various in-vitro and in-vivo plant growth promoting (PGP) traits and for agroactive compounds. *Frontiers in Microbiology*, 7, 1334. doi: 10.3389/fmicb.2016.01334

Backus, E.J., Tresner, H.D. & Campbell, T.H., 1957. The nucleocidin and alazopeptin producing organisms: Two new species of *Streptomyces*. *Antibiotics and Chemotherapy*, 7, pp.532–541.

Beatriz, G.G. et al., 2024. Comparative study between Salkowski reagent and chromatographic method for auxins quantification from bacterial production. *Frontiers in Plant Science*, 15, 1378079. doi: 10.3389/fpls.2024.1378079

Bhatti, A.A., Haq, S. & Bhat, R.A., 2017. Actinomycetes benefaction role in soil and plant health. *Microbial Pathogenesis*, 111, pp.458–467. doi: 10.1016/j.micpath.2017.09.036

Boeck, L.D., Christy, K. & Shah, R., 1971. Production of anticapsin by *Streptomyces griseoplanus*. *Applied Microbiology*, 21, pp.1075–1079. doi: 10.1128/am.21.6.1075-1079.1971

Boubekri, K. et al., 2021. The screening of potassium- and phosphate-solubilizing actinobacteria and the assessment of their ability to promote wheat growth parameters. *Microorganisms*, 9, 470. doi: 10.3390/microorganisms9030470

Caulier, S. et al., 2019. Overview of the antimicrobial compounds produced by *Bacillus* group. *Frontiers in Microbiology*, 10, 302. doi: 10.3389/fmicb.2019.00302

Etesami, H. & Glick, B.R., 2024. Bacterial indole-3-acetic acid: A key regulator for plant growth, plant-microbe interactions, and agricultural resilience. *Microbiological Research*, 281, 127602. doi: 10.1016/j.micres.2024.127602

Fatmawati, U. et al., 2019. Screening and characterization of Actinobacteria isolated from soybean rhizosphere for promoting plant growth. *Biodiversitas*, 20, pp.2970–2977. doi: 10.13057/biodiv/d201027

Fraser, T. et al., 2015. Soil bacterial phoD gene abundance and expression in response to applied phosphorus. *Soil Biology and Biochemistry*, 88, pp.137–147. doi: 10.1016/j.soilbio.2015.04.014

Gaby, J.C. & Buckley, D.H., 2017. The Use of Degenerate Primers in qPCR Analysis of Functional Genes Can Cause Dramatic Quantification Bias as Revealed by Investigation of nifH Primer Performance. *Microbial Ecology*, 74, pp.701-708. doi: 10.1007/s00248-017-0968-0.

Gangola, S., 2018. Impact assessment of pesticides on soil health through conventional and metagenomic approaches and their biodegradation using indigenous microbes. *Doctoral dissertation*, G.B. Pant University of Agriculture and Technology, Pantnagar, Uttarakhand.

Katz, L. & Baltz, R.H., 2016. Natural product discovery: past, present, and future. *Journal of Industrial Microbiology & Biotechnology*, 43, pp.155–176. doi: 10.1007/s10295-015-1723-5

Koirala, A. et al., 2025. Bacterial isolation from natural grassland on nitrogen-free agar yields many strains without nitrogenase. *Microorganisms*, 13, 96. doi: 10.3390/microorganisms13010096

Madhaiyan, M. et al., 2022. Genomic and phylogenomic insights into the family *Streptomycetaceae* lead to the proposal of six novel genera. *International Journal of Systematic and Evolutionary Microbiology*, 72(10). doi: 10.1099/ijsem.0.005570

Mahyarudin, M., Rusmana, I. & Lestari, Y., 2015. Metagenomic of Actinomycetes based on 16S rRNA and nifH genes in soil and roots of four Indonesian rice cultivars using PCR-DGGE. *HAYATI Journal of Biosciences*, 22, pp.113–121. doi: 10.1016/j.hjb.2015.10.001

Meenakshi, S. et al., 2024. Actinomycetes: Isolation, Cultivation and its Active Biomolecules. *Jouernal Pure Application Microbiology*, 18, pp.118-143. doi: 10.22207/JPAM.18.1.48

Mohamed, A.S. et al., 2020. A new trial for bioformation of antimicrobial agent controlling multi-drug resistance. *Azhar Journal of Pharmaceutical Sciences*, 62, pp.71–97. doi: 10.21608/ajps.2020.118377

Nouioui, I. et al., 2018. Genome-based taxonomic classification of the phylum Actinobacteria. *Frontiers in Microbiology*, 9, 2007. doi: 10.3389/fmicb.2018.02007

Nouioui, I. et al., 2019. Streptacidiphilus bronchialis sp. nov., a ciprofloxacin-resistant bacterium from a human clinical specimen; reclassification of Streptomyces griseoplanus as Streptacidiphilus griseoplanus comb. nov. and emended description of the genus Streptacidiphilus. *International Journal of Systematic and Evolutionary Microbiology*, 69, pp.1047-1056. doi: 10.1099/ijsem.0.003267

Nurkanto, A. & Agusta, A., 2015. Molecular identification and morpho-physiological characterization of Actinomycetes with antimicrobial properties. *Jurnal Biologi Indonesia*, 11(2), pp.195–203.

Olanrewaju, O. et al., 2021. Genome mining of three plant growth-promoting Bacillus species from maize rhizosphere. *Applied Biochemistry and Biotechnology*, 193, pp.3949–3969. doi: 10.1007/s12010-021-03660-3.

Passari, A.K. et al., 2016. Detection of biosynthetic gene and phytohormone production by endophytic Actinobacteria associated with *Solanum lycopersicum* and their plant-growth-promoting effect. *Research in Microbiology*, 167(8), pp.692–705. doi: 10.1016/j.resmic.2016.07.001.

Ragot, S. et al., 2017. Soil phoD and phoX alkaline phosphatase respond to multiple factors. *FEMS Microbiology Ecology*, 93(1), fiw212. doi: 10.1093/femsec/fiw212.

Ritung, S. et al., 2015. *Sumber Daya Lahan Pertanian Indonesia: Luas, Penyebaran, dan Potensi Ketersediaan*, Jakarta: IAARD Press, pp.9–10.

Suleiman, M.K. et al., 2019. Divulging diazotrophic bacterial community structure in Kuwait desert ecosystems and their N2-fixation potential. *PLoS ONE*, 14, e0220679. doi: 10.1371/journal.pone.0220679

Silva, G.C. et al., 2022. The potential use of Actinomycetes as microbial inoculants and biopesticides in agriculture. *Frontiers in Soil Science*, 2, 833181. doi: 10.3389/fsoil.2022.833181

Tang, J. et al., 2023. Biosynthetic pathways and functions of indole-3-acetic acid in microorganisms. *Microorganisms*, 11, 2077. doi: 10.3390/microorganisms 11082077

Vijayabharathi, R. et al., 2014. Biological activity of entomopathogenic actinomycetes against lepidopteran insects (Noctuidae: Lepidoptera). *Canadian Journal of Plant Science*, 94, pp.759–769. doi: 10.4141/CJPS2013-298

Walpola, B.C. & Hettiarachchi, R.H.A.N., 2020. Comparison of Qualitative and Quanititave Methods for Isolation of Phosphate Solubilizng Microorganism. *Vidyodaya Journal of Science*, 23, pp.14-22.

Widawati, S. et al., 2022. Characterization of plant growth promoting bacteria isolated from water in mangrove ecosystem. *IOP Conference Series: Earth and Environmental Science*, 976, 012039. doi: 10.1088/1755-1315/976/1/012039

Xu, N. et al., 2016. Effect of biochar additions to soil on nitrogen leaching, microbial biomass and bacterial community structure. *European Journal of Soil Biology*, 74, pp.1–8. doi: 10.1016/j.ejsobi.2016.02.004

Journal of Tropical Biodiversity and Biotechnology
Volume 10, Issue 04 (2025): jtbb19647
DOI: 10.22146/jtbb.19647

Research Article

First Record on Microbial Colonies in Freshwater Sponges in East Java, Indonesia, and Their Estimated Pollutant Degradation Genes

Edwin Setiawan[1], Michael Einstein Hermanto[2], Ahmad Yanuar[3], Catur Riani[4], Wuttichai Mhuanthong[5], Fitra Adi Prayogo[6], Dyah Wulandari[7]*, Anto Budiharjo[8,9]*, Laurensius M. Jackie[10]

1)Department of Biology, Institut Teknologi Sepuluh Nopember, Kampus ITS Sukolilo, Surabaya, Indonesia, 60111
2)Postgraduate Alumni of Biology Department, Institut Teknologi Sepuluh Nopember, Kampus ITS Sukolilo, Surabaya, Indonesia, 60111
3)PT. Milieu Elang Abadi, Pondok Wage Indah II Waru, Sidoarjo 61257, Indonesia
4)School of Pharmacy, Institut Teknologi Bandung, Jl. Ganesa No.10 Bandung, Indonesia, 40132
5)National Center for Genetic Engineering and Biotechnology (BIOTEC) | BioTec. Bioresources Technology Unit, Thailand
6)Biomedical Sciences Study Program, Karya Husada University, Jl. R. Kompol Soekanto No.46, Semarang, Indonesia, 50276
7)Food Technology Department, Faculty of Agricultural Technology, Soegijapranata Catholic University (SCU), UNIKA Semarang, Indonesia, 50219
8)Molecular and Applied Microbiology Laboratory, Central Laboratory of Research and Service, Diponegoro University, Jl. Prof. Sudharto SH, Semarang, Indonesia, 58275
9)Biotechnology Study Program, Faculty of Science and Mathematics, Diponegoro University, Jl. Prof. Soedarto, SH, Semarang, Indonesia, 50275
10) Department of Biology, Faculty of Science and Mathematics, Diponegoro University, Jl. Prof. Soedarto, SH, Semarang, Indonesia, 50275
* Corresponding author, email: dyahwulandari@unika.ac.id ; anto.budiharjo@live.undip.ac.id

Keywords:
East Java Indonesia
Eunapius carteri
Oncosclera asiatica
Freshwater sponges
Microbial colonies
Submitted:
30 January 2025
Accepted:
28 May 2025
Published:
24 October 2025
Editors:
Miftahul Ilmi
Tanti Agustina

ABSTRACT

Sponges are known to harbor diverse and abundant microbial colonies. Nevertheless, studies on the diversity and abundance of microbial colonies in freshwater sponges have not been as extensive as those of marine sponges. This study investigates the microbial colonies of two freshwater sponge species, *Eunapius carteri* and *Oncosclera asiatica*, from the Kaliporong River in Indonesia. High microbial diversity was observed, with *E. carteri* harboring over 1,400 unique microbial species (Operational Taxonomic Units or OTUs) and *O. asiatica* hosting over 400. Proteobacteria were the dominant bacterial group in both sponges, comprising over 90 % of *O. asiatica* and over 50 % in *E. carteri* colonies. Functional profiling revealed a high potential for xenobiotic degradation in both sponge species, particularly through pathways involving Cytochrome P450 and the degradation of benzoate, caprolactam, and aminobenzoate. *O. asiatica* shows more of these degradation pathways than *E. carteri*. For example, benzoate degradation, involving over 60 genes or enzymes, was more pervasive in *O. asiatica* (5.81 %) than in *E. carteri* (5.03 %). These findings highlight the significant role of freshwater sponges in supporting diverse microbial populations with potential for bioremediation, particularly in polluted environments like the Kaliporong River. Further research is needed to understand the specific functions of these microbial colonies in freshwater sponges and their impact on the ecosystem.

How to cite:
Setiawan, E. et al., 2025. First Record on Microbial Colonies in Freshwater Sponges in East Java, Indonesia, and Their Estimated Pollutant Degradation Genes. *Journal of Tropical Biodiversity and Biotechnology*, 10(4), jtbb19647. doi: 10.22146/jtbb.19647

INTRODUCTION

Sponges are mostly found in the marine ecosystem, inhabiting both shallow and deep-sea environments. Notably, tropical regions, particularly Indonesian waters, are considered biodiversity hotspots for sponge exploration, surpassing sub-tropical and polar regions in species richness (Putra et al. 2023). According to the World Porifera Database (WPD, 9,490 sponge species have been identified to date, with estimates suggesting the actual number may surpass 20,000 due to many species remaining unidentified, cryptic, or difficult to classify (de Voogd et al. 2024). Research on sponges has gained momentum over the past two decades, partly because sponges represent the earliest branch of the animal lineage (Animalia) and exhibit a simple level of biological organization (Pisani et al. 2015; Adamska 2016; Feuda et al. 2017). Therefore, sponges are suitable for studying animal evolution and the origin of multicellular life. Sponges also possess an important role in ecology, especially in marine ecosystem. In addition to support coral reef survival, they serve as a bioeroder for coral restoration and recycles chemical elements (Pawlik & McMurray 2020). They can also serve as an alternative source of biochemical or biopharmaceutical compound (Rajendran 2016; see detail in Varijakzhan et al. 2021) as they harbor symbiotic organisms such as microbes.

Microbes are known as a diet component of sponges but many extracellular microbes also inhabit sponge tissues, living as symbiotic bacteria. According to the symbiotic relationships, sponges are categorized in two groups: High Microbial Abundance (HMA) and Low Microbial Abundance (LMA) sponges (Gloeckner et al. 2014; Moitinho-Silva et al. 2017). The difference between these two groups is that symbionts assist in the nourishment. HMA sponges have smaller filtering structures but process large volumes of water, while LMA sponges possess larger filtering organs (Poppell et al. 2014) as they have less symbiotic microbes. LMA sponges invest more energy in developing feeding structures since their nutrition needs are less supported by microbial symbionts. Meanwhile, HMA sponges receive substantial nutritional support from their abundant microbial symbionts and, as a result, do not require large filter-feeding structures. Proteobacteria, Poribacteria and Actinobacteria are well-known symbiotic microbes commonly found in sponges. These microorganisms are known to dominate in marine sponges, whereas freshwater sponges remain comparatively understudied.

Freshwater sponges are classified as a minor group of sponges that inhabit freshwater ecosystem and possess unique characters. A key feature of freshwater sponges is their ability to survive fluctuating or extreme environmental conditions, such as drought, and to disperse over long distances. This resilience is due to their production of gemmules—specialized asexual reproductive structures (see detail in Manconi & Pronzato 2016). Ecologically, freshwater sponges link energetic pathway between pelagic and benthic community in the freshwater ecosystem by hosting zoo-chlorella and serving as prey for spongivorous insects (e.g., Hall et al. 2021; Ruengsawang et al. 2022). Studies on microbes, especially bacteria group in freshwater sponges not as extensive as those on marine sponges. Similarly, knowledge of microbial symbionts in freshwater sponges remains limited to a few bacteria groups (Keller-Costa et al. 2014). The microbial symbionts in freshwater sponges are not as diverse as marine sponges (see review in Lo Giudice & Rizzo 2024; Setiawan et al. 2024). However, after utilization of next generation sequencing (NGS) on symbiotic bacteria diversity, freshwater sponges also harbor a comparable number of microbes with marine sponges; for example, in India, it is discovered that Firmicutes, Proteobacteria, Cyanobacteria and Actinobacteria were the most abundant groups of freshwater sponges (Gaikwad et al. 2016). The presence of Actinobacteria suggests that freshwater sponges also hold potential for the discovery of novel bioactive compounds.

There has not any study yet on freshwater sponges in Indonesia in terms of microbial diversity. For this reason, we aim to compare and explore community symbiotic bacteria from two well-identified freshwater sponges in East Java Indonesia namely as *Eunapius carteri* (Bowerbank, 1863) and *Oncosclera asiatica* (Manconi & Ruengsawang, 2012) that are categorized under order Spongillida (Manconi & Pronzato, 2002) based on profiling of 16s rRNA gene utilizing Illumina Novaseq platform. *E carteri* is a, globular sponge that attaches to hard substrates in muddy environments, which has a flat, encrusting form and adheres to rocky substrates in river systems such as Kaliporong, near Surabaya city in East Java Province Indonesia (Setiawan et al. 2023).

MATERIALS AND METHODS

Materials

For microbiome isolation, DNA extraction buffer was made using Tris base (Himedia, Mumbai, India), EDTA (Biorad, California, US), sodium phosphate (Merck, Darmstadt, Germany), sodium chloride (Himedia, Mumbai, India), CTAB (Himedia, Mumbai, India), and proteinase K (Intron, South Korea). Sodium dodecyl sulphate (SDS), chloroform, isoamyl alcohol, isopropanol, ethanol, and distilled water were used for DNA extraction. MO-BIO PowerClean® DNA Clean-Up Kits (Qiagen, Germany) was used to purify and Qubit dsDNA HS Assay Kit (Thermo Fisher Scientific, US) to quantify DNA extracts. Agarose gel and sodium borate (SB) buffer were used to assess DNA quality.

As for PCR, Phusion® High-Fidelity PCR Master Mix (Biolabs, New England) were used to amplify the DNA using 515F (5'-GTGCCAGCMGCCGCGGTAA) and 806R (5'-GGACTACHVHHHTWTCTAAT) primer. Agarose, Tris Acetate EDTA (TAE), florosafe DNA stain (1st BASE), 1 Kb Plus DNA ladder (Invitrogen, Thermo Fisher Scientific, US), and DNA loading dye (Thermo Fisher Scientific, US) were used for electrophoresis. Moreover, Mo-Bio UltraClean PCR Clean-Up Kit (Qiagen, Germany) was used for amplicon pool cleaning.

Methods

Sample Collection

Samples of *E. carteri* (EC) (Figure 1B) and *O. asiatica* (SS) (Figure 1C) were collected freshly (in triplicates and coded as EC1. EC2, EC3; SS1, SS2, SS3) from the Kaliporong in Surabaya, East Java (Figure 1A). Sponges were collected during the river's lowest tide (approximately 20–30 cm depth) using hand collection. The six specimens were immediately placed in sterile containers and temporarily frozen prior to microbiome extraction.

Microbiome Isolation

Microbiome was extracted using the SDS-based DNA extraction method (Vesty et al. 2017). A total of 0.25 g of frozen sponges were homogenized by mechanical grinding with the addition of 500 µL of DNA extraction buffer [100 mM Tris-HCl (pH 8.0), 100 mM sodium EDTA (pH 8.0), 100 mM sodium phosphate (pH 8.0), 1.5 M NaCl, 1 % (wv^{-1} cetyltrimethylammonium bromide (CTAB)), and 20 µL of proteinase K (10 mg ml^{-1})] (Vesty et al. 2017). Furthermore, each sample of sponges (EC1, EC2, EC3; SS1, SS2, SS3) was moved to microtubes and shaken at 225 rpm for 30 min at 37 °C temperature. SDS was added to each microtube, then incubated at 65 °C for 2 h with gentle inverting every 20 min.

Samples were then centrifuged at 6000×g for 10 min. The supernatants were collected in the new microtubes and added an equal volume of chloroform : isoamyl alcohol (24 : 1, v v^{-1}). The mixtures were centrifuged at

6000×g for 5min and then the upper phase was recovered in the new microtubes. Isopropanol was added to 60 % of the total mixture volume. The mixture was then incubated at room temperature for 1 hour and subsequently centrifuged at 14,000×g for 20 min. The DNA pellet was washed using 70 % (v v^{-1}) cold ethanol and resuspended in distilled water. Finally, all DNA extracts were purified using MO-BIO PowerClean® DNA Clean-Up Kits and quantified using Qubit dsDNA HS Assay Kit, run on 1 % agarose gel in sodium borate buffer to check the quality of DNA.

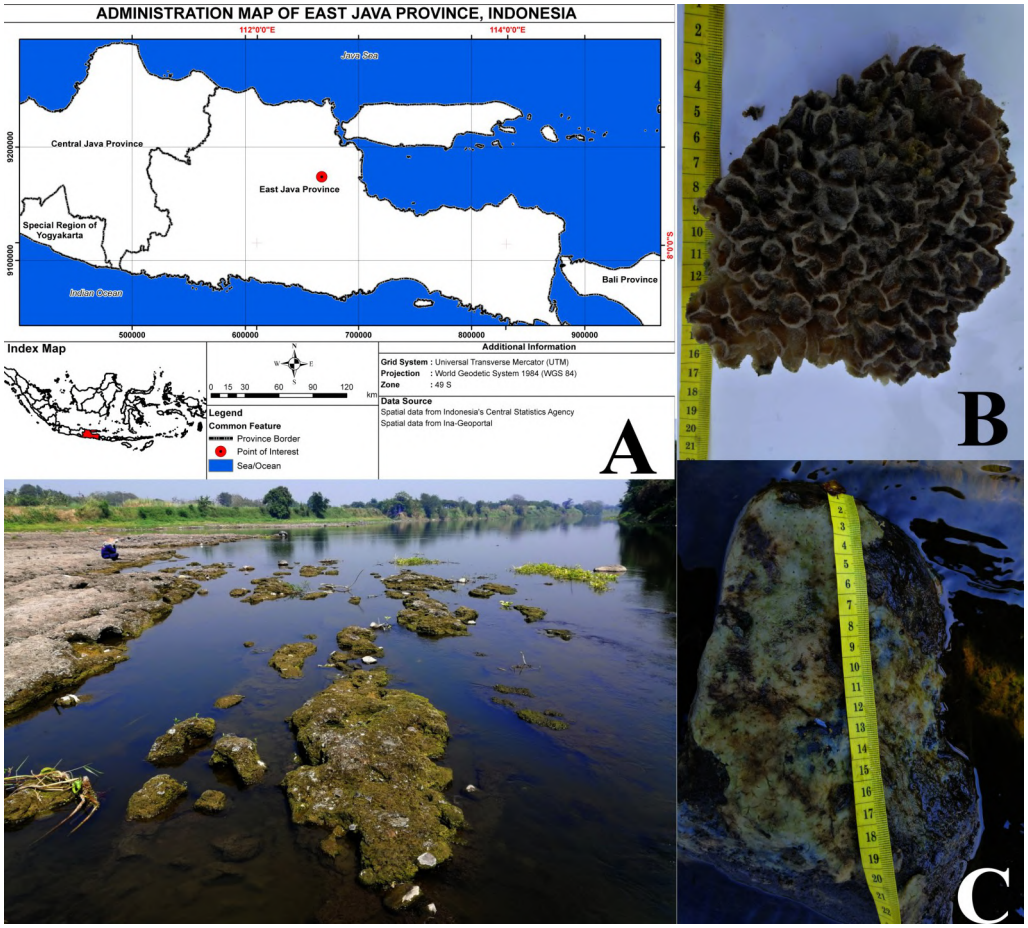

Figure 1. Sampling site and freshwater sponges: a. *Eunapius carteri*; b. *Oncosclera asiatica*.

16S rRNA Sequencing

16S rRNA rRNA gene region (V4) were amplified using specific primers 515F (5'-GTGCCAGCMGCCGCGGTAA) and 806R (5'-GGACTACHVHHHTWTCTAAT) with the barcode (Walters et al. 2016). All PCR reactions were carried out with Phusion® High-Fidelity PCR Master Mix (New England Biolabs). The cycling conditions of the PCR program were as follows: 3 min at 94 °C for activation, followed by 35 cycles of 94 °C for 45 s for denaturation, 50 °C for 60 s for annealing, and 72 °C for 90 s for elongation, with a final elongation cycle of 72 °C for 10 min and hold at 4 °C. The PCR amplicons were mixed in the same volume of 1X loading buffer (contained SYB green) and examined by 2 % TAE agarose gel electrophoresis run at 100 V for 30 min. Expected band size for 515F-806R is 400-450 bp. Low-biomass samples may yield faint or no visible bands. Amplicon with bright main strips were chosen for further experiments. The amplicon pool was cleaned using Mo-Bio UltraClean PCR Clean-Up Kit and the concentration was measured A260/A280 ratio should be between 1.8-2.0 for the best results of final pool. For Sequencing of the 16S rRNA amplicon was performed by the Illumina HiSeq platform to produce 250 bp paired end reads.

Data Analysis

First step, paired-end reads were merged using FLASH (V1.2.7). Chimera sequences or artifacts were detected and removed using UCHIME (Edgar 2016) with the Gold referenced database. The overall processed were performed by Qiime (Version 1.7.0). OUT clustering was performed by Uparse software with 97 % similarity. Next, the representative sequence of each OTU was assigned for its taxonomy against the SILVA SSUrRNA database (Yilmaz et al. 2014) by RDP classifier (Wang & Cole 2024). OTUs abundances were normalized to the sequencing depth of the sample with the fewest reads. Subsequent analyses of alpha and beta diversity were conducted using the normalized data. To compare the microbial diversity between two sponges, alpha diversity indices including observed OTUs, Shannon diversity index, chao1 estimator, and PD whole tree were calculated. In addition, beta diversity analysis was performed to evaluate differences of samples in species complexity using both weighted and unweighted UniFrac methods.

Weighted UniFrac incorporates taxon abundances to highlight microbial shift by dominant taxa, whereas unweighted UniFrac relies on presence–absence to detect changes in rare lineages. Principal Coordinate Analysis (PCoA) has been performed from UniFrac distance matrix and visualized via ggplot2 package in R software. The Adonis test (using the Adonis function from the Vegan package) was conducted to statistically test the difference in microbial profiles between *Eunapius carteri* and *Oncosclera asiatica*. To expand the scope of our study, we performed the functional gene prediction from 16S rRNA data by Picrust (detail in PICRUSt2.pdf, Douglas et al. 2020). Moreover, The KEGG (Kyoto Encyclopedia of Genes and Genomes database) was used to analyze the biodegradation pathways that reflect on the predictive functional profiling.

RESULTS AND DISCUSSION

Results

Sequencing Results

We obtained in total 975,160 read ranging from 123,494 to 178,854 sequences from six samples. These consist of 503,072 reads from *E. carteri* ranging from 164,505 to 178,985 sequences (Sequence Read Archive/ SRA accession number SRX15600599, SRX15600600, SRX15600601) and 472,088 reads from *O. asiatica* ranging from 123, 494 to 178, 854 sequences (Sequence Read Archive/ SRA accession number SRX15600602, SRX15600603, 15600604). After trimming in QC process for avoiding chimeras and singletons, 739,774 reads that consist of 372,610 sequences from *E. carteri* and 367,164 sequences from *O. asiatica* were yielded.

In addition to alpha diversity, we evaluated microbial community structure using Adonis (PERMANOVA) and Welch t-tests. The Adonis Unweighted UniFrac results yielded a pseudo-F value of 2.039 with a p-value of 0.107, while Adonis Weighted UniFrac analysis resulted in a pseudo-F value of 3.052 and a p-value of 0.088. Although these p-values were above the typical threshold of statistical significance ($p < 0.05$), they suggest a trend toward distinct colony compositions between the two sponge species, particularly when microbial abundance is taken into account.

Welch's t-tests further supported differences in colony richness and structure. Statistically significant differences were observed in Shannon diversity ($p = 0.019$), observed OTUs ($p = 0.040$), Chao1 richness estimator ($p = 0.042$), and Faith's phylogenetic diversity (PD Whole Tree; $p = 0.050$). These results indicate that *E. carteri* samples consistently host a more phylogenetically rich and diverse bacterial colonies than *O. asiatica*. While beta diversity metrics indicate compositional differences, these alpha diversity tests underscore the significantly richer microbial diversity in the *E. carteri* sample.

Alpha and Beta Diversity of Microbial Communities

Three samples of *E. carteri* showed values of 1138; 1030; and 624 OTUs, in contrast to the *O. asiatica* samples, which showed significantly lower values of 257; 221; and 470 OTUs—approximately one-third as many. Similarly, Shannon diversity index values for *E. carteri* were higher at 3.82, 3.51, and 4.12 compared to *O. asiatica*, which were 0.49, 0.42, and 1.93. The higher microbial diversity of *E. carteri* was further supported by chao1 richness estimates at 1210, 1114, and 700, compared to *O. asiatica*, which showed lower values of 298, 353, and 536. Similarly, PD whole tree values were higher in *E. carteri* (118, 89, and 76) than on *O. asiatica* (52, 43, and 41). Although the average alpha diversity indices of *E. carteri* are higher than those of *O. asiatica*, the results from the Welch's t-test are not significantly different due to the low number of replicates (Figure 2).

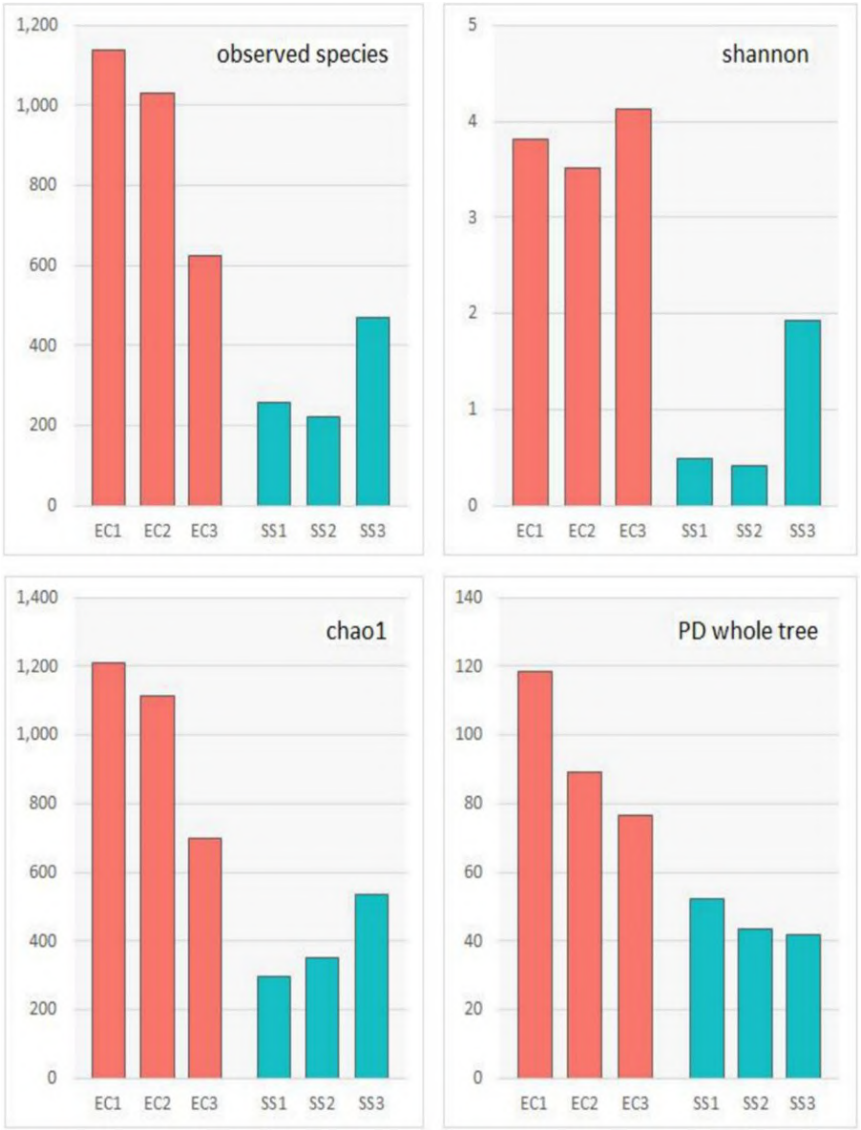

Figure 2. Comparison of alpha diversity index across samples. Four alpha diversity metrics; (A) observed OTUs, (B) Shannon diversity index, (C) Chao1 richness estimator, and (D) Faith's phylogenetic diversity (PD whole tree), computed for each of six samples (EC1–EC3 and SS1–SS3), with the x-axis representing individual sample IDs, and the y-axis showing the diversity value for each metric.

The microbiome composition of symbiont from *O. asiatica* samples is more uniform than *E.carteri*. This was further observed by beta diversity displayed on principal coordinate analysis (PCoA) plot (Figure 3). The assessment of species richness using rarefaction plot, based on the sampling results, indicates sufficient sampling depth. This is evidenced by the sampled sequenc-

es from *O. asiatica*, which show greater saturation compared to *E. carteri* (Figure 4). Moreover, unique OTUs from *E. carteri* are higher than *O. asiatica* samples, reflecting more diverse and unique symbionts of *E. carteri* than O. *asiatica* (Figure 5, Table 1).

The Principal Coordinates Analysis (PCoA) plots illustrate the beta diversity of microbial colonies in freshwater sponges *E. carteri* and *O. asiatica.* PCoA plot based on the weighted UniFrac distances (left) indicates clear separation between the microbial communities of SS and EC in the first principal component (PC1), which explains 80.43 % of the variation. Meanwhile, PCoA plot based on the unweighted UniFrac distances (right), which consider only the presence or absence of taxa, also indicating distinct clustering between SS and EC groups along PC1, accounting for 35.39 % of the variation. Both plots demonstrate compositional differences between the microbial colonies in the two sponge groups observed in this study.

The assessment of species richness using rarefaction curves (Figure 4) confirmed the sufficient sequencing depth in both sponge species. However, the *E. carteri* samples showed steeper curves and a broader range of observed OTUs, indicating a richer and more diverse microbial community than *O. asiatica.* The plateauing of rarefaction curves across all samples indicates a mini-

Table 1. Number of detected OTU based on cleaned sequences among selected samples of freshwater sponges (EC= *E. carteri*; SS= *O. asiatica*) and the diversity indexes.

Summary of Sequencing Data and Alpha Diversity Index									
Sample ID	No. Raw Read	No. Cleaned Read	Observed Species	Shannon	Simpson	Chaol	ACE	Goods Coverage	PD Whole Tree
EC1	176.985	118.366	1.138	3,815	0.793	1.211	1.229	0.998	118,615
EC2	161.582	124.926	1.03	3,507	0.689	1.114	1.149	0.998	89,366
EC3	164.505	129.318	624	4,124	0.879	701	732	0.999	76,609
SS1	169.74	125.43	257	0,486	0.091	299	308	0.999	52,432
SS2	123.494	94.618	221	0,422	0.078	353	328	0.999	43,393
SS3	178.854	147.116	470	1,93	0.38	536	522	0.999	41,696

Adonis Unweighted Unifrac						
Group 1	**Group 2**	**Sample size**	**Permutations**	**pseudo-F**	**p-value**	**q-value**
EC	SS	6	999	2.038758189	0.107	0.107

Adonis Weighted Unifrac						
Group 1	**Group 2**	**Sample size**	**Permutations**	**pseudo-F**	**p-value**	**q-value**
EC	SS	6	999	3.051691559	0.088	0.088

Welch t-test result EC vs SS			
feature	**t_statistic**	**p_value**	**p_adj**
shannon	5.480285	0.01866	0.050368151
observed_OTUs	3.518411	0.040448	0.050368151
chao1	3.559903	0.041973	0.050368151
PD_whole_tree	3.808369	0.050478	0.050477551

mal gain in new OTUs with increasing sequencing depth, suggesting that most microbial diversity was adequately captured.

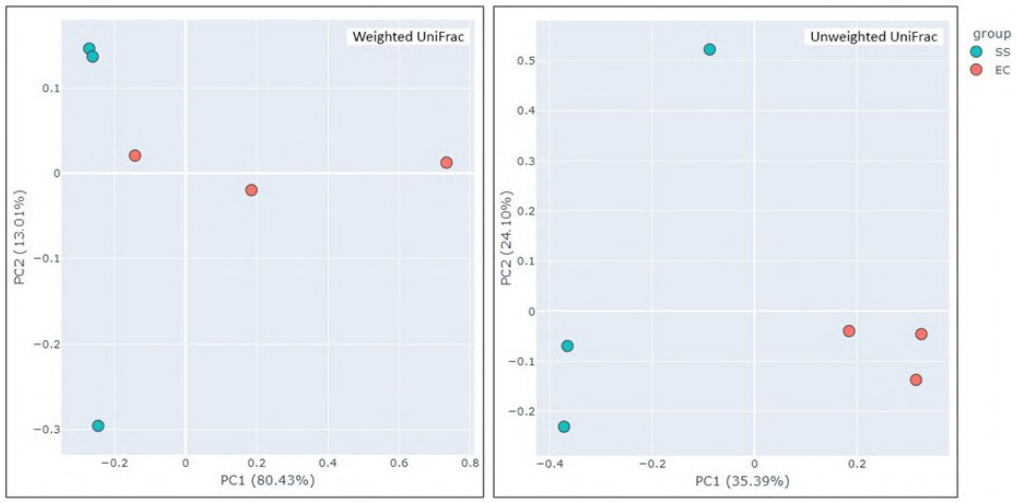

Figure 3. Beta Diversity Analysis Using Weighted and Unweighted UniFrac Metrics.

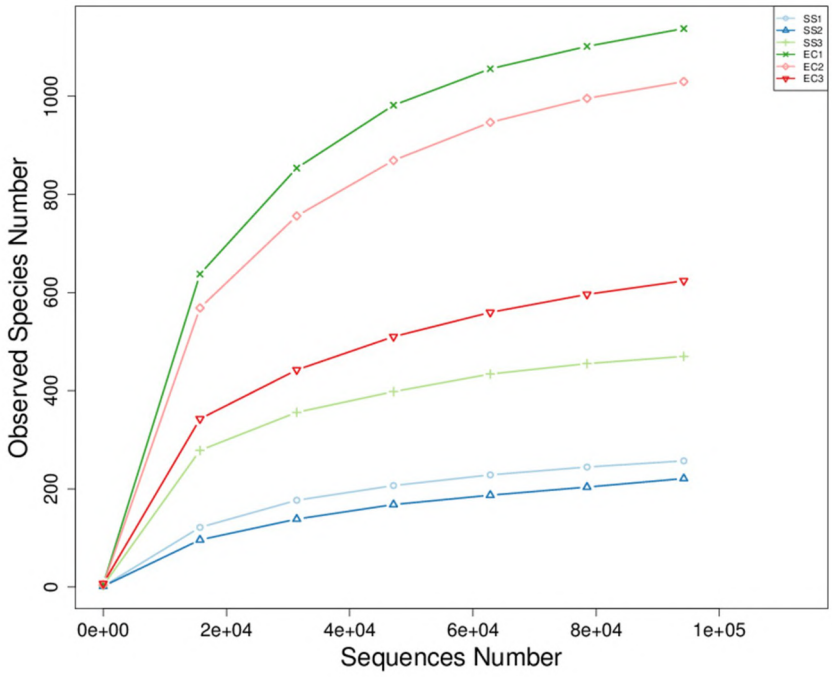

Figure 4. Rarefaction curves showing observed species richness of microbial colonies in *E. carteri* and *O. asiatica*.

Further, the Venn diagram (Figure 5) highlights the shared and unique in microbial colonies among the samples. *E. carteri* displayed more unique OTUs than *O. asiatica*, supporting earlier studies suggesting it harbors a more diverse and distinct microbiome. The shared OTUs between both sponge species likely represent a core microbial colony characteristic of the Kaliporong River environment, while the unique OTUs underline species-specific bacterial associations. These figures collectively reinforce the conclusion that *E. carteri* harbors a broader and more exclusive bacterial diversity than *O. asiatica*.

Our study revealed higher values of taxonomic richness of microbial colony, highlighting biogeographic patterns at the family/genus/species levels from two freshwater sponges *E. carteri* (Bowerbank, 1863) and *O. asiatica*

(Manconi & Ruengsawang, 2012) in Kaliporong river, Surabaya, East Java, Indonesia. Recent findings of previously undocumented freshwater sponge species and their associated microbial communities in Indonesia suggest that their biodiversity is still largely underexplored. Further investigations should explore the potential bioactive compounds produced by freshwater symbionts, which may contribute to the development of new antibiotics or antiviral agents.

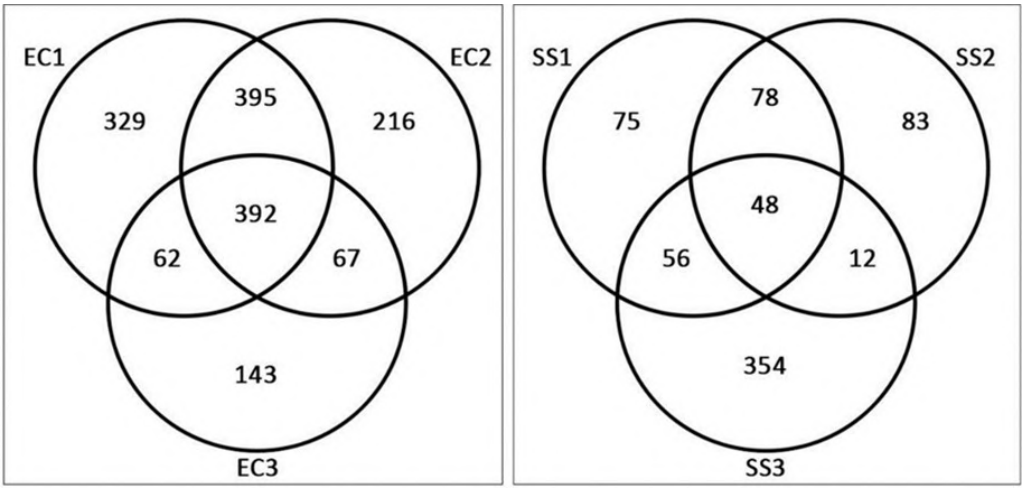

Figure 5. Venn diagram shows the number of shared and unique OTUs of microbial colonies in *E. carteri* and *O. asiatica.*

Bacterial Composition Profile (Phylum/Class and Genus)

We identified 28 bacteria phyla in the freshwater sponges under study with the majority being Proteobacteria phylum in both *E. carteri* (50 %) and *O. asiatica* (90 %). Although Proteobacteria dominated the symbiotic communities in both sponge species, each hosted a distinct bacterial phylum composition. In addition to Proteobacteria, Firmicutes, Bacteroidetes, and Actinobacteria were also detected in both species. Nevertheless, *E. carteri* harbors a larger population of Cyanobacteria and unknown bacteria group, whereas *O. asiatica* shows a higher relative abundance of Firmicutes and Bacteroidetes (Figure 6). This figure showed the comparison of bacterial profiles between EC and SS samples. Furthermore, Aeromonas, Pseudomonas, and unclassified genera were dominant in *E. carteri*, whereas *O. asiatica* exhibited a higher prevalence of Pseudomonas and Ralstonia (Figure 7).

Predictive Functional Profiling

Xenobiotic degradation and metabolism accounted for 0.96 of the total predicted functions in *E. carteri* and 1.12 % in O. asiatica, based on the 52 second-level pathway categories from the KEGG Orthology (KO) database (Figure 8). Given the large number of KOs associated with xenobiotic degradation and metabolism pathways in the KEGG database, the top ten KOs were selected for further analysis, including K01692, K00626, K01825, K00632, K01782, K00121, K00128, K01951, K00088, and K00799. The curation of these top KO numbers is related to major xenobiotic degradation and metabolism pathways, such as the pathway of xenobiotic and drug metabolism by cytochrome P450, degradation of benzoate, degradation of caprolactam, and degradation of aminobenzoate (Figure 9). Xenobiotic metabolism by cytochrome P450 had the highest relative abundance among the selected pathways, with at least seven associated genes or enzymes identified (E1.1.1.1, CBR1, frmA, ALDH3, GST, EPHX1, HPGDS). This is followed by drug metabolism by cytochrome P450 and by other enzymes. In general, the relative abundance of degradation pathways present in *E. carteri* samples was lower

than *O. asiatica* samples. Notably, benzoate degradation, another pathway with relatively high abundance, was represented at 5.03 % in *E. carteri* and 5.81 % in *O. asiatica*, involving at least 60 associated genes or enzymes.

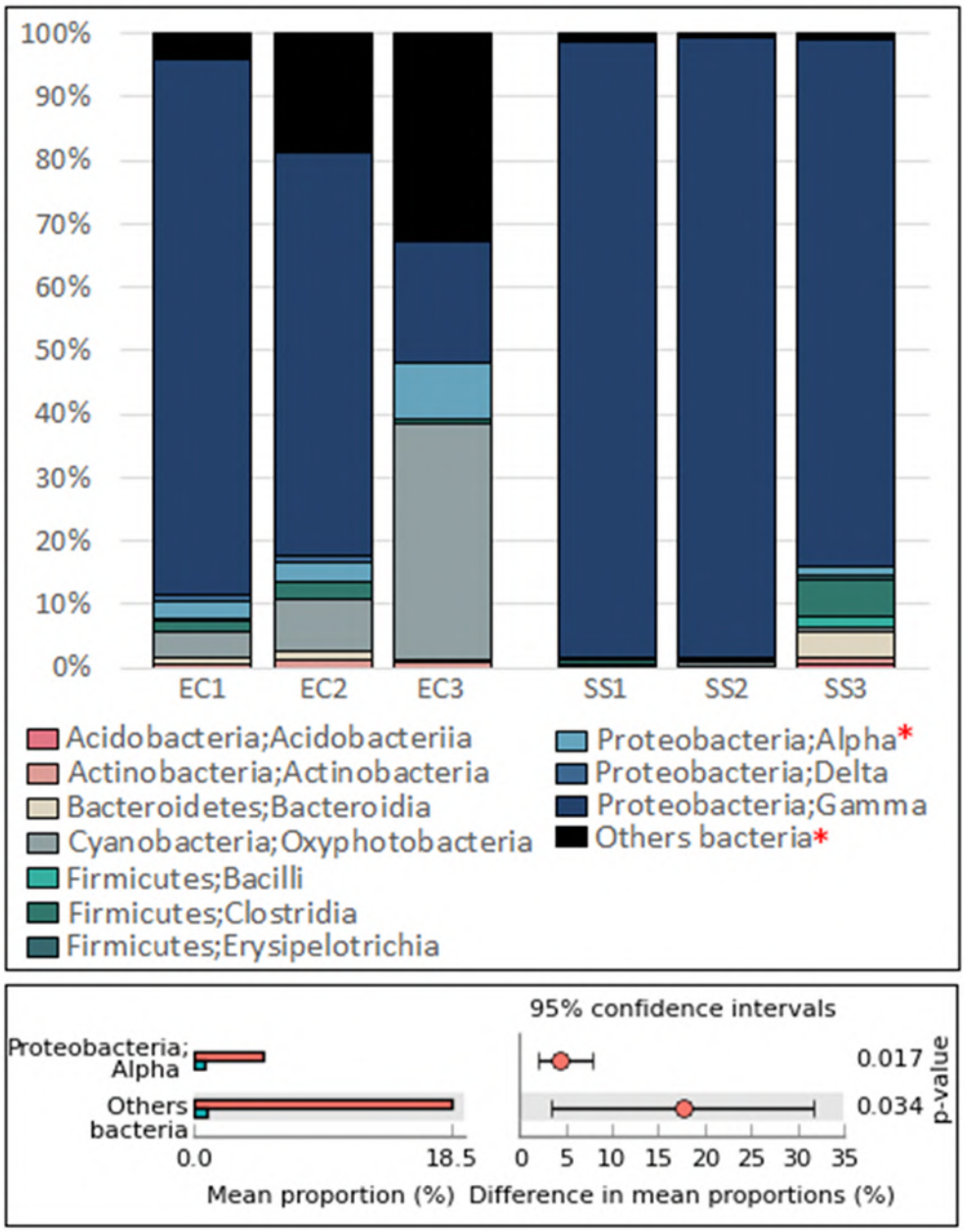

Figure 6. Comparison of relative abundance phyla in *E. carteri* and *O. asiatica*.

Discussion

The estimated bacterial symbiont diversity in our *E. carteri* samples, with 996 observed OTUs, aligns closely with findings from *E. carteri* in India, which reported 980 OTUs (Gaikwad et al. 2016). However, different composition of symbiotic bacteria in those two different locations were detected, since in India, Firmicutes constituted the highest proportion, followed by Cyanobacteria and Actinobacteria. By contrats, our *E. carteri* harbors the largest composition of Proteobacteria, followed by Cyanobacteria and unidentified bacteria. This difference may be attributed to variations in habitat or environmental conditions that influence the composition of symbiotic bacteria (Weigel & Erwin 2016; see detail in Hill & Sacristán-Soriano 2017; Ferreira et al. 2020). Furthermore, the approximately one-third lower OTU count in *O. asiatica* (335) might be due to differences in sponge morphology. *E. carteri* exhibits more encrusting, lobate, and arborescent forms, whereas *O. asiatica* has a massive,

thinner structure and exclusively attaches to rock substrates. Consistent with the influence of morphology, other Spongillids with encrusting and lobate forms have also been shown to harbor significantly higher OTU diversity of symbiotic bacteria in *Corvospongilla lapido* (2900 OTU) (Gaikwad et al. 2016) and *Trochospongilla pennsylvanica 2* (approximately 1800 OTU) (Laport et al. 2019). Moreover, gradual colonization, functional redundancy of symbiotic microbe and more specifically, water exposure on host, also influence microbe diversity and its OTU number (Webster & Thomas 2016), as sponges obtain nourishment by filtering water from the surroundings.

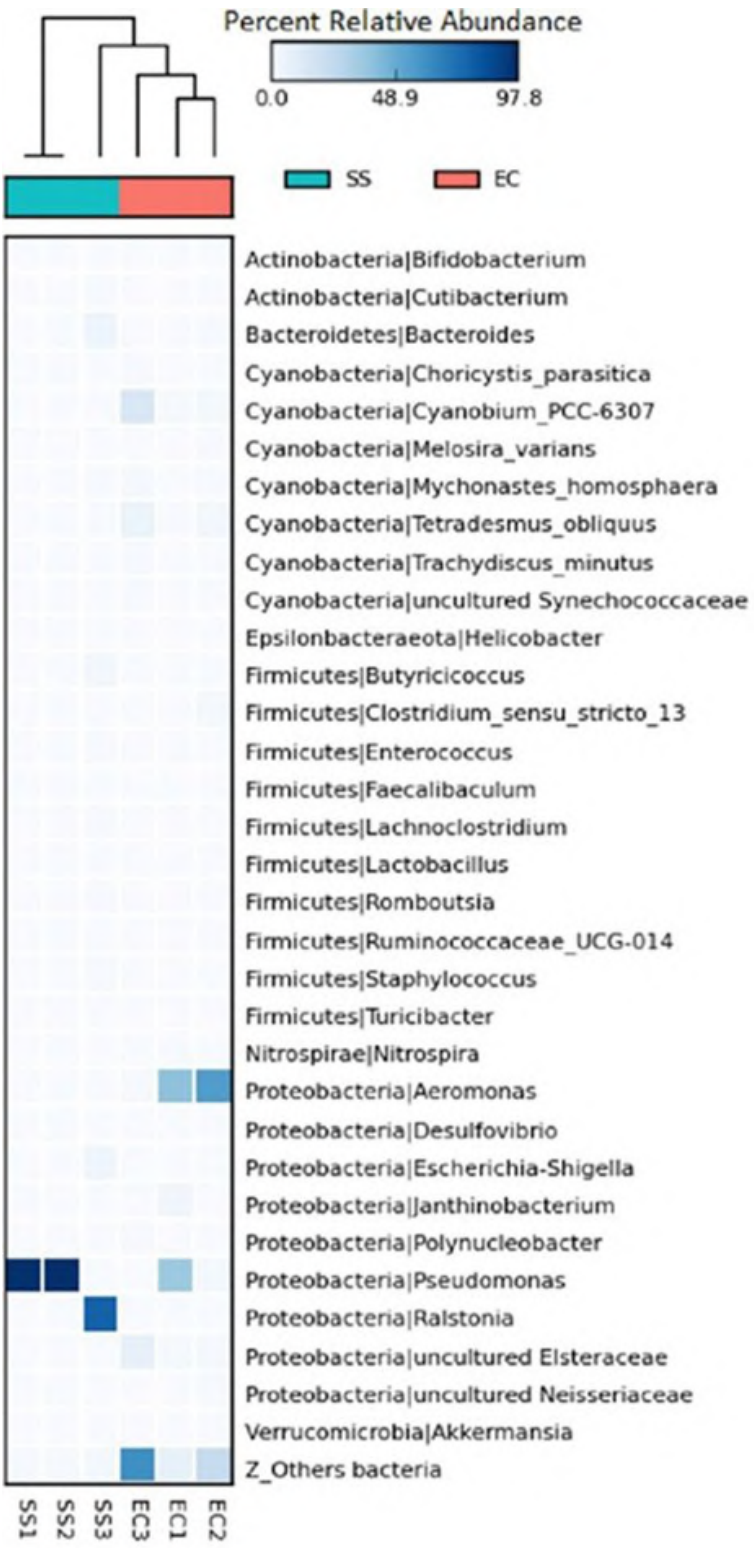

Figure 7. Heatmap of relative abundance of microbial profile at the genus-level. The heatmap shows the percent relative abundance of bacterial genera across six samples, similarly clustered as shown by the dendrogram.

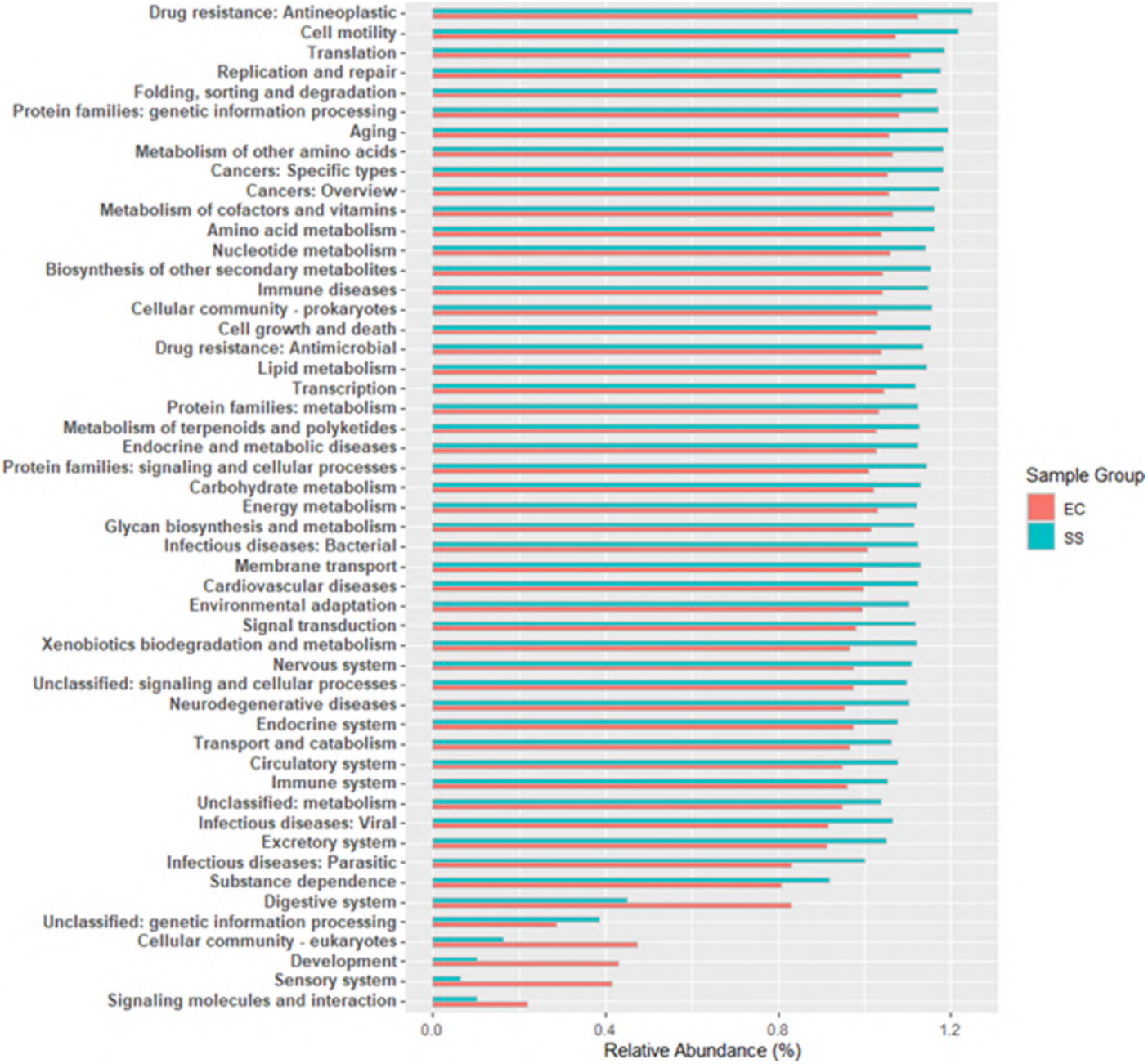

Figure 8. Predicted second-level pathways in KEGG for each group of *E. carteri* and *O. asiatica*.

Domination of gammaproteo bacterial on both of our species aligns with findings on symbionts of the spongillid *Ephydatia fluviatilis* (Keller-Costa et al. 2014). Gammaproteo bacteria has been recognized as one of the major components of marine, intertidal and freshwater environment (Francis et al. 2021). Besides possessing a vital role on carbon, nitrogen, and sulfur cycling (Nikrad et al. 2014; Baker et al. 2015), this microbial classis is also known for its medicinal, industrial, and environmental properties. The biggest genus of symbiont *O. asiatica* (Pseudomonas) plays an important role in antibiotic production, waste degradation, enzyme, and pigment and biosurfactant production, i.e., *P. aeruginosa* (Anayo et al. 2019). Likewise, the second biggest symbiont of *O. asiatica*, genus Ralstonia also plays an important role in biomaterial production like acrylamide (Aisami & Gusmanizar 2019) and poly [hydroxyalkanoate] (Priyadarshi et al. 2014).

In contrast to *O. asiatica*, the genus Aeromonas from gammaproteobacterial and unidentified bacterial phylum dominates *E. carteri*. Aeromonas is known for its important role in regulating the population of copepods (Gugliandolo et al. 2008; Chaix et al. 2017), which is an important food source

on freshwater food chain and ecosystem. Photosynthetic bacteria from Phylum Cyanobacteria represent the third major group of symbionts in our *E. carteri*, supporting previous findings that identified that Cyanobacteria as major components in *E. carteri* in India (Gaikwad et al. 2016). In addition to their marine counterparts, freshwater sponges also rely on Cyanobacteria for nitrogen fixation and protection against UV radiations (Kenny et al. 2019; Hall et al. 2021).

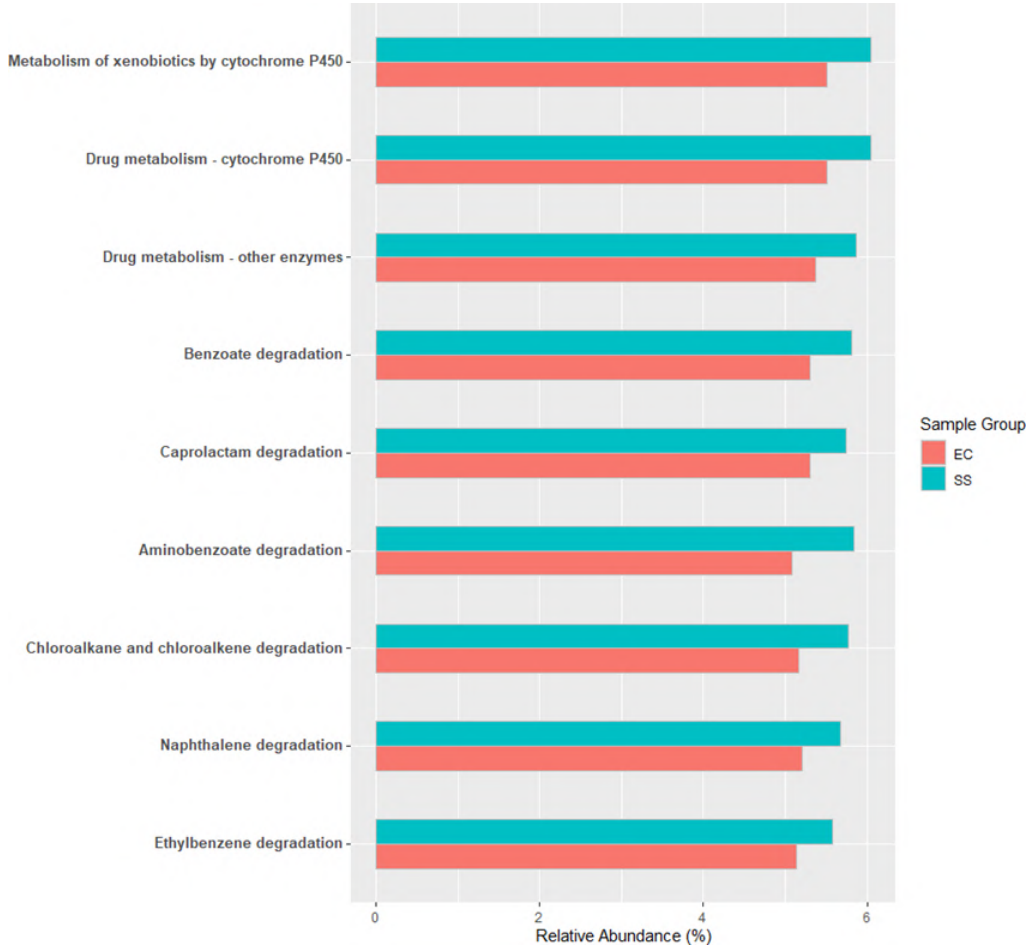

Figure 9. Predicted xenobiotic degradation pathways in KEGG for each group of *E. carteri* and *O. asiatica*.

Functional prediction analysis was performed to investigate the functional pathways in different freshwater sponges. Among the predicted functions, xenobiotic and drug metabolism via cytochrome P450 showed the highest relative abundance in both *O. asiatica* and *E. carteri* samples. Cytochrome P450 enzymes are known to play key roles in xenobiotic degradation and are also linked to major secondary metabolite pathways (Senate et al. 2019; Kunakom et al. 2023). Although *O. asiatica* has lower diversity than *E. carteri*, *O. asiatica* has a higher xenobiotic degradation capability due to the high abundance of the genus Pseudomonas and other contributing genus. Many bacteria do not contain cytochrome P450 (Kelly & Kelly 2013). However, there are some groups of bacteria such as *Pseudomonas putida* that can perform oxidative dehalogenation with a P450CAM intermediation (Greule et al. 2018). Other Pseudomonas, such as *P. aeruginosa* CYP168A1 was characterized as a fatty acid hydroxylase (Tooker et al. 2022). *Ralstonia metallidurans* also reported with one-component P450 system, expressing phthalate dioxygenase reductase (Alviz-Gazitua et al. 2022). The presence of GST was related in the degradation of xenobiotics, carcinogens, antioxidant, and peroxides (Zhang et al. 2021).

Cyanobacteria have been reported to contain a high concentration of

intracellular GSH (Narainsamy et al. 2016; Allocati et al. 2018; Rai et al. 2021; Cassier-Chauvat et al. 2023). This might explain the high amount of P450 degradation system in *E. carteri*. In addition, benzoate degradation was another pathway with relatively high abundance. Benzoate is an aromatic ester, an intermediate in the biodegradation of complex aromatic compounds such as toluene; and a precursor of catechol and protocatechuate, and also commonly used as model compounds to study bacterial metabolism of aromatic compounds (Muñoz-García et al. 2019; Yadav et al. 2021). Prediction results show that key genes such as benA-xylX, benB-xylY, benC-xylZ, and benD-xylL convert benzoate to catechol. Other genes, such as catA, catB, catC, pcaB, pcaC pcaD, pcaI, and pcaF confirm the degradation of benzoate through the catechol-ortho cleavage pathway (Yadav et al. 2021).

Several studies (Nanjani et al. 2022) have reported that Pseudomonas, specifically *P. aeruginosa* D6 and *P. putida* P8 can degrade textile dyes from the benzoate group via both ortho- and meta-cleavage pathways. Aminobenzoate degradation is also closely related to benzoate degradation. The abmG and antA genes detected indicate the presence of both aerobic and anaerobic degradation of 2- Aminobenzoate (anthranilate). The antABC gene encodes an anthranilate dioxygenase enzyme that converts anthranilate to catechol, which is further degraded via ortho cleavage or meta cleavage pathways. The abmG gene encodes 2-Aminobenzoate-CoA ligase that converts 2-Aminobenzoate to 2-Amino-benzoyl-CoA. 2-Amino-benzoyl-CoA is converted into Benzoyl-CoA, which ultimately enters the benzoate degradation pathway (Arora 2015). The enrichment of xenobiotic degradation pathways, particularly in O. asiatica, suggests that this species and its microbiome may contribute significantly to detoxifying polluted river systems. This functional potential aligns with the detection of abundant cytochrome P450-related pathways and benzoate degradation genes. Taken together, these findings highlight the promise of *O. asiatica* as a valuable natural resource for freshwater bioremediation, especially in environments facing anthropogenic contamination.

Our study revealed higher values of taxonomic richness of microbial community, highlighting biogeographic patterns at the family/genus/species levels from two freshwater sponges *E. carteri* (Bowerbank, 1863) and *O. asiatica* (Manconi & Ruengsawang, 2012) from Kaliporong river in near Surabaya, East Java province Indonesia.

This research has shown that biodiversity of freshwater sponges has been underexplored, as indicated in this new record of species of freshwater sponges and their microbial community. Further investigations should explore the potential bioactive compound from the freshwater symbionts, which could contribute to the fulfilment of the demand for antibiotics or antiviral agents.

CONCLUSION

Our analysis of 16S rRNA gene sequences enabled the identification of major taxonomic groups and the estimation of bacterial symbiont diversity associated with selected freshwater sponges *E. carteri* and *O. asiatica*. These data enhance our knowledge of freshwater sponge microbial colonies in freshwater sponges, which are reliable indicators of the state of their aquatic environment.

AUTHORS CONTRIBUTION

E.S., C.R., A.B. designed the research. A.Y., L.M.J., F.P. collected the data and did the Laboratory works. W.M. analyzed the bioinformatic data. D.W., E.S., A.B. wrote the manuscript and supervised all the process.

ACKNOWLEDGMENTS

This study was funded by the Directorate of Research and Community Service (DPRM) of Institut Teknologi Sepuluh Nopember, Surabaya; Universitas Diponegoro, Semarang; and Institut Teknologi Bandung, Bandung; for the consortium grant schemed as Program Penelitian Kolaborasi Indonesia (PPKI) PTNBH 2021 number 1331/PKS/ITS/2021, 117-06/UN7.6.1/PP/2021, and 042/IT1.B07.1/SPP-LPPM/II/2021. The authors also gratefully acknowledge financial support from the Institut Teknologi Sepuluh Nopember for this work, under project scheme of the Publication Writing and IPR Incentive Program (PPHKI) 2025. AB would like to thank FSM - UNDIP for IJR Grant no: 650/UN7.F8/PP/III/2025; and RAR Grant no: 222-055/UN7.D2/PP/IV/2025 and DW would like to thank Diponegoro University for the World Class University Program, Indonesia Endowment Fund for Education 2024 grant No: 61/UN7.A/HK/XII/2024.

CONFLICT OF INTEREST

The authors declare that they have no known competing financial interests that could have appeared to influence the work reported in this paper.

REFERENCES

Adamska, M., 2016. Sponges as models to study emergence of complex animals. *Current Opinion in Genetics & Development*, 39, pp.21-28. doi: 10.1016/j.gde.2016.05.026.

Aisami, A. & Gusmanizar, N., 2019. Characterization of an acrylamide-degrading bacterium isolated from hydrocarbon sludge. *Bioremediation Science and Technology Research*, 7(2), pp.15-19. doi: 10.54987/bstr.v7i2.487

Allocati, N. et al., 2018. Glutathione transferases: substrates, inihibitors and pro-drugs in cancer and neurodegenerative diseases. *Oncogenesis*, 7, 8. doi: 10.1038/s41389-017-0025-3.

Alviz-Gazitua, P. et al., 2022. *Cupriavidus metallidurans* CH34 possesses aromatic catabolic versatility and degrades benzene in the presence of mercury and cadmium. *Microorganisms*, 10(2), 484. doi: 10.3390/microorganisms10020484

Anayo, O.F. et al., 2019. The Beneficial Roles of *Pseudomonas* in Medicine, Industries, and Environment: A Review. In *Pseudomonas Aeruginosa - An Armory Within*. IntechOpen. doi: 10.5772/intechopen.85996.

Arora, P.K., 2015. Bacterial degradation of monocyclic aromatic amines. *Frontiers in Microbiology*, 6, 820. doi: 10.3389/fmicb.2015.00820.

Baker, B.J. et al., 2015. Genomic resolution of linkages in carbon, nitrogen, and sulfur cycling among widespread estuary sediment bacteria. *Microbiome*, 3, 14. doi: 10.1186/s40168-015-0077-6.

Cassier-Chauvat, C. et al., 2023. The Glutathione System: A Journey from Cyanobacteria to Higher Eukaryotes. *Antioxidants*, 12, 1199. doi: 10.3390/antiox12061199

Chaix, G. et al., 2017. Distinct *Aeromonas* Populations in Water Column and Associated with Copepods from Estuarine Environment (Seine, France). *Frontiers in Microbiology*, 8, 1259. doi: 10.3389/fmicb.2017.01259.

de Voogd, N.J. et al., 2024. *World Porifera Database*, viewed 5 January 2025, from https://www.marinespecies.org/porifera.

Douglas, G.M. et al., 2020. PICRUSt2 for prediction of metagenome functions. *Nature Biotechnology*, 38(6), pp.685-688. doi: 10.1038/s41587-020-0548-6.

Edgar, R.C., 2016. UCHIME2: improved chimera prediction for amplicon sequencing. *BioRxiv*, 12, 074252. doi: 10.1101/074252

Ferreira, M.R.S. et al., 2020. Geographical location and habitat predict variation in prokaryotic community composition of *Suberites diversicolor*. *Annals of Microbiology*, 70, 14. doi: 10.1186/s13213-020-01546-z.

Feuda, R. et al., 2017. Improved Modeling of Compositional Heterogeneity Supports Sponges as Sister to All Other Animals. *Current Biology*, 27, pp.3864-3870. doi: 10.1016/j.cub.2017.11.008.

Francis, B. et al., 2021. North Sea spring bloom-associated Gammaproteobacteria fill diverse heterotrophic niches. *Environmental Microbiome*, 16, 15. doi: 10.1186/s40793-021-00385-y.

Gaikwad, S., Shouche, Y.S. & Gade, W.N., 2016. Microbial community structure of two freshwater sponges using Illumina MiSeq sequencing revealed high microbial diversity. *AMB Express*, 6, 40. doi: 10.1186/s13568-016-0211-2.

Gloeckner, V. et al., 2014. The HMA-LMA dichotomy revisited: an electron microscopical survey of 56 sponge species. *The Biological Bulletin*, 227, pp.78-88. doi: 10.1086/BBLv227n1p78.

Greule, A. et al., 2018. Unrivalled diversity: the many roles and reactions of bacterial cytochromes P450 in secondary metabolism. *Natural Product Reports*, 35, pp.757-791. doi: 10.1039/c7np00063d.

Gugliandolo, C. et al., 2008. Pathogenic *Vibrio*, *Aeromonas* and *Arcobacter* spp. associated with copepods in the Straits of Messina (Italy). *Marine Pollution Bulletin*, 56, pp.600-606. doi: 10.1016/j.marpolbul.2007.12.001

Hall, C. et al., 2021. Freshwater sponge hosts and their green algae symbionts: a tractable model to understand intracellular symbiosis. *PeerJ*, 9, e10654. doi: 10.7717/peerj.10654.

Hill, M.S. & Sacristán-Soriano, O., 2017. Molecular and Functional Ecology of Sponges and Their Microbial Symbionts. In *Climate Change, Ocean Acidification and Sponges: Impacts Across Multiple Levels of Organization*. Cham: Springer, pp.105-142. doi: 10.1007/978-3-319-59008-0_5.

Keller-Costa, T. et al., 2014. The freshwater sponge Ephydatia fluviatilis harbours diverse *Pseudomonas* species (Gammaproteobacteria, Pseudomonadales) with broad-spectrum antimicrobial activity. *PLoS ONE*, 9, e88429. doi: 10.1371/journal.pone.0088429

Kelly, S.L. & Kelly, D.E., 2013. Microbial cytochromes P450: biodiversity and biotechnology. Where do cytochromes P450 come from, what do they do and what can they do for us? *Philosophical Transactions of the Royal Society B: Biological Sciences*, 368(1612), 20120476. doi: 10.1098/rstb.2012.0476.

Kenny, N.J. et al., 2019. Symbiosis, Selection, and Novelty: Freshwater Adaptation in the Unique Sponges of Lake Baikal. *Molecular Biology and Evolution*, 36, pp.2462-2480. doi: 10.1093/molbev/msz151.

Kunakom, S. et al., 2023. Cytochromes P450 involved in bacterial RiPP biosyntheses. *Journal of Industrial Mirobiology and Biotechnology*, 50(1), kuad005. doi: 10.1093/jimb/kuad005.

Laport, M.S., Pinheiro, U. & Rachid, C.T.C.D.C., 2019. Freshwater Sponge *Tubella variabilis* Presents Richer Microbiota Than Marine Sponge Species. *Frontiers in Microbiology*, 10, 2799. doi: 10.3389/fmicb.2019.02799.

Lo Giudice, A. & Rizzo, C., 2024. Freshwater Sponges as a Neglected Reservoir of Bacterial Biodiversity. *Microorganisms*, 12(1), 25 doi: 10.3390/microorganisms12010025.

Manconi, R. & Pronzato, R., 2016. How to survive and persist in temporary freshwater? Adaptive traits of sponges (Porifera: Spongillida): A review. *Hydrobiologia*, 782, pp. 11-22. doi: 10.1007/s10750-016-2714-x.

Moitinho-Silva, L. et al., 2017. Predicting the HMA-LMA Status in Marine Sponges by Machine Learning. *Frontiers in Microbiology*, 8, 752. doi: 10.3389/fmicb.2017.00752.

Muñoz-García, A. et al., 2019. Influence of salinity on the degradation of xenobiotic compounds in rhizospheric mangrove soil. Environmental Pollution, 249, pp.750-757. doi: 10.1016/j.envpol.2019.03.056.

Nanjani, S. et al., 2022. Transcriptome profiling reveals upregulation of benzoate degradation and related genes in *Pseudomonas aeruginosa* D6 during textile dye degradation. *Environmental Research*, 212, 113288. doi: 10.1016/j.envres.2022.113288.

Narainsamy, K. et al., 2016. Oxidative-stress detoxification and signalling in cyanobacteria: The crucial glutathione synthesis pathway supports the production of ergothioneine and ophthalmate. *Molecular Microbiology*, 100(1), pp.15-24. doi: 10.1111/mmi.13296

Nikrad, M.P., Cottrell, M.T. & Kirchman, D.L., 2014. Uptake of Dissolved Organic Carbon by Gammaproteobacterial Subgroups in Coastal Waters of the West Antarctic Peninsula. *Applied and Environmental Microbiology*, 80, pp.3362-3368. doi: 10.1128/aem.00121-14.

Pawlik, J.R. & McMurray, S.E., 2020. The Emerging Ecological and Biogeochemical Importance of Sponges on Coral Reefs. *Annual Review of Marine Science*, 12, pp.315-337. doi: 10.1146/annurev-marine-010419-010807.

Pisani, D. et al., 2015. Genomic data do not support comb jellies as the sister group to all other animals. *Proceedings of the National Academy of Sciences*, 112, pp.15402-15407. doi: 10.1073/pnas.1518127112.

Poppell, E. et al., 2014. Sponge heterotrophic capacity and bacterial community structure in high-and low-microbial abundance sponges. *Marine Ecology*, 35, pp.414-424. doi: 10.1111/maec.12098.

Priyadarshi, S., Shukla, A. & Borse, B.B., 2014. Polyhydroxyalkanoates: role of *Ralstonia eutropha*. *International Journal of Biomedical and Advance Research*, 5(2), pp.68-76. doi: 10.7439/ijbar.v5i2.639

Putra, S. et al., 2023. Two centuries of sponges (phylum Porifera) taxonomic studies in Indonesia (1820–2021): checklist and bibliography. *Zootaxa*, 5298, pp.1-74. doi: 10.11646/zootaxa.5298.1.1.

Rai, R. et al., 2021. Regulation of antioxidant defense and glyoxalase systems in cyanobacteria. *Plant Physiology and Biochemistry*, 168, pp.353-372. doi: 10.1016/j.plaphy.2021.09.037.

Rajendran, I., 2016. Typification of Chemical Compounds of Marine Sponge Metabolites. In *Marine Sponges: Chemicobiological and Biomedical Applications*. New Delhi: Springer India, pp.167-256. doi: 10.1007/978-81-322-2794-6_11.

Ruengsawang, N., Sangpradub, N. & Manconi, R., 2022. Aquatic Insects in Habitat-Forming Sponges: The Case of the Lower Mekong and Conservation Perspectives in a Global Context. *Diversity*, 14(11), 911. doi: 10.3390/d14110911

Senate, L.M. et al., 2019. Similarities, variations, and evolution of cytochrome P450s in *Streptomyces* versus *Mycobacterium*. *Scintific Reports*, 9, 3962. doi: 10.1038/s41598-019-40646-y.

Setiawan, E. et al., 2023. Revisit Study of Freshwater Sponges *Eunapius carteri* (Bowerbank, 1863) and a New Record of *Oncosclera asiatica* Manconi and Ruengsawang, 2012 (Porifera: Spongillida) in Porong River, East Java, Indonesia. *HAYATI Journal of Biosciences*, 30, pp.232-245. doi: 10.4308/hjb.30.2.232-245.

Setiawan, E. et al., 2024. A Mini Review on Analysis of Potential Antibacterial Activity of Symbiotic Bacteria from Indonesian Freshwater Sponge: An Unexplored and A Hidden Potency. *Journal of Tropical Biodiversity and Biotechnology*, 9(1), jtbb82682. doi: 10.22146/jtbb.82682.

Tooker, B.C. et al., 2022. *Pseudomonas aeruginosa* cytochrome P450 CYP168A1 is a fatty acid hydroxylase that metabolizes arachidonic acid to the vasodilator 19-HETE. *Journal of Biological Chemistry*, 298, 101629. doi: 10.1016/j.jbc.2022.101629.

Varijakzhan, D. et al., 2021. Bioactive compounds from marine sponges: Fundamentals and applications. *Marine Drugs*, 19(5), 246. doi: 10.3390/md19050246.

Vesty, A. et al., 2017. Evaluating the impact of DNA extraction method on the representation of human oral bacterial and fungal communities. *PLoS ONE*, 12(1), e0169877. doi: 10.1371/journal.pone.0169877

Walters, W. et al., 2016. Improved Bacterial 16S rRNA Gene (V4 and V4-5) and Fungal Internal Transcribed Spacer Marker Gene Primers for Microbial Community Surveys. *mSystems*, 1, e00009-15. doi: 10.1128/mSystems.00009-15.

Wang, Q. & Cole, J.R., 2024. Updated RDP taxonomy and RDP Classifier for more accurate taxonomic classification. *Microbiology Resource Announcements*, 13(4), e01063-23. doi: 10.1128/mra.01063-23.

Webster, N.S. & Thomas, T., 2016. The sponge hologenome. *ASM Journals MBio*, 7(2), pp.10-1128. doi: 10.1128/mbio.00135-16.

Weigel, B.L. & Erwin, P.M., 2016. Intraspecific Variation in Microbial Symbiont Communities of the Sun Sponge, *Hymeniacidon heliophila*, from Intertidal and Subtidal Habitats. *Applied and Environmental Microbiology*, 82, pp.650-658. doi: 10.1128/aem.02980-15.

Yadav, R., Rajput, V. & Dharne, M., 2021. Functional metagenomic landscape of polluted river reveals potential genes involved in degradation of xenobiotic pollutants. *Environmental Research*, 192, 110332. doi: 10.1016/j.envres.2020.110332.

Yilmaz, P. et al., 2014. The SILVA and "all-species living tree project (LTP)" taxonomic frameworks. *Nucleic Acids Research*, 42(D1), pp.D643-D648. doi: 10.1093/nar/gkt1209.

Zhang, W. et al., 2021. Intracellular GSH/GST antioxidants system change as an earlier biomarker for toxicity evaluation of iron oxide nanoparticles. *NanoImpact*, 23, 100338. doi: 10.1016/j.impact.2021.100338.

Journal of Tropical Biodiversity and Biotechnology
Volume 10, Issue 04 (2025): jtbb16953
DOI: 10.22146/jtbb.16953

Research Article

Biomonitoring Application at IMTA Cage at Two Different Farming Areas: An Effort Towards Productive Sustainable Aquaculture

Sapto P. Putro[1]*, Leonita Y. Sriyanto[2], Rizki S. Titisari[2], M. Helmi[3], Fuad Muhammad[2], Erwin Adriono[4]

1)Center of Marine Ecology and Biomonitoring for Sustainable Aquaculture, Diponegoro University 50275, Tembalang, Semarang, Indonesia
2)Department of Biology, Faculty of Science and Mathematics, Diponegoro University 50275, Tembalang, Semarang, Indonesia
3)Department of Oceanography, Faculty of Fishery and Marine Science, Diponegoro University 50275, Tembalang, Semarang, Indonesia
4)Department of Computer Engineering, Faculty of Engineering, Diponegoro University 50275, Tembalang, Semarang, Indonesia
* Corresponding author, email: saptoputro@live.undip.ac.id

Keywords:
Aquatic Ecosystems
C-organic
Karimunjawa
Macrobenthos Structure
N-total
Teluk Awur Coastal Regions
Submitted:
11 October 2024
Accepted:
11 July 2025
Published:
31 October 2025
Editors:
Miftahul Ilmi
Annisaa Widyasari

ABSTRACT

The evaluation of the application of the Integrated Multi-Trophic Aquaculture (IMTA) system is needed due to potential environmental disturbance caused by organic enrichment. The aim of this study is to assess the potential environmental disturbance by applying biomonitoring, measuring the relationship between macrobenthic structure and organic matter in farmed zones in Karimunjawa and Teluk Awur, Jepara, Indonesia. The study was conducted at two coastal areas: Teluk Awur (Station 1: MSTP Area; Station 2: Coast of Panjang Island) and Karimunjawa (Station 1: Monoculture Zone; Station 2: Polyculture Zone). Sediment sample analysis at Teluk Awur stations revealed an average organic carbon (C-organic) content of 3.3 mg C gdw^{-1} and an average total nitrogen (N-total) content of 0.7 mg N gdw^{-1}, whilst those at Karimunjawa had an average of 5.0 mg C gdw^{-1} and 0.8 mg N gdw^{-1}, respectively. The total abundance of macrobenthic communities from Karimunjawa (55,812 ind m^{-2}) was higher than in Teluk Awur coastal area (48,676 ind m^{-2}), implying a better sediment property for the microbenthic habitat. Dominant species in Teluk Awur were *Peronidia* sp. (3655 ind m^{-2}), *Divalucina* sp. (2709 ind m^{-2}), and *Turritella* sp. (3913 ind m^{-2}), whilst in Karimunjawa they were *Fustiaria* sp. (3569 ind m^{-2}), *Bittium* sp. (4687 ind m^{-2}), *Rissoina* sp. (5029 ind m^{-2}), and *Cerithium* sp. (3784 ind m^{-2}). The most influential abiotic factor affecting macrobenthic structure was N-total (BIO-ENV, Primer 6.1.5; r = 0.117). Anthropogenic activities such as fishing and tourism are suspected to influence changes in organic chemical compounds.

How to cite:
Putro, S.P. et al., 2025. Biomonitoring Application at IMTA Cage at Two Different Farming Areas: An Effort Towards Productive Sustainable Aquaculture. *Journal of Tropical Biodiversity and Biotechnology*, 10(4), jtbb16953. doi: 10.22146/jtbb.16953

INTRODUCTION

Integrated Multi-Trophic Aquaculture (IMTA) optimises ecological interactions by co-cultivating species at different trophic levels, repurposing organic and inorganic waste from higher-level feeders to sustain lower-level extractive species. This approach mitigates environmental issues like eutrophication while enhancing production efficiency (Lothmann & Sewilam 2023; Tucciarone et al. 2024). Furthermore, IMTA relies on functional complementarity, where seaweeds absorb inorganic nutrients, and deposit feeders like sea cucumbers and bivalves process organic waste from finfish or shrimp farming. Studies confirm sea cucumbers assimilate fish farm residues, improving nutrient recycling and reducing aquaculture's environmental footprint (Cutajar et al. 2022; Cotou et al. 2024). Beyond ecological benefits, IMTA fosters economic resilience by diversifying farm outputs and accessing premium markets for sustainable seafood. Its circular economy model maximises resource use, supports secondary product extraction such as biofuels, and promotes long-term sustainability (Alvarado-Ramírez et al. 2023; Checa et al. 2024).

Dissolved organic chemicals in the water result from the remnants of metabolic processes and decay products formed from plants, dead benthic animals, and animal faeces in shallow coastal waters, which then sink to the bottom. Dissolved organic chemicals such as organic carbon and phosphate accumulate in the bottom substrate of the water, causing their concentration in the sediment to be higher than in the overlying water (Javed et al. 2024). The composition of organic matter in sediments varies greatly depending on the depositional environment. Organic carbon is more easily dissolved into clay-shaped sediments (Latifah et al. 2013).

Most organic chemical content is found more in fine muddy sediments where water movement is slower, allowing organic matter to settle more easily in the sediment. In coastal environments, the surface layers of sediment have a significant impact on recycling nutrients and breaking down organic matter (Middelburg et al. 1996; Rius et al. 2018). They exhibit dual behaviour, serving as either repositories or sources of carbon and nutrients for the water column (Berner 1989). Organic matter within the sediment can undergo burial or a series of reactions leading to the breakdown of sedimentary carbon (Froelich et al. 1979; Rius et al. 2018). Dissolved organic chemicals in sediments play an important direct and indirect role for the biota living in benthic substrates, serving as a source of energy (food), materials for bacteria, plants, animals, vitamins, and substances that can accelerate and inhibit the organisms growth. The ratio of carbon and nitrogen has a very important role as a provider of nutrients in sediments. Carbon acts as a source of energy, while nitrogen is required for protein builder for organism growth (Misbahudin & Hasan 2013).

Macrobenthos are among the benthic biota that depend heavily on organic chemicals. Macrobenthos are organisms living on the seabed substrate and serve as bioindicators environmental quality detection in aquatic ecosystems. Macrobenthos play crucial roles in the functioning of marine ecosystems, such as the decomposition of organic matter and the transfer and recycling of nutrients within food webs (Xu et al. 2019). Macrobenthos can be divided based on their location into macrobenthic infauna and epifauna. Macrobenthos infauna are groups living within the sediment (subsurface deposit feeders), making holes (burrowers), or making tubes (tube builders). In shallow coastal habitats, benthic infauna play central roles in the biotic and abiotic functioning of coastal water bodies, being key components of benthic-pelagic coupling, enhancing biogeochemical cycling, and often serving as a direct harvest for coastal fisheries (Wolkovich et al. 2010; Day et al. 2020). Macrobenthic epifauna live on the sediment surface, some acting as deposit feeders and consumers of dissolved organic matter (Putro et al. 2014a). Macrobenthos have a strong correlation with the availability of organic chemicals

in the sediment, because macrobenthos absorb organic chemicals as a source of nutrients. Dissolved organic matter will have an important effect both directly and indirectly on macrobenthos density (Choirudin et al. 2014).

This study was conducted in the waters of Teluk Awur coastal regions and Karimunjawa Islands. Teluk Awur waters have two stations that have been selected, namely at the MSTP Dock and Panjang Island, while in Karimunjawa Islands two stations have also been selected, namely the Monoculture Zone, and the Polyculture Zone. This study aims to compare the two waters, each characterised by different sediment and aquatic environmental properties, to explore potential differences in sediment organic chemical composition and assess these through the macrobenthos community structure.

MATERIALS AND METHODS

Research Sites

This research was carried out at two aquatic ecosystems: Teluk Awur coastal area located at coordinates 6°37'01 "S110°38'20 "E (Station 1: MSTP Dock Area; Station 2: Coast of Panjang Island) and Karimunjawa Islands located at coordinates 110°25'42. 2 "E, 5°52'56.6 "S (Station 1: Monoculture Zone; Station 2: Polyculture Zone), as shown in Figure 1.

Sample Collection and Laboratory Analysis

Sampling was performed between May and June 2023. The methods used in this study were purposive sampling method and exploratory survey method with direct sampling technique. The materials used in this study were macro-

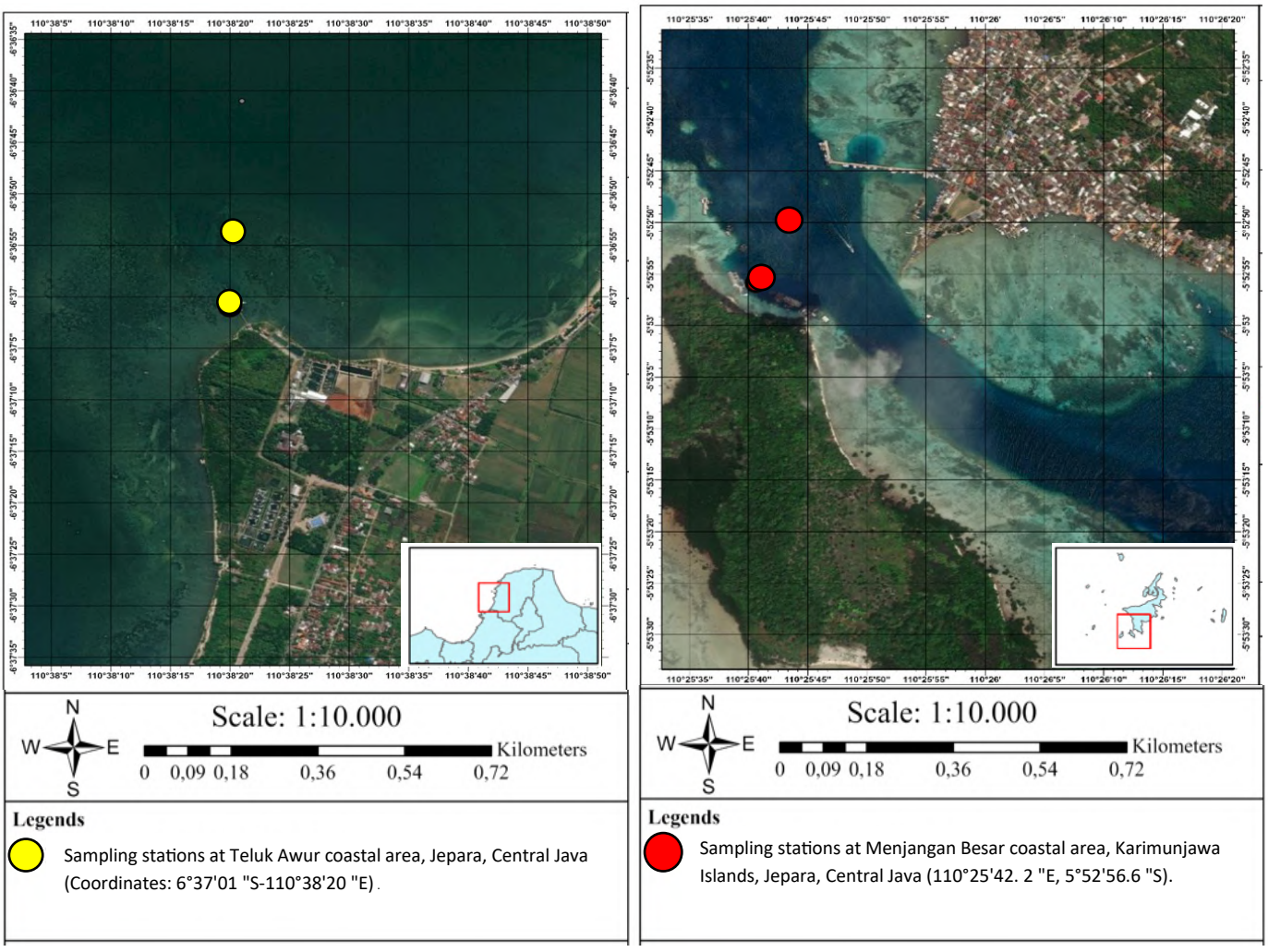

Figure 1. Sampling sites, comparing two stations at Teluk Awur, Jepara and two stations at Menjangan Besar coastal areas, Karimunjawa.

benthic animal samples, sediment, 10 % formalin solution, and 70 % ethyl alcohol. The tools used in this study included an Ekman grab, a Horiba Water Quality Checker, a 500 µm sieve, a Canon MZ-25 stereomicroscope, a jar, a sample jar, tweezers, gloves, labels, and a camera.

Three replicate samples were collected from each location using an Ekman grab with and area of 43 m². The Ekman grab was placed on the sea floor, and the substrate dredged to collect macrobenthos within the grab. After collection, the samples were then poured into the jar and given a 10 % formalin solution to keep the samples preserved. The physical and chemical parameters of water that were measured including temperature, DO, pH, and salinity, using the Horiba Water Quality Checker.

The process of observation and identification of macrobenthos samples were conducted at the Ce-MEBSA Laboratory (Center of Marine Ecology and Biomonitoring for Sustainable Aquaculture) Integrated Laboratory, Diponegoro University. The sediments were gently filtered through a 500 µm sieve, washed under water, and macrobenthos samples carefully sorted carefully and identified to the lowest taxonomic level (species) under a microscope. The macrobenthos samples was identified using taxonomic keys and references, including: "Polychaetes" by Rouse (2001), "The Polychaete Worms: Definitions and Keys to the Orders, Families and Genera" by Fauchald (1977), "Polychaetes and Allies: The Southern Synthesis" by Beesley et al. (2000), "An Illustrated Guide to the Marine Decapod Crustaceans of Florida" Part 1 by Lawrence G. Abele and Won Kim (1986), and " The Mollusks: A Guide to the Their Study, Collection, and preservation" by Charles F. Sturm et al. (2006) and journals such as "Spatial and temporal distribution of macrobenthic polychaetes (Animalia: Annelida) comparing mangrove forest and aquaculture zone at Karimunjawa Island, Jepara District, Indonesia" by Putro et al. (2025), and "The influence of different substrate types on the diversity of macrofouling organisms at the submerged coastal ecosystem of Karimunjawa Islands, Indonesia" by Putro et al. (2024). After the process of identification, based on research by Putro et al. (2025), the macrobenthos samples were put into a labelled sample bottles containing 70 % ethyl alcohol for preservation. Sediment samples obtained were processed to determine the organic composition and grain composition of the substrate. The organic composition of carbon (C) and nitrogen (N) in the sediment was processed by Gas Chromatography-mass Spectrometry (GC-MS) method at the Integrated Laboratory Unit, Diponegoro University, Semarang.

Data Analysis

Statistical processing was conducted using Microsoft Excel and BIO-ENV in Primer software v.6.1.5. The correlation between the biotic and abiotic components was calculated using BIO-ENV in Primer software. The biotic data were transformed using log (X+1) and then analysed using Bray Curtis similarity. Abiotic data were applied with a square root transformation and then normalised. The normalised abiotic data and Bray-Curtis similarity-analysed biotic data were then processed using BIO-ENV to determine correlations between abiotic and biotic components.

RESULTS AND DISCUSSION

Macrobenthos

A total of 104,488 individuals of macrobenthos per square metre (ind m^{-2}) were collected in this study. Details of macrobenthic community structure collected from Teluk Awur coastal regions and Karimunjawa Islands are presented in Table 1. In the sampling areas of Teluk Awur and the Karimunjawa Islands, 72 species of macrobenthos of 47 families and of the 8 classes that include Bivalves (15 species), Gastropods (49 species), Scaphopods (1 species),

Amphineures (1 species), Polychaetes (1 species), Echinoideans (2 species), Tubothalameans (1 species), and Crustaceans (1 species).

The results from the table above showed that the macrobenthic community structure in both sites was dominated by Gastropods (especially from Family Cerithiidae, Potamididae, Turritellidae, Naticidae, Rissoinidae, and Pyramidelidae) and Bivalves (especially from Family Veneridae, Tellinidae, and Lucinidae). The dominating species in Teluk Awur were *Peronidia* sp. (3655 ind m^{-2}), *Divalucina* sp. (2709 ind m^{-2}), and *Turritella* sp. (3913 ind m^{-2}), whilst the dominating species in Karimunjawa were *Fustiaria* sp. (3569 ind m^{-2}), *Bittium* sp. (4687 ind m^{-2}), *Rissoina* sp. (5029 ind m^{-2}), and *Cerithium* sp. (3784 ind m^{-2}), as shown in Figure 2. The aquatic environment's circumstances have a direct correlation with the diversity and availability of marine biological resources, especially with physical-chemical water parameters and organic matter availability (Kushadiwijayanto et al. 2021; Putro et al. 2024). Gastropods are the dominant taxa in both Teluk Awur and Karimunjawa (Figure 2 and 3). According to Supratman et al. (2018), the reason for the high abundance of gastropods is their diverse range of habitats, which includes muddy to sandy beaches, mangroves, and unstable environments like mining sites. According to Imamsyah et al. (2020), the existence of gastropods in maritime environments can indicate favourable environmental conditions and preserve ecological stability. Gastropods possess significant economic value and serve as bioindicators of environmental quality (Savic et al. 2016; Litaay et al. 2017; Reguera et al. 2018; Baroudi et al. 2020). Bivalve constitute the second most dominant taxon (Figures 2 and 3). Bivalves are filter-feeding, sentinel benthic creatures that exhibit resilience to fluctuating environmental circumstances and possess the capacity to gather various compounds from their surroundings (Helmholz et al. 2016; Strehse & Master 2020). Bivalves are a group of invertebrate organisms that live in intertidal areas and have the ability to live in accordance with the physical and chemical factors of the environment (Rudi et al. 2017). Polychaeta, Crustacea, and Amphineura are classes found in small numbers, especially in Teluk Awur. The low numerical abundance of Crustacea and Amphineura in many aquatic systems can be linked to the interplay between hydrodynamic forces and organic matter deposition. In areas where hydrodynamic energy is low, there is facilitation of organic matter accumulation from both terrestrial plant detritus and marine thallophytes. Bernardes et al. (2020) demonstrated that such conditions, often found in marine protected areas, provide shelter for certain decapod crustaceans; however, they also tend to promote habitat heterogeneity. This patchiness in organic retention creates microhabitats that can lead to localized zones of hypoxia and substrate alteration, which may not be optimal for all taxa, particularly for specialized groups of crustaceans whose recruitment and survival can be limited when organic enrichment disrupts sediment stability and oxygen exchange. Additionally, the fine-scale distribution of organic matter and sediment characteristics strongly influences the microdistribution of benthic macroinvertebrates. Burgazzi et al. (2020) reported that spatial and environmental factors—including the amount and quality of organic deposits—play a critical role in shaping community composition. For Amphineura, which includes taxa sensitive to alterations in the sediment-water interface, increased organic content may result in adverse conditions such as enhanced microbial decomposition and oxygen depletion. Although Hosokawa et al. (2021) noted that sediment physical characteristics, particularly water content impacted by hydrodynamic forces, affect the taxonomic density of benthic communities, they primarily focused on diversity indices for sediment quality assessments and may not have directly addressed the implications on benthic invertebrate density related to hydrodynamic conditions. In addition, Polychaeta are considered sensitive to organic matter, resulting in rapid changes in abundance (Putro et al. 2014a).

Table 1. Composition of macrobenthic collected at each site.

No	Class	Family	Species	Average Macrobenthos Community Abundance (ind m^{-2})			
				Teluk Awur		Karimunjawa	
				MSTP Dock Area	Coast of Panjang Island	Monoculture Zone	Polyculture Zone
MOLLUSCS							
1.	Bivalvia	Veneridae	*Periglypta* sp.	344	645	215	430
2.			*Circe* sp.	86	0	0	172
			Gafrarium sp.	860	344	215	516
3.		Cyrenidae	*Polymesoda* sp.	0	0	43	0
4.		Arcidae	*Anadara* sp.	602	344	0	258
5.		Pholadidae	*Pholas* sp.	43	0	86	0
6.		Cardiidae	*Trachycardium* sp.	43	0	86	0
			Vasticardium sp.	258	0	559	43
7.		Tellinidae	*Tellina* sp.	774	0	258	86
			Angulus sp.	2451	559	602	301
			Peronidia sp.	2537	1118	602	430
8.		Placunidae	*Placuna* sp.	86	0	0	0
9.		Lucinidae	*Divalucina* sp.	2150	559	86	86
10.		Mytillidae	*Brachidontes* sp.	43	0	0	0
11.		Psammobiidae	*Gari* sp.	43	0	129	0
12.	Gastropoda	Nassariidae	*Nassarius* sp.	559	43	817	731
13.		Melongenidae	*Pugilina* sp.	301	0	129	43
14.		Turbinidae	*Turbo* sp.	172	0	129	43
15.		Trochidae	*Trochus* sp.	43	0	43	129
			Austrocochlea sp.	0	0	86	43
			Gibbula sp.	172	43	129	0
16.		Cerithiidae	*Monodonta* sp.	645	86	86	430
			Clypeomorus sp.	946	43	129	473
			Bittium sp.	1075	86	1634	3053
			Cerithium sp.	602	43	2236	1548
17.		Muricidae	*Thais* sp.	129	0	516	86
			Murex sp.	43	0	0	0
			Paciocinebrina sp.	86	0	473	473
18.		Neritidae	*Ergalatax* sp.	86	0	172	215
			Nucella sp.	215	0	903	129
			Nerita sp.	1204	129	129	172
			Smaragdia sp.	0	0	43	86
			Clithon sp.	172	0	43	0
19.		Potamididae	*Terebralia* sp.	1935	43	2064	559
			Cerithidea sp.	2236	86	2322	645
			Telescopium sp.	1032	0	43	0
			Cerithideopsilla sp.	2236	215	774	301
			Pirenella sp.	1462	0	301	43
20.		Columbellidae	*Pyrene* sp.	86	0	129	0
21.		Conidae	*Conus* sp.	0	0	0	86
22.		Eulimidae	*Melanella* sp.	1290	172	1763	215
23.		Rhizoridae	*Rhizorus* sp.	129	129	86	43
24.		Turritellidae	*Tachyrhynchus* sp.	946	129	473	172
			Turritella sp.	3096	817	430	473
25.		Clypeasteridae	*Clypeaster* sp.	0	0	0	86
26.		Littorinidae	*Littoraria* sp.	43	0	86	0
27.		Cyclophoridae	*Cyclophorus* sp.	86	0	0	430
28.		Cypraeidae	*Cypraea* sp.	172	0	258	129
			Palmadusta	0	0	344	688
29.		Naticidae	*Neverita* sp.	1419	129	129	1032
30.		Planaxidae	*Fissilabia* sp.	387	0	301	0
			Planaxis sp.	645	0	86	215

Table 1. Contd.

No	Class	Family	Species	Average Macrobenthos Community Abundance (ind m^{-2})			
				Teluk Awur		Karimunjawa	
				MSTP Dock Area	Coast of Panjang Island	Monoculture Zone	Polyculture Zone
31.	Gastropoda	Rissoinidae	*Phosinella* sp.	1505	129	817	1720
31.		Rissoinidae	*Rissoina* sp.	1333	86	2406	2623
32.		Cerithiopsidae	*Cerithiopsis* sp.	731	0	215	645
33.		Pyramidellidae	*Boonea* sp.	129	86	258	129
33.		Pyramidellidae	*Syrnola* sp.	1634	129	1806	1462
34.		Amathinidae	*Amathinidae* sp.	129	172	129	86
35.		Margaritidae	*Margarites* sp.	387	0	430	172
36.		Trochaclididae	*Acremodonta* sp.	258	0	215	0
37.		Haliotidae	*Haliotis* sp.	0	0	0	86
38.		Cymatiidae	*Gyrineum* sp.	301	0	473	258
39.		Pisaniidae	*Engina* sp.	43	0	172	215
40.		Strombidae	*Lambis* sp.	0	0	0	86
41.	Scaphopoda	Dentaliidae	*Dentalium* sp.	387	258	1978	258
42.		Fustiariidae	*Fustiaria* sp.	860	387	2107	1462
43.	Amphineura	Chitonidae	*Chiton* sp.	0	0	0	43
			ANNELIDS				
44.	Polychaeta	Terebellidae	*Terebellides* sp.	0	0	43	0
			ECHINODERMS				
45.	Echinoidea	Clypeasteridae	*Clypeaster* sp.	0	0	0	86
46.		Laganidae	*Laganum* sp.	0	0	0	43
			FORAMINIFERA				
47.	Tubothalamea	Peneroplidae	*Peneroplis* sp.	0	0	43	43
			ARTHROPODS				
48.	Crustacea	Leucosiidae	*Bellidilia* sp.	0	0	0	43
		TOTAL		41667	7009	31259	24553

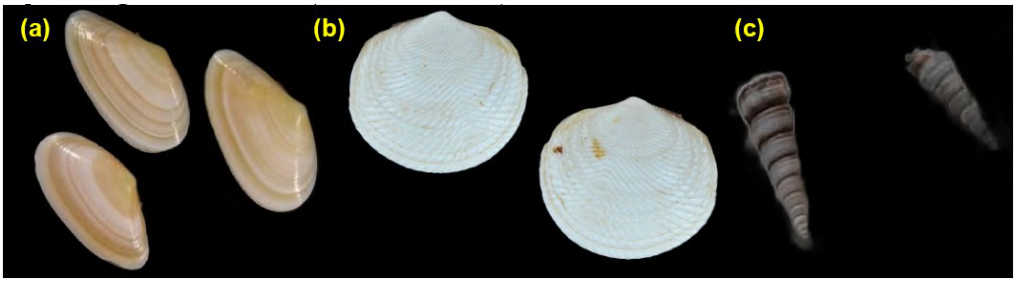

Figure 2. The dominating taxa at Teluk Awur site: (a) *Peronidia* sp. (3655 ind m^{-2}), (b) *Divalucina* sp. (2709 ind m^{-2}), and (c) *Turritella* sp. (3913 ind m^{-2})

Aquatic organisms are significantly affected by organic soluble chemical compounds in water. Organic matter (C-organic) encompasses all organic materials originating from living or deceased plant and animal tissues (Strosser 2010; Reyes & Crisosto 2016; Gmach et al. 2020). The C-organic content serves as a source of productivity and germplasm utilised by aquatic organisms. Total nitrogen (TN) in sediment is a frequently neglected metric that more accurately assesses the ecosystems' responses to anthropogenic nitrogen influx (Gillett 2010). Nitrogen is essential for protein synthesis in organismal growth. The carbon-to-nitrogen ratio plays a crucial role in nutrient availability in sediments (Nopsagiarti et al. 2020).

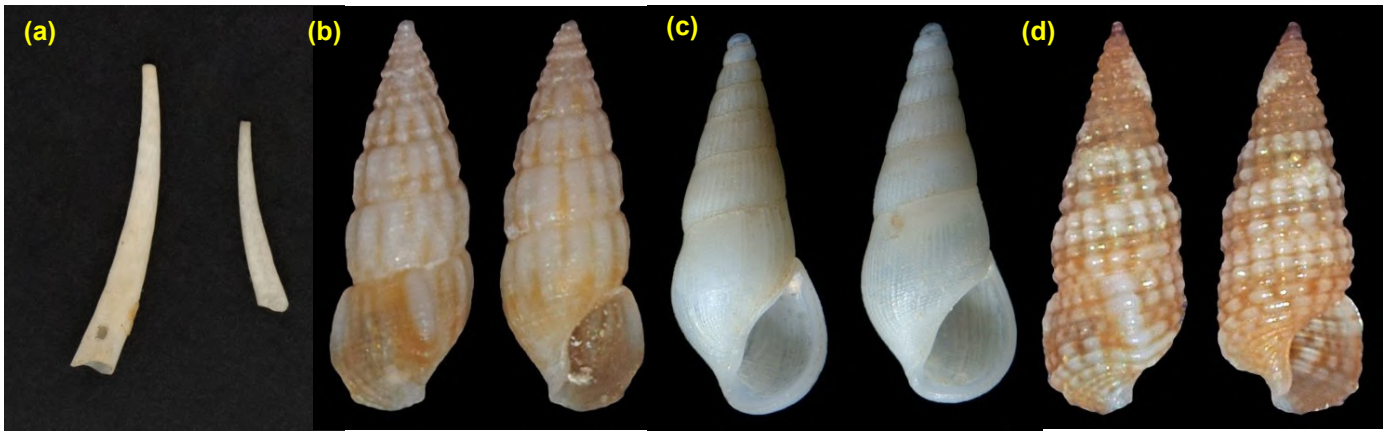

Figure 3. The dominating taxa at Karimunjawa site: (a) *Fustiaria* sp. (3569 ind m^{-2}), (b) *Bittium* sp. (4687 ind m^{-2}), (c) *Rissoina* sp. (5029 ind m^{-2}), and (d) *Cerithium* sp. (3784 ind m^{-2}).

Analysis of the Correlation between Macrobenthos Community Structure and Chemical Soluble-Organic Compound

Based on data on organic matter dissolved in sediments, Teluk Awur coastal region has an average C-organic of 3.3 mg C gdw^{-1} and an average N-total of 0.7 mg N gdw^{-1}, while the Karimunjawa Islands exhibit an average C-organic of 5.0 mg C gdw^{-1} and an average N-total of 0.8 mg N gdw^{-1}, as shown in Figure 4. These results show a decrease compared to previous research by Putro et al. (2023), which reported organic matter in the Monoculture Zone average of 3.5 mg C gdw^{-1}, while N-total had a lower average value of 0.5 mg N gdw^{-1}. The decrease in organic matter content in sediments can be caused by high-

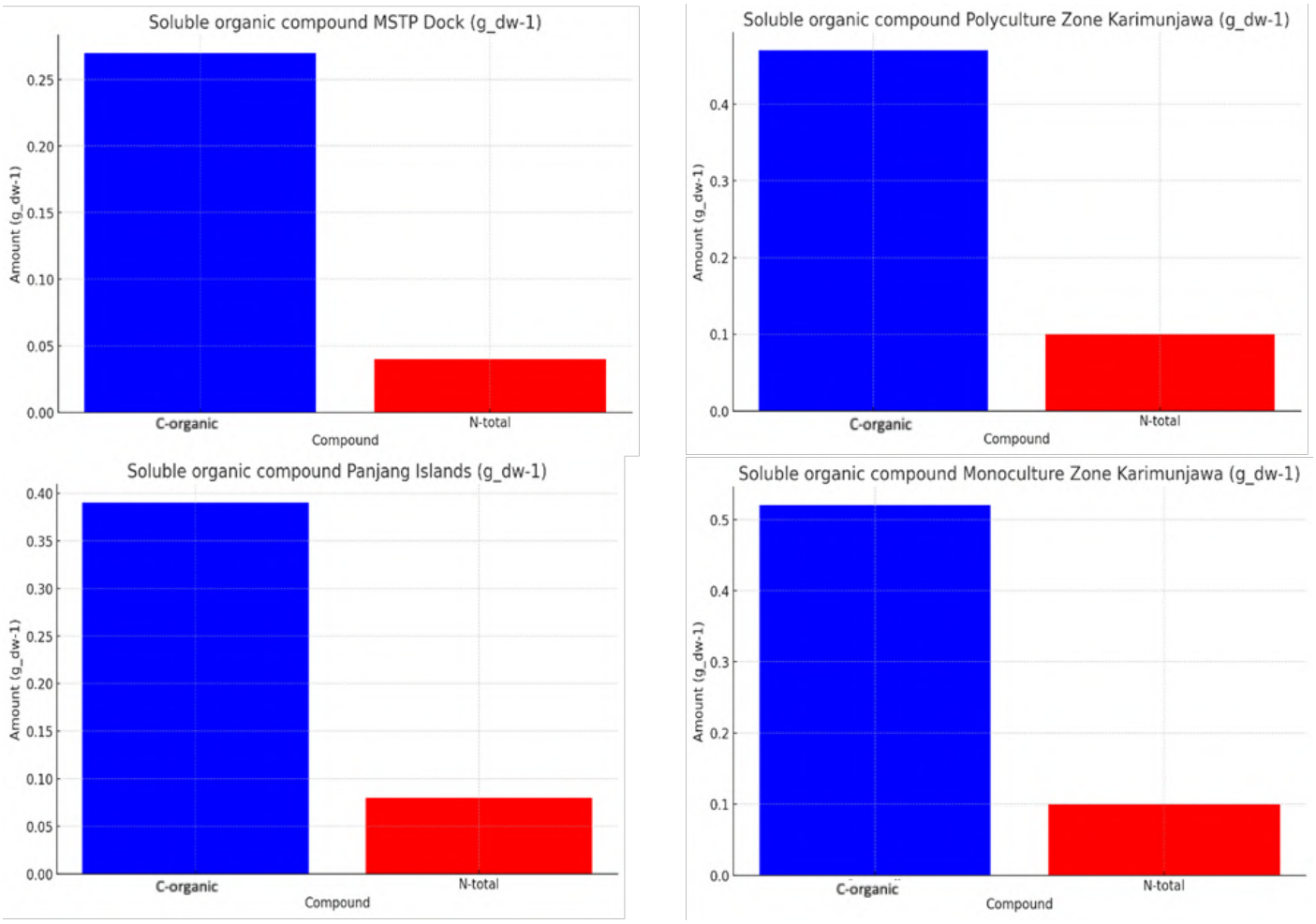

Figure 4. Percentage diagram of soluble organic compound each site: (a) MSTP Dock-Teluk Awur; (b) Panjang Island-Teluk Awur; (c) Menjangan Besar-Karimunjawa Islands; (d) Menjangan Besar-Karimunjawa Islands.

er levels of anthropogenic activity and waste disposal.

High dissolved organic matter in the sediment substrates can greatly influence the variation of macrobenthos organisms. Karimunjawa waters have higher dissolved organic matter than Teluk Awur, resulting in greater variation in macrobenthos abundance. According to another previous research (Misbahudin & Hasan 2013), if the content of organic matter in the substrate is high, it will greatly affect the distribution and abundance of macrobenthos organisms. Sediments with high levels of organic matter generally support abundant deposit feeders, on the other hand, sediments that have low levels of organic matter are generally supported by abundant suspension feeders (Putro et al. 2014b).

Analysis using BIO-ENV (Primer v6.1.5) was conducted to analyse the level of relationship between physico-chemical data of sediment and water on macrobenthos community abundance. Abiotic data, including sediment and water parameters, were square root transformed, normalised using Euclidean distance similarity, and analysed using the Weighted Spearman correlation method.

Table 2. Results of BIO-ENV analysis to determine the correlation between biotic and abiotic parameters.

No. Vars	Correlation coefficients (r)	Selections
1	0.117	2
2	0.010	2,3
1	0.010	3
2	0.008	3,4
3	-0.041	2-4
1	-0.044	4
2	-0.064	2,4
1	-0.071	1
2	-0.151	1,3
3	-0.156	1,3,4

Caption for the selected variable: 1) C-organic, 2) N-total, 3) DO (mg L^{-1}), 4) Salinity (ppt).

Correlation analysis between biotic and abiotic parameters revealed that total nitrogen (N-total) most strongly influences microbenthic community abundance compared to other abiotic parameters (r=0.117), as shown in Table 2. The high nutrient content in the water can lead to plankton blooms, which subsequently contribute to an increase in macrobenthos abundance (Mustofa 2015). Organic matter also serves as a primary food source for marine biota, particularly those inhabiting the substrate, making its presence crucial for benthic organisms. In the context of aquaculture, the presence of organic matter and nutrient balance plays a key role in the sustainability of the Integrated Multi-Trophic Aquaculture (IMTA) system. Sediment analysis indicates that the waters of Teluk Awur have an average organic carbon (C-organic) content of 3.3 mg C gdw^{-1} and an average total nitrogen (N-total) content of 0.7 mg N gdw^{-1}. Meanwhile, the waters of Karimunjawa exhibit higher C-organic content, averaging 5.0 mg C gdw^{-1} and N-total at 0.8 mg N gdw^{-1}. This contributes to differences in macrobenthos community abundance, where the total abundance in Teluk Awur (48,676 ind m^{-2}) is lower than that in Karimunjawa (55,812 ind m^{-2}).

The macrobenthic community structure in both locations is dominated by Gastropods and Bivalves. The high density of Gastropods is likely due to their ability to adapt to environmental physical and chemical factors. The abiotic factor that most influences macrobenthos structure dynamics is N-total, as indicated by the BIO-ENV analysis (Primer 6.1.5; r=0.117). Compared to monoculture and polyculture systems, IMTA has the potential to create a

more balanced ecosystem by managing organic waste more efficiently. In monoculture systems, accumulating organic matter and unutilized nutrients often leads to eutrophication and ecosystem imbalance. While polyculture systems involve more than one species, their trophic relationships are not always optimised. IMTA, on the other hand, integrates multiple organisms at different trophic levels, allowing waste from one species to be utilsed by another, thereby reducing negative environmental impacts.

CONCLUSIONS

The presence of organic matter is crucial for the life of benthic organisms in aquatic environments. The sediment sample analysis at Teluk Awur revealed an average organic carbon (C-organic) content of 3.3 mg C gdw^{-1} and an average total nitrogen (N-total) content of 0.7 mg N gdw^{-1}, while Karimunjawa exhibited an average C-organic content of 5.0 mg C gdw^{-1} and an average N-total content of 0.8 mg N gdw^{-1}. The total abundance of microbenthic communities in Teluk Awur waters (48,676 ind m^{-2}) was considerably lower than the total abundance in Karimunjawa waters (55,812 ind m^{-2}). The macrobenthic community structure in both sites was dominated by Gastropods and Bivalves. The high density of Gastropods is likely due to their ability to adapt to physical and chemical environmental factors. Among all abiotic factors, total nitrogen (N-total) most influenced the dynamics of macrobenthos structure (BIO-ENV, Primer 6.1.5; r=0.117). This study demonstrates that hydrodynamics and organic matter availability in the marine ecosystem influence macrobenthic structure. In particular, farming practice using IMTA/polyculture and monoculture exhibited differences in relation to their community structure. This implies that IMTA is a promising system as a multifaceted approach to sustainable aquaculture. By integrating species from different trophic levels into a single production system, IMTA not only closes nutrient cycles and reduces environmental impacts but also diversifies production and enhances economic resilience. Continued interdisciplinary research and technological advancements are essential to overcome current challenges and fully harness the potential of IMTA in contributing to global aquaculture sustainability.

AUTHOR CONTRIBUTION

S.P.P. conceptualized and designed the study, including the selection of IMTA farm sites in Karimunjawa and Teluk Awur, and supervised the overall research and manuscript preparation. L.Y.S. and R.S.T. carried out field sampling at the coastal stations, performed macrobenthic community identification, and analyzed sediment samples. M.H. provided expertise in oceanographic parameters, assisted in the environmental interpretation of water and sediment data. F.M. conducted statistical analyses and interpreted relationships between macrobenthic structures and sediment composition. E.A. contributed to data visualization, spatial mapping, and the computational processing of environmental and biological datasets. All authors contributed to the interpretation of results, critically revised the manuscript for intellectual content, and approved the final version for submission.

ACKNOWLEDGMENTS

The authors would like to thank Directorate of Research and Community Service, Directorate General of Research and Development, Ministry of Higher Education, Science, and Technology and the Institute for Research and Community Service (LPPM), Diponegoro University for financially supporting this study under the scheme of Applied Research Grant (Penelitian Terapan), Contract No. 359-095/UN7.D2.1/PP/V/2025. The study was supported by Marine and Fishery Service (DKP), Central Java Province; Cen-

ter for Brackish Water Aquaculture Development (BBPBAP) Jepara; Center of Marine Ecology and Bio-monitoring for Sustainable Aquaculture (CeMEBSA), Diponegoro University; Karimunjawa National Park (BTNK) Jepara; and the Marine Science Techno Park (MSTP) UNDIP.

CONFLICT OF INTEREST

The authors declare that they have no conflict of interests that could have influenced the work or the publication of this paper.

REFERENCES

Abele, L.G. & Kim, W., 1986. *An Illustrated Guide to the Marine Decapod Crustaceans of Florida (Vol. 8, No. 1)*. Florida State University.

Alvarado-Ramírez, L. et al., 2023. Sustainable production of biofuels and bioderivatives from aquaculture and marine waste. *Frontiers in Chemical Engineering*, 4, 1072761. doi: 10.3389/fceng.2022.1072761

Baroudi, F. et al., 2020. Snail as sentinel organism for monitoring the environmental pollution. *a review. Ecological Indicator*, 113, 106240. doi: 10.1016/j.ecolind.2020.106240

Beesley, P.L., Ross, G.J. & Glasby, C.J., 2000. *Polychaetes & allies: the southern synthesis (Vol. 4)*, Australia: CSIRO publishing.

Bernardes, V. et al., 2020. Comparison of the spatio-temporal distribution of the roughneck shrimp rimapenaeus constrictus (stimpson, 1874) (crustacea, penaeoidea) from monthly samples collected 20 years apart: effects of a marine protected area in southeastern brazil. *Marine Ecology*, 41(5), e12605. doi: 10.1111/maec.12605

Berner, R., 1989. Biogeochemical cycles of carbon and sulfur and their effect on atmospheric oxygen over phanerozoic time. *Palaeogeography, Palaeoclimatology, Palaeoecology*, 75(1-2), pp.97–122. doi: 10.1016/0031-0182(89)90186-7

Burgazzi, G. et al., 2020. Communities in high definition: spatial and environmental factors shape the micro-distribution of aquatic invertebrates. *Freshwater Biology*, 65(12), pp.2053-2065. doi: 10.1111/fwb.13599.

Checa, D. et al., 2024. Circularity assessment in aquaculture: The case of integrated multi-trophic aquaculture (IMTA) systems. *Fishes*, 9(5), 165. doi: 10.3390/fishes9050165

Choirudin, I., Supardjo, M. & Muskananfola, M., 2014. Study of the correlation between sediment organic matter concentration and macrozoobenthos abundance in the Wedung River estuary, Demak Regency. *Management of Aquatic Resources Journal (MAQUARES)*, 3(3), pp.168–176. doi: 10.14710/marj.v3i3.6708

Cotou, E. et al., 2024. Growth performance and environmental quality indices and biomarkers in a co-culture of the European sea bass with filter and deposit feeders: a case study of an IMTA system. *Fishes*, 9(2), 69. doi: 10.3390/fishes9020069

Cutajar, K. et al., 2022. Stable isotope and fatty acid analysis reveal the ability of sea cucumbers to use fish farm waste in integrated multi-trophic aquaculture. *Journal of environmental management*, 318, 115511. doi: 10.1016/j.jenvman.2022.115511

Day, L. et al., 2020. Benthic prey production index estimated from trawl survey supports the food limitation hypothesis in coastal fish nurseries. *Estuarine, Coastal and Shelf Science*, 235, 106594. doi: 10.1016/j.ecss.2020.106594

Fauchald, K., 1977. *The polychaete worms, definitions and keys to the orders, families and genera, Los Angeles, CA (USA): Natural History Museum of Los Angeles County.*

Froelich P.N. et al., 1979. Early oxidation of organic matter in pelagic sediments of the eastern equatorial Atlantic suboxic diagenesis, *Geochimica et Cosmochimica Acta*, 43, pp.1075–1090. doi: 10.1016/0016-7037(79)90095-4

Gillett, D.J., 2010. *Effects of Habitat Quality on Secondary Production in Shallow Estuarine Waters and the Consequences for the Benthic-Pelagic Food Web.* The College of Willam & Mary, Virginia Institute of Marine Science. doi: 10.25773/V5-7YBD-6034

Gmach, M. et al., 2020. Processes that influence dissolved organic matter in the soil: A review. *Scientia Agricola*, 77(3), e20180164. doi: 10.1590/1678-992x-2018-0164

Helmholz, H. et al., 2016. Seasonal and annual variations in physiological and biochemical responses from transplanted marine bioindicator species Mytilus spp. during a long term field exposure experiment. *Science of the Total Environment*, 565, pp.626–636. doi: 10.1016/j.scitotenv.2016.04.202

Hosokawa, S. et al., 2021. The use of diversity indices for local assessment of marine sediment quality. *Scientific Reports*, 11, 14991. doi: 10.1038/s41598-021-94636-0

Imamsyah, A., Arthana, I.W. & Astarini, I. A., 2020. The influence of physico-chemical environment on the distribution and abundance of mangrove gastropods in Ngurah Rai Forest Park Bali, Indonesia. *Biodiversitas*, 21 (7), pp.3178–3188. doi: 10.13057/biodiv/d210740

Javed, M.U. et al., 2024. Algal-based hollow fiber membrane bioreactors for efficient wastewater treatment: A comprehensive review. *Fermentation*, 10(3), 131. doi: 10.3390/fermentation10030131

Kushadiwijayanto, A.A. et al., 2021. Diversity of Molluscs (Bivalves and Gastropods) in Kabung Island, West Kalimantan, Indonesia. *Jurnal Ilmu Kelautan SPERMONDE*, 7(2), pp.34–37. doi: 10.20956/jiks.v7i2.14727

Latifah, I., Yanuar, P. & Nora, H., 2013. Analysis of organic carbon content in sediments in the upper Jeneberang River using the soil and water assessment tools model. *Jurnal Teknik Hidraulik.*, 4(2), pp.117–128. doi: 10.32679/jth.v4i2.505

Litaay, M., Deviana, M. & Priosambodo, 2017. Biodiversity and distribution of gastropods at seagrass meadow of Balangdatu Waters Tanakeke Island South Sulawesi Indonesia. *International Journal of Applied Biology*, 1 (2), pp.65–75. doi: 10.20956/ijab.v1i2.3134

Lothmann, R. & Sewilam, H., 2023. Potential of innovative marine aquaculture techniques to close nutrient cycles. *Reviews in Aquaculture*, 15(3), pp.947-964. doi: 10.1111/raq.12781

Middelburg, J.J. et al., 1996. Organic matter mineralization in intertidal sediments along an estuarine gradient. *Marine Ecology Progress Series*, 132, pp.157–168. doi: 10.3354/meps132157

Misbahudin, & Hasan, I., 2013. *Analisis Data Penelitian dengan Statistik*, Jakarta: PT. Bumi Aksara.

Mustofa, A., 2015. Kandungan Nitrat dan Pospat Sebagai Faktor Tingkat Kesuburan Perairan Pantai. *Jurnal Disprotek*, 6(1), pp.13–19. doi: 10.34001/jdpt.v6i1.193

Nopsagiarti, T., Okalia, D. & Marlina, G., 2020. Analysis of soil C-organic, nitrogen and C/N on Beken Jaya Agrotourism. *Journal of Agrosciences Technol*ogy, 5(1), pp.11–18. doi: 10.24853/jat.5.1.11-18

Putro, S.P. et al., 2014a. Response of trophic groups of macrobenthos to organically enriched sediments: A comparative study between temperate and tropical regions. Aquatic Science and Technology, 2(1), pp. 15-29. doi: 10.5296/ast.v2i1.4807

Putro, S.P. et al., 2023. The Roles of Macrobenthic Molluscs Structure in Assessing Ecological Status at Mangrove and Aquaculture Areas. *Journal of Science and Engineering (JT-UTM).*, 85 (6), pp.27–35. doi: 10.11113/jurnalteknologi.v85.20068

Putro, S.P. et al., 2024. The influence of different substrate types on the diversity of macrofouling organisms at the submerged coastal ecosystem of Karimunjawa Islands, Indonesia. *Biodiversitas Journal of Biological Diversity*, 25(8), pp.3394-3400. doi: 10.13057/biodiv/d250810

Putro, S.P. et al., 2025. Spatial and temporal distribution of macrobenthic polychaetes (Animalia: Annelida) comparing mangrove forest and aquaculture zone at Karimunjawa Island, Jepara District, Indonesia. *Biodiversitas Journal of Biological Diversity*, 26(1), pp.178-189. doi: 10.13057/biodiv/d260119

Putro, S.P., Febria, I. & Muhammad, F., 2014b. Comparative Study of Characteristics of Sediment and Water Quality in Aquaculture Farming Systems Area with Coastal Area Adjacent to Industrial Activities. *Journal of Science & Mathematics*, 22(3), pp.79–83.

Reguera, P., Couceiro, L. & Fernandez, N., 2018. A review of the empirical literature on the use of limpets Patella spp. (Mollusca: Gastropoda) as bioindicators of environmental quality. *Ecotoxicology and Environmental Safety*, 148, pp.593–600. doi: 10.1016/j.ecoenv.2017.11.004

Reyes, T.G. & Crisosto, J.M., 2016. Characterization of dissolved organic matter in river water by conventional methods and direct sample analysis-time of flight mass spectrometry. Journal of Chemistry, 2016(1), 1537370. doi: 10.1155/2016/1537370

Rius, A.T. et al., 2018. Macrobenthic diversity and sediment-water exchanges of oxygen and ammonium: Example of two subtidal communities of the eastern English Channel, *Journal of Sea Research*, 136 (June 2017), pp.15–27. doi: 10.1016/j.seares.2018.02.007

Rouse, G.W. & Pleijel, F., 2001. *Polychaetes*, Oxford University Press.

Rudi, R., Sahami, F. & Kasim, F., 2017. Keanekaragaman Bivalvia di Kawasan Pantai Desa Katialada. *NIKé Jurnal Ilmiah Perikanan dan Kelautan*, 5(1), pp.12-17.

Savic, A. et al., 2016. Assemblages of freshwater snails (Mollusca: Gastropoda) from the Nisava River, Serbia: Ecological factors defining their structure and spatial distribution. *Acta Zoologica Bulgarica*, 68(2), pp.35–242.

Strehse, J.S. & Maser, E., 2020. Marine bivalves as bioindicators for environmental pollutants with focus on dumped munitions in the sea: A review. *Marine Environmental Research*, 158, 105006. doi: 10.1016/j.marenvres.2020.105006

Strosser, E., 2010. Methods for determination of labile soil organic matter: An overview. *Journal of Agrobiology*, 27(2), pp.49–60. doi: 10.2478/s10146-009-0008-x

Sturm, C.F., Pearce, T.A. & Valdés, Á., 2006. *The Mollusks: A Guide to Their Study, Collection, and Preservation*, Pittsburgh, PA, U.S.A.: American Malacological Society.

Supratman, O., Arthur, M.F. & Jemi, F., 2018. Kelimpahan dan Keanakeragaman Gastropoda Pada Zona Intertidal di Pulau Bangka Bagian Timur. *Jurnal Enggano*, 3(1), pp.10-21. doi: 10.31186/jenggano.3.1.10-21

Tucciarone, I. et al., 2024. Sustainable aquaculture over the last 30 years: An analysis of the scientific literature by the Text Mining approach. *Reviews in Aquaculture*, 16(4), pp.2064-2076. doi: 10.1111/raq.12950

Wolkovich, E.M. et al., 2010. Grass invasion causes rapid increases in ecosystem carbon and nitrogen storage in a semiarid shrubland. *Global Change Biology*, 16(4), pp.1351-1365. doi: 10.1111/j.1365-2486.2009.02001.x

Xu, Y. et al., 2019. Spatial pattern of benthic macroinvertebrate communities and their relationship with environmental variables on the East China Sea shelf. *Deep Sea Research Part II: Topical Studeis in Oceanography*, (104633), pp.169–170. doi: 10.1016/j.dsr2.2019.07.021

Journal of Tropical Biodiversity and Biotechnology
Volume 10, Issue 04 (2025): jtbb19562
DOI: 10.22146/jtbb.19562

Research Article

The Effects of Rearing Media on the Growth and Microbiome Diversity in the Digestive Tract of Black Soldier Fly (*Hermetia illucens*) Larvae

Senny Helmiati[1]*, Nur Indah Septriani[2], Tiara Putri Faralovrisya[1], Julian Ransangan[3]
1)Fisheries Department, Faculty of Agriculture Universitas Gadjah Mada, A-4 Building, Flora Street, Bulaksumur Yogyakarta Indonesia 55281
2)Faculty of Biology, Universitas Gadjah Mada, Teknika Selatan Street, Sekip Utara, Yogyakarta Indonesia
3)Higher Institution Centre of Excellent (HICoE), Borneo Marine Research Institute, Universiti Malaysia Sabah, Jalan UMS, Kota Kinabalu, Sabah, 88400, Malaysia
* Corresponding author, email: senny@ugm.ac.id

Keywords:
Black Soldier Fly Larvae
Growth
Microbiome
Substrate
Submitted:
25 January 2025
Accepted:
12 June 2025
Published:
03 November 2025
Editors:
Ardaning Nuriliani
Liya Audinah

ABSTRACT

This study aimed to determine the nutritional content and rearing substrate and identify types of microbiota in the digestive tracts of BSF larvae. The substrates used include BSFB (fruit waste), BSFC (fermented bread waste), BSFP (bread waste), BSFS (palm kernel meal), and BSFSO (organic waste). Data on the nutritional content of the substrates and body, the length of the intestinal epithelium of BSF larvae, and the diversity of 32 microbiomes in the digestive tract of BSF larvae were analyzed statistically using analysis of variance with a significance level of 95%. The high and low nutrient content of BSF larvae is influenced by the substrate used. BSF larvae utilized the protein in the substrate to form their body proteins. BSF larvae grown on BSFS substrate showed the highest increase in length of digestive tract epithelium compared to other substrates. Differences in substrate types are one of the factors that affect the diversity of bacterial communities. The most dominant phylum in BSFB, BSFC, BSFS and BSFSO was Proteobacteria, with relative abundances of 62.53 %, 59.63 %, 56.35 %, and 61.35 %, respectively. The most dominant genus in BSFP was *Dysgonomonas* (69.04 %). Differences in substrate type are one of the factors influencing the diversity of bacterial communities within the digestive tract of BSF larvae. These results provide information for formulating specific substrates that promote beneficial gut bacteria, optimize nutrient conversion, and reduce rearing costs.

How to cite:
Helmiati, S. et al., 2025. The Effects of Rearing Media on the Growth and Microbiome Diversity in the Digestive Tract of Black Soldier Fly (*Hermetia illucens*) Larvae. *Journal of Tropical Biodiversity and Biotechnology*, 10(4), jtbb19562. doi: 10.22146/jtbb.19562

INTRODUCTION

Aquaculture production is highly dependent on the quantity and quality of feeds. Feed contributes largely to the overall operational cost, accounting for 60-70 % of the total aquaculture production cost. The biggest portion of feed is the protein source. Traditionally, the popular source of protein for aquaculture feeds is fishmeal. However, recent developments have shown that the use of fishmeal in feed production has decreased due to depletion of many fishery stocks, increase costs, and environmental concerns (Mohan et al. 2022). Fortunately, various alternative protein sources have been found to equally or more effectively improve feed utilisation and fish growth, among which is the black soldier fly.

The black soldier fly (BSF) (*Hermetia illucens* L.) larvae have been used as a component of fish feed formulations and have received special attention from fish farmers. According to Henry et al. (2015), BSF larvae have a complete nutrient profile that is suitable for fish. BSF larvae contain 10-13 % ash, 38-42 % protein, and 28-35 % fat, as well as amino acids and fatty acids. However, studies have shown that the nutrient profile of BSF larvae is affected by the composition of the media or substrates used in the production (Mirwandhono et al. 2022). BSF larvae can be cultivated using organic waste or agro-industrial products. BSF larvae act as natural bio-converters, which can convert organic waste for growth into nutrient-rich biomass efficiently. Bioconversion using insects is a promising strategy to convert organic waste into biomass that can be used for various applications and converted into high value-added products, thereby overcoming environmental, social, and economic problems (Eke et al. 2023).

According to Allegretti et al. (2017), BSF larvae are capable of extracting energy from animal and plant waste, and converting them to biomass (Zarantoniello et al. 2019). The use of BSF larvae has gained popularity in Indonesia and many parts of the world as a sustainable and cost-effective alternative to traditional livestock feed. This is driven by the high protein content of maggots, which makes them an excellent nutritional supplement for poultry, fish, and other livestock (Sumbung 2020).

The rearing substrate and the culture conditions have been shown to influence the development process of BSF larvae (Yuwono & Mentari 2018). Furthermore, it has also been shown to significantly affect the overall composition of microbial community in the gut of the larvae. The maintenance media and gut microbiota in BSF larvae can contribute to a deeper understanding of how substrate composition affects insect physiology and microbial ecology. The quantity and quality of the substrate have also been shown to affect the survival and nutrient content of BSF larvae (Wardhana 2016). However, studies have also shown that not all substrates can guarantee the provision of appropriate nutrients for BSF larval development (Wang & Shelomi 2017). Studies have optimized the mass rearing of BSF larvae on several organic substrates for maximum biomass yields (Bruno et al. 2019). According to Lestari et al. (2020), a mixture of 25 % fermented rice bran, 25 % fermented coconut dregs, 25 % fermented tofu dregs, and 25 % fermented palm kernel cake was the best culture medium for BSF larvae. Osimani et al. (2021) showed that BSF larvae reared on silverskin coffee substrate enriched with *Schizochytrium limacinum* or *Isochrysis galbana harbours*, *Lactobacillus*, *Leuconostoc* and *Weissella* as the main component of its microbiota. Many previous studies investigated the digestive system of different developmental stages of the BSF (Bruno et al. 2019). However, no studies have examined the microbiota histology of the BSF larvae's digestive system and its growth in relation to different media/types of feed with varying proximate compositions. The present study aimed to determine the effect of the nutrient content of rearing substrate on BSF larval growth, the condition of the larval epithelium, and the

types of microbiota present in the larval gut.

MATERIALS AND METHODS

Materials

The materials used in this study included substrates of BSFB (fruit waste), BSFC (fermented bread waste), BSFP (bread waste), BSFS (palm kernel meal), BSFSO (organic waste), BSF eggs, 10 % NBF, ethanol (70 %, 75 %, 96 % and absolute ethanol), alcoholic acid, xylol, paraffin, distilled water, sterile water, haematoxylin eosin dye, tissue paper, Canada balsam, DNA purification kit, and agarose gel electrophoresis.

Methods

The substrates used in this study included fruit waste (BSFB), fermented bread waste (BSFC), bread waste (BSFP), palm kernel meal (BSFS), and organic waste (BSFSO). These substrates were subjected to proximate analysis prior to use. The moisture content was determined using the thermogravimetric method, ash content using the ashing method, crude protein using micro-Kjeldahl method, crude fat using the Soxhlet method, and crude fibre using strong acid and base methods.

BSF larvae rearing

The rearing substrate was weighed at approximately 120 g per a clean plastic container measuring 32 x 19 x 11 cm^3 (L x W x H) and added with 120 ml of sterile distilled water, stirred, and evenly distributed throughout the container. The BSF eggs were obtained from PT Tribumi Yogyakarta. The BSF eggs were then sprinkled on the substrate and kept until they hatched after 7 days. After hatching, the larvae were kept for 11 days.

Proximate and amino acid analysis of BSF larvae

A total of 55 g of BSF larvae were prepared for proximate analysis. The BSF larvae were ground until smooth using a grinder and then prepared for analysis. The proximate analysis was conducted as described for proximate analysis for substrates. Amino acid analysis was conducted using HPLC, UPLC, and LC-MS/MS methods.

Histologically analysis of digestive tract of BSF larvae

Histological analysis of the digestive tract of the BSF was conducted using the Haematoxylin-Eosin method described by (Bruno et al. 2019). Briefly, the intestinal organs of the BSF larvae were soaked in 10 % NBF for 3 hours, followed by washing with distilled water. First, the fixed intestinal organs were cut to approximately 3 mm and placed into embedding cassettes. Next, the fixed specimens were dehydrated by first removing excess water using clean tissue paper and then soaking them in a series of ethanol 70 % solutions. After that, the dehydrated fixed tissues were cleared of remaining alcohol by soaking them. After complete clearing, the fixed tissues were then impregnated in Toluol:paraffin (3:1) for 30 minutes, then in Toluol:paraffin (2:2), (1:3), and finally in 100 % paraffin for 50 minutes each. After the paraffin impregnation, the tissues were then embedded in paraffin and sectioned at a thickness 5 µm using a rotary microtome (Microm HM 310). The tissue sections were floated in warm distilled water (50 °C) to flatten them before being placed on glass slides. The slides were stained using the haematoxylin and eosin staining method described by Bancroft and Layton (2019). After staining, slides were mounted with Canada balsam and covered with a cover glass. Finally, the slides were examined under a compound microscope (Leica, ICC 50) at 40x and 100x magnifications.

Measurement of the length of the digestive tract epithelium

The length of the digestive tract (epithelium) of the BSF larvae was measured using ImageJ software. Briefly, the ImageJ was first calibrated to the magnification used when capturing the microscope images. Then, a ruler image matching the photo resolution and magnification was inserted into ImageJ and used to set the scale. This involved drawing a straight line from one point to another on the ruler image, ensuring proper alignment and setting the known distance. Once calibrated, ImageJ was used to measure epithelial length of the digestive tract of BSF larvae by drawing a line across the epithelium and selecting the measurement options.

Gut microbiome analysis of BSF larvae

BSF larvae were fasted for 24 hours, washed with sterile distilled water, and then stunned using cold water at -20 °C. The BSF larvae were surface sterilised with 75 % alcohol and washed with sterile distilled water. The guts of BSF larvae were then aseptically removed for use in DNA extraction using the Promega's Wizard® Genomic DNA Purification Kit. The presence of DNA was verified on 0.8 % agarose gel electrophoresis whereas the DNA purity was determined spectrophotometrically using a Nanodrop spectrophotometer at wavelengths of 260 nm and 280 nm, respectively. In this study, only DNA samples with purity and concentration of 1.8~2.0 (ratio of absorbance at wavelengths of 260 nm and 280 nm) and ≥ 20 ng μL^{-1}, respectively were proceeded with PCR amplification and sequencing. The PCR amplification was achieved using universal bacterial/archaeal primers 515f (GTGCCAGCMGCCGCGGTAA) and 806r (GGACTACHVGGGTWTCTAAT) that target the variable regions (V3 and V4) of the 16S rRNA.

This PCR amplification and amplicon sequencing were carried out by a service company (NovogeneAIT) in Singapore. The same amount of PCR products from each sample was pooled, end-repaired, A-tailed, and further ligated with Illumina adapters. Libraries were sequenced on a paired-end Illumina MiSeq platform to generate 250bp paired-end raw reads. Sequencing libraries were generated using NEBNext® Ultra™ II FS DNA PCR-free Library Prep Kit (New England Biolabs, USA). The library was checked with Qubit and real-time PCR for quantification and Bioanalyzer for size distribution detection. Quantified libraries were pooled and sequenced on Illumina MiSeq platforms according to the effective library concentration and the required data output. The bioinformatics analysis pipeline included sequence assembly using FLASH (V1.2.11, http://ccb.jhu.edu/software/FLASH/) (Magoc & Slazberg 2011). Data filtering was performed using the fastp (Version 0.23.1) software to obtain high-quality Clean Tags (Bokulich et al. 2012). Chimeras were removed using VSEARCH (V2.16.0) package (Edgar 2013). OTU production was performed using UPARSE software (v7.0. 1001, http://drive5.com/uparse/) (Edgar 2013). Species Annotation 16S was conducted using SILVA database (http://www.arb-silva.de/) (Quast et al. 2012). Top 10 taxa were selected to plot a histogram of relative abundance in Perl with SVG output. Heatmap visualisations of abundance were generated using R; Venn and flower diagrams were produced in R and in Perl using SVG functions. Alpha diversity was calculated with QIIME (Version 1.9.1) and displayed using R (version 4.0.3). PCoA analysis was performed and visualised using the ade4 package and ggplot2 packages in R software (version 4.0.3). The entire analysis was conducted using Python 3.6.13, R 4.0.3, and Perl 5.26.2.

Data analysis

Data on nutrient contents of substrates of BSF larvae, amino acid composition, length and weight of BSF larvae, and the length of gut epithelium were

statistically analysed using analysis of variance (ANOVA) at a 95 % significance level. The significant difference between treatments was tested using the Duncan Multiple Range Test. The gut microbiome diversity in BSF larvae was determined using the next-generation sequencing (NGS) method and statistically analysed using analysis of variance at a 95 % significance level.

RESULTS

The feed or rearing substrates used in this study included BSFB (fruit waste), BSFC (fermented bread waste), BSFP (bread waste), BSFS (palm kernel meal), and BSFSO (organic waste). These substrates have different proximate compositions, including protein, moisture, ash, carbohydrate, lipid, and energy, as shown in Table 1.

Identification of the condition of the BSF larvae rearing medium was necessary to improve its productivity. According to Table 1, the nutritious essential substance of the rearing media of BSF larvae includes protein, moisture, ash, carbohydrate, lipid, and energy ranging from 5.42 ± 0.33 to 17.85 ± 0.17 %, 8.30 ± 0.17 to 46.84 ± 0.23 %, 1.95 ± 0.08 to 7.39 ± 0.05 %, 35.44 ± 0.01 to 83.40 ± 0.17 %, 0.00 ± 0.00 to 7.13 ± 0.06 %, and 202.32 ± 0.36 to 317.34 ± 0.01 kcal g^{-1}, respectively.

Substrates for BSF larvae have different nutrient contents. The high and low nutrient content of BSF larvae is influenced by the substrate used. BSF larvae utilized the protein in the substrate to form their body proteins. According to Table 2, the nutrient content of BSF larvae include protein, moisture, ash, carbohydrate, lipid, and energy ranging between 35.15 ± 1.48 to 49.25 ± 0.49 %, 23.90 ± 0.57 to 33.76 ± 0.20 %, 1.85 ± 0.07 to 6.39 ± 0.24 %, 8.60 ± 0.42 to 27.85 ± 0.49 %, 3.04 ± 0.49 to 7.85 ± 0.07 %, and 302.45 ± 0.09 to 321.30 ± 0.02 kcal g^{-1}, respectively.

Measuring the amino acid compositions in BSF larvae was crucial for ensuring their effectiveness and reliability as a high-quality protein source, optimizing their production, and enhancing our understanding of their nutritional and biological characteristics. Therefore, the levels of amino acids like alanine, arginine, aspartate, glycine, glutamate, histidine, isoleucine, cysteine, leucine, lysine, methionine, tryptophan, valine, phenylalanine, proline, serine, threonine, and tyrosine in BSF larvae were measured in this study.

The profiles of both essential and non-essential amino acids in BSF larvae are listed in Table 3. The most abundant essential amino acids are leucine, lysine, and valine, whereas the most abundant non-essential amino acids are alanine, glutamate, and proline. BSFP produced the highest total amino acid content, followed by BSFSO, BSFB, BSFC, and BSFS.

Table 1. Nutrient content of BSF larvae rearing substrates.

Nutrient content	Media				
	BSFB	BSFC	BSFP	BSFS	BSFSO
Protein (%)	5.42 ± 0.33^{e}	12.57 ± 0.08^{c}	11.91 ± 0.29^{d}	17.85 ± 0.17^{a}	15.01 ± 0.01^{b}
Moisture (%)	8.30 ± 0.17^{e}	23.09 ± 0.07^{b}	21.24 ± 0.05^{d}	21.69 ± 0.14^{c}	46.84 ± 0.23^{a}
Ash (%)	2.86 ± 0.16^{c}	3.37 ± 0.04^{b}	2.44 ± 0.01^{d}	7.39 ± 0.05^{a}	1.95 ± 0.08^{e}
Carbohydrate by different (%)	83.40 ± 0.17^{a}	53.82 ± 0.07^{c}	57.52 ± 0.05^{b}	50.35 ± 0.47^{d}	35.44 ± 0.01^{e}
Lipid (%)	0.00 ± 0.00^{d}	7.13 ± 0.06^{a}	6.86 ± 0.25^{a}	2.73 ± 0.10^{b}	1.18 ± 0.02^{c}
Energy (kcal g^{-1})	316.29 ± 0.00^{a}	309.81 ± 0.08^{b}	317.34 ± 0.01^{a}	281.39 ± 0.35^{c}	202.32 ± 0.36^{d}

Notes: BSFB (fruit waste), BSFC (fermented bread waste), BSFP (bread waste), BSFS (palm kernel meal), and BSFSO (organic waste); Energy = {(protein x 4.5 kcal g^{-1}) + (lipid x 9.1 kcal g^{-1}) + (carbohydrate x 3.5 kcal g^{-1})}/100 (NRC 1993). All values are presented in average value ± standard deviation. The superscript letters in each line show a significant difference ($P<0.05$).

Table 2. Nutrient content of BSF larvae.

Nutrient content	Substrates				
	BSFB	BSFC	BSFP	BSFS	BSFO
Protein (%)	35.15 ± 1.48^{d}	49.25 ± 0.49^{a}	44.60 ± 0.14^{b}	44.83 ± 0.33^{b}	39.95 ± 1.20^{c}
Moisture (%)	30.93 ± 0.18^{b}	33.76 ± 0.20^{a}	31.20 ± 0.23^{b}	23.90 ± 0.57^{c}	22.73 ± 0.95^{c}
Ash (%)	2.85 ± 0.16^{d}	1.85 ± 0.07^{e}	4.75 ± 0.21^{b}	3.87 ± 0.08^{c}	6.39 ± 0.24^{a}
Carbohydrate by different (%	24.74 ± 1.26^{b}	8.60 ± 0.42^{d}	11.55 ± 0.21^{c}	23.19 ± 1.38^{b}	27.85 ± 0.49^{a}
Lipid (%)	6.34 ± 0.21^{b}	6.50 ± 0.14^{b}	7.85 ± 0.07^{a}	4.22 ± 0.57^{c}	3.04 ± 0.49^{d}
Energy (kcal g^{-1})	302.45 ± 0.09^{c}	310.87 ± 0.05^{b}	312.56 ± 0.00^{b}	321.30 ± 0.02^{a}	304.91 ± 0.04^{c}

Notes: BSFB (fruit waste), BSFC (fermented bread waste), BSFP (bread waste), BSFS (palm kernel meal), and BSFSO (organic waste). Energy = {(protein x 4.5 kcal g^{-1}) + (lipid x 9.1 kcal g^{-1}) + (carbohydrate x 3.5 kcal g^{-1})}/100 (NRC 1993). All values are presented in average value ± standard deviation. The superscript letters in each line show a significant difference (P<0.05).

Table 3. Amino acid composition of BSF larvae.

Amino acid	Substrate				
	BSFB	BSFC	BSFP	BSFS	BSFSO
Alanine	7758.94 ± 18.42^{d}	11431.61 ± 30.72^{b}	14497.46 ± 30.85^{a}	5379.41 ± 15.64^{e}	10126.3 ± 16.49^{c}
Arginine	3478.54 ± 0.47^{c}	2566.80 ± 1.20^{d}	4752.37 ± 7.62^{a}	1790.05± 1.20^{e}	4127.51 ± 5.24^{b}
Aspartate	4706.28 ± 2.47^{d}	5263.71 ± 8.42^{c}	9019.08 ± 13.59^{a}	1063.57 ± 0.36^{e}	5758.66 ± 6.41^{b}
Glisin	5722.79 ± 16.23^{c}	5489.31 ± 12.17^{d}	8421.25 ± 18^{a}	4009.99 ± 13.17^{e}	7087.68 ± 7.80^{b}
Glutamate	9516.67 ± 5.25^{c}	7512.52 ± 15.97^{d}	14012.09 ± 29.19^{a}	3712.53 ± 4.67^{e}	11928.04 ± 5.25^{b}
Histidine	946.61 ± 0.45^{d}	1446.47 ± 1.59^{b}	2615.78 ± 4.87^{a}	ND	1052.79 ± 1.37^{c}
Isoleusine	3211.86 ± 1.30^{c}	2083.59 ± 2.08^{d}	3590.42 ± 0.82^{a}	2075.75 ± 7.28^{d}	3282.51 ± 25.78^{b}
Cystein	718.78 ± 1.40^{e}	2365.97 ± 1.85^{c}	4465.76 ± 2.49^{a}	1462.97 ± 0.50^{d}	3728.57 ± 3.83^{b}
Leucin	5577.33 ± 10.85^{c}	4226.68 ± 5.23^{d}	7405.18 ± 11.72^{a}	3515.13 ± 12.44^{e}	6984.11 ± 13.51^{b}
Lysine	4602.71 ± 6.44^{c}	4297.13 ± 1.94^{d}	7031.22 ± 14.04^{a}	2567.39 ± 6.67^{e}	5494.71 ± 9.60^{b}
Methionine	75.08 ± 0.04^{a}	88.8 ± 0.014^{a}	547.34 ± 27.06^{a}	91.58 ± 0.035^{a}	123.61 ± 0.27^{a}
Tryptophan	486.35 ± 2.36^{d}	671.44 ± 5.81^{c}	991.36 ± 0.87^{a}	907.94 ± 1.83^{b}	999.13 ± 2.83^{a}
Valine	4945.97 ± 7.36^{c}	3931.11 ± 2.7^{d}	6328.97 ± 2.48^{a}	3565.23 ± 4.41^{e}	5482.99 ± 0.77^{b}
Phenylalanin	2420.72 ± 3.88^{d}	2660.59 ± 4.37^{c}	4400.95 ± 7.07^{a}	929.75 ± 0.47^{e}	3289.81 ± 8.54^{b}
Proline	6568.85 ± 11.00^{d}	4127.37 ± 10.71^{e}	7474.07±7.16^{b}	7035.82 ± 23.34^{c}	8447.56 ± 11.32^{a}
Serine	4375.89 ± 5.77^{c}	4204.41 ± 5.79^{d}	6585.47 ± 0.48^{a}	2609.18 ± 4.7^{e}	5358.67 ± 3.65^{b}
Treonine	2587.15 ± 4.95^{c}	2059.23 ± 2.14^{d}	3883.52 ± 6.75^{a}	610.19 ± 1.06^{e}	2587.15 ± 4.95^{b}
Tyrosin	2336.63 ± 0.46^{d}	3399.03 ± 4.70^{b}	5992.48 ± 10.55^{a}	ND	3288.2 ± 2.63^{c}
Total (mg kg^{-1})	70037.15 ± 2592.89	67825 ± 2632.73	112014.8 ± 3750.83	41326.48 ± 1951.50	89148 ± 3143.34

Notes: BSFB (fruit waste), BSFC (fermented bread waste), BSFP (bread waste), BSFS (palm kernel meal), and BSFSO (organic waste). ND = not detected. All values are presented in average value ± standard deviation. The superscript letters in each line show a significant difference (P<0.05).

Based on Figure 1, the provision of BSFS substrate showed the highest length of digestive tract epithelium in BSF larvae. Additionally, the administration of a substrate in the form of BSFSO also showed that the length of the digestive tract epithelium was not much different from the results shown by the BSFS substrate.

Based on the results obtained in this study, the administration of BSFS substrate resulted in the highest intestinal epithelium length in the BSF larvae (Figure 2). In addition, the BSFSO substrate produced a gut epithelium length comparable to that of BSFS, followed by BSFB, BSFC, and BSFP substrates. Increased epithelium lengths indicate the addition of the absorption surface as a tissue response to the high fiber and cellulose content in BSFS and BSFSO substrates.

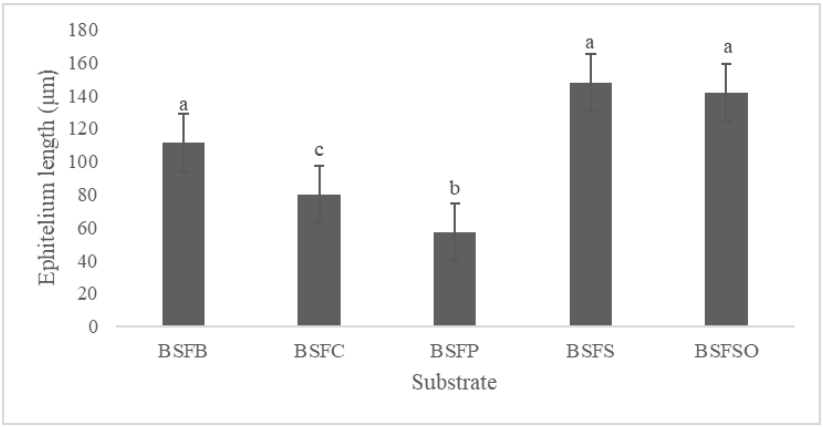

Figure 1. Length of digestive tract epithelium of BSF larvae. Remarks: BSFB (fruit waste), BSFC (fermented bread waste), BSFP (bread waste), BSFS (palm kernel meal), and BSFSO (organic waste).

In this study, the bacterial community in the BSF larvae digestive tract was observed using amplicon sequencing. The dominance of bacterial communities among the five groups of BSF larvae fed with different substrates directly influenced bacterial diversity. The bacterial community phyla in the digestive tract of BSF larvae reared on several media are listed in Table 4.

Table 4. The complexity of bacteria community phyla in the digestive tract of BSF larvae.

Phyla	Substrate				
	BSFB	BSFC	BSFP	BSFS	BSFSO
Actinobacteriota (%)	0.23	0.62	0.17	0.00	0.85
Bacteroidota (%)	22.32	25.29	63.33	21.08	23.77
Campylobacterota (%)	0.00	0.36	0.34	0.00	0.00
Desulfobacterota (%)	0.00	1.04	1.00	0.00	0.35
Firmicutes (%)	11.32	11.07	2.28	22.37	9.95
Fusobacteriota (%)	3.56	1.99	19.83	0.13	3.73
Proteobacteria (%)	62.53	59.63	10.8	56.35	61.35

Notes: BSFB (fruit waste), BSFC (fermented bread waste), BSFP (bread waste), BSFS (palm kernel meal), and BSFSO (organic waste).

Bacteroidota, Firmicutes, Fusobacteriota, and Proteobacteria are types of phyla found on all substrates. BSF larvae reared on BSFC and BSFP substrates had greater bacterial species complexity than those reared on other media. Table 4 shows that Proteobacteria is the dominant bacterial phylum in the digestive tract of BSFB (62.53 %), BSFP (59.63 %), BSFS (56.35 %), and BSFSO (61.35 %). Meanwhile, the BSFC substrate was dominated by the phylum Bacteroidota (63.33 %). Based on Figure 3, the most dominant bacterial phylum found in the digestive tract of BSF larvae is Proteobacteria, while the least frequently found is Desulfobacterota.

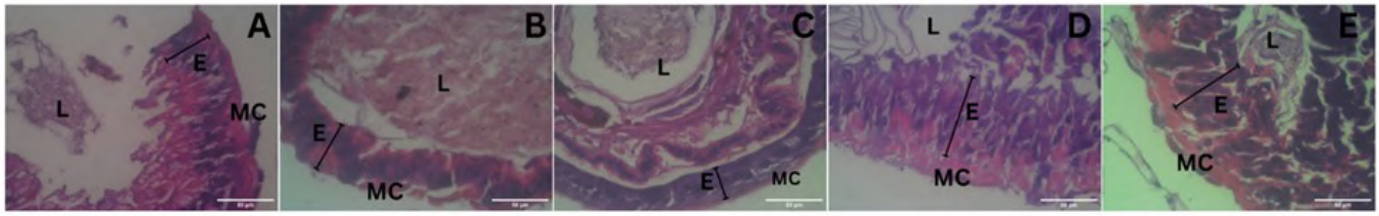

Figure 2. Histology of the BSF larvae digestive tract. Notes: Remarks: L (lumen), E (epithelium), MC (muscle cell), and line (epithelium length). Magnification: 40x. Scale bar: 50 µm. A (BSFB/fruit waste), B (BSFC/fermented bread waste), C (BSFP/bread waste), D (BSFS/palm kernel meal), and E (BSFSO/organic waste).

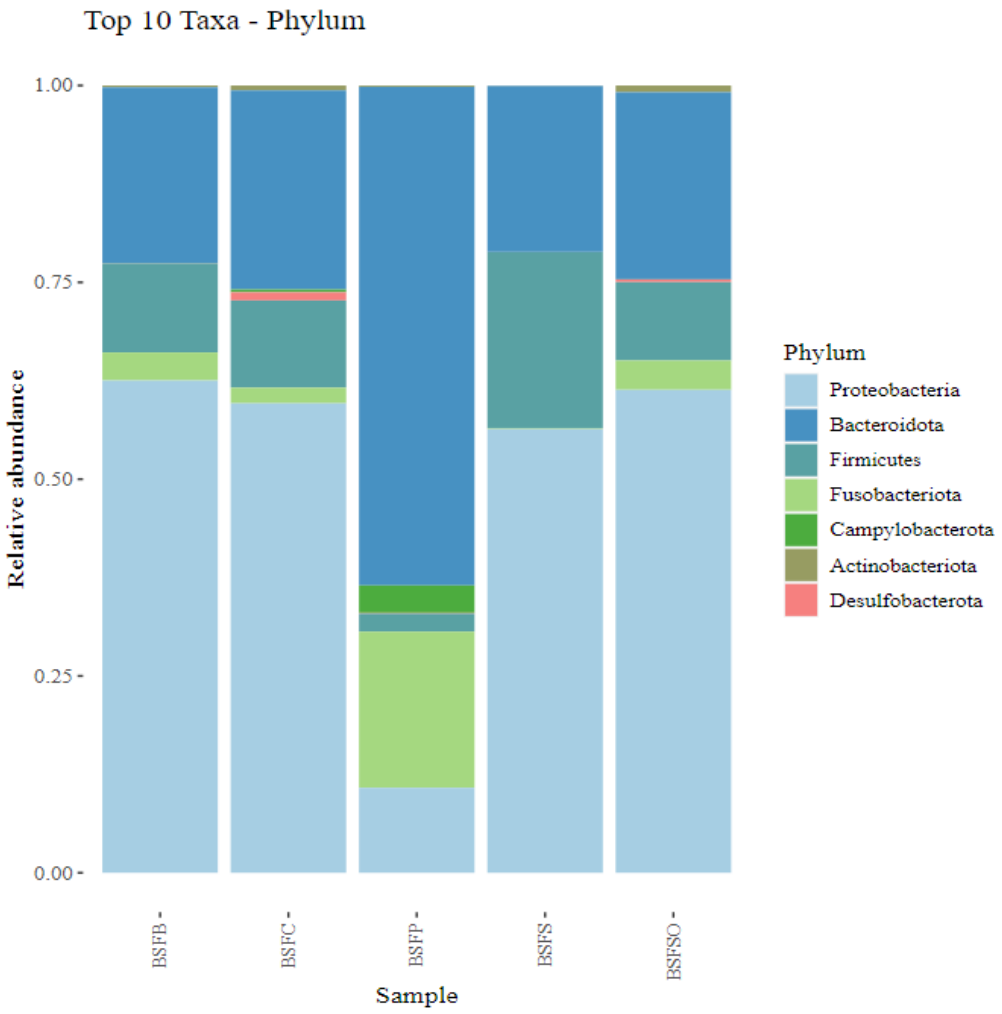

Figure 3. Bacterial communities in the digestive tract of BSF larvae based on phyla. Remarks: BSFB (fruite waste); BSFC (fermented bread waste); BSFP (bread waste); BSFS (palm kernel meal); BSFSO (organic waste).

Bacteroides, *Dysgonomonas*, *Fusobacterium*, *Morganella*, *Phascolarctobacterium*, and *Providencia* are some of the genera found on all substrates. Table 5 shows that *Morganella* is the dominant bacterial genus in the digestive tract of BSF larvae reared on BSFB (64.43 %), BSFC (76.65 %), BSFS (51.69 %), and BSFSO (29.47 %). Meanwhile, the BSFP substrate was dominated by the genus *Dysgonomonas* (69.04 %). Based on Figure 4, the most dominant bacterial genus found in the digestive tract of BSF larvae is *Morganella*, while the least frequently found are *Citrobacter* and *Sebaldella*.

Table 5. Genus of bacterial community in the digestive tract of BSF larvae.

Genus	Substrates				
	BSFB	BSFC	BSFP	BSFS	BSFSO
Bacteroides (%)	3.14	5.63	0.20	0.31	3.56
Citrobacter (%)	0.25	0.00	0.00	0.00	29.19
Dysgonomonas (%)	24.07	8.8	69.04	25.6	25.93
Fusobacterium (%)	4.34	2.65	17.13	0.19	4.63
Morganella (%)	64.43	76.65	1.17	51.69	29.47
Phascolarctobacterium (%)	1.19	3.58	0.43	10.99	4.42
Providencia (%)	2.16	1.74	3.57	0.56	2.3
Sebaldella (%)	0.00	0.00	4.72	0.00	0.00
Sedimentibacter (%)	0.42	0.39	0.00	10.66	0.48
Others	0.00	0.49	3.74	0.00	0.00

Notes: BSFB (fruit waste), BSFC (fermented bread waste), BSFP (bread waste), BSFS (palm kernel meal), and BSFSO (organic waste).

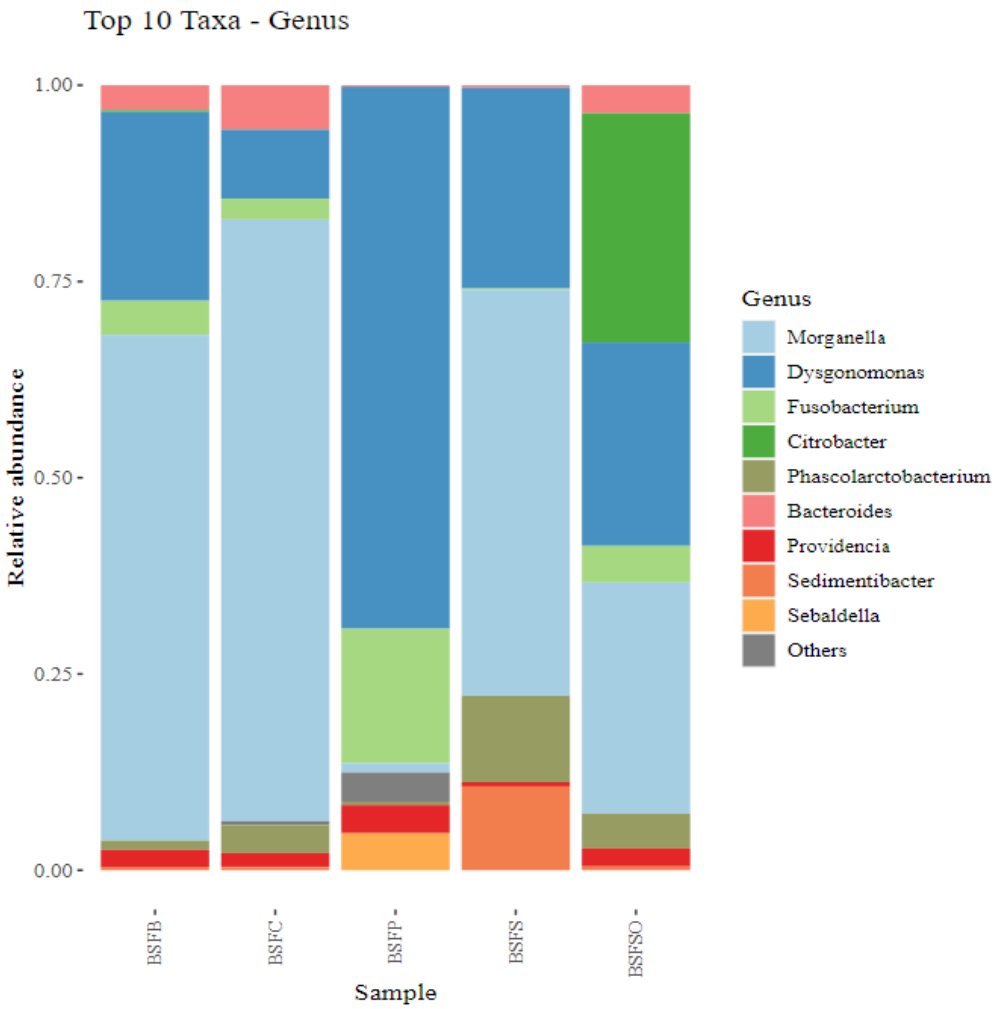

Figure 4. Bacterial communities in the digestive tract of BSF larvae based on genus. Notes: BSFB (fruit waste), BSFC (fermented bread waste), BSFP (bread waste), BSFS (palm kernel meal), and BSFSO (organic waste).

Table 6 shows that the bacterial community in the five BSF larvae gut samples was relatively similar as indicated by the narrow range between the maximum and minimum index values. The bacterial/OTU evenness by Shannon index ranged from 2.803 to 3.528. The dominant bacteria/OTU indicated by Simpson index ranged from 0.800 to 0.949. Meanwhile, the dominant bacteria/OTU in each sample, as indicated by Inverse Simpson index, ranged from 5.00 to 19.90.

Table 6. Alpha diversity indices of the bacteria from BSF larvae digestive tract.

Sample	Alpha Diversity Indices		
	Shannon	Simpson	InvSimpson
BSFSO	3.52	0.949	19.988
BSFS	3.03	0.907	10.777
BSFP	2.84	0.891	9.175
BSFB	2.80	0.837	6.140
BSFC	2.91	0.800	5.001

Notes: BSFB (fruit waste), BSFC (fermented bread waste), BSFP (bread waste), BSFS (palm kernel meal), and BSFSO (organic waste).

Based on the PCoA diagram (Figure 5), the species composition of the five samples varies. The examination of the composition of various samples (97 % similarity) reflects differences and distances between samples. The results showed that the samples were widely separated. The differences between the groups were explained by the sum of the first dimension (51.53 %)

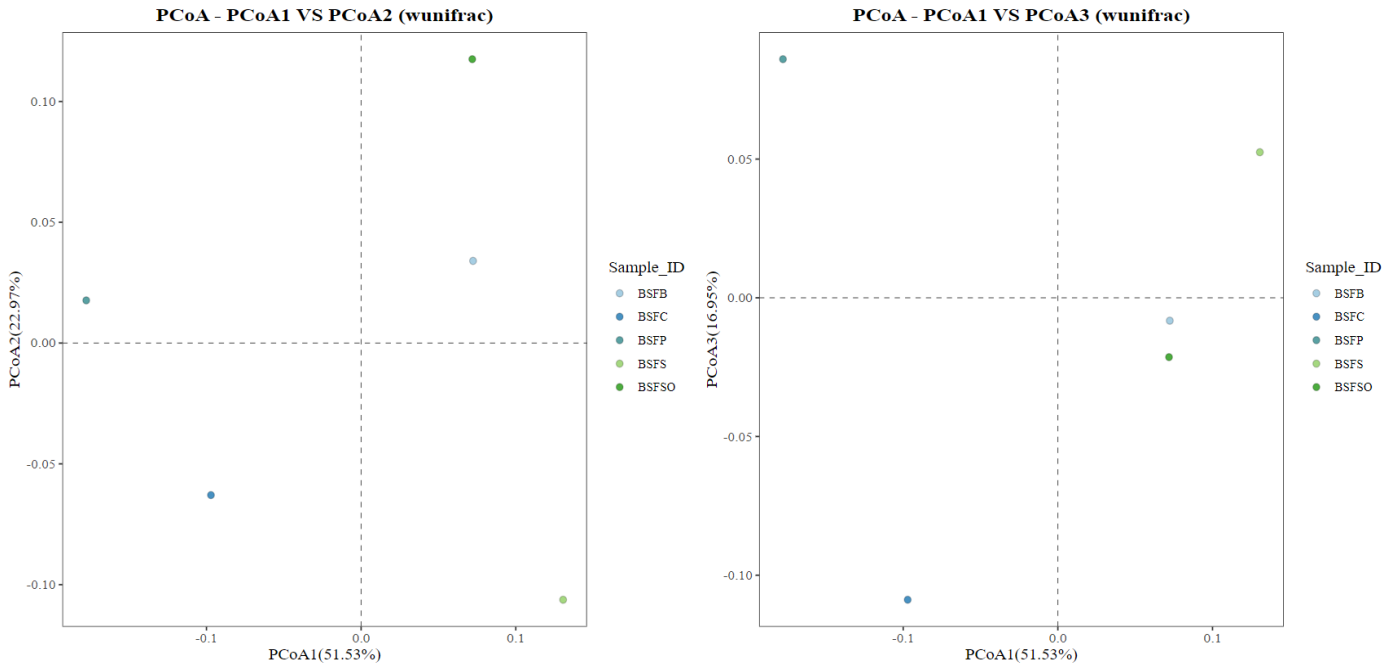

Figure 5. Principal component analysis of microbial composition between samples. Notes: BSFB (fruit waste), BSFC (fermented bread waste), BSFP (bread waste), BSFS (palm kernel meal), and BSFSO (organic waste).

and the second dimension (22.97 %) reaching 74.5 %.

Among 649 identified OTUs, the 12 OTUs (1.85 %) were common core microbiomes in the digestives tracts (guts) of BSF larvae, as they overlapped to all three-colour samples (Figure 6). The 28 OTUs (4.35%) were present in the microbiomes of BSFC and BSFP guts; 2 OTUs (0.38%) in BSFP and BSFS; 3 OTUs (0.51%) in BSFS and BSFSO; 12 OTUs (1.85%) in BSFSO and BSFB; and 2 OTUs (0.38%) in BSFB and BSFC digestive tracts.

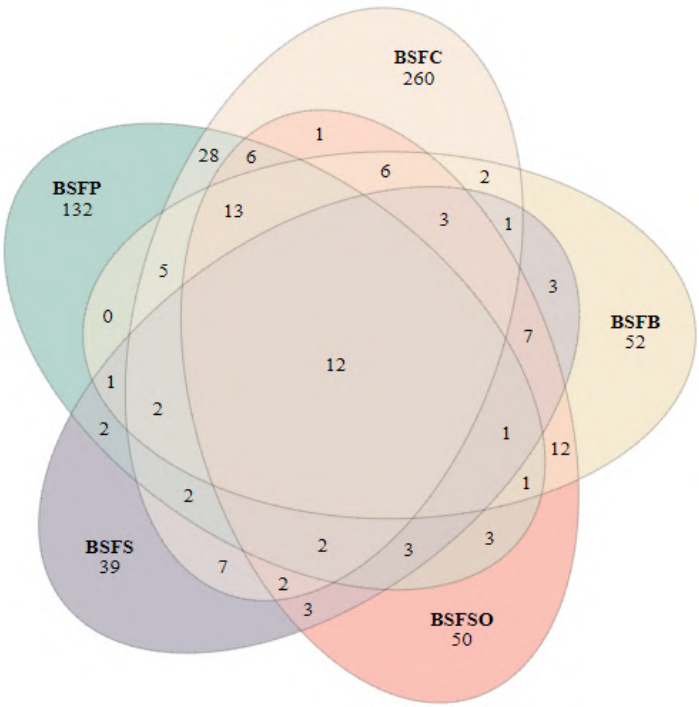

Figure 6. Venn diagram of the number of OTUs in the digestive tracts of BSF larvae. Notes: BSFB (fruit waste), BSFC (fermented bread waste), BSFP (bread waste), BSFS (palm kernel meal), and BSFSO (organic waste).

Based on Figure 7, the heatmap analysis revealed that the microbiome of BSF larvae had various bacterial communities based on the substrates, as

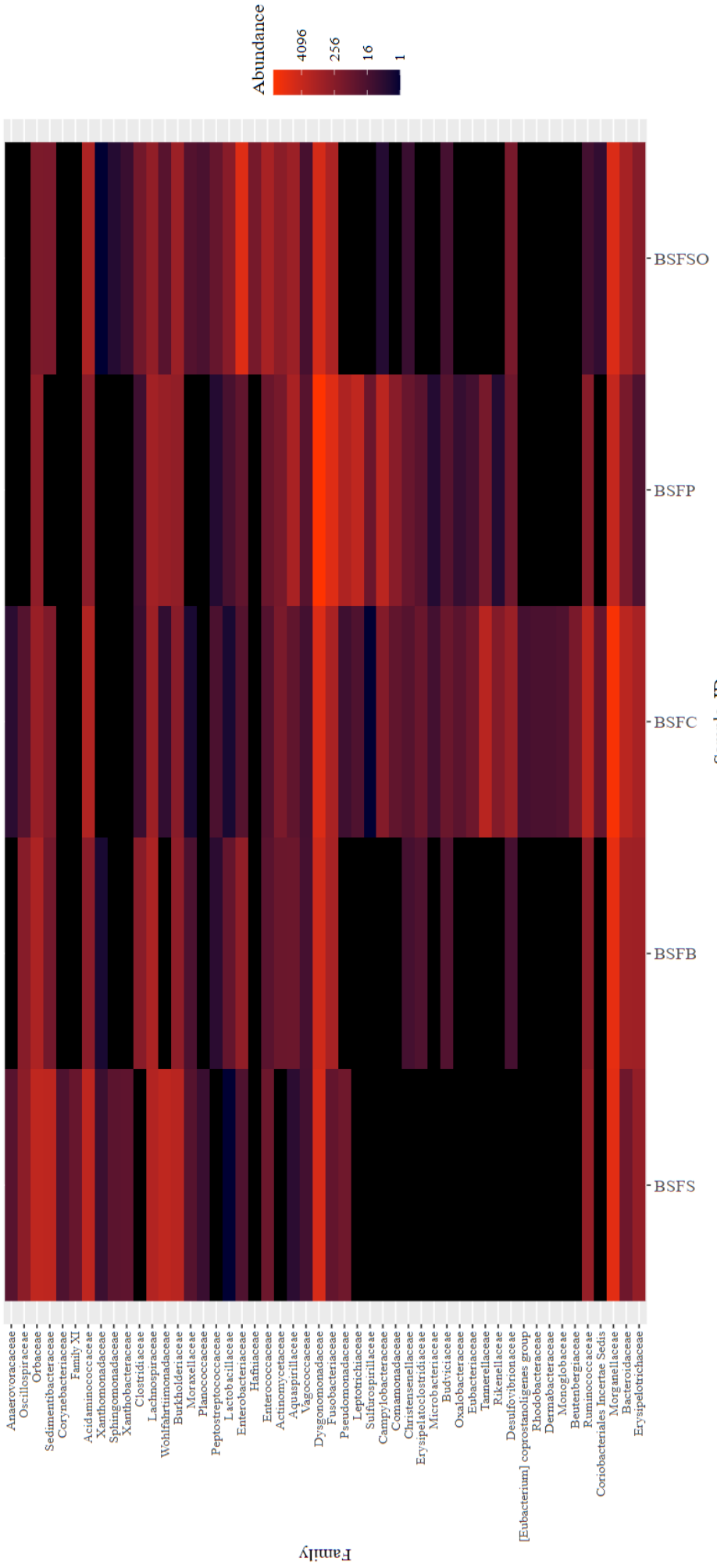

Figure 7. The heatmap of bacterial communities at the family level in the digestive tracts of BSF larvae. Notes: BSFB (fruit waste), BSFC (fermented bread waste), BSFP (bread waste), BSFS (palm kernel meal), and BSFSO (organic waste).

indicated by different dominant families. According to the heatmap, the families Morganellaceae, Dysgomonadaceae, Wolfahrtiimonadaceae, Sedimentibactaceae, Orbaceae, Acidaminococcaceae, Bukholdericeae, and Lachnospiraceae were dominant in BSFS. The families Morganellaceae, Dysgomonadaceae, Orbaceae, Fusobacteriaceae, Orbaceae, Clostridiaceae, Bukholdericeae, and Enterobacteriaceae were dominant in BSFB. The families of Morganellaceae, Dysgomonadaceae, Fusobacteriaceae, Tannerellaceae, Acidaminococcaceae, Orbaceae, Lachnospiraceae, Bacteroidaceae, Ruminococcaceae, and Bukholdericeae were dominant in BSFC. The families of Dysgomonadaceae, Fusobacteriaceae, Leptotrichiaceae, Campylobacteraceae, Morganellaceae, Aquaspirillaceae, and Lachnospiraceae were dominant in BSFP. The families of Morganellaceae, Enterobacteriaceae, Dysgomonadaceae, Fusobacteriaceae, Aquaspirillaceae, and Bacteroidaceae were dominant in BSFO.

DISCUSSION

Substrates are the primary source of microbial diversity. Microbial communities interact with different diets and impact larval growth and health (Zheng et al. 2013). Additionally, they act as selective barriers that support the formation of microorganisms in the digestive tract to meet the specific nutrient requirements of the host (Eke et al. 2023).

The nutrient contents in BSF larvae vary depending on the substrate used. BSF larvae rely on the protein found in the substrate to develop their own body proteins. It's essential to take into account the substrate's nutrient composition to maximize the growth of BSF larvae. The composition and dynamics of the bacterial community in BSF larvae can be used to improve the performance of larvae assisted by microbiome engineering (Vendemeyer et al. 2023).

Identifying the conditions of the media for rearing BSF larvae is necessary to enhance their productivity. According to Eke et al. (2023), microbial flora colonizing the rearing substrate, nutrient content of the consumed substrate, and the digestive tract of BSF larvae are parameters influencing their productivity, alongside factors like temperature, lighting conditions, and humidity. Previous studies have shown that the nutritional content of the substrate can affect the growth, development, and nutritional quality of BSF larvae (Albalawneh et al. 2024). For example, substrates rich in protein tend to result in larvae with higher protein content, which are desirable for applications in animal feed and bioconversion of organic waste (Spranghers et al. 2017). Additionally, the moisture content of the substrate can impact larval growth rates and overall biomass production (Frooninckx et al. 2024).

Hermetia illucens can use a number of organic materials for its growth. However, not all substrates are able to guarantee the proper provision of nutrients for larval development (Wang & Shelomi 2017). Figure 1 shows that BSF larvae grown on organic substrates (BSFSO) produce the highest increase in length of digestive tract epithelium compared to other substrates. The nutrient content of the substrate greatly influences the length and weight of BSF larvae, because good nutrient content will have a positive effect on increasing the length and weight of BSF larvae (Raharjo et al. 2016). The increase in digestive tract epithelial length indicates an increase in absorption surface as a tissue response to the high fibre and cellulose content in BSFS and BSFSO substrates.

The midgut epithelium of the adult BSF (Figure 2) is primarily composed of columnar cells that are responsible for digestive processes. The activity of this organ is supported by endocrine and stem cells. Additionally, the midgut epithelium is notably thicker in BSF, an adaptation that is believed to enhance its ability to process a wide variety of substrates and protect against potential damage from harsh or contaminated food sources. According to research by Bonelli et al. (2020), the morphology of the digestive tract epitheli-

um, especially the brush border on columnar cells, shows different lengths and depends on the substrate.

The bacterial communities in the digestive tracts of BSF larvae in this study showed differences in the taxonomic diversity and richness between samples. The substrate treatment of BSF larvae showed the highest alpha species diversity and richness according to the Shannon index. The highest diversity was in the guts of BSFSO (black soldier fly fed with organic waste). Differences in substrate types are among the factors that contribute to the diversity of bacterial communities. BSF larvae fed with different feeds had different bacterial communities. This shows that the type of food directly influences the diversity of bacteria in the guts (Jeon et al. 2011). Each substrate has different physicochemical conditions and nutrient content, thereby giving possibility for many microorganisms to grow. According to Cifuentes et al. (2020), bacterial community dynamics are correlated with rearing performance and physicochemical properties and composition of the residue. The dominance of bacterial communities among the groups of BSF larvae given different feed revealed that the type of substrate time could slightly change bacterial diversity. According to the previous research, the dominant species (*Bacteroides*, *Dysgonomonas*, *Morganella*, *Entererococcus*, *Providencia*, *Klebsiella*, *and Bacillus*) showed significant variability in BSF larvae, possibly related to feed variations (Klammsteiner et al. 2020). The composition and number of bacterial communities in insects' guts are influenced not only by nutrition but also by the insect species.

The most dominant phylum in BSFB, BSFP, BSFS, and BSFSO was Proteobacteria with relative abundance of 62.53 %, 59.63 %, 56.35 %, and 61.35 %. Meanwhile, the most dominant phylum in BSFP was Bacteroidota (63.3 %). Bacteriodota was the second most dominant in BSFB, BSFC and BSFSO with relative abundance of 22.32 %, 25.29 % and 23.77 %, respectively. This study showed that the most dominant phylum in BSFC, BSFS, BSFSO and BSFB was Proteobacteria. Other studies showed that Proteobacteria and Bacteroidota were also found as the most dominant phyla of bacterial communities in the gut of BSF larvae fed with chicken manure substrate (Shumo et al. 2021), chicken feed and camelina commercial feed (Schreven et al. 2022), canteen waste and household waste (Gold et al. 2020). The enhanced proportions of these two phyla demonstrate an abundance of such bacteria to regulate hydrolytic enzyme activities for organic breakdown. Bacteroidota was largely responsible for the degradation of high molecular weight organic matter, such as proteins and carbohydrates (Zhang et al. 2014).

Gut bacterial communities of BSF larvae at the phylum level are mostly composed of *Proteobacteria*, *Bacteroidota*, *Firmicutes* and *Fusobacteria*. Jeon et al. (2011) reported some differences, which included *Bacteroidetes*, *Proteobacteria*, *Firmicutes*, *Fusobacteria*, *and Actinobacteria*. Those bacteria have important role in the gut of BSF larvae. *Proteobacteria* was observed as a potential microbial signature of disease and *Firmicutes* was considered to play an important role in the digestion of animal manure (Zhan et al. 2020).

At the genus level, *Morganella* was the most abundant in BSFB (64.43 %), BSFC (76.65 %), BSFS (51.69 %) and BSFSO (29.47 %), whereas the most dominant genus in BSFP was *Dysgonomonas* (69.04 %). The second abundant in BSFB (24.07 %), BSFC (8.8 %), BSFS (25.6 %) and BSFSO (25.93 %) was *Dysgonomonas*. Other studies showed that *Morganella* and *Dysgonomonas* were also found as the most dominant genera of bacterial communities in the gut of BSF larvae fed on fruit, vegetable waste, and supermarket/restaurant waste (Wynants et al. 2019). Symbiotic microorganisms are important for host survival and reproduction as they perform essential metabolic roles such as nutrient digestion (Engel & Moran 2013; Gold et al. 2020). *Morganella morganii*

can express urease which in turn leads to the production of high levels of biogenic amines (Özogul & Özogul 2004; Gold et al. 2020). *Dysgonomonas*, as a major genus in the gut of BSF larvae, could be involved in the digestion, playing a significant role in breaking down complex polysaccharides, proteins and lipids. *Dysgonomonas* could contribute to nutrient decomposition in the residue (Bruno et al. 2019).

The bacterial communities also play a significant role in host growth, digestion and immunity, and the prevention of gut colonisation by pathogens. The characteristics of the bacterial community in the larval gut can be influenced by changing the food (Vogel et al. 2018). Meanwhile, symbiosis with hosts may change surrounding microbial ecosystems (Hammer et al. 2017). Clearly, the gut flora of many insects is an open system where exogenous microorganisms can colonize and interact with the internal gut microbiome.

CONCLUSION

This research provides valuable insights into the relationship between rearing media and gut microbiota in Black Soldier Fly larvae, contributing to a deeper understanding of how substrate composition influences insect physiology and microbial ecology. By revealing the potential of specific organic waste types to enhance larval development and microbial diversity, the study supports the development of more efficient, sustainable insect farming systems. These findings can inform future efforts to formulate tailored substrates that promote beneficial gut bacteria, optimize nutrient conversion, and reduce rearing costs. Further research should explore the functional roles of dominant microbial taxa and investigate how manipulating the microbiome could enhance BSF resilience, disease resistance, and feed efficiency at larger production scales.

AUTHOR CONTRIBUTION

S.H. contributed to the research design and was responsible for all research activities and finalising the manuscript. N.I.S. has contributed to histological preparation, measurement of the digestive tract epithelium length, and manuscript improvement. T.P.F. has contributed to the analysis of nutrient content and the types of microbiota in the intestines. J.R. has contributed to the analysis of nutrient content and manuscript improvement.

ACKNOWLEDGMENTS

This research was funded by Doctoral Competency Improvement Program Universitas Gadjah Mada, under Contract Number: 7743/UN1P.II/Dit-Lit/PT.01.03/2023.

CONFLICT OF INTEREST

The authors declare no conflict of interest.

REFERENCES

Allegretti, G., Schmidt, V., & Talamini, E., 2017. Insects as feed: species selection and their potential use in brazilian poultry production. *Poultry Science Journal*, 73(4), pp.928-937. doi: 10.1017/S004393391700054X.

Albalawneh, A. et al., 2024. Evaluating the influence of nutrient-rich substrates on the growth and waste reduction efficiency of black soldier fly larvae. *Sustainability*, 6(22), 9730. doi: 10.3390/su16229730.

Bancroft, J.D. & Layton, C., 2019. *Theory and practice of histological techniques (eight Edition): The hematoxylins and eosin*, China: Elsevier.

Bonelli, M. et al., 2020. Black soldier fly larvae adapt to different food substrates through morphological and functional responses of the midgut. *International Journal of Molecul Sciences*, 21(14), 4955. doi: 10.3390/ijms21144955.

Bokulich, N.A. et al., 2012. Quality-filtering vastly improves diversity estimates from Illumina amplicon sequencing. *Nature Methods*, 10(1), pp.57-59. doi: 10.1038/nmeth.2276.

Bruno, D. et al., 2019. The intestinal microbiota of hermetia illucens larvae is affected by diet and shows a diverse composition in the different midgut regions. *Applied and Environmental Microbiology*, 85, e01864-18. doi: 10.1128/AEM.01864-18.

Cifuentes, Y., 2020. The gut and feed residue microbiota changing during the rearing of hermetia illucens larvae. *Antonie Van Leeuwenhoek*, 113(9), pp.1323-1344. doi: 10.1007/s10482-020-01443-0.

Edgar, R.C., 2013. UPARSE: highly accurate OTU sequences from microbial amplicon reads. *Nature Methods*, 10(10), pp.996-998. doi: 10.1038/nmeth.2604.

Eke, M. et al., 2023. Deciphering the functional diversity of the gut microbiota of the black soldier fly (hermetia illucens): recent advances and future challenges. *Animal Microbiome*, 5, 40. doi: 10.1186/s42523-023-00261-9.

Engel, P. & Moran, N.A., 2013. The gut microbiota of insects – diversity in structure and function. *FEMS Microbiology Reviews*, 37(5), pp.699–735. doi: 10.1111/1574-6976.12025.

Frooninckx, L. et al., 2024. Optimizing substrate moisture content for enhanced larval survival and growth performance in hermetia illucens: exploring novel approaches. *Discover Animals*, 1, 7. doi: 10.1007/s44338-024-00005-2.

Gold, M. et al., 2020. Identification of bacteria in two food waste black soldier fly larvae rearing residues. *Frontiers in Microbiology*, 11, 582867. doi: 10.3389/fmicb.2020.582867.

Hammer, T.J. et al., 2017. Caterpillars lack a resident gut microbiome. *Proceedings of the National Academy of Sciences USA*, 114, pp.9641–9646.

Henry, M. et al., 2015. Review on the use of insects in the diet of farmed fish: past and future. *Animal Feed Science and Technology*, 203, pp.1-22. doi: 10.1016/j.anifeedsci.2015.03.001.

Jeon, H. et al., 2011. The intestinal bacterial community in the food waste-reducing larvae of hermetia illucens. *Current Microbiology*, 62(5), pp.1390-1399. doi: 10.1007/s00284-011-9874-8.

Klammsteiner, T. et al., 2020. The core gut microbiome of black soldier fly (hermetia illucens) larvae raised on low-bioburden diets. *Frontiers in Microbiology*, 11, 993. doi: 10.3389/fmicb.2020.00993.

Lestari, A. et al., 2020. Maggot black soldier fly (hermetia illucens) nutritional content using various culture media. *Jurnal Peternakan Integratif*, 8(3), pp.202-211. doi: 10.32734/jpi.v8i3.12534.

Magoc, T. & Salzberg, S.L., 2011. FLASH: fast length adjustment of short reads to improve genome assemblies. *Bioinformatics*, 27(21), pp.2957-2963. doi: 10.1093/bioinformatics/btr507.

Mirwandhono, R.E. et al., 2022. An assessment of mass production and nutrient composition of black soldier fly maggot on different agriculture by-product to fermented growth media. *IOP Conference Series: Earth and Environmental Science*, 1001, 012011. doi: 10.1088/1755-1315/1001/1/01201.

Mohan, K. et al., 2022. Use of black soldier fly (hermetia illucens L.) larvae meal in aquafeeds for a sustainable aquaculture industry: A review of past and future needs. *Aquaculture*, 553, 738095. doi: 10.1016/j.aquaculture.2022.738095.

NRC (Nutrient Requirement Council)., 1993. Nutrient requirement of fish. National Academy Press, Washington DC.

Osimani, A., 2021. Microbial dynamics in rearing trials of hermetia illucens larvae fed coffee silverskin and microalgae. *Food Research International*, 140, 110028. doi: 10.1016/j.foodres.2020.110028.

Özogul, Y. & Özogul, F., 2004. Effects of slaughtering methods on sensory, chemical and microbiological quality of rainbow trout (onchorynchus mykiss) stored in ice and MAP. *European Food Research and Technology*, 219, pp.211–216. doi: 10.1007/s00217-004-0951-0.

Quast, C. et al., 2012. The SILVA ribosomal RNA gene database project: improved data processing and web-based tools. *Nucleic Acids Research*, 41 (1), pp.590-5596. doi: 10.1093/nar/gks1219.

Raharjo, E.I., Rachimi, & Muhammad, A., 2016. Pengaruh kombinasi media ampas kelapa sawit dan dedak padi terhadap produksi maggot (hermetia illucens). *Jurnal Ruaya : Jurnal Penelitian dan Kajian Ilmu Perikanan dan Kelautan*, 4(2), pp.41-46. doi: 10.29406/jr.v4i2.702

Schreven, S.J.J., 2022. Black soldier fly larvae influence internal and substrate bacterial community composition depending on substrate type and larval density. *Applied and Environmental Microbiology*, 88(10), e0008422. doi: 10.1128/aem.00084-22.

Shumo, M., 2021 A molecular survey of bacterial species in the guts of black soldier fly larvae (hermetia illucens) reared on two urban organic waste streams in Kenya. *Frontiers in Microbiology*, 12, 687103. doi: 10.3389/fmicb.2021.687103.

Spranghers, T., 2017. Nutritional composition of black soldier fly (hermetia illucens) prepupae reared on different organic waste substrates. *Journal of The Science of Food and Agriculture*, 97, pp.2594–2600. doi: 10.1002/jsfa.8081.

Sumbung, A., 2020. Utilization of black soldier fly larvae (hermetia illucens) as feed supplement in poultry farming. *Journal of Animal Nutrition*, 45 (3), pp.215-222.

Vendemeyer, D. et al., 2023. Bacterial biota composition in gut regions of black soldier fly larvae reared on industrial residual streams: revealing community dynamics along its intestinal tract. *Frontiers in Microbiology*, 14, 1276187. doi: 10.3389/fmicb.2023.1276187.

Vogel, H. et al., 2018. Nutritional immunology: diversification and diet-dependent expression of antimicrobial peptides in the black soldier fly hermetia illucens. *Developmental & Comparative Immunology*, 78, pp.141-148. doi: 10.1016/j.dci.2017.09.008.

Wang, Y. & Shelomi, M., 2017. Review of black soldier fly (hermetia illucens) as animal feed and human food. *Foods*, 6(10), pp.91. doi: 10.3390/foods6100091.

Wardhana, A.H., 2016. Black soldier fly (hermetia illucens) sebagai sumber protein alternatif untuk pakan ternak. *Wartazoa*, 26(2), pp.69-78.

Wynants, E. et al., 2019. Assessing the microbiota of black soldier fly larvae (hermetia illucens) reared on organic waste streams on four different locations at laboratory and large scale. *Microbial Ecology*, 77, pp.913–930. doi: 10.1007/s00248-018-1286-x.

Yuwono, A.S. & Mentari, P.D., 2018. *Black soldier fly (bsf) penggunaan larva (maggot) dalam pengolahan limbah organic*, Bogor: SEAMEO BIOTROP.

Zarantoniello, M, 2019. A six-months study on black soldier fly (hermetia illucens) based diets in zebrafish. *Scientific Reports*. 9, 8598. doi: 10.1038/s41598-019-45172-5

Zhan, S., Fang, G. & Cai, M., 2020. Genomic landscape and genetic manipulation of the black soldier fly hermetia illucens, *Cell Research*, 30, pp.50-60. doi: 10.1038/s41422-019-0252-6.

Zhang, Z., et al. 2014. Attenuation of veterinary antibiotics in full-scale vermicomposting of swine manure via the housefly larvae (musca domestica). Scientific Reports. 4:6844. |doi: 10.1038/srep06844.

Zheng, L., 2013. A survey of bacterial diversity from successive life stages of black soldier fly (Diptera: Stratiomyidae) by using 16S rDNA pyrosequencing. *Journal of Medical Entomology*, 50, pp.647– 658. doi: 10.1603/ME12199.

Journal of Tropical Biodiversity and Biotechnology
Volume 10, Issue 04 (2025): jtbb18398
DOI: 10.22146/jtbb.18398

Research Article

Morphological Variation of *Anabas testudineus* (Bloch, 1792) in Central Kalimantan: Insights into Habitat-Driven Adaptations

Lia Septya[1], Muhammad Risman Wahid[2]*, Annisa Nurul Ilmi[3], Mudatul Ulfa[1], Rumaisha Rahmaniar[1]

1)Department of Biology, Faculty of Mathematics and Natural Sciences, University of Palangka Raya, Jl. Yos Sudarso, Kampus UPR Tunjung Nyaho, Palangka Raya, Central Kalimantan 73111, Indonesia
2)Department of Biology Education, Faculty of Teacher Training and Education, Universitas Riau, Jl. HR Soebrantas KM.12.5, Simpang Baru, Pekanbaru 28293, Riau, Indonesia
3)Department of Biology, Faculty of Mathematics and Natural Sciences, Mulawarman University, Jl. Barong Tongkok No. 4, Kampus Gunung Kelua, Samarinda, East Kalimantan 75123, Indonesia
* Corresponding author, email: risman.wahid@lecturer.unri.ac.id

Keywords:
Adaptability
Ecosystem
Morphometric
Native Freshwater
Phenotypic Plasticity
Submitted:
15 December 2024
Accepted:
27 July 2025
Published:
07 November 2025
Editors:
Ardaning Nuriliani
Sri Nopitasari

ABSTRACT

Anabas testudineus (Bloch, 1792) is a native freshwater species from Central Kalimantan with high adaptability. This study examines morphological variations based on 25 morphometric and 14 meristic characters, as well as body colour patterns and markings, using 150 samples collected from ten locations across four districts and one city in Central Kalimantan. Morphometric data were standardised and analysed using PCA and Kruskal-Wallis tests to identify the most influential characters in forming fish group clusters. Meristic characters were evaluated descriptively through tabulations of fin and scale count variations in each group. The results revealed three main clusters formed based on the most influential morphometric characters: Mouth to Pectoral Fin Base Distance (H), Anal Fin to Caudal Fin Base Distance (L), Anal Fin Height (V), and Body Width (Y). Meristic analysis showed only one character with similarity across groups, while 13 other characters showed significant differences among fish groups. Regarding colour patterns, ten colour variations were found, showing a tendency for dark colour dominance and five unique body markings. These findings confirm phenotypic adaptations to diverse aquatic habitats, including peat swamps and river ecosystems. This study contributes to the understanding of phenotypic plasticity as a response to environmental differences in *A. testudineus* and provides a basis for future conservation strategies. Further research is needed to confirm the genetic relationships of the observed fish variations.

How to cite:
Septya, L. et al., 2025. Morphological Variation of *Anabas testudineus* (Bloch, 1792) in Central Kalimantan: Insights into Habitat-Driven Adaptations. *Journal of Tropical Biodiversity and Biotechnology*, 10(4), jtbb18398. doi: 10.22146/jtbb.18398

INTRODUCTION

Anabas testudineus is classified under the Order Perciformes, Suborder Anabantoidei, and Family Anabantidae (ITIS 2024; Laan et al. 2014; Eschmeyer et al. 2024). *Anabas testudineus* (Bloch, 1792), commonly known as "The Climbing Perch" and locally called "Papuyu," is a native species found in the freshwater habitats of Central Kalimantan (Froese & D. Pauly 2024; Eschmeyer et al. 2024). This species is highly adaptable, capable of "walking" as it is labelled as an obligate air-breather due to adaptation of its labyrinth organ (Ndobe et al. 2019; Nuralam & Luthfi 2019; Li et al. 2024), tolerating saline waters (Waltham et al. 2023) and surviving in dry or hypooxic environments (Hughes & Singh 1970). According to the IUCN (2019), *A. testudineus* is added as "Least Concern", reflecting its excellent adaptability. Widely distributed across Kalimantan, this species has high daily consumption demand from wild-caught stocks and is considered as a key fishery commodity in the region (Slamat et al. 2019; Parvez et al. 2020; Hanafie et al. 2023; Septya & Wanto 2024).

Morphological adaptation serves as a mechanism by which individuals respond to environmental changes; therefore, the measurement and calculation of body shape-related parameters are essential for identifying individuals or populations within a particular species. Commonly used parameters include measurements of body proportions such as total length, fin length, and the distances between fins. Meanwhile, meristic parameters refer to counts of soft fin rays, fin spines, and the number of fish scales. The results of these measurements can reveal specific characteristics that group certain individuals into the same morphological cluster (Kumaladewi et al. 2022). The use of morphometric (Armbruster 2024) and meristic characters in studies of fish classification and clustering is commonly carried out through statistical analysis (Manon et al. 2023). These parameters are used to differentiate and cluster fish groups because they respond differently to environmental changes in each species (Adedeji et al. 2024).

The interconnected aquatic habitats of tropical climates allow fish populations to adapt and specialize in morphological characteristics (Chukwuka & Adeogun 2024). Morphological adaptation is crucial because each habitat has distinct environmental characteristics, such as vegetation type, food availability, and the characteristics and velocity of water currents. For example, a greater body size proportion in a fish species correlates with a higher ability to withstand strong currents (Ponomareva et al. 2017; Shuai et al. 2018). A study by Samoilov and Tran Duc Dien (2022) also emphasized that morphological adaptations, such as body and fin shape proportions in *A. testudineus* across different habitat types, significantly affect the fish's locomotion efficiency and support their survival capabilities.

There are two main mechanisms underlying the morphological adaptation of *A. testudineus* to the structure and conditions of its habitat: phenotypic plasticity and natural selection (local adaptation). In the context of phenotypic plasticity, which is influenced by epigenetic mechanisms, individuals grow and develop in response to various environmental stimuli. This response occurs through the activation or suppression of specific gene expression, resulting in phenotypic changes without altering the DNA sequence (Abdelnour et al. 2024; Makvandi-Nejad & Moghadam 2023). Plasticity plays a crucial role in enabling individuals to cope with rapidly changing habitats (Roy et al. 2023). Meanwhile, in the mechanism of local adaptation, individuals with morphological traits best suited to the environment gain a selective advantage (Lin et al. 2017). Genes supporting these adaptive traits are expressed in specific habitats, producing distinct morphological characteristics that enhance the survival of local populations (Hart et al. 2018; Larsen et al. 2011). These conditions result in phenotypic variations in the fish, enhancing

its survival in the environment (Tuset et al. 2018).

Research on the morphology of *A. testudineus* has been conducted in several regions outside of Kalimantan, including Bangladesh (Hossen et al. 2017) and Central Sulawesi (Ndobe et al. 2019). In Kalimantan, studies on morphometric and meristic characteristics have been conducted in the Mahakam River Basin, East Kalimantan (Akbar et al. 2008), and on morphometric characteristics and growth patterns in the Batang River, South Kalimantan (Ahmadi 2019). Additionally, research on morphometric variation has been carried out in five locations in Palangka Raya, Central Kalimantan (Bungas 2014). Based on existing research records, it is evident that information on the comparison of *A. testudineus* morphology across several regions of Central Kalimantan using morphometric and meristic characteristics has not been previously studied. The objective of this study is to examine the clustering of *A. testudineus* species formed from various habitats spread across several areas in Central Kalimantan through the analysis of comparative morphometric and meristic characteristics. Understanding the morphological variation within *A. testudineus* is crucial for identifying intraspecific diversity, formulating habitat-specific conservation strategies, and supporting sustainable fisheries management. Furthermore, these data provide an essential basis for the future development of more effective aquaculture programs. This highlights the need for localized studies to understand how habitat-specific differences shape morphological traits in *A. testudineus*.

MATERIALS AND METHODS

Data Collection

A total of 150 *A. testudineus* samples were collected from 10 sampling sites (across four districts and one city), including Barito Timur (BT), Lamandau (LM), Katingan Hilir (KH), Kahayan (KHY), Muara Teweh (MT), Tumbang Nusa (TN), Tumbang Samba (TS), Tewang Panjang (TP), Rawa I (RW1), and Rawa II (RW2) (Figure 1) between February and November 2024. Based on local information, these fish are relatively difficult to obtain during the rainy season. The selected locations were considered as an initial representation of aquatic habitat diversity in the region, including peat swamp and river ecosystems.

Samples were collected with the assistance of river fishermen and swamp anglers using fish nets and fishing rods. Fish were euthanised through thermal shock by immersion in ice. Photographs of fresh specimens were taken at the Biology Laboratory of the University of Palangka Raya to document body shape, colour patterns, and markings, ensuring that the natural appearance of the fish was preserved before any colour changes occurred. This step was essential for maintaining the accuracy of observations related to body coloration and patterns. Morphometric and meristic measurements were also performed at the Biology Laboratory of the University of Palangka Raya under controlled conditions to ensure consistency and reliability in data collection.

Methods

Morphometric

Morphometric measurements were carried out using a ruler and a millimetre grid sheet with an accuracy of 0.1 cm. A total of 26 characters were used, referring to (Hossen et al. 2017; Srinu et al. 2019; Dasuki et al. 2023), including: Total Length (AA); Standard Length (A); Head Length (B); Head Height (C); Body Height (D); Caudal Peduncle Height (E); Mouth to Dorsal Fin Base Distance (F); Mouth to Eye Distance (G); Mouth to Pectoral Fin Base Distance (H); Mouth to Pelvic Fin Base Distance (I); Dorsal Fin Base to Caudal Fin Base Distance (J); Pelvic Fin to Anal Fin Base Distance (K); Anal Fin to

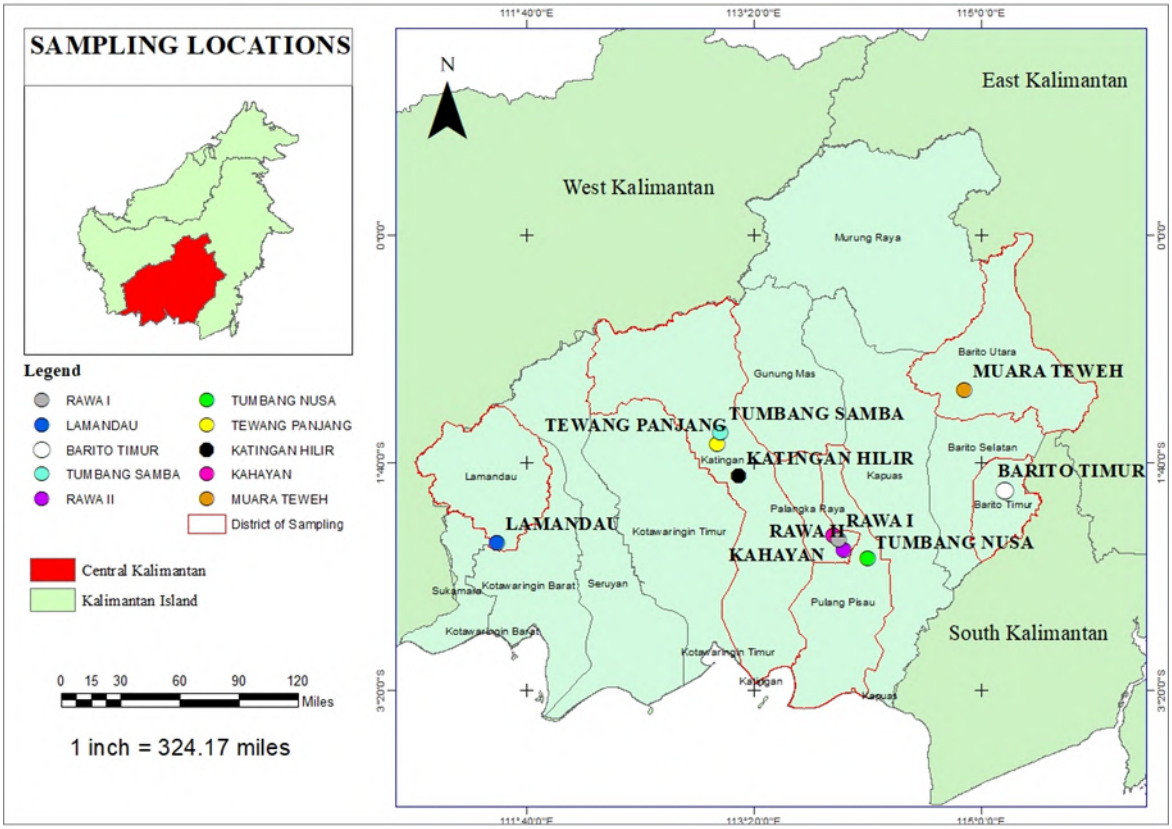

Figure 1. Geographic distribution of sampling locations for *Anabas testudineus* from 10 sites across four districts and one city (Barito Timur, Lamandau, Katingan Hilir, Muara Teweh, and Palangka Raya) in Central Kalimantan, Indonesia.

Caudal Fin Base Distance (L); Eye Diameter (M); Eye to Operculum Distance (N); Pectoral Fin Base Length (O); Pectoral Fin Height (P); Dorsal Fin Base Length (Q); Dorsal Fin Height (R); Caudal Fin Base Length (S); Caudal Fin Height (T); Anal Fin Base Length (U); Anal Fin Height (V); Pelvic Fin Base Length (W); Pelvic Fin Height (X); and Body Width (Y) (Figure 2).

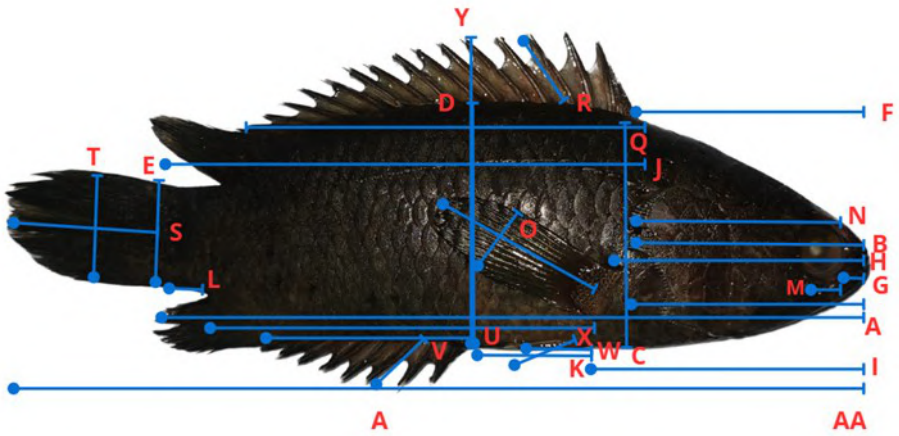

Figure 2. Illustration of the morphometric characters measured on *Anabas testudineus* and distance parameters between anatomical landmarks used in this study. Total Length (AA); Standard Length (A); Head Length (B); Head Height (C); Body Height (D); Caudal Peduncle Height (E); Mouth to Dorsal Fin Base Distance (F); Mouth to Eye Distance (G); Mouth to Pectoral Fin Base Distance (H); Mouth to Pelvic Fin Base Distance (I); Dorsal Fin Base to Caudal Fin Base Distance (J); Pelvic Fin to Anal Fin Base Distance (K); Anal Fin to Caudal Fin Base Distance (L); Eye Diameter (M); Eye to Operculum Distance (N); Pectoral Fin Base Length (O); Pectoral Fin Height (P); Dorsal Fin Base Length (Q); Dorsal Fin Height (R); Caudal Fin Base Length (S); Caudal Fin Height (T); Anal Fin Base Length (U); Anal Fin Height (V); Pelvic Fin Base Length (W); Pelvic Fin Height (X); and Body Width (Y).

Data standardisation, as referenced in (Haryono et al. 2017; Montaña et al. 2020; Lawson et al. 2023), was performed by dividing the value of each character by the total length, followed by the log10 transformation to minimise bias due to sample size differences. Subsequently, the morphometric data from all locations were analysed using Principal Component Analysis (PCA) with RStudio software to identify the most influential morphological characters. Based on these characters, statistical analysis was performed using GraphPad Prism v.10.4.0 with One-Way ANOVA non-parametric (Kruskal-Wallis Test), followed by Dunn's Multiple Comparisons Test to assess significant differences between fish groups.

Meristic

Meristic characters were examined and enumerated using a stereo microscope and scalpel. The meristic characters examined, adapted from (Hossen et al. 2017; Srinu et al. 2019; Dasuki et al. 2023), included: Dorsal Fin Spines (DFS), Dorsal Fin Soft Rays (DFSR), Pelvic Fin Hard Spines (PFHS), Pelvic Fin Soft Rays (PFSR), pectoral fin rays (PFR), Anal Fin Spines (AFS), Anal Fin Soft Rays (AFSR), Caudal Fin Rays (CFR), Predorsal Scales (PS), Cheek Scales (CS), Circumference Scales (CRS), Caudal Peduncle Scales (CPS), Lateral Line Scales (LLS), and Scales Above and Below The Lateral Line (SABLL) (Figure 3).

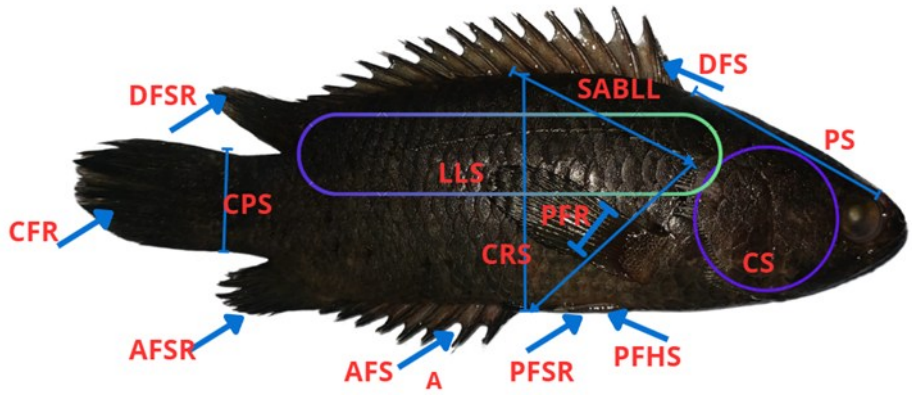

Figure 3. Illustration of the meristic characters measured on *Anabas testudineus* and distance parameters between anatomical landmarks used in this study. Dorsal Fin Spines (DFS), Dorsal Fin Soft Rays (DFSR), Pelvic Fin Hard Spines (PFHS), Pelvic Fin Soft Rays (PFSR), pectoral fin rays (PFR), Anal Fin Spines (AFS), Anal Fin Soft Rays (AFSR), Caudal Fin Rays (CFR), Pre-dorsal Scales (PS), Cheek Scales (CS), Circumference Scales (CRS), Caudal Peduncle Scales (CPS), Lateral Line Scales (LLS), and Scales Above and Below the Lateral Line (SABLL).

RESULTS AND DISCUSSION

In Table 1, the mean values and standard deviations of each morphometric character measurement are presented. The results show that the mean values for each character do not exhibit significant differences among the fish groups. However, some morphometric characters, such as Total Length (AA) and Standard Length (A), show clearer variation between the different fish groups. The difference is caused by the use of samples that are not restricted based on the size or age of the fish.

Based on the results of the morphometric analysis, the PCA scatter plot (Figure 4a) shows a clustering pattern according to the tested morphometric character variables. Three clusters were formed, as follows: Cluster 1 consists of the KHY, TP, and TN groups, with variations within these groups that tend to be homogeneous, representing that the fish in this cluster share similar morphometric characteristics. Cluster 2 includes the KH, BT, TS, LM, MT, TP, and TN groups. The TP and TN fish groups appear in both clusters

Table 1. Mean and Standard Deviation of Morphometric Characters of *A. testudineus*.

Morphometric Characters	TS	RWI	RW2	TN	KHY	TP	MT	KH	BT	LM
AA	13.02 ± 1.07	9.38 ± 0.67	6.97 ± 0.87	12.78 ± 0.56	12.14 ± 0.63	11.86 ± 0.64	10.46 ± 0.74	9.82 ± 0.52	13.54 ± 2.21	13.28±1.41
A	10.8 ± 1.01	7.58 ± 0.64	5.65 ± 0.66	10.315 ± 0.49	9.67 ± 0.58	9.73 ± 0.56	8.42 ± 0.64	8.04 ± 0.43	11.31 ± 1.75	11.1±1.17
B	2.62 ± 0.53	2.8 ± 0.2	1.92 ± 0.3	3.315 ± 0.25	4.03 ± 4.22	2.33 ± 0.5	2.72 ± 0.2	2.42 ± 0.2	3.39 ± 0.5	3.34±0.25
C	2.55 ± 0.39	2.38 ± 0.19	1.78 ± 0.35	3.09 ± 0.27	2.98 ± 0.36	2.41 ± 0.35	2.1 ± 0.15	2.1 ± 0.08	2.7 ± 0.49	2.76±0.32
D	3.35 ± 0.32	3.14 ± 0.16	2.26 ± 0.32	3.67 ± 0.25	3.5 ± 0.24	3.13 ± 0.32	2.66 ± 0.2	2.56 ± 0.12	3.85 ± 0.63	3.68±0.33
E	1.79 ± 0.16	1.34 ± 0.1	1.01 ± 0.13	1.68 ± 0.13	1.55 ± 0.13	1.59 ± 0.12	1.38 ± 0.08	1.72 ± 0.14	2.02 ± 0.33	1.9±0.2
F	3.37 ± 0.37	2.68 ± 0.19	2.02 ± 0.26	3.39 ± 0.29	3 ± 0.2	3 ± 0.24	2.94 ± 0.22	2.74 ± 0.2	3.92 ± 0.63	3.61±0.31
G	0.76 ± 0.07	0.56 ± 0.04	0.53 ± 0.05	0.65 ± 0.09	0.64 ± 0.08	0.62 ± 0.07	0.61 ± 0.03	0.62 ± 0.04	0.77 ± 0.08	0.74±0.04
H	3.56 ± 0.29	2.74 ± 0.16	2.11 ± 0.24	3.43 ± 0.2	3.17 ± 0.19	3.21 ± 0.24	3 ± 0.23	2.74 ± 0.04	3.8 ± 0.55	3.67±0.32
I	3.82 ± 0.31	2.86 ± 0.1	2.35 ± 0.27	3.75 ± 0.19	3.45 ± 0.25	3.45 ± 0.18	3.23 ± 0.21	3.06 ± 0.2	4.08 ± 0.59	3.9±0.6
J	7.16 ± 0.5	5.26 ± 0.24	3.6 ± 0.58	6.89 ± 0.38	6.63 ± 0.61	6.47 ± 0.44	5.38 ± 0.33	5.28 ± 0.29	7.55 ± 1.12	7.6±0.83
K	2.17 ± 0.24	1.42 ± 0.11	1.07 ± 0.2	2.05 ± 0.26	2.01 ± 0.27	1.9 ± 0.21	1.65 ± 0.17	1.7 ± 0.26	2.26 ± 0.44	2.12±0.21
L	1.17 ± 0.15	0.7 ± 0.06	0.56 ± 0.13	0.83 ± 0.17	1.07 ± 0.8	0.96 ± 0.19	0.86 ± 0.08	1.02 ± 0.04	1.14 ± 0.2	1.1±0.19
M	0.74 ± 0.05	0.66 ± 0.04	0.56 ± 0.06	0.76 ± 0.07	0.78 ± 0.03	0.7 ± 0.04	0.67 ± 0.04	0.6 ± 0	0.78 ± 0.08	0.75±0.05
N	2.78 ± 0.24	2.58 ± 0.23	1.72 ± 0.26	2.92 ± 0.22	2.63 ± 0.23	2.53 ± 0.16	2.5 ± 0.13	2.16 ± 0.1	3.01 ± 0.34	2.97±0.23
O	2.55 ± 0.27	2.18 ± 0.09	1.55 ± 0.2	2.53 ± 0.42	2.4 ± 0.2	2.3 ± 0.23	2.13 ± 0.15	1.84 ± 0.1	2.5 ± 0.48	2.76±0.39
P	0.92 ± 0.1	0.88 ± 0.04	0.56 ± 0.16	1.08 ± 0.13	0.98 ± 0.13	0.88 ± 0.17	0.66 ± 0.04	0.86 ± 0.1	1.07 ± 0.26	1.1±0.14
Q	5.69 ± 0.79	4.38 ± 0.28	3.25 ± 0.5	5.64 ± 0.43	5.6 ± 0.9	5.27 ± 0.51	4.39 ± 0.34	4.08 ± 0.22	5.85 ± 0.81	5.87±0.7
R	1.1 ± 0.1	0.98 ± 0.09	0.65 ± 0.14	1.25 ± 0.11	1.3 ± 0.14	1.09 ± 0.14	1.06 ± 0.09	0.8 ± 0.06	1.32 ± 0.2	1.23±0.16
S	1.79 ± 0.16	1.6 ± 0.16	1.02 ± 0.14	1.69 ± 0.15	1.55 ± 0.19	1.59 ± 0.12	1.38 ± 0.08	1.72 ± 0.14	2.05 ± 0.32	1.9±0.2
T	2.36 ± 0.28	1.9 ± 0.23	1.25 ± 0.31	2.32 ± 0.41	2.45 ± 0.3	2.13 ± 0.28	2.08 ± 0.11	1.9 ± 0.12	2.28 ± 0.62	2.3±0.31
U	3.31 ± 0.45	3.42 ± 0.27	2.16 ± 0.38	3.95 ± 0.26	3.69 ± 0.37	3.53 ± 0.37	2.45 ± 0.22	2.12 ± 0.09	3.42 ± 0.54	3.06±0.54
V	0.9 ± 0.09	0.78 ± 0.09	0.41 ± 0.12	1.02 ± 0.12	1 ± 0.08	0.86 ± 0.12	0.83 ± 0.07	0.66 ± 0.08	0.99 ± 0.13	1±0.18
W	1.8 ± 0.24	1.44 ± 0.08	1.01 ± 0.24	1.91 ± 0.27	1.95 ± 0.21	1.67 ± 0.22	1.53 ± 0.1	1.24 ± 0.04	1.87 ± 0.23	1.76±0.28
X	1.95 ± 0.18	1.46 ± 0.04	0.88 ± 0.15	1.53 ± 0.22	1.54 ± 0.24	1.59 ± 0.19	1.64 ± 0.11	1.44 ± 0.04	2.04 ± 0.29	1.95±0.22
Y	4.45 ± 0.39	4.12 ± 0.22	2.93 ± 0.45	4.92 ± 0.3	4.81 ± 0.35	4.22 ± 0.42	3.74 ± 0.25	3.36 ± 0.08	5.17 ± 0.82	4.91±0.44

because the individual variation in these two groups is relatively larger. The TP and TN groups seem somewhat dispersed across the two clusters but are not completely separated. This indicates that the morphometric characteristics of these two locations are similar to Cluster 1, while also sharing some similarities with Cluster 2. Meanwhile, Cluster 3, or the isolated cluster, consists of the RW1 and RW2 groups. These groups are distinctly separated from the others, though there are differences between the two groups. This suggests significant morphological differences between Cluster 1 and Cluster 2.

The results of the PCA variable analysis show that four morphometric characters were most influential in clustering the fish, namely: Mouth to Pectoral Fin Base Distance (H), Anal Fin to Caudal Fin Base Distance (L), Anal Fin Height (V), and Body Width (Y). Subsequently, a Kruskal-Wallis test was conducted to examine significant differences between the groups, with the following results: For variable C (Figure 4c), it was found that TS significantly differed from RW1 (P=0.0041), RW2 (P<0.0001), TN (P<0.0001), and KHY (P<0.0001); The RW1 group significantly differed from TP (P=0.0367) and BT (P=0.0349); The RW2 group significantly differed from TP (P=0.0001), MT (P=0.0020), BT (P=0.0007), and LM (P=0.0049); The TN group showed significant differences from TP (P=0.0010), MT (P=0.0124), BT (P=0.0048), and LM (P=0.0374). Meanwhile, KHY exhibited significant differences from TP (P=0.0006), MT (P=0.0091), BT (P=0.0035), and LM (P=0.0262). The RW2, KHY, and TN groups tended to have higher mean ranks compared to the other groups.

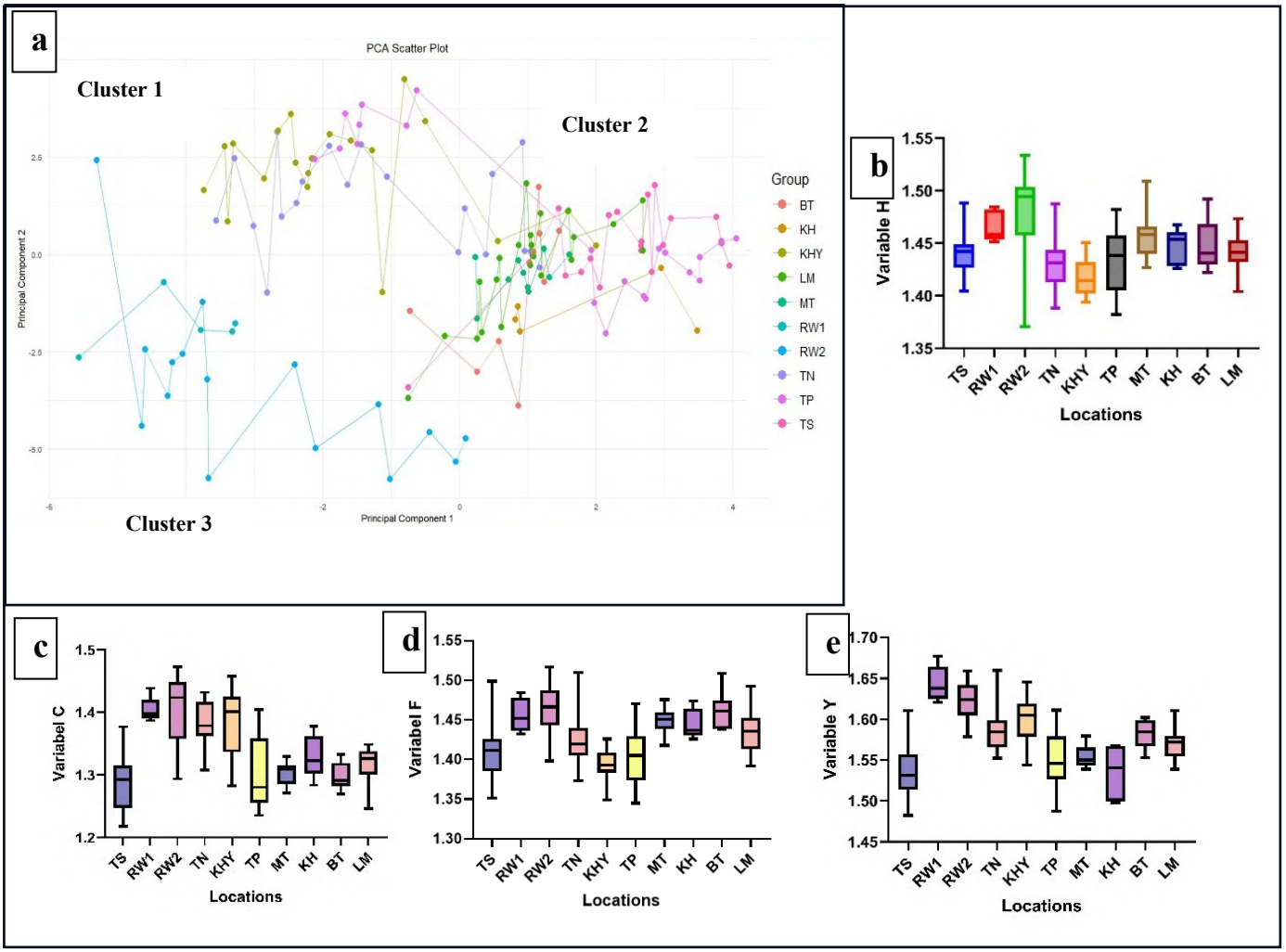

Figure 4. Analysis Morphometric of *Anabas testudineus*: a). Scatter Plot PCA; b) boxplot variable H; c) boxplot variable C; d) boxplot variable F; e) boxplot variable Y.

For variable F (Figure 4d), the TS group significantly differed from RW2 (P=0.0031) and BT (P=0.0107). The RW1 group significantly differed from KHY (P=0.0093); The RW2 group showed significant differences with KHY (P<0.0001) and TP (P=0.0002); The KHY group significantly differed from MT (P=0.0005), BT (P<0.0001), and LM (P=0.0024); Additionally, the TP group showed significant differences with MT (P=0.0216) and BT (P=0.0012). Overall, the KHY group stood out with the most significant differences compared to the other groups for this variable. For variable H (Figure 4b), the test results for this variable showed significant differences between several group pairs. The TS group significantly differed from RW2 (P=0.015). The RW1 group significantly differed from KHY (P=0.0056). The RW2 group showed significant differences with TN (P=0.0001), KHY (P<0.0001), and TP (P=0.0023). Additionally, the KHY group significantly differed from MT (P=0.0041). These results confirm the presence of important differences between certain groups.

In variable Y (Figure 4e), among all fish groups, TS, RW1, and RW2 are the three groups showing the most significant differences compared to other groups. The TS group exhibits highly significant differences ($p<0.001$) with RW1, RW2, and KHY, as well as significant differences ($p<0.05$) with TN and BT. The RW1 group shows highly significant differences ($p<0.001$) with TS and significant differences ($p<0.05$) with TP, MT, KH, and LM. The RW2 group demonstrates highly significant differences ($p<0.001$) with TS and TP, as well as moderately significant differences ($p<0.01$) with MT, KH, and LM. By analysing the intergroup comparison results for each variable (C, F, H, and Y), it is evident that TS, RW1, RW2, and KHY are the groups with the most significant differences compared to others, and the significance values align with the formation of three clusters in the PCA scatter plot.

Meristic

Eight meristic fin characters (dorsal, caudal, pectoral, ventral, and anal) were tabulated using fin formulas (Mawa et al. 2021) and summarized into five main characters (Table 2). Meanwhile, six meristic scale count characters were presented using the minimum and maximum counts within each fish group. The Pelvic Fin characters (PFHS and PFSR) showed consistent counts across all fish groups. On the other hand, the remaining ten meristic characters tended to exhibit differences in counts between fish groups.

Body Shape, Coloration and Pattern

Ten colour variations found across all samples are described as follows (Figure 5): (A) The fish has a dark brown to golden-yellow coloration. Its body shape is oval, appearing more robust rather than compressed, with a rounded head; (B) This fish exhibits a dark olive-green coloration with a smooth gradient along its body, giving it a muted, earthy appearance. The body is elongated and Its body is more elongated and oval-shaped, appearing more robust than Fish A; (C) The fish has a solid dark coloration, primarily black, with no visible patterns, and its body is oval-shaped, sturdy, and slightly flattened on the sides; (D) With the brightest coloration among the others, this fish has a dominant pale-yellow hue that gradually fades. The body features faint dark vertical stripes that contrast with the light yellow colour. There is also a slight reddish tint in some areas. A distinct black spot is visible on the caudal fin, adding a unique pattern to the fish's appearance; (E) The fish has a light greyish colour on its back, with a yellowish hue on its underside. In certain lighting, there is a subtle light greenish tint visible on the body. Its body shape is elongated and relatively slender, contributing to its streamlined appearance; (F) This fish has a mix of black and dark green on its back, which lightens towards the ventral region. Its body is adorned with scattered black speckled patterns, extending from the lower middle part of

Table 2. Results of the Meristic Character Analysis of *Anabas testudineus*.

Meristic Characters	Locations									
	TS	RW1	RW2	TN	KHY	TP	MT	KH	BT	LM
Dorsal Fin (DFS and DFSR)	D.XII-XIX, 8-10	D.XVII-XVIII, 8-9	D.XVII-XVIII, 7-10	D.XVI-XIX, 8-10	D.XVII-XXII, 8-11	D. XVII-XIX, 8-10	D.XVII-XIX, 8-10	D.XVII, 7-9	D.XVIII-XIX, 9-11	D.XVII-XVIII, 9-10
Pelvic Fin (PFHS and PFSR)	P2.I, 5	P2.I, 5	P2.I, 5	P2.I, 5	P2.I, 5	P2.I, 5	P2.I, 5	P2.I, 5	P2.I, 5	P2.I, 5
Pectoral Fin (PFR)	P.14-16	P.13-15	P.11-15	P.13-15	P.13-17	P.14-15	P.13-15	P.14-15	P.15-16	P.14-15
Anal Fin (AFS and AFSR)	A.VIII-XI, 8-11	A.IX-XI, 9-12	A.X-XI, 8-10	A.X-XI, 9-13	A.X-XI, 9-11	A.X-XI, 8-19	A.X.XI, 9-10	A.VIII-X, 8-9	A.X-XI, 9-11	A.VIII-X, 9-10
Caudal Fin Rays (CFR)	C.15-18	C.13-16	C.14-16	C.15-16	C.15-17	C.12-17	C.16-16	C.16-16	C.15-16	C.16-16
Predorsal Scales	15-20	13-16	14-18	14-19	15-19	15-18	15-18	14-15	17-19	15-21
Cheek Scales	50-62	52-59	40-57	48-80	48-59	20-56	49-54	37-41	46-62	52-60
Circumference Scales	26-34	26-30	23-28	25-31	27-31	25-35	26-32	23-24	28-34	24-32
Caudal Peduncle Scales	15-18	11-16	9-12	12-17	12-17	14-17	15-19	13-16	15-19	16-20
Lateral Line Scales	30-38	30-35	25-29	27-43	32-40	31-35	31-35	26-28	32-39	33-40
Scales Above and Below The Lateral Line	15-19	16-18	13-16	16-19	15-29	15-18	15-18	15-16	16-20	16-20

the body towards the caudal fin. The body shape is round, compact, and broad in the middle; (G) This fish exhibits a uniform black coloration across its body. Its body shape is elongated, appearing similar to Fish "C" but slimmer and more noticeably flattened giving it a sleeker profile; (H) This fish exhibits a laterally compressed body with an overall oval profile. Its coloration is predominantly dark brown to olive green. Faint stripes are present on the ventral surface, and a black spot is located in the caudal region.

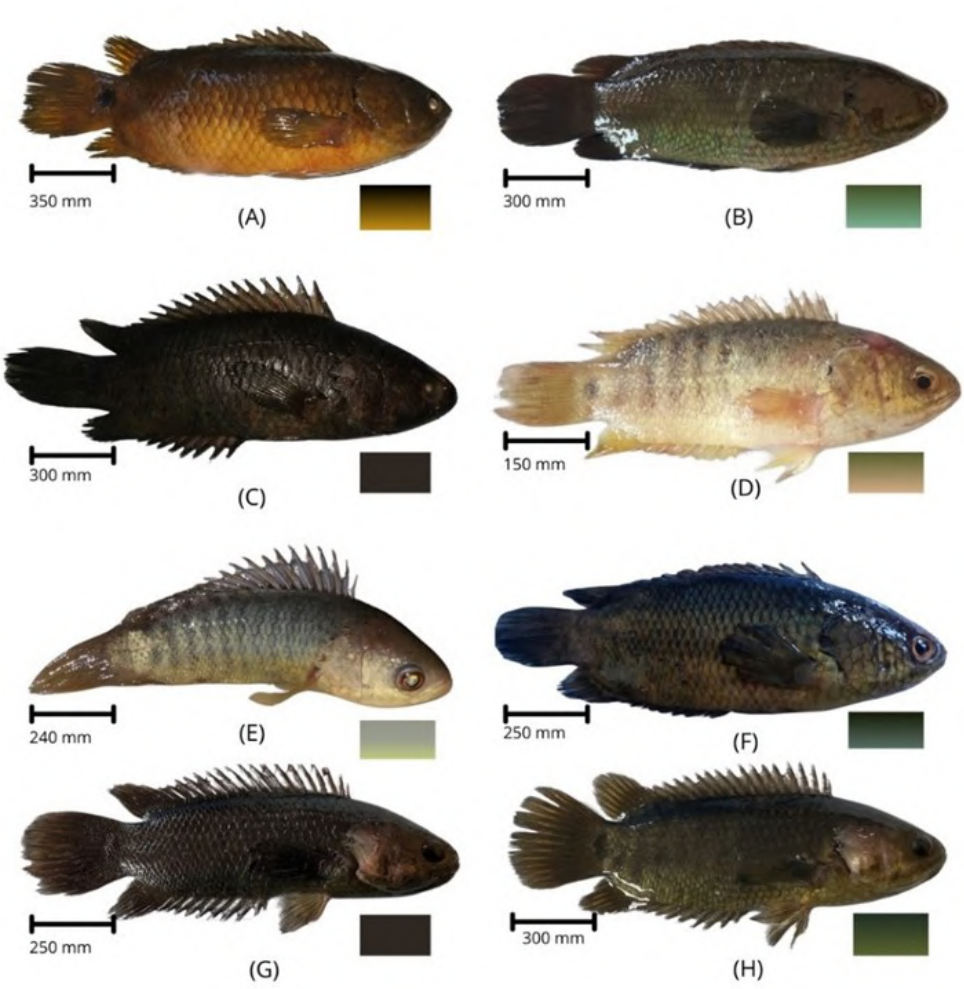

Figure 5. Coloration and Body Shape Differences of *Anabas testudineus*.

Observations of *Anabas testudineus* (Figure 6) show variation in patterns and markings between individuals. These variations include: (a) a pattern of black spots at the base of the caudal fin; (b) black spots scattered in the ventral area extending towards the caudal region; (c) irregular striping patterns on the dorsal part, with one black spot on the caudal fin; (d) blotchy patterns scattered across the entire body; and thick vertical lines extending from the anterior to the posterior dorsal, towards the ventral region of the body. Although similar patterns can be found in different groups, differences can be observed based on the combination of patterns and colours within specific groups. Furthermore, the combination of patterns and colours tends to be consistent within individuals in a particular group of fish.

DISCUSSION

Morphometrics, Meristics, and Morphology Adaptations

Based on the observation of the collected samples, three main groupings were identified (Figure 4a): Cluster 1 (KHY, TN, and TP), Cluster 1 refers to the main river and its tributaries, forming an ecosystem derived from the same water flow. The Kahayan River (KHY) is characterized by a dendritic tidal

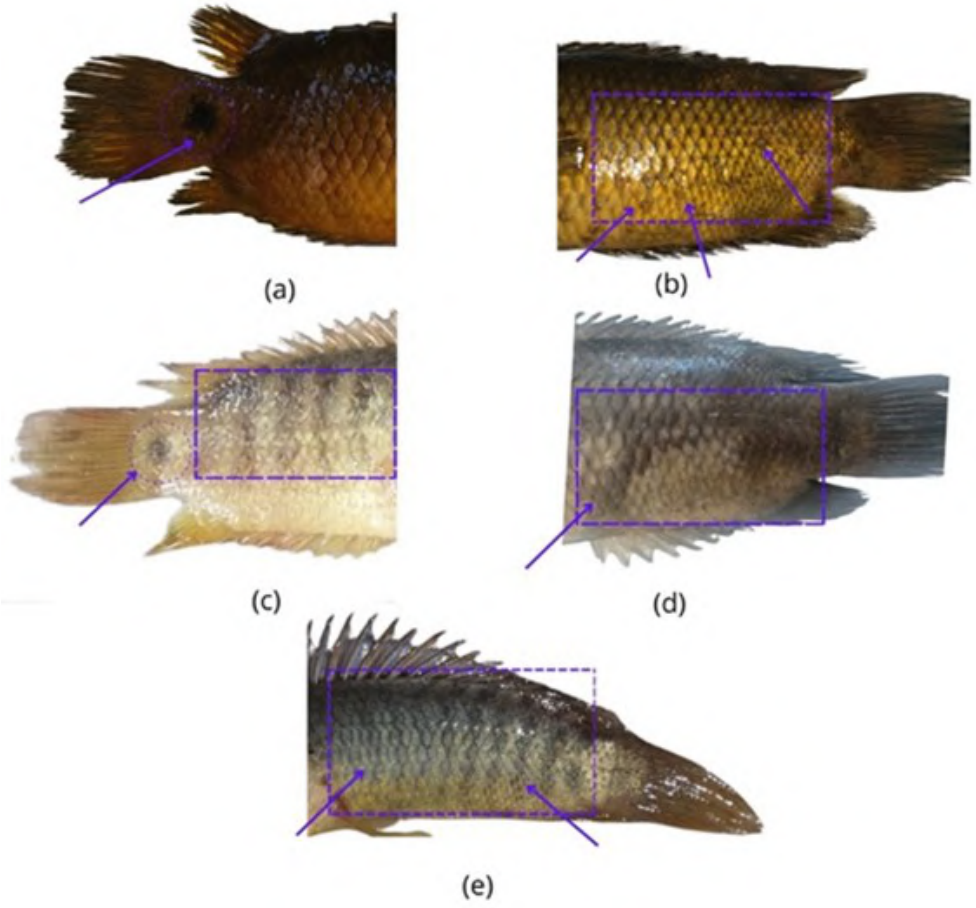

Figure 6. Pattern Differences of *Anabas testudineus*.

pattern, with its upstream fed by tributaries, transitioning to peat swamps in the middle section, and tidal swamps downstream. During the rainy season, the river overflows into floodplain areas, while in the dry season, the water recedes (Maimunah et al. 2020; Fera et al. 2022; Yanti 2023).

Cluster 2 (BT, KH, LM, MT, TP, TS, TN): This cluster includes the majority of locations, showing a tendency for similar morphology. Although the group consists of locations that are geographically dispersed and might have a wider variety of habitats, the ecosystems in each location likely share similarities in flora, fauna, and environmental conditions. This leads to the formation of fish groups with diverse morphology but still showing traits connected to more general environments, such as large rivers and estuaries. In line with the region's physiographic conditions, the Kahayan River, as the main river, has a relatively low slope extending to its middle section. This influences the reach of tidal flows (particularly during the dry season), which can extend far inland. Conversely, during the rainy season, the river frequently overflows into lowland areas along its course. Meanwhile, Tumbang Nusa (TN) and Tewang Panjang (TP) are two areas within the branching streams of the Kahayan River (Figure 7) and are part of its watershed. Therefore, fish from these locations exhibit relatively similar morphological groupings due to their shared origin.

Cluster 3 (RW1 and RW2), These two locations represent swamps situated in the city of Palangka Raya. The fish groups in these locations display distinct morphological clustering, likely due to the specific environmental conditions and vegetation types associated with peat swamps (Kissinger et al. 2022). Interestingly, some geographically distant locations fall into the same cluster, while nearby locations belong to different clusters (Figure 7). Several factors can explain this phenomenon: Habitat Variability vs. Geographical Distance: Even though some locations are geographically far apart, their eco-

logical habitats may be very similar. For example, two distant sites with comparable water conditions, water quality, or vegetation types may lead to fish developing similar morphological adaptations. Conversely, closely located sites might exhibit significant habitat differences, such as variations in salinity, depth, current, or flora and fauna diversity, causing fish to adapt with differing morphologies (Urbina et al. 2011; Sun et al. 2023). For instance, based on observations in *Anabas* species, fish inhabiting fast-flowing water tend to develop slimmer body proportions, whereas those in still-water environments exhibit more compact body shapes. Similarly, in gobies, a streamlined body structure has been shown to enhance fast-start performance, which facilitates predator evasion—particularly in climbing fish (Diamond et al. 2021). Genetic Flow and population exchange: The migratory behaviour of A. testudineus (Pavlov et al. 2020), enables genetic exchange when populations meet (Glover et al. 2017). On the other hand, fish populations in nearby locations may face ecological barriers that hinder genetic exchange due to limited interactions, resulting in distinct morphological traits between groups.

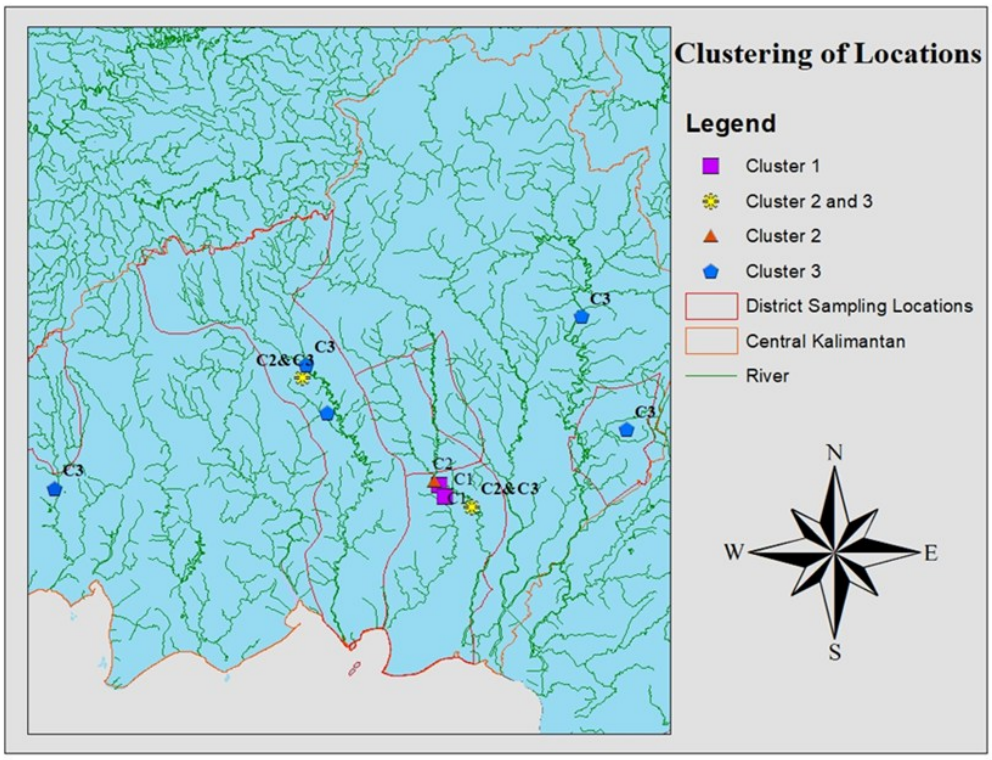

Figure 7. Clustering of Locations of *Anabas testudineus*.

Variation in environmental conditions can trigger phenotypic plasticity in fish. Genes involved in morphological adaptation become activated, enhancing the organism's ability to cope with diverse environmental challenges. This process is mediated by epigenetic mechanisms such as DNA methylation, which does not alter the DNA nucleotide sequence but acts as an "on-off switch" for the expression of specific genes (Makvandi-Nejad & Moghadam 2023). Plasticity is not always permanently heritable; for morphological traits to become part of evolutionary adaptation, long-term natural selection acting on the underlying genetic variation of the plastic response is required. Nevertheless, transgenerational plasticity mechanisms exist, referring to the ability of parents to modify the phenotype of their offspring without genetic alteration. Parental environmental experiences can influence the genotype expression in their offspring, enabling them to develop physiological traits better suited to prevailing environmental conditions (Roy et al. 2023). Thus, the interaction between environmental and genetic factors plays a key role in gen-

erating and maintaining morphological variation in fish of the same species across different habitats.

The analysis of meristic characters obtained from all sampling locations also revealed a significant tendency for morphological differences in *A. testudineus*. This is demonstrated by the variation in the number of fins and scales at each location, with most differences being significantly distinct (Table 2). In fact, the differences that formed correlate with differences in morphometric characters. This indicates the role of morphological adaptation to habitat differences in each fish population, such as food, dissolved oxygen levels, salinity, and human activities (Svanbäck 2004; Smith 2020; Abdelnour et al. 2024).

Variation in Colour and Pattern

All of the specimens observed exhibited variations in body colour patterns. Generally, the colour and pattern on fish serve as adaptations related to their feeding habits when acting as predators and as a form of protection when they are prey. These patterns help fish camouflage by resembling the surrounding vegetation or substrate. Fish use their body colour and patterns as a form of aposematism in their efforts to defend themselves in the environment (Caro & Ruxton 2019; Halpin & Rowe 2019). Ten different colours were found, ranging from dark, slightly dark, to light tones. This study revealed that the collected specimens tend to exhibit darker colour variations (Figure 5).

The formation of colour variation in *A. testudineus* is most likely due to phenotypic adaptation influenced by the dark-coloured peat swamp ecosystem waters. The colour of an animal's body affects how well an individual can blend and camouflage with its environment, even allowing them to minimise detection by predators (Stevens & Ruxton 2019). This is why fish are more active with darker body colours in waters that tend to be similarly coloured. Conversely, light-coloured bodies in dark waters result in more restricted movement for the fish (Lehtonen et al. 2023). On the other hand, bright colours can serve as a signal and warning to potential predators that the fish may be dangerous (Mappes et al. 2005; Rowe & Halpin 2013; Hamasaki et al. 2022). In addition, body colouration and patterns can serve as signals for mating success and the establishment of dominance over other males (Endler 1984; John et al. 2021). According to (Blakeslee et al. 2009; Peroš et al. 2025) body colouration also plays a role in how fish determine their shoaling group and social hierarchy structure.

In addition to colour differences, five distinct body pattern variations were found in *A. testudineus* (Figure 6). Animals with specific patterns that move quickly within a visual field can create a "Flicker Fusion" phenomenon (Umeton et al. 2017). This phenomenon causes a visual illusion where rapidly moving patterned objects create a visualisation that appears unclear. In fish, this effect allows them to appear as a single colour or a different visual representation, making it difficult for predators to target them as prey. In the specimens observed, fish with patterns on their bodies were more commonly found in those with lighter colour patterns. Although patterns were also found in fish with darker colour patterns, they appeared more prominently on areas of the body that were lighter in colour. This suggests that the function of the patterns is related to environmental conditions.

Adaptive morphology involving variations in body colouration and patterning across different ecosystems also occurs in other fish species. Colour polymorphism has been observed in the *L. vittata* species complex across habitats with varying salinity levels (Rodriguez-Silva et al. 2023). *Rhadinocentrus ornatus* exhibits colour variation in habitats with differing light conditions. Light plays a crucial role in signalling within aquatic environments, thereby influencing the development of competing phenotypes in this species (Hancox

et al. 2013). A study by Fark et al. (2022) revealed green and brown colour variations in *Symphodus roissali* and *S. rostratus* in Mediterranean marine waters, which are likely driven by the heterogeneous (mosaic) nature of their habitats. Brown-coloured individuals predominantly inhabit rocky substrates, while green morphs are more frequently found in seagrass-dominated areas. All of these highlight morphological adaptations in response to environmental stimuli.

Based on these findings, and supported by various studies demonstrating the relationship between habitat differences and the emergence of morphological variation, phenotypic plasticity is likely to play a key role in shaping the future evolutionary trajectory of fish. Amid widespread environmental degradation caused by anthropogenic activities and climate change, the selective value of certain morphological traits may shift significantly. Therefore, morphological adaptation may serve as a foundational step in evolutionary change, particularly as a response mechanism when phenotypic plasticity alone is no longer sufficient to cope with environmental challenges.

CONCLUSIONS

This study reveals morphological variation in *A. testudineus* found across ten locations. Based on morphometric analysis, three main clusters were identified based on significant morphological characters, namely the Distance from Mouth to Pectoral Fin Base (H), Distance from Anal Fin to Caudal Fin Base (L), Height of Anal Fin (V), and Body Width (Y). These variations reflect phenotypic adaptations as compensation for habitat differences. Meanwhile, the meristic results showed a dominant difference in most characters between the fish groups. Colour variation was also found as part of habitat adaptation, with a tendency toward darker colours and varied patterns. Overall, this morphological and meristic study of *A. testudineus* contributes valuable insights into the environmental influence on speciation and morphological adaptation in freshwater fish species. Further research is needed to confirm the relationship between morphological variation and genetic and ecological factors, as well as its implications for future conservation strategies for this species.

AUTHOR CONTRIBUTION

L.S conceptualised and designed the study, conducted field sampling, analysed data, and wrote the manuscript. M.R.W. assisted in field sampling, laboratory work, data processing, and contributed to data interpretation and manuscript review. A.N.I, supervised the research process and contributed to manuscript editing and finalisation. M.U, assisted in field sampling, data collection, and initial data entry. R.R. provided support during data collection and prepared samples for analysis. All authors have reviewed and approved the final manuscript for publication.

ACKNOWLEDGMENTS

The authors would like to thank the Faculty of Biology, University of Palangka Raya, for providing laboratory facilities during this research. The authors also express their gratitude to the local communities and fishermen in Central Kalimantan for their support in facilitating sample collection across various habitats.

CONFLICT OF INTEREST

The authors declare no conflict of interest. This research was conducted independently, and all funding was provided by the authors themselves.

REFERENCES

Abdelnour, S.A. et al., 2024. Environmental epigenetics: Exploring phenotypic plasticity and transgenerational adaptation in fish. *Environmental Research*, 252, 118799. doi: 10.1016/j.envres.2024.118799

Adedeji, H. A. et al., 2024. Comparative Analysis of Morphometric and Meristic Characters in Oreochromis niloticus (Linnaeus, 1758), Nile Tilapia across Diverse Ecological Zones in Nigeria. *Asian Journal of Fisheries and Aquatic Research*, 26(7), pp.80–90. doi: 10.9734/ajfar/2024/v26i7785.

Ahmadi, 2019. Morphometric characteristic and growth patterns of climbing perch (*Anabas testudineus*) from sungai batang river, Indonesia. *International Journal of Hydrology*, 3(4), pp.270-277. doi: 10.15406/ijh.2019.03.00189

Akbar, H., 2008. *Studi Karakter Morfometrik-Meristik Ikan Betok (Anabas testudineus Bloch) di DAS Mahakam Tengah Propinsi Kalimantan Timur*. Institut Pertanian Bogor.

Armbruster, J.W., 2024. A new genus for the Blackfin Sucker, Thoburnia atripinnis (Cypriniformes: Catostomidae). *Zootaxa*, 5536(2), pp.325–335. doi: 10.11646/zootaxa.5536.2.8

Blakeslee, C. et al., 2009. The effect of body coloration and group size on social partner preferences in female fighting fish (Betta splendens). *Behavioural Processes*, 80(2), pp.157–161. doi: 10.1016/j.beproc.2008.11.005

Bungas, K., 2014. Keragaman Fenotip Ikan Betok (*Anabas testudineus* Bloch) di Perairan Rawa Gambut. *Jurnal Ilmu Hewani Tropika*, 3(1), pp.33-38.

Caro, T. & Ruxton, G., 2019. Aposematism: Unpacking the Defences. *Trends in Ecology & Evolution*, 34(7), pp.595–604. doi: 10.1016/j.tree.2019.02.015

Chukwuka, A.V. & Adeogun, A.O., 2024. Habitat-driven otolith shape morphology in Oreochromis niloticus (pelagic) and Chrysichthys nigrodigitatus (benthic) from distinct zones of a tropical coastal lagoon syste. *Regional Studies in Marine Science*, 78, 103760. doi: 10.1016/j.rsma.2024.103760

Dasuki, A. et al., 2023. Distinguishing Hybrids of Golden Thailand and Malaysian Strains of Climbing Perch, *Anabas testudineus* (Bloch, 1792), Using Multivariate Analyses of Morpho-Meristic Traits. *Asian Fisheries Science*, 36(3), pp.171–181. doi: 10.33997/j.afs.2023.36.3.006.

Diamond, K.M. et al., 2021. Interactions among multiple selective pressures on the form–function relationship in insular stream fishes. *Biological Journal of the Linnean Society*, 134(3), pp.557–567. doi: 10.1093/biolinnean/blab098

Endler, J.A., 1984. Natural and sexual selection on color patterns in poeciliid fishes. In *Evolutionary ecology of neotropical freshwater fishes*. Dodrecht: Springer. doi: 10.1007/978-94-015-7682-6_7

Eschmeyer, W.N., Laan, R.V.D. & Fricke, R., 2024, 'Eschmeyer's Catalog of Fishes, California Academy of Science', in *California Academy of Sciences*, viewed 15 November 2024, from http://researcharchive.calacademy.org/research/ichthyology/catalog/fishcatmain.asp

Fark, S.N. et al., 2022. Multispecies colour polymorphisms associated with contrasting microhabitats in two Mediterranean wrasse radiations. *Journal of Evolutionary Biology*, 35(4), pp.633–647. doi: 10.1111/jeb.13999

Fera, N. et al., 2022. *Buku Pintar Dinas Kelautan dan Perikanan Provinsi Kalimantan Tengah 2022*, Pemprov Kalimantan Tengah: Dinas Kelautan dan Perikanan.

Froese, R. & D. Pauly, 2024, 'The Global Database of Fishes FishBase, Wide Web electronic publication', in *FishBase*, viewed 25 November 2024, from https://www.fishbase.se/summary/Anabas-testudineus.html

Glover, K.A. et al., 2017. Half a century of genetic interaction between farmed and wild Atlantic salmon: Status of knowledge and unanswered questions. *Fish and Fisheries*, 18(5), pp.890–927. doi: 10.1111/faf.12214.

Halpin, C.G. & Rowe, C., 2019. Aposematism as a Defence Against Predation. In *Encyclopedia of Animal Behavior*. Elsevier, pp.182–190. doi: 10.1016/B978-0-12-809633-8.20858-3.

Hamasaki, K., Takahashi, Y. & Dan, S., 2022. Body colourations affect predation risk from fish in fiddler crabs. *Journal of Experimental Marine Biology and Ecology*, 557, 151818. doi: 10.1016/j.jembe.2022.151818.

Hanafie, A. et al., 2023. Study of Growth And Survival of Climbing Perch (*Anabas Testudineus* Bloch) With Different Sex Ratio In Biofloc System. *Russian Journal of Agricultural and Socio-Economic Sciences*, 134(2), pp.185–201. doi:10.18551/rjoas.2023-02.22.

Hancox, D., Wilson, R.S. & White, C.R., 2013. Visual habitat geometry predicts relative morph abundance in the colour-polymorphic ornate rainbowfish. *Proceedings of the Royal Society B: Biological Sciences*, 280(1752), 20122377. doi: 10.1098/rspb.2012.2377

Haryono et al., 2017. Karakterisitk Morfologi dan Habitat Ikan Brek (Barbonymus balleroides Val. 1842) di Sungai Serayu Jawa Tengah. *Jurnal Biologi Indonesia*, 13(2), pp.223–232. doi: 10.47349/jbi/13022017/223.

Hart, J.C. et al., 2018. Convergent evolution of gene expression in two high-toothed stickleback populations. *PLOS Genetics*, 14(6), e1007443. doi: 10.1371/journal.pgen.1007443

Hossen, M. B. et al., 2017. Morphometric and Meristic Variation of Indigenous and Thai Koi, *Anabas testudineus* Available in Coastal Region of Bangladesh. *International Journal of Innovative Research*, 2(1), pp.01-08.

Hughes, G.M. & Singh, B.N., 1970. Respiration in An Air-Breathing Fish, the Climbing Perch, *Anabas Testudineus*. *Journal of Experimental Biology*, 53 (2), pp.281–298. doi: 10.1242/jeb.53.2.281.

ITIS., 2024. '*Anabas testudineus* (Bloch, 1792)', in *Integrated Taxonomic Information System*, viewed 3 Desember 2024 from https://www.itis.gov/servlet/SingleRpt/SingleRpt?search_topic=TSN&search_value=172585#null

IUCN., 2019. *Anabas testudineus* (errata version published in 2020). The IUCN Red List of Threatened Species 2019: e.T166543A174787197. doi: 10.2305/IUCN.UK.2019- 3.RLTS.T166543A174787197.en

John, L. et al., 2021. Body coloration as a dynamic signal during intrasexual communication in a cichlid fish. *BMC Zoology*, 6(1), 9. doi: 10.1186/s40850-021-00075-9

Kissinger, Pitri, R.M.N. & Nasrulloh, A.V., 2022. Implementation of Plant Selection Based-On Plant Growth on Revegetation of Peatland in South Kalimantan. *International Journal of Environment, Agriculture and Biotechnology*, 7(2), pp.137-142. doi: 10.22161/ijeab.72.15

Kumaladewi, P. et al., 2022. Morphometric and Meristic Analysis of Rasbora in East Java Province. *Journal of Aquaculture and Fish Health*, 11(3), 298–305. doi: 10.20473/jafh.v11i3.30956

Laan, R.V.D., Eschmeyer, W.N. & Fricke, R., 2014. Family-group names of recent fishes. *Zootaxa*, 3882(1), pp.1–230. doi: 10.11646/zootaxa.3882.1.1.

Larsen, P.F. et al., 2011. Gene expression analysis for the identification of selection and local adaptation in fishes. *Journal of Fish Biology*, 78(1), pp.1–22. doi: 10.1111/j.1095-8649.2010.02834.x.

Lawson, L.P. et al., 2023. Diversification of spiny-throated reed frogs (Anura: Hyperoliidae) with the description of a new, range-restricted species from the Ukaguru Mountains, Tanzania. *PLoS ONE*, 18(2), e0277535. doi: 10.1371/journal.pone.0277535.

Lehtonen, T.K., Candolin, U. & Wong, B.B.M., 2023. Environmental variation promotes colour morph-specific behavioural differences in a cichlid fish. *Animal Behaviour*, 197, pp.123–130. doi: 10.1016/j.anbehav.2023.01.005.

Li, P. et al., 2024. Terrestrial locomotion characteristics of climbing perch (*Anabas testudineus*). *Journal of Experimental Biology*, 227(11), jeb247238. doi: 10.1242/jeb.247238.

Lin, J.E. et al., 2017. Modeling local adaptation and gene flow in sockeye salmon. *Ecosphere*, 8(12), e02039. doi: 10.1002/ecs2.2039

Manon, M.R.K. et al., 2023. Intraspecific phenotypic differences in climbing perch *Anabas testudineus* (Bloch, 1792) populations may be linked to habitat adaptations. *Heliyon*, 9(7), e17685. doi: 10.1016/j.heliyon.2023.e17685.

Maimunah et al., 2020. Analisis Karakteristik Morfometri DAS Maluka Menggunakan Citra Satelit Shuttle Radar Topography Mission. *Jurnal Geografika (Geografi Lingkungan Lahan Basah)*, 1(1), pp.12-19. doi: 10.20527/jgp.v1i1.2293

Makvandi-Nejad, S. & Moghadam, H., 2023. Genetics and Epigenetics in Aquaculture Breeding. In *Epigenetics in Aquaculture*. Wiley, pp.439–449. doi: 10.1002/9781119821946.ch19

Mappes, J., Marples, N. & Endler, J., 2005. The complex business of survival by aposematism. *Trends in Ecology & Evolution*, 20(11), pp.598–603. doi: 10.1016/j.tree.2005.07.011.

Mawa, Z. et al., 2021. Estimation of Relative Growth of *Anabas testudineus* through multiple linear dimensions. *Egyptian Journal of Aquatic Biology and Fisheries*, 25(1), pp.935-952. doi: 10.21608/ejabf.2021.153232

Montaña, C.G. et al., 2020. Functional and trophic diversity of fishes in the Mekong-3S river system: comparison of morphological and isotopic patterns. *Environmental Biology of Fishes*, 103(2), pp.185–200. doi: 10.1007/s10641-020-00947-y.

Ndobe, S. et al., 2019. Meristic characters and length-weight relation of climbing perch (*Anabas testudineus*) from wetlands in Sigi District, Central Sulawesi, Indonesia. *IOP Conference Series: Earth and Environmental Science*, 370, 012001. doi: 10.1088/1755-1315/370/1/012001.

Nuralam, E. & Luthfi, M.J., 2019. 'The Anatomy of Respiratory Organ of Climbing Perch (*Anabas testudineus*)', viewed 20 November 2024, from https://ejournal.uin-suka.ac.id/saintek/icse/article/view/2566

Parvez, I. et al., 2020. Genetic variation of native and introduced climbing perch *Anabas testudineus* (Bloch, 1792) derived from mitochondrial DNA analyses. *Ecological Genetics and Genomics*, 17, 100067. doi: 10.1016/j.egg.2020.100067.

Pavlov, E.D. et al., 2020. Effect of Urea and Thiourea on Migration Activity of Climbing Perch *Anabas testudineus*. *Journal of Ichthyology*, 60(6), pp.885–890. Doi: 10.1134/S0032945220060053.

Peroš, M. et al., 2025. Male bluegill vary in color and behavior relative to their position in a lek. *Frontiers in Ethology*, 3, 1513231. doi: 10.3389/fetho.2024.1513231

Ponomareva, V.Y., Pavlov, D.S. & Kostin, V.V., 2017. Development and application of methods for investigating the ratio of rheoreaction types of fish in a circular tank. *Inland Water Biology*, 10(1), pp.103–111. doi: 10.1134/S1995082917010151

Rodriguez-Silva, R. et al., 2023. Color polymorphism in the Cuban endemic livebearing fish *Limia vittata* (Teloestei, Poeciliidae): Potential roles of sexual and natural selection. *Ecology and Evolution*, 13(1), e9768. doi: 10.1002/ece3.9768

Rowe, C. & Halpin, C., 2013. Why are warning displays multimodal?. *Behavioral Ecology and Sociobiology*, 67(9), pp.1425–1439. doi: 10.1007/s00265-013-1515-8.

Roy, S. et al., 2023. Transgenerational Phenotypic Plasticity in Fishes. In *Biotechnological Tools in Fisheries and Aquatic Health Management*. Springer Nature Singapore, pp.59–75. doi: 10.1007/978-981-99-2981-8_4

Samoilov, K.Y. & Tran, D.D., 2022. Morphological Plasticity and Biological Patterns of the Climbing Perch *Anabas testudineus* from Different Types of Water Bodies in Khánh Hòa Province, Vietnam. *Inland Water Biology*, 15(3), pp.217–226. doi: 10.1134/S1995082922020109

Septya, L. & Wanto, W.A., 2024. An Inventory and Analysis of Conservation Status of Freshwater Fish Species in Palangka Raya City Traditional Markets. *Jurnal Biologi Tropis*, 24(2), pp.623–629. doi: 10.29303/jbt.v24i2.6930.

Shuai, F. et al., 2018. Habitat effects on intra-species variation in functional morphology: Evidence from freshwater fish. *Ecology and Evolution*, 8 (22), pp.10902–10913. doi: 10.1002/ece3.4555

Slamat, S. et al., 2019. The Breeding of Climbing Perch (*Anabas Testudineus*) With Meristic Phylogenetic Hybridization Technique Sampled From Three Types of Swamp Ecosystems. *Tropical Wetland Journal*, 5(2), pp.31–39. doi: 10.20527/twj.v5i2.72.

Smith, M., 2020. Evolution. In *Gene Environment Interactions*. Academic Press, pp.55–78. doi: 10.1016/B978-0-12-819613-7.00003-7.

Srinu, G., Padmavathi, P. & Chatla, D., 2019. Identification and Validation of *Anabas* spp. (Osteichthyes: Anabantidae) Through Morphology and DNA Barcoding From Lake Kolleru, Andhra Pradesh, India. *Journal of Coastal Research*, 86(sp1), pp.142-148. doi: 10.2112/SI86-022.1.

Stevens, M. & Ruxton, G.D., 2019. The key role of behaviour in animal camouflage. *Biological Reviews*, 94(1), pp.116–134. doi: 10.1111/brv.12438.

Sun, L. et al., 2023. Relation between fish morphological differentiation and pressure drag difference. *Ecological Indicators*, 156, 111071. doi: 10.1016/j.ecolind.2023.111071.

Svanbäck, R., 2004. *Ecology and Evolution of Adaptive Morphological Variation in Fish Populations*. Umeå University.

Tuset, V.M. et al., 2018. Morpho-functional diversity in Diaphus spp. (Pisces: Myctophidae) from the central Atlantic Ocean: Ecological and evolutionary implications. *Deep Sea Research Part I: Oceanographic Research Papers*, 138, pp.46–59. doi: 10.1016/j.dsr.2018.07.005.

Umeton, D., Read, J.C.A. & Rowe, C., 2017. Unravelling the illusion of flicker fusion. *Biology Letters*, 13(2), 20160831. doi: 10.1098/rsbl.2016.0831.

Urbina, M.A., Forster, M.E. & Glover, C.N., 2011. Leap of faith: Voluntary emersion behaviour and physiological adaptations to aerial exposure in a non-aestivating freshwater fish in response to aquatic hypoxia. *Physiology & Behavior*, 103(2), pp.240–247. doi: 10.1016/j.physbeh.2011.02.009.

Waltham, N.J. et al., 2023. New Australian frontier in freshwater fish invasion via Torres Strait Islands. *Biodiversity and Conservation*, 32(14), pp.4551–4571. doi: 10.1007/s10531-023-02716-6

Yanti, E.V., 2023. Dinamika Musiman Kualitas Air di Daerah Aliran Sungai Kahayan Kalimantan Tengah. *ZIRA'AH*, 42(2), pp.107-118.

Journal of Tropical Biodiversity and Biotechnology
Volume 10, Issue 04 (2025): jtbb14522
DOI: 10.22146/jtbb.14522

Research Article

Antioxidant, Antibacterial, and Wound Healing Capacities of *Merremia Borneensis* Leaves from Brunei Darussalam

Nurhazirah Nurazmy[1], Nurul Ashifah Shafie[1], May Poh Yik Goh[2], Farazimah Yakop[2], Hussein Taha[1,3], Norhayati Ahmad[1,2,3]*

1)Environmental and Life Sciences Programme, Faculty of Science, Universiti Brunei Darussalam, Jalan Tungku Link BE1410, Brunei Darussalam
2)Herbal Research Group, Universiti Brunei Darussalam, Jalan Tungku Link, Gadong BE 1410, Brunei Darussalam
3)Institute for Biodiversity & Environmental Research, Universiti Brunei Darussalam, Jalan Tungku Link BE1410, Brunei Darussalam
* Corresponding author, email: norhayati.ahmad@ubd.edu.bn

Keywords:
Akar Bilaran
Antibacterial
Antioxidant
Ethnomedicinal
Merremia borneensis
Wound Healing
Submitted:
05 July 2024
Accepted:
01 June 2025
Published:
10 November 2025
Editors:
Ardaning Nuriliani
Sri Nopitasari

ABSTRACT

Merremia borneensis has important applications in traditional folk medicine. However, the ethnomedicinal value of the plant has yet to receive scientific validation. Bioactivities of *M. borneensis* leaves from Brunei Darussalam were evaluated by analysing the antioxidant, wound healing, and antibacterial activities of the methanol extract and its chloroform, ethyl acetate, and hexane partitioned extracts. The DPPH radical scavenging assay was used to assess the antioxidant capacities of the extracts. The disc diffusion assay was adopted to investigate the antimicrobial activities of the extracts against *Bacillus subtilis*, *Pseudomonas aeruginosa*, *Escherichia coli*, and *Staphylococcus aureus*. The wound healing activities of the methanol extract were analysed using *in vivo* analysis on male Wistar rats. The ethyl acetate and methanol extracts demonstrated high radical scavenging activities of over 90 %. Antibacterial activities of both methanol and ethyl acetate extracts were evident against all four bacterial strains, whereas the chloroform extract only showed activity against *E. coli*. The hexane extract showed weak antioxidant activity and no detectable antibacterial activity. In the wound healing study, topical treatment with 50 % w w^{-1} of the methanol extract in pure petroleum jelly base yielded complete wound closure at post-wounding day 15. Both 10 % and 50 % w w^{-1} dosages accelerated wound contraction and showed augmented formation of collagen structures. Overall, the Bruneian *M. borneensis* leaf extracts showed substantial antioxidant and antibacterial activities, while topical treatment with *M. borneensis* showed improved wound healing progress in the treated animals.

How to cite:
Nurazmy, N. et al., 2025. Antioxidant, antibacterial, and wound healing capacities of *Merremia borneensis* leaves from Brunei Darussalam. *Journal of Tropical Biodiversity and Biotechnology*, 10(4), jtbb14522. doi: 10.22146/jtbb.14522

INTRODUCTION

The use of plants as medicines began in ancient times, as humans started to investigate the use of leaves, bark, flowers, seeds, and other plant parts as medicine to overcome diseases (Petrovska 2012). Most traditional knowledge of plants was passed down orally from one generation to the next, and as a result much of it has been left unrecorded (Jantan 2004). According to traditional medicinal practitioners who have used plants to treat diseases, plant products can generally be referred to as functional foods since edible medicinal plants with therapeutic values can be consumed by people as a source of nutrients as well as a means to prevent various ailments (Rahmatullah et al. 2010).

Antioxidant properties have been widely reported in medicinal plants (Krishnaiah et al. 2011). Antioxidants hold the potential to treat human diseases such as cardiovascular and inflammatory diseases as they prevent cellular oxidative stress that may cause degenerative diseases if untreated (Tepe et al. 2005; Othman et al. 2011; Krishnaiah et al. 2011). Antioxidants are believed to elevate the body's defence system due to their activity against reactive oxygen species (ROS) or free radicals that can accelerate ageing and tissue damage (Metussin et al. 2017).

Many medicinal plants have also been exploited for their effectiveness against pathogenic microorganisms, which are attributable to their secondary metabolites (Selvamohan et al. 2012). The concentration of secondary metabolites in every plant tissue varies depending on the plant parts, with the leaves usually accumulating more bioactive compounds that function to hinder the growth of disease-causing microbes (Selvamohan et al. 2012). In the pharmaceutical industry, plant extracts are claimed to have mechanisms that differ from those undergone by antibiotics, and thus are potentially useful in the fight against drug-resistant microbial pathogens (Selvamohan et al. 2012). The emergence of resistant microbes has prompted scientific investigations to uncover new antimicrobial agents from medicinal plants (Elumalai et al. 2011).

Plants are also known for their use in wound management and treatment. The presence of various phytoconstituents, such as essential oils, alkaloids, tannins, saponins, terpenoids, flavonoids, and phenols, has displayed wound-healing activities, including their roles as biological targets in important mechanisms such as the alteration of cellular cues and behaviours (Edeoga et al. 2005; Thakur et al. 2011). The efficacy of phytochemicals in combating bacterial infections is able to assist in the progression of inflammatory and angiogenic functions in skin regeneration. Other properties, such as antioxidant and anti-inflammatory activities, are known to induce accelerated wound healing (Shah & Amini-Nik 2017).

Merremia borneensis Merr., from the family Convolvulaceae, is a shrub commonly found in Southeast Asia. It is locally referred to as 'akar bilaran' in Brunei Darussalam. The flowers, sticky-latex-containing stems and leaves of the plant have been shown to possess various biological activities (Shah & Hossain 2014; Hossain & Shah 2015). The plant is regarded as an important medicinal herb in many countries. In particular, the natives in Sarawak, Malaysia have claimed the effective use of the leaves to treat breast cancer (Hossain & Shah 2015). *M. borneensis* was found to contain an abundance of nutrients and minerals including vitamins A, B and C, iron, phosphorus, and calcium (Shah & Hossain 2014). The leaves of the plant were also revealed to comprise a wide variety of bioactive phytochemicals, including alkaloids, amino acids, flavonoids, glycosides, phytosterols, saponins, steroids, tannins, and triterpenoids, which may be associated with the medicinal properties of the leaves (Shah & Hossain 2014). The essential oil and extracts of the *M. borneensis* leaves from Malaysia were previously shown to possess good anti-

oxidant potential attributable to their high flavonoid content (Hossain & Shah 2015). In another study, the methanol extract of the leaves from the Bruneian variety of *M. borneensis* was found to contain palmitic acid whereas the aqueous extract showed the presence of 3-hydroxy benzyl alcohol, coumarancoumarin, and catechol (Awang-Jamil et al. 2021). The methanol extract exhibited marked inhibitory effects against *Saccharomyces cerevisiae* whereas the aqueous extract was not active against *E. coli*, *P. aeruginosa*, *B. subtilis* and *S. aureus* (Awang-Jamil et al. 2021). Antibacterial studies were not carried out for the methanol leaf extract of *M. borneensis* (Awang-Jamil et al. 2021). In view of the knowledge gap that still remains for the bioactivity of *M. borneensis*, this study aims to further elucidate the antibacterial activities of additional extracts of the leaves of *M. borneensis* from Brunei Darussalam as well as their antioxidant and wound healing potentials in pursuit to identify novel bioactive compounds that could potentially be used to improve currently available treatment agents.

MATERIALS AND METHODS

Materials

Quercetin, 1,1-diphenyl-2-picrylhydrazyl (DPPH), sodium phosphate monobasic (NaH_2PO_4), sodium phosphate dibasic (Na_2HPO_4), and streptomycin (EC223-286-0) were purchased from Sigma-Aldrich (St. Louis, MO, USA). Hexane, methanol, chloroform, ethyl acetate, xylene, sodium chloride (NaCl), and potassium chloride (KCl) were obtained from Merck (Kenilworth, New Jersey, USA). Nutrient broth, nutrient agar, and Mueller Hinton agar were obtained from Oxoid Ltd (Basingstoke, Hampshire, England). Formaldehyde, haematoxylin, and paraffin wax were obtained from Scharlau (Spain), Thermo Scientific (England), and Fluka (Switzerland), respectively. Only analytical grade chemicals were used.

Preparation of plant extracts

Healthy, mature *M. borneensis* leaves were collected at Bandar Seri Begawan, Brunei Darussalam. Particular effort was made to ensure that infected, yellowing, and old leaves were excluded. Species verification was performed by a botanist. The leaves were dried under a shade for several weeks and a grinder was used to grind the dried samples into coarse powder. Soxhlet extraction was carried out on 100 g of the powdered sample with 1 L of methanol, according to Hasan et al. (2012) with slight modification, followed by vacuum filtration (Hasan et al. 2012). The filtrate was concentrated via rotary evaporation, and the resulting concentrate was dried in a fume hood until a semi-solid methanol extract was obtained. The methanol extract (5.51 g) was consecutively partitioned with 50 mL of chloroform, ethyl acetate, and *n*-hexane. The process was repeated twice, with a total of 150 mL of each of the solvents. The resulting fractions were then collected and concentrated via rotary evaporation, followed by further drying in a fume hood.

DPPH radical scavenging activity

The DPPH radical scavenging activity was determined according to the method described by Sumaya-Martinez et al. (2005) with slight modification. Methanolic solutions of quercetin were prepared at concentrations ranging from 5 to 25 µg mL^{-1} to create a standard curve. The methanol, *n*-hexane, chloroform, and ethyl acetate extracts were each re-suspended in methanol to achieve a concentration of 1000 µg mL^{-1}. For each reaction, a 0.2 mL aliquot of either the quercetin solution or the re-suspended extract was combined with 1 mL of methanolic DPPH solution. In addition, 100 % methanol was used as the control. The mixture was vortexed and incubated in light-safe conditions for 30 minutes. The absorbances were measured at 517 nm via UV

spectrophotometry. The percentage radical scavenging activity of the extracts was calculated based on the formula below, where $Abs_{control}$ is the measured absorbance for the control and Abs_{sample} is the measured absorbance for either the quercetin solution or the re-suspended extract:

$$\text{DPPH scavenging activity (\%)} = (Abs_{control} - Abs_{sample}/Abs_{control}) \times 100\ \% \quad (1)$$

The standard curve of quercetin was used to determine the quercetin equivalent concentrations of each plant extract. All assays were conducted in triplicate.

Antibacterial activity

The antibacterial activities of the extracts against two gram-positive bacteria, *Bacillus subtilis* (ATCC 6633) and *Staphylococcus aureus* (ATCC 29213), and two gram-negative bacteria, *Escherichia coli* (ATCC 25922) and *Pseudomonas aeruginosa* (ATCC 27853) were determined via the disc diffusion assay. Each bacterium was cultured onto nutrient agar before being cultured in nutrient broth at 37 °C for 24 hours. A UV spectrophotometer was used to measure and adjust the turbidity of each bacterial culture to an absorbance of 0.07 to 0.1 at 600 nm, which was equivalent to that of the McFarland 0.5 turbidity standard. Mueller Hinton agar plates were individually inoculated with each bacterium. Based on our preliminary data, antibacterial activities were observed between the workable concentrations of 12.5 to 500 µg mL^{-1}. Therefore, the extracts of *M. borneensis* were reconstituted in methanol at concentrations of 12.5, 50, 100, 300 and 500 µg mL^{-1} to determine their antibacterial effects at different concentrations. Then, 10 µL of each concentration was loaded onto 6 mm paper discs, and placed onto the inoculated Mueller Hinton agar plates. The treated plates were subjected to 24-hour incubation at 37 °C. Methanol and streptomycin (20 µg mL^{-1}) was used as negative and positive controls, respectively. The study was conducted in triplicate. Plant extracts with antibacterial activity produced a clear zone around the disc and the mean diameter was measured in mm.

Wound healing activity

Approval for all animal-related work was obtained from the University Research Ethics Committee [approval letter reference number: FOS/E2(g)]. All relevant activities were conducted based on the guidelines on the use of animals for scientific purposes as well as internationally accepted guidelines. The animals were carefully handled to ensure minimal harm and were closely monitored for signs of distress and pain.

Animals

Male Wistar rats that were 180 to 200 g and 8 to 9 weeks of age were selected for the assay. The rats were provided a standard pellet diet (Cat # 1324, Altromin, Germany) and water *ad libitum*. The animals were kept in the University Animal Facility with a standard 12/12-hour light/dark cycle and maintained at 25 ± 2 °C. Before commencement of the animal study, each animal was assessed for its general health and condition. The welfare and provisions of the animals were attended to throughout the duration of the experiment.

Formulation of ointment

Herbal ointment containing a low dosage of 10 % (w w^{-1}) and a high dosage of 50 % (w w^{-1}) of the methanol *M. borneensis* leaf extract was prepared in petroleum jelly. The herbal ointments were stored at -20 °C until use.

Animal groupings

Animals for the wound excision model were randomly assigned to three groups, with n=6 per group. Animals in Group 1 (control) received petroleum jelly as the only treatment. Group 2 and Group 3 received treatment with the low and high dosage ointments, respectively. All animals were treated according to their group allocation throughout the experimental period of 15 days.

Excisional wound induction

Prior to excision of the wound, the animals were subjected to anaesthesia via diethyl ether inhalation. The wound excision was carried out as previously described (Shafie 2020). The ointments were applied directly to the wound site of the animals daily from day 1 to day 15 post wounding.

Wound area determination

Digital photographs of the wound site were taken with the label and a 10 mm scale bar for reference on post-excision days 1, 3, 5, 7, 11, 13 and 15 (Figure 1). The wound areas were analysed using ImageJ (National Institute of Health, USA) (Figure 2). Briefly, the known distance was first used to calibrate the lengths measured on the software. The wound edge was then outlined using the freehand selection tool, followed by measurement of the wound area by the software.

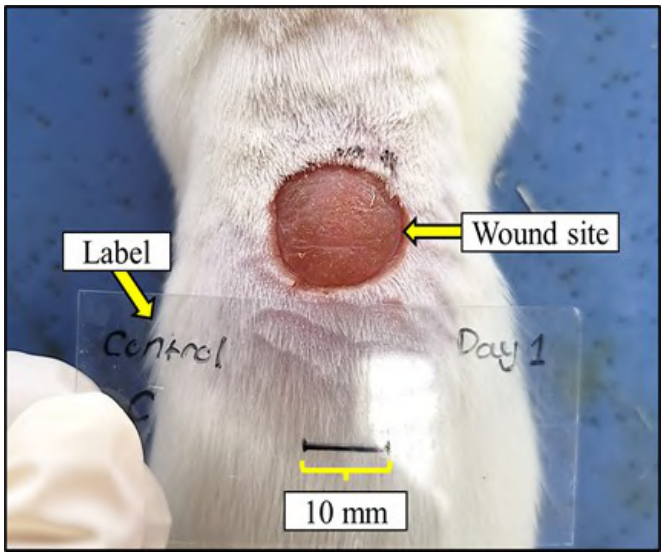

Figure 1. Wound site of anaesthetized rat with label containing post-wounding day, name, and scale bar reference of 10 mm.

A percentage of wound contraction was calculated based on the wound contraction rate as previously defined (Shi et al. 2013):

$$\% \text{ Wound Contraction} = \frac{(\text{Initial Wound Area} - \text{Final Wound Area})}{\text{Initial Wound Area}} \text{ X } 100\% \quad (1)$$

Histological Analysis

Rats were euthanised by means of CO_2 asphyxiation at the end of the experiment, on post-wounding day 15. The entire wound site, including a margin of surrounding healthy skin, was excised. The tissue was immediately fixed in a fixative, most commonly 10 % neutral buffered formalin, to preserve tissue structure. Paraffin-embedded tissue samples were sectioned at a thickness of 10 µm. The tissue sections were then mounted onto glass slides, and subjected to haematoxylin and eosin (H&E) staining for qualitative morphological assessment of granulation tissues. Representative sections that accurately reflected the tissue sample from each group were used for comparison.

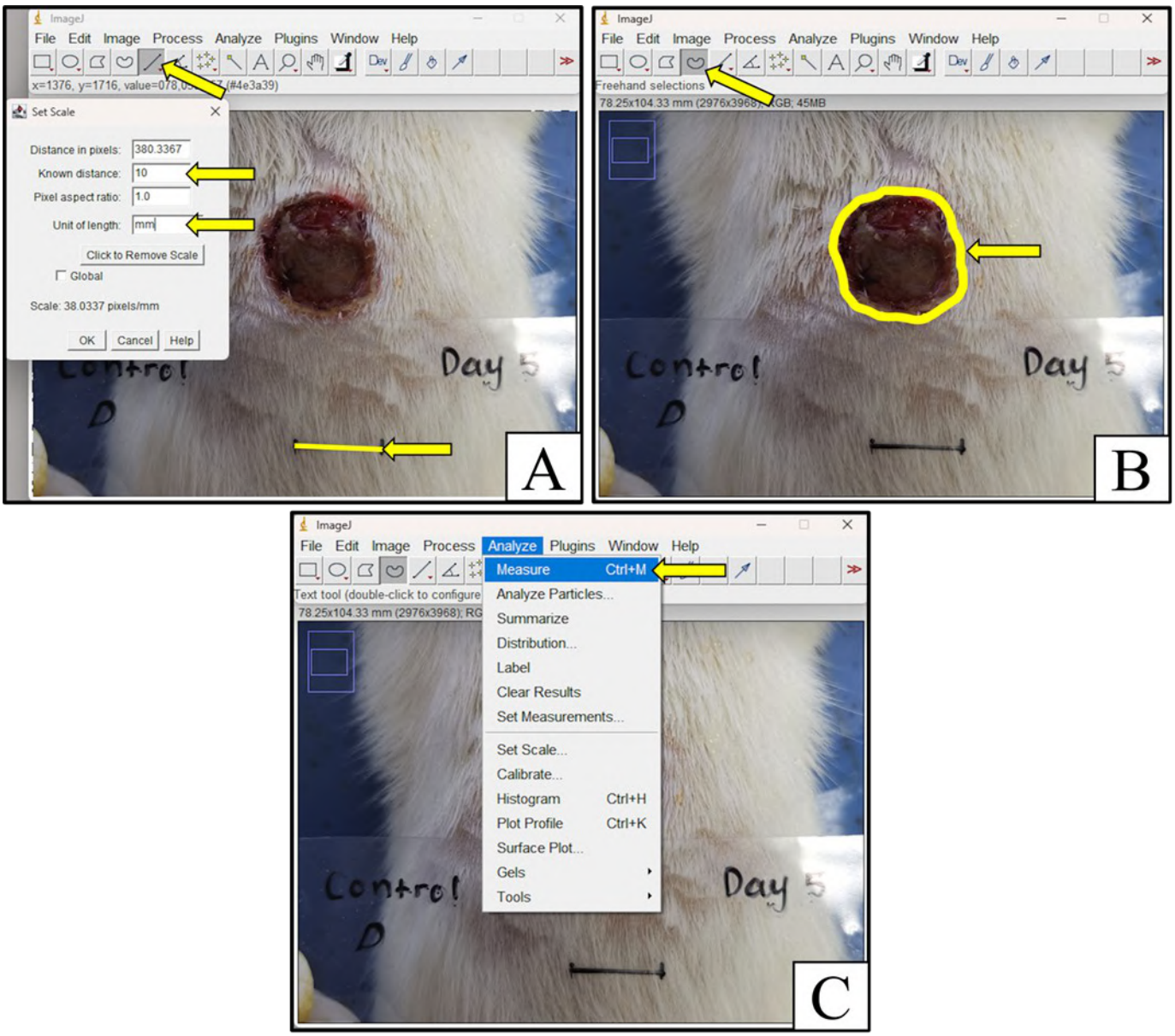

Figure 2. Image processing for quantitative calculation using ImageJ software. The steps in quantifying the area of wound include: (A) calibration with known distance; (B) outlining wound edge using free hand selection; (C) measurement of wound area.

Statistical analyses

The R-3.2.1 software was used to perform the statistical analyses for this study. Differences between the control and treatment groups were analysed using one-way analysis of variance (ANOVA), followed by the post hoc comparisons using Tukey's Honest Significant Difference test. Statistical significance was indicated by a p-value of less than 0.05. All results were expressed as mean ± the standard error of the mean (SEM) or standard deviation (SD).

RESULTS

Extraction yields

The Soxhlet extraction yielded 15.56 % of crude methanol extract from the ground leaf samples. Subsequent solvent partitioning yielded 27 %, 12.7 % and 10.71 % of hexane, chloroform, and ethyl acetate extracts, respectively, from the crude methanol extract.

DPPH radical scavenging activity

At the concentration of 1000 µg mL^{-1}, all extracts of the *M. borneensis* leaves investigated herein showed significant DPPH scavenging activity. The

DPPH radical scavenging assay measures the free radical scavenging ability of antioxidant compounds, which can be observed by a change from dark violet to pale yellow colour (Kalita et al. 2013). The radical scavenging efficacy of each extract is shown in Figure 3. The ethyl acetate and methanol extracts were observed to be the most effective at scavenging the free radicals, whereas the hexane extract showed the least activity. Statistical comparisons showed that the potency of the methanol extract at scavenging free radicals was not significantly different compared to the ethyl acetate extract ($p > 0.05$). This implies that the ethyl acetate extract was the best partition extract of the methanol extract, with similar DPPH radical scavenging activity. This finding also indicates that ethyl acetate was ideal for antioxidant isolation from the *M. borneensis* leaves.

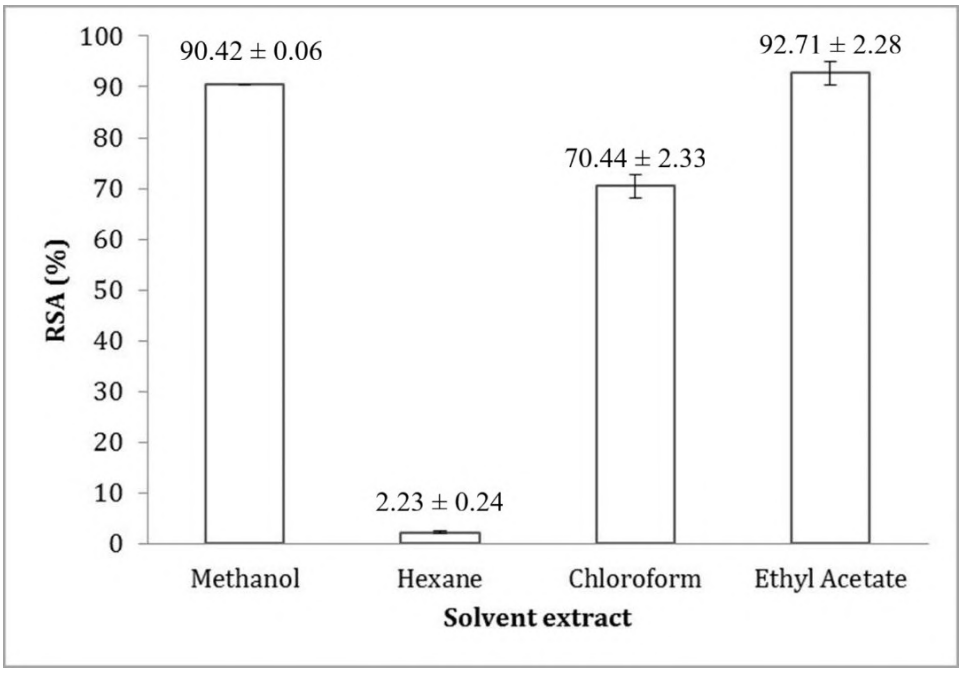

Figure 3. Radical scavenging activity (RSA) of *M. borneensis* leaf extracts. Values shown are average ± SD of triplicates. The ethyl acetate and methanol extracts showed the highest radical scavenging activity compared to the chloroform extract that showed moderate activity and the hexane extract that showed the lowest activity.

Quercetin, which was used as a reference standard in this study, is a known plant flavonol from the flavonoid group of polyphenols, and can scavenge free radicals via the transfer or donation of hydrogen atoms and electrons, respectively (Apak et al. 2007). The quercetin equivalent concentration for the DPPH radical scavenging activity of 1000 µg mL^{-1} of each extract was obtained from the quercetin standard curve (regression line $y = 3.8193x - 4.045$; $R^2 = 0.9981$). In decreasing order, the quercetin equivalent concentrations of the extracts were 25.33 ± 0.06 (ethyl acetate), 24.73 ± 0.02 (methanol), 19.50 ± 0.61 (chloroform) and 1.64 ± 0.60 µg mL^{-1} (hexane). This was similar to the trend observed for the percentage of radical scavenging activity of the extracts mentioned above.

Antibacterial activity

The *in vitro* antimicrobial activities of the extracts of the *M. borneensis* leaves at 12.5 to 500 µg mL^{-1} against the gram-positive bacteria, *S. aureus* and *B. subtilis*, and the gram-negative bacteria, *P. aeruginosa* and *E. coli*, are shown in Table 1. All four bacterial strains showed susceptibility to the methanol and ethyl acetate extracts. However, only *E. coli* was inhibited by the chloroform extract. No inhibition was observed for the hexane extract against all the

Table 1. Zones of inhibition of plant extracts and reference standard.

Extracts	Microorganisms	Streptomycin	Zone of inhibition (mm)				
			12.50 µg mL^{-1}	50 µg mL^{-1}	100 µg mL^{-1}	300 µg mL^{-1}	500 µg mL^{-1}
Methanol	*E. coli*	23.00 ± 4.21	ND	7.89 ± 1.54*	8.89 ± 1.54*	10.11 ± 2.37*	11.44 ± 1.59*
	P. aeruginosa	23.44 ± 3.40	ND	8.22 ± 1.30 *	9.11 ± 0.78*,b	11.56 ± 2.51*,b	11.78 ± 1.56*
	B. subtilis	31.56 ± 2.07	ND	ND	7.67 ± 1.12*	8.11 ± 1.45*	8.67 ± 1.87*
	S. aureus	22.44 ± 1.33	ND	7.44 ± 0.53*	7.61 ± 0.93*,b	8.56 ± 1.13*,b	10.33 ± 1.66*
Ethyl acetate	*E. coli*	24.22 ± 2.51	ND	7.56 ± 0.53*	9.11 ± 1.05*	10.56 ± 1.74*	11.67 ± 2.40*
	P. aeruginosa	22.56 ± 1.67	ND	ND	7.22 ± 0.44*,a	8.00± 0.87*,a	12.00 ± 1.87*
	B. subtilis	33.78 ± 1.72	ND	ND	7.22 ± 0.44*	8.22 ± 0.97*	9.33 ± 0.87*
	S. aureus	23.00 ± 1.87	ND	ND	9.11 ± 0.78*,a	10.44 ± 0.88*,a	11.33 ± 0.87*
Chloroform	*E. coli*	24.56 ± 0.88	7.00 ± 0.43*	7.44 ± 0.53*	8.56 ± 1.42*	9.00 ± 1.66*	10.22 ± 1.79*
	P. aeruginosa	24.67 ± 0.50	NA	NA	NA	NA	ND
	B. subtilis	36.33 ± 2.69	NA	NA	NA	NA	ND
	S. aureus	23.89 ± 0.93	NA	NA	NA	NA	ND
Hexane	*E. coli*	20.89 ± 2.67	NA	NA	NA	NA	ND
	P. aeruginosa	24.00 ± 0.00	NA	NA	NA	NA	ND
	B. subtilis	36.00 ± 0.87	NA	NA	NA	NA	ND
	S. aureus	29.11 ± 1.17	NA	NA	NA	NA	ND

Note: Values shown are average ± SD of three experiments (each with triplicates). ND means not detected. NA means not applicable (antibacterial assay was not conducted when no antibacterial activity was detected at 500 µg mL^{-1}).

*indicates significant difference ($P<0.05$) in zone of inhibition compared to the positive control (streptomycin); [a] indicates significant difference ($P<0.05$) in zone of inhibition compared to the methanol extract at the corresponding concentration; [b] indicates significant difference ($P<0.05$) in zone of inhibition compared to the ethyl acetate extract at the corresponding concentration.

tested bacteria.

The results demonstrated that the methanol extract was potent against *S. aureus*, *P. aeruginosa*, and *E. coli* even at the low concentration of 50 µg mL^{-1}. Similarly, the ethyl acetate extract also inhibited *E. coli* at a minimum concentration of 50 µg mL^{-1}. Interestingly, the chloroform extract was able to inhibit *E. coli* at the lowest concentration of 12.5 µg mL^{-1}.

Macroscopic and quantitative evaluation of wound contraction

At day 3 post excision, the animals treated with 10 and 50 % w w^{-1} of the extract demonstrated 18.9 ± 6.4 and 19.0 ± 3.1 % wound contraction compared to 17.7 ± 4.0 % from animals treated with vehicle only (Table 2). The progress of wound healing at day 3 corresponded to the homeostasis and inflammatory phase of wound healing (Reinke & Sorg 2012; Landén et al. 2016).

Table 2. Effect of *M. borneensis* extract on wound contraction. The table shows the percentage of wound contraction (mean ± SEM) in rats treated with a vehicle control or *M. borneensis* extract (10 % and 50 % w w^{-1}) over a 15-day period. Data points were collected at 3, 7, and 15 days after wound creation. Each group consisted of six animals. Overall, wounds treated with 50 % w w^{-1} *M. borneensis* extract showed complete wound closure at day 15 of post-wound excision.

Animal Group	Percentage of Wound Contraction (%)		
	Day 3	Day 7	Day 15
Vehicle Control	17.7 ± 4.0	66.4 ± 3.2	99.4 ± 0.4
M. borneensis 10 % w w^{-1}	18.9 ± 6.4[a]	75.3 ± 4.3[a]	99.9 ± 0.1[a]
M. borneensis 50 % w w^{-1}	19.0 ± 3.1[a]	73.2 ± 3.4[a]	100 ± 0.0[a]

Note: Data represent mean ± SEM percentage of wound contraction of vehicle (saline) control and *M. borneensis* treated groups (n=6 per group). [a] represents significant ($P<0.05$) compared to the vehicle control.

At day 5, the percentage reduction of wound area was significant in both treatment groups, indicating the progression into the proliferation phase. This observed reduction is indicative of active re-epithelialisation, the restoration of the vascular network, and the development of robust granulation tissues. These processes are essential components of the proliferative stage of wound healing, as described by Landén et al. (2016) and Flanagan (2000), where new tissue formation and structural repair dominate.

At day 7, the wounds of the animals treated with both 10 % and 50 % w w^{-1} extracts dosages further contracted to 75.3 ± 4.3 and 73.2 ± 3.4 %, respectively, both of which were higher compared to vehicle control animals (66.4 ± 3.2 %) We observed scab formation at the wound site in the low dosage group which detached earlier than that in the high dosage group. Proliferation of granulation tissue, characterized as newly formed skin around the wound, was also prominent at post-wounding day 7.

All treatment and control groups displayed secondary scar formation. The wound size of all the animals was further reduced as granulation tissue continued to develop. Towards the end of the experiment, the animals from the high dosage group achieved complete wound closure (100 % wound shrinkage) at day 15 (Table 2; Figure 4C). Meanwhile, animals in the low dosage and control groups displayed 99.9 ± 0.1 and 99.4 ± 0.4 % wound contraction, respectively. There were no signs of irritation and infection observed in any of the animal groups throughout the experimental period.

Histopathological analysis of granulation skin tissue

The granulation tissue of each group was visually compared based on stratification of the epidermal layer and distribution of inflammatory and fibroblast cells as shown in Figures 5 and 6, respectively. This qualitative assessment of the organisation and cellular composition of newly formed granulation tissue enables a comparative assessment of the effects of different treatments on the healing process. Ultimately, this analysis can be used to correlate histological features with the observed macroscopic healing outcomes, thereby providing a deeper understanding of the wound healing activities on a tissue level when treated with *M. borneensis* extract.

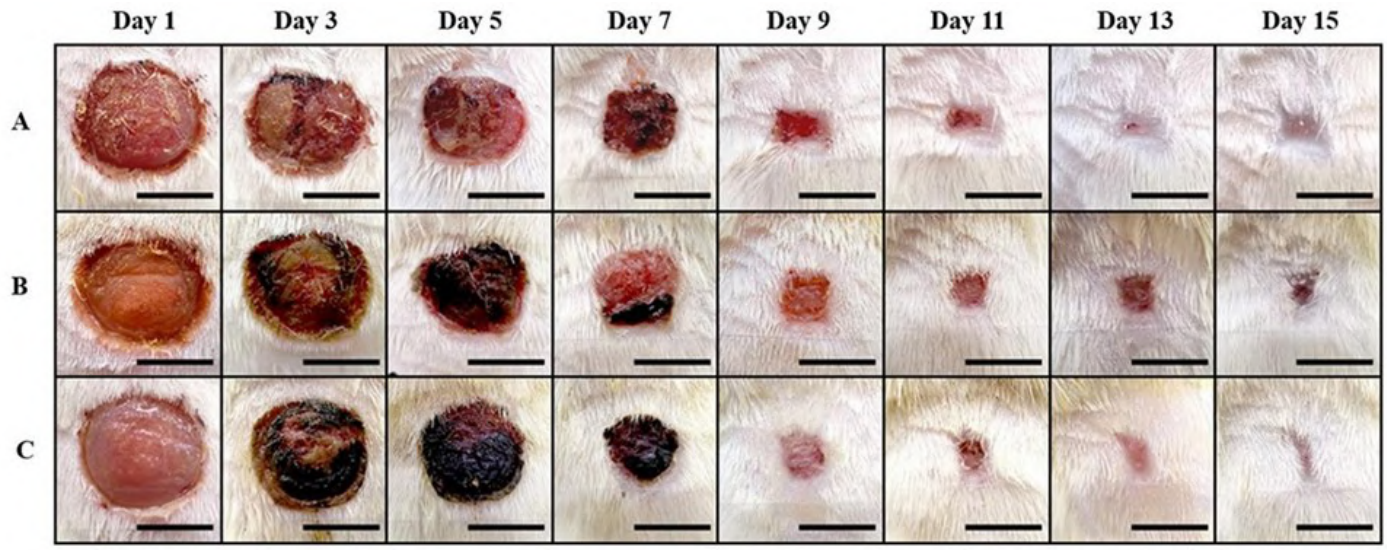

Figure 4. Progress of wound healing in the animals from the (A) vehicle control, (B) low dosage (10 % w w^{-1}) and (C) high dosage (50 % w w^{-1}) of *M. borneensis* extract groups, measured at days 1, 3, 5, 7, 9, 11, 13 and 15 post wound excision. The scale bar represented 1 mm.

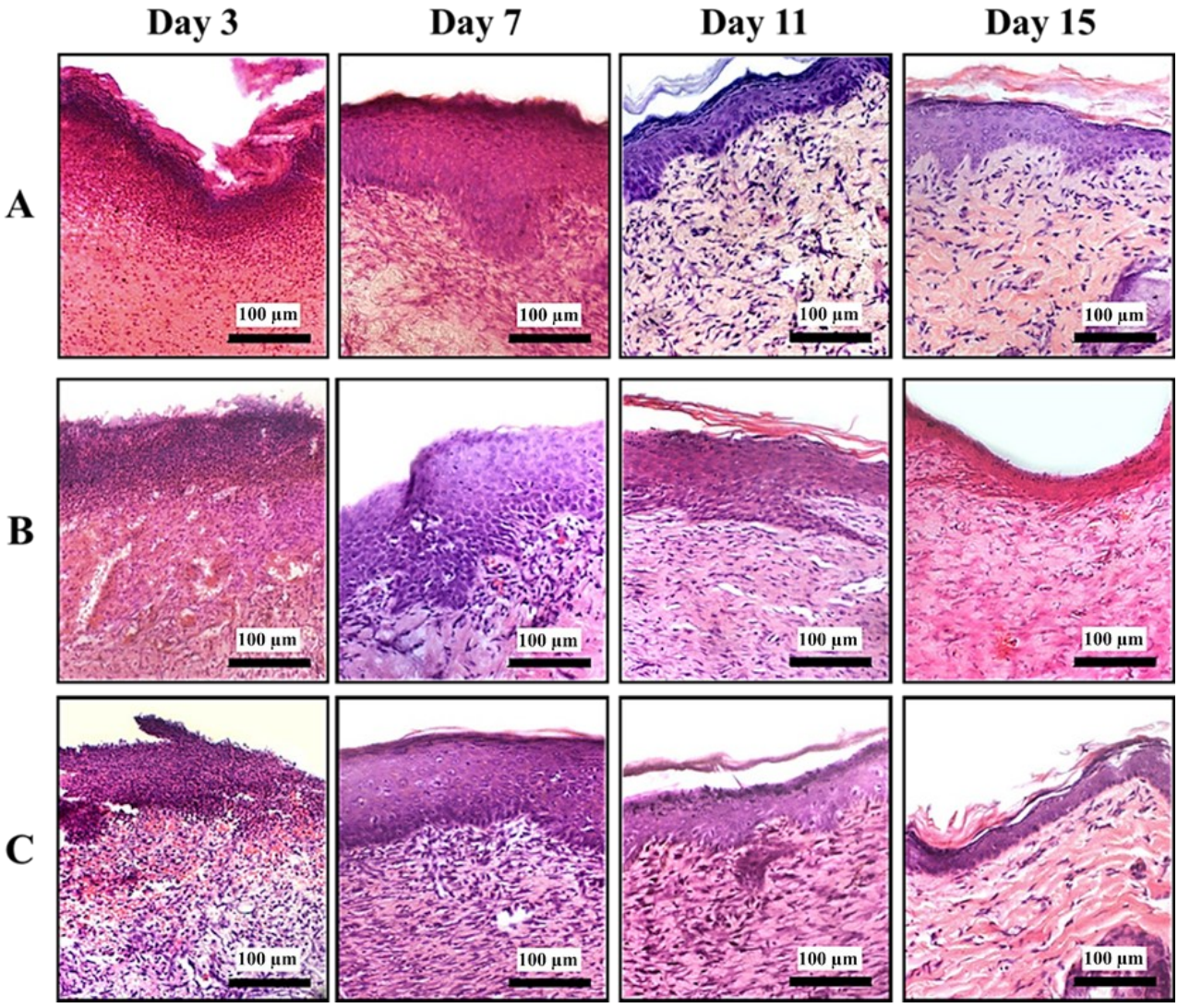

Figure 5. Morphology of the epidermal layer in (A) vehicle control, (B) low dosage (10 % w w^{-1}), and (C) high dosage (50 % w w^{-1}) of *M. borneensis* extract treatment groups, measured at days 3, 7, 11, and 15 post-wound excision, stained with H&E. The epidermal layer is the outermost layer of the skin. Inflammatory cells are seen with darkly stained nuclei. Note the changes in epidermal thickness and the presence of inflammatory cells across different time points and treatment groups. (Magnification x200).

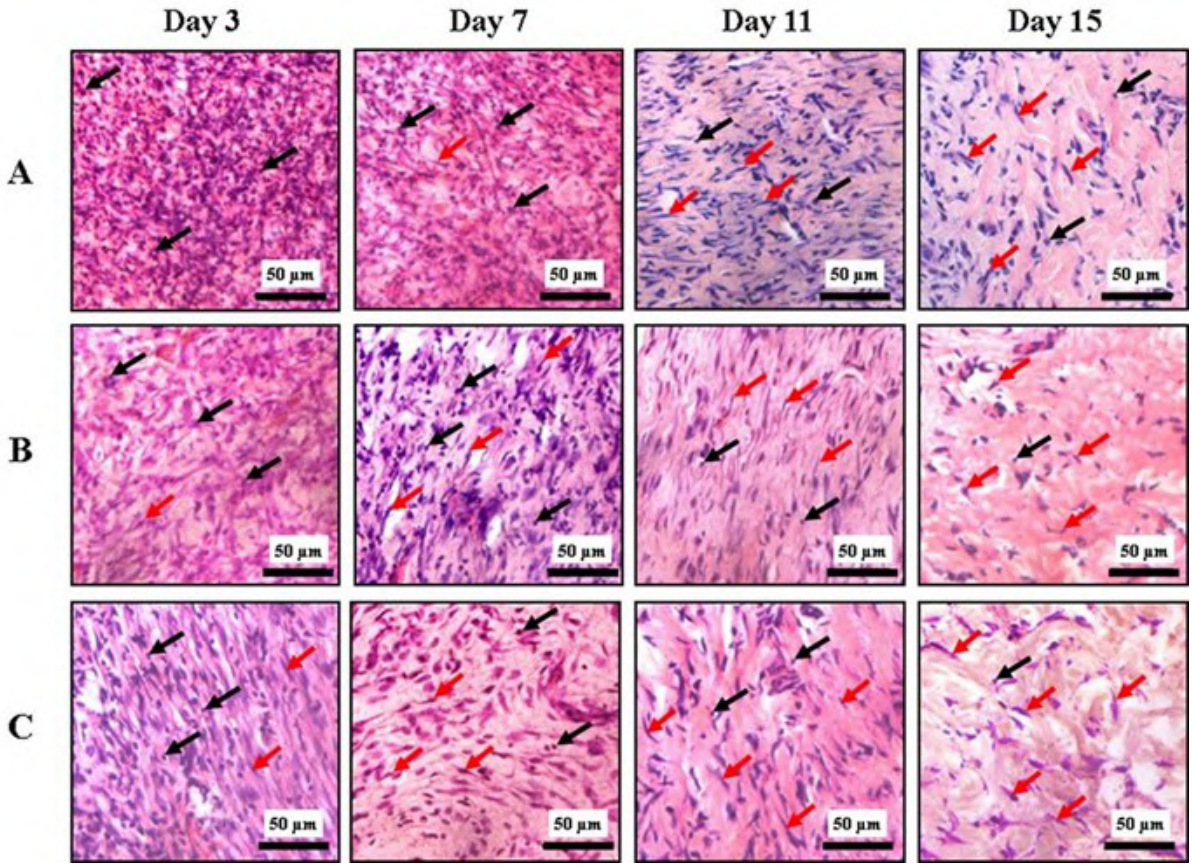

Figure 6. Histological analysis of granulation tissue of (A) vehicle, (B) low dosage (10 % w w^{-1}) and (C) high dosage (50 % w w^{-1}) of *M. borneensis* extract treatment groups, measured at days 3, 7, 11 and 15 post wound excision stained with H&E. Red arrows show fibroblast cells; black arrows show inflammatory cells. (magnification x400).

Three days after wound excision, formation of a thick epidermal layer (Figure 5), and infiltration of inflammatory cells as distinguished by the dark purple-stained mononucleated cells (Figure 6) were generally evident in the granulation tissue of all animals. Infiltration of inflammatory cells was more evident in the control-treated animals (Figure 6A) compared to those in the treatment groups. Infiltration of fibroblasts was also observed in both treatment groups (Figure 6B and Figure 6C). Additionally, the high dosage-treated animals began to show parallel alignment of fibroblasts and formation of new blood vessels.

At post-wounding day 7, a notable stratification at the epidermis-dermis interface and an increase in epidermal thickness compared to day 3 based on qualitative assessment of tissue morphology (Figure 5). The granulation tissues of all animals were also infiltrated with fibroblasts. Inflammatory cells were prominent in the control groups, whereas, the distribution of inflammatory cells appeared reduced in both the extract-treated groups (Figure 6B and Figure 6C). Angiogenesis, which is characterised by formation of new blood vessels, was also observed in animals treated with low dosage extract (Figure 6B), while the high dosage-treated animals displayed obvious fibroblast alignment that was usually accompanied by collagen deposition (Figure 6C).

Subsequently, qualitative observation of granulation tissue morphology exhibited reduced epidermal thickness, clear fibroblast alignment, and collagen fibre deposition were observed in all of the animal groups at post-wounding day 11 (Figure 5). Additionally, blood vessels were profound in the granulation tissue of the control group while inflammatory cells were reduced compared to post-wounding day 7 (Figure 6A). The 50 % w w^{-1} extract-treated animals showed further deposition of collagen which conformed into a compact and wavy arrangement as well as formation of hair follicles (Figure 6C).

By day 15, thinning of the epidermal layer was observed qualitatively in the granulation tissue of all groups (Figure 5A and 5C). We also observed the presence of matured hair follicle shafts especially in the control and high-dosage treatment groups. The granulation tissue of the control group showed profound fibroblasts distribution alongside increased collagen deposition that formed a compact and wavy arrangement of collagen fibres (Figure 6A). Meanwhile, qualitative assessment of the granulation tissue showed that the fibroblasts in both extract-treated animals were generally reduced while more collagen was deposited as the "immature" granulation tissue transformed into "mature" granulation tissue, resulting in a highly compact and wavy arrangement especially in the 50 % w w^{-1} extract-treated animals (Figure 6B and 6C) (Velnar et al. 2009; Jamadagni et al. 2016; Landén et al. 2016).

DISCUSSION

Antioxidant activity of *M. borneensis* leaf extracts

An earlier report on the leaf extracts of *M. borneensis* obtained from Malaysia revealed that the extracts derived from the methanol crude extract through solvent-solvent partitioning had decreasing free radical scavenging activities in the particular order of chloroform > ethyl acetate > hexane (Hossain & Shah 2015). This present study revealed that the ethyl acetate and methanol leaf extract of the *M. borneensis* from Brunei Darussalam had more profound antioxidant activity than the other two solvents. This result suggests that, for the leaf samples used in this study, the phytochemicals extracted in ethyl acetate and methanol have higher composition of antioxidant compounds compared to chloroform and hexane, unlike the results obtained by Hossain and Shah (2015). The variation in the antioxidant activities of the extracts noted between our study and that carried out by Hossain and Shah (2015) might be due to disparities in genetic makeup or environment, both of which could have resulted in varying phytochemical compositions in plants (Akhtar & Mirza 2018). Furthermore, other influences such as differences in plant age, plant tissue used and extraction techniques could also strongly affect the yield of antioxidant compounds (Karabegović et al. 2014; Upadhya et al. 2015).

In this study, a correlation seems to be observed between solvent polarity and antioxidant activity. Enhanced radical scavenging activity was observed with an increase in extraction solvent polarity. The correlation might be due to the presence of antioxidant compounds such as catechins, flavonoids, flavones, isoflavones, anthocyanins, and other phenols that are polar in nature (Alothman et al. 2009; Isabelle et al. 2010). As previously reported, the leaves of *M. borneensis* contained a substantial number of flavonoids along with other compounds as mentioned earlier (Shah & Hossain 2014). Polar flavonoids would be easily extracted with polar solvents due to their higher affinity towards polar solvents (Nawaz et al. 2020). Furthermore, polar phytochemicals such as flavonoids and anthocyanins have been reported to be effective scavengers of free radicals (Hwang et al. 2012; Hassanpour & Doroudi 2023). Their ability to scavenge free radicals could be derived from the presence of phenolic hydroxyl groups in their structures that can donate hydrogen atoms to quench reactive oxygen species such as DPPH (Baliyan et al. 2022; Ge & Ma 2023). Overall, this suggests that ethyl acetate, which is the solvent with high polarity, was able to extract a high amount of polar antioxidant compounds from the leaves of *M. borneensis* that are effective in decomposing free radicals.

Antibacterial activities of *M. borneensis* leaf extracts

Our results suggest that *E. coli* has the highest susceptibility to the leaf extracts of *M. borneensis* in comparison to the other bacterial strains, especially the chloroform extract. Meanwhile, *P. aeruginosa* and *S. aureus* were more

sensitive to the methanol extract than the other extracts. In comparison, *B. subtilis* was the least susceptible strain since a concentration of at least 100 µg $mL^{-1}$of either the methanol or ethyl acetate extract was required to yield detectable bacterial inhibition. Overall, the chloroform, ethyl acetate, and methanol extracts presented good antibacterial potencies and thus may be good sources of potent antimicrobial compounds (Mtunzi et al. 2017).

Our study also demonstrated that the hexane extract was ineffective on all the bacterial strains studied herein. The inactivity observed in the hexane extract against the bacterial strains does not necessarily denote a complete absence of antibacterial compounds. The non-activity might be due to low composition of antibacterial compounds present per volume, or the presence of antagonistic compounds that might have disrupted the antibacterial actions of the bioactive compounds (Akhtar & Mirza 2018). A previous study showed that the aqueous extract of the leaves of *M. borneensis* from Brunei Darussalam lacked inhibitory activity against *B. subtilis*, *S. aureus*, *E. coli* and *P. aeruginosa* (Awang-Jamil et al. 2021). This shows that the ethyl acetate and methanol leaf extracts of the Bruneian *M. borneensis* possess higher levels of antibacterial compounds in comparison to the chloroform and aqueous extracts.

Correlation between the extraction solvent polarity and antibacterial activity could not be established, as the antibacterial activities did not consistently increase with solvent polarity across all the tested bacterial strains. This suggests that solvent polarity did not significantly affect the extraction of antibacterial components from the *M. borneensis* leaves. Furthermore, this finding also suggests that the antioxidant activity did not correlate to the antibacterial activity of the leaf extracts of *M. borneensis*. This finding concurs with the results from previous studies conducted by Adamu et al. (2014), Vitalini et al. (2016), and Jang et al. (2016), whereby the antioxidant activities of various herbal extracts were shown to have poor correlations with their antibacterial activity.

Nevertheless, the rich flavonoid content of the methanol, ethyl acetate, and chloroform extracts may have contributed to their superior antibacterial effects against the tested bacterial strains whereas the lack of antibacterial activities observed in the hexane extract could be due to its low flavonoid content (Hossain & Shah 2015). Indeed, flavonoids have been reported to impart potent antibacterial activity particularly via C5, C7, C3′, and C4′ hydroxylation as well as geranylation or prenylation at C6 (Shamsudin et al. 2022). Furthermore, flavonoids have also been proposed to inhibit bacterial growth by targeting the porins and disrupting the permeability and functions of bacterial cell membranes (Xie et al. 2015). Other than that, flavonoids were also reported to deter nucleic acid synthesis in bacteria as well as hinder energy metabolism, biofilm formation and attachment and overall pathogenicity of the bacteria (Xie et al. 2015). This highlights the potential role of flavonoids in the antibacterial property of the *M. borneensis* leaves and the multifaceted mechanisms that may be involved in the antibacterial activities observed in the extracts.

Plant extracts are generally less potent against gram-negative bacteria than gram-positive bacteria (Parekh & Chanda 2006). It has been suggested that the external membranes of gram-negative bacteria are less permeable to antimicrobial compounds (Wetungu et al. 2014). Nevertheless, this phenomenon was not observed in our study although further studies are required. Based on our results, the study suggests that the structural difference between the cell wall of gram-positive and that of the gram-negative bacteria may not be the sole factor to influence the susceptibility of a bacterial strain to antibacterial compounds. This speculation was found to be in accord with the previous report by Elisha et al. (2017). According to another study by Yan et al. (2024), the potencies of most plant flavonoids against gram-

negative bacteria were higher than those against gram-positive bacteria. Aside from the cell membrane, plant flavonoids may also target other action sites in gram-negative bacteria such as DNA gyrase to inhibit the bacteria (Yan et al. 2024). This aligns with the findings from our study as discussed earlier. Additionally, it re-emphasises the complexity of the mode of action that may be involved in the inhibitory activity of the flavonoids or other antibacterial compounds in the *M. borneensis* leaves.

Wound healing activity of *M. borneensis* leaf extracts

Macroscopic evaluation of the wound revealed enhanced wound healing activity in the extract-treated animals compared to the control group. The formation of a secondary scar, as the wound size reduced after day 7, acts to provide protection to the wound surface and also the environment for further proliferation (Phillips 2000). The overall observations suggest that the *M. borneensis* extract was able to induce early proliferation on granulation tissues in the extract-treated animals.

Microscopic evaluation of the granulation tissues of the control and treatment groups was also carried out at specified post-wounding time points. At the initial phase, the granulation tissue of all animals generally showed hallmarks of the homeostasis and inflammatory stage of wound healing with the establishment of a thick epidermal layer, and infiltration of inflammatory cells. The distribution of inflammatory cells observed in the granulation tissue on day 3 is attributable to its role in cleansing and guarding the wound from micro-organisms and foreign bodies (Flanagan 2000). The advanced infiltration of fibroblasts and parallel alignment of fibroblasts and development of new blood vessels visible in the extract-treated animals signifies, yet again, the early initiation of the proliferation phase of wound healing in the extract-treated animals (Flanagan 2000). Subsequently, the inflammatory cells persisted in the control animals as fibroblasts began infiltrating the granulation tissues. Meanwhile, fibroblast alignment was evident in the extract-treated groups as collagen deposition proceeded at the proliferation stage of wound healing. The presence of fibroblasts and cytokines induce the apoptosis of the inflammatory cells, resulting in their resolution (Tough et al. 1999; Landén et al. 2016). The reduction in epidermal thickness observed in all animals on the following evaluation days may be due to the migration of keratinocytes from the basal layer of the basal membrane to the surface, where they would differentiate, followed by maturation and compression into a flattened layer of remnant dead cells known as the cornified layer (Pastar et al. 2014).

Overall, treatment with either dosage of the extract showed enhanced wound healing progress. Both treatment groups enhanced contraction of wounds starting at day 3 post-wounding. The high dosage-treated animals displayed better wound healing progress compared to the low dosage-treated animals as indicated by the advanced collagen arrangements observed on day 7 compared to the other groups. The seventh post-wounding day coincided with the proliferation phase which is characterised by the development of new tissue made up of collagen (Landén et al. 2016). The enhanced collagen deposition at post-wounding day 7 in the *M. borneensis* extract treated-animals implies that the extract was able to improve the rate of wound healing by bringing forward the proliferation phase in the extract-treated animals ahead of the control-treated animals.

This advanced progression observed in the extract-treated animals, especially from the inflammatory to proliferation phase, can be attributed to the antioxidant and antimicrobial properties of the extract as these properties facilitate wound recovery by scavenging radical oxygen species and inhibiting pathogens that may have resulted at the wound site following inflammations and infections (Shah & Amini-Nik 2017). Other than preventing oxidative

stress and infections, the flavonoid-rich extract of *M. borneensis* may also expedite the wound healing process by up-regulating the expression of wound-repairing promoters such as the proangiogenic mediators, basic fibroblast growth factor (bFGF) and vascular endothelial growth factor (VEGF), and pre-procollagen, collagen type 3 (COL3A1), in the granulation tissue (Johnson & Wilgus 2014; Kuivaniemi & Tromp 2019; Subramanian et al 2023). Furthermore, flavonoids have been reported to regulate the expression of other biomarkers such as Wnt/β-catenin, Hippo, Transforming Growth Factor-beta (TGF-β), Hedgehog, c-Jun N-Terminal Kinase (JNK), NF-E2-related factor 2/antioxidant responsive element (Nrf2/ARE), Nuclear Factor Kappa B (NF-κB), MAPK/ERK, Ras/Raf/MEK/ERK and phosphatidylinositol 3-kinase (PI3K)/Akt that are essential in the pathways involved in wound healing (Zulkefli et al. 2023). Thus, it suggests that the flavonoid content of the *M. borneensis* leaves may have played a critical role in the wound recovery capacity of the *M. borneensis* extract as shown in this study.

CONCLUSION

This study demonstrated that the *M. borneensis* leaves from Brunei Darussalam extracted with ethyl acetate and methanol possessed marked antioxidant activities whereas the chloroform and hexane extract demonstrated significantly lower and weak antioxidant activities respectively. The methanol and ethyl acetate leaf extracts of *M. borneensis* from Brunei Darussalam also showed substantial inhibitory activities against *B. subtilis*, *S. aureus*, *E. coli* and *P. aeruginosa*. However, the chloroform extract was effective against *E. coli* only. The wound healing study showed that topical treatment with 50 % w w^{-1} of the methanol extract of the *M. borneensis* leaves could result in complete wound recovery in the treated animals by post-wounding day 15. Accelerated wound contraction and improved collagen formation were also obvious in groups that received either dosage of the treatment. The wound healing property of the *M. borneensis* leaf extract may be associated with its antioxidant and antibacterial properties. The overall result from this study suggests that the *M. borneensis* leaves from Brunei Darussalam may be a good source of wound healing, antibacterial and antioxidant agents that can be utilised for multiple applications.

AUTHORS CONTRIBUTION

H.T and N.A. designed the research and supervised the entire process whereas F.Y. supervised part of the project. N.N. and N.A.S. collected and analysed the data, M.P.Y.G. compiled and prepared the manuscript.

ACKNOWLEDGMENTS

This study was supported by a research grant under the Institute for Biodiversity and Environmental Research, Universiti Brunei Darussalam reference: UBD/RSCH/1.13/FICBF(b)/2018/001.

CONFLICT OF INTEREST

The authors declare that there is no conflict of interest.

REFERENCES

Adamu, M., Naidoo, V. & Eloff, J.N., 2014. The antibacterial activity, antioxidant activity and selectivity index of leaf extracts of thirteen South African tree species used in ethnoveterinary medicine to treat helminth infections. *BMC veterinary research*, 10, 52. doi: 10.1186/1746-6148-10-52.

Akhtar, N. & Mirza, B., 2018. Phytochemical analysis and comprehensive evaluation of antimicrobial and antioxidant properties of 61 medicinal plant species. *Arabian journal of chemistry*, 11(8), pp.1223-1235. doi: 10.1016/j.arabjc.2015.01.013.

Alothman, M., Bhat, R. & Karim, A.A., 2009. Antioxidant capacity and phenolic content of selected tropical fruits from Malaysia, extracted with different solvents. *Food chemistry*, 115(3), pp.785-788. doi: 10.1016/j.foodchem.2008.12.005.

Apak, R. et al., 2007. Comparative evaluation of various total antioxidant capacity assays applied to phenolic compounds with the CUPRAC assay. *Molecules*, 12(7), pp.1496-1547. doi: 10.3390/12071496.

Awang-Jamil, Z. et al., 2021. Phytochemicals and antimicrobial analysis of selected medicinal plants from Brunei Darussalam. *Biodiversitas Journal of Biological Diversity*, 22(2), pp.601-606. doi: 10.13057/biodiv/d220211.

Baliyan, S. et al., 2022. Determination of Antioxidants by DPPH Radical Scavenging Activity and Quantitative Phytochemical Analysis of Ficus religiosa. *Molecules (Basel, Switzerland)*, 27(4), 1326. doi: 10.3390/molecules27041326.

Edeoga, H.O., Okwu, D.E. & Mbaebie, B.O., 2005. Phytochemical constituents of some Nigerian medicinal plants. *African journal of biotechnology*, 4 (7), pp.685-688. doi: 10.5897/AJB2005.000-3127.

Elisha, I.L. et al., 2017. The antibacterial activity of extracts of nine plant species with good activity against Escherichia coli against five other bacteria and cytotoxicity of extracts. *BMC complementary and alternative medicine*, 17(1), 133. doi: 10.1186/s12906-017-1645-z.

Elumalai, E.K. et al., 2011. Antibacterial activity of various leaf extracts of Merremia emarginata. *Asian pacific journal of tropical biomedicine*, 1(5), pp.406-408. doi: 10.1016/S2221-1691(11)60089-0.

Flanagan, M., 2000. The physiology of wound healing. *Journal of wound care*, 9(6), pp.299-300. doi: 10.12968/jowc.2000.9.6.25994.

Ge, Q. & Ma, X., 2013. Composition and antioxidant activity of anthocyanins isolated from Yunnan edible rose (An ning). *Food Science and Human Wellness*, 2(2), pp.68-74. doi: 10.1016/j.fshw.2013.04.001.

Hasan, H.A. et al., 2012. Chemical composition and antimicrobial activity of the crude extracts isolated from Zingiber officinale by different solvents. *Pharmaceut Anal Acta*, 3, 9. doi: 10.4172/2153-2435.1000184.

Hossain, M.A. & Shah, M.D., 2015. A study on the total phenols content and antioxidant activity of essential oil and different solvent extracts of endemic plant Merremia borneensis. *Arabian Journal of Chemistry*, 8(1), pp.66-71. doi: 10.1016/j.arabjc.2011.01.007.

Hassanpour, S.H. & Doroudi, A., 2023. Review of the antioxidant potential of flavonoids as a subgroup of polyphenols and partial substitute for synthetic antioxidants. *Avicenna journal of phytomedicine*, 13(4), pp.354–376. doi: 10.22038/AJP.2023.21774.

Hwang, J.W. et al., 2012. Anthocyanin effectively scavenges free radicals and protects retinal cells from H 2 O 2-triggered G2/M arrest. *European Food Research and Technology*, 234, pp.431-439. doi: 10.1007/s00217-011-1648-9.

Isabelle, M. et al., 2010. Antioxidant activity and profiles of common fruits in Singapore. *Food Chemistry*, 123(1), pp.77-84. doi: 10.1016/j.foodchem.2010.04.002.

Jamadagni, P.S. et al., 2016. Experimental and histopathological observation scoring methods for evaluation of wound healing properties of Jatyadi Ghrita. *Ayu*, 37(3-4), 222. doi: 10.4103/ayu.AYU_51_17.

Jang, D. et al., 2016. Composition, antioxidant and antimicrobial activities *of Eleutherococcus senticosus* fruit extracts. *Journal of Applied Pharmaceutical Science*, 6(3), pp.125-130. doi: 10.7324/JAPS.2016.60322.

Jantan, I., 2004. Medicinal plant research in Malaysia: scientific interests and advances. *Jurnal Sains Kesihatan Malaysia*, 2(2), pp.27-46.

Johnson, K.E. & Wilgus, T.A., 2014. Vascular Endothelial Growth Factor and Angiogenesis in the Regulation of Cutaneous Wound Repair. *Advances in wound care*, 3(10), pp.647–661. doi: 10.1089/wound.2013.0517.

Kalita, P. et al., 2013. Estimation of total flavonoids content (TFC) and anti oxidant activities of methanolic whole plant extract of Biophytum sensitivum Linn. *Journal of Drug delivery and Therapeutics*, 3(4), pp.33-37. doi: 10.22270/jddt.v3i4.546.

Karabegović, I.T. et al., 2014. The effect of different extraction techniques on the composition and antioxidant activity of cherry laurel (Prunus laurocerasus) leaf and fruit extracts. *Industrial Crops and Products*, 54, pp.142-148. doi: 10.1016/j.indcrop.2013.12.047.

Krishnaiah, D., Sarbatly, R. & Nithyanandam, R., 2011. A review of the antioxidant potential of medicinal plant species. *Food and bioproducts processing*, 89(3), pp.217-233. doi: 10.1016/j.fbp.2010.04.008.

Kuivaniemi, H. & Tromp, G., 2019. Type III collagen (COL3A1): Gene and protein structure, tissue distribution, and associated diseases. *Gene*, 707, pp.151–171. doi: 10.1016/j.gene.2019.05.003.

Landén, N.X., Li, D. & Ståhle, M., 2016. Transition from inflammation to proliferation: a critical step during wound healing. *Cellular and Molecular Life Sciences*, 73, pp.3861-3885. doi: 10.1007/s00018-016-2268-0.

Metussin, N. et al., 2017. Evaluation of antioxidant capacity of Aidia borneensis leaf infusion, an endemic plant in Brunei Darussalam. *Food Research*, 2(1), pp.12-19. doi: 10.26656/fr.2017.2(1).109.

Mtunzi, F.M. et al., 2017. Solvent–solvent fractionations of Combretum erythrophyllum (Burch.) leave extract: Studies of their antibacterial, antifungal, antioxidant and cytotoxicity potentials. *Asian Pacific journal of tropical medicine*, 10(7), pp.670-679. doi: 10.1016/j.apjtm.2017.07.007.

Nawaz, H. et al., 2020. Effect of solvent polarity on extraction yield and antioxidant properties of phytochemicals from bean (Phaseolus vulgaris) seeds. *Brazilian Journal of Pharmaceutical Sciences*, 56, e17129. doi: 10.1590/s2175-97902019000417129.

Othman, S.F.C. et al., 2011. Antioxidant study of garlic and red onion: a comparative study. *Pertanika Journal of Tropical Agricultural Science*, 34(2), pp.253-261.

Parekh, J. & Chanda, S., 2006. In-vitro antimicrobial activities of extracts of Launaea procumbens roxb.(Labiateae), Vitis vinifera l.(Vitaceae) and Cyperus rotundus l.(Cyperaceae). *African Journal of Biomedical Research*, 9(2). doi: 10.4314/ajbr.v9i2.48780.

Pastar, I. et al., 2014. Epithelialization in wound healing: a comprehensive review. *Advances in wound care*, 3(7), pp.445-464. doi: 10.1089/wound.2013.0473.

Petrovska, B.B., 2012. Historical review of medicinal plants' usage. *Pharmacognosy reviews*, 6(11), pp.1-5. doi: 10.4103/0973-7847.95849.

Phillips, S.J., 2000. Physiology of wound healing and surgical wound care. *ASAIO journal*, 46(6), pp.S2-S5. doi: 10.1097/00002480-200011000-00029.

Rahmatullah, M. et al., 2010. A survey of medicinal and functional food plants used by the folk medicinal practitioners of three villages in Sreepur Upazilla, Magura district, Bangladesh. *American Eurasian Journal of Sustainable Agriculture*, 4(3), pp.363-373.

Reinke, J.M. & Sorg, H., 2012. Wound repair and regeneration. *European surgical research*, 49(1), pp.35-43. doi: 10.1159/000339613.

Selvamohan, T., Ramadas, V. & Kishore, S.S.S., 2012. Antimicrobial activity of selected medicinal plants against some selected human pathogenic bacteria. *Advances in Applied Science Research*, 3(5), pp.3374-3381.

Shafie N.A., 2020. *The Potential Antidiabetic and Wound Healing Effects of Anisophyllea disticha and Merremia borneensis in an Animal*. Universiti Brunei Darussalam.

Shah, A. & Amini-Nik, S., 2017. The role of phytochemicals in the inflammatory phase of wound healing. *International journal of molecular sciences*, 18 (5), 1068. doi: 10.3390/ijms18051068.

Shah, M.D. & Hossain, M.A., 2014. Total flavonoids content and biochemical screening of the leaves of tropical endemic medicinal plant Merremia borneensis. *Arabian Journal of Chemistry*, 7(6), pp.1034-1038. doi: 10.1016/j.arabjc.2010.12.033.

Shamsudin, N.F. et al., 2022. Antibacterial Effects of Flavonoids and Their Structure-Activity Relationship Study: A Comparative Interpretation. *Molecules (Basel, Switzerland)*, 27(4), 1149. doi: 10.3390/molecules27041149.

Shi, H.X. et al., 2013. The anti-scar effects of basic fibroblast growth factor on the wound repair in vitro and in vivo. *PloS One*, 8(4), e59966. doi: 10.1371/journal.pone.0059966

Subramanian, S. et al., 2023. Wound healing properties of a new formulated flavonoid-rich fraction from Dodonaea viscosa Jacq. leaves extract. *Frontiers in pharmacology*, 14, 1096905. doi: 10.3389/fphar.2023.1096905.

Sumaya-Martinez, M.T. et al., 2005. Effect of Maillard reaction conditions on browning and antiradical activity of sugar–tuna stomach hydrolysate model system. *Food Research International*, 38(8-9), pp.1045-1050. doi: 10.1016/j.foodres.2005.03.015.

Tepe, B. et al., 2005. Antimicrobial and antioxidant activities of the essential oil and various extracts of Salvia tomentosa Miller (Lamiaceae). *Food chemistry*, 90(3), pp.333-340. doi: 10.1016/j.foodchem.2003.09.013.

Thakur, R. et al., 2011. Practices in wound healing studies of plants. *Evidence-based complementary and alternative medicine*, 2011, 438056. doi: 10.1155/2011/438056.

Tough, D.R. et al., 1999. Stimulation of naive and memory T cells by cytokines. *Immunological reviews*, 170(1), pp.39-47. doi: 10.1111/j.1600-065x.1999.tb01327.x.

Upadhya, V., Pai, S.R. & Hegde, H.V., 2015. Effect of method and time of extraction on total phenolic content in comparison with antioxidant activities in different parts of Achyranthes aspera. *Journal of King Saud University-Science*, 27(3), pp.204-208. doi: 10.1016/j.jksus.2015.04.004.

Velnar, T., Bailey, T. & Smrkolj, V., 2009. The wound healing process: an overview of the cellular and molecular mechanisms. *Journal of international medical research*, 37(5), pp.1528-1542. doi: 10.1177/147323000903700531.

Vitalini, S. et al., 2016. Chemical profile, antioxidant and antibacterial activities of Achillea moschata Wulfen, an endemic species from the Alps. *Molecules*, 21(7), 830. doi: 10.3390/molecules21070830.

Wetungu Martin, W., Matasyoh, J.C. & Kinyanjui, T., 2014. Antimicrobial activity of solvent extracts from the leaves of Tarchonanthus camphoratus (Asteraceae). *Journal of Pharmacognosy and Phytochemistry*, 3(1), pp.123-127.

Xie, Y. et al., 2015. Antibacterial activities of flavonoids: structure-activity relationship and mechanism. *Current medicinal chemistry*, 22(1), pp.132–149. doi: 10.2174/0929867321666140916113443.

Yan, Y. et al., 2024. Antibacterial Activity and Mechanisms of Plant Flavonoids against Gram-Negative Bacteria Based on the Antibacterial Statistical Model. *Pharmaceuticals*, 17(3), 292. doi: 10.3390/ph17030292.

Zulkefli, N. et al., 2023. Flavonoids as Potential Wound-Healing Molecules: Emphasis on Pathways Perspective. *International journal of molecular sciences*, 24(5), 4607. doi: 10.3390/ijms24054607.

Journal of Tropical Biodiversity and Biotechnology
Volume 10, Issue 04 (2025): jtbb19682
DOI: 10.22146/jtbb.19682

Research Article

Food Plants and Feeding Behaviour of Lowland Anoa (*Bubalus depressicornis* Smith, 1827) in Tanjung Peropa Wildlife Reserve, Southeast Sulawesi

Abdul Haris Mustari[1]*, Poppy Desita Sari Guna Wiyanda[1], Ola Prajab Aso[1]
1)Department of Forest Resources Conservation and Ecotourism, Faculty of Forestry and Environment, IPB University, Bogor, West Java 16680
* Corresponding author, email: abdulmu@apps.ipb.ac.id

Keywords:
Anoa
Browser
Endemic species
Feeding behaviour
Food plant
Submitted:
02 February 2025
Accepted:
27 April 2025
Published:
14 November 2025
Editors:
Furzani Binti Pa'ee
Tanti Agustina

ABSTRACT
Lowland anoa is endemic to Sulawesi, inhabiting the tropical rain forests on the island. The animal's food plants included leaves, shoots and growing tips of branches, young twigs, and fallen fruit of many plant species. This study aimed to reveal the food plants and feeding behaviour of lowland anoa in their natural habitat in Tanjung Peropa Wildlife Reserve, Southeast Sulawesi. The potential food plants and faecal samples of anoa were collected, and epidermis left in the faecal samples was analysed and identified microscopically. Based on the characteristics of the plants' epidermis, the plant species could be identified. A total of 55 species of food plants was identified in the faecal samples of anoa. The chief food items of the anoa were dicotyledonous plants representing 84 %, monocots 11 %, and ferns 5 %. Parts of the food plants eaten by the animals were mainly leaves and stems constituted 78 %, while fruit composed 22 % of the diet. Intact fruit seeds found in the faecal samples suggest that anoas play significant roles as seed dispersers, and propagate many species of fruit trees in the tropical rain forest of Sulawesi.

How to cite:
Mustari, A.H., Wiyanda, P.D.S.G. & Aso, O.P., 2025. Food Plants and Feeding Behaviour of Lowland Anoa (*Bubalus depressicornis* Smith, 1827) in Tanjung Peropa Wildlife Reserve, Southeast Sulawesi. *Journal of Tropical Biodiversity and Biotechnology*, 10(4), jtbb19682. doi: 10.22146/jtbb.19682

INTRODUCTION

Lowland anoa (*Bubalus depressicornis*) is endemic to Sulawesi, Indonesia. This species is classified as an endangered species (IUCN 2025), listed on Appendix I of CITES (UNEP-WCMC 2021), and is protected by Indonesian law (Indonesian Ministry of Forestry 2018). The lowland anoa is the smallest of the world's living buffaloes, yet the biggest of Sulawesi's forest ungulates; body weight is 80-100 kg, and shoulder height is 80-100 cm (Mustari 2019). Data on food plants and feeding behaviour of anoa in their natural habitats are limited due to its secretive nature, inhabiting the most remote tropical rain forests on Sulawesi. The habitat of lowland anoa includes beach, lowland, and mountain forests up to 3000 masl (Mustari 2019). Lowland anoa was frequently observed visiting mangrove forests, licking soils, and foraging on leaves and fallen fruit of mangrove trees during low tides (Mustari 2019). Qualitative descriptions of the diet of anoa based on browsing signs left by the animals in the natural habitats have been reported by field biologists (Arini & Wahyuni 2016; Tangkoro et al. 2018; Mustari 2019; Aziz et al. 2023).

Parts of plants eaten by anoa include leaves, fruit, flowers, shoots, and stems (Ranuntu & Mallombasang 2015; Mustari 2019). Food plants of anoa include many species of woody plants, herbs, shrubs, aquatic plants, grasses, ferns, and lianas (Mustari 2019). In captivity, dietary ecology has been studied to reveal feeding behaviour and nutritional content of anoa's feed (Arini & Kafiar 2014; Mustari et al. 2015; Rusiyantono et al. 2019). Every plant species has unique cuticle characteristics, and most plant cuticle is not completely digested in the ruminant digestive processes, allowing food plants to be identified microscopically in faecal samples of grazing or browsing herbivores (Ginantra et al. 2016; Adinda et al. 2023). This study is the first to describe food plants of anoa using epidermal fragments in the faecal samples. This study aimed to identify and reveal food plants and feeding behaviour of anoa in their natural habitats. Relative proportions of the food plants were assessed based on their fragments. The results of this study will contribute to the better understanding of the diets of anoas in their natural habitats. Information on natural diets serves as a reference for providing feed in anoa ex-situ conservation facilities.

MATERIALS AND METHODS

This study was conducted in Kalobo Forest of Tanjung Peropa Wildlife Reserve in Southeast Sulawesi. The conservation forest covers an area of 389.27 km^2, extending from 0 m to 900 m elevation (Figure 1). Food plants that were potentially eaten by anoa were collected, including food plants that showed signs of being browsed and food plants that were directly observed being eaten by the animals. The browsing signs of the lowland anoa could be determined by identifying the footprints of the animals nearby or under the food plants. The only sympatric species in the study sites were the sulawesi warty pig (*Sus celebensis*) and the babirusa (*Babyrousa celebensis*), both of which have distinct footprints and browsing signs.

The food plants browsed by the animals were classified as potential food plants eaten by the animals, while the food plants identified in the faecal samples were the actual food plants consumed by the lowland anoa. Food plants eaten by anoa were identified using microscopic epidermal fragments from the faecal samples (Figure 2). Five fresh faecal samples (50 g each) of anoa were randomly collected every month during 2001 and 2002. A total of 61 faecal samples were collected during the rainy (32 samples) and the dry (29 samples) seasons. In the study site at the south-eastern tip of the mainland of Sulawesi, the rainy season occurred from January to June, and the dry season

was from July to December. The faecal samples were preserved in 70 % ethanol.

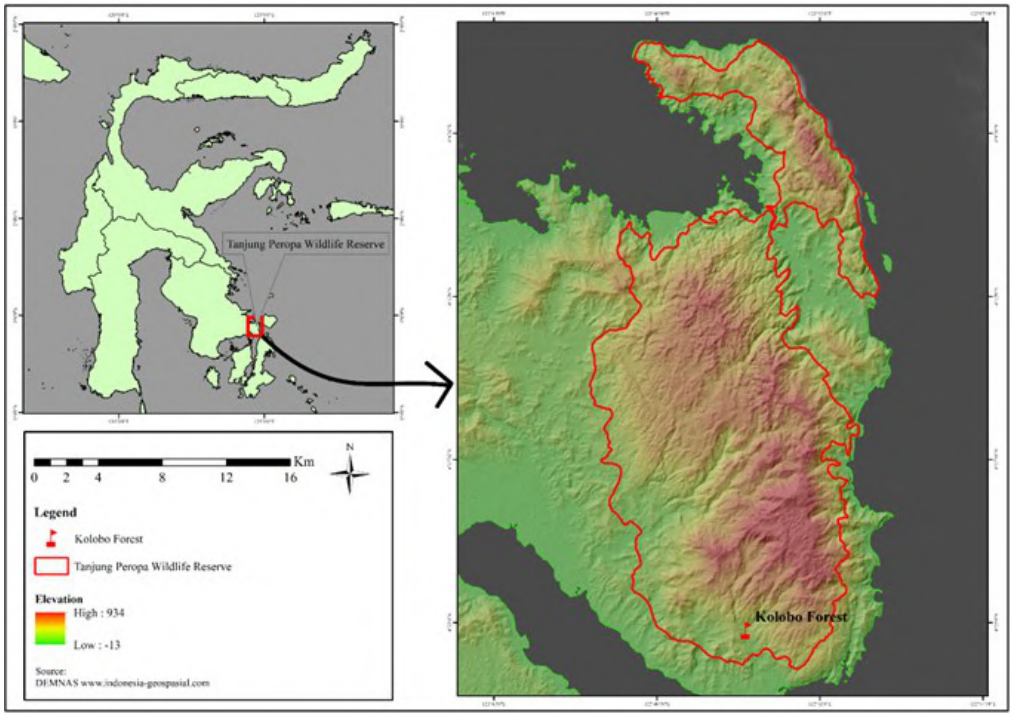

Figure 1. Tanjung Peropa Wildlife Reserve at the southeastern tip of the mainland of Sulawesi.

Figure 2. Lowland anoa (*Bubalus depressicornis*) and its faeces (Photo: Abdul Haris Mustari).

Reference slides

Food plants potentially eaten by the lowland anoa were collected, and the botanical names were confirmed at the Herbarium Bogoriense of the Indonesian Institute of Science (LIPI). Preparation of the reference slides followed the procedures described by (Stewart 1965, 1967; Jarman & Phillips 1989). The materials (leaves, stems, flowers, seeds, and fruit bark) were cut into 5 mm lengths and put into a conical flask containing 10 % nitric acid. The flask containing the plant part was heated intermittently over a Bunsen burner for about five minutes or until the epidermis separated from underlying tissue. When the epidermis separated, water was added to the flask to prevent further disintegration; then the contents of the flask were transferred to a beaker where the epidermal fragments usually floated to the surface. Subsequently, the epidermal fragments were picked up with a small brush and put into a small quantity of safranin stain in a watch glass. After a few minutes, the fragments were removed to a dilute solution of glycerine, which removed excess stain. Finally, the fragments were mounted in glycerine jelly under a 3.8

x 1.9 cm cover slide, and were then ready to be used a reference slide in identifying the food plants' fragments in the faeces of anoa.

Faeces slides

Preparation of the faecal slides followed the procedures described by (Stewart 1965, 1967; Jarman & Phillips 1989). Faecal samples that had been preserved in 70 % ethanol were placed onto a slide using a Pasteur pipette. Sub-samples of approximately 10 g were soaked with water to soften for several hours before being mounted on the slides. The sub-samples were mounted with glycerine jelly under a 3.8 x 1.9 cm cover slide. The faecal slides were examined with a binocular light-transmission microscope under x10 to x100 magnification (Jarman & Phillips 1989). Plant epidermal fragments recorded in the faecal slides were firstly categorised into monocots (grasses, sedges, bamboos) and dicots (herbs, lianas, and woody plants), and then into the parts of the plants: leaves, fruit, seed, stem and woody material (Figure 4). Characteristics of the plant epidermis were first differentiated and classified as monocots and dicots, then species were identified. The species represented by each fragment was recognised, where possible, by characteristics of the epidermis as found in reference slides. The relative proportions of species or their parts in the diet were taken to be represented by the relative amounts of epidermal area that they contributed to the total area of epidermis recognised. Based on these proportions, the percentage of epidermal cover formed by each plant species' fragments could be determined (Jarman & Phillips 1989).

RESULTS AND DISCUSSION

Food plants

Observation of the feeding sites of the animals showed that food plants of anoa included monocots (grasses, sedges, and young leaves and new sprouts of bamboos), dicots (herbs, lianas, and fruit of dicots), and ferns. The food plants that were frequently browsed by anoa included balandete (*Merremia peltata*), wehuko (*Ficus variegata*), kaleuwi (*Hypobathrum microcarpum*), bamboos (*Bambusa* spp.), tawa huko (*Gnetum gnemon*), we wai (*Flagellaria indica*), tokoalinda (*Elatostema rostratum*), and puta (*Barringtonia racemosa*).

The anoa also consumed fruit of many species, particularly figs (*Ficus* spp.), dongi (*Dillenia ochreata*), konduri (*Parkia roxburghii*), toho (*Artocarpus* sp.), kalaero (*Diospyros pilosanthera*), kasu meeto (*Diospyros malabarica*), kabuko (*Syzygium* sp.), menambo (*Garcinia tetrandra*), huhubi (*Artocarpus dasyphylla*), and tembeuwa (*Kjellbergiodendron celebicum*) (Figure 3).

Diet composition

Most fragments of food plants in the faecal samples of the anoa could be recognised (82 %), suggesting that the method of analysing epidermal fragments in the faecal samples of anoa is suitable for studying diets of anoa. The 'unidentified' fragments in the faecal samples were categorised into dicot fruit, dicot, monocot, and fern leaves. Food plant fragments identified (both seasons combined) constituted the following proportions of the diet, respectively: dicots 84 %, monocots 11 %, and ferns 5 %. Leaves and stems constituted 78 %, while fruit made up 22 % of the diets (Figure 5).

A total of 55 species of food plants were identified in the faecal samples; of the dicots, *Merremia peltata* (35.8 %), fig fruit *Ficus* spp. (10.9 %), *Physalis angulata* (7.5 %) and *Schizostachyum* spp. (4.4 %) are the predominant species consumed by anoa (Table 1). Fragments of *Merremia peltata* were not only predominant in proportion but also had the highest frequency of occurrence (100 %), with fragments of this species being found in every faecal sample analysed. Identification of fragments in the faecal samples revealed that, in general, fruit fragments (except seeds) were more difficult to identify than leaf

(a) (b) (c)

Figure 3. Among the food plants of anoa in the natural habitats: a. Balandete (*Merremia peltata*), b. Dongi (*Dillenia ochreata*), c. Wehuko (*Ficus variegata*). (Photo: Abdul Haris Mustari).

fragments, and monocot fragments were relatively easier to identify than dicots and fruit. The main food plants eaten by the anoa for the monocot category were bamboo (43 %), followed by sedges (39 %), while grasses constituted 7 % of the diet.

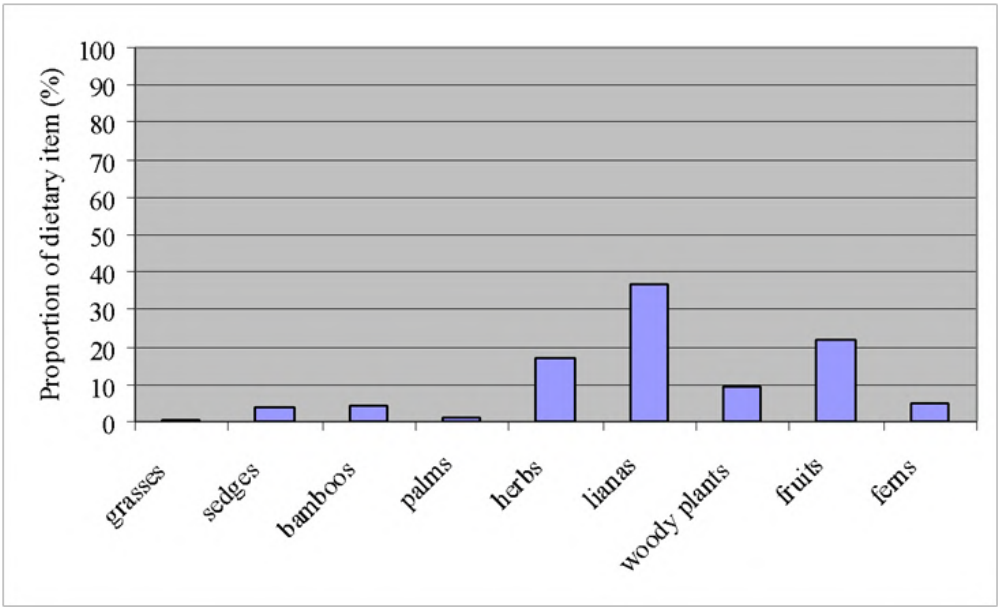

Figure 4. Proportions of food plants in the diet of anoa.

Anoas are the smallest of the living buffaloes; body weight is 80-100 kg for lowland anoa, and less than 80 kg for mountain anoa (Mustari 2019). The tamaraw (*Bubalus mindorensis*), which is endemic to Mindoro Island of the Philippines, has a body weight of 200-274 kg, while the Asian water buffalo (*Bubalus bubalis* and *B. arnee*), and African buffalo (*Syncerus caffer*) can weigh of up to 1000 kg (Wilson & Mittermeier 2011). Based on the predominance of dicotyledonous in the diets, anoa's food plants differed from those of other members of the Bubalina including water buffalo (*Bubalus bubalis*), tamaraw (*B. mindorensis*), and African buffaloes (*Syncerus caffer*), all feeding predominantly on monocotyledonous, mainly grasses (Poaceae), inhabiting the relatively open areas including savannahs. Water buffaloes are associated with wet grasslands and swamps; their favourite foods are lush grass and vegetation growing in or beside rivers and lakes (Nowak 1991). Although it uses various types of habitats, the tamaraw prefers forest edge areas, which make it easier to forage in more open places such as grasslands (Tabaranza et al. 2022). African buffalos are found in the open grassy and swampy areas or in

Table 1. Proportion of total fragment area and frequency of occurrence of fragments in faecal samples of food plants eaten by anoa. (lf = leaf, fr = fruit, D = dicot, M = monocot).

No	Vernacular name	Botanical name	Family name	Proportion (%)			Frequency of occurrence (%)
				Rainy season	Dry season	Rainy and Dry seasons	
1	Balandete (lf)	*Merremia peltata*	Convolvulaceae	28.7	43.7	35.8	100
2	Pokae (fr)	*Ficus* sp.	Moraceae	2.6	20.0	10.9	59
3	Unknown (fr)	*Monocots fruit*	Poaceae	16.1	1.9	9.3	57
4	Unknown (lf/D)	*Dicots leave*	-	10.9	6.3	8.7	64
5	Tameau langgai	*Physalis angulata*	Solanaceae	11.7	3.0	7.5	52
6	Kowuna (lf)	*Schizostachyum* spp.	Poaceae	3.8	5.0	4.4	74
7	Paku hada (lf)	*Microlepia* sp.	Dennstaedtiaceae	5.3	2.5	4.0	59
8	Rara (lf)	*Scleria purpurascens*	Cyperaceae	3.3	2.0	2.7	44
9	Wehuko (lf)	*Ficus variegata*	Moraceae	2.4	1.1	1.8	30
10	Holea (lf)	*Cleistanthus sumatranus*	Phyllanthaceae	1.1	1.4	1.2	23
11	Wako (lf)	*Caryota mitis*	Arecaceae	1.4	1.0	1.2	28
12	Tawa huko (lf)	*Gnetum gnemon*	Gnetaceae	1.4	0.9	1.2	21
13	Kapu (fr)	*Ficus* spp.	Moraceae	0.2	1.6	0.8	8
14	Kaleuwi (lf)	*Hypobathrum microcarpum*	Rubiaceae	0.3	1.4	0.8	30
15	We wai (lf)	*Flagellaria indica*	Flagellariaceae	0.9	0.7	0.8	31
16	Ulu pulu manu (lf)	*Leptaspis banksii*	Poaceae	1.1	0.2	0.7	18
17	Woro woro (lf)	*Saurauia* sp.	Actinidiaceae	1.1	0.1	0.7	8
18	Gelagah (lf)	*Saccharum spontaneum*	Poaceae	1.2	0.0	0.6	5
19	Taena (lf)	*Timonius* sp.	Rubiaceae	0.3	1.0	0.6	20
20	Dongi (fr)	*Dillenia ochreata*	Dilleniaceae	0.2	1.0	0.6	16
21	Taluede (lf)	*Stenochlaena palustris*	Blechnaceae	0.3	0.9	0.6	11
22	Lempeni (lf)	*Ardisia humilis*	Primulaceae	0.5	0.3	0.4	16
23	Pepundi hao (lf)	*Uvaria littoralis*	Annonaceae	0.3	0.4	0.4	7
24	Waru (lf)	*Hibiscus tiliaceus*	Malvaceae	0.1	0.6	0.3	5
25	Tokoalinda (lf)	*Elatostema rostratum*	Urticaceae	0.6	0.0	0.3	7
26	Kura langga (lf)	*Pachystachys coccinea*	Acanthaceae	0.3	0.3	0.3	11
27	Pundikia (stem)	*Musa* sp.	Musaceae	0.5	0.0	0.3	5
28	Kura donga (lf)	*Axonopus compressus*	Poaceae	0.5	0.0	0.3	8
29	Kosimbo (lf)	*cf. Hedychium*	-	0.4	0.0	0.2	2
30	Tarapasi (lf)	*Syzygium lineatum*	Myrtaceae	0.3	0.1	0.2	3
31	Hao tambololi (lf)	*Trichosanthes* sp.	Cucurbitaceae	0.1	0.4	0.2	3
32	Haonggonduri	*Mimosa* sp.	Fabaceae	0.4	0.0	0.2	2
33	Loluna (lf)	*Cordia myxa*	Boraginaceae	0.4	0.0	0.2	8
34	Puta (lf)	*Barringtonia racemosa*	Lecythidaceae	0.0	0.4	0.2	10
35	Pangi (fr)	*Pangium edule*	Achariaceae	0.0	0.4	0.2	5
36	Tia (lf)	*Archidendron palauense*	Fabaceae	0.0	0.4	0.2	10
37	Holea mbute (lf)	*Cleistanthus* sp.	Phyllanthaceae	0.3	0.0	0.2	3
38	Lombinga (lf)	*Dendrocnide stimulans*	Urticaceae	0.3	0.0	0.2	7
39	Paku (lf)	*Blechnum orientale*	Blechnaceae	0.1	0.1	0.1	11
40	Wonggia (lf)	*Syzygium polycephalum*	Myrtaceae	0.0	0.2	0.1	5
41	Kokapi (lf)	*Drynaria sparsisora*	Polypodiaceae	0.0	0.2	0.1	3
42	Pae pae (lf)	*Isachne albens*	Poaceae	0.1	0.1	0.1	5
43	Hokio (lf)	*Acronychia trifoliolata*	Rutaceae	0.1	0.1	0.1	26
44	Huhubi (lf)	*Artocarpus dasyphylla*	Moraceae	0.1	0.0	0.1	3
45	Unknown (lf/fern)	Fern	-	0.1	0.0	0.1	3
46	Hilanggoku (lf)	*Cyrtococcum patens*	Poaceae	0.1	0.0	0.1	3
47	Ombana (lf)	*Sumbaviopsis albicans*	Euphorbiaceae	0.0	0.1	0.1	2
48	Kole (lf)	*Mitrephora cf polypyrena*	Annonaceae	0.0	0.1	0.0	2
49	Toho (fr)	*Artocarpus* sp.	Moraceae	0.0	0.1	0.0	2
50	Kabuko (fr, bark)	*Syzygium* sp.	Moraceae	0.1	0.0	0.0	2
51	Menambo (fr, bark)	*Garcinia tetrandra*	Clusiaceae	0.1	0.0	0.0	2
52	Unknown (lf/M)	*Monocots*	Poaceae	0.0	0.1	0.0	2

Table 1. Contd.

No	Vernacular name	Botanical name	Family name	Proportion (%)			Frequency of occurrence (%)
				Rainy season	Dry season	Rainy and Dry seasons	
53	Rotan (fr/M)	*Calamus* sp.	Arecaceae	0.0	0.0	0.0	2
54	D.heterophylla (lf)	*Derris trifoliata*	Fabaceae	0.0	0.0	0.0	2
55	Akar akaran (lf)	*Mikania cordata*	Asteraceae	0.1	0.0	0.1	2

grassy savannah habitats in Africa (Sinclair 1977).

Anoas are forest-dwelling ungulates inhabiting the tropical rain forests on Sulawesi, their diets are mainly leaves of dicotyledonous plants. This study also showed that anoa consume a high proportion of fruit, which is up to 22 %. Parts of plants eaten by anoa included leaves, fruit, flowers, shoots, stems, and grass bulbs of many plant species. In captivity, anoa has a habit of choosing forage firstly started with fruit, then leaves or young shoots, and finally grasses (Mustari 1996).

Seasonal change in the diets

There was an increase in fruit components in the diet of anoa in February and September, which were the peaks of the fruiting seasons (Figure 6). Most of the fruit trees produced fruit in the rainy season, which reached a peak in February, yet many of the fruit trees, such as figs (*Ficus* spp.) produced fruit both in rainy and dry seasons (Table 2). Fruit components, especially seeds of figs, were found significantly in the faeces of anoa. Fruit fragments were recorded in the faecal samples indicating that anoas played a significant role as seed dispersers, propagating the food plants, as do other frugivores inhabiting Sulawesi's tropical rain forests, including sulawesi warty pig (*Sus celebensis*), sulawesi black macaques (*Macaca* spp.), and red knobbed hornbill (*Rhyticeros cassidix*) (Mustari 2020). As many as 24 seeds of *Parkia roxburghii* were counted in a single defecation (fresh weight 500 g) of anoa. A fruit of *Parkia roxburghii* contained 7 seeds, meaning that every faeces excreted by an anoa required approximately 3.5 fruits. Other seeds that were found in the dung of the animals were *Artocarpus dasyphylla*, *Ficus* spp., *Artocarpus* sp., and *Diospyros* sp.

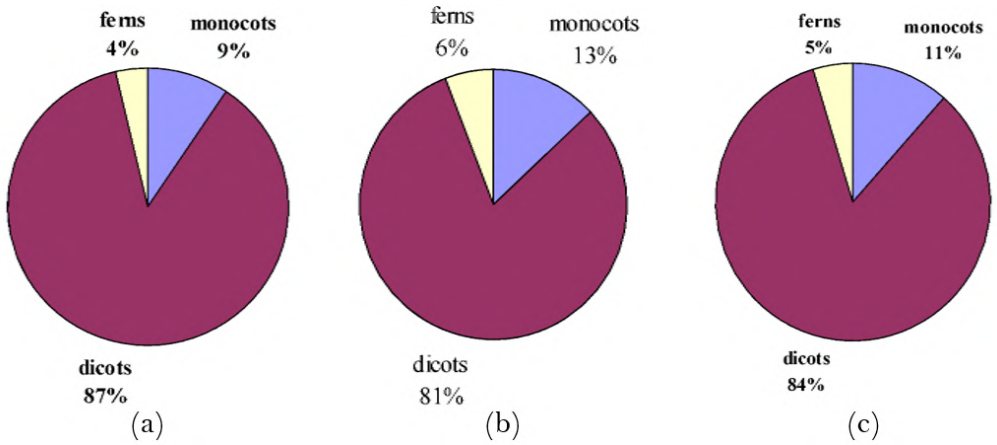

Figure 5. Proportions of monocots, dicots, and ferns in the diet of anoa: (a) rainy season, (b) dry season, (c) both seasons combined.

In general, young leaves and shoots have higher protein and lower crude fibre content than older leaves (McDonald et al. 1995). High-quality foods contain easily digestible carbohydrates and proteins, while low-quality foods are usually old, tough, and woody or fibrous and indigestible. High-

quality foods are young, soft, and green (Jarman & Sinclair 1979). That anoa has developed a feeding strategy that is different from those of other buffaloes could be partly explained by the fact that, in general, among related species with similar digestive capabilities, smaller species require better-quality food than do large species because of the former's higher metabolic rate, although individuals of larger species require larger absolute quantities of food (Jarman & Sinclair 1979).

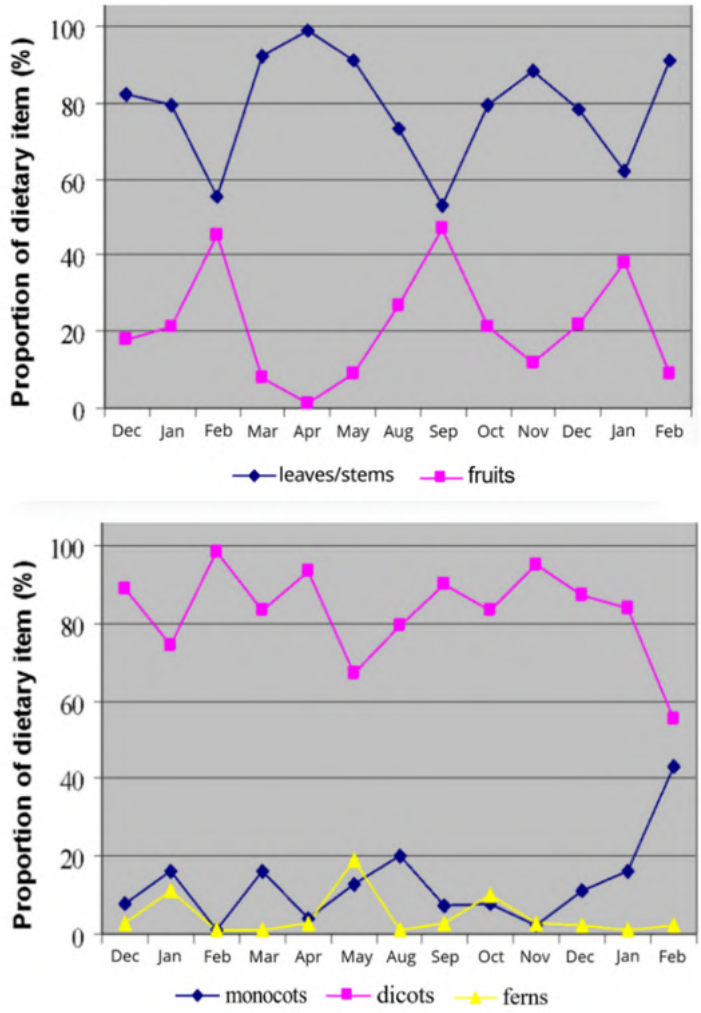

Figure 6. Monthly proportions of monocots, dicots, ferns, leaves/stems, and fruits in the diet of anoa from 2001 to 2002.

Seedlings and undergrowth provide the greatest food sources for anoa, including seedlings of woody plants, herbs, lianas, sedges, bamboos, and grasses. In bamboo forest, the main foods of the anoa are leaves, shoots, and sprouts of the bamboos (*Schizostachyum lima* and *Schizostachyum* cf *brachycladum*). Young leaves and shoots of these bamboos were available all year round. Fruit fragments could be found in the diets of anoa, suggesting that the generative part of the plants plays an important role in the diet of the animals. Most of the fruiting trees produced fruit in the rainy season; the fruiting trees started flowering immediately at the early weeks start of the rainy season in December. A total of 34 fruit species have been recorded as eaten by anoa. Footprints and faeces of anoa were frequently observed under the fruiting trees of figs (*Ficus* spp.), dongi (*Dillenia ochreata*), konduri (*Parkia roxburghii*), toho (*Artocarpus* sp.), kasu meeto (*Diospyros malabarica*), kalaero (*Diospyros pilosanthera*), kabuko (*Syzygium* sp.), menambo (*Garcinia tetrandra*), and huhubi (*Artocarpus dasyphylla*). Fragments of fruit, such as seeds, fruit coats, and flesh, could be identified in the faecal samples. These fragments

Table 2. Phenology of fruiting trees that are potentially eaten by the lowland anoa (* = fruiting, fl = flowering, fl* = flowering and fruiting). Rainy season = January to May, Dry season = July to November; June and December are transitional periods. Most of the fruiting trees started flowering and/or fruiting in the early part of the rainy season in December and January.

Vernacular name	Botanical name	Month											
		Jan	Feb	Mar	Apr	May	Jun	Jul	Aug	Sep	Oct	Nov	Dec
Pepunding-gasu	*Alphonsea javanica*	*	*	*	*	*							fl*
Rema	*Arenga pinnata*	*	*	*	*	*	*	*	*	*	*	*	fl*
Huhubi	*Artocarpus dasyphylla*	*	*	*									fl*
Toho	*Artocarpus* sp.	*	*	*									fl*
We Kilala	*Calamus* sp.			*	*								
Dongi	*Dillenia ochreata*	*	*	*	*	*	*	*	*	*	*	*	fl*
Kalaero	*Diospyros pilosanthera*	*	*	*	*	*							fl*
Kasu meeto	*Diospyros malabarica*	*	*	*	*	*							fl*
Rau	*Dracontomelon mangiferum*	*	*	*						*	*		fl*
Mehere	*Drypetes cf globosa*	*	*										fl*
Kapu Lesea Hoa	*Ficus drupacea*	*	*	*	*	*							fl*
Kapu Wone	*Ficus hirta*	*	*	*	*	*							fl*
Elemeo	*Ficus* sp.	*	*										fl*
Pokae	*Ficus* sp.	*	*	*	*	*						*	fl*
Roramo	*Ficus* sp.	*	*	*									fl*
Wehuko	*Ficus variegata*					*							
Pedengisi	*Garcinia balica*	*	*	*	*	*							fl*
Dede Meiho	*Garcinia cf. dioica*	*	*	*									fl*
Mandula	*Garcinia dulcis*	*	*	*									fl*
Menambo	*Garcinia tetrandra*	*	*	*		fl							
Tembeuwa	*Kjellbergiodendron celebicum*	*	*	*	*	*							
Pundikia	*Musa* sp.	*	*	*	*	*	*	*	*	*	*	*	fl*
Pangi	*Pangium edule*	*	*	*	*	*	*	*	*	*	*	*	fl*
Konduri	*Parkia roxburghii*			fl	*	*	*	*	*	*			
Wewu	*Planchonia valida*	*	*	*									fl*
Oloho	*Spondias pinnata*				*	*							
Kabuko	*Syzygium* sp.	*	*	*									
Pepundi Hao	*Uvaria littoralis*	*	*										fl*

could be easily recognised with the naked eye, such as seeds of *Ficus* spp., *Artocarpus dasyphylla*, and *Parkia roxburghii*; even without the help of a microscope, these intact seeds could be identified in the faeces of anoa. These findings suggests that anoas play an important role in the regeneration of Sulawesi's tropical forest.

The lowland anoa has a high variety of food plants and is predominantly dicots, representing 84 % in the diet, suggesting that this species is browser. A key factor of conserving this species is maintaining the high diversity of food plants that are available in the natural habitats covering many habitat

types, including mangrove, beach, lowland, and lower mountain forests. Lowland anoa's diet also covered many species of fruits, constituting 22 % confirming that this species plays significant roles as seed dispersers in the tropical rain forest of Sulawesi and maintains the natural regeneration of the forests. The conservation implications of these findings are that biodiversity of plants and the pristine primary forests are the key factors in conserving the lowland anoa in the natural habitats.

CONCLUSIONS

Parts of plants browsed by the animals were leaves, shoots, and growing tips of the branches and twigs. A total of 55 species of food plants were identified in analyses of faeces of anoa. The chief foods of the animals were dicotyledons, which constituted 84 %, monocots 11 %, and ferns 5%. Leaves and stems constituted 78 %, while fruit composed 22 % of the diet. Intact seeds of fruit were found in the anoa faecal samples, indicating that anoa plays a significant role as seed dispersers. This study showed that a high diversity of food plants is a key factor in conserving lowland anoa in the natural habitats.

AUTHOR CONTRIBUTION

A.H.M. designed the research, collected and analysed the data, and wrote the manuscript, P.D.S.G.W. analysed the data, and O.P.A. analysed the data.

ACKNOWLEDGMENTS

We would like to thank the officers of the Nature Resources Conservation Bureau (BKSDA) of Southeast Sulawesi and the Ministry of Forestry and Environment of Indonesia. We would like to thank Prof. Peter Jarman of UNE Australia, who supervised this research, and Om Tie in Amolengo Village, who assisted as a field guide during the data collection in Tanjung Peropa Wildlife Reserve. The financial support of this study was provided by the Australian Development Scholarship (ADS).

CONFLICT OF INTEREST

The authors have no financial and personal relationships with other people or organisations that could have influenced this work.

REFERENCES

Adinda, S.K., Ariyanti, N.S. & Dorly, D., 2023. Identifikasi berdasarkan anatomi tumbuhan pakan dalam feses gajah sumatra (*Elephas maximus sumatranus*) di Taman Nasional Way Kambas. *Jurnal Sumberdaya Hayati*, 9(3), pp.125–133.

Arini, D.I.D. & Kafiar, Y., 2014. Prefered feed of anoa (*Bubalus* sp.) at Manado Forestry Research Institute Captivity. *Jurnal Wasian*, 1(2), pp.83–90. doi: 10.62142/3fnp9b11

Arini, D.I.D. & Wahyuni, N.I., 2016. The abundance of anoa (*Bubalus* sp.) plant at Bogani Nani Wartabone National Park. *Jurnal Penelitian Kehutanan Wallacea*, 5(1), pp.91–102. doi: 10.18330/jwallacea.2016.vol5iss1pp91-102.

Aziz, I.R. et al., 2023. Identification, abundance and diversity of forage plants for Anoa (*Bubalus* spp.) in Abdul Latief Forest Park. *Acta Ecological Sinica*, 43(1), pp.202–208. doi: 10.1016/j.chnaes.2022.09.008.

Ginantra, I.K., Muksin, I.K. & Suaskara, I.B.M., 2016. Menggunakan fragmen epidermis di feses untuk identifikasi tumbuhan pakan herbivor: studi seleksi tumbuhan pakan oleh rusa timor (*Cervus timorensis*) di Pulau Menjangan Bali. *Prosiding Seminar Nasional from Basic Science to Comprehensive Education*, pp.194–199.

IUCN, 2025, *The IUCN Red List of Threatened Species Version 2025-1*, viewed 8 April 2025, from https://www.iucnredlist.org.

Jarman, P. & Sinclair, A.R.E., 1979. Feeding Strategy and the Pattern of Resource Partitioning in Ungulates. In *Serengeti: Dynamics of An Ecosystem*. Chicago: Chicago University Press, pp.130-163.

Jarman, P. & C. M. Phillips. 1989. Diets in a Community of Macropods Species. In *Kangaroos, Wallabies and Rat-Kangaroos*. Australia: Surrey Beatty & Sons Pty Limited, pp.143-149.

McDonald, P. et al., 1995. *Animal nutrition*. The 5th Ed. England, Longman Scientific & Technical.

Mustari, A.H., 1996. Population of lowland anoa (*Bubalus depressicornis*, Smith) in Tanjung Amolengu Wildlife Reserve, Southeast Sulawesi, Indonesia. *Media Konservasi*, 5(1), pp.1-3.

Mustari, A.H., Prilianti, A.U. & Masy'ud, B., 2015. Pakan dan perilaku makan anoa (*Bubalus* sp.) di Taman Margasatwa Ragunan, Jakarta Selatan. *Media Konservasi*, 20(3), pp.261–268. doi: 10.29243/medkon.20.3.%p

Mustari, A.H., 2019. *Ekologi, perilaku dan konservasi anoa*, IPB Press.

Mustari, A.H., 2020. *Manual identifikasi dan bio-ekologi spesies kunci di Sulawesi*, IPB Press.

Nowak, R.M., 1991. *Walker's mammals of the world*. The 5th Ed. Baltimore, The Johns Hopkins Univ Pr.

Indonesian Ministry of Forestry, 2018. Peraturan Menteri Lingkungan Hidup dan Kehutanan Republik Indonesia Nomor P.106/Menlhk/Setjen/Kum.1/12/2018 (Permenlhk). Tentang Perubahan Kedua Atas Peraturan Menteri Lingkungan Hidup dan Kehutanan Nomor P.20/Menlhk/Setjen/Kum.1/6/2018 Tentang Jenis Tumbuhan dan Satwa yang Dilindungi. https://jdih.maritim.go.id/id/peraturan-menteri-lingkungan-hidup-dan-kehutanan-no-p106menlhksetjenkum1122018-tahun-2018.

Ranuntu, R.A. & Mallombasang, S.N., 2015. Studi populasi dan habitat anoa (*Bubalus* sp.) di kawasan Hutan Lindung Desa Sangginora Kabupaten Poso. *E-Jurnal Mitra Sains*, 3(2), pp.81-94.

Rusiyantono, Y., Mumu, M.I. & Duma, Y., 2019. The ability to adapt for ex situ conservation of anoa (*Bubalus* sp) through regulation of feeding pattern. *Journal of Physics: Conference Series*, 1214(1), 012042. doi: 10.1088/1742-6596/1242/1/012042

Sinclair, A.R.E., 1977. *The african buffalo*, University Chicago Pr.

Stewart, D.R.M., 1965. The epidermal characters of grasses, with special reference to East African plains species. *Botanische Jahrbücher fur Systematik, Pflanzengeschichte und Pflanzengeographie*, 84(1), pp.63-174.

Stewart, D.R.M., 1967. Analysis of plant epidermis in faeces: a technique for studying the food preferences of grazing herbivores. *Journal of Applied Ecology*, 4(1), pp.83-111. doi: 10.2307/2401411

Tangkoro, I.T.P., Labiro, E. & Korja, I.N., 2018. Komposisi jenis-jenis pakan anoa di kawasan hutan pendidikan Universitas Tadulako Kecamatan Bolano Lambunu Kabupaten Parigi Moutong. *Jurnal Warta Rimba*, 6(2), pp.1–9.

Tabaranza, D.G.E. et al., 2022. Retracing the largest land mammal in the Philippines. *Sylvatrop: The Technical Journal of Philippine Ecosystems and Natural Resources*, 32(2), pp.35–54.

UNEP-WCMC. 2021. Index of Cites Spescies. CITES Secretariat, Geneva, Switzerland and UNEP-WCMC. Cambridge. United Kingdom. E-Appendices-2021-02-14.pdf (cites.org).

Wilson, D.E. & Mittermeier, R.A., 2011. *Handbook of the Mammals of the World*. Lynx Edicions, Barcelona.

Journal of Tropical Biodiversity and Biotechnology
Volume 10, Issue 04 (2025): jtbb18058
DOI: 10.22146/jtbb.18058

Research Article

The *Citrus sinensis* Peel Extract Elevates the Cytotoxicity Effect of Doxorubicin and Inhibits 4T1 Cell Migration

Shofa Khamdanatuz Zufairo'[1,2], Desty Restia Rahmawati[1], Amaliya Permata Putri[1], Anif Nur Artanti[1,3], Faaza Aulia Rahman[1], Edy Meiyanto[4], Ratna Asmah Susidarti[1,5]*

1)Cancer Chemoprevention Research Center (CCRC), Faculty of Pharmacy Universitas Gadjah Mada, Yogyakarta, Indonesia, 55281
2)Master Student of Biotechnology Study Program, Graduate School, Universitas Gadjah Mada, Yogyakarta, Indonesia, 55284
3)Departement of Pharmacy, Vocational College, Universitas Sebelas Maret, Surakarta, 57126, Indonesia
4)Laboratory of Macromolecular Engineering, Department of Pharmaceutical Chemistry, Faculty of Pharmacy, Universitas Gadjah Mada, Yogyakarta, Indonesia, 55281
5)Laboratory of Medicinal Chemistry, Department of Pharmaceutical Chemistry, Faculty of Pharmacy, Universitas Gadjah Mada, Indonesia, 55281
* Corresponding author, email: ratna_asmah@ugm.ac.id

Keywords:
Citrus sinensis
Co-chemotherapy
Doxorubicin
Sinensetin
TNBC
Submitted:
03 December 2024
Accepted:
27 April 2025
Published:
17 November 2025
Editors:
Ardaning Nuriliani
Annisaa Widyasari

ABSTRACT

Combination therapy using natural-based substances is an effective approach to increase the efficacy of doxorubicin (Dox) while reducing its toxicity towards normal cells. This general chemotherapeutic agent treats various cancer cells, including triple-negative breast cancer (TNBC). *Citrus sinensis* peel extract (CPE) contains sinensetin (Sin), which exhibits anti-cancer effects, offering good prospects as a co-chemotherapy agent. This research aims to evaluate the co-chemotherapeutic potency of CPE-contained Sin when combined with Dox and also study its influence on 4T1 cell migration. Assays performed in this experiment included cell viability assay using MTT in individual and combination manner, clonogenic assay to analyse the proliferation inhibition effects of the treatments, scratch wound healing assay to assess the cells' migration status, and gelatine zymography to evaluate cells' matrix metalloproteinase-9 (MMP-9) activity. This experiment confirmed that CPE and Sin had cytotoxic effects on 4T1 cells with the IC_{50} of 536 µg mL^{-1} and 120 µM, respectively, while Dox performed cytotoxicity on 4T1 cells with an IC_{50} of 2 µM. The combination of CPE and Dox showed synergistic effects with the combination index (CI) <1.0. CPE and its co-administration with Dox permanently suppressed the colony formation of 4T1 cells after 10 days of treatment removal. CPE and Sin inhibited the 4T1 cell migration strongly compared to Dox. CPE in its single and mixture form with Dox inhibited the MMP-9 activity. These results suggest that CPE, when combined with Dox, could be a promising co-chemotherapy regimen for TNBC treatment, potentially reducing the risk of metastasis and relapse.

How to cite:
Zufairo', S.K. et al., 2025. The *Citrus sinensis* Peel Extract Elevates the Cytotoxicity Effect of Doxorubicin and Inhibits 4T1 Cell Migration. *Journal of Tropical Biodiversity and Biotechnology*, 10(4), jtbb18058. doi: 10.22146/jtbb.18058

INTRODUCTION

Triple-negative breast cancer (TNBC) is known for progesterone receptor (PR), oestrogen receptor (ER), and human epidermal growth factor receptor 2 (HER-2) negativity, which makes anti-oestrogen based-chemotherapeutic agents ineffective in treating this type of cancer (Manjunath & Choudhary 2021). TNBC comprises 10-15 % of all breast cancer incidence and is responsible for 40 % of the mortality caused by breast cancer worldwide (Rosińska et al. 2024). Patients with TNBC often have a poor prognosis due to the aggressiveness of the disease, such as the high rate of proliferation, metastases, and relapse (Vuger et al. 2020). Chemotherapeutic agents that are neither hormonal nor HER-2 targeted-based are needed to treat this type of cancer.

Some chemotherapy agents have been used to treat TNBC. Doxorubicin (Dox) is an oncological agent generally used to treat diverse cancer types, including TNBC (Amalina et al. 2023). Dox is a non-anti-estrogenic chemotherapy agent that induces DNA damage or double-strand breaks (DSB) in cancer cells due to the intercalation process of Dox molecules in their DNA, leading them to apoptosis (Kciuk et al. 2023). However, the use of Dox still faces some challenges, which are related to cancer cells' resistance, relapse, and migration (Wardhani et al. 2021; Kciuk et al. 2023). Therefore, there is a need for a co-chemotherapy agent to enhance the effectiveness of chemotherapy regimens, such as DOX, in treating cancer cells, especially in TNBC.

Citrus sinensis, a commercially available fruit, is known for its anti-cancer properties (Chu et al. 2017). The *Citrus sinensis* peel extract (CPE) contains several beneficial compounds that could act as anti-cancer agents. Some of these compounds are flavonoids, including sinensetin, hesperidin, hesperetin, and naringenin (Meiyanto et al. 2012; Zufairo' et al. 2023). Sinensetin (Sin) is a polymethoxy flavone that comprises as much as 1.083 % of 120 mg *Citrus sinensis* peel extract (Xu et al. 2019). It has been studied for its anti-cancer potential in several cancer cells. Previous studies have shown that Sin can reduce the viability of lung cancer cells, promote apoptosis in liver cancer cells, suppress metastasis of luminal breast cancer, and inhibit the inflammation caused by cisplatin without affecting the cisplatin's efficacy (Samidurai et al. 2020; Indriyanti et al. 2023; Li et al. 2023; Zhu et al. 2024). These promising features make CPE with Sin in it a potential co-chemotherapy agent that can be combined with Dox, enhancing its effectiveness in restraining cell progression, particularly in TNBC cells.

This study focused on assessing the effects of CPE combined with Dox on TNBC progression, particularly regarding proliferation, relapse, and its potential to inhibit cell migration. 4T1 cells were used for the TNBC model. Some assays used to assess parameters regarding proliferation, relapse, and migration were cell viability assay using MTT, colony formation assay, scratch wound healing assay, and gelatine zymography respectively.

MATERIALS AND METHODS

Materials

Citrus sinensis peel was retrieved from the local fruit market in Sleman, Yogyakarta, and determined at the Department of Pharmaceutical Biology, Faculty of Pharmacy, Universitas Gadjah Mada. Doxorubicin hydrochloride (Dox) was purchased from Wako, Japan (Cat. No. 046-21523). Sinensetin (Sin) was obtained from Sigma, USA (Cat. No. SML 1787-5MG). Each substance for treatment, including the extract, was dissolved in DMSO (Sigma, USA) to prepare a stock solution. These stocks were then diluted into several concentrations using complete medium for treatment purposes.

Methods

Citrus sinensis Peel Preparation

The *Citrus sinensis* peel was cleaned and dried using an oven at the tempera-

ture 60 °C for six hours, as previously described (Zufairo' et al. 2023). Dried *Citrus sinensis* was ground, sifted, and homogenised overnight using 70 % ethanol with a ratio of 1:10. The centrifugation process was conducted to distinguish the pellet and supernatant. The supernatant was collected and dried until a brown viscous extract was obtained. This extract was labelled as *Citrus sinensis* peel extract (CPE).

Cell Culture

The Cancer Chemoprevention Research Center (CCRC), Faculty of Pharmacy of Universitas Gadjah Mada, kindly provided 4T1 cells. Cells were grown in Dulbecco's modified Eagle's medium (Gibco, USA). 10 % FBS (Gibco, USA) and 1 % penicillin-streptomycin (Gibco, USA) were mixed into the medium. Cells were incubated under standard conditions, which were 37 °C and 5 % CO_2.

Cell Viability Assay

4T1 cells were cultured into a 96-well plate at approximately 5 x 10^3 cells/well, incubated under standard conditions for 24h, and treated with a serial concentration of CPE (10-500 µg mL^{-1}), Sin (10-500 µM) (Sigma, USA), and Dox (0.1-10 µM) (Wako, Japan) in single and combination way (with the concentration of $^1/_2$, $^1/_4$, and $^1/_8$ of IC_{50} for each compound). All treatments were done in triplicate. Treated cells were washed with PBS 1X and were given 3-(4,5-dimethyl thiazolyl-2)-2,5-diphenyl tetrazolium bromide (MTT) (Sigma, USA). Cells incubated with MTT (0.5 mg mL^{-1} in complete medium) were then treated with 10% SDS (in 0.01 M HCl) (Sigma, USA) to stop the reaction. The cells were then incubated under dark conditions overnight to be analysed using a microplate reader at 595 nm. As previously described, absorbance data were used to calculated cell viability and IC_{50} (Haryanti et al. 2022). The combination index (CI) was generated by calculating cell viability in combination treatment (Reynolds & Maurer et al. 2005).

Clonogenic Assay

The 4T1 cells were cultured into a 6-well plate (5 x 10^3 cells/well) and incubated for 24 h under standard conditions. The cells were subjected to a single and combination dose of CPE and Dox and incubated for 24 hours. The treated medium on the cells was then replaced by a fresh and complete medium and maintained for 10 days under standard conditions. All treatments were performed in triplicates. Cells were exposed to PBS 1X for rinsing, treated with formalin 10 % (Sigma, USA) for fixation, and stained using gentian violet 1 % (Sigma, USA). Dyed cells were documented and counted to analyse the colony formation of treated cells compared to the untreated ones. The ImageJ was used to analyse and count colonies from images of treated and untreated cells. The number of colonies formed was presented as % colony compared to untreated graphics.

Migration Assay

A cell suspension containing 4T1 cells (approximately 8 × 10^4 cells/well) was added to a 24-well plate and incubated for 24 h. Cells were then given a starvation medium for 24 h, which contained 0.5 % FBS. Cells were wounded by performing a scratch using yellow tips, treated using CPE, Sin, and Dox in a single form, and then incubated for 24 and 48 hours. All treatments were done in triple. Afterward, scratched cells were photographed under 100x inverted-microscope magnification and analysed using ImageJ (NIH Image, USA) to measure the scratched area. The scratched area of each treatment was used to calculate % closure at 24 and 48 h after treatments. The result was analysed against the untreated cells.

MMP-9 Activity Assay

Matrix metalloproteinase-9 (MMP-9) activity was analysed via gelatine zymography. 4T1 cells with approximately 5 x 10^5 cells/well were cultivated in a 6-well plate for 24 hours. Cells were given CPE, Dox, and their combination in starvation medium (0.5 % FBS) and maintained for 24 hours. The treatment media were collected and separated using SDS-PAGE (8 % gel, 0.1 % gelatin). The marker used in this assay was PM5100 Excelband™ 3-color pre-stained protein ladder (SMOBIO, Taiwan). The gel was renatured in 2.5 % Triton X-100 (Sigma, USA) for 30 minutes, washed, and incubated for 24 hours in an incubation buffer (40 mM Tris-HCl pH 8, 10 mM $CaCl_2$, 0.02 % NaN_3). After staining with 0.05 % Coomassie Brilliant Blue G-250 (Sigma, USA) for 2 hours, the gel was destained until clear bands appeared, indicating MMP-9 gelatinolytic activity. Band intensity was quantified using ImageJ.

Statistical Analysis

All the treatments in the assays used in this work were carried out in triplicate. Data normality was confirmed using the Shapiro–Wilk test. Normal data was then analysed statistically by independent t-test using GraphPad Prism 10.1.2, which has 95 % reliability.

RESULTS AND DISCUSSION

CPE and Sin Cytotoxic Activity Towards 4T1 Cells

Cell viability assay was conducted using MTT to assess the capacity of CPE and Sin to perform their cytotoxic activity. The result revealed that CPE and Sin performed cytotoxicity effects towards 4T1 cancer cells with the IC_{50} of 536 µg mL^{-1} and 120 µM, respectively (Figure 1a and 1b). On the other hand, Dox, a general chemotherapy agent, exerted a strong cytotoxic effect on 4T1 with the IC_{50} of 2 µM (Figure 1c). Therefore, based on the IC_{50} value of each agent, it is confirmed that CPE and Sin exerted low and moderate cytotoxicity effects, respectively, whereas Dox produced a strong cytotoxic effect (Ikawati et al. 2023).

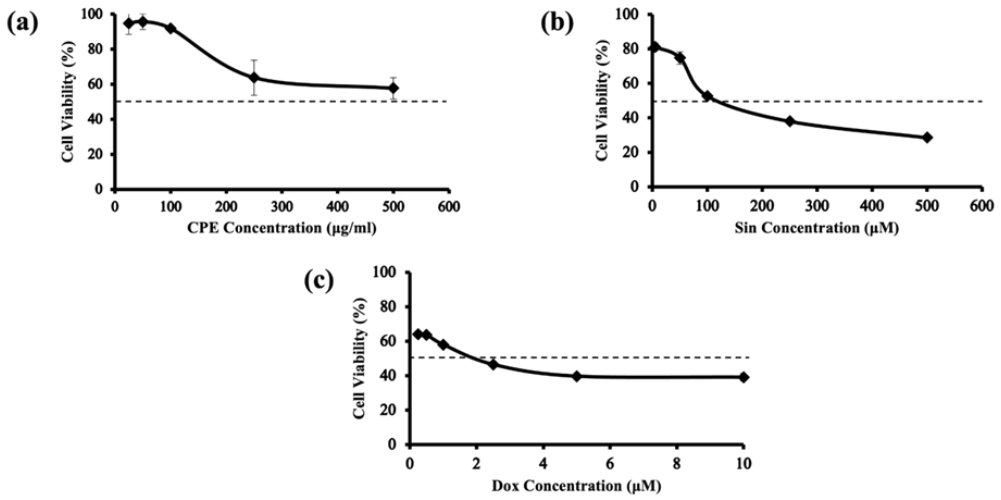

Figure 1. The cell viability status of 4T1 cells after treatment using CPE, Sin, and Dox. CPE (a) and Sin (b) have low and moderate cytotoxicity, while Dox (c) has exhibited a strong cytotoxic effect, both towards 4T1 cells. Quantitative data were presented as the mean of three independent experiments; the error bars indicate the standard error.

CPE Synergistically Enhances Dox Cytotoxic Activity on 4T1 Cells

Cell viability was known to diminish along the higher combination dose of CPE and Dox used (Figure 2a). The combination treatment of 268 µg mL^{-1} CPE with 1 µM Dox was shown to have the lowest cell viability compared to

the other dose of CPE and Dox combination. Generally, the combination index (CI) of CPE-Dox, calculated from cell viability data, exhibited a synergism on 4T1 cells. The CI within the range of 0.1-0.3 was categorised as strong synergism, 0.3-0.7 was categorised as synergism, and the range of 0.7-0.9 was categorised as moderate to slight synergism (Reynolds & Maurer 2005). All CI values for both CPE concentrations combined with various concentrations of Dox were used, which are 0.25, 0.5, and 1 µM, categorised to have strong to moderate synergistic effects with all the CI values <0.1 (Figure 2b).

(a)

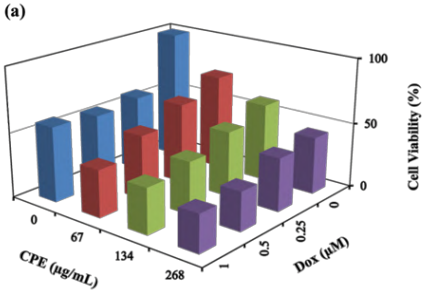

(b)

CPE concentration (µg/mL)	Dox (µM)		
	0.25	0.5	1
67	0.71	0.35	0.18
134	0.38	0.28	0.26
268	0.46	0.37	0.38

Figure 2. CPE-Dox cytotoxic effect. The cell viability of 4T1 after being treated by several combinations of CPE-Dox (a) and the CI value resulting from the cell viability calculation (b) indicates the synergistic status of CPE-Dox. Each numerical data set was presented as the average of three independent experimental replicates (n=3).

CPE and Its Combination with Dox Shows Permanent Effects in the Repressing 4T1 Colony Formation

The permanent effect of treatment is expected to be exerted by chemotherapy and the candidates of co-chemotherapeutic agents to prevent the recurrence caused by the uncontrolled proliferation featured by cancer cells, especially on TNBC. A clonogenic assay was performed in this study to analyse the inhibition capacity of colony formation owned by CPE, Dox, and their combination after 10 days without treatment (Figure 3a and b). All treated cells showed the suppression of colony formation, which is very significant compared to the untreated cells. The combination treatment between CPE 250 µg mL^{-1} and Dox 1 µM performed higher inhibition than CPE and Dox in their single form. The combination of CPE and Dox generated only one small colony, while each of CPE and Dox in a single form generated two small colonies. These results indicate that CPE, in both single and combination form, showed irreversible effects in suppressing the 4T1 cell proliferation by inhibiting colony formation.

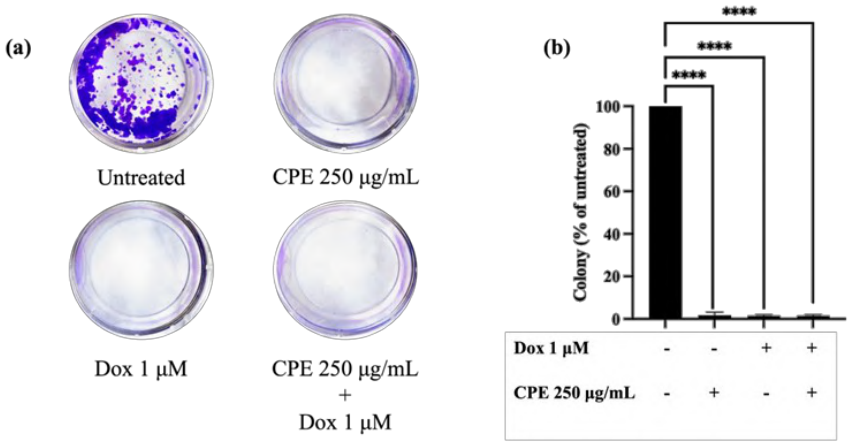

Figure 3. The colony formation of treated and untreated 4T1 cells. The appearance of colony formation of treated and untreated 4T1 cells (a), the colony formed of

treated cells presented as graphic (b). Each numerical data set reflects the average of three independent experiments. The standard deviation is represented by the error bars. ****p<0.0001.

CPE and Sin Exert Migration Inhibition Activity on 4T1 Cells

Triple-negative breast cancer (TNBC) is known as a highly metastatic type. Migration is a crucial step in the metastatic activity of cancer cells. Therefore, migration is one of several aspects that need to be targeted by chemotherapeutic and co-chemotherapeutic agents. A scratch wound healing assay was conducted in this study to evaluate the migration inhibition capacity of CPE, Sin, and Dox on 4T1 cells. Both CPE and Sin generally showed migration inhibition compared to the untreated cells (figure 4a and b). Both doses of CPE and Sin significantly inhibited 4T1 cell migration for 24 and 48 hours compared to untreated group. However, in the case of Sin treatments, the migration inhibition was stronger only with a higher dose (120 µM), even in 24 and 48 hours of treatment, which performed only 8.13 and 15.96 % of closure, respectively. In contrast, 0.5 and 1 µM Dox showed low inhibition on 4T1 cell migration compared to the untreated cells, with a % closure of 82 and 86 %, respectively, in 48 hours. Further analysis, particularly of the molecular aspects, is needed to understand the specific mechanism by which CPE, containing Sin, suppresses the migration of 4T1 cells.

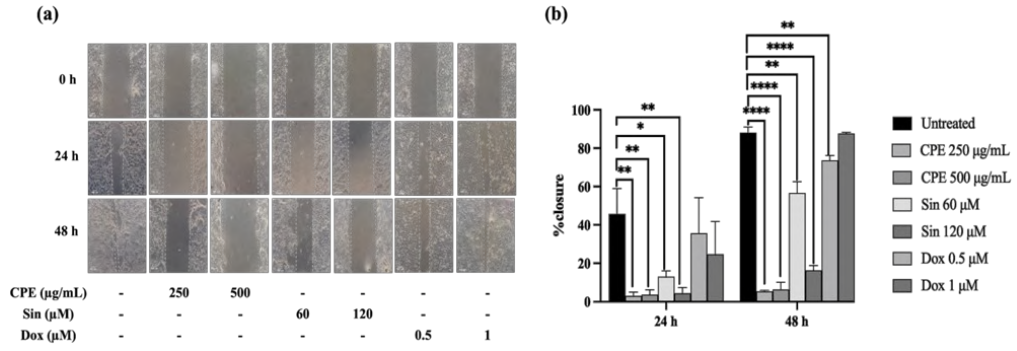

Figure 4. The migration effects of 4T1 cells after being treated by CPE, Sin, and Dox separately compared to untreated cells. The scratched area was observed on all treated and untreated 4T1 cells (a), and the graph showed the percentage of closure of each treated and untreated scratched 4T1 cell (b) from the analysis using ImageJ. Each set of quantitative data represents the average of three independent experiments, with error bars indicating the standard deviation. *p<0.05; ** p<0.01; ****p<0.0001.

CPE and Its Combination with Dox Suppress the Activity of MMP-9 on 4T1 Cells

To elucidate the specific mechanism of CPE-Dox in suppressing the migration of 4T1 cells, their effect on matrix metalloproteinase 9 (MMP-9) activity was examined using gelatine zymography. MMP-9 is a critical protein involved in the migration and metastasis of TNBC. As an enzyme, it degrades the extracellular matrix composed of collagen, facilitating cell detachment and enhancing the potential for cellular migration to other sites. The presence of clear bands in the gel was interpreted as indicative of MMP-9 activity, reflecting its ability to degrade gelatine, a collagen derivative. In this study, MMP-9 activity in 4T1 cells was found to be significantly reduced following treatment with either CPE 250 µg mL^{-1}, Dox 1 µM, or their combination. The reduction in MMP-9 activity was evidenced by the diminished intensity of the bands observed in the gel compared to untreated cells (Figure 5a) and further confirmed through quantification using ImageJ software (Figure 5b). The band intensity for CPE alone was 0.5 times lower than for Dox, with the

lowest band intensity observed in the combination of CPE with Dox. These results demonstrate that CPE, both alone and in combination with Dox, significantly reduces MMP-9 activity.

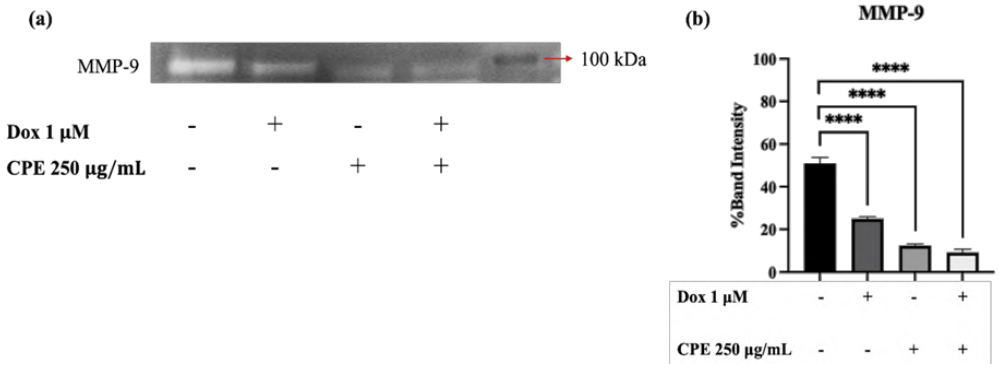

Figure 5. The activity of MMP-9 after CPE, Sin, and Dox treatments on 4T1 cells. Band which represents MMP-9 activity (a), and a graph showing percentage of band intensity from the gelatin zymography results, quantified using ImageJ (b). Each quantitative data set is displayed as the mean of triplicate experiments, with standard deviation as the error bars. ****p<0.0001.

Discussion

This work confirms that CPE enhances the cytotoxicity of Dox on the 4T1 or TNBC model. From this study, CPE demonstrated low cytotoxic effects when used alone on 4T1 cells. However, when paired with Dox in the same cell model, it shows an excellent synergistic effect. Sin, one of the polymethoxylated flavonoids in CPE, exerts a moderate cytotoxic effect on 4T1 cells. Either CPE or Sin has shown potential to increase the susceptibility of various cancer cell types to chemotherapeutic drugs, enhancing their cytotoxic effects. Previous work has shown that either CPE or Sin can enhance the cytotoxicity effects of doxorubicin and cisplatin on HepG2 (Zufairo' et al. 2023). The result of this work highlights CPE as a promising candidate for combination with other chemotherapeutic drugs.

Maintaining a persistent effect of chemotherapeutic agents is crucial to ensure their long-term efficacy and prevent cancer relapse. This study found that CPE and Dox, either alone or in combination, effectively suppressed the colony formation of 4T1 cells even 10 days after treatment cessation, demonstrating their ability to inhibit cancer cell proliferation over an extended period. CPE is known to contain various beneficial compounds, including hesperetin (Chen et al. 2012; Artanti et al. 2023). These results align with previous studies showing inhibition of colony formation in MCF-7 cells, a model of Luminal-A breast cancer, for 14 days after hesperetin treatment discontinuation (Hermawan et al. 2021). However, in this study, the compound was used as an extract at a specific concentration, and a different breast cancer cell model was employed, specifically 4T1 cells, which represent TNBC. The use of other, more human-relevant TNBC cell lines would allow for a more comprehensive evaluation of CPE's cytotoxic and anti-proliferative effects in the human TNBC model. Nevertheless, these findings reinforce the potential of CPE to enhance and maintain the anti-proliferative effects of standard chemotherapeutic agents, such as Dox. Analysis of several parameters involved in cancer eradication is needed to reveal the mechanism of CPE cytotoxicity in cancer cells, especially TNBC.

Migration is when cancer cells move to surrounding tissue near the primary cancer site. Migration is an important step that is strongly correlated with metastasis activity. Triple-negative breast cancer (TNBC) is known for its strong metastatic activity (Vuger et al. 2020; Schrörs et al. 2020). To test the ability of CPE, Sin, and Dox to suppress TNBC migration, a scratch-

wound healing assay technique was performed on 4T1 cells. This study found that Dox achieved the highest %closure, almost the same as untreated-scratched-4T1 cells, after 24 or 48 hours of treatments. This result is in line with the previous experiment (Amalina et al. 2023). Therefore, it is suggested that a combination of Dox with other agents that can inhibit Dox-induced migration is needed.

Interestingly, CPE exhibited stronger migration inhibition on 4T1 cells after 24 and 48 hours of treatment. Research on various pure citrus flavonoids in cancer cells has shown their ability to attenuate migration (Shi et al. 2013; Nurhayati et al. 2020; Zhu et al. 2024). A molecular approach was also conducted in this study to understand how CPE restricts 4T1 cell migration. Matrix metalloproteinase 9 (MMP-9), a crucial enzyme that facilitates cancer cell migration and invasion by degrading the extracellular matrix (ECM), was analysed for its activity using the gelatine zymography technique (Tafrihani et al. 2023). This study revealed that the activity of MMP-9 in CPE at 250 µg mL^{-1} and its combination with Dox at 1 µM was significantly suppressed compared to the untreated group. These findings suggest the prospect of CPE as a co-chemotherapeutic agent of Dox in suppressing breast cancer cell migration, particularly in TNBC.

CONCLUSION

CPE and Sin, which are CPE constituents, are known to have low and moderate cytotoxicity towards 4T1. CPE has been shown to increase the sensitivity of 4T1, a TNBC model, to Dox in a synergistic manner. CPE alone and in combination with DOX show an irreversible effect on 4T1 cells by inhibiting the formation of new colonies after 10 days without treatment. CPE and Sin can strongly inhibit the migration of 4T1 cells at 24 and 48 hours compared to the Dox-treated and untreated cells. CPE and its combination with Dox were shown to reduce the MMP-9 activity, which potentially reduces the cells' ability to degrade the extracellular matrix (ECM), leading to cell invasion inhibition. This study emphasises the CPE as a prospective-co-chemotherapy agent for several standard chemotherapeutic drugs.

AUTHORS CONTRIBUTION

SKZ, along with APP, collected and analysed the in vitro data. DRR, FAR, and ANA conducted the molecular assays. SKZ wrote the manuscript under the supervision of EM and RAS. RAS and EM contributed to the experimental design and provided supervision for the entire assay and manuscript writing.

ACKNOWLEDGMENTS

We are grateful for the support of the Rekognisi Tugas Akhir (RTA) program (under the official assignment letter number of 5286/UN1.P1/PT.01.03/2024) held by Universitas Gadjah Mada for this work.

CONFLICT OF INTEREST

All contributors to this work stated that there is no conflict of interest.

REFERENCES

Amalina, N.D. et al., 2023. In vitro synergistic effect of hesperidin and doxorubicin downregulates epithelial-mesenchymal transition in highly metastatic breast cancer cells. *Journal of the Egyptian National Cancer Institute*, 35(1), 6. doi: 10.1186/s43046-023-00166-3.

Artanti, A.N. et al., 2023. Cytotoxic Activity and Senescence Modulatory Effect of Hesperetin on Triple-Negative Breast Cancer Cells and Kidney Cells Co-Treatment with Cisplatin. *Indonesian Journal of Cancer Chemoprevention*, 14(3), pp.181-188. doi: 10.14499/indonesianjcanchemoprev14iss3pp181-188.

Chen, Z.T. et al., 2012. Protective effects of sweet orange (*Citrus sinensis*) peel and their bioactive compounds on oxidative stress. *Food chemistry*, 135 (4), pp.2119-2127. doi: 10.1016/j.foodchem.2012.07.041.

Chu, C.C. et al., 2017. Antiproliferative effect of sweet orange peel and its bioactive compounds against human hepatoma cells, in vitro and in vivo. *Journal of Functional Foods*, 33, pp.363-375. doi: 10.1016/j.jff.2017.03.051.

Haryanti, S. et al., 2022. The cytotoxic and anti-migratory properties of *Caesalpinia sappan* and *Ficus septica*, in combination with doxorubicin on 4T1 TNBC cells with nephroprotective potential. *Asian Pacific Journal of Cancer Prevention: APJCP*, 23(2), pp.743-753. doi: 10.31557/APJCP.2022.23.2.743.

Hermawan, A. et al., 2021. Bioinformatics and in vitro studies reveal the importance of p53, PPARG and notch signaling pathway in inhibition of breast cancer stem cells by hesperetin. *Advanced Pharmaceutical Bulletin*, 11(2), pp.351-360. doi: 10.34172/apb.2021.033.

Ikawati, M. et al., 2023. The Synergistic Effect of Combination of Pentagamavunone-1 with Diosmin, Galangin, and Piperine in WiDr Colon Cancer Cells: In vitro and Target Protein Prediction. *Journal of Tropical Biodiversity & Biotechnology*, 8(2), jtbb80975. doi: 10.22146/jtbb.80975.

Indriyanti, R.A. et al., 2023. The effect of Sinensetin and Imperatorin on A-549 lung cancer cell viability in vitro. *Pharmacognosy Journal*, 15(1), pp.38-46. doi: 10.5530/pj.2023.15.6.

Kciuk, M. et al., 2023. Doxorubicin—an agent with multiple mechanisms of anticancer activity. *Cells*, 12(4), pp.26-32. doi: 10.3390/cells12040659.

Li, Y. et al., 2023. Natural flavonoid sinensetin inhibits cisplatin-induced pyroptosis and attenuates intestinal injury. *Biochimica et Biophysica Acta (BBA)-Molecular Basis of Disease*, 1869(3), 166637. doi: 10.1016/j.bbadis.2023.166637.

Manjunath, M. & Choudhary, B., 2021. Triple-negative breast cancer: A run-through of features, classification and current therapies. *Oncology Letters*, 22(1), 512. doi: 10.3892/ol.2021.12773.

Meiyanto, E., Hermawan, A. & Anindyajati, A., 2012. Natural products for cancer-targeted therapy: citrus flavonoids as potent chemopreventive agents. *Asian Pacific Journal of Cancer Prevention*, 13(2), pp.427-436. doi: 10.7314/APJCP.2012.13.2.427.

Nurhayati, I.P. et al., 2020. Cytotoxic and antimetastatic activity of hesperetin and doxorubicin combination toward Her2 expressing breast cancer cells. *Asian Pacific Journal of Cancer Prevention: APJCP*, 21(5), pp.1259-1267. doi: 10.31557/APJCP.2020.21.5.1259.

Reynolds, C.P. & Maurer, B.J., 2005. Evaluating response to antineoplastic drug combinations in tissue culture models. *Chemosensitivity: Volume 1 In Vitro Assays*, 110, pp.173-183. doi: 10.1385/1-59259-869-2:173.

Rosińska, M. et al., 2024. Retrospective Observational Study to Determine the Epidemiology and Treatment Patterns of Patients with Triple-Negative Breast Cancer. *Cancers*, 16(6), 1087. doi: 10.3390/cancers16061087.

Samidurai, D. et al., 2020. Sinensetin isolated from Orthosiphon aristatus inhibits cell proliferation and induces apoptosis in hepatocellular carcinoma cells. *Process Biochemistry*, 88, pp.213-221. doi: 10.1016/j.procbio.2019.09.031.

Schrörs, B. et al., 2020. Multi-omics characterization of the 4T1 murine mammary gland tumor model. *Frontiers in oncology*, 10(6), 1195. doi: 10.3389/fonc.2020.01195.

Shi, M.D. et al., 2013. Nobiletin attenuates metastasis via both ERK and PI3K/Akt pathways in HGF-treated liver cancer HepG2 cells. *Phytomedicine*, 20(8-9), pp.743-752. doi: 10.1016/j.phymed.2013.02.004.

Tafrihani, A.S. et al., 2023. Cardamom essential oil extract suppress the progression of triple-negative breast cancer 4T1 cell line. *The Indonesian Biomedical Journal*, 15(2), pp.150-156. doi: 10.18585/inabj.v15i2.2140.

Vuger, A. T. et al., 2020. Characteristics and prognosis of triple-negative breast cancer patients: a Croatian single institution retrospective cohort study. *Acta clinica Croatica*, 59(1), pp.97-107. doi: 10.20471/acc.2020.59.01.12.

Wardhani, B.W. et al., 2021. TGF-β-induced TMEPAI promotes epithelial–mesenchymal transition in doxorubicin-treated triple-negative breast cancer cells via SMAD3 and PI3K/AKT pathway alteration. *Breast Cancer: Targets and Therapy*, 13, pp.529-538. doi: 10.2147/BCTT.S325429.

Xu, Y. et al., 2019. Simultaneous separation of six pure polymethoxyflavones from sweet orange peel extract by high performance counter current chromatography. *Food Chemistry*, 292, pp.160-165. doi: 10.1016/j.foodchem.2019.04.031.

Zhu, S. et al., 2024. Sinensetin suppresses breast cancer cell progression via Wnt/β-catenin pathway inhibition. *Translational Cancer Research*, 13(1), pp.348-362. doi: 10.21037/tcr-23-1317.

Zufairo', S.K. et al., 2023. *Citrus sinensis* Peel Extract Synergistically Enhances the Cytotoxic Effect of Chemotherapeutic Agents on HepG2 Cells. *Indonesian Journal of Cancer Chemoprevention*, 14(3), pp.151-159. doi: 10.14499/indonesianjcanchemoprev14iss3pp151-159.

Journal of Tropical Biodiversity and Biotechnology
Volume 10, Issue 04 (2025): jtbb11819
DOI: 10.22146/jtbb.11819

Research Article

Porifera and Cnidaria Diversity and Paleoecology in Pleistocene Epoch at Sangiran, Indonesia

Donan Satria Yudha[1]*, Fadhil Arrasyid Ardianto[1]
1)Laboratory of Animal Systematics, Faculty of Biology, Universitas Gadjah Mada, Jl. Teknika Selatan, Sekip Utara, Yogyakarta, 55281, Indonesia
* Corresponding author, email: donan_satria@ugm.ac.id

Keywords:
Cnidaria
Fossils
Pleistocene Period
Porifera
Sangiran Dome
Submitted:
19 January 2024
Accepted:
10 July 2025
Published:
24 November 2025
Editors:
Miftahul Ilmi
Sri Nopitasari

ABSTRACT

The Kalibeng Formation of Sangiran Dome geological outcrop (Indonesia) in is an area where various fossils have been found, including ancient human fossils (*Homo erectus*), vertebrate fauna, and marine biota such as coral reefs. To date, the species diversity of fossil corals and sponges in Sangiran Dome and Indonesia, in general, is not widely known. The Sangiran stratigraphy is divided into several layers, with the lowest layer being the Kalibeng Formation, which was an ancient shallow sea, according to Brasseur et al. (2015). Further study can be conducted on the ancient corals and sponges' in Sangiran to reveal the past environmental conditions, particularly during the Pleistocene period in the Sangiran Dome area. Fossilised corals and sponges with well-preserved conditions can serve as a basis for identifying various genera member of the Phylum Porifera and Cnidaria, using specific morphological characteristics for identification. The objective of this study is to determine the genus diversity also to define diagnostic characteristics, and habitat of corals and sponges' fossils in the Plio-Pleistocene Period at Sangiran. The method used for identifying fossil samples was morphological comparison against type specimens and references. The results indicated that the identified corals and sponges were grouped into seven families that inhabits in the neritic zone. This study concludes that each coral genus (phylum Cnidaria) has distinctive corallite characteristics, while sponge genus (phylum Porifera) has distinctive spicules that are useful for identification.

How to cite:
Yudha, D.S. & Ardianto, F.A., 2025. Porifera and Cnidaria Diversity and Paleoecology in Pleistocene Epoch at Sangiran, Indonesia. *Journal of Tropical Biodiversity and Biotechnology*, 10(4), jtbb11819. doi: 10.22146/jtbb.11819

INTRODUCTION

The Sangiran Early Man Site is a location where various types of fossils have been discovered, including ancient human fossils (*Homo erectus*), vertebrate fauna, and marine biota such as corals and sponges. All fossils found in the Sangiran area and its surroundings were collected, described, and displayed in the Sangiran Early Man Site Museum exhibition room. The site is renowned worldwide as a paleontological research site and a scientific tourism destination. The Sangiran Dome area has been designated as a World Cultural Heritage Area protected by law due to its various geological and historical importance (Sukandarrumidi 2021).

The geological outcrop area of the Sangiran Dome, located in Solo, Central Java, has yielded several fossils of marine life, including foraminifera, mollusks, fish, shark teeth, corals and sponges (Yudha et al. 2013). Corals and sponges belong to the phylum Porifera and Cnidaria, they have been present on Earth since the Ediacaran period, over 600 million years ago until today. It is estimated that they first appeared molecularly around a billion years ago during the Cryogenian period and occur in nowadays Sangiran area during the Pio-Pleistocene Period (Morandini et al. 2016).

Research on identifying the characteristics of fossil corals and sponges (Porifera and Cnidaria) in Indonesia is limited. Therefore, it is necessary to conduct research on the diversity and morphology of corals and sponges' fossils in Indonesia, given the limited number of scientific publications on the subject. This research aims: 1) to identify the genus of corals and sponges' fossil collection of the Laboratory of Bioanthropology and Paleoanthropology, Faculty of Medicine, Public Health and Nursing UGM and Sangiran Early Man Site; 2) to examine morphological characteristics to compare with references and identify the genus of the collected samples; and 3) to provide additional references to the diversity of corals and sponges in Sangiran Dome.

MATERIALS AND METHODS

Materials

The study was carried out using comparative morphological method between present-day specimens with fossil collection. Present-day specimen of corals and sponges used was a collection of the Museum of Biology and Laboratory of Animal Systematics, Faculty of Biology, Universitas Gadjah Mada, and alive or in-situ specimen from Porok Beach, Gunung Kidul, Yogyakarta. Meanwhile corals and sponges' fossil analyzed were collection of the Laboratory Bioanthropology and Paleoanthropology, Faculty of Medicine, Public Health and Nursing UGM (abbreviated as LBP) and Sangiran Early Man Site (abbreviated as SEMS). There were three cnidarian fossil specimen collection of LBP; and twelve sponges and cnidarian fossil specimen collection of SEMS. We did not conduct the excavation to obtain the fossil, meanwhile, we only study fossil collection. Therefore, we were not preparing and processing anything also any geological information depends on specimen records from those institutions. Unfortunately, LBP and SEMS do not have any specific information or geological records on fossil corals and sponges of their collection; therefore, we cannot compare its stratigraphical position. The study focused on the hard parts of its morphological characteristics of the preserved fossils. We used identification guides for corals and sponges, i.e., Sponges of The New Caledonian Lagoon (Levi et al. 1998), *Jenis-Jenis Karang di Indonesia* (Suharsono 2008), and Coral Finder (Kelley 2012).

Methods

Qualitative data were obtained by inspecting morphological characteristics of each fossil coral and sponge samples with the references. Morphological characteristics data of corals obtained from present-day specimens, as well as

studying existing literature and compare original description of each genus using references from the World Register of Marine Species (WORMS) (Levi et al. 1998; Suharsono 2008; Kelley 2012). Present-day specimen used was from class Hexacorallia. The identified parts of corals include shape, surface pore distribution, surface ornamentation, texture, structure, system of waterways, size, and geometry of the inorganic skeleton. Meanwhile morphological characteristics data of sponges obtained from present-day specimens' member of the class Demospongiae. The identified parts of sponges include the colony shape, the present of osculum and ostium, and canal system structure.

RESULTS AND DISCUSSION

Summary of fossil specimens evaluated

There was a total of 15 fossil corals and sponges' specimens were identified from two sites (LBP and SEMS). Identified coral fossil consist of 8 genera, 5 families, 2 orders and 2 classes meanwhile there is only one genus of identified sponge fossil (Table 1). Both corals and sponges' fossil have a skeletal structure of limestone ($CaCO_3$) therefore well preserved.

Systematic Descriptions

Phylum Cnidaria Hatschek, 1888
Subphylum Anthozoa Ehrenberg, 1834
Class Hexacorallia Haeckel, 1896
Order Scleractinia Bourne, 1900
Family Agariciidae Gray, 1847
Pachyseris sp. Milne Edwards & Haime, 1849
Material examined: A corallum (Figure 1) collection of the Sangiran Early Man Site.
Diagnostic characters: The intact foliose colonies have sunken corallites with interconnected columella. The corallites are on one side and are immersed in indistinctly undulating walls. Septa are not visible due to erosion (Figure 1, A.2).

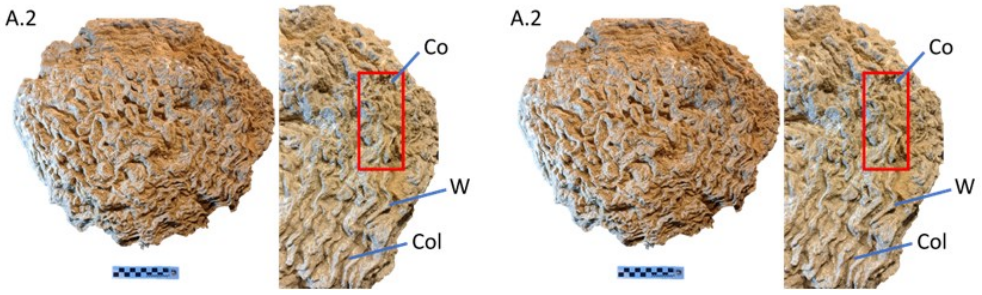

Figure 1. Fossil (A.2) corallum of *Pachyseris* sp., compared with recent specimen from Terraneo et al. (2014). Co = Corallite, Col = Columella, W = Wall.

Table 1. Classification of identified coral and sponge fossil studied.

Phylum	Subphylum	Class	Order	Family	Genus
Cnidaria	Anthozoa	Hexacorallia	Scleractinia	Agariciidae	Pachyseris
				Poritidae	Porites
				Cladocoridae	Cladocora
				Merulinidae	Favites
					Platygyra
				Oculinidae	Petrophyllia
					Oculina
Cnidaria	Anthozoa	Octocorallia	Malacalcyonacea	Tubiporidae	Tubipora
Porifera	–	Demospongiae	Indeterminate	Indeterminate	Indeterminate

Family Poritidae Gray, 1840
Porites sp. Link, 1807
Material examined: A corallum (Figure 2) collection of the LBP UGM, the fossil was found from Sangiran area (Sangiran's finding).
Diagnostic characters: The colonies are massive and the corallites are cerioid, less than 2mm in diameter, making the septa small. The surface appears smooth and hummocky (Figure 2).

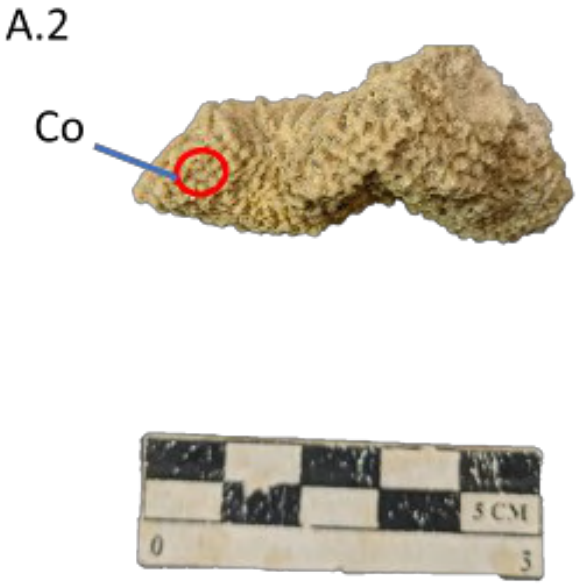

Figure 2. Fossil (A.2) corallum of *Porites* sp., compared with recent specimen from Samiei et al (2013). Co = Corallite

Family Cladocoridae Milne Edwards & Haime, 1857
Cladocora sp. Ehrenberg, 1834
Material examined: A corallum (Figure 3) collection of the Sangiran Early Man Site.
Diagnostic characters: The colonies are corymbose and form tight clumps. The corallites are tube-like and phaceloid in shape, with spacing between them. The septa and columella develop with the conesteum forming fine streaks. (Figure 3, A.2).

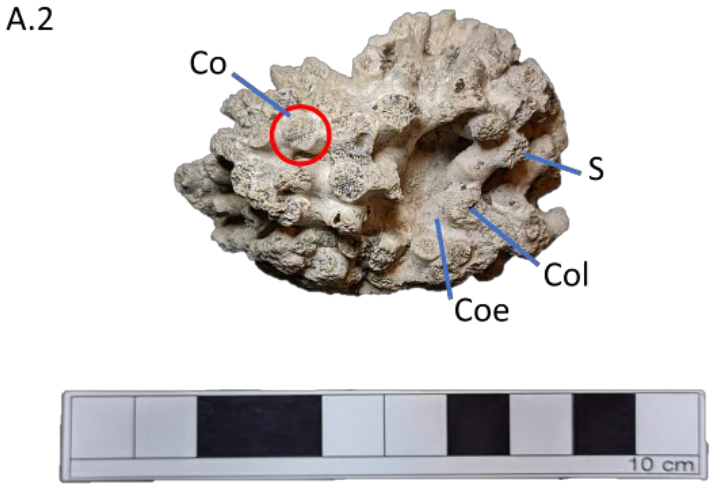

Figure 3. Fossil (A.2) corallum of *Cladocora* sp., compared with recent specimen from Hoeksema and Vicente (2014). Co = Corallite, Col= Columella, Coe = Conesteum , S= Septa.

Family Merulinidae Verrill, 1865
Favites sp. Link, 1807
Material examined: 4 specimens of corallum (Figure 4) collection of the Sangiran Early Man Site.
Diagnostic characters: Colonies are massive, cerioid corallites with smooth septa (Figure 4, B-D). Due to fossilisation, the septa appear to be lost (Figure 4, E) and there are no prominent paliform lobes.

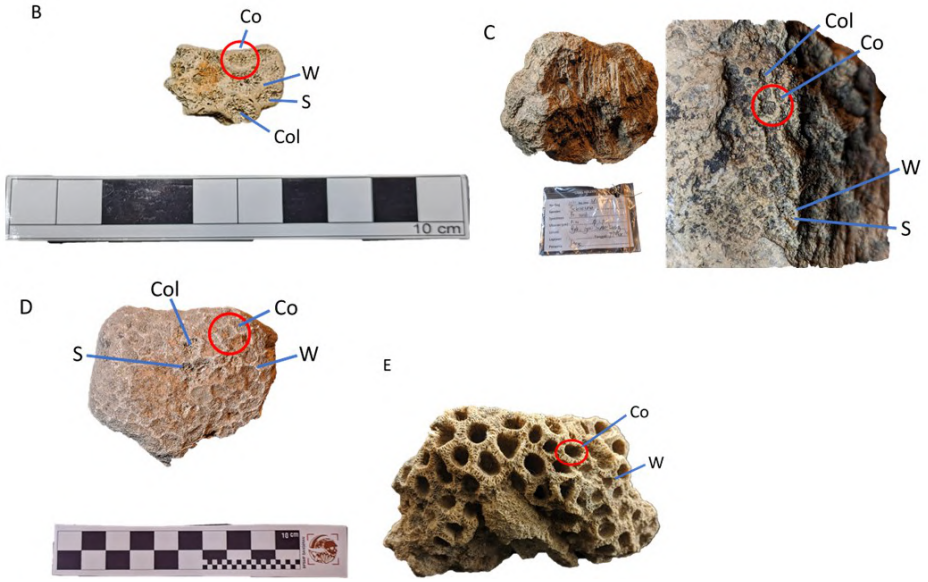

Figure 4. Fossils (B-E) corallum of *Favites* sp., compared with recent specimen from Khalil et al (2021). Co = Corallite, Col= Columella, W= Wall, S= Septa.

Platygyra sp. Ehrenberg, 1834
Material examined: 3 specimens of corallum (Figure 5) collection of the Sangiran Early Man Site.
Diagnostic characters: The colonies are massive and consist of corallites of the meandroid (Figure 5, B-C) and subcerioid to submeandroid (Figure 5, D). The columella appears to be interconnected and the septa are thinly developed with the absence of paliform lobes.

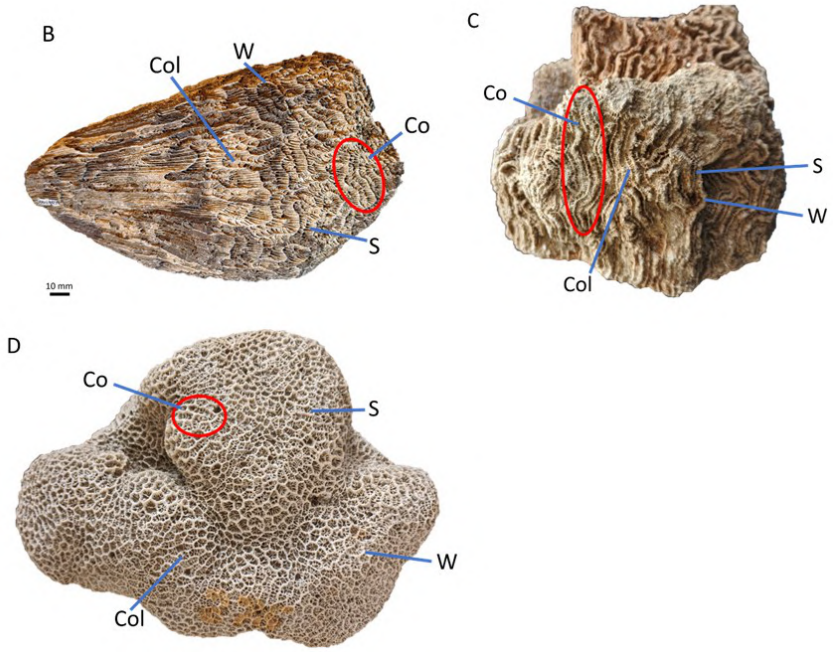

Figure 5. Fossils (B-D) corallum of *Platygyra* sp., compared with recent specimen from Khalil et al (2021). Co = Corallite, Col= Columella, W= Wall, S= Septa.

Family Oculinidae Gray, 1847
Petrophyllia Conrad, 1855
Material examined: A corallum (Figure 6) collection of the Sangiran Early Man Site.
Diagnostic characters: The colonies have a ramose growth form with plocoid-type corallites and irregular branching. The septa and columella develop with a smooth conesteum, particularly when maturing. This coral has both radial corallites and axial corallites (Figure 6).

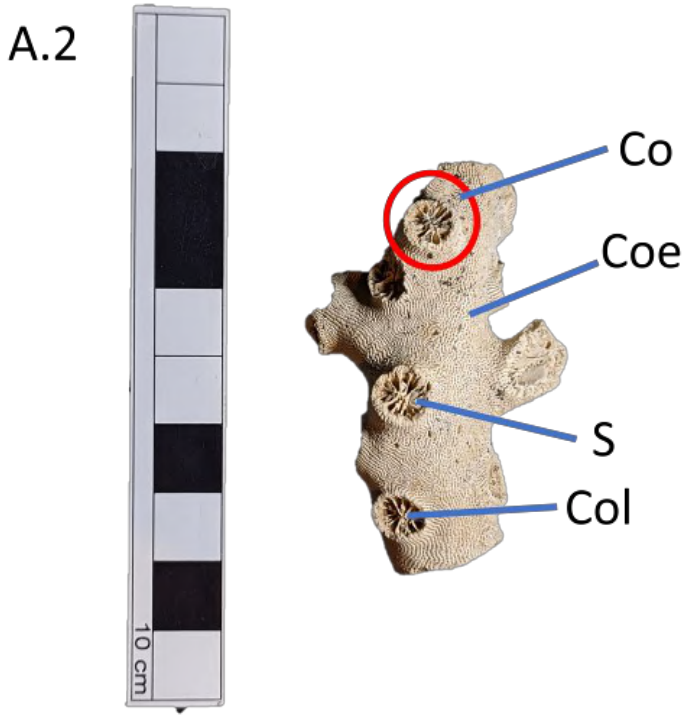

Figure 6. Fossil (A.2) corallum of *Petrophyllia* sp., compared with recent specimen from Cairns and Kitahara (2012). Co = Corallite, Col= Columella, Coe = Conesteum, S= Septa.

Oculina sp. Lamark, 1816
Material examined: A corallum (Figure 7) collection of the Sangiran Early Man Site.
Diagnostic characters: The coral consists of branching colonies of radial corallites with a distance between each corallite. The corallites sink with fine septa and the surface of the conesteum is textured with fine strokes. this coral has only radial corallites (Figure 7).

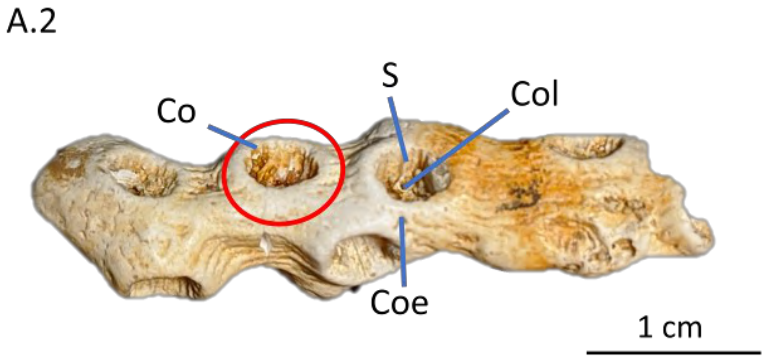

Figure 7. Fossil (A.2) corallum of *Oculina* sp. compared with recent specimen from Hoeksema and Vicente (2014). Co = Corallite, Col= Columella, Coe = Conesteum, S= Septa.

Phylum Cnidaria Hatschek, 1888
Subphylum Anthozoa Ehrenberg, 1834
Class Octocorallia Haeckel, 1866
Order Malacalcyonacea McFadden, van Ofwegen & Quattrini, 2022
Family Tubiporidae Ehrenberg, 1828
Tubipora sp. Linnaeus, 1758
Material examined: 3 specimens of corallum (Figure 8) collection of the LBP UGM, the fossil was found from Sangiran area (Sangiran's finding).
Diagnostic characters: The colonies consist of tubular, towering pipes with phaceloid-type corallites. The walls of the corallites have a porous structure (Figure 8, B-C).

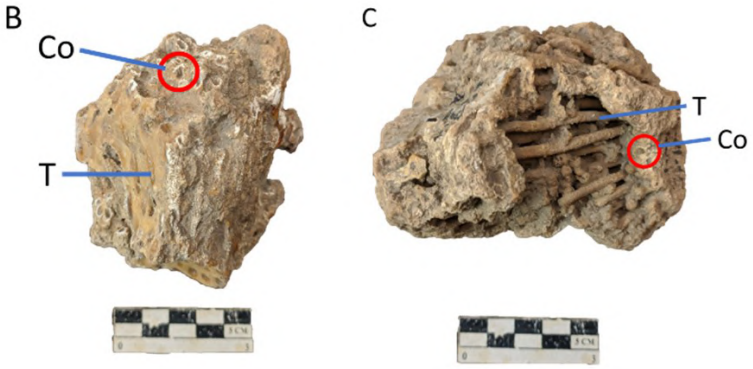

Figure 8. Fossils (B-C) corallum of *Tubipora* sp. compared with description from Richards (2018). Co = Corallite, T= Tabulae.

There was one fragment fossil which was a little bit difficult to identify (Figure 9). First, we identified as *Callyspongia* Duchassaing & Michelotti, 1864 but then, there is a suggestion that the fossil can also be *Clathria basilana* Lévi, 1961. Those two genus were possible due to the similarity of their morphological characters. To identify present-day sponges is by molecular analysis or analyze its spicules or skeleton, therefore we only determine this sponge fossil until class rank which is Class Demospongiae.

Class Demospongiae Sollas, 1885
Material examined: A fragment (Figure 9) collection of the Sangiran Early Man Site.
Diagnostic characters: The upper part features a water outlet (Osc) and the outer side serves as a porous water inlet (Os). The sponge of the tube group has a broad spongocoel with an asconoid water flow type (Figure 9).

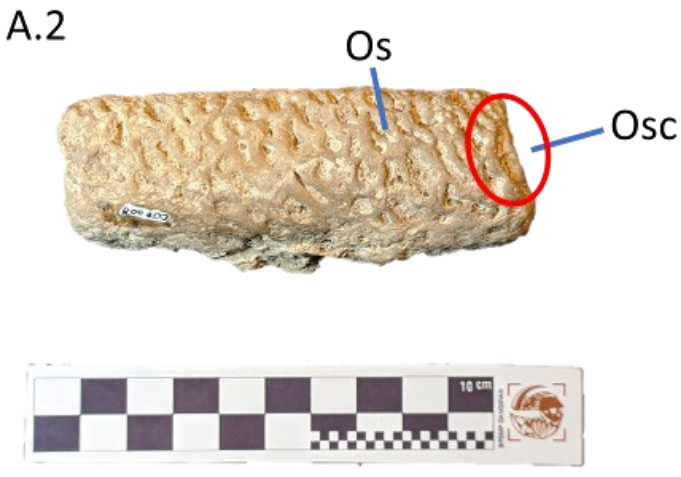

Figure 9. Fossils (A.2) fragment fossil of Demospongiae. Osc= Osculum, Os = Ostia.

Paleo-Environmental Implications

The discovery of coral and sponge fossils in the Kalibeng Formation of the Sangiran Dome provides information about marine condition in the past. Kalibeng Formation of the Sangiran Dome is the oldest layer, found in the center, and aged about 2 million years based on the study of magnetic polarity in the Sangiran area (Sémah et al. 2000).

Understanding the paleoecology of an area based on coral and sponge fossil is based on comparison with recent species or genus, therefore correct determination of coral and sponge's species or genus is a crucial. The ecological niche of these fossil species or genus then compare to the same species or genus which can still be found in the present time (Holocene Period).

Presence of these eight-coral genus and sponge fossils indicates a marine environment, with warm and clear water. A clear environment is required to prevent the callus from being infiltrated and covered by fine-grained sediments. Cnidarians requires sunlight during its life. Presence of cnidarians fossil indicates that in Sangiran during the Lower Pleistocene was shallow marine environment which far from river mouth (delta). These cnidarian fossils can only live in normal marine conditions; therefore, presence of cnidarians fossil also indicate normal salinity. Most corals and sponges tend to live and develop on hard, non-muddy seabed; therefore, these fossils can also be a substrate indicator. Seawater circulation is very important for coral reefs to receive nutrients (Sukandarrumidi 2021).

A total of eight fossil coral genera and one sponge genus were identified from the Kalibeng Formation. The fossil corals and sponge genus identified indicate that the Kalibeng Formation was a shallow marine environment. The upper Kalibeng layer consists of bluish-grey clays and mudstones and also contains marine mollusks (*Arca*, *Chione*, *Nassarius*, *Turritella*), foraminifers, and diatoms deposited during the Early Pleistocene transitions. These mollusks habitats characterize the coastal marine habitats (Faylona 2019).

CONCLUSIONS

There were eight genera of identified coral fossils and one fragment of sponge fossil which indeterminate. The eight genera of coral fossil were *Pachyeseris*, *Porites*, *Cladocora*, *Favites*, *Platygyra*, *Petrophyllia*, *Oculina*, and *Tubipora*. The indeterminate genus of sponge fossil was classified as Class Demospongiae. Palaeoecological reconstruction of the Kalibeng Formation in Sangiran Dome based on the coral and sponges' fossils indicated a shallow marine environment of the neritic zone based on habitat comparisons with present-day similar genus of corals and sponges.

AUTHOR CONTRIBUTION

F.A.A. collected, analysed the data, and wrote the manuscript. D.S.Y. validated data, reviewed, and wrote manuscript. All authors have read and approved the manuscript for publication.

ACKNOWLEDGMENTS

We thank the Laboratory of Bioanthropology and Paleoanthropology, Faculty of Medicine, Public Health and Nursing UGM and Sangiran Early Man Site for the access, permission, and support during research.

CONFLICT OF INTEREST

There are no competing interests.

REFERENCES

Brasseur, B. et al., 2015. Pedo-sedimentary dynamics of the Sangiran dome hominid bearing layers (Early to Middle Pleistocene, central Java, Indonesia): A palaeopedological approach for reconstructing 'Pithecanthropus' (Javanese Homo erectus) palaeoenvironment. *Quaternary International*, 376(1), pp.84-100. doi: 10.1016/j.quaint.2014.05.030.

Cairns, S.D. & Kitahara, M.V., 2012. An illustrated key to the genera and subgenera of the Recent azooxanthellate Scleractinia (Cnidaria, Anthozoa), with an attached glossary. *ZooKeys*, 227, 1–47. doi: 10.3897/zookeys.227.3612

Faylona, M.G.P.G., 2019. The early Pleistocene aquatic palaeoecology and palaeoclimate in Central Java, Indonesia as recorded in mollusc assemblages from the Kalibeng and Pucangan layers of Sangiran Dome. *Palaeontographica Abteilung A*, Band 322, Lieferung 5-6, pp.125-152. doi: 10.1127/pala/2022/0123.

Hoeksema, B.W. & Vicente, O.O., 2014. First record of the Central Indo-Pacific reef coral *Oulastrea crispata* in the Mediterranean Sea. *Mediterranean Marine Science*, 15(2), pp.429-436. doi: 10.12681/mms.751.

Khalil, H.M., Fathy, M.S. & Al Sawy, S.M., 2021. Quaternary corals (Scleractinia: Merulinidae) from the Egyptian and Saudi Arabian Red Sea Coast. *Geological Journal*, 56(8), pp.4150-4188. doi: 10.1002/gj.4145.

Kelley, R., 2012. *Coral finder 3.0: Indo Pacific*. The Australian Coral Reef Society: ByoGuides.

Levi, C. et al., 1998. *Spons Of The New Caledonian Lagoon*. Institut FrancAis De Recherche Scientifique Pour Le Developpement En Cooperation: Editions de l'Orstom.

Morandini, A.C. Custódio, M.R. & Marques, A.C., 2016. Phylum Porifera and Cnidaria. In *Marine and freshwater toxins*. Dordrecht : Springer. doi: 10.1007/978-94-007-6650-1_6-1

Richards, Z., 2018. *The Coral Compactus: Western Australia Hard Coral Genus Identification Guide Version 2*. Western Australian Museum

Samiei, J.V. et al., 2013. Some scleractinian corals (Scleractinia: Anthozoa) of Larak Island, Persian Gulf. *Zootaxa*, 3636(1), pp.101-143. doi: 10.11646/zootaxa.3636.1.5.

Sémah, F. et al., 2000. Did Early Man reach Java during the Late Pliocene? *Journal of Archaeological Science*, 27, pp.763–769.

Suharsono, S., 2008. *Jenis-Jenis Karang di Indonesia*, Jakarta: LIPI Press.

Sukandarrumidi, 2021. *Paleontologi Aplikasi Penuntun Praktis untuk Geologist Muda*, Yogyakarta: Gadjah Mada University Press.

Terraneo, T.I. et al., 2014. *Pachyseris inattesa* sp. n.(Cnidaria, Anthozoa, Scleractinia): a new reef coral species from the Red Sea and its phylogenetic relationships. *ZooKeys*, (433), pp.1-30. doi: 10.3897/zookeys.433.8036

Yudha, D.S. et al., 2013. Keanekaragaman fosil anggota ordo Foraminifera pada Formasi Pucangan di Desa Bukuran dan Krikilan, Kecamatan Kalijambe, Area Situs Manusia Purba Sangiran. *Berkala Ilmiah Biologi*, 12(2), pp.26–33.

Journal of Tropical Biodiversity and Biotechnology
Volume 10, Issue 04 (2025): jtbb14024
DOI: 10.22146/jtbb.14024

Research Article

Short Test Performance of Nitrogen Removal by Anammox Bacteria from Lake Koto Baru, Indonesia, Using Pumice as a Carrier

Zulkarnaini Zulkarnaini[1]*, Reri Afrianita[1], Mahdiah Zulfa[1]
1)Department of Environmental Engineering, Faculty of Engineering, Universitas Andalas, Padang, Indonesia, 25163
* Corresponding author, email: zulkarnaini@eng.unand.ac.id

Keywords:
Anammox
Lake Koto Baru
Pumice
Tropical ambient temperature
Submitted:
23 June 2024
Accepted:
16 June 2025
Published:
01 December 2025
Editors:
Miftahul Ilmi
Annisaa Widyasari

ABSTRACT

Anaerobic ammonium oxidation (anammox) removes ammonium under anaerobic conditions into nitrogen gas using nitrite as an electron acceptor by anammox bacteria belonging to the phylum *Planctomycetota*. The performance of nitrogen removal depends on the species and operating conditions. The purpose of this study was to compare the performance of anammox bacteria from Lake Koto Baru, Indonesia, in nitrogen removal with *Candidatus Brocadia sinica* at tropical ambient temperature using pumice as a carrier. This experiment utilized two up-flow anaerobic sludge blanket reactors with artificial wastewater containing ammonium and nitrite concentrations of 100 mg-N L^{-1} and a hydraulic retention time of 12 hours for 31 days. Run 1 inoculated with *Candidatus Brocadia sinica*; Run 2 used enriched anammox bacteria from Lake Koto Baru, Indonesia. The concentrations of ammonium, nitrite, and nitrate were analyzed twice a week using Nessler's method, spectrophotometry, and screening UV spectrophotometry, respectively. The best nitrogen removal performance occurs in Run 2 using anammox bacteria from Lake Koto Baru, where the maximum nitrogen removal rate, ammonium conversion efficiency, and nitrogen removal efficiency were 0.395 kg-N m^{-3} d^{-1}, 98.12 %, and 92.6 % of 0.341 kg-N m^{-3} d^{-1}, 87 %, 79.8 % of Run 1. These results suggest that anammox bacteria from Lake Koto Baru are highly effective for nitrogen removal in tropical climates and are applicable for wastewater treatment systems in similar regions.

How to cite:
Zulkarnaini, Z., Afrianita, R. & Zulfa, M., 2025. Short Test Performance of Nitrogen Removal by Anammox Bacteria from Lake Koto Baru, Indonesia, Using Pumice as a Carrier. *Journal of Tropical Biodiversity and Biotechnology*, 10 (4), jtbb14204. doi: 10.22146/jtbb.14024

INTRODUCTION

Anaerobic ammonium oxidation (anammox) (Mulder et al. 1995) oxidizes ammonium into nitrogen gas using nitrite as an electron acceptor under anaerobic conditions by anammox bacteria, as in Equation 1 (Van De Graaf et al. 1996). The anammox process is a more sustainable technology in biological nitrogen removal than the nitrification-denitrification process, due to its high ammonium removal rate, lower oxygen demand, and reduced space requirements in full-scale applications. The anammox process has been successfully applied on a laboratory scale, pilot scale, and large scale to treat ammonium-rich wastewater.

$$NH_4^+ + 1{,}146NO_2^- + 0{,}071HCO_3^- + 0{,}057H^+ \text{ à } 0{,}071CH_2O_{0,5}N_{0,15} + 0{,}986N_2 + 0{,}161NO_3^- + 2{,}002H_2O \quad (1)$$

Anammox biomass has three forms to remove the nitrogen in the reactor. They are granular (Ali et al. 2014a), suspended sludge (Lotti et al. 2014b), and biofilm (Oshiki et al. 2013), with the carrier serving as supporting media. Anammox bacterial granules provide excellent biomass retention, adaptability, and a high capacity to withstand shock loading (Lin et al. 2013). However, this form has a problem with the floating biomass due to nitrogen gas production. A carrier can overcome this flotation of biomass to retain anammox bacteria (Kumar et al. 2017). The carriers derived from natural sources include bamboo charcoal (Chen et al. 2012), palm fiber (Zulkarnaini et al. 2019), and sugarcane bagasse (Zulkarnaini et al. 2021). An inert carrier, such as sand (Strous et al. 1997) and zeolite (Feng et al. 2019), has been widely used as a supporting material for anammox growth. Zulkarnaini and Silvia (2021) reported the growth of anammox bacteria in the pores of the ceramic carrier in a two-inflow anammox biofilm reactor. Another potential carrier that comes from nature is pumice, which contains pores.

Indonesia is situated on the volcanic plate of the Eurasia-Australia-Pacific (Ring of Fire), which makes it possess abundant mineral deposits of non-metallic minerals. Pumice is a natural mineral from volcanoes formed due to volcanic gases and rapid cooling materials. The pumice structure comprises cavities formed by air bubbles trapped in lava during the freezing process (Ridha & Darminto 2016). The Pasak River, located in West Sumatra, Indonesia, is one of the sites where pumice was discovered. It is the residue of sand mining carried out by the local community, with around 1–5 kilograms collected daily and accumulated along the riverbanks. The hollow pumice structure has been used as an adsorbent. Pumice can remove nitrogen as an absorbent in the form of nitrate (Indah et al. 2021) and ammonium (Pratiwi et al. 2019) with an efficiency of up to 40-78%. Based on pumice's potential due to its porous structure, it is readily available in nature and can effectively remove nitrogen. Therefore, this study used pumice as a carrier for anammox bacteria to enhance nitrogen removal.

For the first time in Indonesia, anammox bacteria were successfully cultivated from Lake Koto Baru, Indonesia, using a filter bioreactor (FtBR) operated at tropical ambient temperatures of 35 °C (Zulkarnaini 2024). The results show that the nitrogen removal performance is better and more stable at tropical ambient temperatures than at 35 °C. At a tropical ambient temperature, the microbial community revealed *Candidatus Brocadia fulgida* as the predominant species, with a relative abundance of 20.05% (Zulkarnaini et al. 2025). This report demonstrates that anammox bacteria originating from the native environment outperform those from outside sources. Zulkarnaini et al. (2020) reported a decrease in the performance of the anammox bacteria species *Candidatus Brocadia sinica*, characterized by a change in biomass color from red carmine to reddish-brown when the operation was carried out at

tropical ambient temperatures.

Numerous studies have shown that the anammox process operates optimally at warmer temperatures, with 35°C often cited as the ideal condition for achieving maximum nitrogen removal efficiency (Oshiki et al. 2011). However, this presents a significant challenge for wastewater treatment applications, particularly in subtropical and temperate regions, as maintaining such elevated temperatures requires substantial energy input, reducing overall efficiency. In contrast, Lotti et al. (2014a) have demonstrated improved anammox performance at lower temperatures, highlighting the influence of species-specific adaptations. Different anammox bacterial species exhibit varying temperature ranges for optimal nitrogen removal, suggesting that temperature resilience and adaptability are crucial for enhancing the applicability of the anammox process in diverse climatic conditions (Le et al. 2022).

The purpose of this study was to compare the nitrogen removal performance of anammox bacteria originating from Lake Koto Baru, Indonesia, with that of *Candidatus Brocadia sinica*, an anammox bacterium from outside the Indonesian environment, using pumice as a carrier.

MATERIALS AND METHODS

Reactor Configuration

This research utilized two 300 mL acrylic up-flow column reactors that operated continuously, filling 20 mL of inoculum and 20 g of pumice. Pumice was filled into reactors to retain anammox biomass from washout as a carrier during the reactor operation. Run 1 was inoculated with *Candidatus Brocadia sinica*. In contrast, Run 2 used anammox biomass enriched from Lake Koto Baru, Indonesia, containing *Candidatus Brocadia fulgida* (20.04%) and *Candidatus Brocadia caroliniensis* (6.20%) in a FtBR (Zulkarnaini et al. 2025).

The substrate was continuously delivered from the tank to the reactor via a peristaltic pump. The tank was connected to a nitrogen-filled gas bag to maintain anaerobic conditions and stabilize atmospheric pressure.

The schematic of the reactor configuration in this study was shown in Figure 1. The reactors were equipped with filters in the bottom and top parts to prevent biomass washout and were covered with aluminum foil to prevent the growth of phototrophic bacteria. The research was conducted for 31 days, with hydraulic retention time (HRT) of 12 hours. Influent and effluent water samples were collected and analyzed twice a week. Ammonium, nitrite, and nitrate concentrations were analyzed using Nessler's method, spectrophotometry, and screening ultraviolet spectrophotometry, respectively. The reactor was operated at ambient temperature in the laboratory without pH adjustment.

Preparation of pumice

Pumice forms through the expansion of magmatic gases during effusion, giving it a spongy, glassy texture and high internal porosity. Pumice samples from the Pasak River (West Sumatra, Indonesia) were collected for this study. Prior to the experiment, the pumice was repeatedly rinsed with distilled water and air-dried at room temperature. It was then crushed using a basic hammer-type crusher and sieved to a particle size of 8–30 mesh (0.6–2.4 mm) to obtain a uniform material. No acid or base treatment was applied before use.

Seeding Sludge

Inoculum for Run 1 originated from the up-flow column reactor that cultivated *Candidatus Brocadia sinica* at tropical ambient temperature for 1.5 years. The colour of the biomass changed from red carmine to reddish-brown due to temperature operation at a level lower than optimum, 37 °C (Oshiki et al. 2013). Run 2 was inoculated with enriched anammox bacteria from Lake Koto

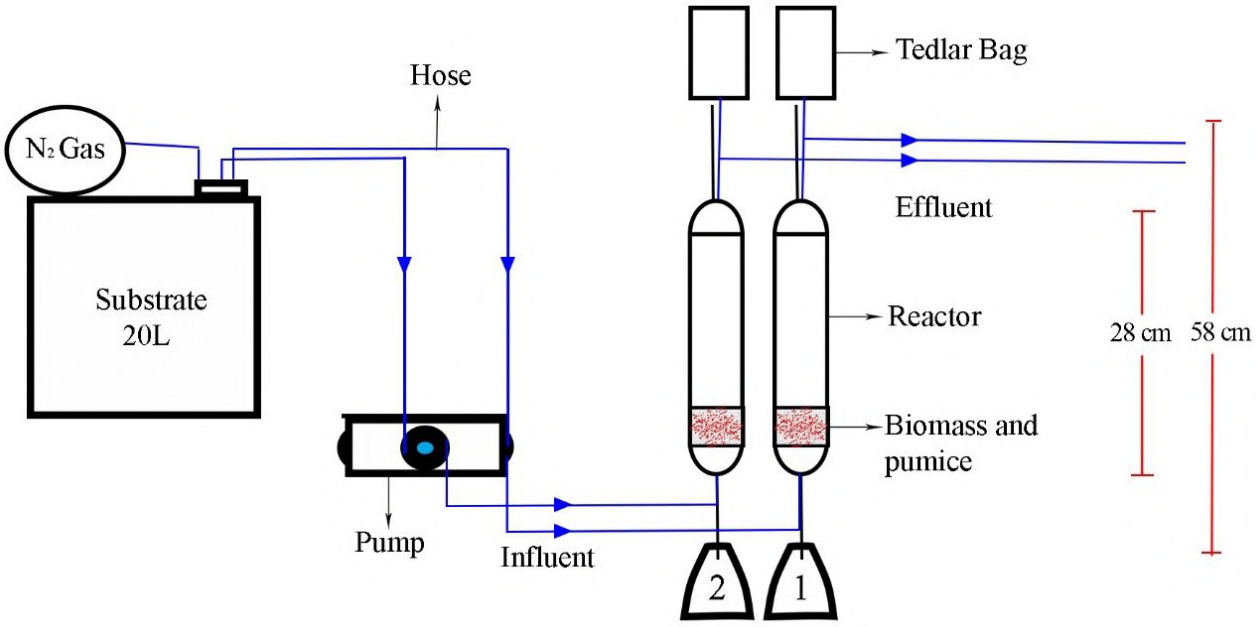

Figure 1. Experimental reactor configuration. Both reactors were filled with pumice; Run 1 was inoculated with *Candidatus Brocadia sinica*, and Run 2 was inoculated with anammox bacteria from Lake Koto Baru.

Baru, Indonesia, using FtBR and had already operated at tropical ambient temperature for one and a half years (Putra et al. 2020). For the reactor's start -up, 20 mL of anammox biomass and pumice were added to each reactor.

Composition of Artificial Wastewater

The artificial wastewater, prepared per liter of groundwater, contained 500 mg $KHCO_3$, 27.2 mg KH_2PO_4, 300 mg $MgSO_4 \cdot 7H_2O$, 180 mg $CaCl_2 \cdot 7H_2O$, 1 mL each of trace element solutions I and II, and 100 mg L^{-1} nitrogen supplied from both $NaNO_2$ and $(NH_4)_2SO_4$ (Zulkarnaini et al. 2024).

Calculation of Nitrogen Removal Performance

The nitrogen removal performance of the anammox process was evaluated following the nitrogen balance method described by Zulkarnaini et al. (2019). They were the nitrogen removal rate (NRR, kg-N m^{-3} d^{-1}), nitrogen removal efficiency (NRE, %), and ammonium conversion efficiency (ACE, %).

RESULTS

Stoichiometry of the anammox process

The anammox process was evaluated using the stoichiometric reaction shown in Equation (1). The nitrite-to-ammonium removal ratio (ΔNO_2^--N/ΔNH_4^+-N) and the nitrate-to-ammonium consumption ratio (ΔNO_3^--N/ΔNH_4^+-N) were determined based on the quantities of ammonium oxidized, nitrite removed, and nitrate produced, respectively.

The average ratio of the ΔNO_2^--N/ΔNH_4^+-N obtained at a stable Run 1 and Run 2 was 1.53 and 1.09, respectively. Run 2 was near the stoichiometry of the anammox process of 1.146, where the anammox process was predominant from the beginning of reactor operation. Higher nitrite oxidation occurred in Run 1. It could be the activity of the denitrification process, where part of the nitrite and nitrate is converted to nitrogen gas under anaerobic conditions in the presence of organic carbon. In various anammox reactors, the NO_2^--N/NH_4^+-N removal ratio typically ranges from 0.5 to 4, depending on reactor configuration, operating conditions, and substrate concentration (Ahn 2006). The comparison of the ΔNO_2^--N/ΔNH_4^+-N ratio from the experiment is shown in Figure 2.

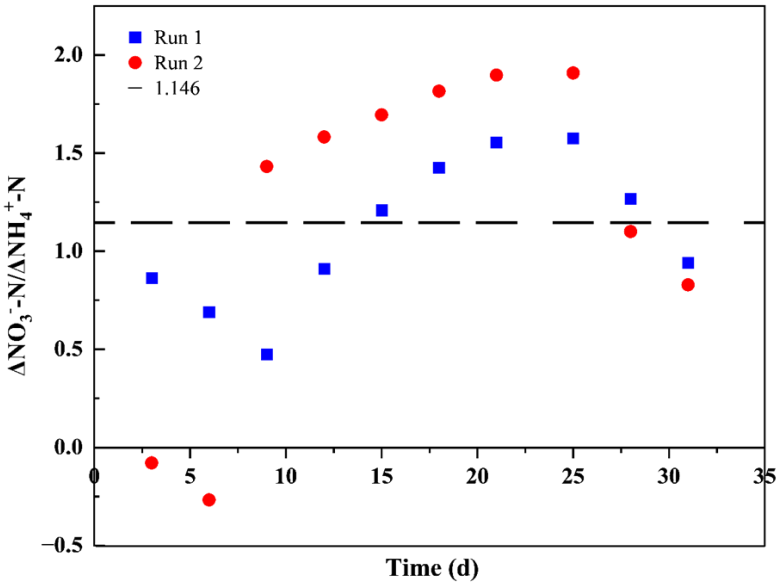

Figure 2. Stoichiometry ratio of ΔNO_3^--N/ΔNH_4^+-N compared with anammox stoichiometry of 1.146 (Lotti et al. 2014b).

Anammox process produces a small amount of NO_3^- instead of N_2. 1 mole of NH_4^+ produces 0.161 NO_3^-. The average ΔNO_3^--N/ΔNH_4^+-N ratio values obtained in this study were 0.05 for Run 1 and -0.14 for Run 2. Both ratios were lower than the anammox stoichiometry. Figure 3 shows the ratio of ΔNO_3^--N/ΔNH_4^+-N during the study. Lower nitrate concentrations can indicate that nitrate was removed due to other processes, such as denitrification. Produced nitrate could be adsorbed by pumice and retained in the reactor; then, denitrification takes place in the pumice.

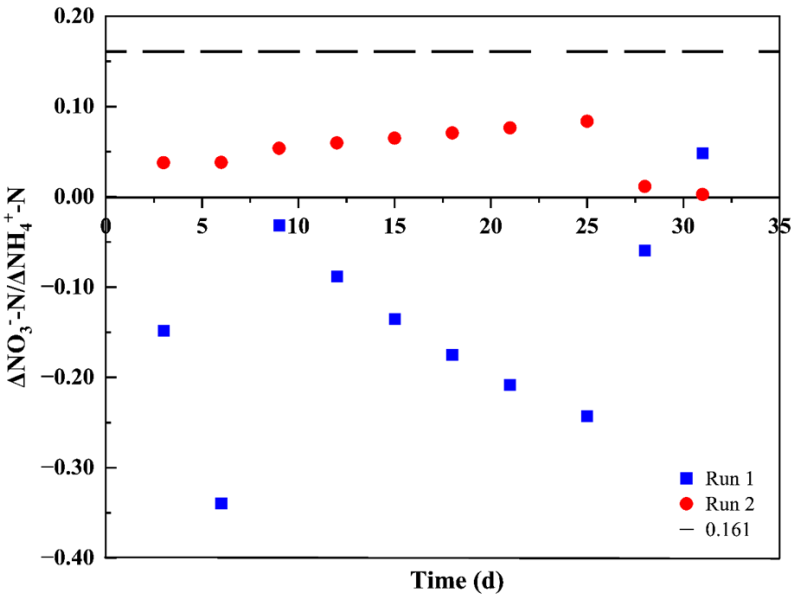

Figure 3. Stoichiometry ratio of ΔNO_3^--N/ΔNH_4^+-N compared with anammox stoichiometry of 0.161 (Lotti et al. 2014b).

Performance of Reactors

The performance of the anammox process in the up-flow column reactor was shown in Figures 4–5. Both reactors were supplied with ammonium and nitrite at concentrations of 100 mg-N L^{-1} each, with a hydraulic retention time (HRT) of 12 hours. Based on ammonium removal efficiency, the start-up process was classified into four stages: the cell lysis phase (effluent ammonium concentration exceeding the influent), the lag phase (gradual decrease in efflu-

ent ammonium), the transition phase (moderate rise in NRR), and the activity elevation phase (rapid increase in NRR). (Chen et al. 2016; Lulrahman et al. 2022). During the cell lysis phase, inhibition causes decay of anammox biomass, resulting in elevated ammonium levels in the effluent. As microorganisms adapt to the new environment, ammonium concentrations gradually decline, followed by a further reduction driven by the enhanced bioactivity of the anammox microorganisms.

Performance of Run 1

Cell lysis phase (days 1–8). As shown in Figure 4(a), the effluent ammonium concentration exceeded the influent, resulting in a negative ammonium removal efficiency. This increase in ammonium was likely due to the lysis of dead anammox biomass. The decay of previously dormant bacteria, leading to cell lysis and the conversion of organic nitrogen to ammonium, may have been triggered by changes in substrate concentration during the experiment as well as conditions from the preceding cultivation process.

At the beginning of operation Run 1, in which *Candidatus Brocadia sinica* was the inoculum and pumice as the carrier, there was no ammonium removal in Run 1. On the contrary, the ammonium concentration in the effluent was higher than in the influent. This increase was nearly double the concentration in the influent.

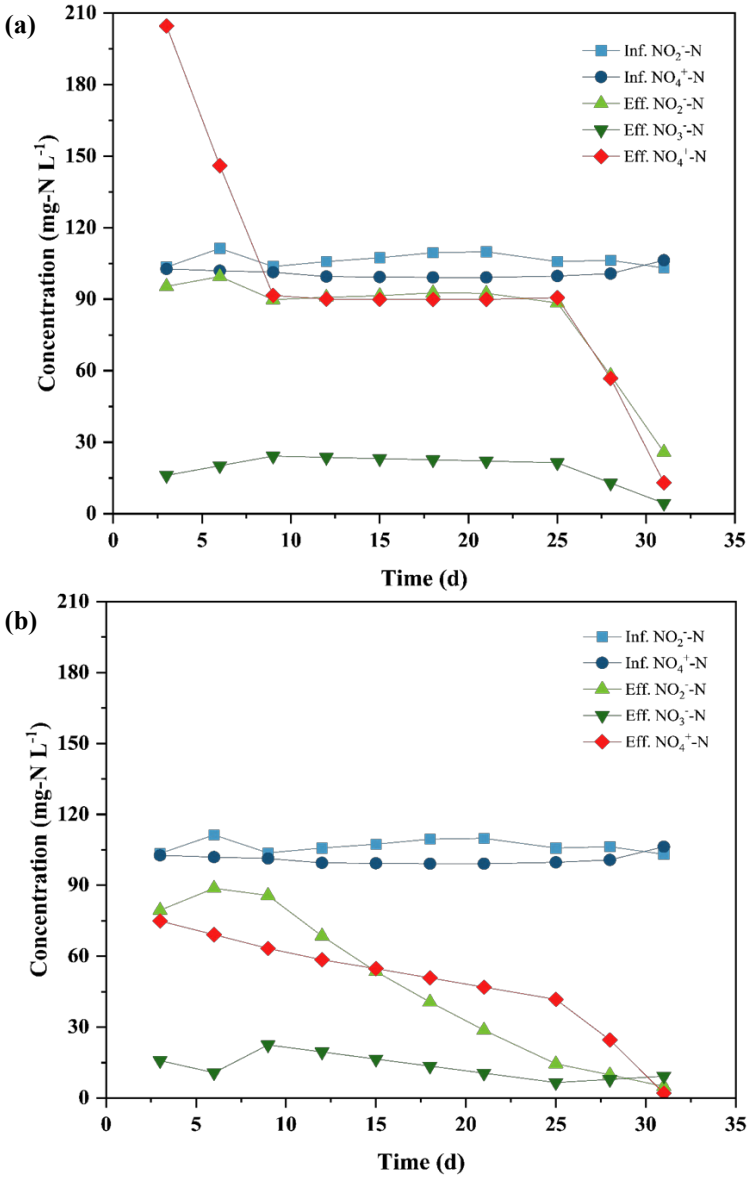

Figure 4. Nitrogen profile of influent and effluent in (a) Run 1 and (b) Run 2.

Anammox activity occurred during the lag phase (days 9-25), where ammonia and nitrite were removed simultaneously, and nitrate was produced. Anammox bacteria adapt to environmental changes over a period of up to 25 days of reactor operation. During the adaptation process, the anammox bacteria undergo a duplication process, with a doubling time of seven days for *Candidatus Brocadia sinica*. Anammox bacteria, classified as slow-growing bacteria, require a considerable amount of time to recover after complete inhibition.

At the activity elevation phase (days 26–31), the anammox process recovered, with a rapid nitrogen removal rate, where both ammonium and nitrite concentrations in the effluent decreased rapidly from 90.60 to 13.00 mg-N L^{-1} and from 88.4 to 25.76 mg-N L^{-1}, respectively. This decrease in ammonium and nitrite concentration indicates the high activity of anammox bacteria. In the anammox process, nitrite functions as an electron acceptor in the conversion of ammonium to nitrogen gas. Figure 4(a) shows the change in nitrogen concentration in Run 1 during the study.

Reactor performance or capability is obtained from changes in nitrogen concentration during the study (Figure 5). Reactor performance was evaluated based on nitrogen loading rate (NLR), NRR, ACE, and NRE. The reactor was fed with NLR 0.40 kg-N m^{-3} d^{-1} during the entire reactor operation. The NRR in the reactor increases gradually from -0.180 kg-N m^{-3} d^{-1} to 0.341 kg-N m^{-3} d^{-1}. The negative NRR at start-up was due to the production of ammonium from the dead biomass. At the end of reactor operation, NRR achieved 0.341 kg-N m^{-3} d^{-1}.

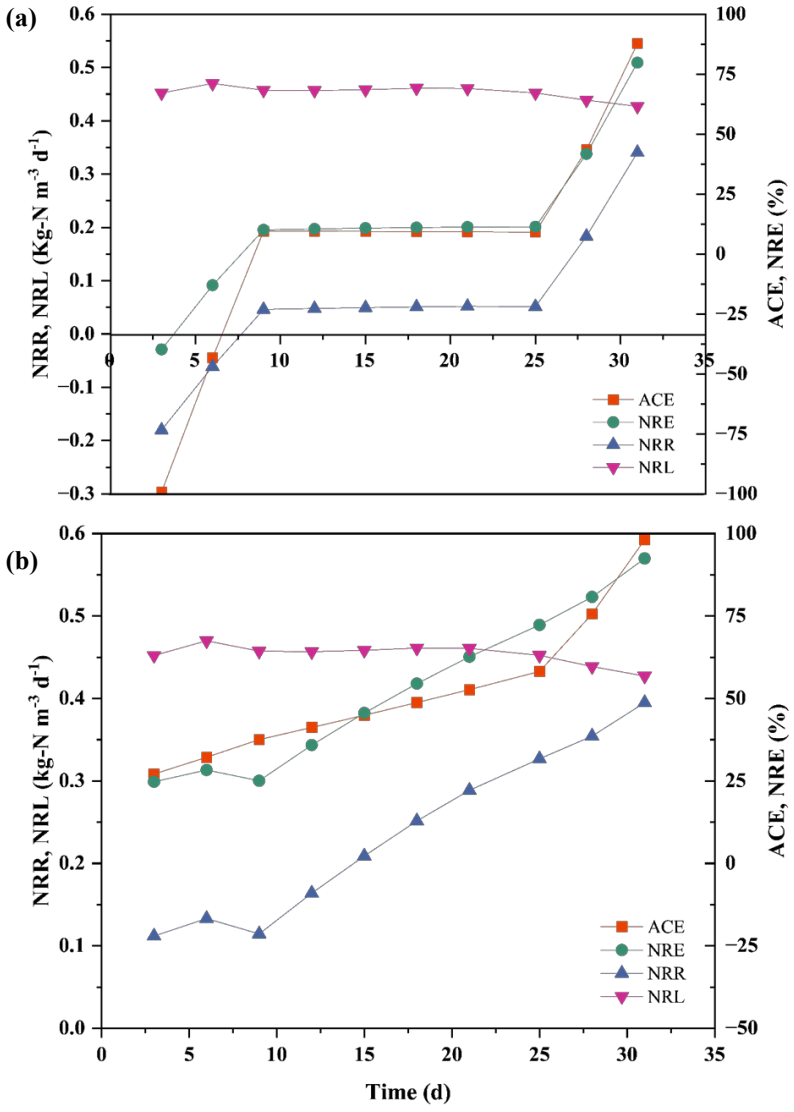

Figure 5. Performance of nitrogen removal in (a) Run 1 and (b) Run 2.

ACE and NRE calculated the reactor's efficiency. ACE was negative, at -99 %, at the beginning of the study, due to ammonium production from decaying anammox biomass. However, ACE continued to increase until the end of the test. On day 31, ACE achieved 88%. The overall nitrogen efficiency was expressed in NRE, with an optimum of 79.8%.

Figure 6 shows the change in biomass color in Run 1. The biomass in the reactor is a reddish-brown color. This color is slightly pale compared to the color characteristics of the anammox bacteria. The colour of anammox biomass is bright red or dark red. The color of the biomass is an indicator of the visibility and performance of anammox bacteria. If the biomass's color changes from red to pale red or black, it is an indicator of reduced activity of the anammox bacteria.

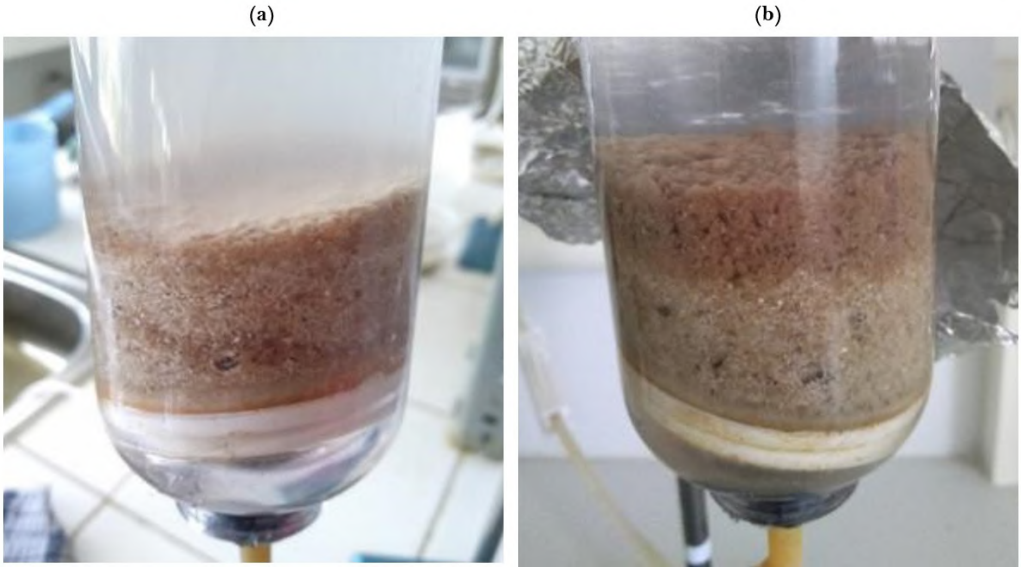

Figure 6 Anammox biomass Run 1, (a) day 1, pumice and anammox biomass mixed as carrier and inoculum, (b) day 31, anammox biomass flows into the upper as a sludge blanket.

Performance of Run 2

Run 2 was a reactor containing *Candidatus Brocadia fulgida* and *Candidatus Brocadia caroliniensis* with pumice as a carrier. These bacteria are also the first reported anammox bacteria to be found in Indonesia. These bacteria are enriched using FtBR with an inoculum sourced from Talago Koto Baru Lake, Tanah Datar, West Sumatra, at tropical ambient temperatures.

Lag Phase (days 1–9), Run 2 does not pass through the cell lysis phase, as well as Run 1, which experiences inhibition and adaptation to changes in the reactor operating environment. However, it is immediately during the lag phase that anammox bacteria adapt to the change in the new environment. The Anammox process has been in operation since the beginning of reactor operation, where both ammonium and nitrite have been removed. Even operated at a lower concentration than the previous operation, 100 mg-N L^{-1}, but the nitrogen loading rate was higher than the previous one due to decreased HRT from 24 to 12 hours.

The transition phase (days 10–25) shows higher nitrogen removal in Run 2. The ammonium concentration decreased gradually from 74.9 mg-N L^{-1} to 41.7 mg-N L^{-1} in the effluent on day 25. Likewise, the effluent's nitrite concentration decreased gradually from 79.46 mg-N L^{-1} to 14.5 mg-N L^{-1}.

During the activity elevation phase (days 26-31), ammonium and nitrite concentrations decreased rapidly to 2.0 mg-N L^{-1} and 4.9 mg-N L^{-1}, respectively, by the end of the experiment. Figure 4(b) shows the change in nitrogen concentration in Run 2. The NLR in the reactor remained stable

throughout the experiment, with a value of ± 0.40 kg-N m^{-3} d^{-1}. Then, NRR increased gradually from 0.112 kg-N m^{-3} d^{-1} to 0.395 kg-N m^{-3} d^{-1} on day 31.

Ammonium was oxidized from the beginning of reactor operation, with an ACE of 27% on day three and increasing gradually to a maximum of 98.12% in the last experiment. Likewise, NRE was stable during the first ten days of operation, ranging from 24.74% to 28.31%, and then increased rapidly, reaching a maximum of 92.47% at the end of the experiment. Run 2 performance in nitrogen removal is the best among both reactors. The nitrogen removal performance in Run 2 was shown in Figure 5(b).

The reactor's biomass is bright red, consistent with the characteristics described by Ali et al. (2014b). The color of the biomass is an indicator of the visibility and performance of anammox bacteria. The red color indicates the development of beneficial bacteria and can also be observed in the good performance of Run 2 in removing nitrogen.

Based on the quantity of bacterial biomass, it has increased from the first day. At the beginning of reactor operation, the anammox biomass inoculated into the reactor was not yet in a granular form. On day 31, it was clear that the anammox bacteria had formed granules. The granules are on the surface of the pumice. The influent flow pushes anammox biomass, causing the granular anammox to be at the top of the pumice.

Similar to Run 1, Run 2 also contained gas bubbles during reactor operation. It indicates the formation of nitrogen gas (N_2) resulting from chemical/metabolic reactions during the anammox process. An illustration of the visual changes that occurred in Run 2 is shown in Figure 7.

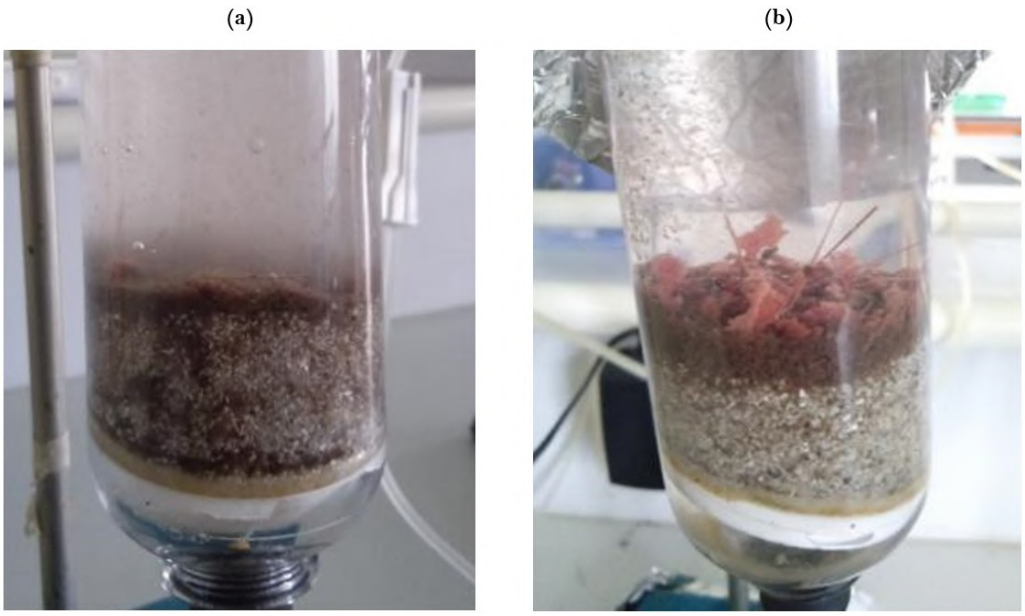

Figure 7 Anammox biomass Run 2, (a) day 1, the mixed pumice and anammox biomass generated bubbles of nitrogen gas as an indicator of a rapid anammox process (b) day 31, bright red anammox biomass grown.

DISCUSSION

The temperature operated lower than 37 °C, high nitrite concentration, and inoculum quality all influenced the anammox process activity during anammox reactor operation. The anammox process occurred at the beginning of both reactor operations, but it differed in the predominant process. In Run 1, another process could involve nitrogen conversions, such as denitrification and organic degradation, that release ammonium. Inhibition and anammox biomass lysis occurred due to the high concentration of supplied nitrite.

The maximum NRR obtained in this study was higher than that reported in previous studies (0.196 kg-N m^{-3} d^{-1}) conducted by Zulkarnaini et al.

(2020) using the same reactor type, HRT, and granular biomass without a carrier. The use of pumice enhanced NRR and improved nitrogen removal. In up-flow column reactor operations, challenges remained, such as seed sludge loss caused by the poor settleability of flocculent sludge. Pumice offers a promising solution, as its porous structure supports the attachment of anammox biomass while enhancing sludge settleability and activity.

Effect of pumice on nitrogen removal

The effect of adding pumice can be seen in Run 1, compared to Zulkarnaini et al. (2020), who used 20 mL of biomass from the *Candidatus Brocadia sinica* species as an inoculum, which was conducted at a tropical ambient temperature with an NRE of 77% and an ACE of 82%. Meanwhile, Run 1 with the same parameters improved NRE values by 79.80% and ACE by 87.77% in a shorter time of 31 days. Based on this comparison, the addition of pumice can improve nitrogen removal performance in the anammox process.

Previously, sand was used in the fluidized bed reactor, where the anammox process was first identified. In this study, pumice was used instead of sand. Two porosity levels can be distinguished when pumice is used as a filter bed material: the porosity of the pumice itself and the porosity of the filter bed. As a result, smaller particles are kept in the pores of the pumice, while larger particles are kept in the filter bed. As a result, clogging occurs more slowly, and the bed's volume is utilised more effectively in a pumice bed than in a sand bed.

In comparison to a sand bed, a pumice bed has more porosity and a larger capacity for particle deposition. The pore was filled with growing anammox biomass. It became thicker, as observed by Zulkarnaini and Silvia (2021), who noted that pores of the ceramic carrier, 1 mm in size, were filled with anammox biomass throughout the carrier's depth.

Pumice stone has been widely applied for nitrogen removal in various nitrogen compounds in different water or wastewater treatments. Helard et al. (2020) utilized pumice as an adsorbent in a fixed-bed column for nitrate removal, achieving a total removal efficiency of 31.42% and an adsorption capacity of 1,394 mg g^{-1} in groundwater. Additionally, pumice has been applied in biofilter tanks for nitrogen removal in recirculating aquaculture systems through the nitrification–denitrification process (Pungrasmi et al. 2016). The interaction and transformation of nitrogen compounds (ammonium, nitrite, and nitrate) are thought to occur through surface adsorption, followed by diffusion into the pumice pores, with hydrogen bonding and electrostatic attraction serving as the primary mechanisms of adsorption (Heibati et al. 2014; Edwin et al. 2023). Therefore, ammonium and nitrite, as substrates for anammox bacteria, will be retained in pumice, where 60% nitrogen removal occurs in the bottom part of the upflow anaerobic sludge blanket (UASB) reactor (Zulkarnaini et al. 2023). The use of pumice as a carrier increased the nitrogen removal in the UASB reactor.

Anammox bacteria naturally tend to form granules. Granulation begins with the presence of nuclei or bio-carriers that facilitate microbial attachment. Cell adhesion to these particles marks the initial stage of biofilm development, which then progresses into thick, dense biofilms on clusters of inert carriers (Yang et al. 2019). Such carriers should possess properties like a high specific surface area and adequate hydrophobicity to enhance sludge aggregation. In reactors with suspended biomass, pumice serves as an effective support medium, promoting anaerobic granule formation, improving biomass sedimentation, preventing washout, and enhancing nitrogen removal efficiency. Given the slow growth rate of anammox bacteria, using pumice as a carrier for attached growth can accelerate start-up and improve reactor performance.

The presence of gas bubbles in the reactor indicates the formation of nitrogen gas (N_2) due to a chemical/metabolic reaction that occurs in the

anammox process (Figure 6(b)). Pumice's porous and amorphous characteristics produce a substantial surface area and skeletal structure with open channels that allow ions and water to move into and out of the crystal structure. The released dinitrogen gas (N_2) bubbles prevent the anammox biomass from floating, a common phenomenon in the anammox process. Granular anammox has two types of internal channels, closed and open channels. In a closed channel, the anammox-produced N_2 gas is trapped in the granule and will float, resulting in a decrease in efficiency and biomass washout. Whereas granular material with open channels remains precipitated at the bottom of the reactor, granular material remains precipitated at the bottom of the reactor. The use of pumice can improve biomass retention and increase the efficiency of nitrogen removal.

Temperature dependence

The temperature of reactor operation influenced the anammox process, which was conducted at a tropical ambient temperature, ranging from 22 to 28 °C. In contrast, the optimum temperature for *Candidatus Brocadia sinica* bacteria is 37 °C. Even though the species has already adapted to tropical ambient temperature for 1.5 years, the lower temperature reduces the performance of bacteria in the ammonium removal process. The changes in the environment caused some bacteria to die. The reddish-brown color of the biomass in Run 1 is evident. The biomass of freshwater anammox species in their optimum state should be red carmine. The bacterial death causes cell lysis and the breakdown of organic nitrogen into ammonium. Therefore, the ammonium concentration increases in the effluent. This phenomenon was also reported by Lulrahman, Silvia and Zulkarnaini (2022) during the start-up of the anammox process to cultivate anammox bacteria using sludge from Penjalinan estuary as inoculum. The increasing ammonium in the effluent only occurred within one week of reactor operation. Then, the ammonium concentration in the effluent decreased to 91.6 mg-N L^{-1}. A small nitrite concentration was removed during this phase, indicating the anammox process was completely inhibited.

In a batch experiment with a limited ammonium concentration, Strous et al. (1999) reported that the anammox process was inhibited entirely by a nitrite concentration of more than 100 mg-N L^{-1}. When the operational reactor conditions change, shock loading occurs due to a higher concentration and lower HRT. Consequently, anammox bacteria undergo cell death.

Potential anammox research and application in a tropical country

The first discovery of anammox bacteria in tropical environments in Indonesia using a novel FtBR is expected to enhance research on anammox in Indonesia and Southeast Asia in the future. Likewise, the application of anammox bacteria to treat domestic wastewater and industrial wastewater, such as tofu waste and industrial fertiliser wastewater.

Effluents from industrial and municipal wastewater treatment plants frequently fail to meet Indonesian effluent quality standards for the nitrogen parameter. Consequently, eutrophication is a common issue in Indonesia's aquatic environment (Komala et al. 2024). Eutrophication, caused by excessive nutrients, primarily nitrogen and phosphorus, can lead to oxygen depletion, fish mortality, foul odors, and toxicity, as observed in Lake Koto Baru (Putra et al. 2020). Efforts have been proposed to apply the anammox process to address these issues (Wijaya & Soedjono 2018). However, despite being discovered over 30 years ago and implemented in full-scale reactors globally, the application of anammox in Indonesia remains limited due to the scarcity of related research.

There is significant potential to implement the anammox process for

wastewater treatment and eutrophication control in tropical environments by utilizing indigenous anammox bacteria. In parallel, developing large-scale anammox reactors could complement or replace existing systems, such as wetlands in the fertilizer industry. Applying the anammox process to domestic and industrial wastewater treatment in tropical countries, particularly Indonesia, could support compliance with national effluent quality standards and help prevent eutrophication —a widespread issue in tropical regions caused by nutrient overloading in water bodies.

This study offers critical insights into the potential of native anammox bacteria from Lake Koto Baru to provide an efficient and sustainable solution for nitrogen removal in wastewater treatment, particularly in tropical regions. By utilizing a local bacterial strain, this research supports the development of regionally adapted environmental technologies that can enhance the performance and economic feasibility of nitrogen removal processes in tropical climates. The successful use of pumice as a carrier in these reactors also highlights its potential as an accessible and cost-effective medium for biofilm development in anammox-based treatment systems. Furthermore, the comparative analysis with *Candidatus Brocadia sinica* demonstrates the viability of indigenous strains, contributing to the broader application of anammox processes in environmental engineering and sustainable water management solutions.

CONCLUSIONS

The use of pumice as a carrier significantly enhances nitrogen removal in both reactors, demonstrating its effectiveness as a biofilm support material for anammox bacteria. The comparison between the two reactors revealed that the enriched anammox bacteria from Lake Koto Baru in Run 2 significantly outperformed *Candidatus Brocadia sinica* in Run 1, with Run 2 achieving a higher nitrogen removal rate (0.395 kg-N m^{-3} d^{-1}), ammonium conversion efficiency (98.12 %), and nitrogen removal efficiency (92.6 %) compared to Run 1's performance (NRR: 0.341 kg-N m^{-3} d^{-1}, ACE: 87 %, NRE: 79.8 %). These findings indicate that the anammox bacteria sourced from Lake Koto Baru exhibit robust nitrogen removal capabilities in tropical conditions, making them highly suitable for wastewater treatment applications in such climates. The results also highlight the potential for utilizing indigenous bacterial strains to optimise nitrogen removal processes, contributing to more sustainable and locally adapted wastewater treatment solutions.

AUTHOR CONTRIBUTION

Z.Z. M.Z. designed the research and supervised all the processes. M.Z. collected and analyzed the data and wrote the manuscript. R.A. revised the manuscript.

ACKNOWLEDGMENTS

The authors would like to express their gratitude to the Polytechnic ATI Padang, Indonesia, for providing the facilities and support during the research work.

COMPETING INTERESTS

There is no competing interests.

REFERENCES

Ahn, Y.H., 2006. Sustainable nitrogen elimination biotechnologies: A review. *Process Biochemistry*, 41(8), pp.1709–1721. doi: 10.1016/j.procbio.2006.03.033

Ali, M., Oshiki, M. & Okabe, S., 2014a. Simple, Rapid and Effective Preservation and Reactivation of Anaerobic Ammonium Oxidizing Bacterium 'Candidatus Brocadia sinica'. *Water Research*, 57, pp.215–222. doi: 10.1016/j.watres.2014.03.036.

Ali, M., Oshiki, M. & Okabe, S., 2014b. Simple, Rapid and Effective Preservation and Reactivation of Anaerobic Ammonium Oxidizing Bacterium 'Candidatus Brocadia sinica'. *Water Research*, 57, pp.215–222. doi: 10.1016/j.watres.2014.03.036.

Chen, C-jun. et al., 2012. Improving Anammox Start-up with Bamboo Charcoal. *Chemosphere*, 89(10), pp.1224–1229. doi: 10.1016/j.chemosphere.2012.07.045.

Chen, H. et al., 2016. Successful Start-up of The Anammox Process: Influence of The Seeding Strategy on Performance and Granule Properties. *Bioresource Technology*, 211, pp.594–602. doi: 10.1016/j.biortech.2016.03.139.

Edwin, T. et al., 2023. Impact of Pyrolysis Temperature on the Removal of Nutrients Using Coarse Rice-Husk Biochar. *Journal of Ecological Engineering*, 24(12), pp.247–257. doi: 10.12911/22998993/173379.

Feng, X. et al., 2019. Nitrogen removal from iron oxide red wastewater via partial nitritation-Anammox based on two-stage zeolite biological aerated filter. *Bioresource Technology*, 279, pp.17–24. doi: 10.1016/j.biortech.2019.01.113.

Van De Graaf, A.A. et al., 1996. Autotrophic growth of anaerobic ammonium-oxidizing microorganisms in a fluidized bed reactor. *Microbiology*, 142 (8), pp.2187–2196. doi: 10.1099/13500872-142-8-2187.

Heibati, B. et al., 2014. Uptake of Reactive Black 5 by pumice and walnut activated carbon: Chemistry and adsorption mechanisms. *Journal of Industrial and Engineering Chemistry*, 20(5), pp.2939–2947. doi: 10.1016/j.jiec.2013.10.063.

Helard, D., Indah, S. & Kiflia, D.P., 2020. Removal of nitrate from groundwater by column using pumice as adsorbent as an effort for water resources conservation. *IOP Conference Series: Materials Science and Engineering*, 846, 012059. doi: 10.1088/1757-899X/846/1/012059.

Indah, S. et al., 2021. Removal of nitrate using modified pumice as adsorbent for reducing groundwater pollution. *E3S Web of Conferences*, 331, 02012. doi: 10.1051/e3sconf/202133102012.

Komala, P.S. et al., 2024. The effect of anthropogenic activities on the spatial distribution of total nitrogen and total phosphate in Lake Maninjau. *Journal of Water and Land Development* 60(I-III), pp.71–78. doi: 10.24425/jwld.2024.149109.

Kumar, M. et al., 2017. Anammox Processes. In *Current Developments in Biotechnology and Bioengineering*. Elsevier, pp.381-407. doi: 10.1016/B978-0-444-63665-2.00015-1.

Le, L.T. et al., 2022. Influence of temperature on anammox reaction and microbial diversity in a bio-carriers reactor under mainstream conditions. *Environmental Technology and Innovation*, 25, 102178. doi: 10.1016/j.eti.2021.102178.

Lin, Y.M. et al., 2013. Apatite accumulation enhances the mechanical property of anammox granules. *Water Research*, 47(13), pp.4556–4566. doi: 10.1016/j.watres.2013.04.061.

Lotti, T. et al., 2014a. Simultaneous Partial Nitritation and Anammox at Low Temperature With Granular Sludge. *Water Research*, 66, pp.111–121. doi: 10.1016/j.watres.2014.07.047.

Lotti, T. et al., 2014b. Physiological and Kinetic Characterization of A Suspended Cell Anammox Culture. *Water Research*, 60, pp.1–14. doi: 10.1016/j.watres.2014.04.017.

Lulrahman, F., Silvia, S. & Zulkarnaini, Z., 2022. Nitrogen Removal by Anammox Process Using Sludge from Muara Penjalinan of Padang City as Inoculum. *Jurnal Teknologi Lingkungan*, 23(2), pp.143–150. doi: 10.29122/jtl.v23i2.5284.

Mulder, A. et al., 1995. Anaerobic ammonium oxidation discovered in a denitrifying fluidized bed reactor. *FEMS Microbiology Ecology*, 16(3), pp.177–183. doi: 10.1016/0168-6496(94)00081-7.

Oshiki, M. et al., 2013. Cultivation of planktonic anaerobic ammonium oxidation (anammox) bacteria using membrane bioreactor. *Microbes and Environments*, 28(4), pp.436–443. doi: 10.1264/jsme2.ME13077.

Oshiki, M. et al., 2011. Physiological characteristics of the anaerobic ammonium-oxidizing bacterium 'Candidatus Brocadia sinica'. *Microbiology*, 157 (6), pp.1706–1713. doi: 10.1099/mic.0.048595-0.

Pratiwi, N.I. et al., 2019. Adsorption and Regeneration of Sungai Pasak Pumice as an Adsorbent for Ammonium Removal in Water. *Jurnal Riset Teknologi Pencegahan Pencemaran Industri* 10(1), pp.38–46. doi: 10.21771/jrtppi.2019.v10.no1.p38-46

Pungrasmi, W., Phinitthanaphak, P. & Powtongsook, S., 2016. Nitrogen removal from a recirculating aquaculture system using a pumice bottom substrate nitrification-denitrification tank. *Ecological Engineering*, 95, pp.357–363. doi: 10.1016/j.ecoleng.2016.06.094.

Putra, R.P. et al., 2020. Start-Up Anammox Process Using Sludge from Koto Baru Lake as Inoculum. *Teknologi Lingkungan*, 21(2), pp.138–146.

Ridha, M. & Darminto, D., 2016. Analisis Densitas, Porositas, dan Struktur Mikro Batu Apung Lombok dengan Variasi Lokasi dan Kedalaman. *Jurnal Fisika dan Aplikasinya*, 12(3), pp.124–130. doi: 10.12962/j24604682.v12i3.1403.

Strous, M. et al., 1997. Ammonium removal from concentrated waste streams with the anaerobic ammonium oxidation (anammox) process in different reactor configurations. *Water Research*, 31(8), pp.1955–1962. doi: 10.1016/S0043-1354(97)00055-9.

Strous, M., Kuenen, J.G. & Jetten, M.S.M., 1999. Key Physiology of Anaerobic Ammonium Oxidation. *Applied and Environmental Microbiology*, 65, pp.3248–3250. doi: 10.1128%2Faem.65.7.3248-3250.1999.

Wijaya, I.M.W. & Soedjono, E.S., 2018. Domestic wastewater in Indonesia: Challenge in the future related to nitrogen content. *International Journal of GEOMATE*, 15(47), pp.32–41. doi: 10.21660/2018.47.06582.

Yang, S. et al., 2019. Improving nitrogen removal in an IFAS nitritation–anammox reactor treating lagoon supernatant by manipulating biocarrier filling ratio and hydraulic retention time. *Biochemical Engineering Journal*, 152, 107365. doi: 10.1016/j.bej.2019.107365.

Zulkarnaini, Afrianita, R. & Putra, I.H., 2020. Application of Anammox Process in Nitrogen Removal Using Up-Flow Anaerobic Sludge Blanket Reactor. *Jurnal Teknologi Lingkungan* 21(1), pp.31–39.

Zulkarnaini, Z., 2024. *Sistem Bioreaktor untuk Pengayaan Bakteri Anaerobic Ammonium Oxidation (Anammox)* IDP000096776 [Patent].

Zulkarnaini, Z. et al., 2024. Diversity of Anammox Bacteria from Landfill Treatment Plant Sludge in Tropical Area. *Applied Science and Engineering Progress*, 17(2), 7299. doi: 10.14416/j.asep.2024.01.003

Zulkarnaini, Z. et al., 2025. Cultivation of anammox bacteria from a tropical lake in Indonesia using a novel filter bioreactor to enhance nitrogen removal efficiency. *Water science and technology*, 91(7), pp.811–826. doi: 10.2166/wst.2025.050.

Zulkarnaini, Z., Komala, P.S. & Almi, A., 2021. Anammox biofilm process using sugarcane bagasse as an organic carrier. *Indonesian Journal of Biotechnology*, 26(1), 25. doi: 10.22146/IJBIOTECH.58554.

Zulkarnaini, Z., Nur, A. & Ermaliza, W., 2019. Nitrogen Removal in the Anammox Biofilm Reactor using Palm Fiber as Carrier in Tropical Temperature Operation. *Jurnal Riset Teknologi Pencegahan Pencemaran Industri*, 10(2), pp.7–15. doi: 10.21771/jrtppi.2019.v10.no2.p7-15.

Zulkarnaini, Z., Rasyidah, A.A. & Ridwan., 2023. Utilization of Waste Plastic Straws as Carrier in the Anammox Process. *Jurnal Teknologi Lingkungan*, 24(1), pp.73–80.

Zulkarnaini, Z. & Silvia, S., 2021. Performance of Nitrogen Removal in Ceramic Anammox Reactor with Two-Inflow. *IOP Conference Series: Materials Science and Engineering*, 1041, 012037. doi: 10.1088/1757-899X/1041/1/012037.

Journal of Tropical Biodiversity and Biotechnology
Volume 10, Issue 04 (2025): jtbb26539
DOI: 10.22146/jtbb.26539

Research Article

Identification of Partial *GDF9* Gene for Genotyping Bligon Goats and Its Origin

Fariz Jordan Fadillah[1], Dina Puspitasari[1], Nanik Prasetya Ningrum[1], Fatimah Az Zahra Chairunissa[1], Arif Irawan[2], Mifta Pratiwi Rachman[1], Kustantinah[2], Sigit Bintara[1], Tety Hartatik[1]*

1)Department of Animal Breeding and Reproduction, Faculty of Animal Science Universitas Gadjah Mada, Yogyakarta, 55281, Indonesia

2)Department of Animal Nutrition and Feed, Faculty of Animal Science Universitas Gadjah Mada, Yogyakarta, 55281, Indonesia

* Corresponding author, email: tety@ugm.ac.id

Keywords:
Bligon goat
GDF9
PCR-RFLP
Restriction enzymes mapping
SNPs

Submitted:
04 September 2023

Accepted:
12 July 2025

Published:
05 December 2025

Editors:
Miftahul Ilmi
Annisaa Widyasari

ABSTRACT

GDF9, a peptide in the *TGF-β* growth factor family, plays a crucial role in oocyte growth and maturation, affecting reproduction through genetic factors. This makes it valuable for livestock selection via SNPs, which are used in genotyping methods like PCR-RFLP. This study aimed to identify SNPs, map restriction enzyme sites, and perform genotyping to explore reproductive traits in Bligon goats. A total of 91 female goats were analysed, including 36 Bligon goats, 26 Peranakan Etawa goats, and 29 Kacang goats, and all of them had single births. PCR amplification was conducted using two pairs of primers for the *GDF9* gene: the forward primer 5'-CTCCTCTTGAGCCTCTGGTG-3' and reverse primer 5'-TCCAGTTGTCCCACTTCAGC-3' for GDF9-3, and forward primer 5'-TGTAAGATCGTCCCGTCACC-3' and reverse primer 5'-CACACTTCCTCTCCCTCTCA-3' for GDF9-6. Sequencing was done after amplification. Six SNPs were identified at positions g.2565C>M, g.2589G>A, g.2634G>A, g.2653G>T, g.2679A>G, and g.2691A>G, with one being synonymous (g.2653G>T) and five non-synonymous, causing amino acid changes. Among these, g.2565C>M was recognized by the restriction enzymes *HpaII* and *MspI*, was recommended for use in PCR-RFLP for genotyping with the *GDF9*-3 primer. The study also found that the genotype frequencies in Bligon, Peranakan Etawa, and Kacang goats were in Hardy-Weinberg equilibrium (HWE), supporting the use of SNP g.2565C>M as a genetic marker. Enzym *MspI* can be used for genotyping the target gene in exon 2 of the *GDF9* gene in three types of goats: Bligon, Peranakan Etawa, and Kacang.

How to cite:
Fadillah, F.J. et al., 2025. Identification of Partial *GDF9* Gene for Genotyping Bligon Goats and Its Origin. *Journal of Tropical Biodiversity and Biotechnology*, 10(4), jtbb26539. doi: 10.22146/jtbb.26539

INTRODUCTION

Efforts to enhance goat productivity focus on improving reproductive traits, such as rapid sexual maturation, high litter sizes, and short kidding intervals. Bligon goat breed known for these traits as a result from crossbreeding of Peranakan Etawa (PE) and Kacang goats and is characterized by its triangular-shaped muzzle, hanging ears, and compact body. These goats are hardy, adaptable, and easy to maintain (Sarwono 2011). Reproductive traits in goats, such as ovulation rate, are influenced by inheritable genes, which can be targeted for improvement through molecular methods (Ginting 2009). Genes like *BMPR1B*, *GDF9*, *BMP15*, *FSHβ*, *FSHR*, *POU1F1*, *PRLR*, and *KISS1* are known to affect reproduction in goats (Ahlawat et al. 2015a). Among them, Growth Differentiation Factor 9 (*GDF9*) plays a vital role in ovulation and oocyte maturation. *GDF9*, produced by oocytes and part of the TGF-β Growth Factor family, is located on chromosome 7, spanning 2 exons and 1 intron, with a total length of about 5644 bp (Arta & Rahayu 2013; Chairunissa et al. 2022).

The *GDF9* gene plays a critical role in controlling reproductive traits, particularly in regulating the number of offspring produced in each cycle (Jia et al., 2015). The number of offspring is influenced by the quantity of eggs ovulated, which is tied to Follicle Stimulating Hormone (FSH) secretion during folliculogenesis. *GDF9* stimulates granulosa cell differentiation, induces receptors for Luteinizing Hormone (LH), and promotes steroidogenesis. Found in both oocytes and granulosa cells, *GDF9* triggers the proliferation of granulosa and cumulus cells before and during ovulation (Arta & Rahayu 2013). A deficiency in *GDF9* impairs follicle growth and granulosa/theca cell function, leading to infertility.

GDF9's influence on reproduction is a polygenic trait, making it valuable for livestock breeding. The use of Single Nucleotide Polymorphisms (SNPs) as genetic markers enhances breeding efficiency (Prihandini & Maharani 2019). SNPs are single base changes that help identify inheritable traits and are commonly used in molecular breeding. Polymerase chain reaction-restriction fragment length polymorphism (PCR-RFLP) is a reliable method for detecting SNPs linked to desirable traits in animals (Wang et al. 2021). This method allows for precise genetic selection and marker-assisted breeding (Liu & Chen 2020) and has been shown to improve selection accuracy and genetic mapping in agricultural species (Kim et al. 2023). Combining SNP analysis with PCR-RFLP has great potential to boost livestock productivity through targeted genetic improvement programs.

PCR-RFLP with the *BsaI* enzyme has been applied in studies like Ghoreishi et al. (2019), where polymorphisms in the *GDF9* gene in Markhoz goats were linked to prolificacy. This study identified three genotypes (CC, CA, AA) with different fragment sizes, demonstrating how restriction enzymes can effectively identify genetic markers and provide insights into traits linked to mutations (Perdana & Hartatik 2022). A study by Hartatik et al. (2023) demonstrated the use of restriction enzymes *BsaI* and *BsmAI* at the g.1956A>C SNP in Exon 1, while *MspI*, *HapII*, and *HpaII* were used to recognize the g.3855A>C SNP in Exon 2 based on GenBank Acc. No. EF446168. Based on this, Irawan et al. (2024) reported that genotyping with PCR-RFLP at the g.3855A/C position in Exon 2 of the *GDF9* gene revealed two genotypes, AA and AC, using the *MspI* enzyme. The *GDF9* gene is a key candidate for traits like litter size, which is important in animal breeding. However, no studies have yet identified specific sequences in Exon 2 using two primers or compared them with the genetic sequences of origin goats. This gap highlights the need for further research, particularly studies on mutation analysis (SNPs and amino acid changes), restriction enzyme mapping, and genotyping of the *GDF9* gene in Bligon goats and their origin breeds, such as PE and Ka-

cang goats. Exploring these areas could provide valuable insights into the genetic basis of litter size and other economically important traits in goats.

MATERIALS AND METHODS

Bloods samples

The materials used in this study consisted of isolated blood samples from 91 animals, consist of 36 Bligon goats, 26 PE goats, and 29 Kacang goats, all of them were female and selected based on single birth type. Approximately one -third of the neck's distal area was obstructed, and blood was collected from the jugular vein. To prevent any contamination during the blood sampling process, a venoject connected to a K3EDTA tube was utilised, and the constrained area was sterilised using alcohol. The venoject was inserted into the blood vessel at an upward angle of 30°, resulting in the collection of a total of 3 ml of blood. The blood stored in the K3EDTA tube was transported to the laboratory while maintaining a low temperature inside an icebox containing ice packs. The blood sampling protocol employed in this study received approval under Ethical Clearance Number 0124/EC-FKH/Eks/2022.

DNA extraction

The DNA extraction was performed following the instructions of the DNA isolation kit (gSYNCTM DNA Extraction Kit, Geneaid, Taiwan) at the Laboratory of Genetics and Animal Breeding, Faculty of Animal Science, Universitas Gadjah Mada.

DNA amplification of GDF9-3 and GDF9-6

The genomic DNA of 91 samples were amplified using PCR method using two sets of primer. The first primer is GDF9-3 (forward primer 5'-CTCCTCTTGAGCCTCTGGTG-3' and a reverse primer 5'-TCCAGTTGTCCCACTTCAGC-3'). The PCR reaction mix were 25 µL total volume, including 12.5 µL of PCR Kit My Taq HS Red Mix (Meridian Bioscience, US), 9.5 µL of DDW, 2 µL of DNA with total 20 ng, and 0.5 µL of each primer with the concentration of 10 pmol μL^{-1}. With the PCR program as follow: pre-denaturation step at 94°C for 5 minutes, followed by 35 cycles of denaturation at 94°C for 30 seconds, annealing at 58°C for 40 seconds, and extension at 72°C for 30 seconds. The final extension was at 72°C for 5 minutes. The second primer set, GDF9-6 (forward primer 5'-TGTAAGATCGTCCCGTCACC-3' and a reverse primer 5'-CACACTTCCTCTCCCTCTCA-3') with similar method as previous primer. The PCR products were then separated by electrophoresis on a 1% agarose gel at 50 volts for 25 minutes.

GenBank accession number EF446168.2 and OP494705.1 were used as reference for the *GDF9* gene target sequence and the primers location scheme were shown in Figure 1.

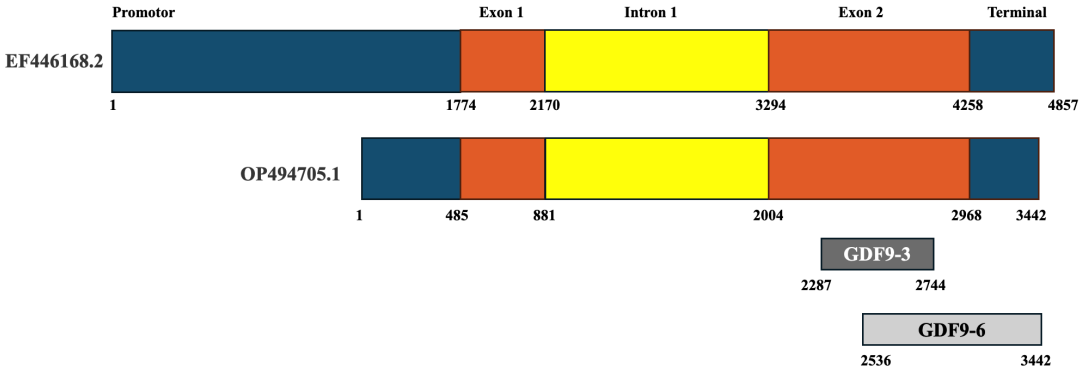

Figure 1. GenBank references EF446168.2 and OP494705.1 of *GDF9* gene and target sequence of two pairs of primers (GDF9-3 and GDF9-6).

Sequencing and SNP identification of targets

The Sanger sequencing process was conducted in LPPT UGM (Yogyakarta, Indonesia). A set of 25 µL of PCR product along with 10 µL of primers was delivered to LPPT, and the results were then aligned using BioEdit software version 7.2.5. SNPs were detected from an electropherogram that showing homozygous and heterozygous sequences. Homozygous SNPs are indicated by a single peak, while heterozygous SNPs are indicated by double peaks. The sequencing approach provides a more accurate confirmation of SNPs, which is then followed by PCR-RFLP analysis for further validation (Figure 3). The sequencing result then were being aligned with the GenBank reference.

Restriction enzyme determination and mapping

We used NebCutter V2.0 website to identify restriction enzymes as well as the restriction site of the SNP. The identification of specific restriction enzymes was able to recognize gene targets and was indicated by the appearance of a red line beneath a sequence (Albakri & Hartatik 2021). The count of cleavage sites was determined using BioEdit v.7.2.5, applied to both the GenBank samples and references.

Genotyping restriction fragment length polymorphism (RFLP)

After identifying the appropriate restriction enzyme from the mapping results, the PCR-RFLP phase was carried out. The SNP g.2565C>M from 91 samples was used for genotyping using PCR-RFLP method. Restriction enzyme digestion was performed in 12 µL reaction volumes, consisting of approximately 3 µL of PCR product with a total of approximately 150 ng DNA, 7.7 µL of ddH2O, 1.2 µL of Buffer 1.1 (New England Biolabs, USA), and 0.1 µL of *MspI* restriction enzyme (10 U μL^{-1}; 1 Unit total). The digestion was incubated for 2 hours at 37°C. The digested products were then analysed by running them on a 3% agarose gel, 50 Volt, and for 30 minutes.

Data analysis

The data analysis employed is descriptive, involving the grouping of alleles and genotypes from the PCR-RFLP results. The allele (1) and genotype (2) frequency analysis can be determined using the formula as follow:

(1) Formula allele frequency

$$X_i = \frac{2N_{ii} + N_{ij}}{2N}$$

$$X_j = \frac{2N_{jj} + N_{ij}}{2N}$$

(2) Formula genotype frequency

$$X_{ii} = \frac{N_{ii}}{N} \times 100\%$$

$$X_{jj} = \frac{N_{jj}}{N} \times 100\%$$

$$X_{ij} = \frac{N_{ij}}{N} \times 100\%$$

Where X_i = frequency of allele i, X_j = frequency of allele j, X_{ii} = genotype ii, X_{jj} = genotype jj, X_{ij} = genotype ij, N = number of individual samples.

Pearson's Chi-square test was used to verify the Hardy–Weinberg equilibrium status for the allele and genotype frequencies using following mathematical model:

$$X^2 = \sum \frac{(O_i - E_i)^2}{E_i}$$

Where X^2 is the Chi-square test value, O_i is the observed frequency, E_i is the expected frequency.

RESULTS AND DISCUSSION

Identification of SNPs *GDF9* gene using GDF-3 and GDF-9 primers

The PCR product using GDF9-3 and GDF9-6 primers were 456 bp and 907 bp, respectively as shown in Figure 2A. Based on the results, four SNPs position were found in GDF9-3 (SNPs: g.2565C>M, g.2589G>A, g.2634G>A, and g.2679A>G) spanned throughout exon 2 (Figure 2B) and three SNPs position were found in GDF9-6 (SNPs: g.2653G>T, g.2679A>G, and g.2691A>G) spanned in exon 2 and the terminal region (Figure 2C). Sequence alignment and electropherograms confirmed the SNP positions, heterozygous from homozygous sequences.

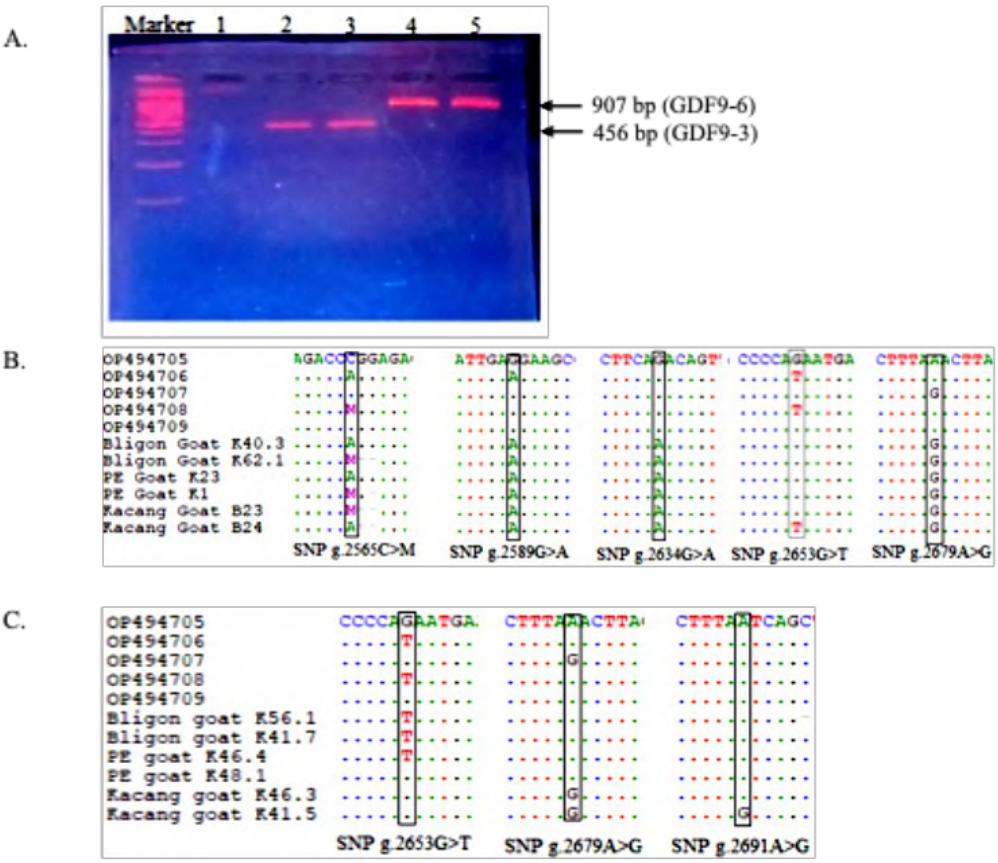

Figure 2. Product size of PCR and alignment results from sequencing in *GDF9* target gene of Bligon, PE, and Kacang goat. Note: A = PCR product (Marker 100 bp), B = GDF9-3 sequence alignment results, and C = GDF9-6 sequence alignment results.

The electrophoregram analysis provides significant insights into the genetic variations within the *GDF9* gene in the studied population. SNP at position g.2565C>M exhibited two genotypes: AA and AC. The AC genotype showed double peaks at both A and C bases, indicating heterozygosity. In contrast, the SNP at position g.2589G>A presented only the AA genotype, characterized by a single peak at base A, indicating homozygosity for the A allele. We have found SNPs at g.2634G>A for Bligon goat found two genotypes (GG and AA), while in the other goats (Kacang and PE) only one genotype (AA). Furthermore, the SNPs at g.2679A>G for Bligon goat found two

genotypes (AA and GG), while in the other goats (Kacang and PE) only one genotype (GG) found in this study. These findings are consistent with Chairunissa et al. (2022) who reported the SNP g.3855A>C (with GenBank reference number EF446168.2) that we found the SNPs at SNP g.2565C>M (with GenBank reference number OP494705.1 in the three local goats in our study). It means that this highlighting the reliability of these genetic markers and their potential utility in breeding programs.

While three SNPs g.2653G>T, g.2679A>G, and g.2691A>G were identified, each displaying two genotypes: TT/GG for g.2653G>T, AA/GG for g.2679A>G, and AA/GG for g.2691A>G were flanked by primer GDF9-6. These genotypes were marked by distinct peaks for bases T/G, A/G, and A/G, respectively, in the electropherogram. These findings are aligned with Zhu et al. (2013), who observed similar SNP variations in different goat breeds, highlighting the functional relevance of these genetic markers across livestock populations. The results have important implications for Marker-Assisted Selection (MAS) in breeding programs. The consistent identification of these SNPs in various studies underscores their potential as reliable markers for selecting animals with desirable traits, especially reproductive traits like litter size. Supporting this, Wouobeng et al. (2020) found that the AA genotype in Markhoz goats was associated with larger litter sizes, and Feng et al. (2011) discovered similar SNP variations in Jining Gray goats, further validating the role of these genetic markers in improving reproductive outcomes.

These findings not only confirm the presence of specific SNPs in the *GDF9* gene but also contribute to improving livestock breeding strategies. The consistent genotyping results from this study, alongside those of Zhu et al. (2013) and Feng et al. (2011), enhance the understanding of how these genetic markers can be utilized to select for reproductive traits, a crucial aspect of livestock management and genetic improvement.

The amino acid analysis revealed one synonymous (nonsense) mutation and five non-synonymous (missense) mutations. The SNP at position g.2565C>M exhibited both homozygous CC and heterozygous AC genotypes. The SNP g.2589G>A resulted in an amino acid substitution, changing Glycine to Arginine. Similarly, the SNP g.2634G>A caused an amino acid change from Aspartic acid to Asparagine. The SNP g.2653G>T led to a premature stop codon (nonsense mutation), while the SNP g.2679A>G resulted in an amino acid change from Asparagine to Aspartic acid. Finally, the SNP g.2691A>G resulted in an amino acid change from Isoleucine to Valine. These amino acid changes are summarized in Table 1.

The SNP g.2565C>M, for example, results in a mutation from Glutamine to Proline, which, although missense, may still affect protein structure and function. Such mutations can influence protein folding, stability, and activity, which in turn may impact the function of *GDF9* a key growth differentiation factor involved in reproductive processes in animals (Zhu et al. 2013). This is consistent with findings from Wang et al. (2018), who noted that SNPs in the *GDF9* gene could alter its expression and functionality, potentially leading to variations in reproductive performance across livestock populations.

Other studies have further explored the role of *GDF9* SNPs in reproductive traits. Ghoreishi et al. (2019) identified a SNP in Markhoz goats (g.183C>A) that did not alter the amino acid Leucine, while Du et al. (2008) found a heterozygous genotype (g.1189G>A mutation) in Guizhou white goats. Among a group of 33 high-productivity brood goats, those with the heterozygous genotype produced three offspring per birth, compared to low-productivity goats with a homozygous genotype. Aboelhassan et al. (2021) also highlighted that *GDF9* gene polymorphism influences fecundity, with

Table 1. Results of amino acid changes in the *GDF9* gene of Bligon, PE, and Kacang goats.

No	SNP Position (OP494705)	Codon	Amino Acid	Mutation	Primer	SNPs status		
						Bligon	PE	Kacang
1	g.2565C>M	CAG CCG	Glutamine Proline	Missense mutation	GDF9-3	Yes	Yes	Yes
2	g.2589G>A	GGA AGA	Glycine Arginine	Missense mutation	GDF9-3	Yes	No	No
3	g.2634G>A	GAC AAC	Aspartic acid Asparagine	Missense mutation	GDF9-3	Yes	No	No
4	g.2653G>T	GAA UAA	Glutamic acid Stop	Nonsense mutation	GDF9-6	Yes	Yes	No
5	g.2679A>G	AAC GAC	Asparagine Aspartic acid	Missense mutation	GDF9-3 and GDF9-6	Yes	No	No
6	g.2691A>G	AUC GUC	Isoleucine Valine	Missense mutation	GDF9-6	No	No	Yes

heterozygous genotypes leading to higher ovulation rates and larger litter sizes in livestock compared to homozygous genotypes in wild populations.

Several previous studies confirmed that missense mutation was found in exon 2 of the *GDF9* gene, such as Hartatik et al. (2023), found SNP g.3855A>M (position from reference EF446168.2) in Bligon goats with an amino acid change from Glutamine to Proline, Zhao et al. (2016) identified SNP g.3905A>C in Kashmir goats, which caused an amino acid change from Valine to Isoleucine, and Feng et al. (2011) detected SNP g.397IG>A in Jining Grey goats, resulting in a Glycine to Aspartic acid change in exon 2 of *GDF9* gene. These studies underscore the importance of identifying SNPs in the exon regions, as they can lead to amino acid changes that may influence reproductive performance, providing valuable information for livestock breeding programs (Perdana 2022).

Restriction enzyme mapping of *GDF9-3* and *GDF9-6*

The restriction enzyme mapping for SNPs in the *GDF9* gene revealed key enzymes suitable for PCR-RFLP genotyping, specifically *MspI* and *HpaII* for SNP g.2565C>M, and *Hpy188I* and *MseI* for SNPs g.2679A>G and g.2691A>G, respectively. *MspI* and *HpaII* enzymes, found at position g.2565C>M, present a unique restriction site with only one cutting site, enabling the identification of three genotypes: CC, AA, and AC. The corresponding fragment sizes for the genotypes are as follows: the AA genotype produces a 456 bp fragment; the AC genotype produces three fragments (456 bp, 307 bp, and 149 bp); and the CC genotype produces two fragments (307 bp and 149 bp). These results make *MspI* an ideal restriction enzyme for genotyping, as highlighted in Table 2.

Restriction enzyme mapping is a useful tool for genetic tagging, as it identifies SNP-associated restriction sites and enables accurate genotyping (Perdana & Hartatik 2022). The use of *MspI* and *HpaII* enzymes is supported by their ability to generate distinct, well-spaced fragment sizes, essential for clear visualization and differentiation of genotypes. The enzymes' specificity is also beneficial, as each enzyme recognizes a single restriction site within the SNP regions. These findings align with earlier studies by Hossain et al. (2020) and Chairunissa et al. (2022), who also used restriction enzymes such as *HhaI*, *DdeI*, and *MspI* for genotyping *GDF9* gene polymorphisms. Furthermore, Hartatik et al. (2023) identified multiple enzymes (*MspI*, *HpaII*) as suitable markers for further genotype identification using PCR-RFLP methods.

The choice to utilize *MspI* and *HpaII* in this study was based on several practical considerations, including their ability to generate sufficiently sized

Table 2. Mapping of restriction enzymes on target *GDF9-3* and *GDF9-6* of Bligon, PE, and. Kacang goat.

Target	Product size	SNP	Enzyme	Recognizing site	Amount of cut	Site of cut	Fragment Size
GDF9-3	456	g.2565C>M	*MspI* *HpaII*	C'CG_G	1 cutter	307	307, 149
GDF9-6	907	g.2679A>G	*Hpy188I*	TC_n'GA	5 cutters	17, 54, 68, 499, 757	17, 37, 14, 431, 258, 150
GDF9-6	907	g.2691A>G	*MseI*	T'TA_A	10 cutters	111, 123, 399, 608, 704, 712, 775, 825, 829, 843	111, 12, 276, 209, 96, 8, 63, 50, 4, 14, 64

bands (over 100 bp), the clear separation of band sizes for easy visualization, and the availability of these enzymes in the lab. In comparison, enzymes like *MseI* and *Hpy188I*, which produce smaller fragment sizes, were less optimal for this study. Overall, the identified restriction enzymes offer reliable markers for genetic analysis and potential applications in livestock breeding programs.

Polymerase chain reaction-restriction fragment length polymerase (PCR -RFLP) of Bligon, PE, and Kacang goats using GDF9-3

The findings from the PCR and PCR-RFLP analysis of the *GDF9* gene are presented in Figure 3, highlighting the genotyping of SNP g.2565C>M in 91 goats using the *MspI* enzyme, which identifies the C|CGG restriction site. The PCR-RFLP analysis identified two distinct genotypes: the homozygous AA genotype, characterised by a 456 bp fragment, and the heterozygous AC genotype, which showed fragments of 149 bp, 307 bp, and 456 bp.

For Bligon goats, most animals exhibited the AA genotype (0.97 frequency), with a smaller proportion showing the AC genotype (0.03). The A allele had a frequency of 0.98, while the C allele had a frequency of 0.02. The Hardy-Weinberg equilibrium (HWE) test for Bligon goats yielded a chi-square (χ^2) value of 0.14, indicating equilibrium. Similarly, in PE goats, the AA genotype was the most common (0.96 frequency), followed by the AC genotype (0.04). The A allele frequency was 0.98, and the C allele frequency

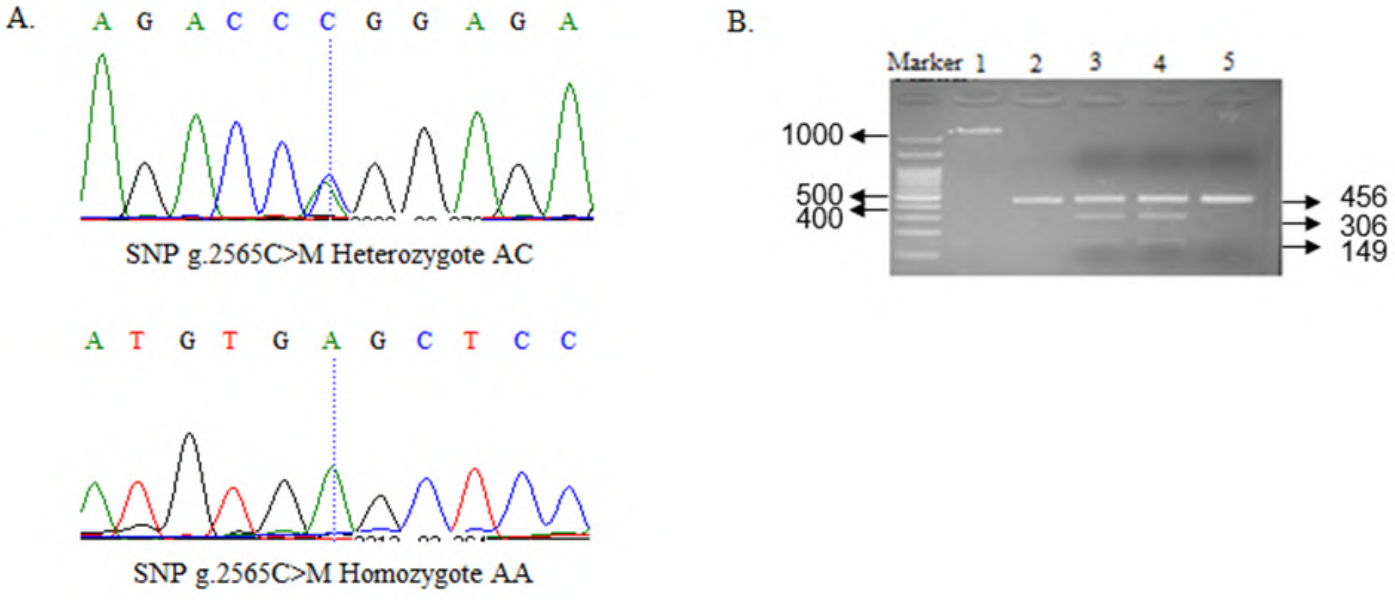

Figure 3. Chromatogram SNP g.2565C>M and PCR-RFLP with *MspI* enzyme. Note: A = Chromatogram of SNP g.2565C>M Heterozygote AC and Homozygote AA, B = Product size of PCR-RFLP in *GDF9* target gene of Bligon, PE, and Kacang goat. 1: DNA isolation, 2: Bligon goat, 3: Bligon goat (K62.1), 4: PE goat (K1), and 5: Kacang goat (B24) (Marker 100 bp, AA= genotype homozygote, AC= genotype heterozygote).

was 0.02, with a chi-square (χ^2) value of 0.01 for HWE. In Kacang goats, the AA genotype frequency was 0.69, while the AC genotype occurred in 0.31 of the animals (Table 3). The A allele had a frequency of 0.84, and the C allele had a frequency of 0.16, with a chi-square (χ^2) value of 0.28 for HWE.

The allele frequencies observed in the populations indicated polymorphism, as the frequency of the common C allele was lower than 0.99, confirming the polymorphic nature of the goat population.

Individuals with the AA genotype exhibited a fragment size of 456 bp, while homozygous AC individuals showed three fragment sizes: 456, 307, and 149 bp. The results from Pearson's Chi-square test indicated that the genotypes did not significantly deviate from Hardy-Weinberg equilibrium (HWE) ($P > 0.05$). Based on Hardy-Weinberg principles, this suggests that the allele and genotype frequencies in the population will remain stable across generations, provided there are no external influences, such as selection, mutations, migration, or inbreeding, that could affect the population randomly (Warwick et al. 1990).

The *MspI* restriction enzyme was used to identify genotypes in goats at position g.2565C>M. Previous studies by Feng et al. (2011), Ahlawat et al. (2015b), Chairunissa et al. (2022), and Hartatik et al. (2023) found two genotypes, AA and AC, in goats using *MspI*. The AA genotype showed a 456 bp fragment, the AC genotype showed fragments of 456, 307, and 149 bp, and the CC genotype showed 307 and 149 bp fragments. In this study, Bligon, PE, and Kacang goats showed only AA and AC genotypes, with AA being the most common. The absence of the CC genotype may be due to the small goat population in the study. The HWE test indicated that the genotypes in these populations were balanced, suggesting no issues like selection, mutation, migration, or inbreeding. More research is needed to explore the potential link between genotype and litter size in these goat populations.

CONCLUSIONS

Based on the research conducted, the restriction enzymes recommended for the target sequence SNP g.2565C>M are *HpaII* and *MspI*. PCR-RFLP analysis showed that only two genotypes (AA and AC) were found in Bligon, PE, and Kacang goats. Additionally, the AA genotype had the highest frequency compared to the heterozygous AC genotype. The HWE analysis showed that the genotype distribution of the *GDF9* gene in the Bligon, PE, and Kacang goat populations is stable. In conclusion, the *MspI* restriction enzyme can be used for genotyping the target gene in exon 2 of the *GDF9* gene in three types of goats: Bligon, PE, and Kacang.

AUTHOR CONTRIBUTION

F.J.F., D.P.S., N.P.N., F.A.C., and A.I. conducted the research and wrote the

Table 3. Genotype frequency, allele frequency, and Hardy–Weinberg equilibrium in Bligon, PE, and Kacang goats.

	Genotype (SNPs g.2565C>M)	N	Genotype frequency	Allele frequency	X^2
Bligon	AA	35	0.97	A = 0.98	
	AC	1	0.30	C = 0.02	0.14
	CC	0	0.00		
PE	AA	25	0.96	A = 0.98	
	AC	1	0.40	C = 0.02	0.01
	CC	0	0.00		
Kacang	AA	20	0.69	A = 0.84	
	AC	9	0.31	C = 0.16	0.28
	CC	0	0.00		

Note: X^2 value for a 0.05 significance level with df = 1 is 3.841.

manuscript. M.P.R., K., S.B., and T.H. performed data analysis and supervised the manuscript.

ACKNOWLEDGMENTS

This publication was financially supported by Rekognisi Tugas Akhir (RTA) Universitas Gadjah Mada in 2023, under assignment letter number 5075/UN1.P.II/Dit-Lit/PT/.01.01.2023. The authors would like to thank Retno Setyawati, the technical assistant at the Genetics and Animal Breeding Laboratory of UGM.

CONFLICT OF INTEREST

The authors have no conflicts of interest related to the research or the funding support for this study.

REFERENCES

Aboelhassan, D. M. et al., 2021. A study on mutation points of GDF9 gene and their association with prolificacy in Egyptian small ruminants. *Journal, Genetic Engineering & Biotechnology*, 19(1), 85. doi:10.1186/s43141-021-00181-8.

Ahlawat, S. et al., 2015a. Review article: Current status of molecular genetics research of goat fecundity. *Small Ruminant Research*, 125, pp.34-42. doi; 10.1016/j.smallrumres.2015.01.027

Ahlawat, S. et al., 2015b. Association analysis of novel SNPs in BMPR1B, BMP15 and *GDF9* genes with reproductive traits in Black Bengal goats. *Small Ruminant Research*, 132(1), pp.92-98. doi: 10.1080/10495398.2016.1167706.

Albakri, M.W. & Hartatik, T., 2021. Restriction mapping of melanocortin 4 receptor in Bos taurus and Bos indicus based on genbank data. *Research Journal of Biotechnology*, 16(1), pp.100–105.

Arta, P.D. & Rahayu, S., 2013. Analysis of Growth Differentiation Factor 9 (GDF-9) gene polymorphism and its relationship with the success of artificial insemination in PO cattle. *Journal of Biotropika*, 1(3), pp.95-100.

Chairunissa, F.A., Bintara, S. & Hartarik, T., 2022. Single nucleotide polymorphism of partial *GDF9* Gene in three local goats of Indonesia compared with several goats in Asia. *Bulletin of Animal Science*, 46(1), pp.41-45. doi: 10.21059/buletinpeternak.v46i1.67188.

Du, Z.Y. et al., 2008. Study on the polymorphisms of exon 2 of *GDF9* gene in Guizhou White goat. *Animal Husbandry & Veterinary Medicine*, 40(1), pp.46–48.

Feng, T. et al., 2011. Polymorphisms of caprine *GDF9* gene and their association with litter size in Jining Grey goats. *Molecular Biology Reports*, 38, pp.5189–5197. doi: 10.1007/s11033-010-0669-y.

Ghoreishi, H. et al., 2019. Identification of mutations in BMP15 and *GDF9* genes associated with prolificacy of Markhoz goats. *Archives Animal Breeding*, 62, pp.565–570. doi: 10.5194/aab-62-565-2019.

Ginting, S.P, 2009. *Prospek pengunaan pakan kompllit pada kambing: Tinjauan manfaat dan aspek bentuk fisik pakan serta respon ternak*. Loka Penelitian Kambing Potong, Sumatra Utara.

Hartatik, T. et al., 2023. Mutation Analysis and Restriction Site Mapping of *GDF9* in Indonesian Bligon Goat. *Tropical Animal Science Journal*, 46(2), pp.163-171. doi: 10.5398/tasj.2023.46.2.163.

Hossain, F., Sharmin, A.S. & Mohammad, S.A.B., 2020. Association of *GDF9* gene polymorphisms with litter size in indigenous sheep of Bangladesh. *Research Agriculture Livestock Fisheries*, 7(1), pp.283-292. doi: 10.3329/ralf.v7i2.48871.

Irawan, A. et al., 2024. Nutrient Digestibility, N Balance, Performance, and Blood Parameters of Kacang Goats Differing in GDF9 Genotype Fed Different Sources of Dietary Fiber. *Tropical Animal Science Journal*, 47 (1), pp.33-41.

Jia, X. et al., 2015. *GDF9* gene polymorphisms and its association with reproductive traits in livestock species. *Animal Reproduction Science*, 159(1), pp.45-53.

Kim, S., Park, J. & Lee, H., 2023. Combining SNP genotyping with PCR-RFLP: A tool for marker-assisted selection in animal breeding. *Animal Genetics*, 54(3), pp.244-253.

Liu, Y. & Chen, Z., 2020. Application of PCR-RFLP for detecting SNP markers in livestock breeding. *Livestock Science*, 234(1), pp.45-51.

Perdana, Y.C., 2022. *Identifikasi keragaman koding sekuen Gen MC4R (target III) serta hubunganya terhadap berat dan ukuran tubuh pada sapi persilangan tiga bangsa*. Universitas Gadjah Mada.

Perdana, Y. C. & Hartatik, T., 2022. Restriction mapping of MC4R gene on Bali Cattle (Bos sondaicus) as genetic marker for breeding program in compared to Bos taurus and Bos indicus. *Journal of Tropical Biodiversity and Biotechnology*, 7(2), jtbb67636. doi: 10.22146/jtbb.67636.

Prihandini P.W & Maharani, D. 2019. Melanocortin-4 receptor (MC4R) gene is the main gene for Fast Growth Selection in Beef Cattle. *Wartazoa*, 29 (2), pp.85-96. doi: 10.14710/jab.v%25vi%25i.20880.

Sarwono., 2011. *Beternak kambing unggul*, Jakarta: Penebar Swadaya.

Wang, L. et al., 2018. Impact of SNPs in the *GDF9* gene on reproductive traits in goats. *Animal Reproduction Science*, 195(1), pp.77-85.

Wang, X., Liu, H. & Zhang, X., 2021. Identification of SNP markers associated with growth traits in livestock using PCR-RFLP. *Journal of Animal Science and Biotechnology*, 12(1), pp.35-42.

Warwick, E.J., Astuti, J.M. & Hardjosubroto, W., 1990. *Pemuliaan Ternak*, Yogyakarta, Indonesia: Universitas Gadjah Mada Press..

Wouobeng, P. et al., 2020. Polymorphism of prolificacy genes (*BMP15*, *BMPR1B*, and *GDF9*) in the native goat (Capra hircus) of Cameroon. *Genetics & Biodiversity Journal*, 4(1), pp.28-43. doi: 10.46325/gabj.v4i1.69.

Zhao, L. et al., 2016. Rac1 modulates the formation of primordial follicles by facilitating STAT3-directed Jagged1, *GDF9* and BMP15 transcription in mice. *Scientific Reports*, 6, 23972. doi: 10.1038/srep23972.

Zhu, Y. et al., 2013. Comparison of SNPs in the *GDF9* gene in different goat breeds. *Journal of Animal Science*, 91(9), pp.4234-4241.

Journal of Tropical Biodiversity and Biotechnology
Volume 10, Issue 04 (2025): jtbb14436
DOI: 10.22146/jtbb.14436

Research Article

Photoprotective Effect of *Samia ricini* (Drury, 1773) Silkworm Cocoon Extract on Viability and Collagen Production in Human Dermal Fibroblast (HDF) Cells Induced by UVB Irradiation

Cintya Angelina[1], Slamet Widiyanto[2]*, Ardaning Nuriliani[3], Sukirno Sukirno[4]
1)Faculty of Biology, Universitas Gadjah Mada. Jl. Teknika Selatan, Sekip Utara, Yogyakarta 55281, Indonesia
2)Laboratory of Animal Physiology, Faculty of Biology, Universitas Gadjah Mada, Yogyakarta, Indonesia 55281
3)Laboratory of Animal Structure and Development, Faculty of Biology, Universitas Gadjah Mada, Yogyakarta, Indonesia 55281
4)Laboratory of Entomology, Faculty of Biology, Universitas Gadjah Mada. Jl. Teknika Selatan, Sekip Utara, Yogyakarta 55281, Indonesia
* Corresponding author, email: slametbio@ugm.ac.id

Keywords:
Human Dermal Fibroblast (HDF) Cell
Photoprotective
Sericin
Silkworm cocoon
UVB irradiation
Submitted:
02 July 2024
Accepted:
10 May 2025
Published:
08 December 2025
Editors:
Miftahul Ilmi
Tanti Agustina

ABSTRACT

UVB radiation (290–320 nm) induces oxidative stress, reducing cell viability and degrading collagen in human dermal fibroblasts (HDF). *Samia ricini*, a non-mulberry silkworm, produces sericin—a natural protein with antioxidant, UV-protective, and anti-aging properties. However, its photoprotective potential remains underexplored, particularly in Indonesia. This study investigates the protective effects of *Samia ricini* cocoon extract (EKUS) against UVB-induced damage in HDF cells, as evaluated by measuring cell viability using the MTT assay and collagen production through the Sirius Red assay. HDF cells seeded at 5×10^3 and 1×10^4 cells/well were irradiated with UVB (280 mJ cm^{-2}) and treated with EKUS at concentrations ranging from 15.625 to 1000 µg mL^{-1}. EKUS showed no cytotoxicity in normal HDF cells across this concentration range. Pre-treatment with 500 µg mL^{-1} EKUS maintained cell viability above 80 % post-UVB exposure. At 1000 µg mL^{-1}, EKUS significantly enhanced cell viability to 123.86 ± 16.77 % and 128.39 ± 13.22 % at 5×10^3 and 1×10^4 cells/well, respectively. In collagen assays, EKUS at 900 µg mL^{-1} increased collagen production to 146.30 ± 27.20 % (5×10^3 cells/well) and 189.04 ± 9.66 % (1×10^4 cells/well), compared to UVB-treated controls. These findings indicate that EKUS exhibits significant photoprotective effects by preserving cell viability and enhancing collagen synthesis in UVB-exposed HDF cells. Additional studies are suggested to confirm its potential in more intricate models.

How to cite:
Angelina, C. et al., 2025. Photoprotective Effect of *Samia ricini* (Drury, 1773) Silkworm Cocoon Extract on Viability and Collagen Production in Human Dermal Fibroblast (HDF) Cells Induced by UVB Irradiation. *Journal of Tropical Biodiversity and Biotechnology*, 10(4), jtbb14436. doi: 10.22146/jtbb.14436

INTRODUCTION

The skin, a crucial organ, plays a major protective role against environmental stressors such as pathogens, infections, chemicals, and ultraviolet (UV) rays. UV radiation consists of UVA (315–400 nm), UVB (290–320 nm), and UVC (100–280 nm). UVB radiation has the potential to damage the DNA and protein structure of skin cells, particularly in the epidermis (Salminen et al. 2022). UVB rays predominantly affect the skin, leading to increased production of matrix metalloproteinases (MMPs) and reduced collagen synthesis, resulting in photoaging (Jung et al. 2014). Photoaging is a condition of damage resulting from chronic exposure to UV light, which contributes to intrinsic skin aging (Pandel et al. 2013). UVB can elevate the production of reactive oxygen species (ROS) in skin cells, which can manifest possible detrimental effects on skin health (Amaro-ortiz et al. 2014). Thus, the skin's defence against increased ROS caused by UVB radiation must be maintained by an antioxidant system, which functions to fight ROS and maintain redox balance in the body (Kumar et al. 2018). UVB radiation is recognized for causing direct DNA damage and the production of ROS, which can lead to cellular senescence, apoptosis, and inflammation. In the case of Human Dermal Fibroblast (HDF) cells, UVB-induced ROS production contributes to the degradation of collagen, a major extracellular matrix protein responsible for skin's structural integrity and elasticity. Prolonged UV exposure disrupts collagen synthesis, leads to the breakdown of collagen fibres, and impairs the normal function of fibroblasts. These processes contribute to the visible signs of skin ageing, such as wrinkling and loss of skin firmness (Cavinato & Jansen-Dürr 2017). The antioxidant system, therefore, plays an essential role in protecting fibroblasts from oxidative damage caused by UV exposure and maintaining collagen homeostasis, which is vital for skin health and resilience.

Sericin, present in numerous silkworm cocoons, exhibits antioxidant properties (Liu et al. 2022) and provides protection against UV rays (Sukirno et al. 2022). Extracts of sericin from mulberry (*Antheraea assamensis*) and non-mulberry (*Philosamia ricin*) silkworm cocoons, at concentrations of 10 and 100 µg mL^{-1}, when administered UVB (120 mJ cm^{-2}) irradiation to HaCaT cells, exhibit UV-protective properties. This is achieved by enhancing cell viability by regulating IL-6 (Interleukin 6) and IL-8 (Interleukin 8), increasing p53, and reducing dysregulation of BCL-2/BAX gene expression (Kumar et al. 2018). Sericin also increases collagen production in HDF cells through MMP-2 regulation without having a cytotoxic effect, as well as increasing cell viability in UVB-irradiated HaCaT cells (Kanpipit et al. 2022). Sericin's antioxidant activity is mainly attributed to its ability to eliminate reactive oxygen species (ROS). Additionally, the presence of arginine and alanine residues enables sericin to interact with tyrosinase, an enzyme involved in melanogenesis, thereby exerting anti-tyrosinase activity. This dual function of antioxidant and enzyme-inhibitory action positions sericin as a promising bioactive compound for skin protection and anti-photoageing applications (Aad et al. 2024). Based on this, sericin derived from silkworm cocoons holds promise as a potential agent for protecting skin from ageing caused by exposure to UVB rays.

However, the protective activity of non-mulberry *Samia ricini* silkworm cocoon sericin extract (EKUS) against skin damage caused by UVB rays has not yet been widely explored in Indonesia. Thus, the aim of this study is to assess the ability of EKUS to protect human dermal fibroblast (HDF) cells from specific doses of UVB radiation. Sericin extract obtained from the *Samia ricini* cocoons has potential as a therapeutic agent aimed at protecting skin cells and treating skin problems caused by UVB exposure. This potential can be applied to the development of more innovative and sustainable skincare products for photoageing prevention.

MATERIALS AND METHODS

Materials

Sirius Red staining, MTT (Thiazolyl blue tetrazolium bromide), and complete DMEM Low Glucose medium, which contains 10 % FBS, 0.5 % fungizone (Gibco), and 2 % penicillin-streptomycin (Gibco), dimethyl sulfoxide (DMSO) (Merck), 0.25 % trypsin-EDTA, aquades, sodium bicarbonate (HEPES), 10 % solution of SDS (sodium dodecyl sulfate) in 0.01 N HCl, ethanol (Merck GmbH), Dulbecco's phosphate buffered saline (PBS), Bouin's solution.

Methods

Cell Culture

Human dermal fibroblast (HDF) cells were obtained from the Department of Dermatology and Venereology, Faculty of Medicine, Public Health, and Nursing at Universitas Gadjah Mada (UGM). The cells were maintained in DMEM (Dulbecco's Modified Eagle's Medium) supplemented with 10 % heat-inactivated fetal bovine serum (FBS), along with 100 U mL^{-1} penicillin and 100 µg mL^{-1} streptomycin (Invitrogen, Carlsbad, CA, USA). The cells were incubated at 37 °C in a humidified environment containing 5 % CO_2. Subculturing was performed using trypsinisation to establish a new culture. This protocol received approval from the Medical and Health Research Ethics Committee of the Faculty of Medicine, Public Health, and Nursing, Universitas Gadjah Mada (KE/FK/1170/EC/2023).

Extraction of *Samia ricini* Cocoon

Cocoons of *Samia ricini* were obtained from the Jantra Mas Sejahtera (JAMTRA) wild silk production facility in Yogyakarta, Indonesia. The extraction method was modified based on the procedure described by Rocha et al. (2017). Cocoon pieces (15 g) were autoclaved in 1000 mL of ultrapure water (aquatridest) at 120 °C for 60 minutes. The resulting solution was vacuum-filtered using a Buchner funnel. The filtrate was aliquoted into multiple glass flasks and subsequently frozen at −86 °C and lyophilised for 48 hours. The crude extract was then ground using a mortar and kept at −20 °C until further use. Based on an average cocoon weight of 0.2–0.3 grams, approximately 50 to 75 cocoons were used in this extraction. The larvae producing these cocoons typically have a body weight range of 2–3 grams during the final instar stage.

For biological assays, serial dilutions of the crude extract (EKUS) were prepared by diluting the stock solution in complete medium, ensuring that the DMSO concentration did not surpass 1 %.

Optimization of UVB Irradiation

Control and treated cells were washed and subsequently covered with phosphate-buffered saline prior to UVB irradiation, and irradiated with UVB light (Broadband/Narrowband Ultraviolet B, Puslit KIM – LIPI) with a wavelength of 290 nm at a distance of 40 cm. After UVB radiation at different dosages (70, 140, 280 mJ cm^{-2}), the cells were rinsed three times with phosphate-buffered saline, then incubated at 37 °C for 24 hours in a humidified atmosphere containing 5 % CO_2. The specific UVB dose is interpreted in terms of exposure time (seconds), which is calculated based on the calibration by Laboratory of Dermatology and Venereology, Faculty of Medicine, Public Health, and Nursing, University of Gadjah Mada.

Cytotoxicity test of cocoon extract on normal HDF cells

HDF cells (5×10^3 and 10^4 cells per well) were plated in a 96-well tissue culture plate and cultured until they reached 80–90 % confluency. EKUS at con-

centrations of 0;15,625; 31,25; 62,5; 125; 250; 500; and 1000 µg mL^{-1} was applied to the cells for 24 hours at 37 °C in a humidified environment with 5 % CO_2. Afterwards, the cells were treated with MTT solution for 4 hours, after which the formazan crystals were dissolved in 10 % SDS. The optical density was measured using a multiplate reader (Bio-Rad) at 570 nm.

Cytoprotective test using the MTT assay

To assess the potential of EKUS in protecting HDF cells from UVB radiation, the cells were pre-treated with 0;15,625; 31,25; 62,5; 125; 250; 500; and 1000 µg mL^{-1} EKUS for 24 hours, followed by exposure to UVB light at dosage 280 mJ cm^{-2} (344 sec), then cultured at 37 °C for 24 hours. Afterward, MTT stock solution was introduced into each well. After incubating the cells for four hours, the medium were removed. The formazan deposits present in each well were solubilised with 10 % SDS, and the absorbance was measured at 570 nm.

Analysis of collagen production with Sirius red assay

The collagen production test followed the method of Szász et al. (2023), with modifications. HDF cells were incubated with EKUS for 48 h, and exposed to UVB (280 mJ cm^{-2}). The culture medium was removed, subsequently, the cells were rinsed with 200 µL of phosphate-buffered saline (PBS) followed by fixation using Bouin's solution at room temperature overnight. Following an additional wash with 200 µL of PBS, cell staining was performed by introducing 50 µL of a 0.1 % Sirius Red (Direct Red 80) solution dissolved in 1 % acetic acid. The plates were allowed to stand at room temperature for 1 hour, after which the wells were rinsed with 0.1 M HCl. Next, each well was treated with a 0.1 M NaOH solution to release the dye attached to the collagens associated with the cells. The optical density (OD) of the solutions was then measured at 550 nm using a Tecan Spark 20M microplate reader.

Statistical analysis

Each measurement was carried out in triplicate, and the results are presented as the mean ± standard error. Statistical analysis was performed using a one-way analysis of variance (ANOVA), subsequently analysed using Duncan's post hoc test to evaluate differences among the means, assuming normality and homogeneity of variances.

RESULTS AND DISCUSSION

Samia ricini (Drury, 1773) Silkworm Cocoon Extraction

The extraction of sericin using autoclaving followed by lyophilisation produced a brownish powder (Figure 1), indicating successful separation of sericin from the *Samia ricini* cocoon. This method is widely regarded as simple and efficient, yielding a clean extract suitable for further applications (Chlapandias et al. 2013). In this study, the extract yield was approximately 4.3 g, equivalent to 28.6 % (w w^{-1}), which is notably higher than the 18 % (w w^{-1}) yield reported by Rocha et al. (2017) using a similar method. This difference may be attributed to variations in the freezing/thawing process prior to lyophilisation, which influences fibroin deposition and sericin separation from the cocoon.

Although effective, autoclaving can degrade sericin due to high heat and pressure. This degradation occurs through peptide bond hydrolysis, breaking the protein into smaller fragments (Gupta et al. 2014). Such changes may reduce its antioxidant activity and overall biofunction, especially with prolonged or excessive heat, which can denature the protein and damage key amino acids critical for its protective role. The extent of degradation is influenced by several parameters, particularly the temperature and duration of the

autoclave cycle. For example, Wang et al. (2021) demonstrated that extraction yields increase with temperature, reporting a maximum yield of 36.5 % ± 0.4 % at 220 °C. However, such high temperatures also increase the risk of protein breakdown. In contrast, extraction at 120 °C, as reported by Gimenes et al. (2014), typically yields between 21 % and 30 %, offering a compromise between yield and protein integrity. Therefore, careful optimisation of autoclaving conditions is essential. In this study, the conditions were controlled to minimise degradation, balancing between maintaining sericin's functional properties and achieving a high yield.

To maintain sericin's bioactivity, it is important to use the lowest effective autoclaving temperature and shortest duration, followed by immediate lyophilisation to reduce heat and moisture exposure. Rocha et al. (2017) showed that this method preserves antioxidant activity. Given sericin's capacity to counteract free radicals and diminish oxidative stress, this study explores the protective effect of *Samia ricini* sericin extract (EKUS) to prevent UVB-triggered damage in HDF.

Figure. 1 *Samia ricini* silkworm cocoon extraction results.

Optimization of UVB Irradiation

An increasing trend in UVB dose appeared to reduce HDF cell viability, although no statistically significant differences were observed ($p > 0.05$) (Figure 2A). HDF cells were subjected to UVB exposure for 86, 172, and 344 seconds, corresponding to energy doses of 70, 140, and 280 mJ cm^{-2}, respectively. At a seeding density of 5×10^3 cells/well, cell viability was recorded as 90.06 % ± 14.42, 85.85 % ± 17.41, and 78.34 % ± 8.85 for each respective dose. Despite the lack of statistical significance, these values indicate a clear dose-dependent downward trend, suggesting potential biological relevance. This trend aligns with findings by Zheng et al. (2019), who reported that UVB-induced reductions in HDF viability depend on both the dose and duration of exposure. UVB radiation is known to exert cytotoxic effects by promoting DNA damage, increasing reactive oxygen species (ROS), impairing collagen homeostasis, and disrupting proteasome activity—mechanisms that contribute to cellular senescence and apoptosis (Cavinato & Jansen-Dürr 2017).

The viability decrease at 280 mJ cm^{-2} did not exceed 50 %, but it still represented a substantial reduction of approximately 24–30 % compared to the control group. This partial yet measurable decline in cell viability was deemed suitable for further analysis, especially for assessing the protective effects of compounds such as EKUS. Using a dose that causes complete cytotoxicity could obscure potential protective responses, while a sub-lethal but biologically significant dose like 280 mJ cm^{-2} provides an optimal condition to evaluate cellular responses to damage and recovery.

The selection of 280 mJ cm^{-2} is further supported by previous studies. Debacq-Chainiaux et al. (2005) described sub-cytotoxic effects at 250 mJ cm^{-2}, which were sufficient to induce stress responses without total loss of viability.

Similarly, Dobrzyńska et al. (2016) reported 200 mJ cm^{-2} as an efficient dose to induce measurable UVB-induced cellular damage in fibroblasts. Based on these findings, 280 mJ cm^{-2} represents a physiologically relevant and biologically effective dose that triggers measurable cell stress and viability reduction while avoiding complete cytotoxicity, making it suitable for evaluating the potential protective effects of EKUS.

Additionally, seeding density was shown to influence UVB response. At a higher cell density of 1×10^4 cells/well, viability initially increased with doses up to 140 mJ cm^{-2} but decreased at 280 mJ cm^{-2} (Figure 2B). These observations suggest that cell-to-cell contact, UV absorption, and the distribution of UV-sensitive components such as chromophores can influence outcomes (Cavinato & Jansen-Dürr 2017). Thus, while statistical significance was not achieved in this initial assay, the biological relevance of the chosen UVB dose is strongly supported by the literature and forms a rational basis for testing the protective efficacy of EKUS in subsequent experiments.

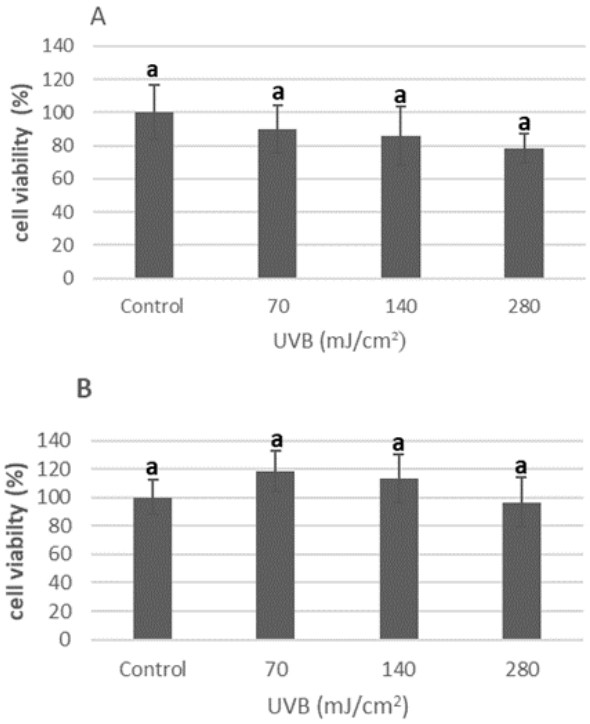

Figure 2. Effect of UVB radiation on HDF cell viability (A) cell density $5x10^3$ cells/well (B) density of 10^4 cells/well evaluated using the MTT assay.

Cytotoxic effect of EKUS on normal HDF cells

EKUS was dissolved in 1 % DMSO because it did not affect drug binding but increased the solubility of the compound (Nguyen et al. 2020). The results of this study indicated that the percentage of live HDF cells in DMSO treatment (Figure 3) at a density of $5x10^3$ and 10^4 cells/well was 84.07 ± 15.97 % and 103.70 ± 12.49 %, respectively. This shows that cells remain viable at a DMSO concentration of 1 %, indicating it is not toxic. This is consistent with the study conducted by Nguyen et al. (2020), which reported that using DMSO at concentration of 0.5-3 % as a drug solvent for the proliferation of skin fibroblast cells does not cause cell death.

EKUS preserved HDF cell viability above 80 % across all tested concentrations (Figure 3). It demonstrated non-toxicity towards HDF cells, with cell viability showing a tendency to rise with increasing EKUS concentration. The data revealed that no meaningful difference was observed ($p\leq0.005$) between EKUS concentrations on cell viability at a density of $5x10^3$ cells/well (Figure 3A.) when contrasted with the control cells. However, HDF cells

treated with EKUS 250, 500 and 1000 µg mL^{-1} increased cell viability by 86.11 ± 12.40 %; 89.93 ± 18.06 % and 117.96 ± 18.78 %, respectively (Figure 3A) High concentrations of EKUS (500-1000 µg mL^{-1}) significantly ($p \leq 0.005$) increased cell viability to <160 % at a cell density of 10^4 cells/well (Figure 3B). This result aligns with previous studies, such as Rocha et al. (2017), which showed that the highest concentration of cocoon extract, when prepared using lyophilisation, exhibited mitochondrial restoration activity in HUVEC cells. The role of sericin in regulating cell growth and viability is concentration-dependent, and in fibroblasts, *S. ricini* sericin has been noted to enhance cell proliferation within 3 days (Sahu et al. 2016). Similarly, sericin extracted from other silk species, such as *Antheraea assamensis*, *Philosamia ricini*, and *Bombyx mori*, has been shown to significantly increase mouse fibroblast proliferation at concentrations up to 400 µg mL^{-1} (Kumar & Mandal 2017). These findings support the conclusion that EKUS promotes cell proliferation without inducing toxicity in HDF cells. However, it is important to consider the potential side effects and long-term toxicity of EKUS, particularly at higher concentrations. Future studies should evaluate these aspects to ensure the safety and efficacy of EKUS for therapeutic use, especially regarding its prolonged exposure or chronic use in clinical applications.

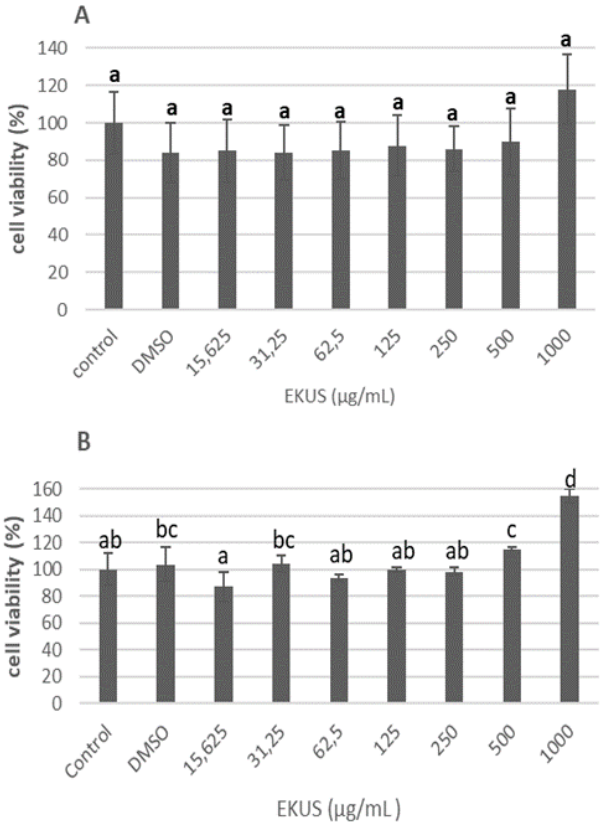

Figure 3. Cytotoxicity effect of EKUS on HDF cells (A) density $5x10^3$ cells/well (B) density 10^4 cells/well.

Protective activity of EKUS on HDF cells against UVB irradiation

The primary objective of this research was to evaluate the cytoprotective activity of EKUS in human dermal fibroblasts (HDF) subjected to UVB radiation at a dose of 280 mJ cm^{-2}. UVB irradiation is known to induce cellular damage through mechanisms like increased ROS production, DNA damage, and the initiation of apoptosis. Sericin, a protein found in silk, has been recognised for its antioxidant properties, which help neutralise free radicals and mitigate UVB-induced damage (Kumar et al. 2018). In this study, EKUS was tested for its ability to protect HDF cells from UVB-induced cell death.

The results indicated a trend towards reduced cell viability with in-

creasing UVB exposure, with a 20–30 % decrease in viability compared to control cells. However, this decline was not found to be statistically significant ($p>0.05$) (Figure 4). This aligns with the work of Sajeeda et al. (2024), who observed that UVB exposure modulates the expression of key apoptotic proteins, including a decrease in the anti-apoptotic protein BCL-2 and an up-regulation of the pro-apoptotic protein BAX in HDF cells. While BAX facilitates cell death, BCL-2 prevents apoptosis by counteracting BAX's activity (Khodapasand et al. 2015). In our study, EKUS treatment, at concentrations below 500 µg mL^{-1}, did not significantly modulate the BCL-2/BAX expression profile, nor did it prevent the DNA damage induced by UVB. This suggests that while EKUS contains antioxidant compounds, they may not be sufficient at these concentrations to fully counteract the dysregulation of these apoptotic pathways.

Interestingly, EKUS at higher concentrations (500–1000 µg mL^{-1}) significantly improved cell viability, maintaining it above 80 % and up to 128.39 % ± 13.22 % at a concentration of 1000 µg mL^{-1}, the highest tested (Figures 4A and 4B). These findings suggest that EKUS can offer significant protection against UVB-induced damage at higher concentrations. This protective effect may be attributed to the cumulative antioxidant activity of sericin, which, at these concentrations, is sufficient to reduce ROS levels and promote cell survival. The antioxidant properties of sericin are mainly due to its ability to neutralize reactive oxygen species (ROS), a function that is amplified by its high levels of polar amino acids like serine and threonine. These amino acids contribute to metal-chelating activity by binding transition metal ions like copper and iron, which are known to catalyse ROS generation via Fenton-type reactions (Aad et al. 2024). These findings are in agreement with previous research by Kumar et al. (2018), who showed that silk sericin extracted from *Philosamia ricini*, a non-mulberry silkworm species, was effective at protecting cells from UV radiation at lower concentrations. However, the discrepancies in protective effects between our study and Kumar et al. (2018) are likely due to differences in extraction methods. The lyophilisation method used in our study may have produced a sericin extract with higher bioactivity compared to the methods used by Kumar et al. (2018), who observed differing effects of sericin based on its extraction method.

Despite these promising findings, the study has several limitations. First, only one cell type, HDF, was utilized in this study. While HDF cells are an important model for studying skin responses, they do not fully capture the complexity of skin's response to UVB radiation, which involves multiple cell types such as keratinocytes. Therefore, the observed protective effects of EKUS may not necessarily extend to other cell types involved in skin damage. Second, this study was conducted entirely in vitro, which limits the translational value of the results. While HDF cell cultures provide a controlled environment for studying cellular mechanisms, they fail to replicate the in vivo complexity of UVB exposure, such as skin's multi-layered structure, the role of immune responses, and the impact of environmental factors. Future research using in vivo models will be essential for a more thorough understanding of the systemic effects and efficacy of EKUS in protecting skin from UVB-induced damage.

While EKUS showed protective effects at higher concentrations, optimizing dosage and treatment time is needed to determine the most effective level for skin protection. Further research should also explore the molecular pathways involved, including antioxidant and anti-inflammatory mechanisms. In conclusion, EKUS effectively protected HDF cells from UVB-induced damage at higher concentrations, significantly improving cell viability. However, limitations such as the use of a single cell type and the absence of in vivo studies highlight the need for further research in more complex models to validate its efficacy and mechanisms.

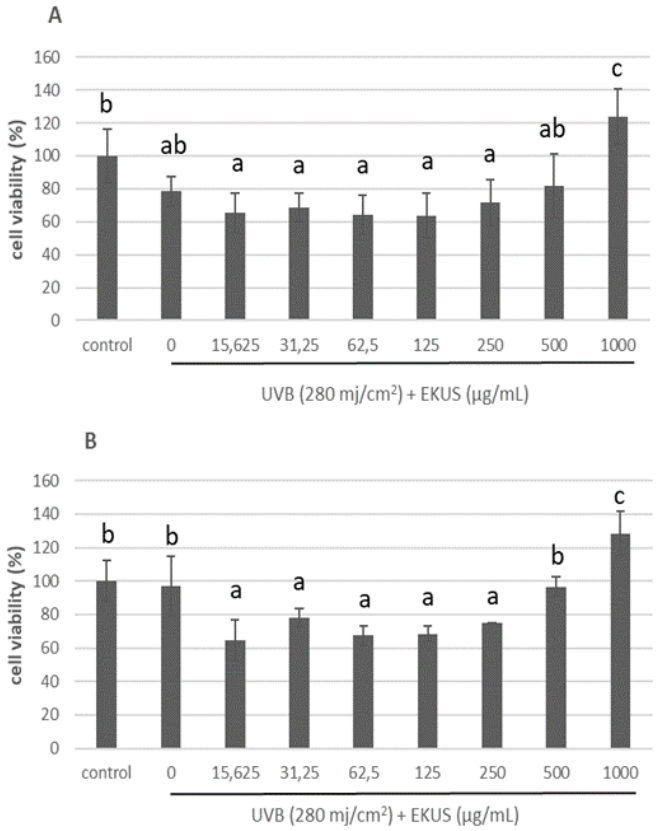

Figure 4. Cytoprotective effect of EKUS against UVB irradiation of 280 mJ cm^{-2} on HDF cells (A) cell density $5x10^3$ cells/well (B) density 10^3 cells/well.

Effect of EKUS on collagen production in UVB irradiated HDF cells

Collagen production is one of the parameters used to determine the protective effect of EKUS on HDF cell damage that is irradiated with UVB using Sirius red staining. Optimal collagen deposition with the right ratio is very important to prevent tissue damage during connective tissue formation (Su et al. 2019). HDF cells were incubated with EKUS for 48 hours, then exposed to UVB light at a dose of 280 mJ cm^{-2} for 344 s. UVB rays cause degradation of collagen synthesis, which causes skin ageing (Jung et al. 2014). In this study, UVB irradiation was able to reduce collagen deposition significantly ($p \leq 0.005$) compared to control cells. In fibroblast cells that only received UVB irradiation, the viability was only 58.08 ± 6.43 % (density $5x10^3$/well) and 62.60 ± 19.16 % (cell density 10^4/well). The results indicated that changes in EKUS concentration significantly impacted ($p \leq 0.005$) collagen deposition ratio in fibroblasts compared to cells that only received UVB irradiation (Figure 5).

EKUS treatment prior to UVB exposure on HDF cells ($5x10^3$ cells/well) began to increase collagen production significantly ($p \leq 0.005$) at concentration of ≥ 600 µg mL^{-1} (Figure 5A). Meanwhile, at a cell density of 10^4/well significantly at a concentration of ≥ 250 µg mL^{-1} (Figure 5B). The most effective EKUS treatment for enhancing collagen production is at a concentration of 900 µg mL^{-1}. This concentration significantly ($p \leq 0.005$) increased collagen production by <198 %. At a cell density of $5x10^3$/well the collage production value was 146.30 ± 27.20 % and at a cell density of 10^4/well the value was 189.04 ± 9.66 %. However, the effect started to decline to 20 % when reaching a concentration of 1000 µg mL^{-1} across two different cell densities (Figure 5). In line with research by Aramwit et al. (2010) silk sericin extracted using the high-heat method at concentrations of >200 µg mL^{-1} can induce collagen production in L929 mouse fibroblast cells after incubation for 24 hours. According to Aramwit et al. (2009), silk sericin enhances collagen

synthesis in fibroblast cells because of its amino acid composition, particularly methionine and cysteine. In experiments conducted by Su et al. (2019) on human fibroblasts, it was demonstrated that mulberry sericin (0.05 %) promotes cell proliferation and enhances the expression of type I and III collagen. Therefore, this study demonstrates that EKUS can protect HDF cells from UVB rays by increasing collagen production.

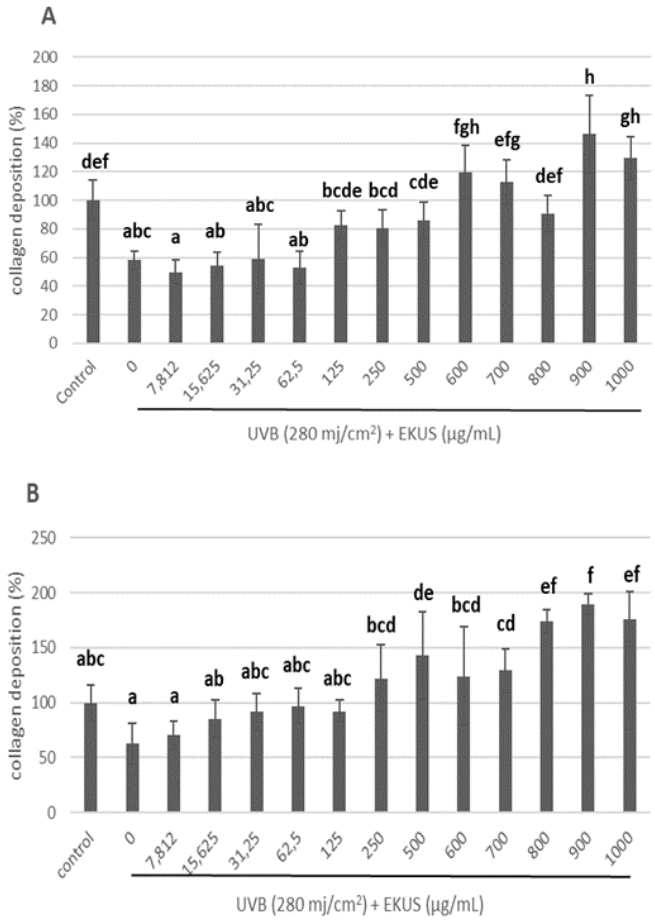

Figure 5. Effect of EKUS on collagen deposition in HDF cells exposed to 280 mJ cm $^{-2}$ UVB radiation (A) density 5x10^{3} cells/well (B) density 10^{4} cells/well.

CONCLUSION

EKUS exhibits protective effects on HDF cells against UVB irradiation by enhancing cell viability within a concentration range of 500 µg mL^{-1} to 1000 µg mL^{-1}. A concentration of 900 µg mL^{-1} of EKUS was found to maximise collagen production in UVB-exposed HDF cells, reaching up to <198 % of the untreated UVB group. Collagen is a key structural protein in the dermis, and its degradation is a hallmark of UV-induced skin damage. UVB radiation elevates levels of reactive oxygen species (ROS), triggering oxidative stress that disrupts fibroblast function and speeds up collagen degradation. EKUS, rich in sericin peptides, likely exerts its photoprotective effects through antioxidant activity that mitigates ROS-induced damage, preserves fibroblast viability, and supports collagen synthesis. By enhancing both cell survival and extracellular matrix integrity, EKUS shows promise as a potential therapeutic candidate for preventing UVB-induced skin ageing.

AUTHORS CONTRIBUTION

C.A. conceived and designed the experiment, conducted the procedures, collected and processed the data, and authored the manuscript. S.W., A.N., S.S. arranged, managed, and directed the experiment, made critical revisions, and endorsed the final version.

ACKNOWLEDGMENTS

The authors acknowledge the financial support for this research by Hibah Rekognisi Tugas Akhir (RTA Grant) University of Gadjah Mada (Number: 2338/UN1/DITLIT/Dit-Lit/PT.01.00/2023).

CONFLICT OF INTEREST

The authors declare that they have no conflict of interest from this manuscript.

REFERENCES

Aad, R., Dragojlov, I. & Vesentini, S., 2024. Sericin Protein: Structure, Properties, and Applications. *Journal of Functional Biomaterials*, 15(11), 322.

Amaro-Ortiz, A., Yan, B. & D'Orazio, J.A., 2014. Ultraviolet radiation, aging and the skin: prevention of damage by topical cAMP manipulation. *Molecules*, 19(5), pp.6202-6219. doi: 10.3390/molecules19056202

Aramwit, P. et al., 2009. The effect of sericin with variable amino-acidcontent from different silk strains on the production of collagenand nitric oxide. *Journal of Biomaterials Science, Polymer Edition*, 20(9), pp.1295-1306 . doi: 10.1163/156856209X453006

Aramwit, P. et al., 2010. The effect of sericin from various extraction methods on cell viability and collagen production. *International Journal of Molecular Sciences*, 11(5), pp.2200-2211. doi: 10.3390/ijms11052200

Cavinato, M. & Jansen-Dürr, P., 2017. Molecular mechanisms of UVB-induced senescence of dermal fibroblasts and its relevance for photoaging of the human skin. *Experimental gerontology*, 94, pp.78-82. doi: 10.1016/j.exger.2017.01.009

Chlapandias, T. et al., 2013. Sericin exhibits ROS scavangingactivity, anti-tyrosinase, anti-elastase, and invitro immunomodulatory activities. *International Journal of Biological Macromolecules*, 58, pp.47-56. doi: 10.1016/j.ijbiomac.2013.03.054.

Debacq-Chainiaux, F. et al., 2005. Repeated exposure of human skin fibroblasts to UVB at subcytotoxic level triggers premature senescence through the TGF-β1 signaling pathway. *Journal of cell science*, 118(4), pp.743-758. doi: 10.1242/jcs.01651

Dobrzyńska, I. et al., 2016. Effects of UVB radiation on the physicochemical properties of fibroblasts and keratinocytes. *The Journal of Membrane Biology*, 249(3), pp.319-325. doi: 10.1007/s00232-016-9870-9

Gimenes, M.L. et al., 2014. High molecular sericin from Bombyx mori cocoons: extraction and recovering by ultrafiltration. *International Journal of Chemical Engineering and Applications*, 5(3), 266. doi: 10.7763/IJCEA.2014.V5.391

Gupta, D., Agrawal, A. & Rangi, A., 2014. Extraction and characterization of silk sericin. *Indian Journal of Fibre & Textile Research (IJFTR)*, 39(4), pp.364-372. doi: 10.56042/ijftr.v39i4.3446

Jung, H. et al., 2014. Pinus Densiflora Extract Protects Human Skin Fibroblasts Against UVB Induced Photoaging by Inhibiting The Expression of MMPs and Increasing Type I Procollagen Expression. *Toxicology Reports*, 1, pp.658–666. doi: 10.1016/j.toxrep.2014.08.010

Kanpipit, N., Nualkaew, N. & Thapphasaraphong, S., 2022. The potential of purple waxy corn cob (Zea mays L.) extract loaded-sericin hydrogel for anti-hyperpigmentation, UV protection and anti-aging properties as topical product applications. *Pharmaceuticals*, 16(1), 35. doi: 10.3390/ph16010035

Khodapasand, E. et al., 2015. Is Bax/Bcl-2 ratio considered as a prognostic marker with age and tumor location in colorectal cancer? *Iranian biomedical journal*, 19(2), 69. doi: 10.6091/ibj.1366.2015

Kumar, J.P. & Mandal, B.B., 2017. Antioxidant potential of mulberry and non-mulberry silk sericin and its implications in biomedicine. *Free Radical Biology and Medicine*, 108, pp.803-818. doi: 10.1016/j.freeradbiomed.2017.05.002

Kumar, J.P. et al., 2018. Protective activity of silk sericin against UV radiation-induced skin damage by downregulating oxidative stress. *ACS Applied Bio Materials*, 1(6), pp.2120-2132. doi: 10.1021/acsabm.8b00558

Liu, J. et al., 2022. Silk sericin-based materials for biomedical applications. *Biomaterials*, 287, 121638. doi: 10.1016/j.biomaterials.2022.121638

Nguyen, S.T., Nguyen, H.T.L. & Truong, K.D., 2020. Comparative cytotoxic effects of methanol, ethanol and DMSO on human cancer cell lines. *Biomedical Research and Therapy*, 7(7), pp.3855-3859. doi: 10.15419/bmrat.v7i7.614

Pandel, R. et al., 2013. Skin photoaging and the role of antioxidants in its prevention. *International Scholarly Research Notices*, 2013(1), 930164. doi: 10.1155/2013/930164

Rocha, L.K. et al., 2017. Sericin from Bombyx mori cocoons. Part I: Extraction and physicochemical-biological characterization for biopharmaceutical applications. *Process Biochemistry*, 61, pp.163-177. doi: 10.1016/j.procbio.2017.06.019

Sahu, N. et al., 2016. Non-mulberry and mulberry silk protein sericins as potential media supplement for animal cell culture. *BioMed Research International*, 2016(1), 7461041. doi: 10.1155/2016/7461041

Sajeeda, A. et al., 2024. Naringenin, a flavanone constituent from Sea buckthorn pulp extract, prevents ultraviolet (UV)-B radiation-induced skin damage via alleviation of impaired mitochondrial dynamics mediated inflammation in human dermal fibroblasts and Balb/c mice models. *Journal of Photochemistry and Photobiology B: Biology*, 256, 112944. doi: 10.1016/j.jphotobiol.2024.112944

Salminen, A., Kaarniranta, K. & Kauppinen, A., 2022. Photoaging: UV radiation-induced inflammation and immunosuppression accelerate the aging process in the skin. *Inflammation Research*, 71(7-8), pp.817-831. doi: 10.1007/s00011-022-01598-8

Su, D. et al., 2019. *Bombyx mori* silk-based materials with implication in skin repair: Sericin versus regenerated silk fibroin. *Journal of Biomaterials Applications*, 34(1), pp.36-46. doi: 10.1177/0885328219844978

Sukirno, S. et al., 2022. The effectiveness of Samia ricini Drury (Lepidoptera: Saturniidae) and Attacus atlas L. (Lepidoptera: Saturniidae) cocoon extracts as ultraviolet protectants of Bacillus thuringiensis for controlling Spodoptera litura Fab. (Lepidoptera: Noctuidae). *International Journal of Tropical Insect Science*, 42(1), pp.255-260. doi: 10.1007/s42690-021-00540-5

Szász, C. et al., 2023. Optimization of Sirius Red-Based Microplate Assay to Investigate Collagen Production In Vitro. *International Journal of Molecular Sciences*, 24(24), 17435. doi: 10.3390/ijms242417435

Wang, X., Chen, Q. & Lü, X., 2014. Pectin extracted from apple pomace and citrus peel by subcritical water. *Food Hydrocolloids*, 38, pp.129-137. doi: 10.1016/j.foodhyd.2013.12.003

Journal of Tropical Biodiversity and Biotechnology
Volume 10, Issue 04 (2025): jtbb14181
DOI: 10.22146/jtbb.14181

Review Article

A Decade of Discovering New *Nepenthes* Species in Southeast Asia: A Review

Sri Wahyu Imamah[1], Maya Safitri[1], Rr Khoirunnisa Asyahidah[1], Siti Arfa Jamlean[1], Khairunnisak[1], Bambang Irawan[1], Firli Rahmah Primula Dewi[1]*

1)Department of Biology, Faculty of Science and Technology, Universitas Airlangga. Jl. Dr. Ir. H. Soekarno, Mulyorejo, Surabaya 60115, Indonesia

* Corresponding author, email: firli.rahmah@fst.unair.ac.id

Keywords:
Conservation
Carnivorous
Identification
New species
Plant diversity
Taxonomy

Submitted:
21 June 2024

Accepted:
15 July 2025

Published:
27 October 2025

Editors:
Miftahul Ilmi
Sri Nopitasari

ABSTRACT

Nepenthes is the largest genus of carnivorous pitcher plants, with the highest diversity in Southeast Asia, where an estimated 50,000 flowering plant species exist. The estimated plant diversity in this region continues to grow with the discovery of many new species in countries such as Myanmar, Thailand, Cambodia, Laos, Vietnam, Malaysia, Singapore, Brunei Darussalam, Indonesia, Timor-Leste, the Philippines, and Papua New Guinea. Approximately 180 species of *Nepenthes* have been identified. The number of species in Southeast Asian countries is likely underestimated due to the lack of taxonomic research on groups with many local endemic species, suggesting that many new *Nepenthes* species remain unidentified. Therefore, this mini-review aims to reveal new *Nepenthes* species discovered in Southeast Asia over the past ten years. Data were collected from various journals, including Phytotaxa, Kalpataru, Philippine Journal of Science, Philippine Journal of Systematic Biology, Plants, Thailand Forest Bulletin, Phytokeys, Journal of Sustainable Natural Resources, Reinwardtia, Kew Bulletin, PeerJ, Carnivorous Plant Newsletter, Malayan Nature Journal, and Journal of Plant Taxonomy and Geography. The collected data were analysed based on the description of *Nepenthes* sp. nov., year of discovery, and distribution area. The identification of new species was based on differences in morphological, anatomical, and molecular characteristics. Thirty-seven new *Nepenthes* species were discovered in Southeast Asia in the past decade. These findings highlight the need for comprehensive surveys in understudied areas. Future efforts should combine molecular and ecological approaches to improve species discovery and guide conservation strategies addressing habitat loss and climate impacts.

How to cite:
Imamah, S.W. et al., 2025. A Decade of Discovering New *Nepenthes* Species in Southeast Asia: A Review. *Journal of Tropical Biodiversity and Biotechnology*, 10(4), jtbb14181. doi: 10.22146/jtbb.14181

INTRODUCTION

Carnivorous plants have fascinated scientists and the general public since the pioneering studies of Charles Darwin. Carnivorous plants are defined as plants that have the ability to absorb decomposed prey products through their leaves or roots to enhance their growth or reproduction. The term holocarnivorous, or true carnivorous, refers to plants that can attract, capture, digest, and utilise the metabolic products for their own growth. For example, *Heliamphora* cannot supply the enzymes for insect digestion and requires the help of microbes in passive traps (Givnish 2015; Thorogood et al. 2018; Mithöfer 2022). There are five families that include carnivorous plants: Droseraceae (which contains three genera), Drosophyllaceae (with only one species), Dioncophyllaceae (with only one genus), Ancistrocladaceae, and Nepenthaceae (with only one genus) (Wójciak et al. 2023).

Nepenthes is a tropical climbing carnivorous plant commonly known as the pitcher plant and is one of the most intriguing groups of carnivorous plants to study in the field of botany. These plants grow singly or in groups in various habitats with nutrient-poor and easily assimilable substrates (Gaume et al. 2016; Setiawan et al. 2018; Mansur et al. 2021). *Nepenthes* belongs to the family Nepenthaceae and was first scientifically described by the French biologist Étienne Geoffroy Saint-Hilaire in 1802 (Bauer et al. 2016).

A distinctive feature that sets *Nepenthes* apart from other plants is its leaves, which have evolved into uniquely shaped pitchers that function to trap and digest insects and other small organisms (Buch et al. 2014). These pitchers typically contain enzymatic fluids that help digest the trapped prey. The modified leaves have several important parts, such as the lid, which prevents rainwater from entering the pitcher, the peristome or pitcher lip, which is slippery and ridged to prevent prey from escaping, and nectar glands that attract insects (King & Cheek 2020). When insects perch on the pitcher, they fall into the trap and are digested by the enzyme mixture in the pitcher fluid. Additionally, the fluid serves as a habitat for a diverse community of dipteran larvae, mites, bacteria, fungi, and protists, which can help the plant obtain nutrients such as nitrogen and phosphate (Buch et al. 2014; Gilbert et al. 2020).

The carnivorous traps of *Nepenthes* are passive, retaining digestive fluids within the pitchers and waiting for potential prey, distinguishing *Nepenthes* from the Drosera group, which has Venus flytraps capable of movement (Saganová et al. 2018). The morphology of *Nepenthes* is highly variable in terms of the size, shape, and colour of the pitchers. Some pitchers can exceed up to 30 cm in length, with striking colour variations ranging from green to red to purple. These adaptations allow *Nepenthes* to thrive in diverse habitats, including humid tropical rainforests and rocky mountainous regions with low soil nutrient content (Murphy et al. 2020).

Nepenthes has various ethnobotanical uses around the world. The boiled roots of *N. ampullaria* and *N. gracilis* are used to treat stomach aches by tribes in Malaysia, while their stems are used for fever and as construction materials due to their durability. The most common use is as a source of water for thirsty hikers (Miguel et al. 2018). The aqueous extract of *Nepenthes khasiana* acts as a reducing agent in the synthesis of gold nanoparticles from gold salts, thanks to its antioxidant phytochemicals. The resulting gold particles exhibit high stability and biocompatibility, making them ideal for diagnostic and drug delivery applications in the field of nanomedicine (Dhamecha et al. 2016).

Numerous valuable metabolites have been identified across various *Nepenthes* species. These molecules play a crucial role in the plants' environmental adaptation. The *Nepenthes* pitcher fluid is inhospitable to microbial growth, partly due to the presence of specialized antimicrobial metabolites. The most extensively documented molecule is plumbagin (5-hydroxy-2-methyl-1,4-

naphthalenedione), which significantly contributes to microbial inhibition in the pitcher fluid. Furthermore, this compound demonstrates diverse potential applications, including agricultural biocontrol, natural food preservation, and various medicinal benefits. Together with its derivatives such as droserone and 5-O-methyldroserone, plumbagin establishes *Nepenthes* as a highly promising source of bioactive compounds for multiple applications (Miguel et al. 2018). However, the *Nepenthes* genus faces severe population threats due to excessive illegal exploitation by collectors for commercial gain (Renjana et al. 2024).

Nepenthes is the genus of pitcher plants with the largest number of species. In 1980, 80 species were recognized; by 2001, this number had increased to 87 species, and by 2012, it had reached 139 species. To date, around 180 species of *Nepenthes* have been identified, with new species discoveries continuing (Setiawan et al. 2018; Mansur et al. 2020). Generally, the discovery of new species in the genus *Nepenthes* is based on the morphological characteristics of the pitchers. Pitchers are actually modified leaves that come in various shapes, sizes, and colors. The morphology of the pitchers has evolved to facilitate the plant's habits, aiding in adaptation and survival in nutrient-poor soils such as those low in nitrogen. Some studies also use the anatomy of *Nepenthes* as a tool for identifying new species (Huda et al. 2022).

Nepenthes is distributed in tropical regions, ranging from southern China, Indonesia, Malaysia, and the Philippines; westward to Madagascar with two species and the Seychelles with one species; southward to Australia with four species and New Caledonia with one species; and northward to India and Sri Lanka with one species. The highest diversity is found in Southeast Asia, particularly Indonesia, which currently hosts 85 species of *Nepenthes* (Fitmawati et al. 2023). Each new discovery enriches our understanding of biodiversity and evolution within this genus. New *Nepenthes* species are often found in remote and under-explored areas, highlighting the importance of ongoing botanical exploration. Recent discoveries in the past decade have increased the number of known species and demonstrate the dynamic process of diversification within this genus (Konwar et al. 2023). Additionally, many *Nepenthes* species face extinction due to a lack of public awareness, fires, and forest degradation. Therefore, reviews related to the presence of *Nepenthes* species are crucial to rekindle public interest in conserving these plants (Lestari et al. 2018).

Based on this statement, this article will discuss the discovery of new species of the genus *Nepenthes* found in Southeast Asia and published in the last 10 years. The results of this review article are expected to provide additional information for future research related to *Nepenthes*.

MATERIALS AND METHODS

This study was conducted at the Department of Biology, Airlangga University during May-June 2024. Data on newly described *Nepenthes* species from the last 10 years were collected from reliable sources. A total of 26 articles containing new species descriptions were identified from 14 scientific journals, including: Phytotaxa, Kalpataru, Philippine Journal of Science, Philippine Journal of Systematic Biology, Plants, Thailand Forest Bulletin, Phytokeys, Journal of Sustainable Natural Resources, Reinwardtia, Kew Bulletin, PeerJ, Carnivorous Plant Newsletter, Malayan Nature Journal, and Journal of Plant Taxonomy and Geography.

The journals were obtained from Google Scholar (https://scholar.google.com/) using the search keyword "new species of *Nepenthes*" with publication year filters set from 2014 to 2023. Google Scholar was selected as the search platform due to its broader and more comprehensive coverage of scientific literature compared to selective journal-based databases

like Web of Science or Scopus (Martín-Martín et al. 2018).

Furthermore, nomenclature validation was performed by accessing the Royal Botanic Gardens, Kew database (https://www.kew.org) to verify data completeness. When species names were not found in the database, additional literature searches were conducted using specific scientific names. All collected data were processed and analysed based on the following parameters: (1) geographical distribution, (2) describing authors, (3) identification methods, (4) discovery year, and (5) year of first formal publication using Microsoft Excel software (Brillo et al. 2024). New species were validated based on significant morphological differences, following taxonomic description criteria in the literature (Cheek & Jebb 2014; Cheek 2015; Cheek et al. 2015; Cheek & Jebb 2016a, 2016b; Cheek et al. 2018).

RESULTS AND DISCUSSION

Based on the first publication of the species, there are 37 new species of the genus *Nepenthes* distributed in Southeast Asia over the last ten years (2014-2023). The description of the new species can be seen in Table 1.

Table 1. Description of a new species in the genus *Nepenthes*.

No.	Species Name	Description	Distribution	Author's Origin	Identification Methods	Year of Discovery Species	References
1.	*Nepenthes armin* Jebb & Cheek, sp. nov	Stems are climbing and rounded-rectangular in shape. There is no covering on the surface except for dense brown simple hairs in leaf axils. The leaves are thinly leathery, petiolate and either narrowly oblong or elliptic-linear in shape. The apex is acute or obtuse-rounded, and the base gradually tapers to the petiole. The upper pitchers are green with faint purple stripes and narrowly cylindrical with smooth indumentum hairs. The peristome is ovoid, the cap is orbicular, and the pitcher is curved.	Philippines	United Kingdom	Morphology	2007	Cheek & Jebb 2014
2.	*Nepenthes tboli* Jebb & Cheek, sp. nov.	Stem form terete; leaves spirally inserted; leaf blade oblong-elliptical; leaf margin hairy, young stems 50 % covered by indumentum; petiole with wings; upper midrib sub cylindrical; outer pitcher surface sparsely patterned with hairs simple; peristome ovate; cap ovate-elliptic; pitcher simple, needle-like, tapering to a point.	Philippines	United Kingdom	Morphology	1993	Cheek & Jebb 2014
3.	*Nepenthes zygon* Jebb & Cheek, sp. nov	Stems climb with internodes; rosette leaves are oblanceolate; climbing stem leaves have an acute tip and are not round; petiole is winged and U-shaped or broad V-shaped in section; leaf base blade curves into the petiole; lower pitchers (tendrils not coiled) are elliptic-cylindrical; peristome is ovate-elliptic; cap is orbicular-elliptic; basal cap appendages are strongly convex and conspicuous on the upper pitcher. Upper pitchers (circular tendrils) are ellipsoid-cylindrical.	Philippines	United Kingdom	Morphology	1997	Cheek & Jebb 2014

Table 1. Contd.

No.	Species Name	Description	Distribution	Author's Origin	Identification Methods	Year of Discovery Species	References
4.	*Nepenthes pantaronensis* Gieray, Gronem., Wistuba, Marwinski, Micheler, Coritico, V.B. Amoroso, spec. Nov.	The stem can reach up to 3 meters in length and is cylindrical in cross-section. The leaves on the bare stem are linear to oval with broad-winged petioles for climbing. Lower pitchers can grow up to 35 cm high and 6 cm wide, while upper pitchers can reach up to 40 cm long and 5 cm wide. The lower one-fifth to one-quarter of the trap is inflating and rounded, narrowing above this section before becoming cylindrical towards the pitcher opening. The inflorescences are panicles. Indumentum, consisting of orange-brown bristles up to 1 cm in length and up to 1 mm in width, is present throughout the foliage, inflorescences, and pitchers.	Philippines	Germany	Morphology	2012	Gronemeyer et al. 2014
5.	*Nepenthes cornuta* Marwinski, Coritico, Wistuba, Micheler, Gronem., Gieray, V.B.Amoroso, spec. nov.	The climbing stem can grow up to 3 meters long. The leaves on the stem have stems of their own and are long and narrow, with a pointed tip and a flared, finger-like base. The leaf's stem partly encloses the stem. The pitcher's opening is oval and can be up to 2.8 cm wide. The lower part of the pitcher is rounded, while the upper part is narrower. The lower third of the pitcher is swollen, and it tapers towards the tendril, giving it a distinctive horn-like shape. There are two flowering stalks in the inflorescence. The developing pitcher bud is covered with tiny and orange-brown hairs.	Philippines	Germany	Morphology	2012	Gronemeyer et al. 2014
6.	*Nepenthes talaandig* Gronem., Coritico, Wistuba, Micheler, Marwinski, Gieray, V.B.Amoroso, spec. nov.	The climbing stem can grow up to 8 meters long. The leaves of the climbing stem are elliptical, with four longitudinal veins evenly distributed on each side of the midrib and numerous pinnate veins running obliquely toward the leaf margin. The tip of the leaf blade is pointed. The lower pitcher is egg-shaped and slightly narrows towards the opening. The rosette pitchers are also egg-shaped and much smaller than the lower pitchers. The upper pitcher is slender, with the lower third of the trap slightly expanding. The pitcher narrows toward the middle of the cylinder before widening towards the oblique opening. The inflorescence is in the form of a panicle, with sparse bracts and indumentum.	Philippines	Germany	Morphology	2012	Gronemeyer et al. 2014

Table 1. Contd.

No.	Species Name	Description	Distribution	Author's Origin	Identification Methods	Year of Discovery Species	References
7.	*Nepenthes amabilis* Wistuba, Gronem., Micheler, Marwinski, Gieray, Coritico, V.B.Amoroso, spec. nov.	The plant has short green stems with minimal space between them. Its leaves spread out and have broad, winged petioles. The top pitcher has short, climbing stems and is cylindrical, with a slightly funnel-like lower third and a distinct puckered area below the peristome. The inflorescence is a panicle with a 15 cm long leaf and an additional 15 cm long rachis bearing two flowers on pedicels that are 20 mm long. The foliage, inflorescence, and pitchers are covered in a noticeable layer of brownish hairs up to 1 mm long, especially along the edges of young leaves.	Philippines	Germany	Morphology	2012	Gronemeyer et al. 2014
8.	*Nepenthes halmahera* Cheek, sp. nov	Upper and lower surfaces lack indumentum except for sessile globose glands and a few simple short hairs on the distal midrib. The petiole is winged and canaliculate. Lower pitchers (short shoots) are ellipsoid-cylindrical with a narrowly ovate mouth and an ovate-elliptical cap with short and dense overall hairs. Bifurcated pitchers are present. Upper pitchers (climbing stems) are green and ovate-cylindrical, with 5 – 10 % of the outer surface covered in simple golden-brown hairs. The mouth is ovate, concave, and oblique, with a pale, waxy greenish-white inner surface and red spots. The peristome is flattened cylindrical, and the cap is ovate-elliptical. The pitchers are oblong. The inflorescence is terminal on the central axis.	Halmahera, Maluku Utara, Indonesia	United Kingdom	Morphology	2013	Cheek 2015
9.	*Nepenthes weda* Cheek, sp. nov.	Stems horizontal, underground, having vertical rosette shoots along the stem; leaves petiolate, coriaceous; rosette shoot leaves anemophilous; shoot leaves short with elliptical-oblong blade; edge densely dark brown hairy; upper surface of blades glabrous, yellow-brown; climbing stem leaves with very narrow elliptical blades; upper surface of blades shiny; petioles canalized; xanthophyll rosette shoots located above the ground, dense dark red, broadly sub cylindrical; mouth ovoid; lower pitchers (short stems) brownish-red, narrowly elliptic; upper pitchers of stems climbing is dark red or greenish-yellow, more or less speckled with brownish red.	Halmahera, Indonesia	United Kingdom	Morphology	2012	Cheek 2015

Table 1. Contd.

No.	Species Name	Description	Distribution	Author's Origin	Identification Methods	Year of Discovery Species	References
10.	*Nepenthes barcelonae* Tandang & Cheek, sp. nov	Stems are climbing; leaves are sessile and oblong-ligulate in shape. The upper pitchers are dimorphic and dichromic, slightly curved, and cylindrical, with an inconspicuous mouth that is spherical. The peristome is shiny, dark red, and subcylindrical, with the outer edge gradually thinning to membranous and appearing wavy. Additionally, the cap is ovoid. The primary upper pitchers are produced at the bottom of the stem, while the secondary upper pitchers are made from stems over 1.5m high. The plant also has racemose inflorescences.	Philippines	United Kingdom	Morphology	2014	Cheek et al. 2015
11.	*Nepenthes krabiensis* Nuanlaong, Onsanit, Chusangrach & Suraninpong, sp. nov	Dioecious shiny climbing herb with axillary buds present at the top of the plant. The leaves are green above and brown below, with an indumentum of brown hair. When young, the leaves are shiny and light green in a rosette. The lower pitcher is green to orange with red stripes outside and red blotches on the inside. The peristome is green to red with a green-to-red cap on the upper surface and a conspicuous central rib with two tufted wings. The upper pitcher is light green with a red spot on the inner surface, a white peristome, and a light green cap. The tendrils are whorled. Male and female inflorescences are clustered.	Thailand	Thailand	Morphology and Anatomy	2015	Nuanlaong et al. 2016
12.	*Nepenthes minima* Jebb & Cheek, sp. nov	Stems are short, cylindrical, or slightly rounded. They have a mix of branched and star-shaped hairs. The leaves have petioles and elliptic-oblong blades with pointed tips. The upper pitchers are green, slightly curved along the central axis, and narrowly funnel-shaped with a narrowly ovate mouth and cap. Female flowers have 4-6 tepals; the seeds are slender and spindle-shaped, pale yellow, with smooth centres.	Sulawesi Tenggara	United Kingdom	Morphology	2016	Cheek & Jebb 2016b
13.	*Nepenthes aenigma* Nuytemans, W. Suarez, Calaramo, sp. nov.	The plant has stems that can grow up to 5 meters in length. The stems are smooth, and they can be round or three-sided. There are dormant buds located 3 to 5 mm above each leaf base. The creeping stems produce short stems above ground, producing traps buried in the leaf litter. The leaves are attached directly to the stem and are long and narrow with rounded or pointed tips. The midrib of the leaf emerges suddenly from the tendrils. The upper pitchers are fewer in number compared to the middle pitchers; they are cylindrical and slightly curved forward with a broad, funnel-shaped base. Inflorescences develop from the axils, and the plant is mostly bare. The cap is pale green with small red spots, and the peristome is cream to reddish. The tendrils on the middle trap are red, while the upper trap has red and green tendrils.	Philippines	Germany	Morphology	2009	Gronemeyer et al. 2016

Table 1. Contd.

No.	Species Name	Description	Distribution	Author's Origin	Identification Methods	Year of Discovery Species	References
14.	*Nepenthes justinae* Gronem., Wistuba, Mey, V.B.Amoroso, sp. nov.	The climbing stem leaves are ovate. The lower pitchers are rounded in the lower 2/3 and slightly infundibulate in the upper 1/3. The outside of the lower pitcher is yellow with purple blotches, while the inside is greenish-white, sometimes coated with angular purple blotches. The peristome is dark red and unevenly streaked with yellow. The entire surface of the lower pitcher is covered with dense and very short brown hairs.	Philippines	Germany	Morphology	2004	Gronemeyer et al. 2016
15.	*Nepenthes maryae* Jebb & Cheek, sp. nov	Please remember the following information: The climbing stem is terete, and its indumentum is densely covered with hairs. The leaf blades of the climbing stem are coriaceous, sessile, and lanceolate-oblong. The upper pitchers (coiled tendrils) are cylindrical with a rhombic mouth. The nectar glands are dense, and the surface has hairs and inconspicuously branched bracts in male inflorescences present at the proximal part.	Central Sulawesi, Indonesia	United Kingdom	Morphology	2000	Cheek & Jebb 2016a
16.	*Nepenthes malimumuensis* Lagunday, Acma, Cabana, Sabas, V.B. Amoroso, sp. nov	The leaves have winged stalks. The lower pitcher is cylindrical and slightly funnelled towards the opening, which is oval and leads to the lid. The peristome has short, triangular tooth-like projections with concave nectar glands nearby. The closing nectar gland is ovoid. The cover of the pitcher is filiform. The outer part of the lower pitcher is green with red blotches, and the inside is similarly coloured. The upper pitcher is funnel-shaped in the lower third and tapers towards the tendril. The female inflorescence is a panicle. The indumentum consists of multicellular trichomes with short pseudo-branches arising from basal, glandular to non-glandular cells found on the tendril, outer part of the pitcher, and inflorescence.	Philippines	Philippines	Morphology	2014	Lagunday et al. 2017
17.	*Nepenthes manobo* Lagunday, Acma, Cabana, Sabas, V.B. Amoroso, sp. nov	The leaves are directly attached and broadly linear. Wings cover the entire front of the trap. The peristome is ribbed, slightly flattened, and tapers backward to form a vertically oriented neck. The cap is oval, with evenly distributed large and small round nectar glands on the lower surface. The exterior of the pitcher is wholly red or yellow. The bottom of the pitcher forms a hip. The pitcher's opening tapers obliquely towards the lid. The peristome is ribbed and cylindrical in cross-section. The male inflorescence is a panicle. The indumentum, present on flowers, outside pitchers, and leaves, is a multicellular trichome that can be glandular or non-glandular.	Philippines	Philippines	Morphology	2014	Lagunday et al. 2017

Table 1. Contd.

No.	Species Name	Description	Distribution	Author's Origin	Identification Methods	Year of Discovery Species	References
18.	*Nepenthes alfredoi* V.B. Amoroso and Lagunday sp. nov	The leaf blade is broad and ovate with a blunt to rounded tip. The opening of the pitcher is ovate. The outer surface of the lower pitcher is green with red blotches, while the inner surface is green. The tendrils and midribs are red. The peristome is cylindrical. The upper pitcher is funnel-shaped and slightly swollen in the lower third, tapering towards the back where the tendril is located, and cylindrical in the middle part, with a somewhat funnel-shaped opening.	Philippines	Philippines	Morphology and Anatomy	2016	Amoroso et al. 2017
19.	*Nepenthes biak* Jebb & Cheek, sp. nov.	A short stem, which is not very different from a climbing stem, has cylindrical internodes. The leaves of the short stem are glossy, leathery, and oblanceolate and are spirally inserted. The lower midrib has erect and not curled tendrils, with tufted wings, while the midrib has tendrils that emerge laterally from the base and are not curled. The upper pitcher gradually narrows laterally at the centre in frontal view and has a yellow peristome.	Biak Island, Indonesia	United Kingdom	Morphology	1966	Cheek et al. 2018
20.	*Nepenthes dactylifera* A.S.Rob., Golos, S.McPherson & Barer, spec. nov.	The stems of this plant are rosette-shaped and cylindrical, while the leaves in the rosette are ovate and have broad, oblong-elliptic shapes. The lower pitcher is ellipsoid, cylindrical, and slightly narrower at the top, widening towards the mouth, while the upper pitcher is broadly tubular to infundibular. The plant has a covering of short, fine brown hairs. In terms of colour, the mature stems are usually reddish to black, the leaves are bright green with some red, the lower pitcher is often dark, and the upper pitcher is pale green with a whitish peristome streaked with dark red.	Malaysia, Brunei, and Kalimantan Indonesia	Australia	Morphology	1992	Robinson et al. 2019a
21.	*Nepenthes erucoides* A.S.Rob. & S.G.Zamudio, sp. nov	The pitcher has an elliptical shape, a more comprehensive peristome, and a transparent border. The bracts on most stalk are partial, about 1 mm long, and never emerge from the stalk. Additionally, the filaments are well-developed.	Philippines	Australia	Morphology	2018	Robinson et al. 2019b
22.	*Nepenthes cabanae* Lagunday & V.B. Amoroso, sp. nov.	The plant has a climbing stem with leaves that attach directly to the stem and have parallel nerves running alongside the midvein. The lower or middle pitcher is shaped like a cylinder, and the peristome has a short triangular tooth, approximately 0.3-0.5 mm long, that does not extend beyond the margin.	Philippines	Philippines	Morphology	2015	Lagunday & Amoroso 2019

Table 1. Contd.

No.	Species Name	Description	Distribution	Author's Origin	Identification Methods	Year of Discovery Species	References
23.	*Nepenthes maximoides* Cheek, sp. nov.	Stem climbing round; leaves spiral; axillary buds inconspicuous; indumentum glabrous. Leaves petiolate, leaflets acuminate, base gradually declining to petiole; midrib when young dense. Petiole clasping the stem by ½ its circumference, not radius, winged, T-shaped. Pitcher's upper (tendrils coiled, cap facing away from tendrils), infundibular narrow; the outer surface of pitcher shiny, drying yellowish brown, hairless. The mouth ovate is slightly concave, forming a column under the cap; the peristome is rounded or flattened and inverted U-shaped in a transverse section. Spur 4 mm below the cap insert, straight, erect, the tip bifurcated, the surface instead densely covered with brown hairs.	Philippines	United Kingdom	Morphology		King & Cheek 2020
24.	*Nepenthes malayensis* A.Amin, M.N.Faizal & Dome sp. nov.	Cross-section of climbing stems hairy, broadly angled, and cylindrical towards the shoot; margin of leaf base (climbing stem) clasping the stem ½ of the circumference, not fingered; pitcher cap ovate with a midline indentation in the centre, base cordate; nectar glands present; mouth slightly indented on the back; peristome loosely cylindrical in the middle; lower pitcher emerging from the tendril; lower part ovate, upper part slightly ovate; hip ½ high; lower pitcher 1/3 broadly infundibuliform, broadly cylindrical at the top and constricted towards the mouth; and peristome on the upper pitcher conspicuously reddish-striped with a green band.	Malaysia	Malaysia	Morphology, Anatomy, and Molecular	2019	Tamizi et al. 2020a
25.	*Nepenthes latiffiana* M. N. Faizal, A. Amin & N. Dome, sp. nov.	Rosette tendrils and climbing leaves with a slender circular formation in the middle, covered with small hairs; the colour of the lower pitcher is yellowish-green-brown with a few red blotches on the upper 1/3 of the pitcher body; the lower pitcher cap has blotches; the base of the cap is cordate retuse; the colour of the upper pitcher is light green; the upper pitcher cap is rounded.	Malaysia	Malaysia	Morphology, Anatomy, and Molecular	2019	Ghazalli et al. 2020
26.	*Nepenthes domei* M. N. Faizal, A. Amin, & A. Latiff, sp. nov.	Rosette tendrils and slightly whorled climbing leaves; lower pitcher colour whitish red to deep ruby red with slight red-purple flaws on the inner surface and lid; lower pitcher lid ovate, pitcher lid rounded; upper pitcher colour green; upper pitcher lid ovate.	Malaysia	Malaysia	Morphology, Anatomy, and Molecular	2019	Ghazalli et al. 2020

Table 1. Contd.

No.	Species Name	Description	Distribution	Author's Origin	Identification Methods	Year of Discovery Species	References
27.	*Nepenthes x setiuensis* A.Amin, M.N.Faizal *et* N.Domenothosp.nov.	The lower pitcher's colour is green to dark purple with black-purple blotches; the peristome is black to dark purple; the middle pitcher's shape and colour are similar to the upper pitcher; the mature upper pitcher slightly ovate at bottom narrowing to cylindrical towards the top, mouth rounded to oblong; the colour of upper pitcher dark purple with a combination of black spots; peristome dark purple; shape of upper/lower pitcher lid rounded; upper/lower pitcher lid downy simple white; peristome medium-sized; and inner pitcher wall surface greenish with red spots, waxy surface.	Malaysia	Malaysia	Morphology and Anatomy	2019	Tamizi et al. 2020b
28.	*Nepenthes longiptera* Victoriano spec. nov.	There are upper wings developed, the shape of the upper pitcher is slender at the basal part, the shape of the lower pitcher is cylindrical at the basal part, the upper pitcher lip is oval with a heart-like base, slightly protruding or rounded upwards, the lower pitcher lip is elliptical with an oval base, the stem is rhombic, the leaf shape is oval and sub petiolate, the leaf veins are amplexicaul, auriculate, clasping 2/3 of the stem.	Aceh, Indonesia	Indonesia	Morphology	2019	Victoriano 2021
29.	*Nepenthes pudica* Dančák & Majeský, sp. nov	The short basal shoots are located underground, the stem indumentum is glabrous, the stem colour is brownish green, the shape of the climbing leaves is oblanceolate, the climbing leaves have stalks, the base of the climbing leaves is auriculate and short, the texture of the climbing leaves is thick and stiff, the tips of the climbing shoot leaves are pointed, the mature midrib indumentum is glabrous, the shape of the lower midrib is fingered, the lower midrib is infundibular, and the male flowers are paired. Rosette pitchers are produced only briefly. The lower pitchers emerge abruptly from the uncoiled tendrils and ventricose, broadly ovate to rounded on the underside, and the outer surface red-purple in colour. Upper pitchers are rarely produced; the outer surface is green, and the inner surface near the mouth is yellowish.	North Kalimantan, Indonesia	Czech Republic	Morphology and Anatomy	2012	Dančák et al. 2022
30.	*Nepenthes bracteosa* Suran. & Nuanlaong sp. nov.	The leaf shape is linear to lanceolate, the leaf tip is acute, the lower pitcher cap is ovate, the spur has fine hairs with branches, the male flower has one flower, the androphore is 2.0-2.5 mm long, has bracts on all flowers, and there is no layer of fine hairs on the stem, lamina, leaf margins, and shoots.	Thailand	Thailand	Morphology, Anatomy, and Molecular	2019	Nuanlaong et al. 2022

Table 1. Contd.

No.	Species Name	Description	Distribution	Author's Origin	Identification Methods	Year of Discovery Species	References
31.	*Nepenthes hirtella* Nuanlaong & Suran. Sp. nov.	Leaf shape oblanceolate, leaf tip rounded, lower pitcher cap ovate, spur bearing hairs with branches, male inflorescence bearing one flower or rarely two flowers and a partial peduncle, bract present at the base of the rachis (1-2 flowers) of both male and female inflorescences, and an indumentum covering all vegetative parts.	Thailand	Thailand	Morphology, Anatomy, and Molecular	2019	Nuanlaong et al. 2022
32.	*Nepenthes harauensis* Hernawati, R.Satria & Chi.C.Lee spec. nov.	Stem cylindrical; internodes closed on short shoots; leaves pinnate, pinching the stem, lamina elliptic; tendril inserts pinnate/subapical; 2 longitudinal veins on each side of midrib; lower pitchers ovate then cylindrical above; peristome cylindrical, widening towards the back; cap ovate to orbicular with a simple thickened ridge near the apex; upper pitchers narrowly ovate-cylindrical and widened above, and inflorescence single-flowered.	West Sumatera, Indonesia	Indonesia	Morphology	2021	Hernawati et al. 2022a
33.	*Nepenthes berbulu* H.L.Tan, G.Lim, Mey, Golos, Wistuba, S.McPherson & A.S.Rob., spec. nov.	Leaves oblong-elliptic with rounded tips; cover hairs thick and unevenly coarse; lower pitcher broadly infundibular at the bottom, cylindrical at the top; the size of lower pitcher up to 25 cm long and 6 cm wide; the colour of lower pitcher yellowish-green or dark pink, spotted with dark red or purple. Peristome yellowish green with reddish stripes, sometimes entirely red; lid on lower pitcher orbicular; upper pitcher broadly infundibular below, slightly constricted just above the hip, cylindrical above; the colour of upper pitcher essentially pale green; and lid on upper pitcher orbicular.	Malaysia	Malaysia	Morphology	2022	Tan et al. 2023
34.	*Nepenthes sericea* Golos, Wistuba, G.Lim, Mey, S.Mcpherson & A.S.Rob.	Lower pitchers have a flattened peristome with teeth, an oval cap with fine abaxial hairs (up to 2 mm), hips primarily positioned in the centre (sometimes close to the mouth), and a mottled outer surface. The upper pitchers are mainly white with pinkish, yellowish-green spots towards the tendrils.	Malaysia	United Kingdom	Morphology	2022	Tamizi et al. 2023
35.	*Nepenthes ulukaliana* A.S.Rob., Wistuba, Mey, Golos, G.Lim & S.Mcpherson.	The lower pitcher is amphora-shaped (because the hips are positioned close to the peristome), has short (≤1 mm long) and dense covering hairs, and the front of the peristome is planar.	Malaysia	Bangladesh	Morphology	2023	Tamizi et al. 2023

Table 1. Contd.

No.	Species Name	Description	Distribution	Author's Origin	Identification Methods	Year of Discovery Species	References
36.	*Nepenthes limiana* Wistuba, Mey, Golos, S. McPherson & A.S. Rob., spec. nov.	Stems slightly angular. Leaf lamina of the rosette are generally oblanceolate, sometimes lanceolate, tendrils of the rosette and lower pitchers unrolled, the shape of rosette pitchers variable, ovate or infundibular basally, forming a slightly ovate base with a hip in the centre and cylindrical above, the cap having fine hairs on the lower surface. Lower to middle pitchers are similar to rosette pitchers in shape. The peristome ovate is often slightly widened and furrowed, and the upper pitchers have conspicuous venation and narrow infundibular basal. Cap sub-orbicular to ovate. Inflorescence is a racemose panicle, and the female inflorescence is two-flowered. Indumentum conspicuous and stem colour red.	Malaysia	United Kingdom	Morphology	2022	Golos et al. 2023
37.	*Nepenthes samudera* R. Chiu, E. Goh, D. Lim, & M. Balahadia sp. nov.	Leaf shape oblong spathulate, stem attachment clasping the stem along ¾ of its circumference, tendrils subapical; lower pitcher broadly infundibulate below and cylindrical above; peristome shape cylindrical, peristome colour dark red; pitcher body colour red; male inflorescence 2-flowered; has bractea and filiform.	Sumatera, Indonesia	London	Morphology	2023	Chiu 2023

The discovery of 37 new species of the *Nepenthes* genus over the past 10 years shows yearly variation, as presented in Figure 1. Next, a comparison of the countries that discovered new species can be seen in Figure 2. Although new species of *Nepenthes* are spread in Southeast Asia, researchers who discovered them come from various countries, with the largest number of researchers from the United Kingdom (Figure 3). Identifying and discovering new species of the genus *Nepenthes* involves several methods, namely based on morphological, anatomical, and molecular comparisons (Figure 4).

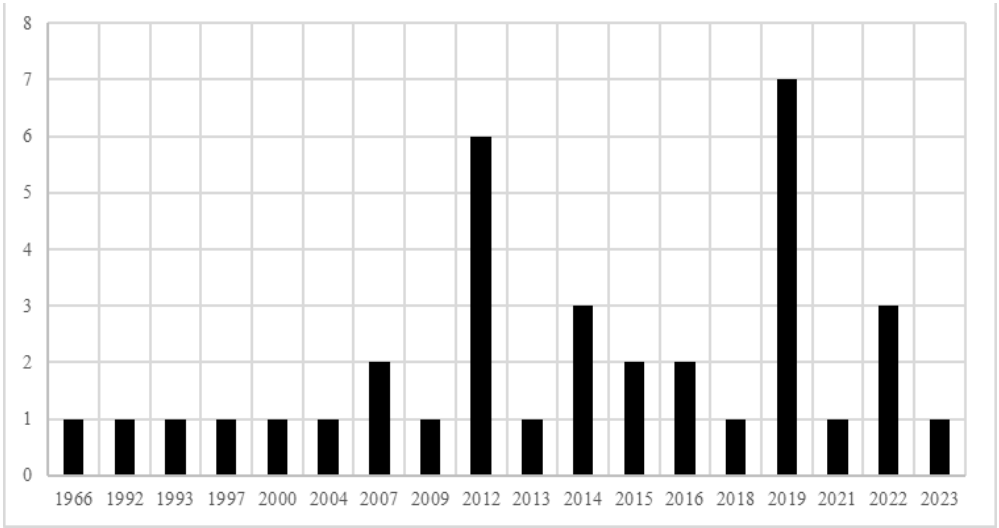

Figure 1. Diagram of the number of new species discovered in the last decade.

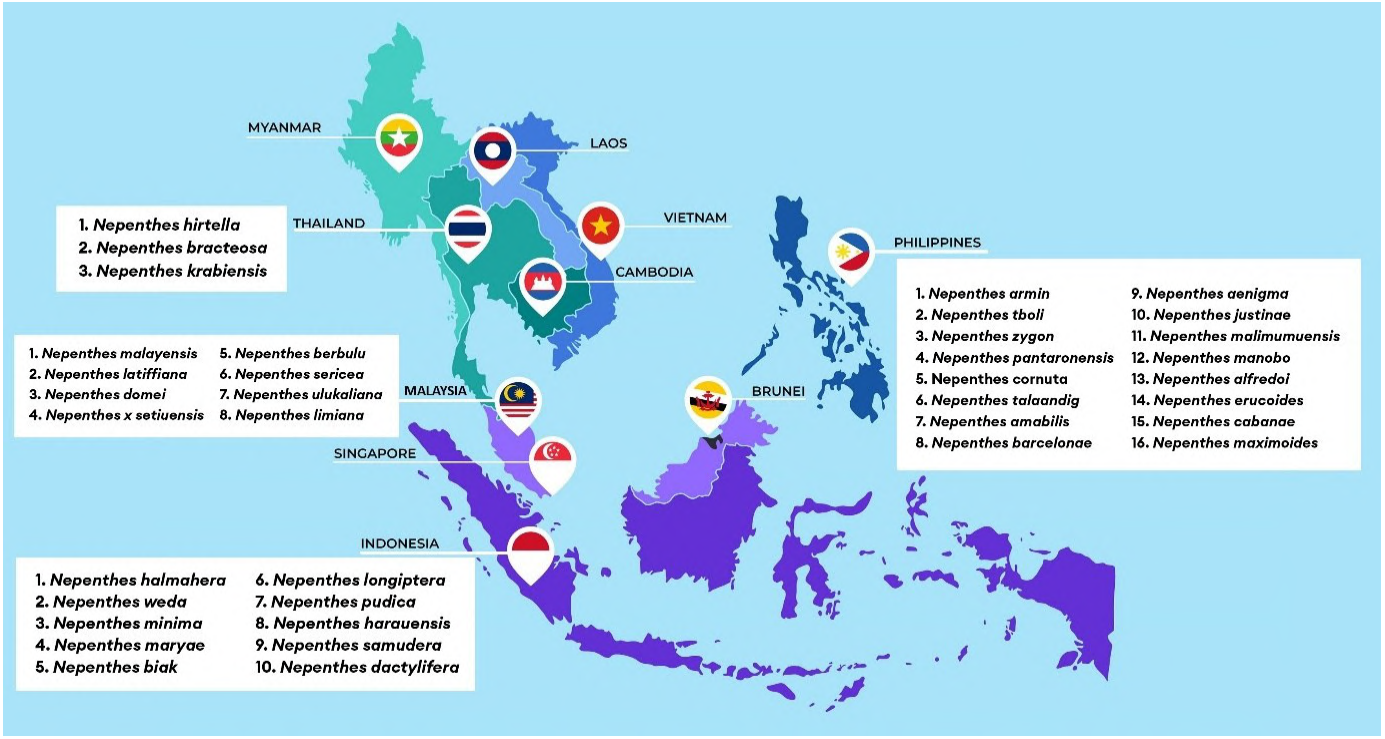

Figure 2. Distribution map of new *Nepenthes* species in Southeast Asia.

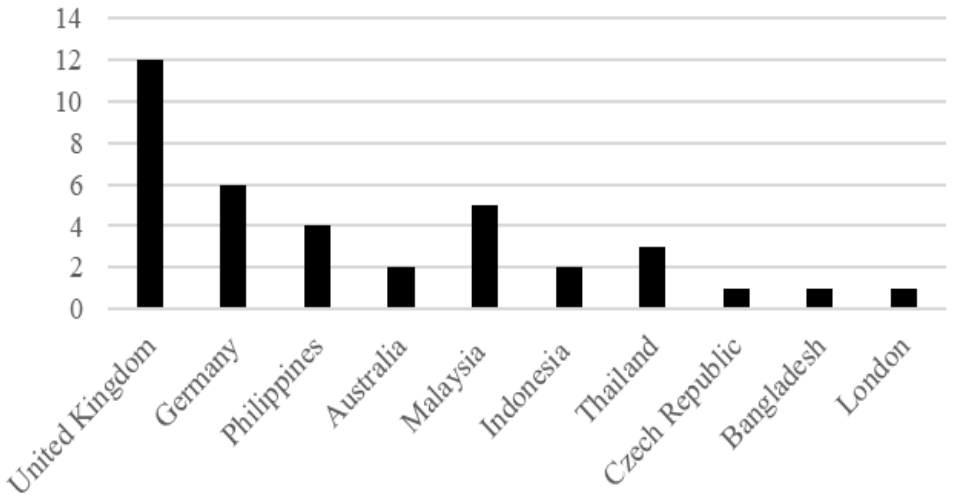

Figure 3. Countries of origin of researchers who discovered new species.

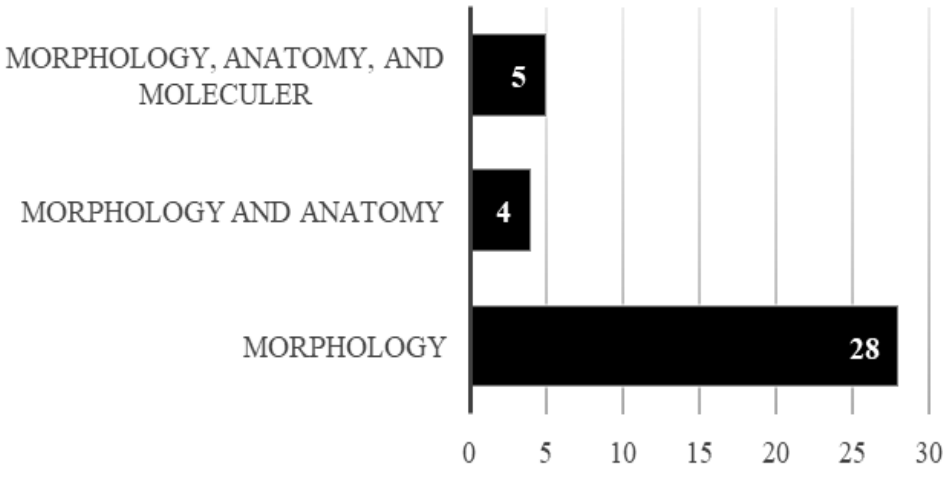

Figure 4. Comparison of new species identification methods.

Discussion

In general, *Nepenthes* has unique and interesting morphological characteristics. *Nepenthes* leaves are lanceolate with elongated tips forming tendrils. These tendrils help the plant climb or drape itself over other plants. One of the most distinctive parts of *Nepenthes* is the trap pouch formed at the end of the tendril. This pouch comes with a flap on top. The inner walls of the pouch are smooth and contain enzymatic fluids and bacteria that help digest the trapped prey. In addition, the relatively small and shallow roots of *Nepenthes* are well suited to their habitat in nutrient-poor soils (Miguel et al. 2018).

Nepenthes play an important ecological role. It helps control insect populations by capturing and digesting them as an additional source of nutrients, particularly nitrogen and phosphorus. This can reduce herbivore pressure on other nearby plants (Buch et al. 2014). The shallow roots of *Nepenthes* also play a role in soil stabilization, especially in vulnerable habitats such as limestone cliffs or peatlands. In addition, as part of the tropical ecosystem, *Nepenthes* contributes to biodiversity by providing habitat for various organisms, including insects, frogs, and even small rodents trapped in their pouches. Some *Nepenthes* species even have symbiotic relationships with animals, such as ants, which help clean the pouches of prey remains and prevent decay (Bazile et al. 2012). *Nepenthes* can also be an indicator of environmental conditions. The presence and health of *Nepenthes* populations often reflect moisture conditions, soil quality, and the level of human disturbance in the habitat (Mansur et al. 2023).

Nepenthes is the only genus in the Nepenthaceae family whose members are all carnivorous plants (Mansur et al. 2024). Research on the genus *Nepenthes* in the last 10 years has resulted in various new species discovered in several countries in Southeast Asia. The Philippines has the highest number of discoveries, reaching 16 new species. Indonesia followed with 10 new species identified. Malaysia also showed a significant contribution with the discovery of eight new species. Meanwhile, Thailand recorded the discovery of three new species. These discoveries reflect the region's incredible biodiversity and researchers' persistent efforts in exploring and documenting the local flora.

Over the past 10 years, research on the *Nepenthes* genus has resulted in numerous discoveries of new species. 2014 recorded the peak of discoveries with seven new species, followed by a decline in 2015 with three species. In 2016, there was another increase with five new discoveries, but this declined to three in 2017 and only one in 2018. Slight stability was achieved in 2019 with three new species, while 2020 saw a resurgence with five discoveries. In 2021, only one new species was discovered, but this number rose to four in 2022 and five in 2023. In 2024, no new species discoveries were recorded. The fluctuation in the number of discoveries each year reflects the challenges and dynamics researchers face in exploring and studying this genus. *Nepenthes* is classified as a protected plant due to its dwindling population in its natural habitat. Discoveries of *Nepenthes* species in Southeast Asia show remarkable diversity, but their habitats are threatened by deforestation, drainage, drought, and climate change (Gaume et al. 2019).

Indonesia has discovered 10 new species that have never been recorded before in the last 10 years, consisting of *N. halmahera*, *N. weda*, *N. minima*, *N. maryae*, *N. biak*, *N. longiptera*, *N. pudica*, *N. harauensis*, *N. oceanic*, *and N. dactylifera*. The worldwide diversity of *Nepenthes* sp. is in line with data from the International Union for Conservation of Nature (IUCN), which records around 122 species, and 116 of them are found in Southeast and South Asia, with 63 of them detected in Indonesia. *Nepenthes* diversity in Indonesia has been sufficiently documented, especially in the main islands such as Sumatra (31 species), Kalimantan (20 species), Papua (12 species), Sulawesi (10 species), Maluku (4 species), and Java (3 species). Among these islands, Sumatra

has the highest number of *Nepenthes* species in Indonesia (Nainggolan et al. 2020).

The Indonesian government has also designated the genus *Nepenthes* as a priority plant for conservation through the Minister of Forestry Regulation No. P.57/Menhut-II/2008. However, there are no adequate species data to support the designation of Nepenthaceae as a priority plant group in Indonesia, so no conservation priorities have been determined at the species level (Hernawati et al. 2022b). Under international convention, the entire *Nepenthes* genus is listed in CITES (Convention on International Trade in Endangered Species) Appendix II, meaning all species within this genus are protected from international trade without proper authorization. This CITES protection applies universally, regardless of individual species' national conservation status. Certain species such as *Nepenthes rajah* and *Nepenthes khasiana* receive even stricter protection under CITES Appendix I, which explicitly prohibits all forms of international commercial trade (https://cites.org/).

The Philippines is now recognized as having the greatest diversity of pitcher plants of the genus *Nepenthes*. Over the past ten years, a number of field expeditions, mainly in Mindanao, have yielded 16 new species, comprising *N. armin*, *N. tboli*, *N. zygon*, *N. pantaronensis*, *N. cornuta*, *N. talaandig*, *N. amabilis*, *N. barcelonae*, *N. aenigma*, *N. justinae*, *N. malimumuensis*, *N. manobo*, *N. alfredoi*, *N. erucoides*, *N. cabanae*, and *N. maximoides*. This high species diversity is related to the wide variety of ultramafic plains exposed in Mindanao, which includes many isolated mountain peaks. Less fertile soil conditions, which tend to be toxic to plants, as well as often poor water availability, together with special climatic factors around ultramafic rocks, all contribute significantly to high levels of speciation and endemism (Galey et al. 2017).

Over the past 10 years, the discovery of new species in Malaysia, especially in Peninsular Malaysia, totalled eight species, consisting of *N. malayensis*, *N. latiffiana*, *N. domei*, *Nepenthes x setiuensis*, *N. hairy*, *N. sericea*, *N. ulukaliana*, and *N. limiana*. According to Ghazalli et al. (2021), there are 14 species of *Nepenthes* recorded in parts of Peninsular Malaysia and are mostly distributed in scrub forests, lowlands, and mountains up to 1000 metres in altitude. Of the 14 *Nepenthes* species recorded, 10 are endemic. The current classification of *Nepenthes* in Peninsular Malaysia is based on morphological characteristics, with clear differences seen between species found at high, middle, and low altitudes (Bunawan et al. 2017).

Thailand is one of the countries in Southeast Asia with 14 recognised species of the genus *Nepenthes* to date. Of these, three new species, including *N. krabiensis*, *N. bracteosa*, and *N. hirtella*, were discovered during the last 10 years. Among these, seven species belonging to the *Pyrophytae* section predominantly occur in highland areas at elevations of 300-760 metres. Members of the *Pyrophytae* section are characterised by several distinct morphological features: tuberous rootstocks, absence of climbing stems and upper pitchers, uncoiled tendrils in upper pitchers, and partial peduncles bearing single flowers (Nuanlaong et al. 2022).

The species identification process for the genus *Nepenthes* typically utilises morphological characteristic differences, particularly pitcher traits, as each species possesses specific morphological features that distinguish it from others (Gilbert et al. 2020; Ghazalli et al. 2021). These distinctive characteristics serve as simple field identification markers for *Nepenthes*, with the most significant variations observed in pitcher morphology and colouration. As modified leaves, the pitchers not only reflect adaptations to nutrient-poor environments but also correlate with dietary specialisation (Setiawan et al. 2018; Huda et al. 2022). However, this approach has limitations. *Nepenthes* are heteroblastic species characterised by leaf ontogenetic dimorphism, which is par-

ticularly pronounced in certain species (Gaume & Di Giusto 2009). This change in leaf form is often associated with the transition from juvenile to mature, flowering stages. Consequently, anatomical studies are now being developed as an alternative approach to address identification ambiguities (Huda et al. 2022).

Nepenthes is a carnivorous plant genus that serves a source of inspiration and value for research development. However, the survival of this plant is threatened, with 17 species classified as endangered and eight as critical based on data from the IUCN. To overcome these threats, it is necessary to conserve exclusively based on the knowledge gathered by scientists (Miguel et al. 2018).

CONCLUSIONS

Nepenthes is a genus of carnivorous plants. This genus belongs to the Nepenthaceae family and can be found in several countries. Based on journals published between 2014-2023, data on newly described *Nepenthes* species were collected from a range of reputable scientific journals that specialise in plant taxonomy, biodiversity, and conservation. These journals include Phytotaxa, Kalpataru, Philippine Journal of Science, Philippine Journal of Systematic Biology, Plants, Thailand Forest Bulletin, Phytokeys, Journal of Sustainable Natural Resources, Reinwardtia, Kew Bulletin, PeerJ, Carnivorous Plant Newsletter, Malayan Nature Journal, and the Journal of Plant Taxonomy and Geography.

A total of 37 new species of *Nepenthes* have been identified across Southeast Asia, particularly in the Philippines, Indonesia, Malaysia, and Thailand. In the Philippines, newly described species include *Nepenthes armin*, *Nepenthes tboli*, *Nepenthes zygon*, *Nepenthes pantaronensis*, *Nepenthes cornuta*, *Nepenthes talaandig*, *Nepenthes amabilis*, *Nepenthes barcelonae*, *Nepenthes aenigma*, *Nepenthes justinae*, *Nepenthes malimumuensis*, *Nepenthes manobo*, *Nepenthes alfredoi*, *Nepenthes erucoides*, *Nepenthes cabanae*, and *Nepenthes maximoides*. In Indonesia, the following new species have been discovered: *Nepenthes halmahera*, *Nepenthes weda*, *Nepenthes minima*, *Nepenthes maryae*, *Nepenthes biak*, *Nepenthes longiptera*, *Nepenthes pudica*, *Nepenthes harauensis*, *Nepenthes samudera*, and *Nepenthes dactylifera*. From Thailand, newly recorded species include *Nepenthes krabiensis*, *Nepenthes bracteosa*, and *Nepenthes hirtella*. Meanwhile, in Malaysia, the new species identified are *Nepenthes malayensis*, *Nepenthes latiffiana*, *Nepenthes domei*, *Nepenthes* × *setiuensis*, *Nepenthes berbulu*, *Nepenthes sericea*, *Nepenthes ulukaliana*, and *Nepenthes limiana*.

Nepenthes plants play an important ecological role by controlling insect populations and stabilising soil in nutrient-poor habitats. Nonetheless, *Nepenthes* populations are threatened by deforestation, climate change, and human activities, so more intensive conservation efforts are needed to protect the survival of this genus.

AUTHOR CONTRIBUTION

S.W.I., M.S., R.K.A., S.A.J., and K. collected, analysed the data and wrote the manuscript; B.I. and F.R.P.D. supervised the entire process.

ACKNOWLEDGMENTS

The authors gratefully acknowledge financial support from the Penelitian Dasar Unggulan (PDU) program, Universitas Airlangga, Indonesia (Grant No. 1747/UN3.LPPM/PT.01.03/2025).

CONFLICT OF INTEREST

This study was conducted without any conflict of interest.

REFERENCES

Amoroso, V.B. et al., 2017. *Nepenthes alfredoi* (Caryophyllales, Nepenthaceae), a new species of pitcher plant from Mindanao, Philippines. *Philippine Journal of Systematic Biology*, 11(2), pp.14–19. doi: 10.26757/pjsb.2017b11018.

Bauer, U. et al., 2016. Carnivorous *Nepenthes* pitcher plants are a rich food source for a diverse vertebrate community. *Journal of Natural History*, 50 (7–8), pp.483–495. doi: 10.1080/00222933.2015.1059963.

Bazile, V. et al., 2012. A Carnivorous Plant Fed by Its Ant Symbiont: A Unique Multi-Faceted Nutritional Mutualism. *PLoS ONE*, 7(5), e36179. doi: 10.1371/journal.pone.0036179.

Buch, F. et al., 2014. Phytochemistry Characterization and heterologous expression of a PR-1 protein from traps of the carnivorous plant *Nepenthes mirabilis*. *Phytochemistry*, 100, pp.43–50.doi: 10.1016/j.phytochem.2014.01.014.

Bunawan, H. et al., 2017. Phylogenetic inferences of *Nepenthes* species in Peninsular Malaysia revealed by chloroplast (trnL intron) and nuclear (ITS) DNA sequences. *BMC Research Notes*, 10(1), pp.4–9. doi: 10.1186/s13104-017-2379-1.

Brillo, S. et al., 2024. A Historical Review of the Molecular Phylogeny of the Philippine *Nepenthes* L. (Nepenthaceae) with Notes for Unsampled Taxa. *Journal of Interdisciplinary Perspectives*, 2(8), pp.422-440. doi: 10.69569/jip.2024.0298.

Cheek, M., 2015. *Nepenthes* (Nepenthaceae) of Halmahera, Indonesia. *Blumea: Journal of Plant Taxonomy and Plant Geography*, 59(3), pp.215–225. doi: 10.3767/000651915X689091.

Cheek, M. & Jebb, M., 2014. Expansion of the *Nepenthes alata* group (Nepenthaceae), Philippines, and descriptions of three new species. *Blumea: Journal of Plant Taxonomy and Plant Geography*, 59(2), pp.144–154. doi: 10.3767/000651914X685861.

Cheek, M. & Jebb, M., 2016a. A new section in *Nepenthes* (Nepenthaceae) and a new species from Sulawesi. *Blumea: Journal of Plant Taxonomy and Plant Geography*, 61(1), pp.59–62. doi: 10.3767/000651916X691510.

Cheek, M. & Jebb, M.H.P., 2016b. *Nepenthes minima* (Nepenthaceae), a new pyrophytic grassland species from Sulawesi, Indonesia. *Blumea: Journal of Plant Taxonomy and Plant Geography*, 61(3), pp.181–185. doi: 10.3767/000651916X693509.

Cheek, M. et al., 2018. *Nepenthes* section insignes in Indonesia, with two new species. *Blumea: Journal of Plant Taxonomy and Plant Geography*, 62(3), pp.174–178. doi: 10.3767/blumea.2018.62.03.03.

Cheek, M. et al., 2015. *Nepenthes barcelonae* (Nepenthaceae), a new species from luzon, philippines. *Phytotaxa*, 222(2), pp.145–150. doi: 10.11646/phytotaxa.222.2.7.

Chiu, R., 2023. *Nepenthes samudera* sp. nov. Largest known *Nepenthes* species from Sumatra, with adaptations for a terrestrial growth habit. December.

Dančák, M. et al., 2022. First record of functional underground traps in a pitcher plant: *Nepenthes pudica* (Nepenthaceae), a new species from North Kalimantan, Borneo. *PhytoKeys*, 201, pp.77–97. doi: 10.3897/phytokeys.201.82872.

Dhamecha, D. et al., 2016. *Nepenthes khasiana* mediated synthesis of stabilized gold nanoparticles: Characterization and biocompatibility studies. *Journal of Photochemistry and Photobiology B: Biology*, 154, pp.108–117. doi: 10.1016/j.jphotobiol.2015.12.002.

Fitmawati et al., 2023. Diversity of Pitcher Plants (*Nepenthes* Spp.) in Riau Archipelago Province, Indonesia. *Sabrao Journal of Breeding and Genetics*, 55(3), pp.927–939. doi: 10.54910/sabrao2023.55.3.27.

Galey, M.L. et al., 2017. Ultramafic geoecology of South and Southeast Asia. *Botanical Studies*, 58(1), 18. doi: 10.1186/s40529-017-0167-9.

Gaume, L. & Di Giusto, B., 2009. Adaptive significance and ontogenetic variability of the waxy zone in *Nepenthes rafflesiana*. *Annals of Botany*, 104(7), pp.1281–1291. doi: 10.1093/aob/mcp238.

Gaume, L. et al., 2016. Different pitcher shapes and trapping syndromes explain resource partitioning in *Nepenthes* species. *Ecology and Evolution*, 6 (5), pp.1378–1392. doi: 10.1002/ece3.1920.

Gaume, L. et al., 2019. The biotic and abiotic drivers of 'living' diversity in the deadly traps of *Nepenthes* pitcher plants. *Biodiversity and Conservation*, 28(2), pp.345–362. doi: 10.1007/s10531-018-1658-z.

Ghazalli, M.N. et al., 2020. *Nepenthes latiffiana* and *N. domei* (Nepenthaceae), two new species of pitcher plants from Terengganu, Peninsular Malaysia. *Webbia. Journal of Plant Taxonomy and Geography*, 75(1), pp.5-28. doi: 10.36253/jopt-7950.

Ghazalli, M.N. et al., 2021. Comparative leaf anatomy of ten *Nepenthes* L. species (Nepenthaceae) from Peninsular Malaysia. *Notulae Scientia Biologicae*, 13(4), 10980. doi: 10.15835/nsb13410980.

Gilbert, K.J. et al., 2020. Tropical pitcher plants (*Nepenthes*) act as ecological filters by altering properties of their fluid microenvironments. *Scientific Reports*, 10, 4431. doi: 10.1038/s41598-020-61193-x.

Givnish, T.J., 2015. New evidence on the origin of carnivorous plants. *Proceedings of the National Academy of Sciences of the United States of America*, 112(1), pp.10–11. doi: 10.1073/pnas.1422278112.

Golos, M.R. et al., 2023. *Nepenthes limiana* (Nepenthaceae), a new pitcher plant from the northern Titiwangsa Range of Peninsular Malaysia. *Carnivorous Plant Newsletter*, 52(3), pp.128–153. doi: 10.55360/cpn523.mg603.

Gronemeyer, T. et al., 2014. Four new species of *Nepenthes* L. (Nepenthaceae) from the central mountains of Mindanao, Philippines. *Plants*, 3(2), pp.284–303. doi: 10.3390/plants3020284.

Gronemeyer, T. et al., 2016. Two new *Nepenthes* species from the Philippines and an emended description of *Nepenthes ramos*. *Plants*, 5(2), pp.195–202. doi: 10.3390/plants5020023.

Hernawati et al., 2022a. *Nepenthes harauensis*, a New Species of Nepenthaceae From West Sumatra. *Reinwardtia*, 21(1), pp.19–23. doi: 10.14203/reinwardtia.v21i1.4306.

Hernawati et al., 2022b. Synopsis of Sumatran *Nepenthes* (Indonesia). *Biodiversitas*, 23(8), pp.4243–4255. doi: 10.13057/biodiv/d230848.

Huda, M.H.N. et al., 2022. Leaf Anatomical Characteristics of *Nepenthes* Species in Western Sarawak, Borneo. *Malaysian Applied Biology*, 51(5), pp.201–210. doi: 10.55230/mabjournal.v51i5.2339.

King, C. & Cheek, M., 2020. *Nepenthes maximoides* (Nepenthaceae) a new, critically endangered (possibly extinct) species in Sect. Alatae from Luzon, Philippines showing striking pitcher convergence with *N. maxima* (Sect. Regiae) of Indonesia. *PeerJ*, 8, e9899. doi: 10.7717/peerj.9899.

Konwar, P. et al., 2023. Identifying conservation priority areas and predicting the climate change impact on the future habitats of endangered *Nepenthes khasiana* Hook.f. utilizing ecological niche modelling. *Journal for Nature Conservation*, 74, 126436. doi: 10.1016/j.jnc.2023.126436.

Lagunday, N.E. et al., 2017. Two new *Nepenthes* species from the unexplored mountains of central mindanao, Philippines. *Philippine Journal of Science*, 146(2), pp.159–165.

Lagunday, NE. & Amoroso, V.B., 2019. *Nepenthes cabanae* (Caryophyllales, Nepenthaceae), a new species of pitcher plant from Central Mindanao, Philippines. *Philippine Journal of Systematic Biology*, 13(1), pp.39-45. doi: 10.26757/pjsb2019a13005.

Lestari, W. et al., 2018. Identification and Cluster Analysis of Pitcher Plant (*Nepenthes* spp.) from South Sumatera Indonesia. *Biosaintifika*, 10(2), pp.245–251.

Mansur, M. et al., 2020. Diversity, Abundance and Ethnobotany of Nepenthes in Mandor Nature Reserve, West Kalimantan, Indonesia. *Planta Carnivora …* [Preprint], (June).

Mansur, M. et al., 2021. Ecology of *Nepenthes* clipeata on Gunung Kelam, Indonesian Borneo. *Plant Ecology & Diversity*, 14(3-4), pp.195-204. doi: 10.1080/17550874.2021.1984602.

Mansur, M. et al., 2023. Diversity, Ecology and Conservation Status of *Nepenthes* in West Sumatra Province, Indonesia. *Biotropia*, 30(2), pp.220–231. doi: 10.11598/btb.2023.30.2.1896.

Mansur, M. et al., 2024. Ecology of *Nepenthes* on Mount Talang, West Sumatra, Indonesia. *Tropical Ecology*, 65, pp.460-469. doi: 10.1007/s42965-024-00333-0.

Martín-Martín, A. et al., 2018. Google Scholar, Web of Science, and Scopus: A systematic comparison of citations in 252 subject categories. *Journal of Informetrics*, 12(4), pp.1160–1177. doi: 10.1016/j.joi.2018.09.002.

Miguel, S. et al., 2018. *Nepenthes*: State of the art of an inspiring plant for biotechnologists. *Journal of Biotechnology*, 265, pp.109–115. doi: 10.1016/j.jbiotec.2017.11.014.

Mithöfer, A., 2022. Carnivorous plants and their biotic interactions. *Journal of Plant Interactions*, 17(1), pp.333–343. doi: 10.1080/17429145.2022.2038710.

Murphy, B. et al., 2020. A phylogenomic analysis of *Nepenthes* (Nepenthaceae). *Molecular Phylogenetics and Evolution*, 144, 106668. doi: 10.1016/j.ympev.2019.106668.

Nainggolan, L. et al., 2020. Inventory of pitcher plant (*Nepenthes* sp.) and its existence in north sumatra indonesia. *Journal of Physics: Conference Series*, 1485, 012013. doi: 10.1088/1742-6596/1485/1/012013.

Nuanlaong, S. et al., 2022. Descriptions of two new species of *Nepenthes* (Nepenthaceae) from Thailand and their phylogenetic analysis based on AFLP technique species confirmation. *Kew Bulletin*, 77(1), pp.105–120. doi: 10.1007/s12225-021-09997-6.

Nuanlaong, S. et al., 2016. A new species of *Nepenthes* (Nepenthaceae) from Thailand. *Thai Forest Bulletin (Botany)*, 44(2), pp.128–133. doi: 10.20531/TFB.2016.44.2.08.

Renjana, E. et al., 2024. Exploring a critically endangered pitcher plant *Nepenthes rigidifolia* and predicting its distribution habitat in North Sumatra, Indonesia. *Journal for Nature Conservation*, 80, 126645. doi: 10.1016/j.jnc.2024.126645.

Robinson, A.S. et al., 2019a. Revisions in *Nepenthes* following explorations of the kemul massif and the surrounding region in north-central Kalimantan, Borneo. *Phytotaxa*, 392(2), pp.97–126. doi: 10.11646/phytotaxa.392.2.1.

Robinson, A.S. et al., 2019b. *Nepenthes erucoides* (Nepenthaceae), an ultramaficolous micro-endemic from Dinagat Islands Province, northern Mindanao, Philippines. *Phytotaxa*, 423(1), pp.21–32. doi: 10.11646/phytotaxa.423.1.3.

Saganová, M. et al., 2018. Regulation of enzyme activities in carnivorous pitcher plants of the genus *Nepenthes*. *Planta*, 248(2), pp.451–464. doi: 10.1007/s00425-018-2917-7.

Setiawan, H. et al., 2018. The diversity of *Nepenthes* at the post-mining area in Sintang District, West Kalimantan, Indonesia. *Biodiversitas Journal of Biological Diversity*, 19(5), pp.1820–1827. doi: 10.13057/biodiv/d190532.

Tamizi, A.A. et al., 2020a. *Nepenthes malayensis* (Nepenthaceae), a new species of carnivorous pitcher plant from Peninsular Malaysia. *Kew Bulletin*, 75 (4), 63. doi: 10.1007/s12225-020-09918-z.

Tamizi, A.A. et al., 2020b. *Nepenthes* × *setiuensis* (Nepenthaceae), a new nothospecies of pitcher plant from montane cloud forest of Peninsular Malaysia. *Malayan Nature Journal*, 72(1), pp.27–41.

Tamizi, A.A. et al., 2023. Insights into The Diversity of *Nepenthes* L. (Nepenthaceae) Across Peninsular Malaysia, Including The First Sighting of an Undescribed Taxon with Flared Peristomes and Quadruple-Row Ventral Wings. *Journal of Sustainable Natural Resources*, 4(1), pp.10-36. doi: 10.30880/jsunr.2023.04.01.002.

Tan, H.L. et al., 2023. *Nepenthes berbulu* (Nepenthaceae), a pitcher plant from Peninsular Malaysia with remarkably long lid bristles. *Carnivorous Plant Newsletter*, 52(1), pp.15–43. doi: 10.55360/cpn521.fm322.

Thorogood, C.J. et al., 2018. Convergent and divergent evolution in carnivorous pitcher plant traps. *New Phytologist*, 217(3), pp.1035–1041. doi: 10.1111/nph.14879.

Victoriano, M., 2021. A new species of *Nepenthes* (nepenthaceae) and its natural hybrids from aceh, sumatra, indonesia. *Reinwardtia*, 20(1), pp17–26. doi: 10.14203/REINWARDTIA.V20I1.3932.

Wójciak, M. et al., 2023. Biological Potential of Carnivorous Plants from Nepenthales. *Molecules*, 28(8), 3639. doi: 10.3390/molecules28083639.

Journal of Tropical Biodiversity and Biotechnology
Volume 10, Issue 04 (2025): jtbb21198
DOI: 10.22146/jtbb.21198

Review Article

Molecular Insights into the Genetic Diversity of Marine Zooplankton

Angkasa Putra[1,a,*], Sarifah Aini[1,a], I Nyoman Suyasa[2], Ilham[2,3], Fitriska Hapsari[2], Muhammad Hery Riyadi Alauddin[4], Ani Leilani[2], Heri Triyono[2], Rina[2], Mugi Mulyono[2], Tatty Yuniarti[2], Mira Maulita[2], Yenni Nuraini[2], Ita Junita Puspa Dewi[2], Sinung Rahardjo[2], Sinar Pagi Sektiana[2], Hamdani[2], Made Ariana[2], Taufik Hadi Ramli[5], Lalu Achmad Jani Qhadaffi[2], Ayu Rizki Amalia[2], Cici Maulida[6], Mhd Aidil Huda J.[7], Muh. Azril[8], Hawati[4], Muhammad Misi Muslimin[9]

1) Interdisciplinary Program of Marine and Fisheries Sciences and Convergent Technology, Pukyong National University, 45 Yongso-ro, Nam-gu, Busan 48513, Republic of Korea
2) Jakarta Technical University of Fisheries (Politeknik Ahli Usaha Perikanan), Ministry of Marine Affairs and Fisheries, Jl. AUP No. 1, Pasar Minggu, South Jakarta, Special Region of Jakarta 12520, Republic of Indonesia
3) Marine and Fisheries Polytechnic of Jembrana (Politeknik Kelautan dan Perikanan Jembrana), Ministry of Marine Affairs and Fisheries, Pengambengan, Negara, Jembrana, Bali 82218, Republic of Indonesia
4) Marine and Fisheries Polytechnic of Bone (Politeknik Kelautan dan Perikanan Bone), Ministry of Marine Affairs and Fisheries, Jl. Sungai Musi KM. 9, Watampone, Bone, South Sulawesi 92718, Republic of Indonesia
5) Marine and Fisheries Polytechnic of Karawang (Politeknik Kelautan dan Perikanan Karawang), Ministry of Marine Affairs and Fisheries, Jl. Lingkar Tanjungpura, Karangpawitan, Karawang, West Java 41315, Republic of Indonesia
6) Samudra University, Jl. Prof. Dr. Syarief Thayeb, Langsa Lama, Langsa, Aceh 24416, Republic of Indonesia
7) Matauli College of Fisheries and Marine Sciences (Sekolah Tinggi Perikanan dan Kelautan Matauli), Jl. Ki Hajar Dewantara No. 1, Pandan, Central Tapanuli, North Sumatra 22611, Republic of Indonesia
8) Tidar University, Jl. Kapten Suparman No. 39, Potrobangsan, North Magelang, Magelang, Central Java 56116, Republic of Indonesia
9) Indonesian Muslim University, Jl. Urip Sumoharjo KM. 5, Makassar, South Sulawesi 90231, Republic of Indonesia
a) These authors contributed equally to this work
* Corresponding author, email: angkasaputra80@gmail.com

Keywords:
Genomic Tools
Marine Biodiversity
Molecular Ecology
Zooplankton
Submitted:
01 May 2025
Accepted:
14 July 2025
Published:
21 November 2025
Editors:
Miftahul Ilmi
Tanti Agustina

ABSTRACT

Zooplankton are fundamental components of marine trophic networks and served as bioindicators of environmental changes. Assessing their genetic diversity is essential for biodiversity assessment, ecosystem monitoring, and evidence-based conservation strategies. The conventional morphological identification methods are limited in detecting cryptic species and lack phylogenetic resolution, necessitating the use of molecular approaches. Hence, this review synthesises the recent advancements in genomic tools for investigating marine zooplankton genetic variability, encompassing techniques such as DNA barcoding and metabarcoding, complete mitochondrial genome analysis, as well as environmental DNA profiling. We systematically evaluated the advantages of each method, the application of genetic markers, and their effectiveness in species identification, population genetics, and evolutionary studies. The genetic methods have greatly improved taxonomic resolution, revealed hidden biodiversity, and offered deeper insights into the population structure and community dynamics of marine zooplankton in response to human-induced pressures. Despite these achievements, several challenges persist, including incomplete genetic reference databases, sequencing errors, and the lack of standardised protocols. Accordingly, future research should prioritise the expansion of comprehensive genetic libraries, the refinement of bioinformatics pipelines, and the integration of multi-marker approaches to deepen our understanding of marine zooplankton genetic variation and ecological interactions. Continued improvement in these molecular methodologies will be important for the effective conservation of marine biodiversity, the mitigation of environmental fluctuation impacts, and the promotion of sustainable fisheries management.

How to cite:
Putra, A. et al., 2025. Molecular Insights into the Genetic Diversity of Marine Zooplankton. *Journal of Tropcial Biodiversity and Biotechnology*, 10(4), jtbb21198. doi: 10.22146/jtbb.21198

INTRODUCTION

The oceans and seas encompass over 70 % of the Earth's surface and harbour exceptionally high levels of biodiversity, with zooplankton representing a dominant component of pelagic ecosystems in terms of both abundance and biomass (Azam et al. 1983; Steinberg et al. 2008). Notably, the extensive swarms of Antarctic krill (*Euphausia superba*) in the Southern Ocean sustain complex marine food webs by supporting ecologically and economically important species, including baleen whales, penguins, and seals, thereby highlighting the vital ecological role of zooplankton on a global scale (Atkinson et al. 2004). Zooplankton comprise a taxonomically diverse assemblage, ranging from microscopic copepods to larger taxa, such as euphausiids, decapod larvae, and ichthyoplankton (Ward et al. 2012). As primary consumers, zooplankton mediate the transfer of energy from autotrophic phytoplankton to higher trophic levels, including fish, marine mammals, and seabirds (Putra et al. 2025) (Figure 1). Furthermore, zooplankton contribute significantly to biogeochemical cycling, particularly of carbon and nutrients through the biological pump mechanism. By producing and exporting organic particulate matter, zooplankton facilitate the sequestration of carbon into the deep ocean, thereby, playing a pivotal role in regulating global climate dynamics (Lindeque et al. 2013).

The genetic diversity within marine zooplankton populations is a critical factor in their ability to adapt and survive under environmental pressures (Möllmann et al. 2008). The genetic variation in DNA sequences also enables zooplankton's adaptive responses to ecological fluctuations, incorporating changes in sea temperature, salinity, food availability, as well as exposure to pathogens and pollutants (Bucklin et al. 2021a). The populations with low genetic diversity are more susceptible to extreme habitat dynamics, potentially destabilizing marine ecosystems as a whole (Lindeque et al. 2013). Therefore, understanding zooplankton genetic variability is integral not only for uncovering their evolutionary patterns but also for informing conservation efforts and the sustainable management of marine resources.

However, our understanding of zooplankton genetic variation remains limited, especially in terms of population differentiation across diverse geographical regions and habitats (McGinty & Irwin 2025). The global warming, microplastic pollution, various pollutants (heavy metals, pesticides, and other toxic chemicals), as well as overexploitation further exacerbate pressures on zooplankton populations, leading to significant shifts in community structure (Möllmann et al. 2008). As a result, more precise methods are needed to monitor and to analyse their genetic dynamics (Lenz et al. 2021). In this context, the molecular investigations, using techniques such as DNA barcoding and metabarcoding have become invaluable tools for species identification and the analysis of genetic variation among individuals, revealing details that are usually inaccessible through traditional morphological methods (Lindeque et al. 2013). These approaches also offer deeper elucidation of phylogenetic relationships, geographical distribution, as well as potential adaptation and speciation processes in marine zooplankton (Filatov et al. 2021; Filatov 2023).

With advancements in molecular technologies, our interpretation of zooplankton genetic diversity can be significantly enhanced, enabling crucial insights into the impacts of anthropogenic activities on marine ecosystems. Thus, this scientific article aims to present a inclusive review of the application of molecular methods in marine zooplankton genetic variability studies. It focuses on the latest molecular techniques for identifying and analysing genetic variation, as well as their implications for the management of marine fisheries resources. In addition, this review highlights key challenges in marine zooplankton genetic research and proposes recommendations for future investigations. By advancing our knowledge of genetic diversity through ge-

nomic approaches, more effective and sustainable conservation strategies and marine ecosystem management practices can be developed and implemented.

Figure 1. The Census of Marine Zooplankton hosts an online gallery showcasing visuals of various zooplankton species (available at http://www.cmarz.org/galleries.html). The photographic records were contributed by R.R. Hopcroft and C. Clarke (University of Alaska Fairbanks) and L.P. Madin (Woods Hole Oceanographic Institution). These illustrations were subsequently compiled and visually integrated into a representative figure by the first author (A.P.).

MOLECULAR MARKERS AND DNA-BASED APPROACHES IN MARINE ZOOPLANKTON RESEARCH

Molecular markers

The molecular markers have become indispensable tools in marine zooplankton genetic research, enabling accurate species identification and providing perspectives into phylogenetic relationships, population connectivity, and evolutionary dynamics (González et al. 2020). Derived primarily from DNA sequences, commonly used markers include mitochondrial genes (e.g., COI), nuclear ribosomal genes (e.g., 18S, 28S rRNA), internal transcribed spacers (ITS), and non-coding regions such as microsatellites (Parent et al. 2012; Bucklin et al. 2016). Notably, the COI region is widely applied in DNA barcoding due to its high interspecific variability and low intraspecific variation, facilitating discrimination of morphologically similar taxa (Hebert et al. 2003). Its integration into global databases like BOLD and GenBank enhances cross-taxon comparisons and facilitates the detection of cryptic species (Blanco-Bercial et al. 2011a; Cornils et al. 2017; Porter & Hajibabaei 2018). Although nuclear genes evolve more slowly than mitochondrial genes, they provide a more reliable signal for reconstructing deeper phylogenetic relationships among marine zooplankton clades (Bucklin et al. 2003; Di Capua et al. 2017). Conversely, microsatellites, characterized by high allelic diversity and codominant inheritance, are particularly suited for fine-scale genetic anal-

yses and enable evaluations of gene flow, mating systems, heterozygosity, and demographic structure (Weydmann et al. 2014; Goetze et al. 2015).

Genomic strategies in marine zooplankton investigation

The molecular techniques offer substantial advantages over conventional morphology-based methods in marine zooplankton genetic diversity and ecological studies, primarily by providing enhanced taxonomic resolution and reliable species identification, including for cryptic taxa (Bucklin et al. 2022). These DNA-based approaches reduce subjective biases inherent in morphological identifications and facilitate detection of rare or minute species often overlooked by traditional methods. Among these, the DNA barcoding utilises standardised short genetic markers, typically mitochondrial COI, to identify individual species, whereas DNA metabarcoding analyses mixed DNA from bulk organism samples to characterise entire community compositions. The environmental DNA (eDNA) metabarcoding extends this capability by extracting DNA directly from biospheric matrices such as seawater, empowering non-invasive detection of elusive species without physical specimen collection (Djurhuus et al. 2018; Carroll et al. 2019) (Figure 2).

The application of molecular tools in marine zooplankton research has revealed extensive phylogenetic, taxonomic, and functional diversity, encompassing at least 15 phyla and 41 functional groups, including both holoplankton and meroplankton (Bucklin et al. 2021b). The significant efforts to barcode key taxa such as Copepoda have yielded extensive COI sequence libraries, although geographic and taxonomic gaps remain (Weydmann et al. 2017; Figure 3). Beyond Copepoda, the DNA barcoding has been successfully applied to other major marine zooplankton taxa, including Cnidaria, Ctenophora, Amphipoda, Euphausiacea, Gastropoda, Chaetognatha, and pelagic Tunicata (O'Brien et al. 2024). The representative case studies illustrated the effectiveness of these molecular methods across diverse marine regions with DNA barcoding characterised zooplankton diversity in the Gulf of Alaska (Questel et al. 2025), eDNA metabarcoding elucidated community composition in the Ulleung Basin (Choi et al. 2024), and DNA metabarcoding demonstrated complex assemblages along the South African coast (Singh et al. 2021; Huggett et al. 2022).

At the population genetic level, the molecular markers such as microsatellites and single nucleotide polymorphisms (SNPs) provide insights into genetic structure, gene flow, and microevolutionary dynamics (e.g., genetic drift, natural selection, and local adaptation) within the marine zooplankton species (Bucklin et al. 2018). High-throughput sequencing techniques such as RNA-Seq, have produced extensive SNP datasets with over 110,000 SNPs have been identified and validated in *Calanus sinicus*, enabling more precise population genetic analyses (Yang et al. 2014). Furthermore, the SNP-based investigations have also resolved previous uncertainties from microsatellite-based hybridisation studies among *Calanus* species, confirming the genetic distinctness of *C. finmarchicus* and *C. glacialis* and highlighting the limitations of microsatellite markers (Choquet et al. 2023). Despite their utility, the molecular methods face challenges, including PCR and primer biases that can skew community composition estimates by preferentially amplifying certain taxa (Elbrecht & Leese 2015; Goldberg et al. 2015), as well as issues of DNA degradation and potential false positives in eDNA samples (Takahashi et al. 2023; Wang et al. 2023). The taxonomic resolution is further constrained by incomplete reference databases, especially in underexplored marine regions (Weigand et al. 2019). The complementary quantitative approaches such as qPCR and digital droplet PCR (ddPCR) also offer high-precision detection and quantification, valuable for monitoring invasive species and environmental changes (Wood et al. 2019).

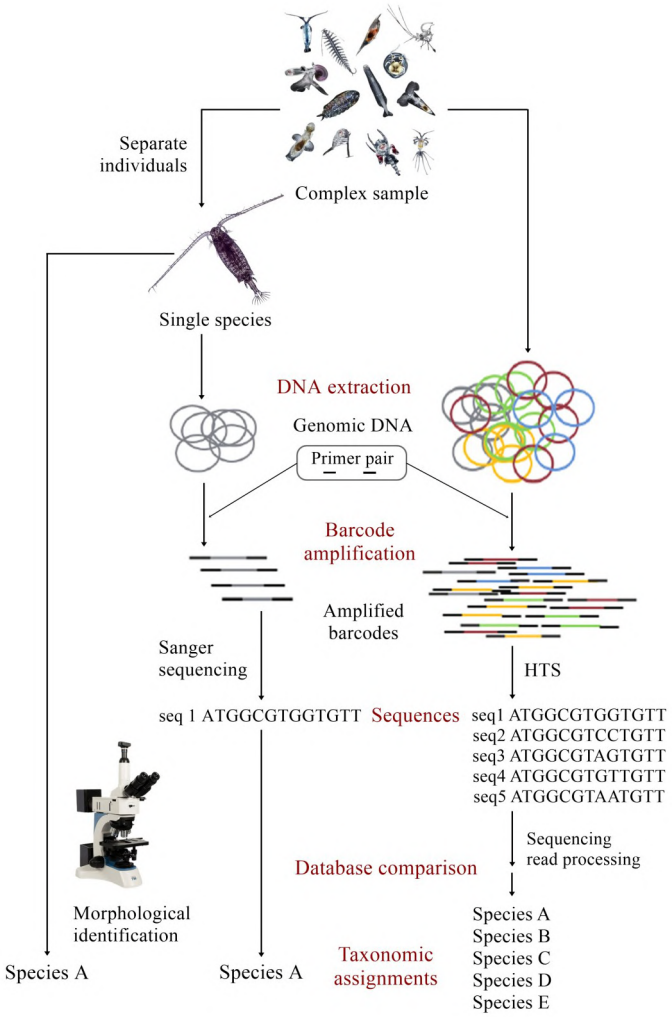

Figure 2. The schematic representation of marine zooplankton sample taxonomy analysis using morphological identification (left arrow), barcoding (middle arrow), or metabarcoding (right arrow). The colored circles represent extracted genomic DNA, consisting of identical copies of the genome (barcoding) or multiple copies of genomes from the species present in the sample (metabarcoding). The amplified products are identical in barcoding, while metabarcoding produces a mixture of amplified products from different genomes. After sequencing the amplification products, taxonomic assignment is made by comparing the obtained sequences with reference databases. The figure was modified by the first author (A.P.) based on studies by Corell and Rodríguez-Ezpeleta (2014) and Bucklin et al. (2016). The complex sample image was sourced from Peijnenburg and Goetze (2013), and the Copepoda image was obtained from micromagus.net.

PATTERNS OF GENETIC DIVERSITY AND PHYLOGEOGRAPHY IN MARINE ZOOPLANKTON

The genetic diversity serves as the foundation for evolutionary potential, ecological adaptability, and long-term population viability in marine zooplankton. This diversity is expressed at multiple hierarchical levels, most notably within species (intraspecific variation) and across geographic ranges (phylogeographic structure). Both are shaped by a combination of environmental pressures and intrinsic biological traits. Notably, the intraspecific genetic variation denotes the extent of genetic differentiation among individuals or subpopulations within a species, primarily driven by mutation, gene flow, and genetic drift (Agashe 2009; Peijnenburg & Goetze 2013). Such variation is crucial for maintaining population resilience and adaptive capacity under fluctuating environmental conditions. It enables species to occupy diverse ecological niches and to maintain ecological functions under stress (de Bruin et al. 2024). Specifically, the copepod populations from distinct habitats, such

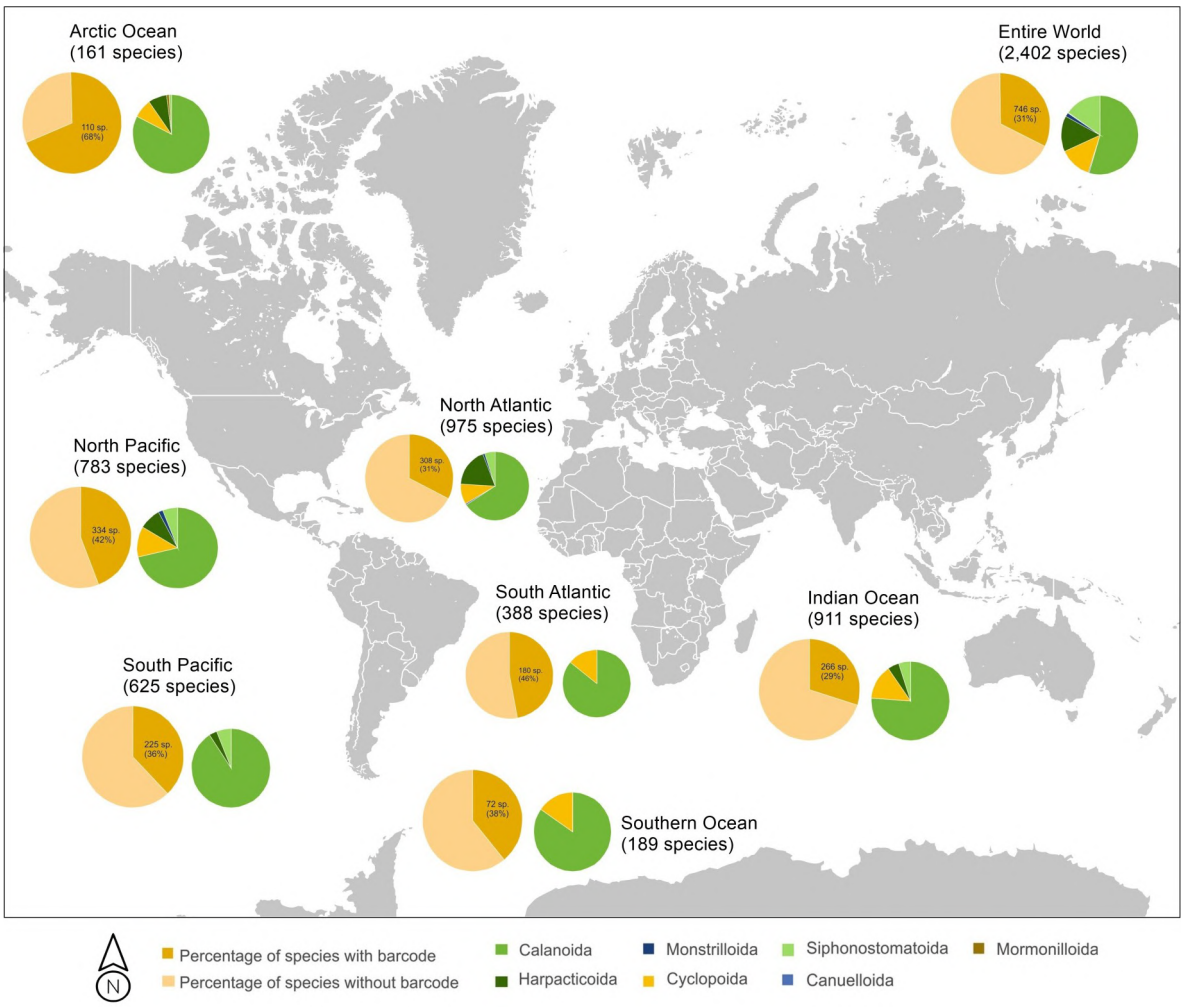

Figure 3. The global distribution of Copepoda with and without COI barcode across various oceanic regions. The recent data indicates that there are currently 12,155 sequences for 752 copepod species, representing approximately 31 % of the total 2402 valid species. The highest number of species is found in the North Atlantic (975 species), Indian Ocean (911 species), and the North and South Pacific (783 and 625 species, respectively), while fewer species are recorded in the South Atlantic (388 species), Southern Ocean (189 species), and Arctic (161 species). The figure was modified by the first author (A.P.) based on Bucklin et al. (2021b).

as estuarine, neritic, and oceanic zones often exhibit localized genetic structuring in response to environmental gradients (Unal & Bucklin 2010; Bashevkin et al. 2020). These patterns suggest that microevolutionary processes contribute significantly to population differentiation, even in highly dispersive marine taxa.

Extending beyond local variation, the phylogeographic structure reflects genetic divergence among marine zooplankton populations separated by geographical or oceanographic barriers. The physical discontinuities, such as current systems, thermal fronts, or bathymetric features can restrict dispersal and limit gene flow, leading to population subdivision over evolutionary timescales (Blanco-Bercial & Bucklin 2016; Bucklin et al. 2021a). The regional adaptation further reinforces this divergence, as populations become genetically fine-tuned to distinct environmental regimes (Gluchowska et al. 2017). Insights from phylogeographic studies have elucidated historical dispersal routes and delineated biogeographic boundaries among marine zooplankton populations. Moreover, these studies have contributed to the development of predictive frameworks for assessing species responses to large-scale environmental perturbations, such as ocean warming, deoxygenation, and acidification (Putra et al. 2025). Building upon these findings, the spatial and temporal dynamics of marine zooplankton genetic diversity are further shaped by a complex interplay of abiotic and biotic determinants (Botterell et

al. 2023). Among abiotic factors, temperature and salinity are particularly influential, as they regulate key physiological processes, including metabolism, fecundity, and larval development (Dam 2013; McGinty et al. 2021; Putra 2025). The thermal gradients can impose intense selective pressures, fostering local adaptation in some populations while contributing to genetic erosion in others (Gluchowska et al. 2017). Similarly, the salinity fluctuations in transitional environments such as estuaries frequently promote genomic divergence between marine and brackish-adapted lineages. In parallel, the life-history of marine zooplankton traits play a pivotal role in modulating the rate and extent of genetic differentiation. The species characterised by rapid generation turnover and high fecundity generally maintains greater levels of genetic variability, enhancing their evolutionary potential. Conversely, the taxa with longer generation times or low reproductive output may be more vulnerable to stochastic genetic drift and demographic bottlenecks, particularly in fragmented or stressed habitats (Spitze 1995; Litchman et al. 2013; Chust et al. 2016). Collectively, these interacting factors influence the persistence, structure, and evolutionary trajectory of genetic diversity across marine zooplankton assemblages.

MOLECULAR PERSPECTIVES ON MARINE ZOOPLANKTON EVOLUTION

While the preceding section examined spatial patterns and ecological drivers of genetic diversity, the molecular approaches provide essential insights into the evolutionary history and adaptive potential of marine zooplankton (Bucklin et al. 2021a). Advances in molecular systematics and population genomics have facilitated precise reconstructions of lineage divergence, post-glacial recolonisation pathways, and microevolutionary responses to environmental pressures. These molecular data have revolutionised understanding of marine zooplankton evolution by enabling fine-scale resolution of phylogenetic relationships and historical population dynamics (Bucklin et al. 2018). Notably, the phylogeographic analyses utilising mitochondrial and nuclear DNA sequences have revealed significant genetic discontinuities across geographic regions, reflecting historical isolation, dispersal barriers, and climate-driven range shifts (Caudill & Bucklin 2004; Bucklin et al. 2022). Such studies have clarified post-glacial colonisation routes, vicariance patterns, and cryptic speciation within morphologically indistinct taxa (Millette et al. 2011; Stepien et al. 2024).

The molecular markers, particularly the mitochondrial COI gene, have been instrumental in delineating evolutionary lineages and resolving taxonomic uncertainties among diverse marine zooplankton taxa (Machida et al. 2021). Moreover, the multilocus sequence data and emerging phylogenomic methods provide comprehensive frameworks for interpreting diversification tempo and mode in the context of paleoceanographic fluctuations. These molecular reconstructions enable mapping of evolutionary trajectories and assessment of past environmental impacts on current genetic structure (Blanco-Bercial et al. 2011b; El-Khodary et al. 2020). Beyond historical reassessments, the genetic tools illuminate mechanisms of adaptive evolution in marine zooplankton. These include selective pressures, such as thermal stress, salinity variation, and trophic shifts drive genomic changes (Dam 2013). The recent high-resolution genomic studies employing SNP markers and transcriptomic analyses have identified loci linked to physiological tolerance and ecological performance (Bucklin et al. 2018; Trubovitz et al. 2020). These findings demonstrate rapid adaptive shifts mediated by selection on genes associated with stress response, reproduction, and metabolic regulation (Johnston et al. 2022; Zhao et al. 2023). Remarkably, populations in high-salinity or thermally variable environments often exhibit unique allelic variants or differential gene expression that enhance fitness under extreme conditions. This molecular evi-

dence underscores the critical role of microevolutionary processes in sustaining population viability amid accelerating climate change. Hence, integrating genetics and environmental genomics provides a robust framework for evaluating marine zooplankton resilience, elucidating the molecular basis of adaptation and the adaptive potential of populations facing unprecedented environmental changes.

GENETIC CONNECTIVITY AND DISPERSAL DYNAMICS IN MARINE ZOOPLANKTON

Gene flow and dispersal mechanisms

The genetic connectivity is fundamental to the population dynamics and evolutionary processes of marine zooplankton (Cowen et al. 2007). Dispersal, largely driven by ocean currents and modulated by species-specific biological traits, shapes gene flow and population structure (Treml et al. 2008). The molecular evidence shows that allele distributions align closely with oceanographic variables, such as current patterns, temperature, and salinity, which can restrict gene flow and promote local adaptation and population differentiation (Filatov 2023; Peluso et al. 2024). The speciation in marine zooplankton often occurs sympatrically, driven by ecological niche specialization rather than geographic isolation, as demonstrated by integrative genomic and evolutionary analyses (Norris & Hull 2012; Filatov et al. 2021). Moreover, zooplankton dispersal is strongly influenced by life history characteristics, particularly during vulnerable larval stages (Chust et al. 2016; de Bruin et al. 2024). The ontogenetic vertical migration, where different life stages occupy distinct depth layers modulates interaction with stratified ocean currents, affecting dispersal trajectories and connectivity (Kobari & Ikeda 2001; Bandara et al. 2021). The daily vertical migration also impacts spatial distribution and genetic exchange by shifting populations between surface and deeper waters to balance feeding and predator avoidance (Bandara et al. 2021). The larval duration correlates positively with dispersal potential, as species exhibiting extended larval phases tend to possess more genetically homogeneous populations owing to broader gene flow, whereas shorter larval stages result in more localised genetic structuring (Modica et al. 2017; Bashevkin et al. 2020). The reproductive strategies further influence connectivity, with broadcast spawners facilitating extensive gene flow through planktonic gamete dispersal, while the brooding species typically show reduced connectivity and greater population differentiation (Riginos et al. 2014). The recent advances in high-throughput genomic sequencing and eDNA analyses have enhanced resolution in detecting these connectivity patterns and dispersal dynamics over large spatial scales (Yan et al. 2023; Rawoot et al. 2024).

Mitochondrial genome contributions to connectivity and dispersal in marine zooplankton

The mitogenome is extensively used to assess zooplankton connectivity due to its maternal inheritance, lack of recombination, and relative stability, making it a robust marker for population structure and dispersal analyses (Avise 1989; Havird et al. 2016; Fields et al. 2018). The next-generation sequencing (NGS) technologies have improved mitogenome resolution, allowing detailed reconstructions of zooplankton population history and migration patterns beyond classic mitochondrial markers (Cowen & Sponaugle 2009; Bucklin et al. 2018). The animal mitogenomes typically comprise 37 genes, including ribosomal RNAs, transfer RNAs, and protein-coding genes, with marine zooplankton exhibiting considerable intra- and interspecific variability within their mitogenomes (Boore 1999). Despite the ecological significance of many marine zooplankton species, the comprehensive mitogenome assemblies remain limited, with several notable taxa sequenced and additional data pending

characterization (Genome 10K Community of Scientists 2009; GIGA Community of Scientists 2014). The relatively slower accumulation of mitogenomic data in marine zooplankton compared to vertebrates highlights the need for expanded sequencing efforts (Table 1).

Table 1. Mitochondrial genomes of marine zooplankton species and their corresponding lengths.

Taxon and species	Length (bp)	Reference
Copepoda		
Calanus finmarchicus	>29,462	Weydmann et al. 2017
Calanus glacialis	>27,342	Weydmann et al. 2017
Calanus hyperboreus	17,910	Kim et al. 2013
Calanus sinicus	>20,460	Minxiao et al. 2011
Paracyclopina nana	15,981	Ki et al. 2009
Tigriopus californicus	14,600	Burton et al. 2007
Tigriopus japonicus	14,628	Machida et al. 2002
Tigriopus sp.	14,301	Jung et al. 2006
Euphausiacea		
Euphausia pacifica	16,898	Shen et al. 2011
Euphausia superba	>15,498	Shen et al. 2010
Ostracoda		
Vargula hilgendorfii	15,923	Ogoh & Ohmiya 2004
Amphipoda		
Onisimus nanseni	14,734	Ki et al. 2010
Decapoda		
Acetes chinensis	15,740	Kim et al. 2012
Cnidaria		
Aurelia aurita	16,937	Shao et al. 2006
Cassiopea frondosa	15,949	Kayal et al. 2011
Chrysaora quinquecirrha	16,775	Hwang et al. 2014
Ctenophora		
Mnemiopsis leidyi	10,000	Pett et al. 2011
Pleurobrachia bachei	11,016	Kohn et al. 2012
Chaetognatha		
Sagitta decipiens	11,121	Miyamoto et al. 2010
Sagitta enflata	12,631	Miyamoto et al. 2010
Sagitta ferox	12,153	Li et al. 2016
Sagitta nagae	11,459	Miyamoto et al. 2010
Paraspadella gotoi	11,423	Helfenbein et al. 2004
Pterosagitta draco	10,426	Wei et al. 2016
Spadella cephaloptera	11,905	Papillon et al. 2004

Role of metagenomics in understanding zooplankton diversity

The metagenomics, involving the direct sequencing of genetic material from environmental samples, has become a powerful method to characterise marine zooplankton diversity without isolating individual organisms (Monchamp et al. 2022). Unlike PCR-based metabarcoding, which targets specific genetic markers (e.g., mitochondrial COI, nuclear 18S rRNA) through amplification, the metagenomics employs untargeted shotgun sequencing, capturing the entire genomic content and thus avoiding primer bias and amplification errors (Tringe & Rubin 2005; Singer et al. 2020). Initially developed for microbial community analysis in aquatic ecosystems, the metagenomics is increasingly applied to eukaryotes, including zooplankton (Grossart et al. 2020). This approach enables comprehensive taxonomic and functional profiling, improving detection of rare, cryptic, and novel taxa beyond the capabilities of metabarcoding (Tang et al. 2015). From a population connectivity perspective, the metagenomics provides high-resolution insights into gene flow and genetic structure within zooplankton communities (Song et al. 2021). When

combined with oceanographic models and eDNA analyses, it facilitates the elucidation of dispersal patterns and real-time monitoring of community genetic dynamics (Monchamp et al. 2022). Thus, the metagenomics represents a transformative tool for assessing marine biodiversity and sustainably managing its ecosystems (Di Capua et al. 2024).

ANTHROPOGENIC IMPACT ON MARINE ZOOPLANKTON GENETIC DIVERSITY

The anthropogenic activities, primarily fossil fuel combustion and deforestation, are the main drivers of current climate change, exceeding the influence of natural factors (National Academy of Sciences 2020). Rising sea temperatures caused by global warming affect zooplankton distribution, population dynamics, and genetic connectivity (Viitasalo & Bonsdorff 2022; Ratnarajah et al. 2023). Elevated temperatures accelerate metabolism, alter life history traits, and shift spawning phenology, thereby modifying genetic structures over time (Bashevkin et al. 2020). Concurrent ocean acidification, resulting from increased atmospheric CO_2, impairs larval survival, particularly in calcifying taxa such as pteropods, reducing genetic diversity by increasing mortality and selection pressure (Putra et al. 2025). Additionally, altered ocean circulation and enhanced stratification fragment populations, limiting gene flow and promoting genetic isolation (Treml et al. 2008). Collectively, these factors could disrupt evolutionary trajectories and constrain the adaptive capacity of marine zooplankton (Johnson et al. 2022) (Figure 4).

Furthermore, the marine pollution from industrial, agricultural, and domestic sources significantly threatens zooplankton genetic diversity (Botterell et al. 2023). The microplastics, prevalent throughout oceans, are ingested by zooplankton, imposing selective pressures that can alter gene expression and diminish genetic variability (Cole et al. 2013). Notably, metagenomic and eDNA-based approaches have revealed shifts in zooplankton community composition and function linked to microplastic exposure, suggesting ecosystem-level genetic restructuring (Ali et al. 2025). The chemical contaminants, such as heavy metals, pesticides, and persistent organic pollutants bioaccumulate in marine zooplankton, causing DNA damage and mutagenesis, which reduce genetic diversity through strong environmental selection (van Straalen & Timmermans 2002; Goswami et al. 2014). This genetic erosion undermines population resilience and adaptability, threatening marine ecosystem stability (Belfiore & Anderson 2002). Additionally, overfishing disrupts trophic interactions by depleting predator populations, which can lead to marine zooplankton population outbreaks and decreased genetic diversity due to dominance by fewer species (Möllmann et al. 2008; Vereshchaka 2024). Human-induced habitat degradation, including coastal reclamation, eutrophication, coral reef destruction, and seagrass loss reduces spawning and nursery grounds critical for zooplankton reproduction and development (Song et al. 2021). Such habitat loss induces genetic bottlenecks and fragmentation, restricting gene flow and increasing population isolation (Li & Roossinck 2004; Botterell et al. 2023). Consequently, reduced genetic connectivity impairs adaptive capacity, escalating vulnerability to environmental changes and destabilizing marine ecosystems (Ezard & Travis 2006) (Figure 4).

CHALLENGES AND RESEARCH OUTLOOK

The molecular analyses have provided valuable insights into the marine zooplankton genetic diversity, yet several technical and logistical challenges continue to affect data quality and reliability. Importantly, sampling in dynamic ocean environments requires meticulous planning to capture spatial and temporal variability, as zooplankton communities fluctuate across depths and seasons, complicating representative sampling. The morphological similarity among co-occurring species hinders individual separation for sequencing, alt-

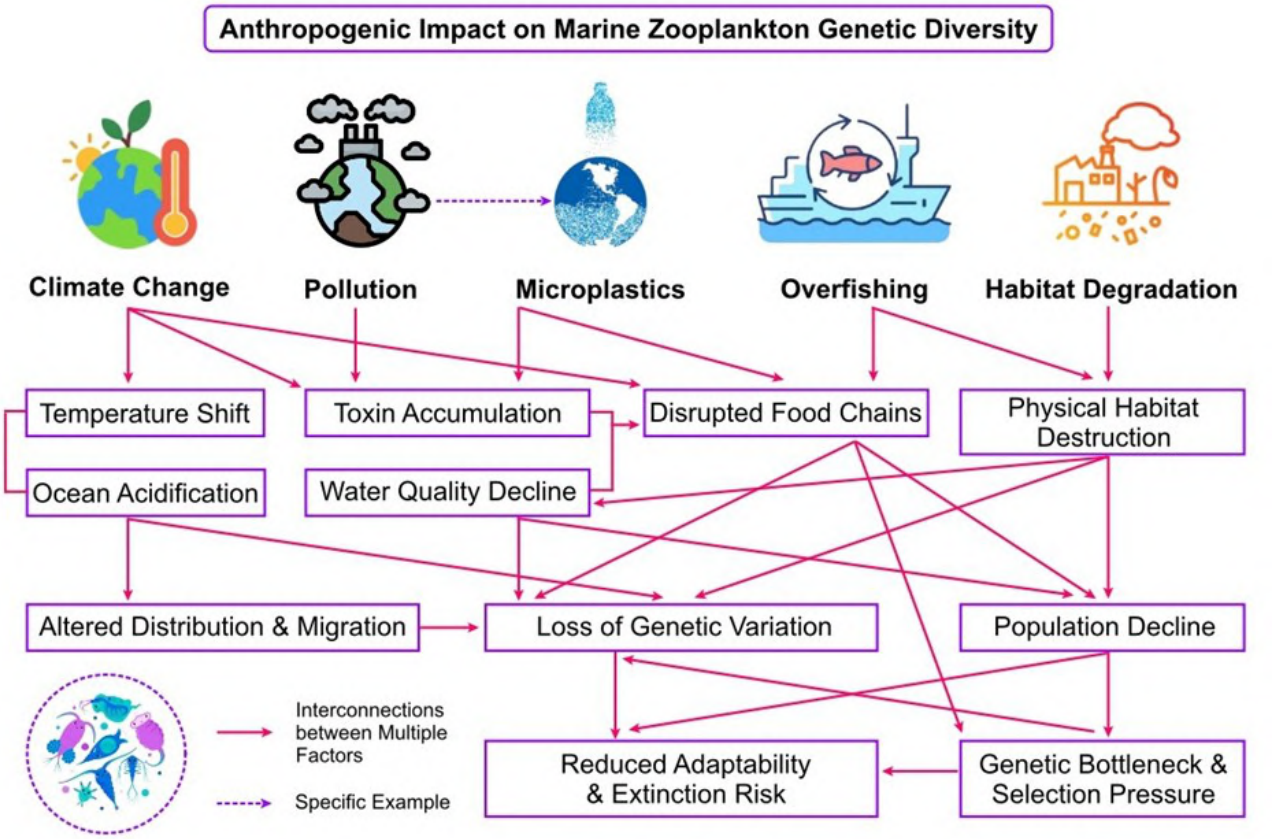

Figure 4. This diagram illustrates the interconnected relationships between various factors influencing the genetic diversity of marine zooplankton. The environmental changes driven by anthropogenic activities, such as climate change, pollution, overfishing, and habitat degradation, can result in significant ecological disturbances. The disruptions in the food chain, increased selective pressures, and declining zooplankton populations can reduce genetic variation, heighten extinction risks, and diminish the adaptive capacity of marine ecosystems to global changes. The illustration was constructed by the first author (A.P.).

hough metabarcoding and metagenomics offer promising alternatives constrained by incomplete reference databases, particularly in understudied regions like the Southern Hemisphere. Risks of contamination from microorganisms and phytoplankton further complicate molecular analyses, necessitating rigorous sample preparation and sequence quality control. Moreover, the high costs and infrastructure demands of NGS restrict accessibility, especially in resource-limited settings. The standardisation of bioinformatics workflows remains critical to ensure reproducibility and integration of data across studies and laboratories. Despite advances in monitoring marine ecosystem responses, zooplankton molecular data have yet to be fully integrated into conservation policies, highlighting the need for effective zooplankton indicators to support biodiversity goals and adaptive management.

Looking forward, the future research must address these challenges by expanding global reference libraries such as comprehensive COI databases, supported by sustainable taxonomic verification and voucher specimen management. Integrating genetic data with ecological and functional traits will deepen understanding of zooplankton population structure, connectivity, and adaptation to environmental drivers like temperature and salinity. Advances in metagenomics, mitogenomics, and affordable NGS technologies promise broader and more detailed analyses, especially in developing countries. Field-deployable tools for real-time genetic monitoring will enhance responsiveness to climatic shifts and biodiversity changes. The multidisciplinary collaboration across genetics, ecology, oceanography, and bioinformatics, combined with artificial intelligence applications, will improve data accuracy, reduce analytical bias, and refine models of marine zooplankton distribution and ad-

aptation. This integrated approach will be pivotal for effective marine ecosystem monitoring and sustainable fisheries management.

CONCLUSION

The genomic tools have substantially advanced the study of marine zooplankton by enabling accurate species identification, uncovering cryptic diversity, and providing high-resolution insights into biodiversity patterns, population connectivity, and genetic responses to environmental change. These molecular approaches also support long-term monitoring of zooplankton populations and enhance understanding of their ecological and biogeographic dynamics. Integrating genetic data is essential for evidence-based ocean management, facilitating biodiversity assessment, ecosystem response prediction, and conservation consistent with sustainable resource use. The genetic information is particularly valuable for anticipating the impacts of climate change and environmental degradation on marine ecosystems. Despite these advances, key challenges persist, including limited sampling representativeness, incomplete reference databases, and the lack of standardized, reproducible bioinformatics pipelines. Open-access repositories such as BOLD and GenBank serve as key infrastructures, with continuous expansion and curation being crucial for the progress of molecular biodiversity research. Nevertheless, the ecological relevance of genetic variation in marine zooplankton remains poorly resolved. Thus, a multidisciplinary framework integrating genetic, ecological, and evolutionary perspectives is therefore required to elucidate zooplankton functional roles in ocean ecosystems. Emerging technologies, including mitogenomics, metagenomics, and artificial intelligence, hold promise for revealing the functional diversity and adaptive mechanisms that underpin marine zooplankton responses to environmental change.

AUTHORS CONTRIBUTION

A.P. and S.A.: Conceptualisation, methodology, resources, investigation, data curation, formal analysis, validation, visualisation, writing – original draft, review & editing. I.N.S.: Methodology, validation, supervision, writing – review & editing. Ilham, F.H., and M.H.R.A.: Methodology, resources, data curation, formal analysis. A.L., H.T., Rina, M.Mulyono, T.Y., M.Maulita, Y.N., I.J.P.D., S.R., and S.P.S.: Resources, investigation, data curation, validation. Hamdani, M.Ariana, T.H.R., L.A.J.Q., A.R.A., C.M., and M.A.H.J.: Resources, investigation, funding acquisition. M.Azril, Hawati, and M.M.M.: Resources, investigation, validation. The authors have read and approved the final version of the manuscript for publication.

ACKNOWLEDGMENTS

The concept and initiative for this scientific review were formulated during the final stage of the first author's (A.P.) Master of Science program, following constructive discussions with the second author (S.A.). A.P. and S.A. sincerely thank the PKNU Research Grant for Graduate Scholarship and the PhiNX Scholarship from Pukyong National University for the support provided during their Master's degree. Furthermore, they gratefully acknowledge the Interdisciplinary Program of Marine and Fisheries Sciences and Convergent Technology at Pukyong National University for its continued support and provision of resources throughout the Ph.D. program. The corresponding author (A.P.) also extends sincere appreciation to fellow co-authors from the Politeknik Ahli Usaha Perikanan, Politeknik Kelautan dan Perikanan Jembrana, Politeknik Kelautan dan Perikanan Bone, Politeknik Kelautan dan Perikanan Karawang, Universitas Samudra, Sekolah Tinggi Perikanan dan Kelautan Matauli, Universitas Tidar, and Universitas Muslim Indonesia for their productive collaboration in various scientific sessions and

discussions. This collaboration played a crucial role in the successful preparation and publication of this article. In addition, we appreciate the anonymous reviewers for their valuable critiques, suggestions, and recommendations, which have significantly contributed to enhancing the quality of this article.

CONFLICT OF INTEREST

The authors declare that there are no financial or non-financial conflicts of interest that could have influenced the results of this study.

REFERENCES

Agashe, D., 2009. The stabilizing effect of intraspecific genetic variation on population dynamics in novel and ancestral habitats. *The American Naturalist*, 174(2), pp.255-267. doi: 10.1086/600085.

Ali, S.S. et al., 2025. Microplastics as persistent and vectors of other threats in the marine environment: Toxicological impacts, management, and strategical roadmap to end plastic pollution. *Environmental Chemistry and Ecotoxicology*, 7, pp.229-251. doi: 10.1016/j.enceco.2024.12.005.

Atkinson, A. et al., 2004. Long-term decline in krill stock and increase in salps within the Southern Ocean. *Nature*, 432, pp.100-103. doi: 10.1038/nature02996.

Avise, J.S., 1989. Gene trees and organismal histories: A phylogenetic approach to population biology. *Evolution*, 43(6), pp.1192-1208. doi: 10.1111/j.1558-5646.1989.tb02568.x.

Azam, F. et al., 1983. The ecological role of water-column microbes in the sea. *Marine Ecology Progress Series*, 10(3), pp.257-263. doi: 10.3354/meps010257.

Bandara, K. et al., 2021. Two hundred years of zooplankton vertical migration research. *Biological Reviews*, 96(4), pp.1547-1589. doi: 10.1111/brv.12715.

Bashevkin, S.M. et al., 2020. Larval dispersal in a changing ocean with an emphasis on upwelling regions. *Ecosphere*, 11(1), e03015. doi: 10.1002/ecs2.3015.

Belfiore, N.M. & Anderson, S.L., 2002. Effects of contaminants on genetic patterns in aquatic organisms: A review. *Mutation Research/Fundamental and Molecular Mechanisms of Mutagenesis*, 489(2-3), pp.97-122. doi: 10.1016/S1383-5742(01)00065-5.

Blanco-Bercial, L. & Bucklin, A., 2016. New view of population genetics of zooplankton: RAD-seq analysis reveals population structure of the North Atlantic planktonic copepod *Centropages typicus*. *Molecular Ecology*, 25(7), pp.1566-1580. doi: 10.1111/mec.13581.

Blanco-Bercial, L. et al., 2011a. Molecular phylogeny of the Calanoida (Crustacea: Copepoda). *Molecular Phylogenetics and Evolution*, 59(1), pp.103-113. doi: 10.1016/j.ympev.2011.01.008.

Blanco-Bercial, L. et al., 2011b. Comparative phylogeography and connectivity of sibling species of the marine copepod *Clausocalanus* (Calanoida). *Journal of Experimental Marine Biology and Ecology*, 404(1-2), pp.108-115. doi: 10.1016/j.jembe.2011.05.011.

Boore, J.F., 1999. Animal mitochondrial genomes. *Nucleic Acids Research*, 27(8), pp.1767-1780. doi: 10.1093/nar/27.8.1767.

Botterell, Z.L.R. et al., 2023. An assessment of the ecosystem services of marine zooplankton and the key threats to their provision. *Ecosystem Services*, 63, 101542. doi: 10.1016/j.ecoser.2023.101542.

Bucklin, A. et al., 2003. Molecular systematic and phylogenetic assessment of 34 calanoid copepod species of the Calanidae and Clausocalanidae. *Marine Biology*, 142, pp.333-343. doi: 10.1007/s00227-002-0943-1.

Bucklin, A. et al., 2016. Metabarcoding of marine zooplankton: Prospects, progress, and pitfalls. *Journal of Plankton Research*, 38(3), pp.393-400. doi: 10.1093/plankt/fbw023.

Bucklin, A. et al., 2021a. New insights into biodiversity, biogeography, ecology, and evolution of marine zooplankton based on molecular approaches. *ICES Journal of Marine Science*, 78(9), pp.3281-3287. doi: 10.1093/icesjms/fsab198.

Bucklin, A. et al., 2021b. Toward a global reference database of COI barcodes for marine zooplankton. *Marine Biology*, 168, 78. doi: 10.1007/s00227-021-03887-y.

Bucklin, A. et al., 2022. COI metabarcoding of zooplankton species diversity for time-series monitoring of the NW Atlantic Continental Shelf. *Frontiers in Marine Science*, 9, 867893. doi: 10.3389/fmars.2022.867893.

Bucklin, A. et al., 2018. Population genomics of marine zooplankton. In: Oleksiak, M. & Rajora, O. (eds.) Population Genomics: Marine Organisms. Springer, Cham. doi: 10.1007/13836_2017_9.

Burton, R.S. et al., 2007. Three divergent mitochondrial genomes from California populations of the copepod *Tigriopus californicus*. *Gene*, 403(1-2), pp.53-59. doi: 10. 1016/j.gene.2007.07.026.

Carroll, E.L. et al., 2019. Multi-locus DNA metabarcoding of zooplankton communities and scat reveal trophic interactions of a generalist predator. *Scientific Reports*, 9, 281. doi: 10.1038/s41598-018-36478-x.

Caudill, C.C. & Bucklin, A., 2004. Molecular phylogeography and evolutionary history of the estuarine copepod, *Acartia tonsa*, on the Northwest Atlantic Coast. *Hydrobiologia*, 511, pp.91-102. doi: 10.1023/B:HYDR.0000014032.05680.9d.

Choi, J.H., Kim, S. & Kim, C.-g., 2024. Evaluating zooplankton species diversity using environmental DNA and bulk-DNA metabarcoding in the Ulleung Basin of the Southeastern Korean Peninsula in the summer. *Frontiers in Marine Science*, 11, 1351148. doi: 10.3389/fmars.2024.1351148.

Choquet, M. et al., 2023. Unmasking microsatellite deceptiveness and debunking hybridization with SNPs in four marine copepod species of *Calanus*. *Molecular Ecology*, 32(24), pp.6854-6873. doi: 10.1111/mec.17183.

Chust, G. et al., 2016. Dispersal similarly shapes both population genetics and community patterns in the marine realm. *Scientific Report*, 6, 28730. doi: 10.1038/srep28730.

Cole, M. et al., 2013. Microplastic ingestion by zooplankton. *Environmental Science & Technology*, 47(12), pp.6646-6655. doi: 10.1021/es400663f.

Corell, J. & Rodríguez-Ezpeleta, N., 2014. Tuning of protocols and marker selection to evaluate the diversity of zooplankton using metabarcoding. *Revista de Investigación Marina*, 21(2), pp.20-39.

Cornils, A. et al., 2017. Global phylogeography of *Oithona similis* s.l. (Crustacea, Copepoda, Oithonidae) - A cosmopolitan plankton species or a complex of cryptic lineages? *Molecular Phylogenetics and Evolution*, 107, pp.473-485. doi: 10.1016/j.ympev.2016.12.019.

Cowen, R.K. & Sponaugle S., 2009. Larval dispersal and marine population connectivity. *Annual Review of Marine Science*, 1, pp.443-466. doi: 10.1146/annurev.marine.010908.163757.

Cowen, R.K. et al., 2007. Population connectivity in marine systems: An overview. *Oceanography*, 20(3), pp.14–21. doi: 10.5670/oceanog.2007.26.

Dam, H.G., 2013. Evolutionary adaptation of marine zooplankton to global change. *Annual Review of Marine Science*, 5, pp.349-370. doi: 10.1146/annurev-marine-121211-172229.

de Bruin, T. et al., 2024. Intraspecific demographic and trait responses to environmental change drivers are linked in two species of ciliate. *BMC Ecology and Evolution*, 24, 47. doi: 10.1186/s12862-024-02241-2.

Di Capua, I. et al., 2017. Molecular phylogeny of Oncaeidae (Copepoda) using nuclear ribosomal internal transcribed spacer (ITS rDNA). *PLoS ONE*, 12(4), e0175662. doi: 10.1371/journal.pone.0175662.

Di Capua, I. et al., 2024. Integrative approach to monitoring metazoan diversity and distribution in two Mediterranean coastal sites through morphology and organismal eDNA. *Scientific Reports*, 14, 19291. doi: 10.1038/s41598-024-69520-2.

Djurhuus, A. et al., 2018. Evaluation of marine zooplankton community structure through environmental DNA metabarcoding. *Limnology and Oceanography*, 16(4), pp.209-221. doi: 10.1002/lom3.10237.

Elbrecht, V. & Leese, F., 2015. Can DNA-based ecosystem assessments quantify species abundance? Testing primer bias and biomass–sequence relationships with an innovative metabarcoding protocol. *PLoS ONE*, 10(7), e0130324. doi: 10.1371/journal.pone.0130324.

El-khodary, G.M. et al., 2020. Phylogenetic identification and assessment of the nutritional value of different diets for a copepod species isolated from Eastern Harbor coastal region. *Egyptian Journal of Aquatic Research*, 46(2), pp.173-180. doi: 10.1016/j.ejar.2020.03.003.

Ezard, T.H.G. & Travis, J.M.J., 2006. The impact of habitat loss and fragmentation on genetic drift and fixation time. *OIKOS*, 114(2), pp.367-375. doi: 10.1111/j.2006.0030-1299.14778.x.

Fields, P.D. et al., 2018. Mitogenome phylogeographic analysis of a planktonic crustacean. *Molecular Phylogenetics and Evolution*, 129, pp.138-148. doi: 10.1016/j.ympev.2018.06.028.

Filatov, D.A. et al., 2021. The mode of speciation during a recent radiation in open-ocean phytoplankton. *Current Biology*, 31(24), pp.5439-5449. doi: 10.1016/j.cub.2021.09.073.

Filatov, D.A., 2023. How does speciation in marine plankton work? *Trends in Microbiology*, 31(10), pp.989-991. doi: 10.1016/j.tim.2023.07.005.

Genome 10K Community of Scientists., 2009. Genome 10K: A proposal to obtain whole-genome sequence for 10 000 vertebrate species. *Journal of Heredity*, 100(6), pp.659-674. doi: 10.1093/jhered/esp086.

GIGA Community of Scientists., 2014. The Global Invertebrate Genomics Alliance (GIGA): Developing community resources to study diverse invertebrate genomes. *Journal of Heredity*, 105(1), pp.1-18. doi: 10.1093/jhered/est084.

Gluchowska, M. et al., 2017. Variations in the structural and functional diversity of zooplankton over vertical and horizontal environmental gradients en route to the Arctic Ocean through the Fram Strait. *PLoS ONE*, 12(2), e0171715. doi: 10.1371/journal.pone.0171715.

Goetze, E. et al., 2015. Temporal stability of genetic structure in a mesopelagic copepod. *PLoS ONE*, 10(8), e0136087. doi: 10.1371/journal.pone.0136087.

Goldberg, C.S., Strickler, K.M. & Pilliod, D.S., 2015. Moving environmental DNA methods from concept to practice for monitoring aquatic macroorganisms. *Biological Conservation*, 183, pp.1-3. doi: 10.1016/j.biocon.2014.11.040.

González, C.E. et al., 2020. Genetic diversity and novel lineages in the cosmopolitan copepod *Pleuromamma abdominalis* in the Southeast Pacific. *Scientific Reports*, 10, 1115. doi: 10.1038/s41598-019-56935-5.

Goswami, P. et al., 2014. Monitoring of genotoxicity in marine zooplankton induced by toxic metals in Ennore estuary, Southeast coast of India. *Marine Pollution Bulletin*, 88(1-2), pp.70-80. doi: 10.1016/j.marpolbul.2014.09.025.

Grossart, H.P. et al., 2020. Linking metagenomics to aquatic microbial ecology and biogeochemical cycles. *Limnology and Oceanography*, 65(S1), pp.S2-S20. doi: 10.1002/lno.11382.

Gupta, S. et al., 2024. *Genomic intelligence: Metagenomics and artificial intelligence*, London: CRC Press.

Havird, J.C. et al., 2016. Sex, mitochondria, and genetic rescue. *Trends in Ecology & Evolution*, 31(2), pp.96-99. doi: 10.1016/j.tree.2015.11.012.

Hebert, P.D.N. et al., 2003. Barcoding animal life: Cytochrome c oxidase subunit 1 divergences among closely related species. *Proceedings of the Royal Society of London. Series B: Biological Sciences*, 270(1), pp.S96-999. doi: 10.1098/rsbl.2003.0025.

Helfenbein, K.G. et al., 2004. The mitochondrial genome of *Paraspadella gotoi* is highly reduced and reveals that chaetognaths are a sister group to protostomes. *Proceedings of the National Academy of Sciences of the United States of America*, 101(29), pp.10639-10643. doi: 10.1073/pnas.0400941101.

Huggett, J.A. et al., 2022. Metabarcoding of zooplankton to derive indicators of pelagic ecosystem status. *South African Journal of Science*, 118(11/12), Art. #12977. doi: 10.17159/sajs.2022/12977.

Hwang, D.S. et al., 2014. Complete mitochondrial genome of the jellyfish, *Chrysaora quinquecirrha* (Cnidaria, Scyphozoa). *Mitochondrial DNA*, 25 (1), pp.25-26. doi: 10.3109/19401736.2013.775272.

Johnson, S.B. et al., 2022. Speciation of pelagic zooplankton: Invisible boundaries can drive isolation of oceanic ctenophores. *Frontiers in Genetics*, 13, 970314. doi: 10.3389/fgene.2022.970314.

Johnston, N.M. et al., 2022. Status, change, and futures of zooplankton in the Southern Ocean. *Frontiers in Ecology and Evolution*, 9, 624692. doi: 10.3389/fevo.2021.624692.

Jung, S.O. et al., 2006. The complete mitochondrial genome of the intertidal copepod *Tigriopus* sp. (Copepoda, Harpactidae) from Korea and phylogenetic considerations. *Journal of Experimental Marine Biology and Ecology*, 333(2), pp.251-262. doi: 10.1016/j.jembe.2005.12.047.

Kayal, E. et al., 2011. Evolution of linear mitochondrial genomes in medusozoan cnidarians. *Genome Biology and Evolution*, 4(1), pp.1-12. doi: 10.1093/gbe/evr123.

Ki, J.S. et al., 2009. Phylogeography of the copepod *Tigriopus japonicus* along the Northwest Pacific rim. *Journal of Plankton Research*, 31(2), pp.209-221. doi: 10.1093/plankt/fbn100.

Ki, J.S. et al., 2010. Complete mitochondrial genome sequence of the Arctic gammarid, *Onisimus nanseni* (Crustacea; Amphipoda): Novel gene structures and unusual control region features. *Comparative Biochemistry and Physiology Part D: Genomics and Proteomics*, 5(2), pp.105-115. doi: 10.1016/j.cbd.2010.02.002.

Kim, S. et al., 2013. The complete mitochondrial genome of Arctic *Calanus hyperboreus* (Copepoda, Calanoida) reveals characteristic patterns in calanoid mitochondrial genome. *Gene*, 520(1), pp.64-72. doi: 10.1016/j.gene.2012.09.059.

Kim, S. et al., 2012. Complete mitochondrial genome of the northern mauxia shrimp *Acetes chinensis* (Decapoda, Dendrobranchiata, Sergestoidae). *Mitochondrial DNA*, 23(1), pp.28-30. doi: 10.3109/19401736.2011.643878.

Kobari, T. & Ikeda, T., 2001. Ontogenetic vertical migration and life cycle of *Neocalanus plumchrus* (Crustacea: Copepoda) in the Oyashio region, with notes on regional variations in body sizes. *Journal of Plankton Research*, 23(3), pp.287-302. doi: 10.1093/plankt/23.3.287.

Kohn, A.B. et al., 2012. Rapid evolution of the compact and unusual mitochondrial genome in the ctenophore, *Pleurobrachia bachei*. *Molecular Phylogenetics and Evolution*, 63(1), pp.203-207. doi: 10.1016/j.ympev.2011.12.009.

Lenz, P.H. et al., 2021. Transcriptomics and metatranscriptomics in zooplankton: Wave of the future? *Journal of Plankton Research*, 43(1) pp.3-9. doi: 10.1093/plankt/fbaa058.

Li, H. & Roossinck, M.J., 2004. Genetic bottlenecks reduce population variation in an experimental RNA virus population. *Journal of Virology*, 78 (19), pp.10582-10587. doi: 10.1128/JVI.78.19.10582-10587.2004.

Li, P. et al., 2016. Complete mitochondrial genome sequence of the pelagic chaetognath, *Sagitta ferox*. *Mitochondrial DNA*, 27(6), pp.1-2. doi: 10.3109/19401736.2015.1106508.

Lindeque, P.K. et al., 2013. Next Generation Sequencing reveals the hidden diversity of zooplankton assemblages. *PLoS ONE*, 8(11), e81327. doi: 10.1371/journal.pone.0081327.

Litchman, E. et al., 2013. Trait-based approaches to zooplankton communities, *Journal of Plankton Research*, 35(3), pp.473-484. doi: 10.1093/plankt/fbt019.

Machida, R.J. et al., 2002. Complete mitochondrial DNA sequence of *Tigriopus japonicus* (Crustacea: Copepoda). *Marine Biotechnology*, 4, pp.406-417. doi: 10.1007/s10126-002-0033-x.

Machida, R.J. et al., 2021. Comparative analysis of zooplankton diversities and compositions estimated from complement DNA and genomic DNA amplicons, metatranscriptomics, and morphological identifications. *ICES Journal of Marine Science*, 78(9), pp.3428-3443. doi: 10.1093/icesjms/fsab084.

McGinty, N. & Irwin, A., 2025. Global variation in zooplankton niche divergence across ocean basins. *Ecology Letters*, 28(2), e70089. doi: 10.1111/ele.70089.

McGinty, N. et al., 2021. Anthropogenic climate change impacts on copepod trait biogeography. *Global Change Biology*, 27(7), pp.1431-1442. doi: 10.1111/gcb.15499.

Millette, K.L. et al., 2011. Pleistocene-driven diversification in freshwater zooplankton: Genetic patterns of refugial isolation and postglacial recolonization in *Leptodora kindtii* (Crustacea, Cladocera). *Limnology and Oceanography*, 56(5), pp.1725-1736. doi: 10.4319/lo.2011.56.5.1725.

Minxiao, W. et al., 2011. Distinctive mitochondrial genome of Calanoid copepod *Calanus sinicus* with multiple large non-coding regions and reshuffled gene order: Useful molecular markers for phylogenetic and population studies. *BMC Genomics*, 12, 73. doi: 10.1186/1471-2164-12-73.

Miyamoto, H. et al., 2010. Genetic diversity and cryptic speciation of the deep sea chaetognath *Caecosagitta macrocephala* (Fowler, 1904). *Deep Sea Research Part II: Topical Studies in Oceanography*, 57(24-26), pp.2211-2219. doi: 10.1016/j.dsr2.2010.09.023.

Modica, M. V. et al., 2017. Do larval types affect genetic connectivity at sea? Testing hypothesis in two sibling marine gastropods with contrasting larval development. *Marine Environmental Research*, 127, pp.92-101. doi: 10.1016/j.marenvres.2017.04.001.

Möllmann, C. et al., 2008. Effects of climate and overfishing on zooplankton dynamics and ecosystem structure: Regime shifts, trophic cascade, and feedback loops in a simple ecosystem. *ICES Journal of Marine Science*, 65 (3), pp.302-310. doi: 10.1093/icesjms/fsm197.

Monchamp, M.È. et al., 2022. Comparative analysis of zooplankton diversity in freshwaters: What can we gain from metagenomic analysis? *Environmental DNA*, 4(6), pp.1250-1264. doi: 10.1002/edn3.335.

National Academy of Sciences., 2020. *Climate change: Evidence and causes: Update 2020*. Washington, DC: The National Academies Press. doi: 10.17226/25733.

Norris, R.D. & Hull, P.M., 2012. The temporal dimension of marine speciation. *Evolutionary Ecology*, 26, pp.393-415. doi: 10.1007/s10682-011-9488-4.

O'Brien, T.D. et al., 2024. MetaZooGene Atlas and Database: Reference sequences for marine ecosystems. In: R. DeSalle, ed. DNA Barcoding. Methods in Molecular Biology, 2744. Humana, New York, NY. doi: 10.1007/978-1-0716-3581-0_28.

Ogoh, K. & Ohmiya, Y., 2004. Complete mitochondrial DNA sequence of the sea-firefly, *Vargula hilgendorfii* (Crustacea, Ostracoda) with duplicate control regions. *Gene*, 327(1), pp.131-139. doi: 10.1016/j.gene.2003.11.011.

Papillon, D. et al., 2004. Identification of chaetognaths as protostomes is supported by the analysis of their mitochondrial genome. *Molecular Biology and Evolution*, 21(11), pp.2122-2129. doi: 10.1093/molbev/msh229.

Parent, G.J. et al., 2012. Natural hybridization between *Calanus finmarchicus* and *C. glacialis* (Copepoda) in the Arctic and Northwest Atlantic. *Limnology and Oceanography*, 57(4), pp.897-1255. doi:10.4319/lo.2012.57.4.1057.

Peijnenburg, K.T.C.A. & Goetze, E., 2013. High evolutionary potential of marine zooplankton. *Ecology and Evolution*, 3(8), pp.2765-2781. doi: 10.1002/ece3.644.

Peluso, L. et al., 2024. Oceanographical-driven dispersal and environmental variation explain genetic structure in an upwelling coastal ecosystem. *Scientific Reports*, 14, 21942. doi: 10.1038/s41598-024-72841-x.

Pett, W. et al., 2011. Extreme mitochondrial evolution in the ctenophore *Mnemiopsis leidyi*: Insight from mtDNA and the nuclear genome. *Mitochondrial DNA*, 22(4), pp.130-142. doi: 10.3109/19401736.2011.624611.

Porter, T.M. & Hajibabaei, M., 2018. Over 2.5 million COI sequences in GenBank and growing. *PLoS One*, 13(9), e0200177. doi: 10.1371/journal.pone.0200177.

Putra, A. et al., 2025. Impact of global climate shifts on the biodiversity and functionality of marine zooplankton communities. *Journal of Tropical Biodiversity and Biotechnology*, 10(1), jtbb14575. doi: 10.22146/jtbb.14575.

Putra, A., 2025. Zooplankton Community around Seogwipo in Jeju Island, Republic of Korea. Master's thesis, Pukyong National University, Busan, Republic of Korea.

Questel, J.M. et al., 2025. DNA barcoding deep-water zooplankton from the Gulf of Alaska, North Pacific Ocean. *Frontiers in Marine Science*, 12, 1515048. doi: 10.3389/fmars.2025.1515048.

Ratnarajah, L. et al., 2023. Monitoring and modelling marine zooplankton in a changing climate. *Nature Communications*, 14, 564. doi: 10.1038/s41467-023-36241-5.

Rawoot, A. et al., 2024. Strengthening the DNA barcode reference library for marine copepods in South Africa. *African Journal of Marine Science*, 46(4), pp.281-289. doi: 10.2989/1814232X.2022.2108144.

Riginos, C. et al., 2014. Dispersal capacity predicts both population genetic structure and species richness in reef fishes. *The American Naturalist*, 184(1), pp.52-64. doi: 10.1086/676505.

Shao, Z. et al., 2006. Mitochondrial genome of the moon jelly *Aurelia aurita* (Cnidaria, Scyphozoa): A linear DNA molecule encoding a putative DNA-dependent DNA polymerase. *Gene*, 381, pp.92-101. doi: 10.1016/j.gene.2006.06.021.

Shen, X. et al., 2010. The mitochondrial genome of *Euphausia superba* (Prydz Bay) (Crustacea: Malacostraca: Euphausiacea) reveals a novel gene arrangement and potential molecular markers. *Molecular Biology Reports*, 37(2), pp.771-784. doi: 10.1007/s11033-009- 9602-7.

Shen, X. et al., 2011. The complete mitochondrial genome sequence of *Euphausia pacifica* (Malacostraca: Euphausiacea) reveals a novel gene order and unusual tandem repeats. *Genome*, 54(11), pp.911-922. doi: 10.1139/g11-053.

Singer, G.A.C. et al., 2020. The utility of a metagenomics approach for marine biomonitoring. *bioRxiv*, pp.1-13. doi: 10.1101/2020.03.16.993667.

Singh, S. et al., 2021. Metabarcoding of marine zooplankton in South Africa. *African Journal of Marine Science*, 43(2), pp.147-159. doi: 10.2989/1814232X.2021.1919759.

Song, C.U. et al., 2021. Zooplankton diversity monitoring strategy for the urban coastal region using metabarcoding analysis. *Scientific Reports*, 11, 24339. doi: 10.1038/s41598-021-03656-3.

Spitze, K., 1995. Quantitative genetics of zooplankton life histories. *Experientia*, 51, pp.454-464. doi: 10.1007/BF02143198.

Steinberg, D.K. et al., 2008. Bacterial vs. zooplankton control of sinking particle flux in the ocean's twilight zone. *Limnology and Oceanography*, 53(4), pp.1327-1338. doi: 10.4319/lo.2008.53.4.1327.

Stepien, C.A. et al., 2024. Evaluating metabarcoding markers for identifying zooplankton and ichthyoplankton communities to species in the Salish sea: Morphological comparisons and rare, threatened or invasive species. *DNA*, 4(1), pp.1-33. doi: 10.3390/dna4010001.

Takahashi, M. et al., 2023. Aquatic environmental DNA: A review of the macro-organismal biomonitoring revolution. *Science of The Total Environment*, 873, 162322. doi: 10.1016/j.scitotenv.2023.162322.

Tang, M. et al., 2015. High-throughput monitoring of wild bee diversity and abundance via mitogenomics. *Methods in Ecology and Evolution*, 6(9), pp.1034-1043. doi: 10.1111/2041-210X.12416.

Treml, E.A. et al., 2008. Modeling population connectivity by ocean currents, a graph-theoretic approach for marine conservation. *Landscape Ecology*, 23(1), pp.19-36. doi: 10.1007/s10980-007-9138-y.

Tringe, S.G. & Rubin, E.M., 2005. Metagenomics: DNA sequencing of environmental samples. *Nature Reviews Genetics*, 6, pp.805-814. doi: 10.1038/nrg1709.

Trubovitz, S. et al., 2020. Marine plankton show threshold extinction response to Neogene climate change. *Nature Communications*, 11, 5069, doi: 10.1038/s41467-020-18879-7.

Unal, E. & Bucklin, A., 2010. Basin-scale population genetic structure of the planktonic copepod *Calanus finmarchicus* in the North Atlantic Ocean. *Progress in Oceanography*, 87(1-4), pp.175-185. doi: 10.1016/j.pocean.2010.09.017.

van Straalen, N.M. & Timmermans, M.J.T.N., 2002. Genetic variation in toxicant-stressed populations: An evaluation of the "genetic erosion" hypothesis. *Human and Ecological Risk Assessment: An International Journal*, 8(5), pp.983-1002. doi: 10.1080/1080-700291905783.

Vereshchaka, A., 2024. Navigating the zooplankton realm: Oceans of diversity beneath the sea surface. *Diversity*, 16, 717. doi: 10.3390/d16120717.

Viitasalo, M. & Bonsdorff, E. 2022. Global climate change and the Baltic Sea ecosystem: Direct and indirect effects on species, communities, and ecosystem functioning. *Earth System Dynamics*, 13(2), pp.711-747. doi: 10.5194/esd-13-711-2022, 2022.

Wang, L. et al., 2023. Research and prospects of environmental DNA (eDNA) for detection of invasive aquatic species in East Asia. *Frontiers in Marine Science*, 10, 1284953. doi: 10.3389/fmars.2023.1284953.

Ward, B.A. et al., 2012. A size-structured food-web model of the global ocean. *Limnology and Oceanography*, 57(6), pp.1877-1891. doi: 10.4319/lo.2012.57.6.1877.

Wei, S. et al., 2016. The mitochondrial genome of the pelagic chaetognath, *Pterosagitta draco*. *Mitochondrial DNA Part B*, 1(1), pp.515-516. doi: 10.1080/23802359.2016. 1197055.

Weigand, H. et al., 2019. DNA barcode reference libraries for the monitoring of aquatic biota in Europe: Gap-analysis and recommendations for future work. *Science of The Total Environment*, 678, pp.499-524. doi: 10.1016/j.scitotenv.2019.04.247.

Weydmann, A. et al., 2014. Microsatellite markers for the Arctic copepod *Calanus glacialis* and cross-amplification with *C. finmarchicus*. *Conservation Genetics Resources*, 6, pp.1003-1005. doi: 10.1007/s12686-014-0269-6.

Weydmann, A. et al., 2017. Mitochondrial genomes of the key zooplankton copepods Arctic *Calanus glacialis* and North Atlantic *Calanus finmarchicus* with the longest crustacean non-coding regions. *Scientific Report*, 7, 13702. doi: 10.1038/s41598-017- 13807.

Wood, S.A. et al., 2019. A comparison of droplet digital polymerase chain reaction (PCR), quantitative PCR, and metabarcoding for species-specific detection in environmental DNA. *Molecular Ecology Resources*, 19(6), pp.1407-1419. doi: 10.1111/1755-0998.13055.

Yan, Z.G. et al., 2023. Environmental DNA sequencing reveals the regional difference in diversity and community assembly mechanisms of eukaryotic plankton in coastal waters. *Frontiers in Microbiology*, 14, 1132925. doi: 10.3389/fmicb.2023.1132925.

Yang, Q. et al., 2014. Comprehensive transcriptome study to develop molecular resources of the copepod *Calanus sinicus* for their potential ecological applications. *BioMed Research International*, 3, 493825. doi: 10.1155/2014/493825.

Zhao, S.Y. et al., 2023. Rapidly evolving zooplankton in a salinizing world: To what extent does microevolutionary adaptation to one salt increase tolerance to another one? *Limnology and Oceanography*, 68(11), pp.2576-2586. doi: 10.1002/lno.12443.